Technische Universität München

Aspects of BSM physics: from gravity to dark matter to UV instantons

Dissertation

by

Maximilian Ruhdorfer

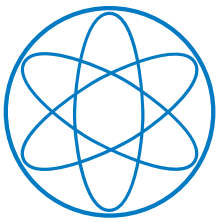

Physik-Department T75, TUM

Technische Universität München

Physik-Department T75

Aspects of BSM physics: from gravity to dark matter to UV instantons

Maximilian Ruhdorfer

Vollständiger Abdruck der von der Fakultät für Physik der Technischen Universität München zur Erlangung des akademischen Grades eines

Doktors der Naturwissenschaften

genehmigten Dissertation.

Vorsitzender:		Prof. Dr. Sherry Suyu
Prüfer der Dissertation:	1.	Prof. Dr. Andreas Weiler
	2.	Prof. Dr. Martin Beneke

Die Dissertation wurde am 11.05.2021 bei der Technischen Universität München eingereicht und durch die Fakultät für Physik am 22.07.2021 angenommen.

Aspects of BSM physics: from gravity to dark matter to UV instantons

Aspekte der BSM Physik: von Gravitation über dunkle Materie zu UV Instantonen

Maximilian Ruhdorfer

Abstract

In this thesis we study possible solutions to a wide range of theoretical and experimental shortcomings of the standard model (SM). The first two parts are devoted to properties and the phenomenology of two well-motivated extensions of the SM: pNGB dark matter in Composite Higgs models and the QCD axion. In the last part we investigate effective field theories (EFTs) of the SM and gravity, construct a non-redundant basis for the most general EFT of the SM coupled to general relativity to all orders and study its renormalization using modern amplitude methods.

Zusammenfassung

In dieser Arbeit untersuchen wir mögliche Lösungen für eine Reihe von Defiziten des Standardmodells (SM) der Teilchenphysik. Die ersten beiden Teile sind den Eigenschaften und der Phänomenologie zweier gut begründeter Erweiterungen des SM gewidmet: pNGB dunkle Materie in Composite Higgs Modellen und dem QCD Axion. Im letzten Teil untersuchen wir effektive Feldtheorien (EFT) des SM und der Gravitation, konstruieren eine redundanzfreie Basis für die allgemeinste EFT des SM gekoppelt an die allgemeine Relativitätstheorie zu allen Ordnungen und charakterisieren ihre Renormierung mittels moderner Amplitudenmethoden.

Contents

Introduction

The discovery of a Higgs boson with mass of approximately 125 GeV in July 2012 by the ATLAS and CMS collaborations [2, 3] constitutes a milestone in modern physics. It concludes a half century long monumental effort both in the theoretical and experimental community to make sense of the "particle zoo", i.e. the overwhelming number and variety of particles that was observed starting in the 1960s. The Higgs was merely the last missing keystone of the Standard Model (SM) of particle physics, which provides an excellent description of all particles and interactions, that we have observed so far. However, even after the completion of the SM many longstanding theoretical questions remain unanswered. For instance the SM can neither explain the lightness of the Higgs boson nor the absence of measurable $\mathcal{CP}$ violation in the strong sector. Furthermore the lack of a candidate for particle dark matter (DM) is proof that there has to exist some form of physics beyond the SM. These and other shortcomings suggest that the SM should be interpreted as an effective field theory (EFT) with a limited range of validity. The more fundamental theory, which supersedes the SM, is then expected to provide answers to the above questions. Finding this extension of the SM is now the main challenge of particle physics.

While we have few hints on the nature of the new physics (NP), our search is not random. We follow well-motivated guiding principles, which have proven useful in the past. One of the most important principles is the concept of naturalness of mass scales. Applied to the electroweak scale, or respectively the Higgs boson mass, this is the well-known hierarchy problem (see Section 2.1 for a thorough discussion). A large hierarchy between the electroweak scale and the scale at which effects of NP appear, which at the latest must occur at the Planck scale where gravity becomes strongly coupled, is unnatural and fine-tuned. Past experience tells us that nature tends to be natural and tuning often has a deeper reason, such as symmetries or dynamic selection. Thus there is good reason to expect new physics not far above the TeV scale.

Nonetheless, despite considerable effort the search for beyond the Standard Model (BSM) physics has so far been unsuccessful. There are no experimental hints of new degrees of freedom. For this reason a careful re-evaluation of our theoretical assumptions and biases is required to make sure that we do not miss NP simply because we are looking at the wrong place. We should look for new physics as broadly as possible. This includes the search for new ways to test the predictions of the SM, since any deviations might hint to BSM physics.

A global search for NP at several fronts is the main theme of this thesis. We approach this goal from two orthogonal but not unrelated directions: gravity in an EFT framework and DM. While the existence of gravity is a fact, we have collected ample evidence for DM during the past 100 years. However, all evidence so far originates exclusively from the gravitational interactions of DM, thus motivating a study of both phenomena as an ideal starting point for the exploration of BSM scenarios. In particular we investigate pseudo-Nambu Goldstone Boson (pNGB) DM and the QCD axion, both well-motivated DM candidates. Additionally we study EFTs of the SM and gravity and construct for the first time the EFT of all known low-energy degrees of

freedom, i.e. the EFT of gravity coupled to SM matter, which we call GRSMEFT.

A particularly active frontier in the quest for new physics is the area of DM searches. Almost 100 years after the discovery of the first solid hints of DM in the velocity dispersion in the Coma cluster in 1930 by Fritz Zwicky [4], its nature is still a mystery to us. During the past decades the focus and experimental target of a majority of DM searches has been weakly interacting massive particle (WIMP) DM. Its popularity originates from the fact that WIMPs generically arise in well-motivated theories addressing the hierarchy problem, such as supersymmetry or Composite Higgs (CH) models, and naturally achieve the observed relic abundance, a phenomenon which is often referred to as the "WIMP miracle". However, the null results in direct detection experiments, such as XENON1T [5], in combination with the increasing sensitivity of indirect searches for present-day annihilation products of DM, e.g. in the cosmic antiproton flux by AMS-02 [6] or gamma rays by Fermi-Lat [7], already put considerable stress on the WIMP. This has sparked a renewed interest in alternative DM scenarios (see Section 2.3 for an overview). While it is important to explore the landscape of DM models, one should not give up on the WIMP too easily, as thermal freeze-out remains a robust and predictive mechanism to explain the "missing mass" in the universe.

In Part I of the thesis we systematically study composite pNGB DM [8], a non-standard WIMP candidate, which can be naturally compatible with the null results in direct detection experiments. pNGB DM naturally emerges e.g. in non-minimal CH models, which are a prominent solution to the hierarchy problem (see Section 2.2). In such models both the Higgs and the DM are composite pNGBs of a new strong sector with a global symmetry $\mathcal{G}$, spontaneously broken to a subgroup $\mathcal{H} \subset \mathcal{G}$ at a scale $f \sim$ TeV. Due to the pNGB nature of the DM its leading coupling to the SM is via momentum dependent interactions with the Higgs. These are extremely suppressed at low momentum transfer and in particular in the elastic scattering of DM on nuclei, making pNGB DM naturally compatible with the strong exclusion limits from direct detection experiments. At the same time, they provide a large enough interaction strength in DM annihilations to set the observed relic abundance via the freeze-out mechanism. In practice this simple picture can be significantly altered due to explicit symmetry breaking effects, which are needed to give a mass to the DM and generically introduce momentum independent interactions. Thus in order to maintain the "Goldstone limit", which is characterized by the dominance of the momentum dependent couplings, a controlled breaking of the Goldstone shift symmetry of the DM is required.

We start the discussion with a short introduction and a presentation of the theoretical background of DM and CH models in Chapters 1 and 2. Subsequently we perform a model independent study of the DM phenomenology of pNGB DM in Chapter 3. Building on these general results we explicitly construct a fully realistic CH model based on the symmetry breaking structure $SO(7)/SO(6)$ in Chapter 4. This symmetry breaking structure gives rise to the Higgs doublet H and a complex DM candidate χ, which is stabilized by an exact $U(1)_{\rm DM} \subset SO(6)$ symmetry of the strong sector. We demonstrate that this model successfully implements electroweak symmetry breaking (EWSB) and study its DM phenomenology, which crucially depends on the source of the explicit breaking of the DM Goldstone symmetry. We identify three qualitatively different scenarios: breaking by the top quark couplings (Section 4.3), breaking by the bottom quark couplings (Section 4.4), breaking by gauging $U(1)_{\rm DM}$ (Section 4.5). These scenarios implement the "Goldstone limit" to a varying degree, each of them leading to an interesting and qualitatively different DM phenomenology.

After having established that Composite Higgs models can indeed feature pNGB DM which

effectively realizes the "Goldstone limit", an alternative direct probe is required, since direct detection signals are structurally suppressed for this type of DM candidate. A promising avenue are searches at particle colliders, which fully exploit the energy growth of the pNGB couplings. In Chapter 5 we assess the potential of current and future particle colliders to detect pNGB DM in weak boson fusion processes.

The focus of Part II is another well-motivated DM candidate, the QCD axion. The QCD axion was originally introduced as a solution to the strong-$\mathcal{CP}$ problem [9–12]: the axion dynamically relaxes the QCD theta angle, thereby explaining the absence of measurable $\mathcal{CP}$ violation in the strong interactions. However, it is at the same time an appealing DM candidate [13–15], whose relic abundance is set non-thermally through the misalignment mechanism or topological defects. The non-observation of WIMP DM has significantly increased the popularity of axion or axion-like particle (ALP) DM, with a large variety of ongoing and proposed experiments, such as the helioscope CAST [16] or the haloscope ADMX [17], trying to detect the axion. The interpretation of the search results in terms of the QCD axion crucially depends on its properties. In the standard approach the axion's low-energy properties are surprisingly well predicted, even though the origin of both the axion and the Peccei-Quinn symmetry breaking mechanism is unknown. In particular its mass can be expressed in terms of measured quantities, such as the pion mass m_π and its decay constant f_π, and the Peccei-Quinn symmetry breaking scale f_a, i.e. $m_a f_a \sim m_\pi f_\pi$ (see Section 7.3). This seems to be a robust prediction, independent of the specific ultra-violet (UV) completion. However, recently it was demonstrated that a non-trivial embedding of QCD in a product gauge group can lead to significant deviations from this expectation due to UV instantons [18, 19]. This is in contrast to the standard expectation that infrared (IR) QCD instantons dominate the mass. Since the axion mass is an important input in experimental efforts to detect the axion, it is essential to have a clear understanding of how robust the above prediction actually is. The goal of Part II of this thesis is to identify the underlying reason for the enhancement of UV instantons in non-trivial UV completions of QCD.

After a short introduction to the topic in Chapter 6 we present the theoretical background of the strong-$\mathcal{CP}$ problem and the axion as its solution in Chapter 7. Subsequently we establish the basics of instantons and the instanton calculus in spontaneously broken gauge theories in Chapter 8. With these ingredients in hand, we investigate in Chapter 9 the contribution to the axion mass from small instantons in partially broken UV completions of QCD.

In Part III we leave the area of DM physics. A particularly convenient and model independent way to parameterize general effects of heavy new physics is the EFT framework, where deviations from the leading theory are encoded in coefficients of higher dimensional operators. There is already a vast literature on the EFT for the SM, or SMEFT. In order to identify the most promising search channels, it is again important to follow some guiding principles in the form of UV complete theories, which can be matched onto the SMEFT. By integrating out the heavy degrees of freedom one gains insight about which effective operators are generated at which loop order. This knowledge will also be crucial for identifying the nature of the NP once we observe deviations from the SM. In this part of the thesis we perform the full one-loop matching of a simple but important benchmark scenario, the SM extended by a heavy singlet scalar, onto the dimension six SMEFT Lagrangian and identify contributions which have been missed in previous computations [20, 21].

While the SMEFT provides an excellent description of all directly observed low-energy degrees of freedom, it does not include gravity. The low-energy description of gravity, Einstein's theory of general relativity (GR), is manifestly non-renormalizable and therefore intrinsically an

EFT. Quantum corrections generate higher-dimensional operators, which have to be included in a consistent formulation. This implies that for a unified low-energy description of the SM coupled to gravity an EFT interpretation is unavoidable. A tower of higher dimensional operators parameterizes deviations from the SM minimally coupled to GR due to heavy physics. In this part of the thesis we want to find the maximal number of independent low-energy departures from GR, what corresponds to a full and non-redundant operator basis in the EFT language. Finding a non-redundant operator basis is a non-trivial task, which has recently been solved within the context of the SMEFT using Hilbert series methods [22, 23]. We generalize these methods to EFTs with gravity and construct an EFT of the SM coupled to gravity, which we call GRSMEFT. The GRSMEFT is the true low-energy description of all fundamental interactions, which have been observed so far. As a next step we study the underlying structure of the GRSMEFT, which might help us to gain a better understanding of gravity. At the quantum level it appears that there are some operators which do not get renormalized at one loop. This is a well-known phenomenon in the SMEFT, where many non-trivial zeroes appear in the dimension six anomalous dimension matrix [24–26]. These can be understood with the help of helicity selection rules [27]. Our goal is to generalize these selection rules to the GRSMEFT in order to gain a better understanding of the one-loop structure of gravity.

The discussion starts with an introduction in Chapter 10 and a review of the EFT framework and Hilbert series methods in Chapter 11. In Chapter 12 we perform the one-loop matching of the SM extended by a scalar singlet onto the SMEFT. Chapters 13 and 14 focus on gravitational EFTs, where we first construct the GRSMEFT in Chapter 13 and subsequently derive helicity selection rules for one-loop renormalization in Chapter 14 and compute a selection of anomalous dimensions in a toy SM coupled to gravity.

We finally conclude in Part IV and summarize our main results. Additionally we give an outlook on still ongoing work and possible future directions.

The thesis is largely based on the following publications:

[28] R. Balkin, M. Ruhdorfer, E. Salvioni and A. Weiler, *Charged Composite Scalar Dark Matter*, JHEP **1711**, 094 (2017), [arXiv:1707.07685].

[29] R. Balkin, M. Ruhdorfer, E. Salvioni and A. Weiler, *Dark matter shifts away from direct detection*, JCAP **1811**, no. 11, 050 (2018), [arXiv:1809.09106].

[30] M. Ruhdorfer, J. Serra and A. Weiler, *Effective Field Theory of Gravity to All Orders*, JHEP **05**, 083 (2020), [arXiv:1908.08050].

[31] M. Ruhdorfer, E. Salvioni and A. Weiler, *A Global View of the Off-Shell Higgs Portal*, SciPost Phys. **8**, 027 (2020), [arXiv:1910.04170].

[32] C. Csáki, M. Ruhdorfer and Y. Shirman, *UV Sensitivity of the Axion Mass from Instantons in Partially Broken Gauge Groups*, JHEP **04**, 031 (2020), [arXiv:1912.02197].

[33] U. Haisch, M. Ruhdorfer, E. Salvioni, E. Venturini and A. Weiler, *Singlet night in Feynmanville: one-loop matching of a real scalar*, JHEP **04**, 164 (2020), [erratum: JHEP **07**, 066 (2020)], [arXiv:2003.05936].

and work in progress

[34] P. Baratella, D. Haslehner, M. Ruhdorfer, J. Serra and A. Weiler, *(Non-)Renormalization of Gravity*, in preparation.

In particular, some figures contained in this thesis have previously appeared in one of these articles.

Part I

Composite dark matter

Chapter 1

Motivation and introduction

The Composite Higgs framework, i.e. the idea that the Higgs arises as a composite pNGB of a new strong sector, is one of the simplest and best-motivated solutions to the hierarchy problem [35]. While the minimal realistic model based on the symmetry breaking structure $SO(5)/SO(4)$ [36] incorporates only the Higgs-doublet as pNGBs, non-minimal realizations contain additional particles which can also provide a solution to the DM puzzle [8]. If besides the Higgs the enlarged symmetry breaking structure $\mathcal{G}/\mathcal{H}$ gives rise to an additional pNGB χ which is a singlet under the SM gauge groups and stable, it constitutes a compelling WIMP DM candidate.

Such a scenario was first explored in the $SO(6)/SO(5)$ model [37], which contains the Higgs-doublet H and a real scalar η as Goldstone bosons (GBs). The possibility that the real scalar η can play the role of DM was extensively explored in [8, 38]. In this setup the DM is stabilized by an exact Z_2 symmetry $P_\eta : \eta \to -\eta$. Even though this is preserved by the two-derivative Lagrangian it is not part of the symmetry of the strong sector, i.e. $P_\eta \notin SO(6)$. This means that P_η can be violated at higher-derivative order, e.g. by a Wess-Zumino-Witten term which appears in the model at four-derivative order with a UV dependent coefficient [37]. Thus one is effectively forced to assume that the symmetry of the UV completion is larger and respects $O(6)/O(5)$ in order to ensure the stability of the DM.

However, an enlarged symmetry breaking structure can also provide a natural stabilization mechanism. E.g. if the DM is a complex scalar charged under an exact $U(1)_{\rm DM} \subset \mathcal{H}$ symmetry in the unbroken subgroup of the strong sector, under which all SM particles are neutral, it is automatically stable. This stabilization mechanism is UV-robust in the sense that any $\mathcal{G}$-invariant high-energy completion of the strong sector will automatically respect $U(1)_{\rm DM}$. Such a mechanism is realized e.g. in a model based on $SO(7)/SO(6)$ which we will study in detail in Chapter 4. The $SO(7)/SO(6)$ coset contains in addition to the Higgs doublet two real scalars η and κ, which are singlets under the custodial $SO(4) \subset SO(6)$. In addition to the custodial $SO(4)$ the unbroken $SO(6)$ also possesses an $SO(2)$ factor, i.e. $SO(4) \times SO(2) \subset SO(6)$, under which η and κ rotate into each other. Combining η and κ into a complex scalar, we obtain a DM candidate χ which is charged under $U(1)_{\rm DM} \simeq SO(2)$, thus implementing the above stabilization mechanism.

Another appealing aspect of pNGB DM in Composite Higgs models is that it is naturally light and weakly coupled at low energies in the same way as the Higgs is and therefore an ideal WIMP candidate. Its leading coupling to the SM is the derivative Higgs portal

$$\frac{1}{f^2}\partial_\mu |H|^2 \partial^\mu |\chi|^2 \,, \tag{1.1}$$

originating from the non-linear sigma model Lagrangian of the GBs. This coupling has the

advantage that it is extremely suppressed at small momentum transfer which characterizes DM-nucleon scattering ($|t|/f^2 \lesssim (100\text{ MeV})^2/(1\text{ TeV})^2 \sim 10^{-8}$), what makes it naturally compatible with the strong exclusions from direct detection experiments. But at the same time the interaction strength for DM annihilation is $s/f^2 \simeq 4m_\chi^2/f^2$ which is large enough to obtain the observed relic abundance for weak scale DM. This feature is one of the reasons why pNGB DM has received increasing attention lately [28, 29, 38–50] within the Composite Higgs framework and in general.

However, explicit symmetry breaking effects can significantly change this simple and appealing picture. Some explicit breaking of the global Goldstone shift symmetry is in fact necessary to generate a potential for the Higgs and Yukawa couplings of the Higgs to the elementary fermions and a mass for the DM candidate χ. This generically also introduces non-derivative couplings of the DM to the SM and in particular the marginal Higgs portal[1]

$$2\,\lambda|H|^2|\chi|^2\,, \tag{1.2}$$

which has been extensively studied in renormalizable scalar singlet DM models [51–53]. It is well-known that WIMP DM which dominantly annihilates through the marginal Higgs portal is mostly ruled out by direct detection (exceptions being the Higgs resonance region, or DM heavier than a few TeV [54] or non-standard but motivated cosmological histories which can open up large regions of parameter space [55]). This implies that in realistic models the marginal Higgs portal coupling has to be suppressed in order to be not ruled out by direct detection. Therefore one has to be as close as possible to the "Goldstone limit" which is characterized by the derivative Higgs portal being the dominant coupling. In Chapter 4 we will demonstrate that this limit can indeed be achieved in the $SO(7)/SO(6)$ model.

We start this part of the thesis with an introduction to the theoretical backgrounds of Composite Higgs models and DM in Chapter 2. Chapter 3 discusses pNGB DM in general and emphasizes some of its main features. In Chapter 4 we explore realistic pNGB DM in the $SO(7)/SO(6)$ Composite Higgs model and identify scenarios which are close to the "Goldstone limit". Finally we present the results of our study of the derivative Higgs portal, the irreducible feature of pNGB DM models, at present and future colliders in Chapter 5. Chapters 3 and 4 are based on [28, 29], whereas the results of Chapter 5 were published in [31].

[1] Note that the more common normalization in marginal Higgs portal models is $\lambda|H|^2|\chi|^2$. We will adopt this normalization in Chapter 5 when we discuss collider constraints on the marginal and derivative Higgs portal. However, in Chapter 3 and 4 we use the normalization in Eq. (1.2).

Chapter 2

Composite Higgs and dark matter

In this chapter we lay the theoretical foundations for the remainder of this part of the thesis. After a brief overview of the hierarchy problem in Section 2.1, we present one of its most popular solutions in Section 2.2: the Composite Higgs framework. Afterwards we discuss the second main ingredient of this part of the thesis: dark matter. We start with a global picture of the DM landscape in Section 2.3 and later focus on one particularly appealing DM candidate, the WIMP, and introduce some fundamental concepts of WIMP DM in Section 2.4.

2.1 The hierarchy problem

There are many equivalent ways to formulate the hierarchy problem (see e.g. [56, 57] for modern essays on the topic and [58–60] for the original formulation). Here we will discuss a variation based on the introduction of [61] which is a formulation that is deeply rooted in the EFT interpretation of the SM.

The foundation of the hierarchy problem is the realization that the SM on its own is an incomplete description of nature. For instance a consistent coupling to gravity is only possible in terms of a low-energy expansion in powers of $(E/M_{\rm Pl})$, which breaks down for energies above the Planck Mass $E > (4\pi)M_{\rm Pl}$. This means that perturbative quantum gravity has to be replaced by a more fundamental theory of quantum gravity with new degrees of freedom or interactions at the latest at the Planck scale. Thus any computation within the SM is only valid up to an energy scale $\Lambda_{\rm SM} \leq M_{\rm Pl}$ where new physics beyond the SM, which does not necessarily have to be related to quantum gravity and might be located far below the Planck scale, appears. This implies that the SM is nothing else but an EFT with a limited range of validity and should, according to the EFT paradigm, not be truncated at the renormalizable level. One should include all local and gauge invariant operators of arbitrary mass dimension d, i.e.

$$\mathcal{L} = \mathcal{L}_{\rm SM} + \sum_{d>4} \sum_{i} c_i^{(d)} \frac{\mathcal{O}_i^{(d)}}{\Lambda_{\rm SM}^{d-4}} \,, \tag{2.1}$$

where on dimensional grounds the higher dimensional operators are suppressed by the scale of new physics $\Lambda_{\rm SM}$. The EFT interpretation nicely explains some further puzzles of the SM. The five dimensional Weinberg operator for example introduces masses for the neutrinos. For an order one operator coefficient the experimental value of $m_\nu \sim 0.1$ eV hints to a suppression scale of $\Lambda_{\rm SM} \sim 10^{14}$ GeV. Such a large scale of new physics would also explain why all low energy observables are so far compatible with the renormalizable SM Lagrangian. The heavy new physics assumption with a cutoff of the order of the GUT scale $\Lambda_{\rm SM} \sim M_{\rm GUT} = 10^{15}$ GeV

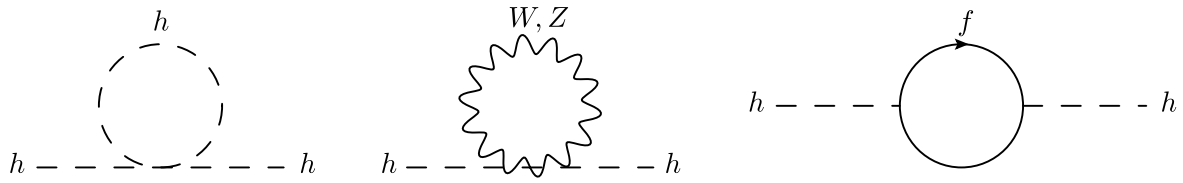

Figure 2.1: Feynman diagrams contributing to the renormalization of the Higgs mass within the SM.

therefore seems to be a plausible and well-motivated scenario. But is heavy new physics also compatible with the renormalizable SM Lagrangian? Let us for the following assume that the scale of new physics is $\Lambda_{\rm SM} \sim M_{\rm GUT}$. The marginal couplings are not directly sensitive to $\Lambda_{\rm SM}$ but the SM also contains one relevant operator, the Higgs mass term. Applying the same logic based on dimensional analysis, which led us to conclude that the $d > 4$ operators are highly suppressed by the scale of new physics, we would expect the Higgs mass term to be of the size

$$c\,\Lambda_{\rm SM}^2 H^\dagger H\,. \tag{2.2}$$

From measuring the Higgs mass we know that $|\mu^2| = m_H^2/2 = (89\text{ GeV})^2 \ll M_{\rm GUT}^2$, i.e. if new physics appears at a high scale the coefficient $c = \mu^2/M_{\rm GUT}^2 \sim 10^{-26} \ll 1$ is unnaturally small. The Hierarchy or Naturalness Problem can thus be phrased as the question why dimensional analysis, which perfectly explains the suppression of higher dimensional operators, fails to predict the order of magnitude of the Higgs mass. Why is there such a large hierarchy between the electroweak and new physics scale, i.e. why is $c = \mu^2/M_{\rm GUT}^2$ so small?

The small value of c is even more puzzling when one considers loop corrections to the Higgs mass term. The diagrams in Figure 2.1 with loops of Higgses, W and Z bosons and the top quark modify the Higgs mass by

$$\delta_{\rm SM} m_H^2 = \frac{\Lambda_{\rm SM}^2}{8\pi^2}\left[3\,y_t^2 - \frac{3\,g_w^2}{4}\left(1 + \frac{1}{2\,\cos^2\theta_w}\right) - 3\lambda\right]. \tag{2.3}$$

The diagrams are quadratically divergent and are therefore sensitive to the scale of new physics, i.e. to the cutoff of the theory. For $\Lambda_{\rm SM} \sim M_{\rm GUT}$ one would consequently need a cancelation between the bare tree level Higgs mass term against the loop contributions of at least 24 digits in order to obtain the observed Higgs mass $m_H = 125$ GeV. Such a cancelation would seem highly unnatural! Note that the sensitivity to $\Lambda_{\rm SM}$ is not merely an artefact of using a cutoff regulator for the loop integral. A cutoff in the EFT language stands for a physical mass threshold such as the mass of a heavy particle. Once these heavy degrees of freedom couple to the SM the Higgs mass will be sensitive to the corresponding mass scale even in regularization schemes where power law divergences are absent, such as dimensional regularization.

One could argue that only the renormalized Higgs mass is observable and is fixed to whatever value we observe in experiments. This is certainly true at a technical level in the EFT framework which should make sense without having exact knowledge of the UV, but the hierarchy problem is actually a question about the nature of the UV completion that gives rise to the SMEFT. We expect that the fundamental theory of electroweak symmetry breaking would predict the Higgs mass in terms of its microscopic input parameters, similar to the Fermi constant G_F which can be predicted in the theory of the weak interaction in terms of the weak coupling constant g_w and the W boson mass m_W. If this is the case the contributions to the Higgs mass can be

parameterized as [61]

$$m_H^2 = \int_0^\infty dE \, \frac{dm_H^2}{dE}(E;p)\,, \tag{2.4}$$

where the integral includes contributions to m_H^2 from all energy scales. Splitting this up into contributions from $E \leq \Lambda_{\rm SM}$, which are computable within the EFT, and BSM contributions from $E \geq \Lambda_{\rm SM}$ we obtain

$$m_H^2 = \int_0^{\Lambda_{\rm SM}} dE \, \frac{dm_H^2}{dE}(E;p) + \int_{\Lambda_{\rm SM}}^\infty dE \, \frac{dm_H^2}{dE}(E;p) = \delta_{\rm SM} m_H^2 + \delta_{\rm BSM} m_H^2\,, \tag{2.5}$$

where $\delta_{\rm SM} m_H^2$ is present in all theories that give rise to the SM and has the generic form that is given by Eq. (2.3). In order to obtain $m_H^2 \ll \Lambda_{\rm SM}^2$ the completely unrelated $\delta_{\rm BSM} m_H^2$ contribution has to cancel $\delta_{\rm SM} m_H^2$ to great accuracy. The required fine-tuning can be quantified in terms of

$$\Delta \geq \frac{\delta_{\rm SM} m_H^2}{m_H^2} \simeq \left(\frac{\Lambda_{\rm SM}}{500\ {\rm GeV}}\right)^2 . \tag{2.6}$$

Order one tuning therefore requires new physics at the TeV scale. New physics at higher scales needs more tuning, which implies that even if we know the fundamental theory we have to measure the input parameters to an equally large precision in order to obtain a prediction for the Higgs mass.

Conceptually there is nothing wrong with a model that exhibits such a large tuning and it could well be that the solution to the hierarchy problem turns out to be anthropic selection. However, past experience tells us that nature tends to be natural and tuning often has some deeper reason, such as symmetries or dynamic selection. For this reason we think it is worth exploring models that aim to explain why the electroweak scale is as low as it is in a natural way without fine-tuning.

2.2 Composite Higgs

The idea behind Composite Higgs models is very simple and dates back to the 1980s [62–68]: instead of an elementary particle the Higgs could be a composite object of finite size l_H, i.e. the Higgs could be a bound state of a new strong sector which confines at the scale $m_* = 1/l_H$. In the following we will first discuss the Composite Higgs framework in general before going into more details concerning partial compositeness and the Goldstone Lagrangian. We conclude this section with a presentation of the minimal Composite Higgs model based on the coset $SO(5)/SO(4)$. For a pedagogic introduction to Composite Higgs models see [61,69–71] and [35] for a review. This section loosely follows and adopts the notation of [61].

2.2.1 The Composite Higgs framework

A composite Higgs naturally solves the Hierarchy problem. Its mass is screened from any energy scales above the confinement scale m_*. The confinement scale on the other hand is dynamically generated by dimensional transmutation similar to the QCD scale $\Lambda_{\rm QCD}$. In UV theories without relevant operators, other than fermion mass terms, the running of the coupling constant g is logarithmic and therefore has to run for an exponentially long time from a weakly coupled regime at a high scale $\Lambda_{\rm UV} \gg m_*$ until it reaches the strongly coupled regime at m_* where it formally diverges

$$\mu \frac{\partial}{\partial \mu} \frac{1}{g^2(\mu)} = -\frac{b_0}{8\pi^2} \qquad \Rightarrow \qquad m_* = \Lambda_{\rm UV} \exp\left(\frac{-8\pi^2}{g^2(\Lambda_{\rm UV})(-b_0)}\right), \tag{2.7}$$

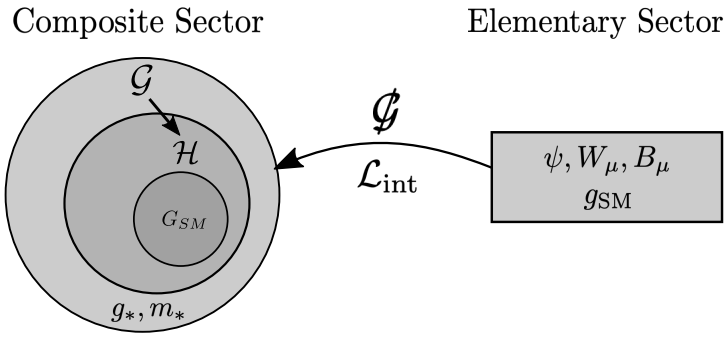

Figure 2.2: Structure of Composite Higgs models. The composite sector with confinement scale m_* and typical coupling of the resonances g_* possesses a global symmetry $\mathcal{G}$ which is spontaneously broken to a subgroup $\mathcal{H}$ which contains the electroweak gauge group of the SM $G_{\text{SM}} = SU(2)_L \times U(1)_Y$. The Higgs is then identified with a $SU(2)_L$ doublet of GBs in the coset $\mathcal{G}/\mathcal{H}$. The global symmetry is explicitly broken by the couplings to the elementary sector, the SM fermions and vectors. This explicit breaking generates the Higgs potential which eventually breaks electroweak symmetry.

where $b_0 < 0$ is the beta function coefficient for an asymptotically free theory. This naturally generates an exponential hierarchy between m_*, which is potentially at the TeV scale, and a large UV scale such as M_{Pl} or M_{GUT} and therefore solves the hierarchy problem.

If the Higgs is a bound state in a new strongly coupled sector its natural mass would be $m_H \sim m_*$ or at most a factor of (4π) below the confinement scale. This suggests that we need $m_* = 1$ TeV or lower in order to make the measured Higgs mass of $m_H = 125$ GeV natural. However, this is problematic for two reasons:

i) In a generic strongly coupled theory the Higgs would be only one of many resonances appearing at m_*. But so far we have not observed any hints of new particles at the TeV scale.

ii) At energies $E \ll m_*$ the heavy resonances can be integrated out generating EFT operators with suppression scale m_*. EFT operators involving the electroweak sector suppressed by a TeV scale cutoff are in conflict with electroweak precision observables.

This essentially forces us to take $m_* \gtrsim 10$ TeV which again introduces some degree of tuning for the Higgs mass. This is often referred to as the little hierarchy problem.

Luckily we can turn to low energy QCD as inspiration for a solution. Composite scalars can be naturally lighter than the other resonances if they are pNGBs of an approximate global symmetry of the strong sector. In QCD the pions for example are the GBs of the approximate chiral $SU(2)_L \times SU(2)_R$ symmetry of the up and down quarks in the QCD Lagrangian which is spontaneously broken to the vectorial combination $SU(2)_L \times SU(2)_R \to SU(2)_V$ by the chiral condensate $\langle \bar{q}q \rangle \propto \Lambda^3_{\text{QCD}}$. Consequently the pion mass is much lower than the confinement scale $m_\pi \simeq 140$ MeV $\ll \Lambda_{\text{QCD}}$.[1]

Finally the picture of Composite Higgs models emerges (see Figure 2.2): we assume that there exists a new strong sector with a global symmetry $\mathcal{G}$ which is spontaneously broken to a subgroup $\mathcal{H}$ when the strong sector confines at m_*. This gives rise to dim $\mathcal{G}-$dim $\mathcal{H}$ massless GBs with symmetry breaking scale f which is much larger than the electroweak scale $f \gg v$.

[1] The mass originates from the small explicit breaking of the chiral symmetry by the non-zero quark masses.

In order to obtain a phenomenologically viable Composite Higgs model this construction has to satisfy the following additional constraints.

1. The electroweak gauge group of the SM $G_{\rm SM} = SU(2)_L \times U(1)_Y$ must be a symmetry of the strong sector and must remain unbroken, i.e. $G_{\rm SM} \subset \mathcal{H}$, such that the SM gauge bosons do not pick up TeV scale masses.

2. The coset $\mathcal{G}/\mathcal{H}$ has to contain a $SU(2)_L$ doublet of GBs which can be identified with the Higgs boson.

Phenomenologically viable Composite Higgs models contain in addition to the composite sector a sector of elementary particles with all SM fermions and gauge bosons,[2] in complete analogy to the elementary photon and leptons in low energy QCD. The SM particles do not fill full $\mathcal{G}$ representations and therefore their coupling to the strong sector or respectively the partial gauging of only the subgroup $G_{\rm SM} \subset \mathcal{G}$ breaks $\mathcal{G}$ explicitly. This means that the Higgs is no longer an exact GB and obtains a potential at the loop level, which triggers electroweak symmetry breaking. The hierarchy between the electroweak scale v and the symmetry breaking scale of the strong sector f is quantified in terms of the ξ parameter

$$\xi = \left(\frac{v^2}{f^2}\right), \tag{2.8}$$

which is determined by the orientation of the $SU(2)_L \times U(1)_Y$ w.r.t. the unbroken group in the true vacuum. As we will see in the following the natural value is $\xi \sim 1$, what requires some tuning to generate a hierarchy between v and f.

2.2.2 Partial compositeness

Now that we know the general structure of the composite sector, it is time to discuss the couplings of the elementary SM particles to the strong sector and in particular how the Yukawa couplings are generated. The most straightforward way to introduce a Yukawa coupling in the UV theory above the confinement scale is in terms of a bilinear quark operator coupled to a scalar operator $\mathcal{O}_S$ of the strong sector. For the third generation quarks this would be of the form

$$\mathcal{L}^{\rm UV}_{\rm int} = \frac{\lambda_t}{\Lambda_{\rm UV}^{d-1}} \bar{q}_L \mathcal{O}_S^c t_R + \frac{\lambda_b}{\Lambda_{\rm UV}^{d-1}} \bar{q}_L \mathcal{O}_S b_R + h.c.\,, \tag{2.9}$$

where $\Lambda_{\rm UV}$ is the cutoff of the strong sector theory and d is the mass dimension of $\mathcal{O}_S$, which has the quantum numbers of the Higgs. In analogy to QCD $\mathcal{O}_S$ can be realized as a bilinear of techniquarks of the new strong sector $\mathcal{O}_S \sim \bar{\psi}^i_R \psi_{L\,i}$ which confines below m_* and forms the Higgs. Therefore the mass dimension of $\mathcal{O}_S$ is typically of the order $d \simeq 3$. However, in this approach it is hard to generate $\mathcal{O}(1)$ Yukawa couplings for the top quark. In order to see this one has to evolve $\lambda_{t,b}$ down to the confinement scale

$$y_{t,b} \simeq \lambda_{t,b}(m_*) = \lambda_{t,b} \left(\frac{m_*}{\Lambda_{\rm UV}}\right)^{d-1}, \tag{2.10}$$

where we assumed that the running is dominated by the canonical mass dimension. $\lambda_{t,b}$ is defined at the UV scale $\Lambda_{\rm UV}$ and cannot be arbitrarily large without violating unitarity. It can be shown that unitarity arguments for scalar operators also imply $d - 1 > 0$ which makes it

[2] Note that the right-handed top can potentially be a composite particle of the strong sector.

challenging to obtain $\mathcal{O}(1)$ Yukawa couplings if there is as anticipated a large hierarchy between $\Lambda_{\rm UV}$ and m_*.

A more solid solution is based on the partial compositeness idea introduced by Kaplan [72] and later rediscovered for models of electroweak symmetry breaking in [73]. In the partial compositeness scenario one assumes that the coupling to the strong sector is linear and of the following form

$$\mathcal{L}_{\rm int}^{\rm UV} = \frac{\lambda_{t_L}}{\Lambda_{\rm UV}^{d_L-5/2}}\bar{q}_L\mathcal{O}_q^L + \frac{\lambda_{t_R}}{\Lambda_{\rm UV}^{d_R-5/2}}\bar{t}_R\mathcal{O}_t^R + \dots\,, \tag{2.11}$$

where $\mathcal{O}_f^{L/R}$ are fermionic operators of the strong sector. These couplings will lead to mixing of the SM fermions with composite resonances in the IR. Here the situation is improved since unitarity bounds for fermionic operators only require $d_{L/R} > 3/2$, such that an operator dimension of $d_{L/R} \sim 5/2$ allows λ_{t_L/t_R} to stay sizable in the IR

$$\lambda_{t_L,t_R}(m_*) = \lambda_{t_L,t_R}\left(\frac{m_*}{\Lambda_{\rm UV}}\right)^{d_{L/R}-5/2}\,, \tag{2.12}$$

which will be able to generate the $\mathcal{O}(1)$ top Yukawa coupling. Note that this can also provide an explanation for the hierarchy of Yukawa couplings. Each quark flavor q_i couples to a different composite operator $\mathcal{O}_{q_i}^{L/R}$. If the operators for the lighter quarks have a dimension $d_{L/R} > 5/2$ their Yukawa couplings are suppressed by powers of $(m_*/\Lambda_{\rm UV})$ and for a large enough hierarchy between m_* and $\Lambda_{\rm UV}$ already a small change in $d_{L/R}$ can cause a huge suppression.

As we already mentioned before, once the strong sector confines the composite operators $\mathcal{O}_f^{L/R}$ generate fermionic resonances of typical mass m_* from the vacuum. These fermionic resonances need to have the same SM quantum numbers as the SM fermions they couple to and are usually referred to as their partners. This implies e.g. that the quark partners have to be colored. Let us now discuss what this implies for the top sector. The situation is completely analogous for all other SM fermions. Below the confinement scale $\mathcal{O}_q^L$ and $\mathcal{O}_t^R$ interpolate multiplets of vector-like fermionic resonances, the top partners, which we will denote by Q and T with $\langle 0|\mathcal{O}_q^L|Q\rangle \neq 0$ and $\langle 0|\mathcal{O}_t^R|T\rangle \neq 0$. Therefore at low energies the interaction Lagrangian in Eq. (2.11) together with the mass terms for the composite resonances schematically takes the form

$$\mathcal{L}_{\rm int}^{\rm IR} = -m_*(\bar{Q}Q + \bar{T}T) - \frac{\lambda_{t_L}}{g_*}m_*(\bar{q}_LQ + h.c.) - \frac{\lambda_{t_R}}{g_*}m_*(\bar{t}_RT + h.c.)\,, \tag{2.13}$$

where we inserted the typical coupling of the composite resonances g_* for dimensional reasons. λ_{t_L,t_R} are understood to be to be taken at the IR scale m_*. Eq. (2.13) induces a mixing between the elementary top quark and its partners such that the observable top quark, just like any other SM fermion, is a linear combination of elementary and composite degrees of freedom

$$|\text{physical ferminon}\rangle = \cos\theta\,|\text{elementary ferminon}\rangle + \sin\theta\,|\text{composite resonance}\rangle \tag{2.14}$$

and thus partially composite, hence the name partial compositeness. Eq. (2.13) generates a mixing angle of the size

$$\sin\theta_i = \frac{\lambda_i}{\sqrt{g_*^2+\lambda_i^2}} \sim \frac{\lambda_i}{g_*}\,, \quad i = t_L, t_R\,, \tag{2.15}$$

where we assumed in the last step that the typical coupling of the composite resonances is large, i.e. $g_* \gg \lambda_{t_L/t_R}$. $\sin\theta_{L/R}$ is a measure for the amount of compositeness of a fermion and is often called the compositeness fraction $\epsilon_{L/R} = \sin\theta_{L/R}$. The top partners couple to further resonances, among others the pNGB Higgs, with coupling strength g_*. This means that also the

physical top quark talks to the Higgs via its mixing with the top partners. Thus the size of the Yukawa couplings can be estimated to be

$$y_t = g_* \sin\theta_{t_L} \sin\theta_{t_R} \sim \frac{\lambda_{t_L}\lambda_{t_R}}{g_*} \,. \tag{2.16}$$

In this picture lighter fermions are less composite, i.e. they have a smaller mixing angle with their composite partners.

2.2.3 Higgs potential and power counting

An important assumption of Composite Higgs models is that all the breaking of the global symmetry $\mathcal{G}$ stems from the couplings with the elementary sector. The elementary sector possesses only a $G_{\rm SM} = SU(2)_L \times U(1)_Y$ symmetry, such that the couplings explicitly break $\mathcal{G}\times SU(2)_L\times U(1)_Y \to [SU(2)_L\times U(1)_Y]_{\rm diag}$ to the diagonal combination of the elementary sector $G_{\rm SM}$ and the $G_{\rm SM} \subset \mathcal{H}$. The gauge sector accomplishes this by only gauging the $SU(2)_L\times U(1)_Y$ subgroup of $\mathcal{G}$. In the fermion sector the linear couplings in Eq. (2.13) break the symmetry since the composite resonances come in full $\mathcal{G}$ representations, whereas the SM fermions only fill incomplete $\mathcal{G}$ multiplets. Due to this explicit breaking of the symmetry the Higgs is no longer an exact GB and obtains a potential at the loop level which is schematically of the form

$$V(H) \sim -\mu^2|H|^2 + \lambda|H|^4 \,. \tag{2.17}$$

The size of the coefficients can be easily estimated by naive dimensional analysis (NDA) and by including the spurions of the symmetry breaking, i.e. the SM couplings

$$\mu^2 \sim \frac{g_{\rm SM}^2}{16\pi^2} m_*^2 \,, \qquad \lambda \sim \frac{g_*^2}{16\pi^2} g_{\rm SM}^2 \,. \tag{2.18}$$

These estimates imply that the natural values for the electroweak scale and the Higgs mass are

$$v \sim \frac{m_*}{g_*} = f \,, \qquad m_h \sim \frac{g_*}{4\pi}\sqrt{2}\, g_{\rm SM} v \,. \tag{2.19}$$

While the Higgs mass is naturally light, its VEV is naturally of the same size as the symmetry breaking scale of the strong sector. However, electroweak precision tests require that $f \geq 3v$, such that some tuning is required, which we can quantify with the ξ parameter defined in Eq. (2.8). Let us add a few more comments about the estimate of the Higgs potential parameters. Eq. (2.18) shows that the largest contribution to the potential comes from the top sector since it has the largest couplings. For this reason contributions from first and second generation quarks as well as the leptons are usually neglected. The contribution from the gauge sector can be important as well even though it seems to be suppressed by the weak gauge coupling. The reason for this is that the strong sector vector resonances which cut off the quadratic divergence and whose mass m_ρ enters instead of m_* in Eq. (2.17) are stronger constrained than the fermionic partners and must have masses of $m_\rho \gtrsim 3$ TeV, compared to $m_* \gtrsim 1$ TeV for the top partners. Besides the gauge sector typically contributes with negative sign to μ^2 and therefore stabilize the electroweak symmetry in contrast to the fermionic contributions which are destabilizing. Thus including the gauge contributions can reduce the residual tuning in the potential.

Before we go on and discuss the Goldstone Lagrangian let us shortly comment on the power counting and dimensional analysis in Composite Higgs models. The usual assumption is that the strong sector can be characterized by one scale and one coupling, i.e. the typical mass of

the composite resonances m_* and their typical coupling g_*. The symmetry breaking scale f is strictly speaking not an energy scale. It has the dimensions of a scalar vacuum expectation value (VEV) and is simply the normalization of the GBs in the non-linear sigma model. In the one scale and one coupling hypothesis the relation to m_* and g_* is fixed by dimensional analysis as we will see in the following

$$m_* = g_* f \,. \tag{2.20}$$

But dimensional analysis can do even more. With its help we can estimate the natural size of EFT operator coefficients. However, the real power of dimensional analysis only manifests itself if one reintroduces units of energy E, length L and time T, s.t. the Lagrangian has dimensions of

$$[\mathcal{L}] = \frac{ET}{L^4} = \frac{[\hbar]}{L^4} \,, \tag{2.21}$$

where we used that $[\hbar] = ET$. With the convention $x^\mu = (ct, x_1, x_2, x_3)$ we see that $[\partial_\mu] = L^{-1}$. Using this we can easily find the dimensions of canonically normalized scalar, fermion and vector fields from their kinetic terms

$$[\phi] = [A_\mu] = \frac{[\hbar]^{1/2}}{L} \,, \qquad [\psi] = \frac{[\hbar]^{1/2}}{L^{3/2}} \,. \tag{2.22}$$

This also implies that in these units a particle mass or a general mass scale has dimensions of $[m] = [m_*] = L^{-1}$. In natural units with $\hbar = c = 1$ couplings are dimensionless but by examining gauge and Yukawa interaction in this units we find that both couplings actually carry dimensions of $[g] = [y] = [\hbar]^{-1/2}$. Note that quartic scalar couplings scale as $(\text{coupling})^2$, i.e. $[\lambda] = [g]^2$. With this information we can express the units of all quantum fields in terms of mass and coupling units

$$[\phi] = [A_\mu] = \frac{[m]}{[g]} \,, \qquad [\psi] = \frac{[m]^{3/2}}{[g]} \,. \tag{2.23}$$

Now we can finally appreciate the difference between a scalar VEV like f and a mass scale like m_* and understand the relation in Eq. (2.20). Note that loop corrections come with an additional factor of $\hbar$ which we can absorb into the loop factor $1/(4\pi)^2$ in natural units, s.t. factors of (4π) formally scale like a coupling constant $[(4\pi)] = [g]$.

In a theory with only one coupling and one scale we can use g_* and m_* to form dimensionless field variables $\hat{\phi}, \hat{\psi}, \hat{A}_\mu$ and dimensionless derivatives $\hat{\partial}_\mu$ with

$$\hat{\phi} = \frac{g_* \phi}{m_*} \,, \quad \hat{\psi} = \frac{g_* \psi}{m_*^{3/2}} \,, \quad \hat{A}_\mu = \frac{g_* A_\mu}{m_*} \,, \quad \hat{\partial}_\mu = \frac{\partial_\mu}{m_*} \,, \tag{2.24}$$

such that we can write the Lagrangian as

$$\mathcal{L} = \frac{m_*^4}{g_*^2} \hat{L}(\hat{\phi}, \hat{\psi}, \hat{A}_\mu) \,. \tag{2.25}$$

In order to extend the power counting to elementary fields we have to normalize the fields with the couplings through which they talk to the strong sector, for example the gauge coupling g for the gauge fields.[3] With this we can write the tree level power counting rule in all generality as

$$\mathcal{L} = \frac{m_*^4}{g_*^2} \hat{L}\left[\frac{\partial_\mu}{m_*}, \frac{g_* \Pi}{m_*}, \frac{g_* \sigma}{m_*}, \frac{g_* \Psi}{m_*^{3/2}}, \frac{g A_\mu}{m_*}, \frac{\lambda \psi}{m_*^{3/2}}\right] , \tag{2.26}$$

[3] Note that this approach does not give the correct normalization for the kinetic terms of the elementary fields.

where Π, σ, Ψ are composite sector pNGBs, scalar resonances and fermionic resonances, respectively, whereas A_μ and ψ are elementary gauge fields and fermions with their corresponding gauge coupling g and linear coupling to the fermionic partners λ. The generalization to loop effects is straightforward.

2.2.4 Goldstone Lagrangian in coset construction

One of the key ingredients of Composite Higgs models is the pNGB nature of the Higgs. In order to describe its dynamics we have to discuss how one can construct the GB Lagrangian. As was found by Callan, Coleman, Wess and Zumino (CCWZ) [74, 75] there is not much freedom in constructing the Lagrangian. Already the knowledge of the coset $\mathcal{G}/\mathcal{H}$ completely fixes the Goldstone interactions due to the non-linear realization of the symmetry. The so called coset construction or CCWZ framework also provides a systematic way to couple the Goldstones to matter fields. In this section we will introduce the basics of the coset construction which are needed for Composite Higgs models. For a pedagogic introduction see the respective chapters in [61, 69]. The following discussion will mostly follow [61].

Let us consider a theory which is invariant under the global action of a compact Lie group $\mathcal{G}$, which is spontaneously broken to a subgroup $\mathcal{H} \subset \mathcal{G}$. This implies the existence of dim $\mathcal{G}$ - dim $\mathcal{H}$ massless GBs, one for each broken generator. It is instructive to assume that the symmetry is broken by the VEV of a scalar field $\Phi(x)$ which transforms linearly under $\mathcal{G}$

$$\Phi(x) \xrightarrow{\mathcal{G}} g \cdot \Phi(x)\,, \tag{2.27}$$

where $g = \exp(i\alpha_A T^A)$ stands for a generic $\mathcal{G}$ element in a linear representation. $T^A = \{T^{\hat{a}}, X^a\}$ are the generators of $\mathcal{G}$ with $T^{\hat{a}}$ being the unbroken and X^a the broken generators. In the following we will assume the normalization $\mathrm{Tr}[T^A T^B] = \delta^{AB}$. The statement that the symmetry is broken by the scalar VEV means that $\langle\Phi\rangle$ is only invariant under $h = \exp(i\alpha_{\hat{a}} T^{\hat{a}}) \in \mathcal{H}$ transformations, whereas $\exp(i\alpha_a X^a) \in \mathcal{G}/\mathcal{H}$ transformations rotate the scalar vacuum $\langle\Phi\rangle$ into a degenerate but non-identical vacuum $\langle\tilde{\Phi}\rangle$. The vacuum manifold can therefore be identified with the coset space $\mathcal{G}/\mathcal{H}$, i.e. any point on the vacuum manifold can be reached by a transformation $U[\boldsymbol{\alpha}] \in \mathcal{G}/\mathcal{H}$[4] with transformation parameters $\boldsymbol{\alpha}$ acting on the VEV, i.e.

$$U\left[\boldsymbol{\alpha}\right]\langle\Phi\rangle = e^{i\alpha_a X^a}\langle\Phi\rangle\,. \tag{2.28}$$

The movement on the vacuum manifold, i.e. the flat directions of the scalar potential, can be interpreted as massless degrees of freedom, i.e. the GBs. Therefore it is natural to parameterize the GBs as fluctuations along the flat directions of the potential, or equivalently along the broken generators. This can be easily achieved by promoting the parameters $\boldsymbol{\alpha}$ in the definition of $U[\boldsymbol{\alpha}]$ to dynamical fields, i.e. $\boldsymbol{\alpha} \to \sqrt{2}\boldsymbol{\pi}(x)/f$, where we also introduced a factor of $\sqrt{2}$ for normalization reasons and the symmetry breaking scale f to make the ratio $\boldsymbol{\pi}(x)/f$ dimensionless. The resulting GB matrix $U[\boldsymbol{\pi}]$

$$U[\boldsymbol{\pi}] = e^{i\frac{\sqrt{2}}{f}\pi_a(x)X^a} \tag{2.29}$$

is therefore a non-linear parameterization of the GBs.

Before we can construct a $\mathcal{G}$ invariant Lagrangian for the GBs we have to figure out how they transform under $\mathcal{G}$ transformations. In order to do so we act with a $\mathcal{G}$ transformation on the parameterization of the vacuum manifold in Eq. (2.28)

$$U\left[\boldsymbol{\pi}\right]\langle\Phi\rangle \xrightarrow{\mathcal{G}} g \cdot U\left[\boldsymbol{\pi}\right]\langle\Phi\rangle \equiv U\left[\boldsymbol{\pi}^{(g)}\right]\langle\Phi\rangle\,, \tag{2.30}$$

[4]Note that $U[\boldsymbol{\pi}]$ is just one representative element of an equivalence class in $\mathcal{G}/\mathcal{H}$, i.e. it is only uniquely defined up to an $\mathcal{H}$ element acting on it from the right.

where we implicitly defined the transformed GB fields. Note that this implicit definition is always valid since $\mathcal{G}$ is a symmetry of the theory and therefore can only rotate the vacuum but we can never depart from the vacuum manifold. The transformation of the GBs is highly non-linear and complicated, but it will turn out that the transformation of $U[\boldsymbol{\pi}]$ is simple. In order to see this one can use the fact that there is a unique decomposition for any global or local group element $g = \exp(i\alpha_A T^A) \in \mathcal{G}$ of the form

$$g = e^{i\alpha_A T^A} = e^{if_a(\alpha)X^a} \cdot e^{if_{\hat{a}}(\alpha)T^{\hat{a}}} \quad \text{with} \quad e^{if_a(\alpha)X^a} \in \mathcal{G}/\mathcal{H}, \quad e^{if_{\hat{a}}(\alpha)T^{\hat{a}}} \in \mathcal{H}\,, \tag{2.31}$$

where $f(\alpha)$ is in general a non-linear function. Applying this to $U[\boldsymbol{\pi}]$ we obtain

$$g \cdot U[\boldsymbol{\pi}] = U[\boldsymbol{\pi}^{(g)}] \cdot h[\boldsymbol{\pi}; g]\,, \tag{2.32}$$

where $h[\boldsymbol{\pi}; g]$ is a local $\boldsymbol{\pi}$ dependent $\mathcal{H}$ element whose exact form can be obtained from the decomposition in Eq. (2.31) which will however not be important for the following discussion. Solving this for $U[\boldsymbol{\pi}^{(g)}]$ we find for the transformed GB matrix

$$U[\boldsymbol{\pi}^{(g)}] = g \cdot U[\boldsymbol{\pi}] \cdot h^{-1}[\boldsymbol{\pi}; g]\,. \tag{2.33}$$

This implies that even though the transformation of the GBs is non-linear, the GB matrix $U[\boldsymbol{\pi}]$ transforms linearly. Therefore it is more convenient to work with $U[\boldsymbol{\pi}]$ instead of the GBs directly.

It is also instructive to discuss the transformation behavior of the GBs under the unbroken symmetry $\mathcal{H}$ which will turn out to be linear. This can be easily derived from the decomposition of the Lie algebra of $\mathcal{G}$ into broken and unbroken generators[5]

$$[T^{\hat{a}}, T^{\hat{b}}] = i\, f^{\hat{a}\hat{b}}{}_{\hat{c}} T^{\hat{c}} \equiv T^{\hat{c}} (t^{\hat{a}}_{\text{adj}})_{\hat{c}}{}^{\hat{b}}\,, \tag{2.34}$$

$$[T^{\hat{a}}, X^b] = i\, f^{\hat{a}b}{}_c X^c \equiv X^c (t^{\hat{a}}_{\pi})_c{}^b\,, \tag{2.35}$$

$$[X^a, X^b] = i\, f^{ab}{}_{\hat{c}} T^{\hat{c}} + i\, f^{ab}{}_c X^c\,, \tag{2.36}$$

where $f^{AB}{}_C$ are the $\mathcal{G}$ structure constants. In Eq. (2.34) we identified the structure constants with the adjoint representation $t^{\hat{a}}_{\text{adj}}$ of $\mathcal{H}$. The matrices $t^{\hat{a}}_{\pi}$ in Eq. (2.35) form another $\mathcal{H}$ representation in which the GBs transform. It can be identified from the decomposition of the adjoint representation of $\mathcal{G}$ under $\mathcal{H}$

$$\mathbf{Adj}_{\mathcal{G}} = \mathbf{Adj}_{\mathcal{H}} \oplus \mathbf{r}_{\pi}\,. \tag{2.37}$$

For the symmetry breaking structure $SO(N+1)/SO(N)$, which we will consider in the following, $\mathbf{r}_{\pi}$ is the fundamental representation of $SO(N)$, i.e. $\mathbf{r}_{\pi} = \mathbf{N}$.

Any invariant that you can form of the GB matrix alone is of the form $\text{Tr}[(U^{-1}U)^n]$, which is independent of the Goldstone fields. This is just another way of saying that the Goldstone fields have a flat potential. In order to get non-trivial Goldstone interactions we have to introduce derivatives. But this introduces a further complication: $\partial_\mu U$ does no longer transform linearly since $h^{-1}[\boldsymbol{\pi}; g]$ in Eq. (2.33) is a local $\mathcal{H}$ element. However, it is still possible to find building blocks which transform linearly. These are the $d_{\mu,\hat{a}}$ and $e_{\mu,a}$ symbols which are the two fundamental quantities in the CCWZ formalism. They are obtained from the projection of the Maurer-Cartan form on the broken and unbroken generators respectively

$$U[\boldsymbol{\pi}]^{-1} i\partial_\mu U[\boldsymbol{\pi}] = d_{\mu,a} X^a + e_{\mu,\hat{a}} T^{\hat{a}} \equiv d_\mu + e_\mu\,. \tag{2.38}$$

[5]Note that in symmetric cosets, such as e.g. $SO(N+1)/SO(N)$, $f^{ab}{}_c = 0$. This implies an algebra automorphism $X \to -X$ which is associated with a $\mathbb{Z}_2$ symmetry of the GBs.

Under a global $\mathcal{G}$ transformation the Maurer-Cartan form transforms as

$$U[\boldsymbol{\pi}]^{-1} i\partial_\mu U[\boldsymbol{\pi}] \xrightarrow{g} h[\boldsymbol{\pi}; g] \cdot \left(U[\boldsymbol{\pi}]^{-1} i\partial_\mu U[\boldsymbol{\pi}] + i\partial_\mu \right) h^{-1}[\boldsymbol{\pi}; g] \,. \tag{2.39}$$

Note that $ih[\boldsymbol{\pi}; g]\partial_\mu h^{-1}[\boldsymbol{\pi}; g]$ is an element of the Lie algebra of the subgroup $\mathcal{H}$ and does therefore only decompose into $T^{\hat{a}}$ generators. This implies that this shift transformation can be entirely attributed to e_μ. We thus find the following transformation behavior of d_μ and e_μ under $\mathcal{G}$ transformations.

$$d_\mu \xrightarrow{g\in\mathcal{G}} h[\boldsymbol{\pi}; g] \cdot d_\mu \cdot h^{-1}[\boldsymbol{\pi}, g] \,, \tag{2.40}$$

$$e_\mu \xrightarrow{g\in\mathcal{G}} h[\boldsymbol{\pi}; g] \cdot (e_\mu + i\partial_\mu) \cdot h^{-1}[\boldsymbol{\pi}, g]. \tag{2.41}$$

If written in components we see that $d_{\mu,\hat{a}}$ transforms like the GB fields in the $\mathbf{r}_\pi$ representation, i.e.

$$d^a_\mu \xrightarrow{g} (h_{\mathbf{r}_\pi}[\boldsymbol{\pi}; g])^a_b \, d^b_\mu \,, \tag{2.42}$$

where $h_{\mathbf{r}_\pi}[\boldsymbol{\pi}; g] \in \mathcal{H}$ is a genuine $\mathcal{H}$ transformation, which if embedded in $\mathcal{G}$ coincides with the $h[\boldsymbol{\pi}; g]$ of Eqs. (2.40) and (2.41). Also note that $e_{\mu,a}$ transforms like a gauge field of a local $\mathcal{H}$ symmetry and in complete analogy with gauge fields one can define a field strength built out of e_μ which transforms linearly (see e.g. [61] for more details).

With the introduction of the d_μ and e_μ symbols we have reduced the problem of finding $\mathcal{G}$ invariants of the GB field and its derivatives to finding invariants of a local $\mathcal{H}$ symmetry built out of the linearly transforming building blocks d_μ and e_μ. At leading order in derivatives there is only one term that we can write down

$$\mathcal{L}_2 = \frac{f^2}{4} \mathrm{Tr}\left[d_\mu d^\mu \right] = \frac{f^2}{4} d_{\mu,a} d^{\mu,a} \,, \tag{2.43}$$

where the factor of $f^2/4$ is needed to obtain a canonically normalized kinetic term for the GBs.

Now that we know how to construct pure Goldstone Lagrangians, the next step is to add matter fields to the picture. Let us start with vector fields A_μ. We will assume that $A_\mu = A^A_\mu T^A$ is the gauge field that is obtained from gauging the whole group $\mathcal{G}$.[6] The simplest way to include gauge fields in the construction, i.e. to extend it to local $\mathcal{G}$ transformations, is to do a minimal substitution and replace the derivative in Eq. (2.38) by a covariant derivative, i.e. $\partial_\mu \to D_\mu = \partial_\mu - iA_\mu$, where we take the gauge coupling to be absorbed in the gauge field. Due to the transformation behavior of gauge fields under local $\mathcal{G}$ transformations

$$A_\mu = A^A_\mu T^A \xrightarrow{g(x)} g(x) \cdot (A_\mu + i\partial_\mu)\, g(x)^{-1} \,, \tag{2.44}$$

the transformation property of the gauged Maurar-Cartan form is identical to Eq. (2.39). This means that we can in the same way define d_μ and e_μ symbols that have the transformation property of Eqs. (2.40) and (2.41) and include the coupling of the GBs to gauge fields

$$U[\boldsymbol{\pi}]^{-1} \left(i\partial_\mu + A_\mu \right) U[\boldsymbol{\pi}] = d_{\mu,a} X^a + e_{\mu,\hat{a}} T^{\hat{a}} \,. \tag{2.45}$$

[6] A partial gauging of $\mathcal{G}$ explicitly breaks the global symmetry such that the GBs are in general only pNGBs. The effects of the explicit breaking can nonetheless be included in a consistent way by formally gauging the full group and treating A_μ as a spurion. In the end one simply sets to zero all fields along ungaged generators, i.e. for the SM electroweak group $SU(2)_L \times U(1)_Y \subset \mathcal{G}$ one makes the substitution $A_\mu \to A^{\mathrm{SM}}_\mu = g W^{a_L}_\mu T^{a_L} + g' B_\mu T^{3_R}$.

The CCWZ framework also allows to construct interactions with matter fields, which we will take to be fermions in the following. These fermions can be taken to transform in irreducible representations $\mathbf{r}_\Psi$ of the unbroken group $\mathcal{H}$,[7] i.e.

$$\Psi^i \xrightarrow{g} (h_{\mathbf{r}_\Psi}[\boldsymbol{\pi}; g])^i_j \, \Psi^j \,. \tag{2.46}$$

With this transformation behavior we can construct $\mathcal{G}$-invariant operators, i.e. operators which are invariant under local $\mathcal{H}$ transformations in this language, using the d_μ and e_μ symbols. At lowest order in derivatives the Lagrangian for a fermion resonance Ψ with mass M is given by

$$\mathcal{L}_f = i\bar{\Psi}\not{\nabla}\Psi - M\bar{\Psi}\Psi \,, \tag{2.47}$$

where the covariant derivative ∇_μ has to be constructed using the e_μ symbol to maintain local $\mathcal{H}$ invariance

$$\nabla_\mu \Psi^i = \left(\partial_\mu \, \delta^i_j - i e^{\hat{a}}_\mu \left(t^{\hat{a}}_{\mathbf{r}_\pi}\right)^i_j\right) \Psi^j. \tag{2.48}$$

Through the e_μ symbol the fermion resonances have interactions with the GBs and the gauge fields. Couplings to the elementary fermions are again obtained with the spurion approach, i.e. by embedding the elementary fermions into incomplete $\mathcal{H}$ representations and treating them as if they transform under the full group.

2.2.5 Minimal Composite Higgs model

With the theoretical background of the previous sections we are now ready to discuss some properties of the minimal Composite Higgs model (MCHM) based on the symmetry breaking structure $SO(5) \times U(1)_X \to SO(4) \times U(1)_X$ [36, 76].[8] The additional $U(1)_X$ is needed to obtain the correct hypercharges for the SM fermions. We embed the electroweak gauge group $SU(2)_L \times U(1)_Y$ into $SO(4) \times U(1)_X$. $SU(2)_L$ is embedded into the $SU(2)_L$ of the group isomorphism $SO(4) \simeq SU(2)_L \times SU(2)_R$ and the hypercharge is identified as the combination $Y = T^3_R + X$, where X is the charge under $U(1)_X$ and T^3_R is the embedding of the $SU(2)$ generator $\frac{\sigma^3}{\sqrt{2}}$ into $SU(2)_R$. Using the explicit form of the $SO(5)$ generators $T^A = \{T^\alpha_L, T^\alpha_R, X^a\}$

$$(T^\alpha_{L,R})_{IJ} = -\frac{i}{2}\left[\frac{1}{2}\epsilon^{\alpha\beta\gamma}(\delta^\beta_I\delta^\gamma_J - \delta^\beta_J\delta^\gamma_I) \pm (\delta^\alpha_I\delta^4_J - \delta^\alpha_J\delta^4_I)\right], \qquad \alpha = 1,2,3, \tag{2.49}$$

$$X^a_{IJ} = -\frac{i}{\sqrt{2}}(\delta^a_I\delta^5_J - \delta^a_J\delta^5_I), \qquad a = 1,\dots,4\,, \tag{2.50}$$

where capital letters $I, J = 1,\dots,5$ denote $SO(5)$ and small letters $a = 1,\dots,4$ $SO(4)$ indices, we can compute the GB matrix $U[\boldsymbol{\pi}]$ for the dim $SO(5)/SO(4) = 4$ GBs π_a

$$U[\boldsymbol{\pi}] = e^{i\frac{\sqrt{2}}{f}\pi_a X^a} = \begin{pmatrix} \mathbb{1}_4 - \left(1 - \cos\frac{\pi}{f}\right)\frac{\boldsymbol{\pi}^T\boldsymbol{\pi}}{\pi^2} & \sin\frac{\pi}{f}\,\frac{\boldsymbol{\pi}}{\pi} \\ -\sin\frac{\pi}{f}\,\frac{\boldsymbol{\pi}^T}{\pi} & \cos\frac{\pi}{f} \end{pmatrix}, \quad \pi = \sqrt{\boldsymbol{\pi}^T\boldsymbol{\pi}}\,. \tag{2.51}$$

[7] The matter fields actually transform linearly in full $\mathcal{G}$ representation, i.e. $\psi \to g \cdot \psi$. However, this can be recast into a linear transformation under the local $\mathcal{H}$ subgroup by multiplying ψ with the GB matrix, i.e. $U[\boldsymbol{\pi}]^{-1}\Psi$ schematically transforms as $U[\boldsymbol{\pi}]^{-1}\psi \to h[\boldsymbol{\pi}; g]U[\boldsymbol{\pi}]^{-1}\psi$. $h[\boldsymbol{\pi}; g]$ is in general a reducible $\mathcal{H}$ representation which can be decomposed into $\boldsymbol{r}_\Psi$.

[8] Note that this is the minimal symmetry breaking structure that includes the custodial group $SO(4) \simeq SU(2)_L \times SU(2)_R$ in $\mathcal{H}$ to protect the ρ parameter. The minimal model containing the Higgs as a Goldstone is based on the symmetry breaking structure $SU(3)/[SU(2)_L \times U(1)_Y]$. However, this model predicts $\mathcal{O}(v^2/f^2)$ corrections to the ρ parameter, which would require an abnormally large f in order not to be in conflict with experiments.

The GBs transform as a bifundamental $(\mathbf{2},\mathbf{2})$ of $SU(2)_L \times SU(2)_R$ and therefore have the right quantum numbers to be identified with the Higgs doublet $H = (h_u, h_d)^T$ via

$$\boldsymbol{\pi} = \frac{1}{\sqrt{2}}\left(-i(h_u - h_u^*), \quad h_u + h_u^*, \quad i(h_d - h_d^*), \quad h_d + h_d^*\right)^T . \tag{2.52}$$

The explicit form of the GB matrix in Eq. (2.51) allows us to determine the d_μ and e_μ symbols via the Maurer-Cartan form

$$U[\boldsymbol{\pi}]^{-1}(i\partial_\mu - gW_\mu^\alpha T_L^\alpha - g' B_\mu T_R^3) U[\boldsymbol{\pi}] = d_\mu^a X^a + e_\mu^{\hat{a}} T^{\hat{a}} , \tag{2.53}$$

where g and g' are the $SU(2)_L$ and $U(1)_Y$ gauge couplings.[9] The leading two-derivative Lagrangian for the GBs in unitary gauge $H = \frac{1}{\sqrt{2}}(0,h)^T$ is then given by

$$\mathcal{L}_2 = \frac{f^2}{4} d_{\mu,a} d^{\mu,a} = \frac{1}{2}(\partial_\mu h)^2 + \frac{g^2}{4}\sin^2\frac{h}{f}\left(|W_\mu|^2 + \frac{1}{2c_w^2} Z_\mu^2\right), \tag{2.54}$$

where $c_w = \cos\theta_w$ is the cosine of the weak mixing angle which is given by $\tan\theta_w = g'/g$. The last term fixes $\langle h\rangle$ in terms of the measured electroweak scale v

$$f^2 \sin^2\frac{\langle h\rangle}{f} = v^2 \simeq (246\ \text{GeV})^2 . \tag{2.55}$$

Note that the non-linear dependence on the Higgs field modifies the Higgs couplings to the vector bosons w.r.t. their SM values when we expand around $\langle h\rangle$

$$\frac{g^2}{4}\sin^2\frac{h}{f}\left(|W_\mu|^2 + \frac{1}{2c_w^2} Z_\mu^2\right) = \frac{g^2 v^2}{4}\left(|W_\mu|^2 + \frac{1}{2c_w^2} Z_\mu^2\right)\left[1 + 2\sqrt{1-\xi}\frac{h}{v} + (1-2\xi)\frac{h^2}{v^2} + \dots\right]. \tag{2.56}$$

The modification of Higgs couplings is a generic prediction of all Composite Higgs Models. Note that the deviation of the couplings from their SM values can be made arbitrarily small by increasing f at the cost of additional tuning in the Higgs potential.

Let us now turn to the elementary fermions. We will only consider the top sector since it gives the largest contribution to the Higgs potential. As was discussed in Section 2.2.2 we assume that the elementary fermions couple linearly to the $SO(5)$ invariant strong sector. In order to construct these couplings we have to specify the $SO(5)$ representation into which we embed the elementary fermions. The choice of embedding is in principle arbitrary and among others embeddings of q_L, t_R into $\mathbf{4}_{2/3}, \mathbf{5}_{2/3}, \mathbf{10}_{2/3}, \mathbf{14}_{2/3}, \dots$ (MCHM$_4$, MCHM$_5$, ...) of $SO(5)_{U(1)_X}$ have been discussed. Usually one chooses one of the smallest representation. However, the minimal choice here, i.e. embedding q_L in the spinorial $\mathbf{4}_{2/3}$ representation, results in large corrections to the $Zb_L\bar{b}_L$ coupling which is in tension with electroweak precision tests. It turns out that large corrections to $Zb_L\bar{b}_L$ can be evaded by embedding q_L in a representation which is invariant under $SU(2)_L \leftrightarrow SU(2)_R$ [77]. The minimal choice which satisfies this requirement is the fundamental representation of $SO(5)$ which decomposes into $\mathbf{5}_{2/3} = (\mathbf{2},\mathbf{2})_{2/3} \oplus (\mathbf{1},\mathbf{1})_{2/3}$ under $(SU(2)_L \times SU(2)_R)_{U(1)_X}$. Both q_L and t_R can therefore be embedded into the $\mathbf{5}_{2/3}$ representation, q_L in the $(\mathbf{2},\mathbf{2})_{2/3}$ part and t_R in the $(\mathbf{1},\mathbf{1})_{2/3}$ part. In the following we will consider this embedding which has the explicit form

$$\xi_L = \frac{1}{\sqrt{2}}\left(ib_L, \quad b_L, \quad it_L, \quad -t_L, \quad 0\right)^T , \qquad \xi_R = \left(0, \quad 0, \quad 0, \quad 0, \quad t_R\right)^T . \tag{2.57}$$

[9] Note that once we introduce composite vector resonances the gauge fields mix with them, s.t. the elementary W and B fields above and the bare couplings g and g' are not the physically observable fields and couplings.

Since the fundamental of $SO(5)$ decomposes as $\mathbf{5}_{2/3} = \mathbf{4}_{2/3} \oplus \mathbf{1}_{2/3}$ under $SO(4) \times U(1)_X$, we consider top partners Q and S in the fundamental and singlet representations of $SO(4)$, respectively. The explicit expression of the fundamental is

$$Q = \frac{1}{\sqrt{2}} \left(iB - iX_{5/3}, \quad B + X_{5/3}, \quad iT + iX_{2/3}, \quad -T + X_{2/3} \right)^T . \tag{2.58}$$

The doublet $(T, B)^T$ transforms as $\mathbf{2}_{1/6}$ under $(SU(2)_L)_Y$, and therefore has the same quantum numbers as q_L, whereas the exotic doublet $(X_{5/3}, X_{2/3})^T \sim \mathbf{2}_{7/6}$ contains an exotic fermion with electric charge equal to $5/3$. The most general fermionic Lagrangian including one layer of resonances Q and S at leading order is of the form

$$\begin{aligned} \mathcal{L}_f \;=\; & i\bar{q}_L \not{D} q_L + i\bar{t}_R \not{D} t_R + \bar{Q} \left(i\not{D} + \not{e} - m_Q \right) Q + \bar{S} \left(i\not{D} - m_S \right) S \\ & + \epsilon_{tQ}\, \bar{\xi}^A_R U_{Aa} Q^a_L + \epsilon_{qQ}\, \bar{\xi}^A_L U_{Aa} Q^a_R + \epsilon_{tS}\, \bar{\xi}^A_R U_{A5} S_L + \epsilon_{qS}\, \bar{\xi}^A_L U_{A5} S_R + \text{h.c.}, \end{aligned} \tag{2.59}$$

where we used that $\xi_{L/R}$ dressed with the GB matrix formally transform in $SO(4)_{U(1)_X}$ representations with $U^{-1}_{aA} \xi^A_{L/R} \sim \mathbf{4}_{2/3}$ and $U^{-1}_{5A} \xi^A_{L/R} \sim \mathbf{1}_{2/3}$. The ϵ coefficients are free parameters which control the breaking of the $\mathcal{G}$ symmetry and will eventually be fixed by the top mass and the Higgs potential parameters. When expanding Q in terms of its components one sees that before EWSB (T, B) mixes with (t_L, b_L) and S with t_R, generating the top Yukawa coupling. In general one expects that there is more than only one layer of fermionic resonances and in principle any $\mathcal{H}$ representation can be present. It will turn out that one needs at least two layers of resonances to cancel the quadratic divergences in the Higgs potential. We will turn to specific models later but for now we will assume that all resonances are heavy so that we can integrate them out. We then parameterize our ignorance of the strong sector resonances in non-local form factors in an effective fermion Lagrangian in momentum space

$$\begin{aligned} \mathcal{L}^{\text{eff}}_{\text{f}} &= \bar{\xi}^A_L \not{p} \left(\delta_{AB}\, \Pi_{L_0} + U_{A5} U^{-1}_{5B}\, \Pi_{L_1} \right) \xi^B_L + \bar{\xi}^A_R \not{p} \left(\delta_{AB}\, \Pi_{R_0}(p^2) + U_{A5} U^{-1}_{5B}\, \Pi_{R_1} \right) \xi^B_R \\ &\quad + M_t\, \bar{\xi}^A_L U_{A5} U^{-1}_{5B} \xi^B_R + h.c. \\ &= \Pi_{L_0} \bar{b}_L \not{p} b_L + \Pi_L\, \bar{t}_L \not{p} t_L + \Pi_R\, \bar{t}_R \not{p} t_R - \Pi_{LR} \left(\bar{t}_L t_R + h.c. \right), \end{aligned} \tag{2.60}$$

with the Higgs dependent form factors

$$\Pi_L = \Pi_{L_0} + \frac{s_h^2}{2}\, \Pi_{L_1}\,, \quad \Pi_R = \Pi_{R_0} + c_h^2\, \Pi_{R_1}\,, \quad \Pi_{LR} = \frac{s_h c_h}{\sqrt{2}} M_t\,, \tag{2.61}$$

where we use the abbreviations $s_h = \sin h/f$ and $c_h = \cos h/f$. The momentum dependent form factors $\Pi_i = \Pi_i(p^2)$ and $M_t = M_t(p^2)$ are obtained by integrating out the fermion resonances in a specific model. Note that Eq. (2.60) also fixes the top mass

$$m_t = \left. \frac{\Pi_{LR}(0)}{\sqrt{\Pi_L(0) \Pi_R(0)}} \right|_{h=\langle h \rangle} . \tag{2.62}$$

From Eq. (2.60) we can also compute the one-loop contribution to the Coleman-Weinberg effective Higgs potential [78]

$$V_f(h) = -2N_c \int \frac{d^4p}{(2\pi)^4} \log \left(p^2 \Pi_L \Pi_R + |\Pi_{LR}|^2 \right). \tag{2.63}$$

The Higgs potential also receives contributions from the gauge sector. In order to compute these contributions we can proceed in the same way as for the fermionic sector, i.e. we construct the

most general Lagrangian of the gauge fields at the two derivative level and parameterize the contributions of composite sector resonances in form factor

$$\mathcal{L}_g^{\text{eff}} = \frac{1}{2}\Big(g^{\mu\nu} - \frac{p^\mu p^\nu}{p^2}\Big)\left(2\Pi_{+-}W_\mu^+ W_\nu^+ + \Pi_{33}W_\mu^3 W_\nu^3 + \Pi_{BB}B_\mu B_\nu + 2\Pi_{3B}W_\mu^3 B_\nu\right) . \tag{2.64}$$

We will discuss the derivation of the form factor in more detail in a later section. Starting from this Lagrangian we obtain the gauge contributions to the one-loop effective potential

$$V_g(h) = \frac{3}{2}\int \frac{d^4p}{(2\pi)^4}\log\left[\Pi_{+-}^2(\Pi_{33}\Pi_{BB} - \Pi_{3B}^2)\right] , \tag{2.65}$$

where the form factors again depend on the Higgs field. Expanding Eqs. (2.63) and (2.65) in the Higgs field one obtains a potential of the form

$$V(h) = \alpha \sin^2\frac{h}{f} + \beta \sin^4\frac{h}{f} , \tag{2.66}$$

which has the minimum

$$\sin^2\frac{\langle h\rangle}{f} = \xi = -\frac{\alpha}{2\beta} , \quad m_h^2 = \left.\frac{\partial^2 V}{\partial h^2}\right|_{h=\langle h\rangle} = \frac{8\beta}{f^2}\xi(1-\xi) . \tag{2.67}$$

As we have already mentioned earlier in order to generate $\xi \ll 1$ one has to tune α and β.

Let us finally comment on the cancelation of divergences in the Higgs potential. In an explicit model one would like to have a finite or at most logarithmically divergent potential. This requires that the form factors $\Pi_i(-p_E^2)$ vanish fast enough for $p_E^2 \to \infty$. One approach to achieve this is to write down the most general theory possible and make the finiteness of the potential a constraint on the free parameters of the theory using Weinberg sum rules [79–81]. For example the contribution to α in the Higgs potential will be of the form

$$\alpha = \int_0^\infty dp_E^2\, p_E^2\, f(p_E^2;\{\alpha_i\}) , \tag{2.68}$$

where f is a function of the form factors and therefore implicitly depends on the parameters of the full model which we denote by $\{\alpha_i\}$. In order for this to be finite one has to impose that

$$\lim_{p_E^2\to\infty} p_E^2\, f(p_E^2;\{\alpha_i\}) = 0 , \tag{2.69}$$

$$\lim_{p_E^2\to\infty} p_E^4\, f(p_E^2;\{\alpha_i\}) = 0 , \tag{2.70}$$

where the first constraint cancels the quadratic and the second the logarithmic divergences. These sum rules have to be understood as constraints on the $\{\alpha_i\}$ and they can be used in a similar way to remove the divergences for β. Typically the sum rules are applied to the gauge and fermion sector independently. Instead of using the Weinberg sum rules one can work e.g. in multi-site models [82, 83] which implement collective-breaking to cancel the quadratic divergences. These are inspired by holographic Composite Higgs models [36, 76], which feature a calculable Higgs potential, and the idea of dimensional deconstruction.

2.3 Dark matter

The first solid hints of DM were already found in the 1930s by Fritz Zwicky [4]. In a study of the velocity dispersion in the Coma cluster he realized that the velocities of several galaxies are too large to be supported by the visible matter alone and suggested the presence of a large amount of non-luminous dark matter.

Another essential piece of evidence to establish the existence of an invisible matter component are the famous galactic rotation curves starting with the ground breaking work by Rubin and Ford in the 1970s [84, 85]. They mapped the rotational velocity of stars in several galaxies as a function of their distance to the galactic center. Newtonian dynamics dictates that the circular velocity is determined by the distance to the center r and the enclosed mass in the orbit $M(r)$

$$v(r) \propto \sqrt{\frac{M(r)}{r}}\,. \tag{2.71}$$

For orbits which extend beyond the Galactic disk the enclosed mass should approximately stay constant, implying a decreasing circular velocity $v(r) \propto r^{-1/2}$. However, Rubin and Ford found a flattening of the rotation curves $v(r)$ beyond the visible part of the galactic disk. Therefore if one assumes that Newtonian dynamics is correct[10] an additional invisible matter component is needed, which extends far beyond the visible galaxy. This observation has subsequently been confirmed in many more galaxies (see e.g. [89]).

Since the 1970s we have collected a considerable amount of evidence for DM on many scales. On galactic scales the rotation curves have been supplemented by data from weak and strong lensing and the observation of the bullet cluster [90], which is naturally explained by collisionless DM. Additionally data from big bang nucleosynthesis (BBN), large scale structure and the CMB are naturally compatible with the ΛCDM model of cosmology[11].

The present-day relic abundance of cold DM can be determined from a fit to CMB data. The latest measurement by the Planck collaboration [92] reports the relic abundance at an impressive precision

$$\Omega_c h^2 = 0.120 \pm 0.001\,, \tag{2.72}$$

where h is the reduced Hubble constant which is related to the expansion rate of the universe via $H_0 = h \cdot 100$ km/s/Mpc. Ω_c is the ratio of the cold DM energy density and the critical energy density of the universe $\rho_{\text{crit}} = 3\,H_0^2/(8\pi G)$ with G being the gravitational constant. Using $h = 0.674 \pm 0.005$ [92] we conclude that $\Omega_c \simeq 0.26$, i.e. roughly one fourth of the total energy density of the universe consists of cold DM. This is about six times as much as the visible baryonic matter in the universe whose abundance is given by $\Omega_b h^2 = 0.0224 \pm 0.0001$ [92].

Despite the plethora of evidence for the existence of DM we know very little about its nature. There is a multitude of possible scenarios ranging from ultralight bosonic fields to heavy compact objects, such as primordial black holes (see [93–95] and references therein for an overview of DM models). Figure 2.3, which is a modified version of Figure 3 in [95], gives a broad overview of the DM model landscape organized according to the mass of the DM candidate. There are very few constraints on the DM mass which is why the proposed scenarios span many orders of magnitude.

[10] Instead of postulating the existence of a DM component the rotation curves can also be explained by modifying gravity on galactic scales [86, 87] (generally referred to as Modified Newtonian Dynamics – MOND). While this can explain flat rotation curves it to date lacks a compelling embedding into a general theory of gravity and needs additional matter to explain the observation of the bullet cluster. Besides MOND without additional matter is strongly disfavored by cosmic microwave background (CMB) and large scale structure data. See [88] for a recent study.

[11] The ΛCDM (Lambda Cold Dark Matter) model assumes a Robertson-Walker universe filled with a cosmological constant, cold DM and ordinary matter. See e.g. [91] for a pedagogic introduction.

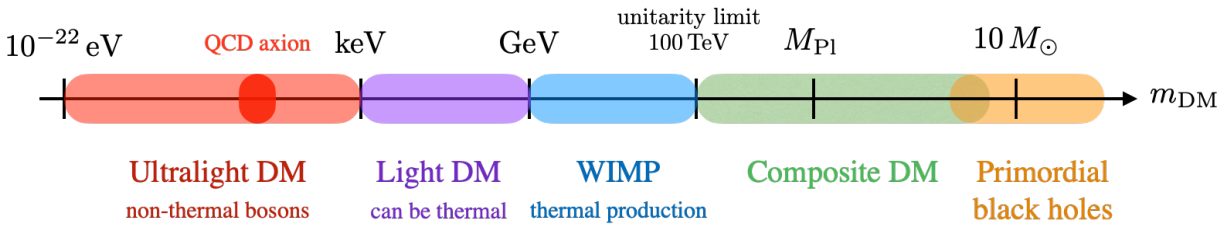

Figure 2.3: Overview of the DM model landscape, ranging from ultralight particle DM to primordial black holes. This Figure is a modified version of Figure 3 in [95].

Bosonic DM can be as light as 10^{-22} eV with the lower bound $m_{\rm DM} \gtrsim 10^{-22}$ eV originating from studies of the Lyman-α forest and dwarf galaxies [96,97], roughly by requiring that the de-Broglie wavelength fits into dwarf galaxies. Such ultralight DM, which among others also includes the QCD axion as DM candidate, behaves as a classical field. The lower mass bound for fermionic DM is more stringent $m_{\rm DM} \gtrsim \mathcal{O}(100)$ eV and is due to the Pauli exclusion principle [98,99]. On the other end of the scale the DM mass is bound from above by the least massive DM halo of observed galaxies which is of the order $10^5 - 10^6\,M_\odot$. While compact massive objects such as boson [100] or axion stars [101] are consistent with such large masses, there are stronger bounds on primordial black holes (see [102, 103] for reviews on the topic). A particularly interesting mass region is $m_{\rm DM} \sim 1$ keV $-$ 100 TeV where the DM could have been in thermal equilibrium with the SM. This scenario is appealing since it is independent of initial conditions and mimics the dynamical mechanism by which the relic abundances of SM particles were set. Lighter DM cannot have been in thermal equilibrium with the SM during freeze-out as it would still have been relativistic and thus washed out density perturbations and dampened the matter power spectrum. This so-called warm DM scenario is tightly constrained by Lyman-α data [104–107]. Thermal DM also cannot be too heavy, since the observed relic abundance requires couplings which violate perturbative unitarity for DM masses $m_{\rm DM} \gtrsim 100$ TeV [108].

Even though the WIMP is only a small fraction of the possible landscape of DM models, as can be seen in Figure 2.3, it remains one of the most popular and well-studied DM scenarios. There is an immense ongoing experimental effort to detect WIMP DM directly in elastic scattering on nuclei or at colliders or indirectly from present-day annihilations.

2.4 WIMP dark matter

WIMPs are one of the most popular DM candidates with masses ranging from $m_{\rm DM} \sim 1$ GeV $-$ 100 GeV (see Figure 2.3) and weak couplings to the SM. What makes the WIMP scenario so appealing is the fact that the couplings to the SM keep the DM in thermal equilibrium with the SM bath in the early universe, thus washing out any arbitrary initial conditions. The present-day relic abundance is then set by the coupling strength to the SM which determines when the DM abundance freezes out.

Before discussing WIMP DM in non-minimal Composite Higgs models we will introduce the basic concepts and tools in this section. We start with a short exposition to thermodynamics in an expanding Friedmann-Lemaitre-Robertson-Walker (FLRW) universe in Section 2.4.1, before discussing the freeze-out mechanism in Section 2.4.2. Finally we shortly describe how to determine elastic scattering cross-sections of DM on nuclei. For a more thorough introduction to cosmology or thermodynamics in an expanding universe we refer the reader to the classic textbooks [91, 109, 110]. For a DM centered presentation see [94, 95, 111].

2.4.1 Thermodynamics in an expanding universe

At large scales the universe is homogeneous and isotropic, which is well described by the FLRW metric

$$ds^2 = dt^2 - a^2(t)\left(\frac{dr^2}{1-k\frac{r^2}{R^2}} + r^2 d\Omega^2\right), \tag{2.73}$$

where $a(t)$ is the so-called scale factor parameterizing the expansion of the universe and $k = -1, 0, +1$ correspond to a closed, flat and open universe with intrinsic curvature scale R, respectively. It turns out that our universe is approximation flat, s.t. we can take $k = 0$ with a dimensionless scale factor which can be normalized to $a(t_0) = 1$. The evolution of the scale factor is governed by the Friedmann Equation, the covariant conservation of the energy momentum tensor $\nabla_\mu T^{\mu\nu} = 0$ and the equation of state for the matter in the universe. This set of equations can be written as

$$H^2 = \left(\frac{\dot{a}}{a}\right)^2 = \frac{8\pi G}{3}\rho\,, \qquad \dot{\rho} + 3\frac{\dot{a}}{a}(\rho + p) = 0\,, \qquad p = \omega\,\rho\,, \tag{2.74}$$

where H is the Hubble parameter, ρ the energy density, p the pressure and a dot denotes the derivative w.r.t. coordinate time. In the ΛCDM standard model of cosmology the universe is filled with non-relativistic matter ($\omega = 0$), radiation ($\omega = \frac{1}{3}$) and vacuum energy ($\omega = -1$), i.e. $\rho = \rho_m + \rho_{rad} + \rho_\Lambda$. In such a universe the Friedmann Equation takes the form

$$H^2 = \frac{8\pi G}{3}\rho_{\text{crit},0}\left[\Omega_{rad}\left(\frac{a_0}{a}\right)^4 + \Omega_m\left(\frac{a_0}{a}\right)^3 + \Omega_\Lambda + \Omega_{curv}\left(\frac{a_0}{a}\right)^2\right], \tag{2.75}$$

where we defined the present-day critical density $\rho_{\text{crit},0} \equiv \frac{3}{8\pi G}H_0^2$ and reintroduced the contribution from a non-vanishing curvature for completeness. The abundance coefficients are defined as $\Omega_i \equiv \rho_{i,0}/\rho_{\text{crit},0}$ and sum up to unity. The exact composition of the universe can e.g. be determined from a fit to CMB data. The Planck collaboration reports the values [92]

$$\Omega_{rad} = 9.4\cdot 10^{-5}\,, \quad \Omega_\Lambda = 0.68\,, \quad \Omega_b = 0.05\,, \quad \Omega_c = 0.27\,, \quad |\Omega_{curv}| \leq 0.01\,, \tag{2.76}$$

where the matter component is composed of baryons and cold DM, i.e. $\Omega_m = \Omega_b + \Omega_c$. This shows that today the universe basically contains only vacuum energy and non-relativistic matter, which is again dominantly composed of cold DM. Both radiation and curvature are negligible today.[12] However, as can be seen from Eq. (2.75), in the early universe before redshift $z_{\text{eq}} \simeq 3400$ or $T_{\text{eq}} \simeq 0.8$ eV radiation was the dominant component. Freeze-out of cold DM generally occurs at much higher temperatures and therefore in a radiation dominated universe for which the Hubble constant is given by $H_{rad} = 1/(2t)$.

The universe is thus filled with various species of interacting particles with most of them being relativistic during the radiation dominated era. Throughout large times of the evolution of the universe the interaction rates of the particles were higher than the expansion rate of the universe and the particles were in local thermal equilibrium.[13] This allows us to use equilibrium thermodynamics to describe the dynamics of the particle bath. The distribution function of the particle species are therefore simply the Fermi or Bose distributions

$$f(\boldsymbol{p}) = \frac{1}{(2\pi)^3}\frac{1}{e^{(E(\boldsymbol{p})-\mu)/T} \mp 1}\,, \qquad E(\boldsymbol{p}) = \sqrt{\boldsymbol{p}^2 + m^2}\,, \tag{2.77}$$

[12] Note that even if our universe is not flat the contribution of curvature to the evolution of the universe has never been important. Its energy density grows slower than the one for matter and radiation for a decreasing scale factor.

[13] Note that thermal equilibrium means chemical and kinetic equilibrium, i.e. number changing interactions occur frequently in both directions and energy and momentum transfer happens efficiently.

where the negative (positive) sign corresponds to bosons (fermions), $E(\boldsymbol{p})$ is the relativistic energy and μ the chemical potential. In the early universe the chemical potential was negligible $\mu \ll T, m$ which is why we will set it to zero in the following. Using the distribution function we can determine the local energy and number density. For relativistic particles these take the form

$$n_i = g_i \int f(\boldsymbol{p}) d^3p = \left[\frac{3}{4}\right] g_i \frac{\zeta(3)}{\pi^2} T^3 \,, \tag{2.78}$$

$$\rho_i = g_i \int f(\boldsymbol{p}) E(\boldsymbol{p}) d^3p = \left[\frac{7}{8}\right] g_i \frac{\pi^2}{30} T^4 \,, \tag{2.79}$$

where the square brackets show the pre-factor for fermions and g_i are the spin degrees of freedom. The number and energy density for non-relativistic particle species is identical for bosons and fermions and exponentially suppressed at $T \ll m_i$

$$n_i = g_i \left(\frac{m_i T}{2\pi}\right)^{3/2} e^{-m_i/T} \,, \tag{2.80}$$

$$\rho_i = m_i n_i + \frac{3}{2} n_i T_i \simeq m_i n_i \,. \tag{2.81}$$

It is also straightforward to show that the pressure in both cases satisfies the equation of state as given in Eq. (2.74). The exponential suppression of non-relativistic particles implies that if all particles are in equilibrium the energy density is dominated by radiation. The total energy density can therefore be characterized in terms of the photon temperature T

$$\rho_{rad} = \frac{\pi^2}{30} g_*(T)\, T^4 \,, \qquad g_*(T) = \sum_{i=\text{bosons}} g_i \left(\frac{T_i}{T}\right)^4 + \frac{7}{8} \sum_{i=\text{fermions}} g_i \left(\frac{T_i}{T}\right)^4 \tag{2.82}$$

where $g_*(T)$, the number of relativistic degrees of freedom, is a sum over all bosons and fermions which are relativistic at the temperature T. In the SM this varies from $g_*(T \geq 100 \text{ GeV}) = 106.75$ when all SM species were still relativistic to today's value of $g_*(T_0) = 3.36$. Note that we also included the possibility that some relativistic species are kinetically decoupled from the photons and have their own temperature T_i. Eq. (2.82) also allows us to determine the expansion rate of a radiation dominated universe in terms of the temperature instead of coordinate time

$$H_{rad} = \left(\frac{8\pi^3 g_*(T)}{90}\right)^{1/2} \frac{T^2}{m_P} \simeq 1.66 \sqrt{g_*(T)} \frac{T^2}{m_P} \,, \tag{2.83}$$

where $m_P^2 = 1/G$ is the Planck mass.

Another important thermodynamic quantity is the entropy density s which is given by (see e.g. [91, 109])

$$s = \sum_i \frac{\rho_i + p_i}{T_i} = \frac{2\pi^2}{45} g_{*s}(T)\, T^3 \,, \qquad g_{*s}(T) = \sum_{i=\text{bosons}} g_i \left(\frac{T_i}{T}\right)^3 + \frac{7}{8} \sum_{i=\text{fermions}} g_i \left(\frac{T_i}{T}\right)^3 \,, \tag{2.84}$$

where we used that the contribution from non-relativistic particles is negligible. $g_{*s}(T)$ is identical to $g_*(T)$ as long as all relativistic species are in kinetic equilibrium. In the SM this is the case until roughly $T_{\nu,dec} \simeq 1$ MeV when neutrinos decouple, s.t. today's value is given by $g_{*s}(T_0) = 3.94$. The expansion of the universe is to a good approximation adiabatic what

implies that the total entropy is conserved. Therefore the entropy density only changes due to the expansion of the universe and it holds that

$$sa^3 = const. \qquad \Rightarrow \qquad g_{*s}(T)^{1/3} T \propto a^{-1} \,. \tag{2.85}$$

Note that the second relation holds in general and not only for a radiation dominated universe. The scaling of the entropy density with the scale factor also allows us to define quantities for which the effect of the expanding universe is modded out. One particularly useful example is the yield for a particle species i which is defined as

$$Y_i = \frac{n_i}{s} \,, \tag{2.86}$$

which does not get diluted due to the expansion of the universe. This means that the yield stays constant for particles which are decoupled from the heat bath.

2.4.2 Freeze-out mechanism and WIMP miracle

Even though the particle bath is in thermal equilibrium during large parts of the evolution of the universe the most interesting phenomena occur when a species leaves equilibrium and decouples from the bath. This happens when the interaction rate Γ_{int} of the process which maintains equilibrium drops below the expansion rate H. In this context equilibrium can be either chemical or kinetic equilibrium. However, the departure from chemical equilibrium usually occurs earlier and sets the relic abundance of the species which decouples. In the following we will study how the departure from chemical equilibrium can set the observed DM relic abundance.

Consider a massive stable particle χ which is initially in thermal equilibrium with the SM bath. If χ were to stay in equilibrium it would follow its equilibrium distribution and once it gets non-relativistic its yield would get exponentially suppressed $n/s \sim (m/T)^{3/2} \exp(-m/T)$ and the abundance for a GeV scale χ would be completely negligible today. However, if decoupling happens shortly after it gets non-relativistic, i.e. at temperatures $T_{\text{FO}}/m \sim \mathcal{O}(10)$, its yield stays constant from this point on $Y_\chi = Y_\chi^{\text{eq}}(T_{\text{FO}})$ and can still be sizable today. This is the so-called freeze-out mechanism and is schematically shown in Figure 2.4. Note that a larger interaction rate maintains equilibrium longer and leads to a smaller abundance. The reactions which keep the DM in equilibrium are annihilation and inverse annihilation

$$\chi\,\bar{\chi} \leftrightarrow \psi\,\bar{\psi} \,, \tag{2.87}$$

where ψ can be any SM or BSM particle into which $\chi\,\bar{\chi}$ can annihilate. Here we concentrate on two-to-two annihilation but in general more complicated processes are possible. One can obtain a rough estimate of when this reaction freezes out by comparing the interaction rate to the expansion rate

$$\Gamma_{\text{int}} = n_\chi^{\text{eq}} \langle \sigma v_{\text{rel}} \rangle \sim H \,, \tag{2.88}$$

where $\langle \sigma v_{\text{rel}} \rangle$ is the thermally averaged annihilation cross-section times the relative velocity summed over all annihilation channels. Using Eq. (2.83) for the Hubble parameter and neglecting $\mathcal{O}(1)$ numbers this lets us estimate the DM yield at freeze out

$$Y_\chi^{\text{FO}} \simeq \frac{\sqrt{g_*(T_{\text{FO}})}}{g_{*s}(T_{\text{FO}})} \frac{1}{m_P T_{\text{FO}} \langle \sigma v_{\text{rel}} \rangle} \,, \tag{2.89}$$

where T_{FO} is determined by Eq. (2.88) and is usually of the size $m_\chi/T_{\text{FO}} \sim 20$. This yield stays constant after freeze out, s.t. the present-day DM energy density is given by $\rho_{\chi,0} = m_\chi s_0 Y_\chi^{\text{FO}}$.

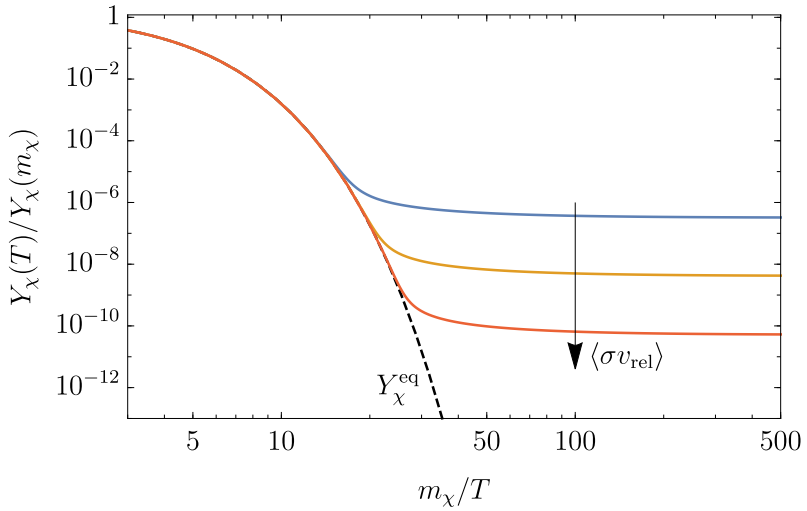

Figure 2.4: Freeze-out mechanism. Once the DM becomes non-relativistic its yield Y_χ follows its exponentially decreasing equilibrium distribution until the interaction rate drops below the expansion rate of the universe and the χ abundance freezes out. Larger annihilation cross-sections $\langle\sigma v_{\rm rel}\rangle$ maintain thermal equilibrium longer and result in a smaller χ abundance.

In order to obtain the observed DM relic abundance one therefore needs an annihilation cross-section of the size

$$\langle\sigma v_{\rm rel}\rangle \sim \frac{1}{10^9\ \text{GeV}^2} \simeq \frac{\alpha_w^2}{1\ \text{TeV}^2}\,, \tag{2.90}$$

where $\alpha_w \simeq 0.03$ is a weak coupling. The second way of writing this cross-section is often called the WIMP miracle what refers to the fact that a weak scale DM candidate with a weak coupling naturally reproduces the observed relic abundance.

In order to match the experimental precision in the determination of the DM relic abundance a more accurate prediction is needed. This requires solving the Boltzmann equation for the phase space distribution function for χ. To obtain the the relic abundance it is sufficient to solve the zeroth order moment of the Boltzmann equation which gives a differential equation for the number density or equivalently the yield. For the present case the Boltzmann equation takes the form (see the classic paper [112] for a thorough derivation)

$$\frac{dn_\chi}{dt} + 3H\,n_\chi = -\langle\sigma v_{\rm rel}\rangle\left[n_\chi^2 - (n_\chi^{\rm eq})^2\right] \quad \text{or equivalently} \quad \frac{dY_\chi}{dx} = -\frac{x\langle\sigma v_{\rm rel}\rangle s}{H(m)}\left[Y_\chi^2 - (Y_\chi^{\rm eq})^2\right], \tag{2.91}$$

where in the formulation with the yield we defined $x = m_\chi/T$. The exact definition of the thermally averaged annihilation cross-section is [112]

$$\langle\sigma v_{\rm rel}\rangle(T) = \frac{1}{16m_\chi^4 T K_2^2(m_\chi/T)} \int_{4m_\chi^2}^\infty ds\, s\,\sqrt{s-4m_\chi^2}\,K_1(\sqrt{s}/T)\,\sigma v_{\rm rel}(s)\,, \tag{2.92}$$

where K_1, K_2 are modified Bessel functions of the second kind. Solving the Boltzmann equation for a temperature independent, i.e. s-wave, annihilation cross-section one finds a refined value for the canonical annihilation cross-section which is often quoted as a benchmark [113]

$$\langle\sigma v_{\rm rel}\rangle_{\rm can} = 2\cdot 10^{-26}\text{cm}^2\text{s}^{-1}\,. \tag{2.93}$$

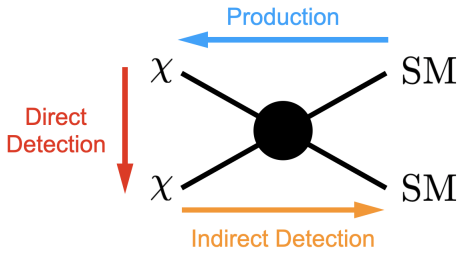

Figure 2.5: The three complementary probes of WIMP DM, indirect detection, direct detection and productions at colliders can be viewed as the three possible directions of reading a DM annihilation Feynman diagram.

2.4.3 DM direct detection

If it does not live in a secluded dark sector thermally produced DM must couple to the SM at least weakly. This makes it possible to search for DM via its couplings to SM particles. There are in general three complementary probes: 1) DM indirect detection, i.e. the search for present-day annihilation products, 2) production of DM at colliders and 3) DM direct detection which denotes the attempt to detect the elastic scattering of DM on detector nuclei. These approaches correspond to the three possible direction in which one can read a DM annihilation Feynman diagram as can be seen in Figure 2.5 and probe the DM interactions at different energy scales.

In the following we will concentrate on direct detection which usually poses one of the most stringent constraints on WIMP models. There is an immense effort to push the experimental sensitivity to the neutrino floor with ongoing experiments such as XENON1T [5] and ambitious proposals for future experiments as e.g. XENONnT [114] or LZ [115, 116]. For an overview of the experimental landscape see the recent review [117].

The idea behind direct detection experiments is very simple and goes back to Goodman and Witten [118]: as the solar system moves through the Milky Way's DM halo we should observe a "wind" of non-relativistic DM particles with a typical velocity of the order of $v \sim 10^{-3}$. In direct detection experiments one tries to detect the rare occasion of a DM particle scattering off a detector nuclei as it flies through the earth. What one actually measures is the recoil of the detector nucleus which for a nucleus of mass m_A and DM of mass m_χ is maximally of the size

$$E_R \leq \frac{|\boldsymbol{q}|^2}{2m_A} \simeq 50 \text{ keV} \left(\frac{m_\chi}{100 \text{ GeV}}\right)^2 \left(\frac{100 \text{ GeV}}{m_A}\right), \tag{2.94}$$

where $|\boldsymbol{q}| \sim m_\chi v$ is the momentum transfer. The energy threshold in such experiments is usually a few keV what explains why there is limited sensitivity for $m_\chi \lesssim 10$ GeV. Due to the small de-Broglie wavelength of the DM, to leading order the WIMP interacts coherently with all nucleons in the detector nucleus. However, once the energy transfer is of the order of the inverse nucleus radius the substructure becomes visible which is parameterized by a form factor $F(E_R)$ in the differential scattering cross-section (see e.g. [117])

$$\frac{d\sigma}{dE_R} = \frac{m_A}{2v^2\mu_{\chi A}^2}\left(\sigma_{\text{SI}}\, F_{\text{SI}}^2(E_R) + \sigma_{\text{SD}}\, F_{\text{SD}}^2(E_R)\right), \tag{2.95}$$

where $\mu_{\chi A} = m_\chi m_A/(m_\chi + m_A)$ is the reduced mass of the DM-nucleus system. The differential cross-section is usually separated into a spin-independent (SI) and spin-dependent (SD) part where σ_{SI} and σ_{SD} are the cross-sections at zero momentum transfer, i.e. in the limit of a point-like nucleus. While the SI cross-section is coherently enhanced by the number of nucleons

the SD cross-section is only sensitive to the total spin of the nucleus. This results in a stronger sensitivity to the SI cross-section in most experiments. For this reason we will concentrate on the computation of $\sigma_{\rm SI}$ in the following.

In order to compute $\sigma_{\rm SI}$ one starts by matching the theory at interest to DM-quark and DM-gluon contact interactions in the limit of small momentum transfer $q^2 \ll \Lambda^2_{\rm QCD}$. For a complex scalar χ as DM candidate the following couplings contribute to $\sigma_{\rm SI}$

$$\mathcal{L} \supset \sum_{\psi=u,d,s,c,b,t} a_\psi \, m_\psi \chi^* \chi \bar{\psi}\psi + \sum_{\psi=u,d,s,c,b,t} \lambda_\psi^V \, i(\chi^* \overleftrightarrow{\partial}_\mu \chi) \bar{\psi}\gamma^\mu \psi + d_G \frac{\alpha_s}{4\pi} \chi^* \chi G^a_{\mu\nu} G^{a\,\mu\nu} \,, \tag{2.96}$$

where $\alpha_s = g_s^2/(4\pi)$ is the strong fine-structure constant and $a_\psi, \lambda_\psi^V, d_G$ are model dependent matching coefficients. Before matching to a theory of nucleons at a scale $E \sim \Lambda_{\rm QCD}$ we have to integrate out the heavy quarks $Q = c, b, t$ what produces another contribution to the effective gluon coupling for each quark flavor

$$m_Q \bar{Q} Q \to -\frac{\alpha_s}{12\pi} G^a_{\mu\nu} G^{a\,\mu\nu} \,. \tag{2.97}$$

Starting from these effective couplings we can now compute the scattering amplitude for elastic (anti-)DM-nucleon scattering $\chi^{(*)}(p)\, N(k) \to \chi^{(*)}(p')\, N(k')$, where $N = p, n$ stands for protons and neutrons and $q = p' - p$ is the momentum transfer. This is accomplished by considering matrix elements of the above QCD operators between nucleon states which relate the quark or gluon contribution to the nucleon mass or vector current via form factors which in the low q limit are given by (see e.g. [95] and references therein)

$$\langle N(k')|m_\psi \bar{\psi}\psi|N(k)\rangle = m_N f^N_{T_\psi} \, \bar{u}_N(k') u_N(k) \,, \tag{2.98}$$

$$\langle N(k')|\alpha_s G^a_{\mu\nu} G^{a\,\mu\nu}|N(k)\rangle = -\frac{8\pi}{9} m_N f^N_{T_g} \, \bar{u}_N(k') u_N(k) \,, \tag{2.99}$$

$$\langle N(k')|\bar{\psi}\gamma^\mu \psi|N(k)\rangle = f^N_{V_\psi} \, \bar{u}_N(k') \gamma^\mu u_N(k) \,, \tag{2.100}$$

where $u_N(k)$ denotes the nucleon polarization spinor. The associated form factors take the values $f^p_{T_u} = 0.021, f^p_{T_d} = 0.041, f^n_{T_u} = 0.019,\ f^n_{T_d} = 0.045$ [119, 120], and $f^{p,n}_{T_s} = 0.043$ [121], leading to $f^{p,n}_{T_g} = 1 - \sum_{\psi=u,d,s} f^{p,n}_{T_\psi} \simeq 0.89$. It is important to note that for the vector current operators proportional to λ^V_ψ, the form factors simply count the valence content of the nucleons, namely $f^p_{V_u} = f^n_{V_d} = 2$ and $f^p_{V_d} = f^n_{V_u} = 1$.

In the non-relativistic limit $u_N(k) \simeq \sqrt{m_N}(\xi_s \,,\, \xi_s)^T$ with two-component spinors ξ_s all these nuclear matrix elements match to the same scalar scattering amplitude

$$\mathcal{M}^{\chi N, \chi^* N} = 4\, m_N m_\chi F_N \xi^\dagger_{s'} \xi_s \,, \tag{2.101}$$

with F_N being given by

$$F_N = \frac{m_N}{2\, m_\chi} \Bigg(\sum_{\psi=u,d,s} f^N_{T_\psi} a_\psi + \frac{2}{27} f^N_{T_g} \Bigg(\sum_{\psi=c,b,t} a_\psi - 3 d_G \Bigg) \Bigg) \pm \sum_{\psi=u,d} f^N_{V_\psi} \lambda^V_\psi \,, \tag{2.102}$$

where $+$ $(-)$ is for (anti-)DM-nucleon scattering. From this it is straightforward to obtain the DM-nucleon cross-section, which we average over the proton and neutron contributions in the detector nucleus

$$\sigma^{\chi N, \chi^* N}_{\rm SI} = \frac{\mu^2_{\chi N}}{\pi} \frac{(Z\, F_p + (A - Z)\, F_n)^2}{A^2} \,, \tag{2.103}$$

where Z and $A - Z$ count the number of protons and neutrons in the nucleus and $\mu_{\chi N}$ is the reduced mass of the DM-nucleon system. This quantity factors out the dependence on the target material and is usually reported in bounds on the SI scattering cross-section. The most recent bounds reach an impressive sensitivity on the cross-section of the order of $\sigma_{\rm SI}^{\chi N,\chi^* N} \sim 10^{-46}$ cm^2 for DM masses around 100 GeV. These strong constraints put considerable stress on conventional WIMP DM models.

The DM-nucleon cross-section in Eq. (2.103) is related to the DM-nucleus cross-section $\sigma_{\rm SI}$ in Eq. (2.95) via

$$\sigma_{\rm SI} = \frac{\mu_{\chi A}}{\mu_{\chi N}} A^2 \sigma_{\rm SI}^{\chi N,\chi^* N} \,, \tag{2.104}$$

where $\mu_{\chi A}$ is the reduced mass of the DM and detector nucleus with atomic number A. Note that if $\sigma_{\rm SI}^{\chi N} \neq \sigma_{\rm SI}^{\chi^* N}$ one should take the average $(\sigma_{\rm SI}^{\chi N} + \sigma_{\rm SI}^{\chi^* N})/2$ in the above equation and when comparing to experimental limits.

Chapter 3

Composite pNGB dark matter

Now that we have introduced the theoretical foundations of Composite Higgs models and DM we are finally in a position to discuss pNGB DM, both in Composite Higgs models and in general. The focus in the following will be on scenarios in which both the Higgs doublet and a scalar DM candidate, singlet under the SM gauge symmetries, arise as GBs from a strongly coupled sector. Here we take the DM to be a complex scalar χ but all results also apply to real DM ϕ after simply replacing $\chi \to \phi/\sqrt{2}$. Our discussion will be based on an effective Lagrangian for the pNGB DM and Higgs which is in general of the form

$$\mathcal{L}_{\text{eff}} = \mathcal{L}_{\text{GB}} + \mathcal{L}_f - V_{\text{eff}} \,, \tag{3.1}$$

where $\mathcal{L}_{\text{GB}}$ contains only the derivative couplings among the GBs which originate from the non-linear sigma model kinetic term. $\mathcal{L}_f$ contains couplings of both the Higgs and DM to the SM fermions. In general these break the global symmetry $\mathcal{G}$ of the strong sector and generate an effective potential V_{eff} for the Higgs and DM. In the following we will systematically discuss the contributions to $\mathcal{L}_{\text{eff}}$. In Section 3.1 we start with the Goldstone couplings and introduce the derivative Higgs portal, which is an irreducible characteristic of pNGB DM. As a next step we shortly discuss the DM phenomenology of this zeroth order approximation of pNGB DM and highlight the appealing features of the "Goldstone limit" in which the χ mass is the only explicit breaking of the DM shift symmetry. Realistic models contain in general additional shift-symmetry breaking non-derivative couplings in $\mathcal{L}_f$ and V_{eff}. In Section 3.2 we study how these non-derivative couplings affect DM phenomenology and examine under which circumstances the "Goldstone limit" can be approximately maintained. In this context we also discuss possible origins of the explicit symmetry breaking effects in Composite Higgs and which couplings they introduce. In all this discussion we motivate our parameter choices based on a Composite Higgs models with the symmetry breaking pattern $SO(7)/SO(6)$. Finally in Section 3.3 we broaden our scope and discuss the most general DM-SM couplings in pNGB DM models not limiting ourselves to a specific symmetry breaking pattern.

This chapter is based on results previously published in [28, 29, 31].[1] All figures and parts of the text are taken from these references.

[1] [28]: R. Balkin, M. Ruhdorfer, E. Salvioni and A. Weiler, *Charged Composite Scalar Dark Matter*,
[29]: R. Balkin, M. Ruhdorfer, E. Salvioni and A. Weiler, *Dark matter shifts away from direct detection*,
[31]: M. Ruhdorfer, E. Salvioni and A. Weiler, *A Global View of the Off-Shell Higgs Portal*.

3.1 Goldstone boson Lagrangian: the derivative Higgs portal

The Higgs and χ kinetic term and the derivative couplings in $\mathcal{L}_{\rm GB}$ arise from the nonlinear sigma model kinetic term. Assuming custodial symmetry for the Higgs and a global $U(1)_{\rm DM}$ which stabilizes the DM, the most general two-derivative Lagrangian invariant under $SU(2)_L \times SU(2)_R \times U(1)_{\rm DM} \subset \mathcal{H}^2$ is given by[3]

$$\mathcal{L}_{\rm GB} \;=\; |D^\mu H|^2 + |\partial^\mu \chi|^2 + \frac{c_H}{2f^2}\partial_\mu |H|^2 \partial^\mu |H|^2 + \frac{c_d}{f^2}\partial_\mu |H|^2 \partial^\mu |\chi|^2 + \frac{c_\chi}{2f^2}\partial_\mu |\chi|^2 \partial^\mu |\chi|^2 . \tag{3.2}$$

We could have written four additional operators,

$$\frac{c_1}{f^2}|D_\mu H|^2|H|^2\,, \qquad \frac{c_2}{f^2}|D_\mu H|^2|\chi|^2\,, \qquad \frac{c_3}{f^2}|\partial_\mu \chi|^2|H|^2\,, \qquad \frac{c_4}{f^2}|\partial_\mu \chi|^2|\chi|^2\,, \tag{3.3}$$

but these can be removed through the $O(1/f^2)$ field redefinition

$$H \to \Big(1 - \frac{c_1}{2f^2}|H|^2 - \frac{c_2}{2f^2}|\chi|^2\Big)H\,, \qquad \chi \to \Big(1 - \frac{c_3}{2f^2}|H|^2 - \frac{c_4}{2f^2}|\chi|^2\Big)\chi\,. \tag{3.4}$$

Notice that for $c_1 = c_2 = c_3 = c_4 = -2/3$ these are the leading terms of

$$\frac{\sin(\pi/f)}{\pi}\,\pi^a \to \frac{\pi^a}{f}\,, \qquad \pi = \sqrt{\boldsymbol{\pi}^T \boldsymbol{\pi}}\,, \tag{3.5}$$

where $\boldsymbol{\pi}$ is the GB vector [37]. This redefinition has customarily been adopted in studies of the $SO(6)/SO(5)$ and $SO(7)/SO(6)$ models because in the basis of Eq. (3.2), which also coincides with the SILH basis [122] when restricted to Higgs interactions, the scalar potential is a simple polynomial and the VEV of the Higgs is equal to $v \simeq 246$ GeV. In those models the coefficients take the values $c_H = c_d = c_\chi = 1$, which we often adopt as reference in the following.

The relevant operator parameterizing the DM interactions with the SM is therefore the "derivative Higgs portal" operator proportional to c_d, i.e.

$$\mathcal{L}_{\rm GB} \supset \frac{c_d}{f^2}\partial_\mu |H|^2 \partial^\mu |\chi|^2\,. \tag{3.6}$$

This operator mediates DM annihilation into SM particles via s-channel Higgs exchange, s.t. the observed relic abundance can be produced via the freeze-out mechanism. The requirement of reproducing the observed DM relic abundance fixes the interaction strength c_d/f^2 as a function of the DM mass, what is shown by the blue curve in Figure 3.1, which was obtained by numerically solving the Boltzmann equation for the DM number density using the public code `micrOMEGAs` [123]. For $m_\chi > m_h$ the relation is particularly simple and is well approximated by

$$1 = \frac{\Omega_{\chi+\chi^*}}{\Omega_{\rm DM}} \simeq \frac{\langle \sigma v_{\rm rel}\rangle_{\rm can}}{\frac{1}{2}\langle \sigma v_{\rm rel}\rangle}\,, \qquad \langle \sigma v_{\rm rel}\rangle \simeq \frac{c_d^2 m_\chi^2}{\pi f^4} \tag{3.7}$$

and hence

$$\frac{f}{c_d^{1/2}} \approx 1.1 \text{ TeV} \left(\frac{m_\chi}{130 \text{ GeV}}\right)^{1/2}, \tag{3.8}$$

[2]More precisely, this is the most general $SU(2)_L \times SU(2)_R \times U(1)_{\rm DM}$ invariant Lagrangian where $SU(2)_R$ is only broken by the gauging of hypercharge.

[3]Note that we do not include in $\mathcal{L}_{\rm GB}$ operators containing $\chi^* \overset{\leftrightarrow}{\partial_\mu} \chi \equiv \chi^* \partial_\mu \chi - \partial_\mu \chi^* \chi$, which vanish trivially in the $SO(6)/SO(5)$ model where $\chi \to \eta/\sqrt{2}$ with real η, and are forbidden in the $SO(7)/SO(6)$ model by custodial $SO(4) \simeq SU(2)_L \times SU(2)_R$ invariance, since H and χ belong to the same irreducible representation of $\mathcal{H} = SO(6)$. Notice also that $\chi^* \overset{\leftrightarrow}{\partial_\mu} \chi$ is odd under the charge conjugation associated to $U(1)_{\rm DM}$.

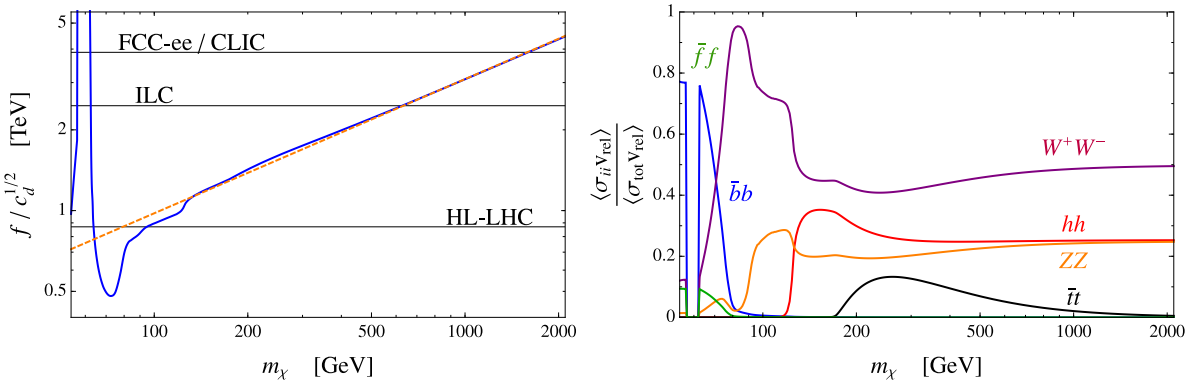

Figure 3.1: *Left panel:* value of the global symmetry breaking scale f that allows to reproduce the observed DM relic density via the derivative Higgs portal in Eq. (3.6), as a function of the DM mass. The solid blue curve shows the full Boltzmann solution obtained using `micrOMEGAs` [123], while the dashed orange curve corresponds to the approximate relation given in Eq. (3.8). The gray lines show the 95% CL lower bounds achievable from the measurement of the hVV couplings at current and future colliders, assuming $c_H = c_d$. *Right panel:* fractions for annihilation to the different SM final states. $\bar{f}f$ denotes the sum over all light quarks and leptons. This figure was adopted from [29].

where $\langle\,\cdot\,\rangle$ as usual denotes thermal average, $\Omega_{\rm DM} = 0.120\,h^{-2}$ [92] and $\langle\sigma v_{\rm rel}\rangle_{\rm can} = 2{\cdot}10^{-26}{\rm cm}^2{\rm s}^{-1}$ is the canonical value for the annihilation cross-section as given in Eq. (2.93). Note that the above estimate includes only the dominant annihilation channels $\chi\chi^* \to WW, ZZ, hh$.[4]

While being strong enough at center of mass energies $s \simeq 4m_\chi^2$ to produce the observed relic abundance, the derivative Higgs portal is strongly suppressed at small momentum transfer. This suppression results in negligibly small cross-sections for DM scattering on heavy nuclei: the amplitude for $q\chi \to q\chi$ scattering mediated by Higgs exchange is proportional to $|t|/f^2 \lesssim (100\text{ MeV})^2/(1\text{ TeV})^2 \sim 10^{-8}$, where 100 MeV is a rough estimate of the maximum momentum transfer. Consequently pNGB DM which couples only via the derivative Higgs portal to the SM is naturally compatible with null results in direct detection experiments.

Before moving on to interactions which violate the global symmetry $\mathcal{G}$ of the strong sector, let us note that Eq. (3.2) contains another important effect due to the pNGB nature of the Higgs. A non-zero value of c_H implies that all Higgs couplings are rescaled by a universal factor. After electroweak symmetry breaking c_H induces a correction to the kinetic term of the bare Higgs field $\tilde{h}$. In unitary gauge $H = (0\,,\,\tilde{h}/\sqrt{2})^T$ the physical Higgs field h is related to $\tilde{h}$ through

$$\tilde{h} = v + \left(1 - \frac{c_H}{2}\frac{v^2}{f^2}\right) h\,. \tag{3.9}$$

A robust and model-independent probe of the pNGB nature of the Higgs is therefore the measurement of the hVV couplings with $V = W, Z$. Figure 3.1 also shows the projected reach of current and future colliders on the symmetry breaking scale f through this observable [124] under the assumption that $c_H = c_d$.

[4]The cross-section for annihilation to $t\bar{t}$ scales as $\sigma_{t\bar{t}}\,v_{\rm rel} \sim N_c m_t^2/(\pi f^4)$, as opposed to $\sigma_{WW,ZZ,hh}\,v_{\rm rel} \sim m_\chi^2/(\pi f^4)$, therefore $t\bar{t}$ is important only for m_χ not much larger than m_t. See the right panel of Figure 3.1.

3.2 Explicit symmetry breaking effects

Let us now discuss the non-derivative couplings which are effects of the explicit breaking of the global symmetry of the strong sector. One result of the explicit breaking has to be the generation of Yukawa couplings between the pNGB Higgs and the elementary fermions. Similar couplings are also possible for the DM. For this reason we consider the most general Lagrangian which couples the pNGBs to the third generation quarks

$$\mathcal{L}_f = -y_t \bar{q}_L \widetilde{H} t_R \left(1 - \frac{c_t}{f^2}|H|^2 - \frac{c_t^\chi}{f^2}|\chi|^2\right) - y_b \bar{q}_L H b_R \left(1 - \frac{c_b}{f^2}|H|^2 - \frac{c_b^\chi}{f^2}|\chi|^2\right) + \text{h.c.}\,, \quad (3.10)$$

with $\mathcal{O}(1)$ coefficients $c_t, c_t^\chi, c_b, c_b^\chi$. The explicit symmetry breaking also generate a scalar potential at one-loop which up to quartic order of the fields has the form

$$V_{\text{eff}} = \mu_h^2|H|^2 + \lambda_h|H|^4 + \mu_{\text{DM}}^2|\chi|^2 + \lambda_{\text{DM}}|\chi|^4 + 2\lambda|H|^2|\chi|^2\,, \quad (3.11)$$

where μ_h^2 and λ_h are fixed by the observed VEV and mass of the Higgs. We restrict the remaining parameter space by the requirement that $\langle\chi\rangle = 0$, such that $U(1)_{\text{DM}}$ is not spontaneously broken and χ is stable. In the next chapter we will see that this in general imposes a mild constraint on the fermionic sector.

In addition to providing a mass for the DM of the size $m_\chi^2 = \mu_{\text{DM}}^2 + \lambda\, v^2$, the explicit symmetry breaking can also considerably affect DM phenomenology. While the annihilation is still dominantly mediated by s-channel Higgs exchange, the $\chi^*\chi h$ coupling has both a derivative and non-derivative contribution which come with opposite signs

$$\mathcal{M}(\chi\chi^* \to \text{SM}) \propto \left(c_d \frac{s}{f^2} - 2\lambda\right) v \simeq \left(c_d \frac{4m_\chi^2}{f^2} - 2\lambda\right) v\,. \quad (3.12)$$

For $m_\chi > m_t$ the $\chi^*\chi\bar{t}t$ interaction proportional to c_t can also contribute significantly to $\chi^*\chi \to \bar{t}t$. However, this is only the case in models where the top couplings are the dominant source of explicit breaking of the χ shift symmetry since otherwise c_t is suppressed or altogether absent making Eq (3.12) a good approximation of the annihilation amplitude to SM particles.

The most dramatic effect can be observed in the DM scattering on nuclei, which is mediated by t-channel Higgs exchange and through the contact interactions c_q^χ. Matching to the effective DM quark contact interaction in Eq. (2.96) we find

$$m_q a_q\, \bar{q}q\chi^*\chi\,, \qquad a_q \approx \frac{2\,\lambda}{m_h^2} + \frac{c_q^\chi}{f^2}\,, \quad (3.13)$$

where we dropped the negligible contribution from the derivative Higgs portal. It is well-known that the marginal Higgs portal coupling is strongly constrained by direct detection experiments. Taking as a benchmark $\sigma_{\chi N} \lesssim 10^{-46}\ \text{cm}^2\text{s}^{-1}$, which is roughly the most recent XENON1T bound for a DM mass of $m_\chi \sim 100$ GeV [5], and assuming that the contribution from c_q is subleading, the portal coupling has to be smaller than $\lambda \lesssim 0.6 \cdot 10^{-2}$. This implies that realistic models need to have a suppressed marginal portal coupling to be compatible with direct detection exclusions. In order to understand how λ can be suppressed let us shortly recapitulate how the explicit symmetry breaking typically enters Composite Higgs models.

There are two irreducible sources of explicit symmetry breaking which generate at least some of the couplings in Eqs. (3.10) and (3.11): the gauging of the SM electroweak group $SU(2) \times U(1)_Y \subset \mathcal{H}$ and the couplings of the elementary fermions to the strong sector. In the

partial compositeness framework the elementary fermions couple linearly to the strong sector, i.e.

$$\mathcal{L}_{\rm mix}^{\rm UV} \sim \lambda_q f\, \bar{q}_L \mathcal{O}_q + \lambda_t f\, \bar{t}_R \mathcal{O}_t + \lambda_{q'} f\, \bar{q}_L \mathcal{O}_{q'} + \lambda_b f\, \bar{b}_R \mathcal{O}_b + \text{h.c.}, \tag{3.14}$$

where we have ignored the flavor structure and put our focus on the masses of the third generation of quarks [125]. The mixing with composite resonances generates the Yukawa couplings to the physical fermions, which are a linear combination of elementary and composite degrees of freedom. The amount of explicit symmetry breaking is directly related to the compositeness fraction of the physical fermions which schematically scale like $\epsilon^t_{L,R} \sim \lambda_{q,t} f/\sqrt{m^2_{*q,t} + \lambda^2_{q,t} f^2}$ and $\epsilon^b_{L,R} \sim \lambda_{q',b} f/\sqrt{m^2_{*q',b} + \lambda^2_{q',b} f^2}$, where $m_{*q,t,q',b}$ are the relevant masses of the resonances in the top and bottom sectors. The Yukawas have the form

$$y_\psi \simeq \frac{M_{*\psi}}{f}\, \epsilon^\psi_L\, \epsilon^\psi_R\,, \qquad (\psi = t, b) \tag{3.15}$$

where $M_{*\psi}$ is a combination of the resonance mass parameters. A larger Yukawa coupling therefore requires a larger compositeness fraction and consequently a larger amount of breaking of the global symmetry.

The Goldstone symmetry of the Higgs has to be broken by both effects to obtain Yukawa couplings and a SM-like potential. However, the situation for χ is different: which couplings break the χ shift symmetry is a priori unknown and they do not have to coincide with the couplings which break the Higgs shift symmetry. There are two straightforward possibilities which we will discuss in great detail in the next chapter. The χ shift symmetry might be broken by the couplings of the SM quarks to the strong sector. In this scenario a dominant breaking by the bottom or lighter quarks is favored, since a breaking due to the top couplings typically introduces $\lambda \sim \lambda_h$, which is in strong tension with direct detection results. A second possibility is the gauging of the stabilizing $U(1)_{\rm DM}$ symmetry which breaks the χ shift symmetry but preserves the Higgs shift symmetry, therefore decoupling Higgs and DM physics. In this case the portal coupling vanishes at one loop, which effectively implements the "Goldstone limit".

3.3 A global view on pNGB DM

In the previous sections we analyzed the DM couplings which one typically expects in a Composite Higgs model based on the symmetry breaking structure $SO(6)/SO(5)$ or $SO(7)/SO(6)$. Here we broaden our scope and consider a more general effective Lagrangian which couples the DM to the SM

$$\mathcal{L} = \mathcal{L}_{\rm SM} + |\partial_\mu \chi|^2 - m_\chi^2 |\chi|^2 + \mathcal{L}_{\rm int}\,. \tag{3.16}$$

Still having in mind a scenario in which both the Higgs and DM are pNGBs of a strong sector, we can write the most general DM-SM interactions up to dimension six as

$$\begin{aligned}
\mathcal{L}_{\rm int} \;=\; & \frac{c_d}{f^2}\, \partial_\mu |\chi|^2 \partial^\mu |H|^2 + \frac{i}{f^2} (\chi^* \overset{\leftrightarrow}{\partial_\mu} \chi) \sum_{\Psi = q_L, u_R, d_R, \ell_L, e_R} b_\Psi \overline{\Psi} \gamma^\mu \Psi + \frac{i g'}{m_*^2} c_B (\chi^* \overset{\leftrightarrow}{\partial_\mu} \chi) \partial_\nu B^{\mu\nu} \\
& - 2\,\lambda |\chi|^2 |H|^2 + \frac{|\chi|^2}{f^2} \big(c_u^\chi\, y_u \bar{q}_L \widetilde{H} u_R + c_d^\chi\, y_d \bar{q}_L H d_R + c_e^\chi\, y_e \bar{\ell}_L H e_R + \text{h.c.} \big) \\
& + \sum_{V = G, W, B} \frac{d_V y^2}{16\pi^2} \frac{g_V^2}{m_*^2} |\chi|^2 V^{\mu\nu} V_{\mu\nu},
\end{aligned} \tag{3.17}$$

where $\chi^* \overset{\leftrightarrow}{\partial_\mu} \chi \equiv \chi^* \partial_\mu \chi - \chi \partial_\mu \chi^*$ and $m_* = g_* f$ with g_* a coupling of the strong sector, while $g_{G,W,B} = g_s, g, g'$. A sum over the fermion generations is understood. Note that the operators in the first line preserve the DM shift symmetries,[5] whereas those in the second and third line explicitly break them (in the last term, y generically indicates the relevant shift symmetry breaking coupling). We additionally assume $\mathcal{CP}$ and custodial invariance what implies that all the coefficients in Eq. (3.17) are real and forbids the operator $(\chi^* \overset{\leftrightarrow}{\partial_\mu} \chi)(H^\dagger \overset{\leftrightarrow}{D_\mu} H)$. Also note that we have neglected $|\chi|^2|H|^4$, since for our purposes it only gives a subleading contribution to λ, with relative suppression $\sim v^2/f^2$. The Lagrangian in Eq. (3.17) is equivalent to the one presented in Refs. [126, 127], with a different choice for the operator basis. Our normalization is such that the b, c and d coefficients have maximal size of $O(1)$, according to the SILH power counting [122].[6] Additional Higgs operators such as $c_H(\partial_\mu |H|^2)^2/(2f^2)$, which modifies all Higgs couplings and has already been mentioned in Section 3.1, have been neglected in Eq. (3.17).

As we have discussed before, the null results in direct detection experiments put the most stringent constraints on these kind of models. Using again a benchmark of $\sigma_{\chi N} \lesssim 10^{-46}$ cm^{2}s^{-1} for DM masses of $m_\chi \sim 100$ GeV [5] we study the bounds this sets on the model parameters (see the DM-nucleon cross-section in Appendix I.F)

$$\frac{f}{b_1^{1/2}} \gtrsim 56 \text{ TeV}, \qquad \frac{m_*}{c_B^{1/2}} \gtrsim 6.5 \text{ TeV}, \qquad \lambda \lesssim 0.6 \cdot 10^{-2}, \tag{3.18}$$

where in the first case we set $b^1_{q_L} = b^1_{u_R} = b^1_{d_R} = b_1$ for the first generation, whereas in the last two cases we took one operator at a time. The first constraint in Eq. (3.18) naively seems to be by far the strongest. However, in Composite Higgs models the coefficient b scales as $b_\Psi \sim \epsilon_\Psi^2$, where ϵ_Ψ is the compositeness fraction of the corresponding fermion field, which is typically small except for the third generation quarks. Assuming comparable compositeness fractions for both fermion chiralities, i.e. $b_{q_L} \sim b_{\psi_R} \sim \sqrt{2}\, m_\psi/(g_* v)$, the bound in Eq. (3.18) translates to $f \gtrsim \mathcal{O}(100)$ GeV for first generation quarks and any interesting g_*. Hence the bound is easily irrelevant in realistic models. The constraint on $m_*/c_B^{1/2}$ is more interesting since it pushes g_* toward the fully strongly coupled regime for $f \sim$ TeV. However, in explicit models this coupling, and all others which include the DM current, are absent if hidden charge conjugation, which transforms $\chi \to -\chi^*$ and leaves the SM fields invariant, is a good symmetry. This is e.g. the case in the $SO(7)/SO(6)$ model. In summary we recover the previous conclusion that direct detection primarily constrains the marginal portal coupling which must be suppressed to comply with null results.

Note that while our original motivation for the Lagrangian in Eqs. (3.16, 3.17) are theories where both the Higgs and the DM arise as composite pNGBs, this EFT can also apply to models such as that of [129], where a complex scalar S is added to the SM as [129–131]

$$\mathcal{L} = \mathcal{L}_{\rm SM} + |\partial_\mu S|^2 + \frac{\mu_S^2}{2}|S|^2 - \frac{\lambda_S}{2}|S|^4 - \lambda_{HS}|S|^2|H|^2 + \frac{\mu_S'^2}{4}(S^2 + \text{h.c.})\,. \tag{3.19}$$

The $U(1)$ symmetry is spontaneously broken be the VEV of the complex scalar $\langle S \rangle = v_s/\sqrt{2}$ and explicitly broken by μ'_S, leaving a remnant $S \to S^*$ invariance. The complex field can therefore be parameterized as $S = (v_s + \sigma)e^{i\phi/v_s}/\sqrt{2}$ with σ being a real radial mode and ϕ

[5] Naively, the derivative Higgs portal operator may not seem shift-symmetric. This is just a consequence of our choice of basis for the Goldstone fields (see e.g. [29]), which is the same adopted in the Strongly Interacting Light Higgs (SILH) Lagrangian [122]. In this basis the shift invariance is not immediate.

[6] If the SM transverse gauge bosons are also composite [128] the enhancements $c_B \sim g_*/g'$ and $d_V \sim 16\pi^2/y^2$ are possible.

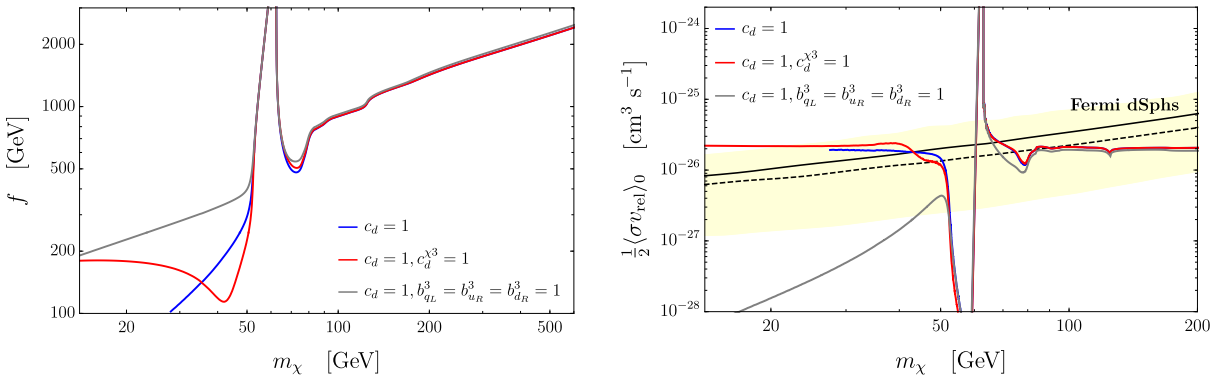

Figure 3.2: *Left:* contours obtained requiring that the thermal relic density of χ matches the observed one, assuming the given values of the EFT coefficients and setting the others to zero. *Right:* the present-day annihilation cross-section to SM particles, calculated along the relic density contours shown in the left panel. The black line (yellow band) is the 95% CL observed upper limit (95% CL uncertainty band on the expected limit) from the dSphs analysis in [7]. The dashed black line corresponds to the observed limit from the analysis of a smaller dSphs sample [145]. The quoted experimental bounds assume annihilation to $b\bar{b}$. This Figure has previously been published in [31].

a real pNGB DM candidate with mass μ_S' stabilized by the remnant $S \to S^*$ symmetry. If the radial mode is heavy, it can be integrated out, yielding an effective Lagrangian which after a field redefinition can be brought into the form of Eq. (3.17) with $c_d/f^2 = \lambda_{HS}/m_\sigma^2$.[7] The marginal portal coupling arises at one loop in this model resulting in a very suppressed DM-nucleon cross-section [133,134]. This model also gives rise to interesting other signatures such as gravitational wave signals from phase transitions in the early universe, which has been studied in [135,136]. For extended models and subsequent studies of models built following this approach see [137–144].

The common feature of all of these models is that the expected direct detection signals are structurally suppressed due to the pNGB nature of the DM, assuming that the marginal Higgs portal coupling λ is suppressed. Depending on the specific realization, the DM-nucleon scattering signal might be in reach at future experiments, e.g. due to effects of DM-quark contact interactions proportional to c_q^χ. However, it could equally well be hidden beneath the neutrino floor, making its detection extremely challenging. In addition the derivative Higgs portal operator proportional to c_d plays an important role in setting the DM relic abundance since it is unsuppressed in DM annihilation. The observed relic abundance is reproduced through the freeze-out mechanism for $f \sim$ TeV and weak scale DM masses as shown in the left panel of Figure 3.2. The Figure also shows that in this mass range couplings to the light quarks have a very limited effect on the relic abundance. Note that for completeness we show results down to $f = 100$ GeV, although it should be kept in mind that for weak-scale f, finding ultraviolet models that are acceptably described at low energies by Eq. (3.17) may be challenging.

Since as we have argued DM-nucleon scattering is not a reliable probe for pNGB DM, indirect detection and collider searches are crucial ingredients to find hints of pNGB DM. At this point we will shortly comment on indirect detection and defer a discussion of collider probes

[7] Note that if the radial mode is relatively light it has to be included in the study of DM phenomenology. However, in this case one can also directly probe the radial mode, which could e.g. be produced on-shell in VBF and decays to a DM pair, as studied in [132] at the LHC.

to Chapter 5 where we will present a collider study on the irreducible coupling in this kind of scenarios, the derivative Higgs portal. The derivative portal mediates s-channel annihilation, implying that looking for present-day annihilations could be a sensitive probe. In the right panel of Figure 3.2 we compare the present-day annihilation cross-section to the bounds obtained by the Fermi-LAT [7, 145] from gamma-ray observations of dwarf spheroidal galaxies (dSphs). For DM mass of $O(100)$ GeV, these bounds (which were computed assuming DM annihilation to $b\bar{b}$) are very close to the canonical thermal cross-section $\langle\sigma v_{\rm rel}\rangle_{\rm can} \approx 2 \cdot 10^{-26}\,{\rm cm}^3\,{\rm s}^{-1}$. We see that the region $m_\chi \lesssim 70$ GeV is already in mild tension with data, and future improvements of the sensitivity will provide a stringent test of pNGB DM. Additionally searches for monochromatic photon annihilation products are relevant for the region $m_h/2 \lesssim m_\chi \lesssim m_w$ where the off-shell Higgs has a branching ratio to photons $\gtrsim 10^{-3}$. We find that in this region the expected cross-section is close to the Fermi-LAT sensitivity [146], if a favorable DM profile (contracted Navarro-Frenk-White) and the accordingly-optimized region of the sky are considered.

Another important channel are annihilations into antiprotons. Recent measurements of the antiproton spectrum by AMS-02 [6] give additional constraints and even show a hint of an excess [147, 148], which could be explained by DM. Recently an explanation in terms of pNGB DM annihilations has been suggested in [149]. However, systematic uncertainties are still larger for antiprotons compared to gamma rays, although it has been argued that they are under control [150]. But as the situation has not settled yet we do not show constraints from antiprotons in Figure 3.2.

Chapter 4

Composite dark matter in SO(7)/SO(6) Composite Higgs model

The previous Chapter discussed pNGB DM from an EFT point of view, referring to explicit models when building the effective Lagrangian and estimating the size of the couplings. In this chapter we want to justify these assumptions by explicitly constructing a fully realistic Composite Higgs model. Our construction will be based on the symmetry breaking structure $SO(7)/SO(6)$ which is the smallest coset containing both the Higgs-doublet and a complex DM candidate stabilized by a remnant global symmetry. As we will show in the following this simple model can give rise to all pNGB DM scenarios which we discussed in the previous chapter. In particular it features varying degrees of the "Goldstone limit", depending on which couplings break the DM shift symmetry. In Section 4.1 we introduce the $SO(7)/SO(6)$ coset and construct the Goldstone Lagrangian which is completely fixed by this symmetry. Then we demonstrate that in this coset DM stabilization can originate from the global symmetries of the strong sector. The fermion couplings in Composite Higgs models are a priori not fixed, leaving a choice as to how to embed them into a representation of the global symmetry group and consequently which part of the symmetry this embedding breaks. In Section 4.2 we shortly outline the different possibilities and what effect they have on DM phenomenology. In broad categories there are three such possibilities which implement the "Goldstone limit" in increasing purity: (1) the embedding of the top quark breaks the DM shift symmetry, (2) the embedding of the bottom quark breaks the DM shift symmetry or (3) the embedding of the quarks do not break the DM shift symmetry at all. In the third case the breaking has to come from a different source which we take to be the gauging of the $U(1)_{\rm DM}$ stabilizing symmetry. We will study in detail these three scenarios in Sections 4.3 to 4.5.

This chapter is based on [28, 29][1] from which all Figures and part of the text have been taken.[2]

[1] [28]: R. Balkin, M. Ruhdorfer, E. Salvioni and A. Weiler, *Charged Composite Scalar Dark Matter*,
[29]: R. Balkin, M. Ruhdorfer, E. Salvioni and A. Weiler, *Dark matter shifts away from direct detection.*

[2] Note that some of the results in Section 4.3 build on findings of the author's Master thesis.

4.1 Goldstone Lagrangian

In the following we assume a strong sector which possesses a global $SO(7)$ symmetry which is spontaneously broken to $SO(6)$ at a scale f. This gives rise to six GBs π^a $a = 1, \ldots, 6$ which transform in the fundamental representation of the unbroken $SO(6)$. Under the custodial $SO(4)$ this decomposes into $H \sim \mathbf{4}$, which we identify with the Higgs doublet, and two real singlets κ, η. Following the Callan-Coleman-Wess-Zumino (CCWZ) construction [74, 75], which is detailed in Appendix I.A, we parameterize the GBs by the matrix $U = \exp(i\sqrt{2}\pi^a X^a/f)$, where X^a are the broken generators. At leading two-derivative order, the GB Lagrangian is given by

$$\mathcal{L}_\pi = \frac{f^2}{4} d_\mu^a d^{a\,\mu}, \tag{4.1}$$

where the CCWZ symbol d_μ is constructed from U and its $SU(2)_L \times U(1)_Y$ covariant derivative. In unitary gauge the GB vector is given by

$$\boldsymbol{\pi} = \Big(0,\ 0,\ 0,\ \tilde{h},\ \eta,\ \kappa\Big)^T, \tag{4.2}$$

where $\tilde{h}$ is the radial mode of the Higgs doublet and its physical excitation will be identified with the observed Higgs boson. After a field redefinition of the GB fields, which is given in Eq. (I.A.4), we obtain the the explicit form of the Goldstone Lagrangian

$$\mathcal{L}_\pi = \frac{1}{2}\Big[(\partial_\mu \tilde{h})^2 + (\partial_\mu \eta)^2 + (\partial_\mu \kappa)^2\Big] + \frac{1}{2}\frac{\big(\tilde{h}\partial_\mu \tilde{h} + \eta \partial_\mu \eta + \kappa \partial_\mu \kappa\big)^2}{f^2 - \tilde{h}^2 - \eta^2 - \kappa^2} + \frac{\tilde{h}^2}{4}\Big[\bar{g}^2 |\bar{W}_\mu^+|^2 + \frac{1}{2}\big(\bar{g}\bar{W}_\mu^3 - \bar{g}'\bar{B}_\mu\big)^2\Big]. \tag{4.3}$$

The bar over the gauge fields and couplings labels them as elementary fields and couplings. The elementary fields couple linearly to strong sector resonances, s.t. the physical fields, i.e. the mass eigenstates, are linear combinations of elementary and composite degrees of freedom. Performing the diagonalization of the mass matrix yields e.g. for the charged gauge fields $\bar{g}\bar{W}_\mu^\pm \to g W_\mu^\pm + \ldots$, where g and $W_\mu^\pm$ are the SM gauge coupling and field, respectively, where we left out terms with composite vector resonances. After the diagonalization we can identify $\langle \tilde{h} \rangle = v \simeq 246$ GeV. If we further assume $\langle \eta \rangle = \langle \kappa \rangle = 0$ and expand around the vacuum, we see that the kinetic terms of the singlets are canonically normalized, whereas for the Higgs canonic normalization is achieved with

$$\tilde{h} = v + \sqrt{1-\xi}\, h\,, \qquad \xi \equiv \frac{v^2}{f^2}\,, \tag{4.4}$$

where h is the physical excitation. This field redefinition rescales all Higgs couplings.

4.2 Fermion couplings and DM stability

Similarly to the gauge sector, we assume that partial compositeness is also realized in the fermion sector [72] with elementary fermions coupled linearly to strong sector operators. For the third generation quarks this takes the schematic form

$$\mathcal{L}_{\text{mix}} \sim \epsilon_q\, \bar{q}_L \mathcal{O}_q + \epsilon_t\, \bar{t}_R \mathcal{O}_t + \epsilon_{q'}\, \bar{q}_L \mathcal{O}_{q'} + \epsilon_b\, \bar{b}_R \mathcal{O}_b + \text{h.c.}\,, \tag{4.5}$$

where the ϵ_i scale as a coupling λ_i times the symmetry breaking scale, i.e. $\epsilon_i \sim \lambda_i f$. Notice that a correct hypercharge assignment requires an enlargement of the symmetry pattern to

$SO(7) \times U(1)_X \to SO(6) \times U(1)_X$, s.t. $Y = T^3_R + X$. Since the SM fermions do not come in complete $SO(7)$ representations,[3] the above interactions will break explicitly at least some of the GB shift symmetries. The minimal requirement on these couplings is that they break the Higgs shift symmetry in order to produce Yukawa couplings for $\tilde{h}$ to the top and bottom and additionally a 1-loop potential of the correct size.

While the structure of the explicit symmetry breaking from the gauge sector is fixed by the embedding of the SM gauge group, the breaking from the fermion sector crucially depends on the form of the couplings in Eq. (4.5), i.e. the $SO(7)$ quantum numbers of the composite operators $\mathcal{O}_i$. However, the $SO(7)_X$ representations of the $\mathcal{O}_i$ are not uniquely fixed and leave room for model dependent assumptions on the symmetry breaking effects. In order to classify different viable options for the quantum numbers, we consider the decomposition of $SO(7)$ representations under its subgroup $SO(4) \times SO(3)$, which we can write in an equivalent form as $SU(2)_L \times SU(2)_R \times SU(2)'$, where we used the local group isomorphisms $SO(4) \simeq SU(2)_L \times SU(2)_R$ and $SO(3) \simeq SU(2)'$. The $SO(3)$ or equivalently $SU(2)'$ subgroup is generated by the broken generators under which the two singlets shift, $X^\eta \equiv X^5$ and $X^\kappa \equiv X^6$, together with

$$T^{\rm DM} \equiv T^{56} = \frac{1}{\sqrt{2}} \, \mathrm{diag}(\mathbf{0}_{4\times4}, \sigma^2, 0) \;\in\; SO(6), \tag{4.6}$$

where we used block notation. The label of the third generator already anticipates its role in the DM stabilization. The first few $SO(7)$ representations decompose under $(SU(2)_L, SU(2)_R, SU(2)')$ as (see for example [151]),

$$\begin{aligned}
\mathbf{1} &= (\mathbf{1},\mathbf{1},\mathbf{1}),\\
\mathbf{7} &= (\mathbf{2},\mathbf{2},\mathbf{1}) \oplus (\mathbf{1},\mathbf{1},\mathbf{3}),\\
\mathbf{8} &= (\mathbf{2},\mathbf{1},\mathbf{2}) \oplus (\mathbf{1},\mathbf{2},\mathbf{2}),\\
\mathbf{21} &= (\mathbf{2},\mathbf{2},\mathbf{3}) \oplus (\mathbf{3},\mathbf{1},\mathbf{1}) \oplus (\mathbf{1},\mathbf{3},\mathbf{1}) \oplus (\mathbf{1},\mathbf{1},\mathbf{3}),\\
\mathbf{27} &= (\mathbf{3},\mathbf{3},\mathbf{1}) \oplus (\mathbf{2},\mathbf{2},\mathbf{3}) \oplus (\mathbf{1},\mathbf{1},\mathbf{5}) \oplus (\mathbf{1},\mathbf{1},\mathbf{1}).
\end{aligned} \tag{4.7}$$

In order to guarantee custodial protection against zero-momentum corrections to the $Zb_L\bar{b}_L$ vertex, which are strongly constrained from LEP data, q_L must be embedded in the $(\mathbf{2},\mathbf{2})_{2/3}$ representation of $(SU(2)_L,\, SU(2)_R)_X$ and t_R either in $(\mathbf{1},\mathbf{1})_{2/3}$ or $(\mathbf{1},\mathbf{3})_{2/3} \oplus (\mathbf{3},\mathbf{1})_{2/3}$ [77].[4] This still leaves several options for the embeddings, such as $q_L \sim \mathbf{7}, \mathbf{21}, \ldots$ and $t_R \sim \mathbf{1}, \mathbf{7}, \ldots$. However, these different embeddings considerably influence the phenomenology of the remaining singlets. Embeddings into a singlet of $SU(2)'$ preserve the shift symmetry of η and κ, thus keeping them massless. This opens up the possibility that e.g. the embedding of the top preserves the shift symmetry but embeddings of lighter quarks break it. Such a scenario will be the topic of Section 4.4. But even if an embedding breaks $SU(2)'$ it might not break it completely. The embedding of a quark into the $(\mathbf{1},\mathbf{1},\mathbf{3})$ representation can be chosen in such a way as to preserve a residual $U(1)$, generated by one among $\{X^\eta, X^\kappa, T^{\rm DM}\}$. Therefore we either keep the shift symmetry of one of the singlets, i.e. it remains massless, or we preserve the $U(1)$ generated by $T^{\rm DM}$ which acts on η and κ. In this case the singlets can be combined into a complex scalar

$$\chi \equiv (\kappa + i\eta)/\sqrt{2}\,, \tag{4.8}$$

which has charge $+1$ under $U(1)_{\rm DM}$ (the normalization is fixed by taking $\sqrt{2}\,T^{\rm DM}$ as the generator), while the quark in this embedding is uncharged since it is embedded along the $U(1)_{\rm DM}$

[3] An exception is the case where t_R is embedded into an $SO(7)$ singlet.

[4] Once we explicitly include b_R in the construction it has to be embedded either in $(\mathbf{1},\mathbf{1})_{-1/3}$ or $(\mathbf{1},\mathbf{2})_{1/6}$ in order to avoid large tree-level corrections to the $Zb_R\bar{b}_R$ coupling.

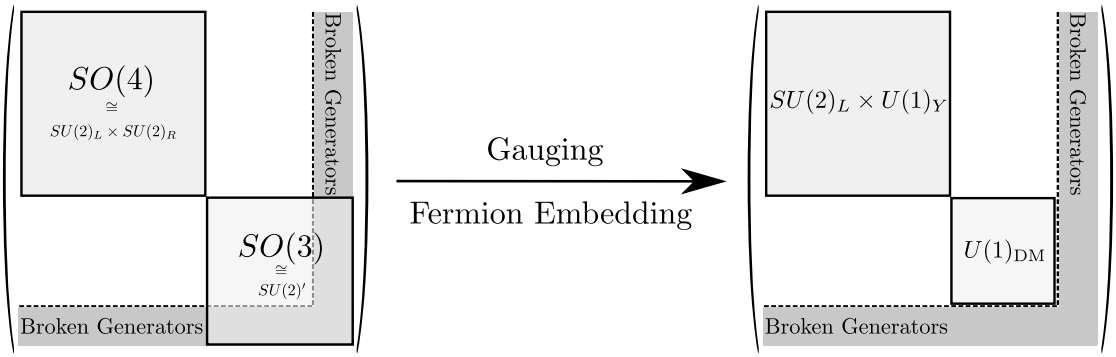

Figure 4.1: Schematic overview of the $SO(7)$ algebra. In the left drawing the structure of the $SU(2)_L \times SU(2)_R \times SU(2)'$ subgroup is displayed, whereas the right drawing shows the symmetries that remain unbroken after the weak gauging of the SM electroweak group and the coupling of the fermions to the strong sector. Note that this also applies if $SU(2)'$ is respected by the fermion embeddings but explicitly broken by the gauging of $U(1)_{\rm DM}$ as we will consider in Section 4.5. This Figure is taken from [28].

generator. In the following we will always take embeddings which preserve the $U(1)_{\rm DM}$. Thus the leading breaking of the χ shift symmetry will be implemented as either an embedding or gauging along the $T^{\rm DM}$ generator. The unbroken $U(1)_{\rm DM}$ ensures the stability of χ, which will be our DM candidate. This setup is schematically shown in Figure 4.1.

Note that so far we have assumed that each elementary fermion couples to only one strong sector operator in a $U(1)_{\rm DM}$-invariant way. However, in general there could be additional, subleading couplings to other operators. If one of them breaks the $U(1)_{\rm DM}$, the DM stability could be compromised. For this reason we have to assume that $U(1)_{\rm DM}$ is either a global symmetry respected by all elementary-composite couplings, or an unbroken gauge symmetry.

In this thesis we consider three discrete choices for the dominant source of DM shift symmetry breaking: the embedding of t_R, the embedding of b_R and weakly gauging $U(1)_{\rm DM}$. Each of them realizes the "Goldstone limit" to a different degree. Before we discus each realization in great detail in the next Sections, we give a short overview of the characteristics of each scenario. A schematic summary of the three scenarios and their main features relevant for DM phenomenology is shown in Figure 4.2.

Leading breaking by top quark couplings. This scenario was first discussed in Refs. [8,38] in the context of real scalar DM in the $SO(6)/SO(5)$ model stabilized by a Z_2 symmetry. In the $SO(7)/SO(6)$ model, which we discuss here, it is realized e.g. for $\mathcal{O}_{q,t} \sim \mathbf{7}_{2/3}$, where q_L is embedded into the $SU(2)'$ preserving part $(\mathbf{2},\mathbf{2},\mathbf{1})_{2/3} \subset \mathbf{7}_{2/3}$. The interactions of $t_R \sim (\mathbf{1},\mathbf{1},\mathbf{3})_{2/3} \subset \mathbf{7}_{2/3}$ explicitly break the χ shift symmetry. Top loops generically make the DM heavier than the Higgs and generate a marginal Higgs portal coupling of similar size as the Higgs quartic λ_h, i.e.

$$\lambda \lesssim \frac{\lambda_h}{2} \simeq 0.065 \qquad \text{and} \qquad m_\chi \gg m_h \,. \tag{4.9}$$

For $f \gtrsim$ TeV these estimates imply $\lambda f^2 \lesssim m_\chi^2$, s.t. according to Eq. (3.12) λ plays a subleading but non-negligible role in DM annihilation. The portal coupling induces a DM-nucleon cross-section of the order $\sigma_{\rm SI}^{\chi N} \sim 10^{-46}$ cm^2, which is currently probed by XENON1T and already in mild tension with data. A thorough study of this model will be performed in Section 4.3.

Leading source of DM shift symmetry breaking		*DM annihilation*	*DM direct detection*
t_R	(Sec. 4.3)	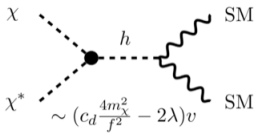	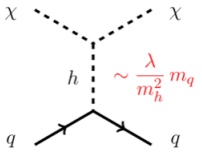
b_R	(Sec. 4.4)	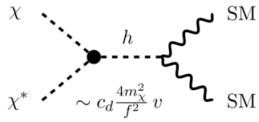	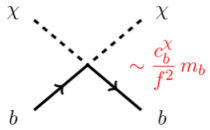
γ_D	$m_{\gamma_D} = 0$ (Sec. 4.5.1)	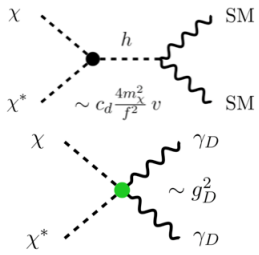	*negligible*
	$m_\chi < m_{\gamma_D}$ (Sec. 4.5.2)	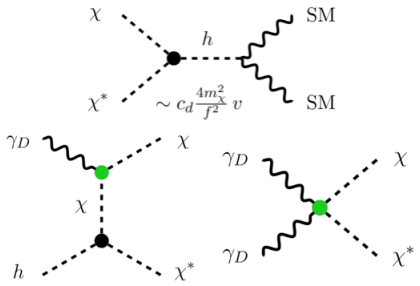	

Figure 4.2: Schematic summary of the three scenarios which we discuss in Sections 4.3 to 4.5. The EFT coefficients c_d, c_b^χ and λ were defined in Eqs. (3.2), (3.10) and (3.11), respectively. In the third scenario we denote with γ_D the dark photon associated to the gauging of $U(1)_{\rm DM}$ with coupling g_D, and mark the gauge interactions in green. This Figure is adopted from [29].

Leading breaking by bottom quark couplings. Although this possibility was also first discussed in [8], here we focus on a different parametric regime. The top couplings preserve $SU(2)'$, what can be achieved by $\mathcal{O}_q \sim \mathbf{7}_{2/3}, \mathcal{O}_t \sim \mathbf{21}_{2/3}$, and the bottom couplings constitute the leading breaking of the χ shift symmetry with $\mathcal{O}_{q',b} \sim \mathbf{7}_{-1/3}$. In this case the one-loop generated portal coupling and DM mass scale differently with the bottom Yukawa,

$$\lambda \propto y_b^2 \qquad \text{and} \qquad m_\chi \propto (y_b\, g_*)^{1/2} f\,, \tag{4.10}$$

where g_* is the strong sector coupling. This implies that λ is small enough ($\lambda \ll 10^{-3}$) to be irrelevant for direct detection, while χ can be sufficiently heavy ($m_\chi \sim 100$ GeV) s.t. the observed relic abundance can be achieved via annihilation through the derivative Higgs portal. The explicit symmetry breaking additionally generates the DM-bottom quark contact interaction proportional to c_b in Eq. (3.10), which yields a small DM-nucleon cross-section $\sigma_{\rm SI}^{\chi N} \sim 10^{-47}$ cm^2 which is in the reach of future direct detection experiments. A detailed study of this scenario

will be the topic of Section 4.4.

Leading breaking by weakly gauging $\mathbf{U(1)_{DM}}$. It is possible to couple all SM quarks to the strong sector in a way which preserves the DM shift symmetry. This can e.g. be achieved with $\mathcal{O}_q \sim \mathbf{7}_{2/3}$ and $\mathcal{O}_{u,d} \sim \mathbf{21}_{2/3}$. In this case we need a BSM source for the explicit breaking in order to generate a mass for the DM. One such possibility is gauging the stabilizing $U(1)_{\rm DM}$ symmetry with coupling constant g_D. This can generate a DM mass at on-loop

$$m_\chi \propto g_D f\,, \tag{4.11}$$

which is naturally of $\mathcal{O}(100)$ GeV, while λ is strongly suppressed as it is only generated at higher loops. This model achieves the closest realization of the "Goldstone limit". The presence of a dark photon γ_D additionally yields a rich and interesting phenomenology which we study in detail in Section 4.5.

4.3 Shift symmetry breaking by top quark coupling

We start our study with the most straightforward scenario: the leading breaking of both the Higgs and DM shift symmetry originates from the couplings of the top quark. This can be achieved by embedding q_L and t_R into the $\mathbf{7}_{2/3}$ representation of the global symmetry in such a way that the $U(1)_{\rm DM}$ remains unbroken. Under $(SU(2)_L, SU(2)_R)^{\rm DM}_X$ the $\mathbf{7}_{2/3}$ decomposes as

$$\mathbf{7}_{2/3} = (\mathbf{2},\mathbf{2})^0_{2/3} \oplus (\mathbf{1},\mathbf{1})^0_{2/3} \oplus (\mathbf{1},\mathbf{1})^{\pm1}_{2/3}\,. \tag{4.12}$$

This allows us to embed q_L into $(\mathbf{2},\mathbf{2})^0_{2/3}$ and t_R into $(\mathbf{1},\mathbf{1})^0_{2/3}$, what keeps them neutral under $U(1)_{\rm DM}$. The t_R embedding into $(\mathbf{1},\mathbf{1})^0_{2/3}$, which picks the direction generated by $T^{\rm DM}$ in the $(\mathbf{1},\mathbf{1},\mathbf{3})_{2/3} \subset \mathbf{7}_{2/3}$, explicitly breaks the $SU(2)'$ to $U(1)_{\rm DM}$ and consequently also the shift symmetry of χ, which will acquire a potential and in particular a mass of the same size as the Higgs. The explicit form of the embeddings, which we will adopt in the following, is given by

$$\xi_L = \frac{1}{\sqrt{2}}\left(ib_L,\quad b_L,\quad it_L,\quad -t_L,\quad 0,\quad 0,\quad 0\right)^T\,,\qquad \xi_R = \left(0,\quad 0,\quad 0,\quad 0,\quad 0,\quad 0,\quad t_R\right)^T\,. \tag{4.13}$$

4.3.1 Strong sector resonances

The strong sector resonances, which couple linearly to the elementary particles, come in full multiplets of the unbroken $SO(6)$ and can be consistently described in the CCWZ framework (see Section 2.2.4). We begin with a discussion of the fermion sector, which will play a dominant role in the following. Since the $\mathbf{7}_{2/3}$ representation, into which we have embedded the elementary fermions, decomposes as $\mathbf{7}_{2/3} = \mathbf{6}_{2/3} \oplus \mathbf{1}_{2/3}$ under $SO(6) \times U(1)_X$, we consider fermionic resonances Q in the $\mathbf{6}_{2/3}$ and S in the $\mathbf{1}_{2/3}$ representation of the unbroken group. The explicit form of the Q multiplet in the fundamental representation can be written as

$$Q = \frac{1}{\sqrt{2}}\left(iB - iX_{5/3},\quad B + X_{5/3},\quad iT + iX_{2/3},\quad -T + X_{2/3},\quad -i\mathcal{Y} + i\mathcal{Z},\quad \mathcal{Y} + \mathcal{Z}\right)^T\,, \tag{4.14}$$

where the doublet $(T,B)^T$ transforms as $\mathbf{2}^0_{1/6}$ under $(SU(2)_L)^{\rm DM}_Y$, and therefore has the same quantum numbers as q_L, whereas the exotic doublet $(X_{5/3}, X_{2/3})^T \sim \mathbf{2}^0_{7/6}$ contains an exotic fermion with electric charge equal to 5/3. The two states $\mathcal{Y}, \mathcal{Z} \sim \mathbf{1}^{\pm1}_{2/3}$ share the SM quantum

numbers of the t_R, but are additionally charged under $U(1)_{\rm DM}$, what strongly constrains their couplings. The singlet S is uncharged under $U(1)_{\rm DM}$. The leading Lagrangian of the fermion sector is thus given by

$$\begin{aligned}\mathcal{L}_f \;=\; & i\bar{q}_L \not{D} q_L + i\bar{t}_R \not{D} t_R + \sum_{i=1}^{N_Q} \bar{Q}_i \left(i\not{D} + \not{e} - m_{Q_i}\right) Q_i + \sum_{j=1}^{N_S} \bar{S}_j \left(i\not{D} - m_{S_j}\right) S_j \\ & + \sum_{i=1}^{N_Q} \left(\epsilon^i_{tQ} \bar{\xi}^A_R U_{Aa} Q^a_{iL} + \epsilon^i_{qQ} \bar{\xi}^A_L U_{Aa} Q^a_{iR}\right) + \sum_{j=1}^{N_S} \left(\epsilon^j_{tS} \bar{\xi}^A_R U_{A7} S_{jL} + \epsilon^j_{qS} \bar{\xi}^A_L U_{A7} S_{jR}\right) + \text{h.c.},\end{aligned} \tag{4.15}$$

where N_Q and N_S are the number of Q and S multiplets coupling to the strong sector. $A\,(a)$ denotes indices in the fundamental representation of $SO(7)\,(SO(6))$. The second line in Eq. (4.15) is the low-energy interpolation of the linear partial compositeness couplings to strong sector operators. Also note the $\xi_{L/R}$ are converted into $SO(6)$ multiplets by dressing them with the GB matrix U. The kinetic term of Q_i also includes the CCWZ e_μ symbol which is needed to make it invariant under local $SO(6)$ transformations, what is required by the CCWZ formalism in order to account for the non-linear realization of $SO(7)$. There are in principle additional terms in the Lagrangian, which arise purely from strong dynamcis with $\mathcal{O}(1)$ coefficients $c^{L/R}_{ji}$, that are of the form

$$\mathcal{L}_d = \sum_{i=1}^{N_Q} \sum_{j=1}^{N_S} c^L_{ji} \bar{S}_{jL} \not{d}^a Q^a_{iL} + \text{h.c.} + (L \to R). \tag{4.16}$$

Since they are couplings within the strong sector, they respect the full non-linearly realized $SO(7)$ symmetry and in particular the GB shift symmetries. For this reason they contain only derivative couplings of the GBs with the strong sector resonances. At the leading order in the $1/f$ expansion one GB couples to two fermions with the coupling strength $\sim c^{L/R} p/f$, where p is the relevant energy scale. While these operators do not contribute to the effective potential of the pNGBs, since they do not break the GB shift symmetry, they can be important in hadron collider processes [152], where $p/f \sim m_*/f \sim O(1)$ with m_* the mass of a resonance. We will return to them in the discussion of the LHC and future collider prospects in Sec. 4.3.4.B. For DM phenomenology, i.e. DM annihilation and DM scattering on heavy nuclei, these interactions scale as $p/f \lesssim m_\chi/f \ll 1$ and are therefore suppressed compared to the couplings in Eq. (4.15), which are of the size $\sim \epsilon/f$. For this reason we will neglect the couplings in Eq. (4.16) in the following.

Gauge sector resonances can be introduced following the generalized hidden local symmetry approch [153], where vector resonances for a symmetry breaking structure $\mathcal{G}/\mathcal{H}$ are implemented as gauge bosons of a local $\mathcal{G}$ symmetry. For $\mathcal{G} = SO(7)$ the adjoint representation decomposes as $\mathbf{21} = \mathbf{15} \oplus \mathbf{6}$ under $SO(6)$. We therefore introduce massive vectors in the adjoint $\rho_\mu \sim \mathbf{15}$ and in the fundamental $a_\mu \sim \mathbf{6}$ of $SO(6)$. The Lagrangian and further details are given in Appendix I.A.

4.3.2 Scalar potential and EWSB

The explicit breaking of the $SO(7)$ symmetry by gauging only a subgroup $SU(2)_L \times U(1)_Y \subset SO(7) \times U(1)_X$ and by the linear coupling of the strong sector to elementary fermions in incomplete $SO(7)$ representations, which are parameterized in Eq. (4.15) by the elementary-composite mixing parameters, which we will collectively denote as ϵ, generates a radiative potential for the GBs. This 1-loop effective potential can be computed along the lines of Coleman-Weinberg

(CW) [78], what yields in unitary gauge and to quartic order in the fields

$$V(\tilde{h},\chi) = \frac{1}{2}\mu_h^2\tilde{h}^2 + \frac{\lambda_h}{4}\tilde{h}^4 + \mu_{\rm DM}^2\chi^*\chi + \lambda_{\rm DM}(\chi^*\chi)^2 + \lambda\tilde{h}^2\chi^*\chi\,. \tag{4.17}$$

This potential is supposed to induce a correct EWSB VEV for the Higgs, i.e. $\langle\tilde{h}\rangle = v \ll f$. Note that while $U(1)_{\rm DM}$ is a global symmetry of the theory, the effective potential could in principle break it spontaneously, which would spoil DM stability. In order to assure the stability of the DM we will only consider parameter choices satisfying $\langle\chi\rangle = 0$. The masses of the pNGBs can be obtained from the second derivative of the potential evaluated at the minimum, i.e.

$$m_h^2 = (1-\xi)\left.\frac{\partial^2 V}{\partial\tilde{h}^2}\right|_{\tilde{h}=v,\,\chi=0} = (1-\xi)2\lambda_h v^2\,, \qquad m_\chi^2 = \left.\frac{\partial^2 V}{\partial\chi\partial\chi^*}\right|_{\tilde{h}=v,\,\chi=0} = \mu_{\rm DM}^2 + \lambda v^2\,, \tag{4.18}$$

where we included $(1-\xi)$ for the Higgs mass in order to account for the non-canoncially normalized kinetic term in the non-linear sigma model after EWSB (cf. (4.3) and (4.4)). Computing the effective potential directly from the gauge and fermion Lagrangian, one finds that $\mu_h^2, \mu_{\rm DM}^2$ and $\lambda_h, \lambda_{\rm DM}, \lambda$ are in general quadratically and logarithmically divergent, respectively, and therefore sensitive to the UV cutoff $\Lambda \lesssim 4\pi f$ of the EFT.[5] However, in order to retain predictivity one usually assumes that the sensitivity to UV scales is cut off by the first set of vector and fermion resonances, which we introduces in Section 4.3.1. One way to achieve this is with a set of generalized Weinberg sum rules (WSRs) [79], which we introduced in Section 2.2.5. The basic idea is that the form factors determining the potential parameters for loops of SM states should vanish sufficiently fast at large momenta to make the potential calculable [80,81]. This can be achieved by imposing non-trivial relations on the model parameter, which are exactly the WSRs.[6]

Let us now first discuss the contributions from the gauge sector to the effective potential. Since the gauge couplings do not break the DM shift symmetry and preserve $U(1)_{\rm DM}$, gauge boson loops will only affect the Higgs potential. The gauge contributions to the mass parameter and Higgs quartic will be denoted as $\mu_{h,g}^2$ and $\lambda_{h,g}$, respectively. In order to obtain a finite contribution, one has to introduce at least one multiplet of vector resonances ρ_μ in the adjoint of $SO(6)$ and one multiplet a_μ in the fundamental of $SO(6)$, with their masses $m_{\rho,a}$ and decay constants $f_{\rho,a}$ related by two WSRs

$$2f_\rho^2 - 2f_a^2 = f^2\,, \qquad f_\rho^2 m_\rho^2 = f_a^2 m_a^2\,, \qquad (\text{WSR } 1+2)_g\,. \tag{4.19}$$

The first relation removes the quadratic sensitivity to the cutoff in $\mu_{h,\,g}^2$ and makes $\lambda_{h,\,g}$ finite, whereas the second relation cancels the remaining logarithmic divergence in $\mu_{h,g}^2$. The WSRs in Eq. (4.19) allow us to get rid of f_a and m_a and express them in terms of f_ρ, m_ρ and f. The first condition additionally requires $f_\rho > f/\sqrt{2}$. In the limit of $g^2/g_\rho^2 \ll 1$, with $g_\rho = m_\rho/f_\rho$ and neglecting the subleading hypercharge contribution we get to leading order

$$\mu_{h,\,g}^2 \approx \frac{9\,g^2}{32\pi^2} m_\rho^2 \frac{f_\rho^2}{f^2} \log\left(\frac{2f_\rho^2/f^2}{2f_\rho^2/f^2 - 1}\right)\,, \tag{4.20}$$

[5] Notice that by naive power counting, the quartic couplings can also be quadratically divergent. However, the structure of the field-dependent mass matrices leads to a quadratically divergent term $\sim \Lambda^2 \mathrm{STr}\, m^2(h,\chi) = \Lambda^2(k_0 + k_h h^2 + k_\chi\chi^*\chi)$ with $k_{0,h,\chi}$ field-independent constants. Thus the leading degree of divergence of the quartics is only logarithmic.

[6] Notice also that, due to the contribution of top quark and SM gauge boson loops, the expression of λ_h in Eq. (4.17) is infrared (IR) divergent. To retain full predictivity, this issue is resolved by adding to $V(\tilde{h},\chi)$ an additional quartic for $\tilde{h}$ that is non-analytic at $\tilde{h}=0$. See Appendix I.D for further details.

what is strictly positive and therefore stabilizes electroweak symmetry. In order to trigger EWSB a second and larger negative contribution is needed, which destabilizes the electroweak symmetry. Such a negative to μ_h^2 contribution is readily obtained from fermion loops, which has to be tuned against $\mu_{h,g}^2$ in order to obtain a realistic Higgs VEV $\langle\tilde{h}\rangle = v \ll f$. The gauge contribution to the Higgs quartic is small compared to the fermionic contribution (see e.g. the discussion in Section 2.2.3).

In the fermionic case the $\mathcal{G}$ breaking spurions are the elementary-composite mixing parameters ϵ, which generate a potential in fermion loops. The ϵ parameters break the shift symmetry of both $\tilde{h}$ and χ and therefore give contributions to all potential coefficients. The WSRs which ensure their cutoff independence take the form

$$\sum_{i=1}^{N_Q} \left|\epsilon_{qQ}^i\right|^2 = \sum_{j=1}^{N_S} \left|\epsilon_{qS}^j\right|^2 , \qquad \sum_{i=1}^{N_Q} \left|\epsilon_{tQ}^i\right|^2 = \sum_{j=1}^{N_S} \left|\epsilon_{tS}^j\right|^2 , \qquad \text{(WSR 1)}_f \tag{4.21}$$

$$\sum_{i=1}^{N_Q} \left|\epsilon_{qQ}^i\right|^2 m_{Q_i}^2 = \sum_{j=1}^{N_S} \left|\epsilon_{qS}^j\right|^2 m_{S_j}^2 , \qquad \sum_{i=1}^{N_Q} \left|\epsilon_{tQ}^i\right|^2 m_{Q_i}^2 = \sum_{j=1}^{N_S} \left|\epsilon_{tS}^j\right|^2 m_{S_j}^2 . \qquad \text{(WSR 2)}_f \tag{4.22}$$

Similar to the gauge contributions, the first sum rule removes the quadratic divergence in $\mu_{h,f}^2$ and $\mu_{\mathrm{DM},f}^2$ and makes $\lambda, \lambda_{\mathrm{DM}}$ and $\lambda_{h,f}$ finite. The residual divergence in mass parameters is canceled by the second sum rule. Note that in order to satisfy these sum rules one needs a set of resonances consisting of at least one multiplet Q in the fundamental representation of $SO(6)$ and one singlet S. This 'one-layer' setup, which we will discuss in Section 4.3.2.A, turns out to be very predictive but leads to a DM candidate, which is phenomenologically ruled out. However, due to its simplicitly it allows for analytical results to which will give us valuable insight. Next we turn to a non-minimal model with two full layers of fermion resonances. In Section 4.3.2.B we find that such a 'two-layer' setup has enough freedom to contain a viable DM candidate.

A One layer of fermionic resonances

Let us consider the Lagrangian in Eq. (4.15) with $N_Q = N_S = 1$. The WSRs in Eqs. (4.214.22) for this scenario take the from

$$\epsilon_{qQ}^2 = \epsilon_{qS}^2 , \qquad \epsilon_{tQ}^2 = \epsilon_{tS}^2 , \qquad m_Q^2 = m_S^2 , \tag{4.23}$$

where we have assumed that all parameters are real and $\mathcal{CP}$ is conserved. We will also assume without loss of generality that all masses are positive, i.e. $m_Q = m_S \equiv m > 0$. Note that Eq. (4.23) does not fix the relative signs of the mixing parameters $\epsilon_{qQ} = \pm\,\epsilon_{qS}$ and $\epsilon_{tQ} = \pm\,\epsilon_{tS}$. However, the case with equal signs restores the $SO(7)$ symmetry in the non-derivative Lagrangian in Eq. (4.15), thus making it possible to remove the GB matrix U with a field redefinition (see for example [154]). Hence the scalar potential vanishes. This effectively forces us to take opposite signs for the mixing parameters, which we take to be $\epsilon_{qQ} = -\epsilon_{qS} \equiv -\epsilon_q$ and $\epsilon_{tQ} = \epsilon_{tS} \equiv \epsilon_t$,[7]. In this case we find for the potential parameter relevant for DM phenomenology

$$\mu_{\mathrm{DM},f}^2 = \lambda_{\mathrm{DM},f} = 0 , \qquad \lambda_f = -\frac{\mu_{h,f}^2}{f^2} = \frac{N_c \epsilon_q^2 \epsilon_t^2 m^2 \log(M_T^2/M_S^2)}{2\pi^2 f^4 (M_T^2 - M_S^2)} , \tag{4.24}$$

[7]Notice that by redefining the phases of the resonances, we can equivalently choose a field basis with same-sign mixings and $m_Q + m_S = 0$. This is a realization of the "maximal symmetry" of [155]. Accordingly, the tuning of the model is minimal, see Eq. (4.29) below.

where $M^2_{T,S} = m^2 + \epsilon^2_{q,t}$ are the tree-level, pre-EWSB, squared masses of the top partners, which mix with q_L and t_R, respectively. Since there are no contributions to $\mu^2_{\rm DM}, \lambda_{\rm DM}$ and λ from the gauge sector, Eq. (4.24) shows the full expressions. A similar calculation yields the contribution to the Higgs quartic

$$\lambda_h \approx \frac{N_c \epsilon_q^2 \epsilon_t^2 m^2 \log(M_T^2/M_S^2)}{\pi^2 f^4 (M_T^2 - M_S^2)}\,, \tag{4.25}$$

for which we have neglected the gauge contribution to the potential. Equations (4.24) and (4.25) suggest the relation $\lambda \approx \lambda_h/2$, which is indeed verified within 20% in our numerical scan of the parameter space. Therefore both the portal coupling and the DM mass are fixed in terms of v and the Higgs mass,

$$\lambda \approx \frac{\lambda_h}{2} \simeq \frac{m_h^2}{4v^2} \simeq 0.065\,, \qquad m_\chi^2 = \lambda v^2 \approx \frac{\lambda_h v^2}{2} \simeq \frac{m_h^2}{4} \simeq (63\text{ GeV})^2\,. \tag{4.26}$$

The DM mass and portal coupling in Eq. (4.26) imply that due to the small mass the derivative couplings play a subleading role in DM phenomenology, s.t. it is well described by a renormalizable Higgs portal model [51–53]. However, in this model the parameter region $\lambda \sim \lambda_h/2$, $m_\chi \sim m_h/2$ has been ruled out by direct detection experiments and bounds on the Higgs invisible width (see e.g. [156]) at the LHC, which are relevant for $m_\chi < m_h/2$.

It is worth having a closer look at the source of the problematic values in Eq. (4.26). In the one-layer setup the second set of WSRs is so restrictive that the form factors Π_{L_1} and Π_{R_1} in Eqs. (I.D.7, I.D.8) vanish and the only contribution comes from the top mass form factor Π_{LR}, which therefore determines the full structure of the potential. As a consequence we obtain a non-generic form of the potential. For this reason it seems plausible that once we allow for more parametric freedom in the form of a second layer of composite resonances, we should be able to significantly depart from the values of Eq. (4.26), while still maintaining full calculability. This hypothesis is also supported by results from a parameter scan of a model, where we do not enforce the second WSR and retain a logarithmic sensitivity to the cutoff, which we take to be $\Lambda = 4\pi f$, in $\mu^2_{h,f}$ and $\mu^2_{{\rm DM},f}$. After this modification the potential has a generic form and exhibits large deviations from Eq. (4.26). Therefore we will consider a full two-layer model in the next Section.

But before turning to the two-layer model, let us point out a few properties of the current setup which at least qualitatively apply in the extended model. If we combine Eq. (4.25) with $m_t \simeq \sqrt{2}\epsilon_q \epsilon_t v/(M_T M_S f)$, which is the top mass at leading order in ξ, we obtain

$$\frac{m_h^2}{m_t^2} \approx \frac{N_c}{\pi^2 f^2} \frac{M_T^2 M_S^2}{M_T^2 - M_S^2} \log(M_T^2/M_S^2)\,. \tag{4.27}$$

This relation shows a well-known feature of CH models, which has also been obtained in the MCHM with the symmetry breaking structure $SO(5)/SO(4)$ [81,157], namely that a light Higgs requires at least one relatively light top partner with a mass comparable to f. We verified that Eq. (4.27) is satisfied numerically to a good accuracy, once small corrections from the gauge contribution, which have been neglected in Eq. (4.27), have been taken into account. We can also estimate the fine-tuning needed to obtain $v \ll f$ using the standard measure [158]

$$\Delta = \Delta_\xi = \max_i \left| \frac{\partial \log \xi}{\partial \log c_i} \right|\,, \tag{4.28}$$

with c_i denoting the model parameters, which are $c_i = \{\epsilon_q, \epsilon_t, m, f_\rho, m_\rho\}$ in the one-layer model. A more immediate estimate can be obtained from Eqs. (4.24)-(4.26) by noticing that the fermion

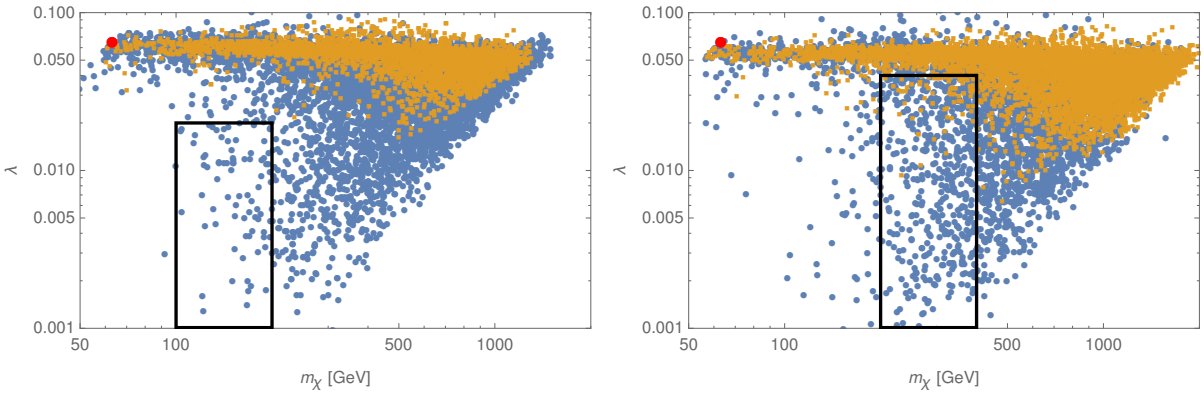

Figure 4.3: Distribution in the (m_χ, λ) plane for the parameter scan of the two-layer model. The left panel assumes $f = 1$ TeV, the right panel $f = 1.4$ TeV. The black boxes roughly indicate the viable regions of parameters for DM. The red dot shows the approximate prediction of the one-layer model, Eq. (4.26). For orange (blue) points, the lightest fermionic resonance is heavier (lighter) than the approximate LHC lower bound of 1 TeV. The Figure is adopted from [28].

contributions alone give $\xi \approx 1/2$. Thus $\mu^2_{h,g}$ has to be adjusted such that $\xi \ll 1$, which requires a fine-tuning of

$$\Delta^{-1} \sim 2\xi\,. \tag{4.29}$$

This is actually the irreducible amount of tuning for models with a Higgs potential, which is entirely generated at the radiative level. Numeric estimates following Eq. (4.28) agree well with Eq. (4.29).

Let us finally remark that the prediction in Eq. (4.26) was previously found by [38] for the realization of the $SO(6)/SO(5)$ model with minimal fermion content.

B Two layers of fermionic resonances

As a next step we consider the fermionic Lagrangian in Eq. (4.15) with $N_Q = N_S = 2$. In this case the first set of WSRs in Eq. (4.21) can be solved in terms of two mixings $\epsilon_{q,t}$ and four angles α, θ, β and ϕ,

$$\frac{\epsilon^1_{qQ}}{\cos\alpha} = \frac{\epsilon^2_{qQ}}{\sin\alpha} = \frac{\epsilon^1_{qS}}{\cos\theta} = \frac{\epsilon^2_{qS}}{\sin\theta} = \epsilon_q\,, \qquad \frac{\epsilon^1_{tQ}}{\cos\beta} = \frac{\epsilon^2_{tQ}}{\sin\beta} = \frac{\epsilon^1_{tS}}{\cos\phi} = \frac{\epsilon^2_{tS}}{\sin\phi} = \epsilon_t\,. \tag{4.30}$$

Two of the angles are fixed by the second set of WSRs in Eq. (4.22), modulo sign ambiguities. Here we choose

$$s^2_{\theta,\phi} = \frac{m^2_{Q_1} - m^2_{S_1} + \left(m^2_{Q_2} - m^2_{Q_1}\right) s^2_{\alpha,\beta}}{m^2_{S_2} - m^2_{S_1}} \qquad (s^2_x \equiv \sin^2 x), \tag{4.31}$$

and without loss of generality we assume $m_{S_2} > m_{S_1}$ and $m_{Q_2} > m_{Q_1}$. We study the resulting parameter space[8] in a numeric scan, which is described in detail in Appendix I.D. We show the resulting distribution in Figure 4.3 in the (m_χ, λ) plane for two choices of the symmetry breaking scale: $f = 1$ TeV and $f = 1.4$ TeV. For both values large deviations from the prediction of the one-layer model are clearly visible. One of the most striking differences is that χ is much heavier

[8] Note that for special values of the parameters, the model can be realized via a three-site construction [82].

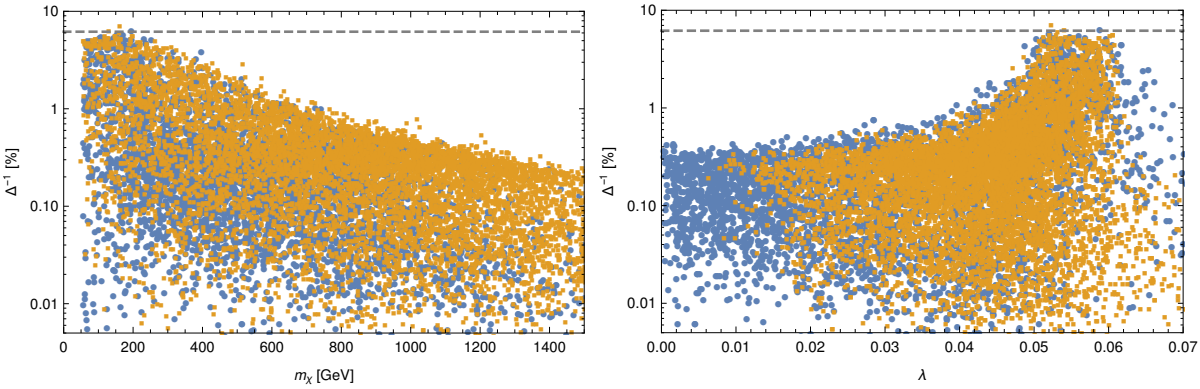

Figure 4.4: Fine-tuning of the two-layer model, shown versus the DM mass (left panel) and versus the portal coupling (right panel). For orange (blue) points, the lightest fermionic resonance is heavier (lighter) than the approximate LHC lower bound of 1 TeV. The scale f is fixed to 1.4 TeV. This Figure has been previously published in [28].

than the one-layer prediction of $m_h/2 \sim 63$ GeV. In particular the $100 - 400$ GeV range is populated which will turn out to be the region where the observed DM relic abundance can be achieved. Another important difference is that the portal coupling λ can be significantly smaller than $\lambda_h/2 \sim 0.065$. This is actually crucial to avoid exclusion by direct detection bounds. It is also clearly visible in Figure 4.3 that a reduction in λ is correlated with the appearance of light top partners, which can be in tension with bounds from LHC searches, which we will take to be approximately 1 TeV. (We will discuss the LHC constraints in detail in Sec. 4.3.4, but this rough estimate suffices for the scope of the present discussion.) In fact for $f = 1$ TeV we do not find any points, which are in the region required to give a viable DM candidate (100 GeV $\lesssim m_\chi \lesssim 200$ GeV and $\lambda \lesssim 0.02$, shown by the black box) and are not in conflict with LHC bounds on top partners. A larger value for f relaxes this tension, as top partners are naturally heavier, and it shifts the DM mass to higher values where the constraints on λ are not as stringent. The minimal value for f with a sizable number of allowed parameter points is approximately $f = 1.4$ TeV, which we will use as a benchmark in the remainder of this Section. For this symmetry breaking scale the viable region shifts to 200 GeV $\lesssim m_\chi \lesssim 400$ GeV and $\lambda \lesssim 0.04$, as shown in the right panel of Figure 4.3.

Increasing f goes at the cost of additional tuning. The minimal tuning for $f = 1.4$ TeV can be estimated as $\Delta^{-1} \sim 2\xi \simeq 6\%$ (cf. Eq. (4.29)). A more refined analysis of the tuning according to the definition in Eq. (4.28) on a point-by-point basis is shown in Figure 4.4. The Figure shows that an increasing departure from the predictions of the one-layer model, i.e. $m_\chi \gg m_h/2$ and $\lambda \ll \lambda_h/2$ requires additional tuning. The additional tuning for a larger m_χ can be explained by noticing that a larger DM mass needs a larger contribution from the form factor Π_{R_1}, which vanishes in the one-layer model (see Eq. (I.D.10)). This in turn comes with the need of a more severe cancellation in the Higgs mass parameter to keep $\xi \ll 1$. However, it is possible to obtain a DM candidate in the viable mass region 200 GeV $\lesssim m_\chi \lesssim 400$ GeV, without significantly exceeding the irreducible contribution of $2\xi \sim 6\%$. However, a portal coupling which satisfies direct detection bounds, i.e. roughly $\lambda \lesssim 0.04$, requires a tuning of at least $\Delta^{-1} \lesssim 1\%$. Note that we have found that once the Higgs VEV and mass are fixed to their observable values there is no additional tuning required for the DM mass, i.e. computing the tuning according to Eq. (4.28) for $\mu^2_{\rm DM}$ instead of ξ for the points in Figure 4.4, results in $\mathcal{O}(1)$ tuning even for DM masses as low as 200 GeV. All in all we expect that the level of fine-tuning in this two-layer model to

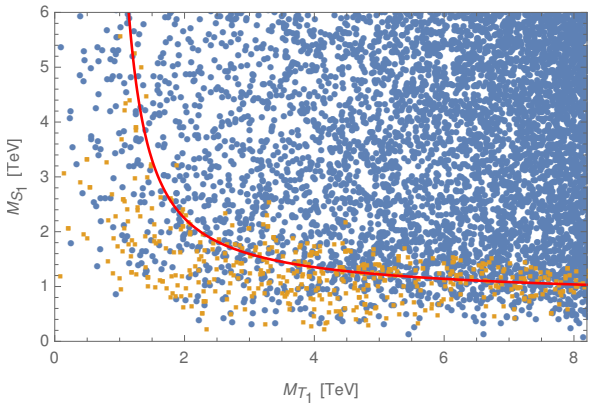

Figure 4.5: Mass of the lightest top partner mixing with the t_R (M_{S_1}) versus mass of the lightest top partner mixing with the q_L (M_{T_1}), neglecting EWSB corrections, in the two-layer model. Orange (blue) points have a Higgs mass within (outside) the range 120 GeV $< m_h <$ 130 GeV. The red line shows the approximate prediction of the one-layer model, Eq. (4.27). We set $f = 1.4$ TeV. This Figure has been adopted from [28].

solve both the Higgs naturalness and DM problem is of the order of 1% or slightly worse. The additional tuning is mainly driven by increasing sensitivity of direct detection experiment and searches for top partners at the LHC.

In Figure 4.5 we explicitly confirm that the relation in Eq. (4.27), which correlates a light Higgs with the existence of at least one light top partner, qualitatively also holds in the two-layer model. Even numerically Eq. (4.27) yields a good approximation if we identify M_T and M_S with the masses of the lightest top partner mixing with q_L and t_R, respectively.

Now that we have qualitatively characterized the current CH model, including estimates of the model parameters, we will discuss its phenomenology in the following Sections. In Section 4.3.3 we discuss the DM phenomenology of the model and in Section 4.3.4 we turn to the top partner phenomenology at the LHC.

4.3.3 Dark matter phenomenology

We will now discuss the DM phenomenology of the complex scalar χ, focussing on the DM relic abundance and the DM-nucleus scattering cross-section. We will conclude this Section with a brief comment on constraints from indirect detection.

A Effective theory for DM annihilation

As we have discussed at length in Section 2.4.2, the relic abundance of weakly coupled DM is set via the freeze-out mechanism. The relic abundance "freezes-out" once the annihilation rate in the early universe drops below the expansion rate of the universe. This takes places at an energy scale of $\sqrt{s} \sim 2m_\chi \ll m_*$, where m_* denotes the characteristic mass of the strong sector resonances. This implies that we can compute the annihilation cross-section in an EFT including only h, χ and the SM fermions and bosons with the heavy top partners integrated out. Additionally assuming that the freeze-out temperature is below the weak scale, i.e. $T_f \ll v$, which is generically the case for WIMP DM, for which $T_f \sim m_\chi/20 \ll v$, we can construct the effective Lagrangian in the broken electroweak phase. We also limit ourselves to operators quadratic in the DM field, which give the leading contribution to DM annihilation. The structure

of the effective Lagrangian is therefore

$$\mathcal{L}_{\text{eff}} = \underbrace{\mathcal{L}_{\text{GB}} + \mathcal{L}_t}_{\text{tree}} \underbrace{- V_{\text{eff}}}_{\text{1-loop}} . \tag{4.32}$$

Note that this has exactly the same form as the general effective Lagrangian, which we considered in Eq. (3.1) of Chapter 3, where we parameterized the general fermion Lagrangian $\mathcal{L}_f$ and effective potential V_{eff} in Eqs. (3.10) and (3.11), respectively. However, while we organized Eq. (3.1) as an expansion in $1/f$ in the electroweak unbroken phase, here we perform an expansion in the physical fields in the electroweak broken phase and give the coupling coefficients to all orders in the v/f expansion. For the first term, which is simply the the non-linear sigma model Lagrangian Eq. (4.3) in terms of physical fields after EWSB, this has the form

$$\begin{aligned}\mathcal{L}_{\text{GB}} = {} & \frac{1}{2}(\partial_\mu h)^2\Big(1 + 2\,a_{hhh}\frac{h}{v} + 2\,a_{hh\chi\chi}\frac{\chi^*\chi}{v^2}\Big) + \partial_\mu\chi\partial^\mu\chi^* + \frac{1}{v}\partial_\mu h\,\partial^\mu(\chi^*\chi)\Big(b_{h\chi\chi} + b_{hh\chi\chi}\frac{h}{v}\Big) \\ & + 2\,a_{hVV}\frac{h}{v}\Big(m_W^2 W_\mu^+ W^{-\,\mu} + \frac{m_Z^2}{2}Z_\mu Z^\mu\Big).\end{aligned} \tag{4.33}$$

The radiatively generated effective potential V_{eff} organized in an expansion of physical fields will be parameterized as

$$V_{\text{eff}} = \frac{1}{2}m_h^2 h^2 + d_{hhh}\,\frac{m_h^2}{2v}\,h^3 + m_\chi^2\chi^*\chi + 2\,d_{h\chi\chi}v\lambda h\chi^*\chi + d_{hh\chi\chi}\lambda h^2\chi^*\chi\,. \tag{4.34}$$

Note that even though the scalar couplings in the potential Eq. (4.34) are loop suppressed, they can be equally important as those in the tree-level interactions in $\mathcal{L}_{\text{GB}}$, whose derivative structure leads to a suppression of $\sim s/f^2 \ll 1$ [8]. Note that except for λ all dimensionless coefficients in Eqs. (4.33, 4.34) are functions of ξ only and are given in Eq. (I.F.10). The couplings of the DM to the top quark are given by

$$\mathcal{L}_t = i\bar{t}\partial\!\!\!/ t - m_t\bar{t}t\Big(1 + c_{tth}\frac{h}{v} + 2\,c_{tt\chi\chi}\frac{\chi^*\chi}{v^2}\Big), \tag{4.35}$$

where the dimensionless coefficients are of the form

$$c_k = c_k^{\text{nl}\sigma\text{m}}(\xi) + O\Big(\xi\frac{\epsilon^2}{m_*^2}\Big), \qquad k = \{tth, tt\chi\chi\}. \tag{4.36}$$

The functions $c_k^{\text{nl}\sigma\text{m}}(\xi)$ encode the model-independent non-linearity in ξ due to the non-linear sigma model construction and are given by

$$c_{tth}^{\text{nl}\sigma\text{m}} = \frac{1-2\xi}{\sqrt{1-\xi}}\,, \qquad c_{tt\chi\chi}^{\text{nl}\sigma\text{m}} = -\frac{\xi}{2(1-\xi)}\,. \tag{4.37}$$

The second term in Eq. (4.36) originates from the mixing of the top quark with the top partners and depends on the model parameters. In general they are suppressed as long as both top chiralities are mostly elementary, i.e. $\epsilon \ll m_*$. However, if one chirality is mostly composite, $\epsilon \sim m_*$ these corrections become important. In previous studies of pNGB DM these corrections were completely neglected [8, 38], but in our scenario we find that they are important in large parts of the parameter space. In Figure 4.6 we see that already for moderate compositeness fractions of t_R these corrections can give an $\mathcal{O}(1)$ modification to $c_k^{\text{nl}\sigma\text{m}}(\xi)$, its value due to the symmetry structure in the non-linear sigma model. In particular $c_{tt\chi\chi}$ is strongly suppressed and even vanishes in the limit of a fully composite t_R, in which case these corrections exactly cancel

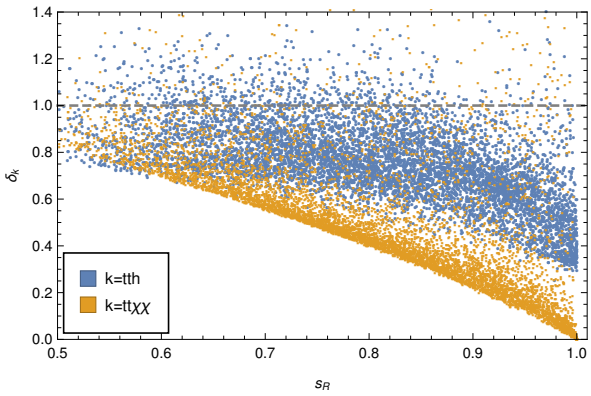

Figure 4.6: Corrections from top partner mixing to the effective $t\bar{t}h$ and $t\bar{t}\chi^*\chi$ couplings, defined as $\delta_{tt\chi\chi} \equiv c_{tt\chi\chi}/c_{tt\chi\chi}^{\mathrm{nl}\sigma\mathrm{m}}$ and $\delta_{tth} \equiv (c_{tth}-1)/(c_{tth}^{\mathrm{nl}\sigma\mathrm{m}}-1)$, as functions of the compositeness fraction s_R of the right handed top (see Eq. (I.D.30) for its definition). The gray dashed line indicates the pure sigma model result, where top partner mixing is neglected. The points shown are obtained from a parameter scan of the two-layer model with $f = 1.4$ TeV, requiring all fermionic resonances to be heavier than the approximate LHC bound of 1 TeV. This Figure has been adopted from [28].

$c_{tt\chi\chi}^{\mathrm{nl}\sigma\mathrm{m}}(\xi)$. This effect can be understood as follows: in our current scenario, i.e. embedding both q_L and t_R into the **7** representation of $SO(7)$ with the explicit embeddings given in Eq. (4.13), only the embedding of t_R breaks the DM shift symmetry. Once the physical t_R becomes fully composite, i.e. it has no overlap with elementary fermions and is a resonance of the strong sector, it preserves the full $SO(7)$ symmetry and in particular does not break the DM shift symmetry. Hence no non-derivative coupling of the DM to the top is allowed and $c_{tt\chi\chi}$ must vanish. The $t\bar{t}h$ receives smaller, but still important, corrections from the top partner mixing.[9]

B Dark matter relic abundance

The precise value of today's DM relic abundance is obtained by solving the Boltzmann equation, but a useful approximate result is given by (see Section 2.4 for an explanation of the symbols and this estimate)[10]

$$\frac{\Omega_{\mathrm{DM}}h^2}{0.1198} \simeq \frac{3\cdot 10^{-26}\mathrm{cm}^3\,\mathrm{s}^{-1}}{\frac{1}{2}\langle\sigma v_{\mathrm{rel}}\rangle(T_f)}\,. \tag{4.38}$$

Note that the factor 1/2 in front of the thermally averaged annihilation cross-section $\langle\sigma v_{\mathrm{rel}}\rangle(T_f)$ at the freeze-out temperature T_f appears because the DM is not self-conjugate and therefore both the number of particles and anti-particles contribute to the relic abundance.

As we have already discussed at length in Chapter 3, the annihilation proceeds mainly through s-channel Higgs exchange into $\chi\chi^* \to t\bar{t}, WW, ZZ, hh$. Even though $\chi\chi^* \to t\bar{t}, hh$ receive additional contributions from contact interactions, we can gain a good intuition by neglecting these contributions in a first approximation. In this case the cross-section is proportional

[9] Notice that the $t\bar{t}h$ coupling does not vanish at full RH top compositeness, because even in that limit the coupling of q_L to the strong sector breaks the h shift symmetry.

[10] Note that the value for the DM relic abundance which we take in Eq. (4.38) does not exactly agree with Eq. (2.72). The reason for this is that when these results were published the most precise measurement of the relic abundance was $(\Omega_{\mathrm{DM}}h^2)_{\mathrm{exp}} = 0.1198 \pm 0.0015$ [159]. Since this was used in all parameter scans and results in this Section, we decided to quote this slightly outdated but almost identical value here.

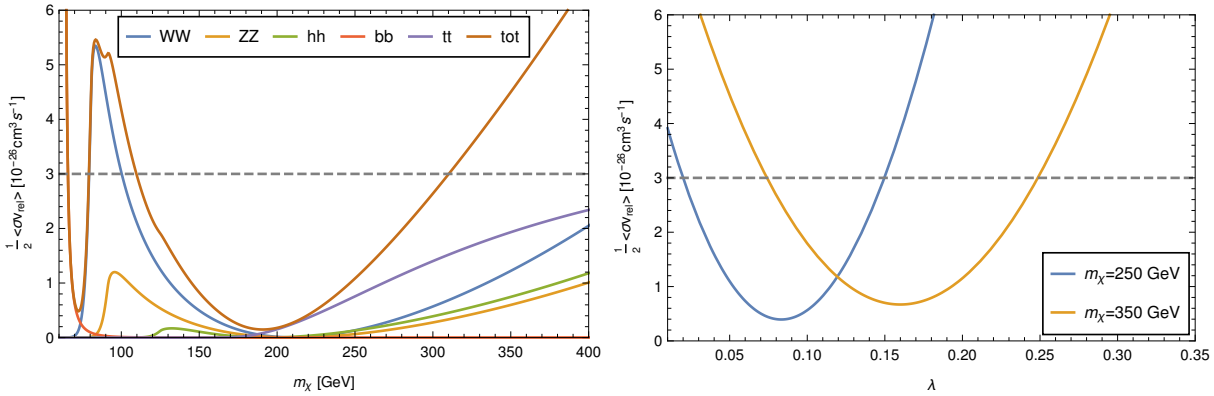

Figure 4.7: Thermally averaged cross section for DM annihilation. The gray dashed line shows the canonical value, which is typically required to reproduce the present relic abundance according to the approximate relation in Eq. (4.38). The scale f was fixed to 1.4 TeV. In the left panel we set the portal coupling to the representative value $\lambda = 0.05$, in the right panel we chose two representative values of the DM mass. In both panels the $t\bar{t}h$ and $t\bar{t}\chi^*\chi$ couplings were set to their sigma model values (Eq. (4.37)), thus neglecting top partner mixing. With this simplification, $\langle\sigma v_{\rm rel}\rangle$ is completely determined by f, m_χ and λ. This Figure has previously been published in [28].

to the squared $\chi\chi^* h$ vertex

$$\sigma v_{\rm rel} \propto \left(\frac{b_{h\chi\chi}}{v} s - 2\, d_{h\chi\chi}\lambda v\right)^2 \approx v^2\left(\frac{s}{f^2} - 2\lambda\right)^2, \tag{4.39}$$

where the first term in the brackets originates from the derivative couplings in Eq. (4.33) and the second term is the marginal Higgs portal contribution from the effective potential in Eq. (4.34). For non-relativistic DM $s \sim 4m_\chi^2$, what is a good approximation at freeze-out, there is a large suppression of the annihilation cross section for $m_\chi^2 \sim \lambda f^2/2$. This is clearly visible for the annihilation cross-section into WW, ZZ and hh in the left panel of Figure 4.7. Note that Eq. (4.39) also implies that for a given f and m_χ there are two values for λ, which yield the same cross-section, i.e. there are two possible values which can give the correct relic abundance. This feature can be seen in the right panel of Figure 4.7. The branch with larger λ is usually excluded by direct detection, but the lower branch can provide a viable scenario. Also note that the value for λ along the lower branch is smaller than the one needed in a pure marginal Higgs portal model to obtain the correct relic abundance.

For $m_\chi > m_t$ the simple scaling in Eq. (4.39) is violated by annihilations into top pairs. In this case the corrections from contact interactions $t\bar{t}\chi\chi^*$ can no longer be ignored. In the left panel of Figure 4.8 we show the effect of $c_{tt\chi\chi}$ on the $\chi\chi^* \to t\bar{t}$ annihilation cross-section, by varying $c_{tt\chi\chi}^{\rm nl\sigma m} \leq c_{tt\chi\chi} \leq 0$, which contains all phenomenologically relevant points. The effect of a suppressed $|c_{tt\chi\chi}|$ due to top partner mixing is to shift the relic abundance contour to larger m_χ for fixed λ or smaller (larger) λ for fixed m_χ along the lower (upper) branch with a larger effect on the lower branch, as can be seen in Figure 4.8. This can be understood by noticing that the contribution from a $t\bar{t}\chi\chi^*$ contact interaction to the amplitude, relative to the $\chi\chi^*$ induced s-channel Higgs exchange via the marginal portal coupling λ scales as $2m_\chi^2/(\lambda f^2)$ for $m_\chi \gg m_h/2$. Along the branch with larger λ, for which $2m_\chi^2 < \lambda f^2$, the ratio is smaller than one and therefore the relative contribution from the contact interaction $c_{tt\chi\chi}$ (and consequently corrections to it) is subleading. However, along the lower branch the contributions from the

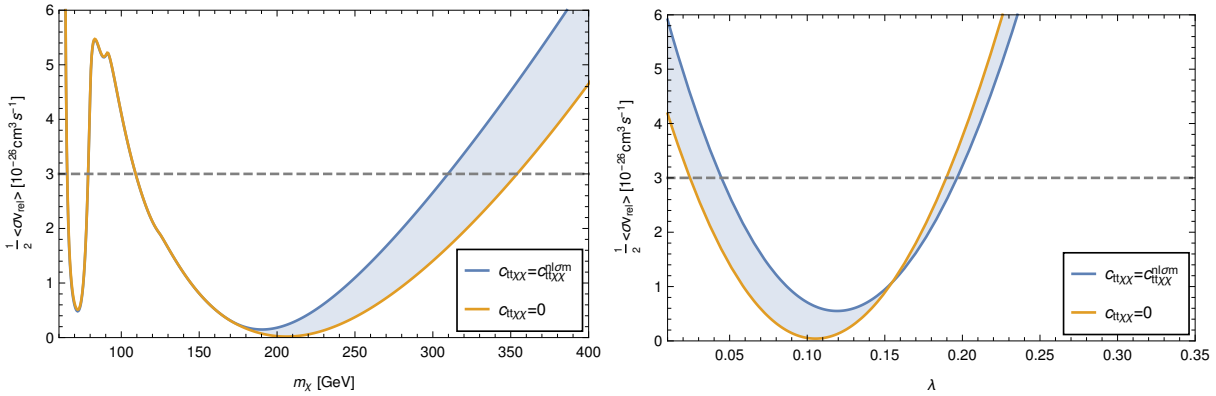

Figure 4.8: Impact on the total annihilation cross section of varying the strength of the $t\bar{t}\chi^*\chi$ contact interaction in the range $c_{tt\chi\chi} \in [c_{tt\chi\chi}^{\rm nl\sigma m}, 0]$. The lower value corresponds to the pure sigma model, where top partner mixing is neglected, whereas the upper value corresponds to a setup with fully composite t_R, where top partner mixing is maximal. The realistic parameter points lie within this range, i.e. they fall within the band shaded in blue. The gray dashed line shows the value required to reproduce the present relic abundance according to the approximate relation in Eq. (4.38). In the left panel we set $\lambda = 0.05$, whereas in the right panel the DM mass was fixed to $m_\chi = 300$ GeV. We took $f = 1.4$ TeV in both panels. This Figure is adopted from [28].

contact interaction are of the same size or even larger than the contribution from the portal coupling and therefore corrections to it are significant. In the following we will see that these corrections are crucial to avoid constraints from direct detection.

C Radiative corrections to pNGB derivative interactions

In the previous discussion on the annihilation cross-section we have included tree-level couplings from the non-linear sigma model Lagrangian and the fermion-pNGB couplings, but also one-loop radiatively generated interactions from the effective potential (see Eq. (4.32)). However, the effective potential only includes radiative corrections from gauge and fermion loops in the limit of vanishing external momenta. Such a simplification is not justified when considering DM annihilation. The relevant momentum scale is $p \sim m_\chi$ and therefore one-loop corrections to derivative operators of $\mathcal{O}(p^2)$ are expected to be important. As an example we will consider the $\chi\chi^* hh$ interaction and we will neglect EWSB effects, i.e. we take $v = 0$ in the following. At $\mathcal{O}(p^0)$ this is simply the marginal Higgs portal in the effective potential $V_{\rm eff} \supset \lambda h^2\chi^*\chi$, which is absent at tree-level but generated by the fermion sector at one-loop. At $\mathcal{O}(p^2)$ we find from Eq. (4.33) that this interaction has the following form

$$\mathcal{L}_{\rm GB} \supset \frac{1}{f^2} h\partial_\mu h(\chi^*\partial^\mu\chi + \chi\partial^\mu\chi^*). \tag{4.40}$$

Notice that the tree-level contribution to this interaction originates from the non-linear sigma model kinetic term. In the absence of explicit symmetry breaking spurions, the non-linear sigma model does not get renormalized, since it is completely fixed by symmetry. This implies that any loop corrections must be proportional to the $SO(7)$-breaking parameters. The one-loop radiative corrections to this interaction arise only from the fermion sector and are therefore proportional to the mixing parameters ϵ, since we require a combination of spurions which break both the Higgs and DM shift symmetry. Consequently the radiatively corrected expression of the two-derivative

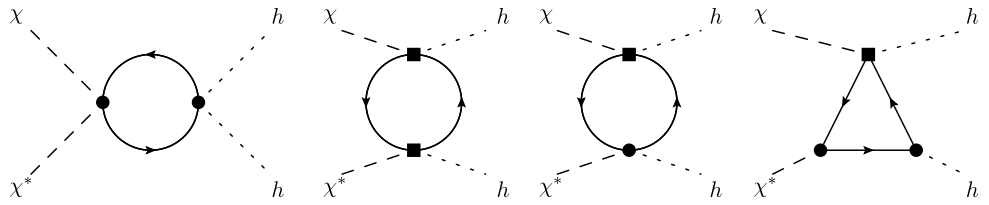

Figure 4.9: Representative set of 1-loop diagrams that contribute to the renormalization of the $\chi^*\chi hh$ interaction at $O(p^2)$. The circles indicate non-derivative interactions arising from elementary-composite mixing terms, whereas the squares denote derivative couplings originating from the e_μ symbol (see Eq. (4.15)). This Figure is adopted from [28].

coupling is of the form

$$i(c_{\text{tree}} + c_{1-\text{loop}})\frac{p^2}{f^2}\,, \qquad c_{\text{tree}} \sim 1\,, \qquad c_{1-\text{loop}} \sim \frac{N_c\epsilon^2}{16\pi^2 f^2}\log\Lambda^2\,. \tag{4.41}$$

Notice that $c_{1-\text{loop}}$ is expected to be logarithmically divergent. In contrast to λ its UV-behavior is not softened by the WSRs in Eqs. (4.21, 4.22). The combination of the log enhancement and the fact that ϵ/f is typically of $\mathcal{O}(1)$, i.e. the Goldstone symmetry is badly broken, suggests that the one-loop contributions could be very important. We find four classes of diagrams, which contribute to the renormalization of the operator in Eq. (4.40), shown in Figure 4.9. The diagrams contain two types of scalar-fermion vertices: non-derivative couplings from the elementary-composite mixing terms and derivative couplings from the e_μ, which is contained in the kinetic terms of the resonances in the $SO(6)$ fundamental, $\sum_i \bar{Q}_i \not{e} Q_i$.[11] For simplicity we neglect external masses, s.t. $s + t + u \simeq 0$ and compute the log divergent $\mathcal{O}(p^2)$ contribution to the $\chi^*\chi \to hh$ amplitude. Even though this is a rough approximation for DM annihilation, where the kinematic variables take the values (assuming $m_\chi^2 \gg m_h^2$) $s \sim 4m_\chi^2$ and $t \sim u \sim -m_\chi^2$, it is nevertheless sufficient for the purpose of estimating the theoretical uncertainty on the cross section, what is the purpose of the present discussion. The contributions from the individual classes of diagrams are given by

$$i\mathcal{A}_1 = \frac{iN_c}{8\pi^2 f^4}\Big(\epsilon_t^2 - \frac{\epsilon_q^2}{8}\Big)s\log\Lambda^2\,, \quad i\mathcal{A}_2 = \frac{iN_c}{8\pi^2 f^4}\Big(-\frac{\epsilon_q^2}{8}\Big)3\,s\log\Lambda^2\,, \quad i\mathcal{A}_4 = \frac{iN_c}{8\pi^2 f^4}(\epsilon_t^2)3\,s\log\Lambda^2\,. \tag{4.42}$$

with the third class of diagrams being proportional to the external masses, and thus negligible within our approximations. Summing the three pieces and making the argument of the logarithm dimensionless by inserting m_*^2, we arrive at the final result

$$i(c_{\text{tree}} + c_{1-\text{loop}})\frac{s}{f^2}\,, \qquad c_{\text{tree}} = 1\,, \qquad c_{1-\text{loop}} = \frac{N_c}{2\pi^2 f^2}\Big(\epsilon_t^2 - \frac{\epsilon_q^2}{8}\Big)\log\frac{\Lambda^2}{m_*^2}\,, \tag{4.43}$$

where we have imposed the conditions from the WSRs and denoted the mass of fermionic resonances by m_*. Note that this result has only a very mild loop suppression of $N_c/(2\pi^2)$ and is log enhanced. After EWSB this interaction contributes to the $h\chi^*\chi$ coupling which enters all s-channel Higgs mediated annihilation channels in the computation of the annihilation cross-section. As we saw in the previous subsection this coupling is actually dominant in the phenomenologically interesting region where λ is suppressed. This means that in order to maintain predictivity we have to keep the size of the radiative corrections under control. This can

[11] Notice that in general the couplings containing the d_μ symbol that appear in Eq. (4.16) also contribute. However, for simplicity we set their coefficients to zero in the computation.

only be achieved by limiting our parameter space to regions where the loop corrections are subleading and by assigning an uncertainty to the annihilation cross-section. In order to keep the corrections to the annihilation cross-section below 50% we have to require that

$$0.5 < \left(1 + \frac{c_{1-\text{loop}}}{c_{\text{tree}}}\right)^2 < 1.5 \qquad \longrightarrow \qquad -0.4 < \frac{1}{f^2}\left(\epsilon_t^2 - \frac{\epsilon_q^2}{8}\right) < 0.3\,, \tag{4.44}$$

where we take $\Lambda \sim 10$ TeV and $m_* \sim 1$ TeV. If we do not assume an approximate cancellation $\epsilon_q^2 \approx 8\,\epsilon_t^2$, which may be regarded as a tuning unless it can be enforced by a symmetry, a further reduction of the uncertainty would lead to values of $\epsilon_{q,t}$ that are too small to reproduce the measured top mass. In conclusion, we will require that Eq. (4.44) is satisfied throughout our phenomenological analysis, and we will correspondingly assign a 50% theoretical uncertainty on the total DM annihilation cross section.

D Constraints from DM direct detection

DM direct detection experiments try to measure the recoil of detector nuclei from an elastic scattering event of DM on a detector nucleus. It consequently probes the DM couplings at low momentum transfer $\sqrt{-q^2} \leq 100$ MeV. Currently the strongest bounds are on the SI DM-nucleon cross-section (see Section 2.4.3) set by the Xenon-based XENON1T [5] experiment.[12] In the current model the elastic scattering on quarks is mediated by three kinds of diagrams: t-channel Higgs exchange, the $\chi^*\chi\bar{q}q$ contact interaction, and diagrams involving the exchange of the $U(1)_{\text{DM}}$ charged top partners $\mathcal{Y}$ and $\mathcal{Z}$. The first two contribute to the scattering with all quarks, whereas the last only affects the scattering with top (sea) quarks. Note that, as we have discussed at length in Chapter 3, the derivative couplings give completely negligible contributions to the DM-nucleon scattering, since $-q^2/f^2 \ll 1$. The Higgs-exchange diagrams are therefore effectively proportional to λ, which for realistic regions of parameter space dominates over the contact and $\mathcal{Y}, \mathcal{Z}$ mediated contributions. The SI cross-section is therefore completely determined by the portal coupling λ, similar to the simple renormalizable Higgs portal model (see e.g. [162]). Matching the Higgs exchange contribution to Eq. (2.96), we directly obtain $\sigma_{\text{SI}}^{\chi N}$ from Eq. (2.103)

$$\sigma_{\text{SI}}^{\chi N} \simeq \frac{f_N^2}{\pi}\frac{\lambda^2 m_N^4}{m_h^4 m_\chi^2} \;\approx\; 1.6 \times 10^{-46}\,\text{cm}^2 \left(\frac{\lambda}{0.02}\right)^2 \left(\frac{300\ \text{GeV}}{m_\chi}\right)^2, \qquad (t_R \text{ breaking}) \tag{4.45}$$

where m_N is the nucleon mass, and $f_N \simeq 0.30$ contains the dependence on the nucleon matrix elements. The exact expression of $\sigma_{\text{SI}}^{\chi N}$ is reported in Appendix I.F. The XENON1T experiment is currently probing cross-section of the size of Eq. (4.45) [5]. This implies that direct detection requires a suppression of the most natural value $\lambda \sim \lambda_h/2 \sim 0.065$ by about a factor of 3, assuming the local DM density to take the the standard value $\rho_0 = 0.3\ \text{GeV}\,\text{cm}^{-3}$. Note that this bound is more stringent than what was state of the art when this project was completed. We will comment on this more stringent bound when discussing the results. All quoted direct detection limits are given at 90% CL.

E Results

We summarize the main results of our phenomenological study in Figure 4.10, for which we set $f = 1.4$ TeV and perform a parameter scan. All points reproduce the experimentally

[12] Note that at the time when these results were published the strongest constraints were set by an older dataset from XENON1T [160] and LUX [161]

measured values for v, m_h, m_t and are compatible with LHC constraints on top partners, which we will be discussed in detail in Section 4.3.4. We additionally implement the constraint in Eq. (4.44) to limit the theoretical uncertainty on the annihilation cross-section due to radiative corrections, which are not included in the calculation, to 50%. The color code for the points in the (m_χ, λ) plane is the following: green marks points which reproduce the observed relic abundance. Red (purple) points represent parameter choices which exceed (undershoot) the observed relic abundance. The calculation of the relic abundance was performed with `micrOMEGAs` [163] to solve the Boltzmann equation, based on the effective Lagrangian in Eq. (4.32) implemented in `FeynRules` [164] (see Appendix I.F for details). Due to the dependence of the contact interactions on the top partner mixing, the relic abundance has to be computed on a point-by-point basis. The direct detection bounds from LUX [161] (brown) and XENON1T [160] (gray), in contrast, are insensitive to the explicit top partner parameters.

The upper panel in Figure 4.10 shows in green the points, which yield a relic abundance within 5% of the observed value, without assuming a 50% uncertainty on the annihilation cross-section. We also show in thick blue the 3σ relic abundance contours for the $t\bar{t}h$ and $t\bar{t}\chi\chi^*$ couplings set to their sigma model values, in which case the contours are completely determined by $\{f, m_\chi, \lambda\}$. The previously discussed two-branch structure for $m_\chi \geq 180$ GeV is due to the structure of the annihilation cross-section given in Eq. (4.39). The DM annihilation in the upper branch is dominated by the marginal portal coupling λ, whereas in the lower the annihilation dominantly proceeds through the derivative portal. Between the two branches the annihilation cross-section approximately cancels, causing the DM to be over-abundant. Outside the two-branches one coupling becomes too strong and the DM is under-abundant. Direct detection rules out the full upper-branch, which is why we will focus on the lower branch in the following. The green points around the lower branch fall, as expected, between the solid blue and dashed blue line, corresponding to $c_{tt\chi\chi} = c_{tt\chi\chi}^{\mathrm{nl}\sigma\mathrm{m}}$ and $c_{tt\chi\chi} = 0$, respectively. $c_{tt\chi\chi} = 0$ is reached in the limit of a fully composite t_R. The suppression of $|c_{tt\chi\chi}|$ reduces the value of λ, which is needed to reproduce the DM relic abundance, for a fixed value of m_χ. Including this effect turns out to be crucial to comply with direct detection bounds. Had we not included top partner mixing, we would have wrongly concluded that all these points are ruled out by LUX [161] and XENON1T [160] data, what highlights the importance of top partner mixing effects.

The lower panel of Figure 4.10 shows the final result, which includes a 50% uncertainty on the annihilation cross-section. Therefore the green points reproduce the observed value of the relic abundance within 50%. Accounting for this uncertainty there is a large number of potentially viable points which which also avoid direct detection bounds. Generically the DM mass for these points is in the range 200 GeV $\lesssim m_\chi \lesssim$ 400 GeV and the portal coupling between roughly $0.01 \lesssim \lambda \lesssim 0.04$. We also show, as a dashed gray curve, the projected XENON1T sensitivity after two years of data taking [114] (whereas the "35d" label on the solid dashed curve refers to an exposure of 35 days [160]). All the currently viable points lie well within the ultimate reach of XENON1T, which will thus be able to test the entire parameter space of the model for $f = 1.4$ TeV.

Note that after the publication of these results XENON1T has released data from an exposure of one year [5]. This rules out another chunk of the parameter space and in particular probes all points which are close to the solid blue line. This implies that a non-tuned version of this model is now in tension with direct detection data. A remedy for this is either choosing a larger symmetry breaking scale, what effectively shifts the relic abundance contour to larger masses for fixed λ, or assuming a different embedding of the elementary fermions. We will discuss the second possibility in Sections 4.4 and 4.5.

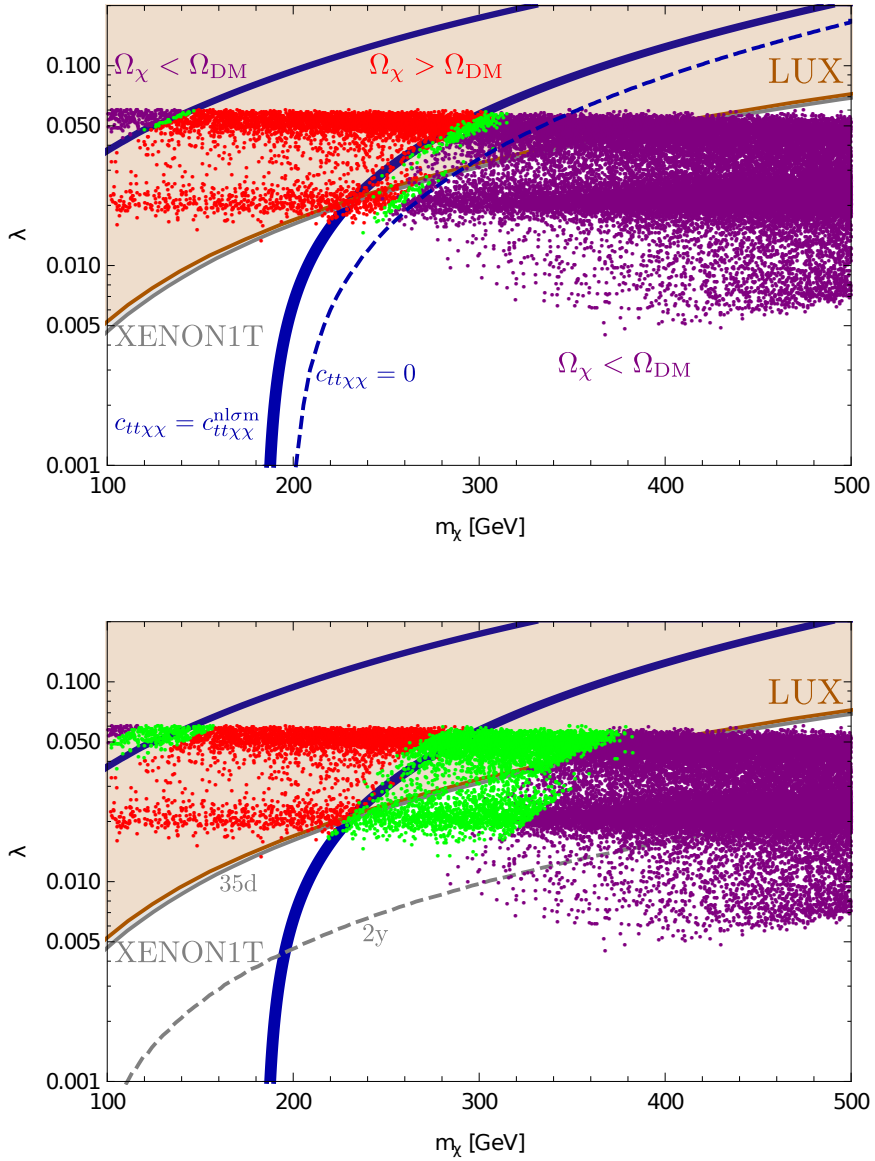

Figure 4.10: Distributions in the (m_χ, λ) plane that summarize our analysis of DM phenomenology. The points have different colors depending on whether they are compatible with (green), exceed (red) or undershoot (purple) the observed value of the DM relic abundance. In the upper (lower) panel, the theoretical uncertainty of 50% on the annihilation cross section is neglected (included). See the main text for further explanations on the meaning of the different curves. Note that after the publication of this Figure in [28] an updated XENON1T direct detection bound [5] has appeared. For a related discussion see the text.

F Indirect detection

Let us shortly comment on bounds from indirect detection experiments on the present-day annihilation cross-section. For a detailed discussion on constraints from the PAMELA antiproton spectrum [165] on real singlet pNGB DM in the $SO(6)/SO(5)$ model see [38]. The annihilation spectrum of the complex DM in our case is very similar to the real DM in [38], which allowed us to check that our viable parameter space is safely compatible with PAMELA data. It is however important to mention that bounds from the cosmic antiproton spectrum have large

systematic uncertainties due to assumptions on the antiproton propagation and astrophysical backgrounds. For example a more conservative approach to setting bounds on the present annihilation cross-section $\langle\sigma v_{\rm rel}\rangle_0$ (see e.g. [166]), yields results which are weaker by an order of magnitude compared to those in [38]. More recent measurements of the antiproton spectrum by AMS-02 [6] set very stringent constraints on the annihilation cross-section [147, 148], probing even the canonical value for the thermal annihilation cross-section in some channels. However, the analysis shows a hint of an excess [147, 148], which could be explained by DM. But as the situation has not settled yet we do not show constraints from antiprotons. Another source of competitive bounds are gamma rays from dwarf galaxies, which are affected by smaller systematics compared to antiprotons. For a more thorough discussion of gamma ray constraints on pNGB DM see Section 3.3.

4.3.4 Collider phenomenology

Before we discuss other embeddings for the elementary fermions we will outline the collider phenomenology of the model at hand, focusing on signals from fermionic top partners at hadron colliders. But let us also mention that searches for top partners are not the only characteristic observables in CH models. The pNGB nature of the Higgs is responsible for deviations of Higgs couplings from their SM value due to corrections of the order of $\mathcal{O}(v^2/f^2)$. In particular the hVV couplings with $V = W, Z$ are rescaled by a factor $c_V = \sqrt{1-\xi}$, which is a deviation of $\approx 1.5\%$ for our benchmark of the symmetry breaking scale of $f = 1.4$ TeV. Such a small deviation is not accessible at the LHC, but will be tested at future lepton colliders (see [167] for a recent overview). Similar deviation also affect the $h\bar{t}t$, $hgg/h\gamma\gamma$ and $Z\bar{t}t$ couplings, which will however be tested with a lower accuracy. Another subleading test can be monojet searches, considering that the coupling of χ to first generation quarks is very weak. A further class of collider probes are searches for the pNGB DM produced through the marginal or derivative Higgs portal. This will be the topic of Chapter 5.

Note that the following is based on LHC data and searches, which were state of the art when these results were published. More recent LHC results will give more stringent bounds than the ones reported here.

A LHC constraints on top partners

A generic feature of CH models is that a light Higgs requires at least some of the top partners to be light, $m_* = g_* f$ with $g_* \sim 1$ (see [168] for an extensive discussion). Our model is no exception in this regard, as can be seen from Figure 4.5. The top partners mix with the SM quarks and are therefore colored, making the direct production of top partners hadron colliders, and in particular the LHC, a sensitive probe of the CH framework [152, 169–171]. Here we will discuss a simplified model with only one fundamental multiplet Q and one singlet S. This corresponds to only one layer of resonances and is a good approximation if the second layer is somewhat heavier, what is satisfied in most of the parameter space.

Our starting point is the fermion Lagrangian in Eq. (4.15) with $N_Q = N_S = 1$. We additionally set the derivative interactions proportional to $c^{L/R} = 0$ in Eq. (4.16) to zero, as we have consistently done during the whole discussion, and will return to them in Section 4.3.4.B. To leading order, i.e. neglecting EWSB effects, the fermion sector is diagonalized by the rotation

$$\begin{pmatrix} t_R \\ S_R \end{pmatrix} \to \begin{pmatrix} \cos\phi_R & -\sin\phi_R \\ \sin\phi_R & \cos\phi_R \end{pmatrix} \begin{pmatrix} t_R \\ S_R \end{pmatrix}, \qquad \begin{pmatrix} q_L \\ Q_L \end{pmatrix} \to \begin{pmatrix} \cos\phi_L & -\sin\phi_L \\ \sin\phi_L & \cos\phi_L \end{pmatrix} \begin{pmatrix} q_L \\ Q_L \end{pmatrix}, \tag{4.46}$$

where $Q \equiv (T, B)^T$ and the mixing angles are $\tan\phi_R = \epsilon_{tS}/m_S$ and $\tan\phi_L = \epsilon_{qQ}/m_Q$. The

remaining fermions in Q, namely the exotic doublet $(X_{5/3}, X_{2/3})^T$ and the $U(1)_{\rm DM}$-charged SM singlets $\mathcal{Y}, \mathcal{Z}$ do not mix with the elementary fermions. The masses of the top partners are therefore given by

$$M_S = \sqrt{m_S^2 + \epsilon_{tS}^2}\,, \qquad M_{T,\,B} = \sqrt{m_Q^2 + \epsilon_{qQ}^2}\,, \qquad M_{X_{5/3},\,X_{2/3},\,\mathcal{Y},\,\mathcal{Z}} = m_Q\,. \tag{4.47}$$

Hence at the bottom of the spectrum we find either a singlet S, or four approximately degenerate states $X_{2/3}, X_{5/3}, \mathcal{Y}$ and $\mathcal{Z}$.[13] From the numerical parameter scans in the two-layer models, shown in Figure 4.11, we conclude that the lightest top partner is typically, but not always, a singlet. The branching ratios for the top partner decays are straightforward to obtain from the Goldstone equivalence theorem by expand the GB matrix U to $\mathcal{O}(1/f)$ and diagonalizing the elementary-composite mixings

$$\begin{aligned} \mathrm{BR}(S \to W^+ b) &= 2\,\mathrm{BR}(S \to Zt) = 2\,\mathrm{BR}(S \to ht) = \frac{1}{2}\,, \\ \mathrm{BR}(T \to ht) &= \mathrm{BR}(T \to Zt) = \mathrm{BR}(X_{2/3} \to ht) = \mathrm{BR}(X_{2/3} \to Zt) = \frac{1}{2}\,, \\ \mathrm{BR}(X_{5/3} \to W^+ t) &= \mathrm{BR}(B \to W^- t) = \mathrm{BR}(\mathcal{Y} \to \chi t) = \mathrm{BR}(\mathcal{Z} \to \chi^* t) = 1\,. \end{aligned} \tag{4.48}$$

Note that the $U(1)_{\rm DM}$ charged top partners always decay into a top and DM χ (see Refs. [172–174] for recent studies of top partner decays into additional Goldstone scalars). These leading order predictions are also satisfied to a good accuracy in the full model, what is explicitly verified in the right panel of Figure 4.11, where the exact branching ratios of the singlet are shown.

There are in general two production mechanisms for top partners at the LHC: QCD pair production $pp \to \psi\bar{\psi}$ where ψ is any top partner, and single production in association with a top or bottom quark via electroweak interactions. For a singlet S the leading process is $pp \to S\bar{b}j$ via the $\bar{b}W^-S$ vertex.[14] In the absence of the derivative couplings proportional to $c^{L,R}$ the bounds from single production [175] are weaker than from QCD pair production [176,177], which we will discuss in the following. For simplicity we will assume the branching fractions from Eq. (4.48). The search in [176] focuses on the $\bar{\psi}\psi \to t(h \to b\bar{b})+X$ process in 1- and 0-lepton final states, yielding the 95% CL constraints $M_S > 1.02$ TeV and $M_{X_{2/3}} > 1.16$ TeV (henceforth, LHC limits will always be quoted at 95% CL). The bound on $X_{2/3}$ is stronger due to the larger branching ratio into th. The search in [177] instead specifically targets the $X_{5/3}$ in the same-sign-dileptons final state, and gives $M_{X_{5/3}} > 1.16$ TeV.[15] In addition to these standard CH signature our model contains more exotic scenarios with the $U(1)_{\rm DM}$ charged top partners $\mathcal{Y}, \mathcal{Z}$. Since these always decay into a top quark and DM, pair production of $\mathcal{Y}, \mathcal{Z}$ gives rise to the signature $t\bar{t}$ + missing transverse energy (MET). The bound depends on the DM mass, which we will take to be $m_\chi = 300$ GeV, i.e. exactly in the middle of the best motivated mass range (see Figure 4.10). Our strategy to obtain the bound on $M_{\mathcal{Y}}, M_{\mathcal{Z}}$ is to start from the 8 TeV analysis of [178], which results in $m_\psi > 0.85$ TeV based on ~ 20 fb^{-1} of data. As a next step we use the Collider Reach [179] method to rescale the bound to a luminosity of ~ 36 fb^{-1} at 13 TeV, obtaining $m_\psi > 1.30$ TeV. Finally we take into account that $\mathcal{Y}, \mathcal{Z}$ are two degenerate Dirac fermions, which both contribute to the signal. For this reason we solve the following equation

[13] EWSB effects do not alter the masses of $X_{5/3}, \mathcal{Y}$ and $\mathcal{Z}$, which remain exactly degenerate, but they do shift $M_{X_{2/3}}$ slightly. The correction can have either sign depending on the parameter point.

[14] Note that the $U(1)_{\rm DM}$ charged top partners $\mathcal{Y}, \mathcal{Z}$ cannot be singly produced.

[15] This is the bound obtained for a purely right-handed $\bar{t}W^-X_{5/3}$ coupling, as appropriate since in this model the left-handed coupling is suppressed by one extra power of v.

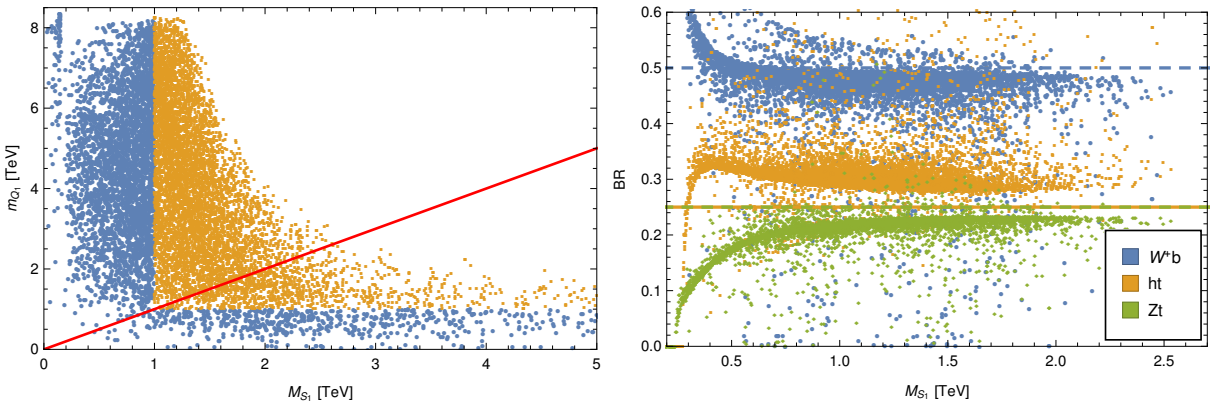

Figure 4.11: Distributions in the model with two fermionic resonance layers. *Left:* mass of the lightest exotic top partner (m_{Q_1}) versus the mass of the lightest singlet top partner (M_{S_1}). For orange (blue) points, the lightest fermionic resonance is heavier (lighter) than the approximate LHC lower bound of 1 TeV. The red line corresponds to $m_{Q_1} = M_{S_1}$. *Right:* branching ratios of the lightest singlet S_1, for the parameter points where it is the lightest fermionic resonance. The dashed lines indicate the leading order predictions, see Eq. (4.48). This Figure has been adopted from [28].

for $M_{\mathcal{Y}}$: $\sigma_{pp\to\bar{\psi}\psi,\,13\text{ TeV}}(m_\psi = 1.30\text{ TeV}) = 2\,\sigma_{pp\to\bar{\psi}\psi,\,13\text{ TeV}}(M_{\mathcal{Y}})$, arriving to $M_{\mathcal{Y}} > 1.42$ TeV.[16] In summary, the current LHC constraints on the top partner masses are, at 95% CL,

$$M_S > 1\text{ TeV}, \qquad M_{X_{5/3},\,X_{2/3}} > 1.2\text{ TeV}, \qquad M_{\mathcal{Y},\,\mathcal{Z}} > 1.4\text{ TeV}. \tag{4.49}$$

These conditions are imposed at every point in the parameter scan presented in Figure 4.10.

B Beyond the lightest top partner

The first manifestation of top partners at the LHC would almost certainly be the lightest top partner. However, if the lightest top partner is a singlet S it is near to impossible to draw conclusions about the symmetry of the CH model and the connection to DM. A smoking gun signature for DM in this CH model are the $U(1)_{\text{DM}}$ charged top partners $\mathcal{Y}$ and $\mathcal{Z}$. If they can be produced and there is a large enough mass splitting $m_Q - M_S$, both the decay to $\chi^{(*)}t$ and the cascade decay $\chi^{(*)}S$ are unsuppressed. Assuming $\epsilon_{tQ}, M_S \ll m_Q$ and taking the limit of full t_R compositeness $\sin\phi_R \to 1$, the branching ratios are given by

$$\text{BR}(\mathcal{Y}\to\chi t) = \text{BR}(\mathcal{Z}\to\chi^* t) \simeq \frac{c_R^2}{c_L^2 + c_R^2}\,, \tag{4.50}$$

where we took nonzero coefficients for the derivative interactions in Eq. (4.16), setting $c^{L/R} = i\,c_{L,R}$ so that $\mathcal{CP}$ is conserved. According to Eq. (4.50) $\mathcal{Y}$ and $\mathcal{Z}$ decay almost democratically into both channels. Therefore one could get an additional handle on the exotic top partners by considering cascade decays of pair produced $\mathcal{Y}$ or $\mathcal{Z}$ into an intermediate singlet S, which finally yields a Z or h in addition to the "stop-like" signature $bW\bar{b}W\chi\chi^*$.

In a scenario where the multiplet in the fundamental Q is lighter than the singlet S, i.e. $m_Q < M_S$, $\mathcal{Y}$ and $\mathcal{Z}$ are at the bottom of the spectrum and would give a $t\bar{t}$ + MET signature

[16] As an independent cross-check, we have recast the constraint on the stop mass extracted from [180], $m_{\tilde{t}} > 1.04$ TeV with ~ 36 fb^{-1}, by solving for $M_{\mathcal{Y}}$ the equation $\sigma_{pp\to\tilde{t}^*\tilde{t},\,13\text{ TeV}}(m_{\tilde{t}} = 1.04\text{ TeV}) = 2\,\sigma_{pp\to\bar{\psi}\psi,\,13\text{ TeV}}(M_{\mathcal{Y}})$, obtaining a consistent bound $M_{\mathcal{Y}} > 1.47$ TeV.

early on. In this case the singlet S could still be accessed via single production $pp \to S\bar{b}j$, whose rate can be sizable for non-vanishing derivative couplings $c_{L,R}$ [152]. This could lead to the "inverse" of the cascade which we considered above, i.e. the singlet could decay into an intermediate $\mathcal{Y}$ or $\mathcal{Z}$, i.e. $S \to \chi^*\mathcal{Y}, \chi\mathcal{Z}$, which would finally yield a monotop signature of the form $t\chi\chi^*\bar{b}j$. Assuming that $\epsilon_{tQ}, m_Q \ll M_S$ the branching ratio for these decays in the limit of full t_R compositeness is

$$\mathrm{BR}(S \to \chi^*\mathcal{Y}) = \mathrm{BR}(S \to \chi\mathcal{Z}) \simeq \frac{1}{6}\,, \tag{4.51}$$

what holds for arbitrary $c_{L,R}$. Hence $\approx 1/3$ of the singly produced singlets yield the monotop final state.

4.4 Shift symmetry breaking by bottom quark coupling

A qualitatively very different DM phenomenology can be obtained by taking another embedding for the elementary fermions. A particularly interesting scenario is reached by assuming that the top quark couplings do not break the DM shift symmetry and the leading breaking originates from the bottom quark couplings. This can be easily achieved by coupling the third generation quarks to composite operators transforming in the $\mathcal{O}_q \sim \mathbf{7}_{2/3}, \mathcal{O}_t \sim \mathbf{21}_{2/3}$ and $\mathcal{O}_{q',b} \sim \mathbf{7}_{-1/3}$ representations under $SO(7) \times U(1)_X$. In this case the t_R couplings preserve the DM shift symmetry if we embed it into $(\mathbf{3},\mathbf{1},\mathbf{1})_{2/3} \oplus (\mathbf{1},\mathbf{3},\mathbf{1})_{2/3} \subset \mathbf{21}_{2/3}$, which is a singlet under the full $SU(2)'$ subgroup. The explicit form of the top embeddings is given by

$$\mathbf{7}_{2/3} \sim \xi_L^{(t)} = \frac{1}{\sqrt{2}}\left(ib_L, \quad b_L, \quad it_L, \quad -t_L, \quad \mathbf{0}_3^T\right)^T, \quad \mathbf{21}_{2/3} \sim \xi_R^{(t)} = \frac{i\,t_R}{2}\begin{pmatrix} 0 & -1 & & & \\ 1 & 0 & & & \\ & & 0 & 1 & \\ & & -1 & 0 & \\ & & & & \mathbf{0}_{3\times 3} \end{pmatrix}, \tag{4.52}$$

where empty entries are zero. In order to model the bottom quark sector, we have to introduce a second embedding for q_L into $\mathcal{O}_{q',b} \sim \mathbf{7}_{-1/3}$, since otherwise we would not be able to write a $U(1)_X$ invariant Yukawa coupling for the bottom. This will however lead to dangerous tree-level corrections to the $Z\bar{b}_L b_L$ coupling, which we will comment on momentarily. The embedding of b_R is along the same lines as t_R in the previous section and will constitute the leading breaking of the DM shift symmetry. The explicit embeddings are of the form

$$\mathbf{7}_{-1/3} \sim \xi_L^{(b)} = \frac{1}{\sqrt{2}}\left(-it_L, \quad t_L, \quad ib_L, \quad b_L, \quad \mathbf{0}_3^T\right)^T, \qquad \mathbf{7}_{-1/3} \sim \xi_R^{(b)} = b_R\left(\mathbf{0}_6^T, \quad 1\right)^T. \tag{4.53}$$

Before continuing the study of this model a few comments are in order. The leading contribution to the Higgs potential comes from the top quark, since its $\mathcal{G}$-breaking couplings have to be sizable to generate an $\mathcal{O}(1)$ Yukawa coupling. This implies that the bottom contribution to the Higgs potential can be neglected in a first order approximation. This effectively decouples Higgs and DM properties and couplings, since the dominant contribution to the DM potential comes from the bottom quark. For this reason we will not discuss the mixing Lagrangian for the top quark and its contribution to the effective potential here and refer to Appendix I.B for details. Here we will purely focus on the bottom couplings and their effect on DM phenomenology and implicitly assume that the top quark and gauge sector take care to generate a realistic effective potential for the Higgs.

4.4.1 Fermion sector and effective potential for DM

Under $SO(6)$, $\mathbf{7}_{-1/3}$ decomposes as $\mathbf{7}_{-1/3} = \mathbf{6}_{-1/3} \oplus \mathbf{1}_{-1/3}$. We therefore expect the bottom quark to couple to resonances $Q^{(b)} \sim \mathbf{6}_{-1/3}$ and $S^{(b)} \sim \mathbf{1}_{-1/3}$ under $SO(6) \times U(1)_X$. The component expression of the "bottom partner" multiplet $Q^{(b)}$ is

$$Q^{(b)} = \frac{1}{\sqrt{2}} \Big(iU_{-4/3} - i\widetilde{T}, U_{-4/3} + \widetilde{T}, iU_{-1/3} + i\widetilde{B}, -U_{-1/3} + \widetilde{B}, -i\mathcal{V} + i\mathcal{W}, \mathcal{V} + \mathcal{W} \Big)^T , \quad (4.54)$$

where under $(SU(2)_L)^{\rm DM}_Y$ we have $(U_{-1/3}, U_{-4/3})^T \sim \mathbf{2}^0_{-5/6}$, $(\widetilde{T}, \widetilde{B})^T \sim \mathbf{2}^0_{1/6}$ and $\mathcal{V}, \mathcal{W} \sim \mathbf{1}^{\pm 1}_{-1/3}$. The elementary-composite mixing Lagrangian for the bottom sector reads

$$\mathcal{L}^{(b)}_{\rm mix} = (\epsilon^m_{qS^{(b)}} \bar{\xi}^{(b)A}_L S^{(b)}_{R,m} + \epsilon^m_{bS^{(b)}} \bar{\xi}^{(b)A}_R S^{(b)}_{L,m}) U_{A7} + (\epsilon^n_{qQ^{(b)}} \bar{\xi}^{(b)A}_L Q^{(b)a}_{R,n} + \epsilon^n_{bQ^{(b)}} \bar{\xi}^{(b)A}_R Q^{(b)a}_{L,n}) U_{Aa} + \text{h.c.}, \quad (4.55)$$

where $\{m, n\}$ run from 1 to $\{N_{S^{(b)}}, N_{Q^{(b)}}\}$, respectively. The complete fermionic Lagrangian is $\mathcal{L}_f = (\text{kin. terms}) + (\text{resonance masses}) + \mathcal{L}^{(t)}_{\rm mix} + \mathcal{L}^{(b)}_{\rm mix}$, where the kinetic terms include both those for the elementary fields and the CCWZ ones for the resonances. $\mathcal{L}^{(t)}_{\rm mix}$ is given in Eq. (I.B.5).

The couplings in Eq. (4.55) radiatively generate a potential for the Higgs and DM. The contribution relevant for DM phenomenology is of the form

$$V^{(b)}_{\rm eff}(\tilde{h}, \chi) \supset \mu^2_{\rm DM} \chi^* \chi + \lambda_{\rm DM} (\chi^* \chi)^2 + \lambda \tilde{h}^2 \chi^* \chi \, . \quad (4.56)$$

The potential parameters are in general divergent, but can be rendered calculable by imposing WSRs (see Section 4.3.2 for a similar discussion in the context of top couplings breaking the DM shift symmetry). In the following we will be content with partial calculability and introduce $N_{Q^{(b)}} = N_{S^{(b)}} = 1$ resonances together with one set of WSRs. This makes the marginal couplings UV-finite, but leaves a residual logarithmic divergence in the mass parameters. This is motivated by the discussion in Section 4.3 where we found that requiring full calculability in a model with only one layer of resonances is often too restrictive and results in a non-generic potential. This is cured at the cost of increased complexity by introducing an additional layer of resonances. However, in Section 4.3 we also found that qualitatively and quantitatively similar results can be obtained by relaxing the requirement of full calculability in a one-layer setup. The WSRs, which make the marginal couplings finite correspond to the relations

$$\epsilon^2_{qS^{(b)}} = \epsilon^2_{qQ^{(b)}} \, , \qquad \epsilon^2_{bS^{(b)}} = \epsilon^2_{bQ^{(b)}} \, . \qquad (\text{WSR})_b \quad (4.57)$$

These relations imply that $\mu^2_{\rm DM}$ vanishes for $m^2_{Q^{(b)}} = m^2_{S^{(b)}}$ (see Appendix I.D). We assume $m_{Q^{(b)}}, m_{S^{(b)}} > 0$ and take $\epsilon_{qS^{(b)}} = +\epsilon_{qQ^{(b)}}$ and $\epsilon_{bS^{(b)}} = -\epsilon_{bQ^{(b)}}$ as solutions to the sum rules, in which case λ does not vanish even for $m_{Q^{(b)}} = m_{S^{(b)}}$. This implies the following parametric scaling of the potential parameters

$$\mu^2_{\rm DM} \simeq a \, \frac{N_c}{16\pi^2} \frac{M^4_{*b}}{f^2} (\epsilon^b_R)^2 \, C_{QS} \, , \quad C_{QS} \equiv \frac{m^2_{Q^{(b)}} - m^2_{S^{(b)}}}{M^2_{*b}} \, , \qquad \lambda \simeq b \, \frac{N_c}{16\pi^2} \frac{M^2_{*b}}{f^2} \, y^2_b , \quad (4.58)$$

where $a, b > 0$ are $O(1)$ coefficients and M_{*b}, defined via Eq. (3.15), is identified with $M_{*b} = m_{Q^{(b)}} + m_{S^{(b)}}$, which implies $|C_{QS}| < 1$. $\epsilon^b_R \leq 1$ is the compositeness fraction of the RH bottom quark and is proportional to spurions which explicitly break the DM shift symmetry.

Bounds from corrections to the $Z\bar{b}_L b_L$ coupling

As we have mentioned before, an important constraint on this scenario are tree-level corrections

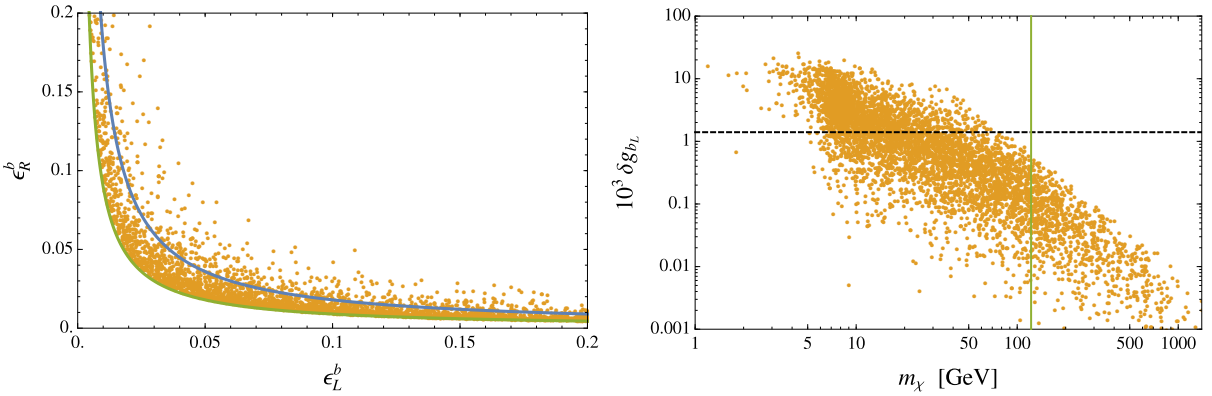

Figure 4.12: Results of the numeric parameter scan of the model where the DM shift symmetry is broken by b_R, for $f = 1$ TeV. *Left panel:* distribution of the mixings for the two chiralities of the bottom quark. The blue (green) curve corresponds to the relation $y_b \simeq \epsilon_L^b \epsilon_R^b M_{*b}/f$ with $M_{*b} = 8\,(16)$ TeV. Notice that $M_{*b} = m_{Q^{(b)}} + m_{S^{(b)}}$ is not a physical mass, and can therefore exceed $4\pi f$. *Right panel:* tree-level correction to the $Z\bar{b}_L b_L$ coupling versus the physical χ mass. The black dashed line indicates the 99% CL experimental upper bound, $10^3\,\delta g_{b_L} < 1.4$, whereas the green vertical line corresponds to the mass for which χ yields the observed DM density by annihilating purely through the derivative Higgs portal. This Figure has been adopted from [29].

to the $Z\bar{b}_L b_L$ coupling, which is not protected by the P_{LR} custodial symmetry [77] since b_L is embedded in $(\mathbf{2},\mathbf{2})_{-1/3}$ and $(\mathbf{2},\mathbf{2})_{2/3}$ of $SU(2)_L \times SU(2)_R \times U(1)_X$. The corrections scale as

$$\frac{g}{c_w} Z_\mu \bar{b}_L \gamma^\mu (g_{b_L}^{\rm SM} + \delta g_{b_L}) b_L\,, \qquad \delta g_{b_L} \simeq +(\epsilon_L^b)^2\,\frac{v^2}{f^2} \tag{4.59}$$

($g_{b_L}^{\rm SM} = -1/2 + s_w^2/3$), where the sign is fixed to be positive. The experimental bound is $-1.7 < 10^3\,\delta g_{b_L} < +1.4$ at 99% CL [181].[17] The corrections to the $Z\bar{b}_L b_L$ coupling crucially depend on the compositeness fraction of the LH bottom quark. A maximally composite b_L, i.e. $\epsilon_L^b \sim 1$ and $\epsilon_R^b \sim y_b f/M_{*b}$, on the one hand leads to very light DM with $m_\chi \approx 4$ GeV $(M_{*b}/8$ TeV$)(1$ TeV$/f)$, for which we used $m_b = m_b^{\overline{MS}}(2\text{ TeV}) \simeq 2.5$ GeV, but on the other hand it is robustly ruled out by $Z\bar{b}_L b_L$ unless $f \gg 1$TeV. The reverse scenario of large b_R compositeness $\epsilon_R^b \sim 1$, $\epsilon_L^b \sim y_b f/M_{*b}$ easily satisfies the $Z\bar{b}_L b_L$ bound but yields parametric scalings for $\mu_{\rm DM}^2$ and λ that are similar to those already discussed in the case where the DM shift symmetry is broken by t_R couplings. We are therefore mainly interested in the intermediate range $\epsilon_L^b \sim \epsilon_R^b \sim \sqrt{y_b f/M_{*b}}$, where corrections to $Z\bar{b}_L b_L$ are mild ,$10^3\,\delta g_{b_L} \sim +\,\text{few} \times 0.1\,(8\text{ TeV}/M_{*b})\,(1\text{ TeV}/f)$.

In order to justify these estimates we show the results of a numeric parameter scan in Figure 4.12. For this scan we took $f = 1$ TeV and required that the top and bottom contributions give a realistic Higgs potential. In order to prevent spontaneous breaking of $U(1)_{\rm DM}$ we choose $m_{Q^{(b)}} > m_{S^{(b)}}$, what gives $0 < C_{QS} < 1$ and $\mu_{\rm DM}^2 > 0$. As cutoff for the residual logarithmic divergence we took $\Lambda = 10\,f$. We additionally approximately accounted for LHC constraints [182] by only showing points with masses of the lightest resonance larger than 1.2 TeV. The left panel of Figure 4.12 clearly shows that the intermediate region of $\epsilon_L^b \sim \epsilon_R^b$ is densely populated. In the right panel we show the tree-level corrections to $Z\bar{b}_L b_L$, i.e. δg_{b_L}, as a function of the DM

[17] In this model b_R is embedded in a $(\mathbf{1},\mathbf{1})_{-1/3} \subset \mathbf{7}_{-1/3}$, so the $Z\bar{b}_R b_R$ coupling is protected by P_{LR} and very suppressed. Therefore it makes sense to set $\delta g_{b_R} = 0$ in the electroweak fit. Since δg_{b_L} is weakly correlated with the remaining precision observables, we can then simply quote its one-parameter bound.

mass. We find that for $m_\chi \gtrsim 80$ GeV, and in particular $m_\chi \approx 122$ GeV where the observed relic abundance is obtained purely from annihilation through the derivative portal, the $Z\bar{b}_L b_L$ bounds are always satisfied.

4.4.2 Dark matter phenomenology

In Section 4.4.1 we found that constraints from tree-level corrections to the $Z\bar{b}_L b_L$ coupling favor a mild compositeness fraction of b_L. For this reason we focus on the region of parameter space where both chiralities have comparable compositeness fractions, i.e. $\epsilon_L^b \sim \epsilon_R^b \sim \sqrt{y_b f/M_{*b}}$. For this scaling we can obtain an estimate on the DM mass and portal coupling from Eq. (4.58)

$$m_\chi \simeq \sqrt{\mu_{\rm DM}^2} \approx 120 \text{ GeV} \left(\frac{M_{*b}}{8 \text{ TeV}}\right)^{3/2} \left(\frac{1 \text{ TeV}}{f}\right)^{1/2}, \tag{4.60a}$$

$$\lambda \approx 3 \times 10^{-4} \left(\frac{M_{*b}}{8 \text{ TeV}}\right)^{2} \left(\frac{1 \text{ TeV}}{f}\right)^{2}, \tag{4.60b}$$

where we took $C_{QS} \sim 0.2$. This implies that while it is possible to obtain an $\mathcal{O}(100)$ GeV DM mass, the portal coupling is strongly suppressed and negligible for both annihilation ($\lambda f^2 \ll m_\chi^2$) and elastic scattering on nuclei. The relic abundance is set via annihilations through the derivative portal, yielding the observed value for $f \sim$ TeV. However, the breaking of the DM shift symmetry by the bottom quark also induces non-derivative contact interactions of the form $\chi^*\chi b\bar{b}$. These are actually the dominant contribution to DM-nucleon scattering, whose cross-section is

$$\begin{aligned}\sigma_{\rm SI}^{\chi N} &\simeq \frac{\tilde{f}_N^2}{\pi} \frac{m_N^4}{4 f^4 m_\chi^2} \\ &\approx 1.0\text{-}5.6 \times 10^{-47} \text{ cm}^2 \left(\frac{1 \text{ TeV}}{f}\right)^4 \left(\frac{100 \text{ GeV}}{m_\chi}\right)^2, \quad (b_R \text{ breaking})\end{aligned} \tag{4.61}$$

where the shown range accounts for the theory uncertainty on the couplings of the first and second generation quarks. The lower value assumes that only the bottom quark breaks the DM shift symmetry, i.e. $c_b^\chi = 1$ and $c_q^\chi = 0$ for all $q \neq b$ (case I), what yields a nucleon form factor $\tilde{f}_N \simeq 0.066$. The higher value corresponds to all down-type quarks breaking the DM shift symmetry, i.e. $c_{d,s,b}^\chi = 1$ and $c_{u,c,t}^\chi = 0$ (case II), which is what one would get by duplicating the symmetry breaking pattern of the third generation quarks to all three generations. This scenario gives $\tilde{f}_N \simeq 0.15$. Even though the resulting cross-section is very suppressed, it will be tested by next-generation direct detection experiments such as LZ [115].

We show a summary of the DM phenomenology in the current model and the corresponding constraints in the (m_χ, f) plane in Figure 4.13. We use the effective Lagrangian from Section 3.1 and 3.2 and set $c_d = c_b^\chi = 1$, $c_t^\chi = \lambda = 0$. The blue line shows the contour in parameter space which reproduces the observed relic abundance. The red-shaded region is ruled out by XENON1T direct detection results [5] if we assume case I. The excluded region corresponding to case II is represented by the dashed line. The solid (dashed) gray line is the projected sensitivity of LZ [115] to case I (case II). For light DM, i.e. $m_\chi < m_h/2$, there are additional constraints from searches for invisible Higgs decays. The current 95% CL bound is $\text{BR}(h \to \chi^*\chi) < 0.13$ [183], ruling out the orange-shaded region, which extends almost up to $f \simeq 1.4$ TeV for light χ. At HL-LHC this bound is projected to improve to $\text{BR}(h \to \chi^*\chi) < 0.08$ [184], corresponding to the dotted orange curve, will extend the reach to $f \simeq 1.6$ TeV. The purple region shows the parameter values which are probed in searches for present-day DM annihilation in dwarf

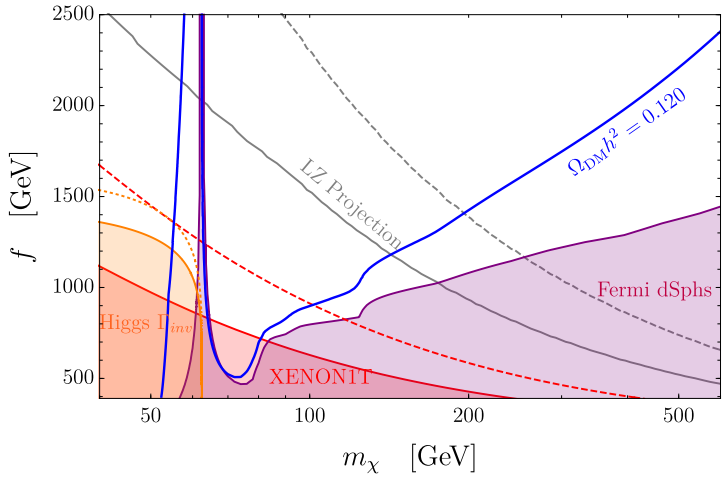

Figure 4.13: Parameter space of the model where the bottom quark gives the leading breaking of the DM shift symmetry. The coefficients of the effective Lagrangian, discussed in Sections 3.1 and 3.2, are set to $c_d = c_b^\chi = 1$, $c_t^\chi = \lambda = 0$. For the exclusion contours from direct and indirect detection we have assumed that all of the observed DM is composed of χ particles, irrespective of the thermal value of the χ density predicted at each (m_χ, f) point. This Figure is an updated version of the one published in [29].

spheroidal galaxies (dSphs) by the Fermi-LAT collaboration [145].[18] We set this bound by comparing the total DM annihilation cross-section in our setup to the limit reported by Fermi for the $b\bar{b}$ final state and should therefore only be taken as an approximation. Note that most of the best-motivated parameter space from our numeric scans, i.e. 80 GeV $\lesssim m_\chi \lesssim$ 200 GeV and 0.8 TeV $\lesssim f \lesssim$ 1.4 TeV, is currently untested but within reach of LZ.

4.5 Shift symmetry breaking by gauging of $\mathbf{U(1)}_{\mathrm{DM}}$

Another possibility is to assume that all fermions respect the DM shift symmetry. Such a scenario is possible in the $SO(7)/SO(6)$ model by coupling the SM quarks to strong sector operators in the $\mathcal{O}_q \sim \mathbf{7}_{2/3}$ and $\mathcal{O}_{u,d} \sim \mathbf{21}_{2/3}$ representation for all generations (see Appendix I.B for details about this embedding). In such a model the fermion and gauge sector still break the Higgs shift symmetry and are responsible for radiatively generating a realistic Higgs potential. However, at the same time they do not contribute to $\mu^2_{\rm DM}, \lambda_{\rm DM}$ and λ. This means we need an additional breaking of the DM shift symmetry from BSM physics to at least generate a DM mass. A simple possibility for complex DM is to gauge the stabilizing $U(1)_{\rm DM}$ symmetry under which all SM particles are uncharged. In the $SO(7)/SO(6)$ model the $U(1)_{\rm DM}$ generator $T^{\rm DM}$ together with the two generators under which the real and imaginary part of the DM χ shift $X^{\rm Re}, X^{\rm Im}$, generate $SU(2)' \sim \{X^{\rm Re}, X^{\rm Im}, T^{\rm DM}\} \subset SO(6)$ (see the discussion in Section 4.2). Gauging only $U(1)_{\rm DM} \subset SU(2)'$ will explicitly break $SU(2)'$ along the directions generated by $X^{\rm Re}, X^{\rm Im}$. Consequently loops of the new dark photon γ_D will generate a mass for the DM in the same way as the photon generates a mass for the pions.

[18] As we have already mentioned in Section 3.3 and 4.3.3.F there are additional indirect detection constraint [147, 148] can from the antiproton spectrum measured by AMS-02 [6]. However, these constraints are plagued by larger systematic uncertainties, whose size is still under debate. For this reason we only show the more conservative and robust bounds from dSphs.

In practical terms we take the gauging of $U(1)_{\rm DM}$ into account by modifying $\mathcal{L}_{\rm GB}$ in the following way

$$|\partial^\mu \chi|^2 \quad \to \quad |(\partial^\mu - i g_D A_D^\mu)\chi|^2 - \frac{1}{4} F_D^{\mu\nu} F_{D\mu\nu} + \frac{1}{2}\, m_{\gamma_D}^2 A_{D\mu} A_D^\mu \,, \tag{4.62}$$

where we took χ to have unit charge and included a possible mass term for the dark photon, which might e.g. arise via the Stückelberg mechanism without spontaneously breaking $U(1)_{\rm DM}$. At one loop this generates no portal coupling λ but a DM mass of the size

$$m_\chi = \sqrt{\mu_{\rm DM}^2} \simeq \sqrt{\frac{3\alpha_D}{2\pi}}\, m_\rho \approx 100 \text{ GeV} \left(\frac{\alpha_D}{10^{-3}}\right)^{1/2} \left(\frac{m_\rho}{5 \text{ TeV}}\right), \qquad \lambda = 0 \,, \tag{4.63}$$

where $\alpha_D \equiv g_D^2/(4\pi)$ and we cut off the loop integral at m_ρ, the mass of the vector resonance which mixes with the elementary dark photon (see Appendix I.C). This estimate is valid as long as $m_{\gamma_D} \ll m_\rho$, which we will assume in the following. The vanishing of λ at one-loop is due to the fact that the Higgs is uncharged under $U(1)_{\rm DM}$. Thus this model is almost a perfect realization of the "Goldstone limit" in Section 3.1 and is therefore effectively inaccessible in direct detection experiments.

However, the introduction of the dark photon as additional degree of freedom has important phenomenological consequences. Note in particular that in Eq. (4.62) we did not add a kinetic mixing term of the hypercharge gauge boson and the dark photon of the form $\varepsilon B_{\mu\nu} F_D^{\mu\nu}/2$. The choice $\varepsilon = 0$ is motivated by the $SO(7)/SO(6)$ model, which forbids the kinetic mixing due to the presence of an accidental symmetry under C_D, the $U(1)_{\rm DM}$ charge conjugation operator.[19] The action of C_D on the low-energy states is $A_D^\mu \to -A_D^\mu$, $\chi \to -\chi^*$ and leaves SM states invariant. An important consequence of this discrete symmetry is that it makes γ_D stable for $m_{\gamma_D} < 2m_\chi$ when the decay $\gamma_D \to \chi\chi^*$ is kinematically forbidden. For a complete discussion of kinetic mixing and details on the implementation of C_D as an $\mathcal{O}(6)$ transformation, which we will call P_6, we refer the reader to Appendix I.E.

The dark sector in this model can therefore be completely described by four parameters $\{m_\chi, f, \alpha_D, m_{\gamma_D}\}$. In the following we will extensively discuss the phenomenology of this setup, first concentrating on the possibility of a massless the dark photon in Section 4.5.1, before continuing with the case of a massive dark photon in Section 4.5.2.

4.5.1 Phenomenology for massless dark photon

Specializing to a massless dark photon fixes one of the model parameters $m_{\gamma_D} = 0$ and leaves three additional ones $\{m_\chi, f, \alpha_D\}$. A massless dark photon behaves as radiation at all temperatures and therefore contributes to the number of present-day relativistic degrees of freedom. This is strongly bounded by CMB observations but crucially depends on the temperature of the dark photon bath. For this reason we start with a short summary of the thermal history of the dark sector and determine when it decouples from the SM.

At early times elastic $\chi f \to \chi f$ scattering on SM fermions f mediated by the Higgs keeps the dark sector, consisting of χ and γ_D, in kinetic equilibrium with the SM bath. However, these processes become inefficient at temperatures $T \ll m_\chi$ and eventually drop below the Hubble expansion rate. When this happens the dark and visible sectors decouple, each having their separate temperature. The decoupling temperature $T_{\rm dec}$ is defined via [185] $H(T_{\rm dec}) = \gamma(T_{\rm dec})/2$, where $H(T) = \pi\sqrt{g_*(T)}\, T^2/(3\sqrt{10} M_{\rm Pl})$ is the Hubble parameter for a radiation-dominated

[19] This assumes that the subleading spurionic embeddings of the SM fermions respect the C_D invariance. See Appendix I.E for details.

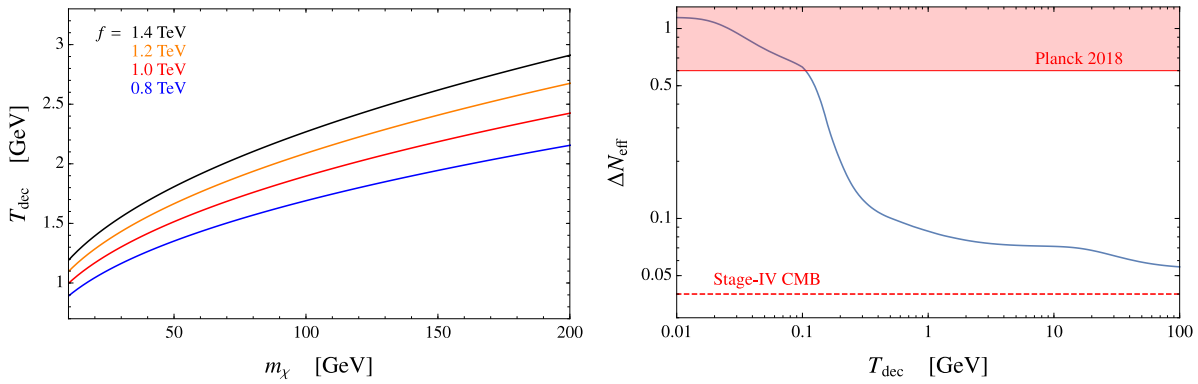

Figure 4.14: *Left panel:* temperature at which the dark sector kinetically decouples from the visible sector. *Right panel:* contribution of the dark photon to ΔN_{eff} at photon decoupling, calculated from Eq. (4.64). In the evaluation of $g_{*s,\mathrm{vis}}(T_{\mathrm{dec}})$ we assumed 150 MeV as temperature of the QCD phase transition. The region shaded in red corresponds to the current CMB constraint $\Delta N_{\mathrm{eff}} \lesssim 0.6$, while the dashed red line shows the projected Stage-IV CMB bound $\Delta N_{\mathrm{eff}} \lesssim 0.04$. This Figure has been adopted from [29].

Universe[20], and $\gamma(T)$ is the momentum relaxation rate, which scales as $\gamma \sim (T/m_\chi) n_f \langle \sigma_{\chi f} v_{\mathrm{rel}} \rangle$. This scaling can be understood in the following way: the typical momentum transfer per collision is $\delta p \sim T$, whereas the non-relativistic WIMP momentum satisfies $p^2/(2m_\chi) \sim T$, i.e. $p \sim (m_\chi T)^{1/2}$. Momentum transfer is a stochastic process, i.e. the fraction of transferred momentum per reaction is roughly $(\delta p/p)^2 \sim T/m_\chi$, requiring m_χ/T collisions to get an $\mathcal{O}(1)$ momentum transfer which is needed to maintain kinetic equilibrium. Therefore if $\gamma(T) \sim (\delta p/p)^2 n_f \langle \sigma_{\chi f} v_{\mathrm{rel}} \rangle$ drops below the Hubble expansion rate kinetic equilibrium is lost. Using the full expression for $\gamma(T)$ from [185] we compute the decoupling temperature T_{dec} as a function of m_χ and f. The resulting temperature is typically between 1 and 3 GeV, as we show in the left panel of Figure 4.14. After the dark photon decouples from the SM bath, the entropy in each sector is separately conserved. Using that $g_{\mathrm{dark}}(T_{\mathrm{dec}}) = g_{\mathrm{dark}}(T) = 2$, since the DM is already non-relativistic at kinetic decoupling, we can obtain the dark sector temperature by using Eq. (2.84) and Eq. (2.85). The temperature of the dark photon is in general lower than that of the photon bath and the contribution to the relativistic degrees of freedom today, quantized in terms of the photon temperature, is suppressed. This is usually discussed in terms of the effective number of light neutrino species N_{eff}. In our model the contribution of the dark photon to N_{eff} is given by [186]

$$\Delta N_{\mathrm{eff}} = N_{\mathrm{eff}} - 3.046 = \frac{8}{7} \frac{g_{\mathrm{dark}}(T)}{2} \left(\frac{T}{T_\nu} \right)^4 \left(\frac{g_{\mathrm{dark}}(T_{\mathrm{dec}})}{g_{\mathrm{dark}}(T)} \frac{g_{*s,\mathrm{vis}}(T)}{g_{*s,\mathrm{vis}}(T_{\mathrm{dec}})} \right)^{4/3}, \tag{4.64}$$

where $T \sim 0.3$ eV is the photon temperature at decoupling, $N_{\mathrm{eff}} = 3.046$ is the SM prediction, $T/T_\nu = (11/4)^{1/3}$ and $g_{*s,\mathrm{vis}}(T) = 3.91$. As shown in the right panel of Figure 4.14, as long as $T_{\mathrm{dec}} \gg 100$ MeV the current bound $\Delta N_{\mathrm{eff}} \lesssim 0.6$ [92] (95% CL) is easily satisfied. A typical decoupling temperature of 1 - 3 GeV results in a ΔN_{eff} in the range $\Delta N_{\mathrm{eff}} \approx 0.07$ - 0.09, what is significantly below the sensitivity of present CMB measurements but can be probed in future Stage-IV CMB measurements, which are expected to constrain $\Delta N_{\mathrm{eff}} \lesssim 0.04$ at 95% CL [187]. Note that similar but weaker constraints can be obtained from BBN [188].

[20] Note that $g_*(T)$ is the total number of relativistic degrees of freedom including both the visible and dark sectors.

Let us also note that the Compton scattering in the dark sector $\chi\gamma_D \to \chi\gamma_D$ delays kinetic decoupling of the DM from the dark photon compared to the standard WIMP scenario [186,189]. This results in a suppressed matter power spectrum on small scales and prevents the formation of DM halos below a minimal mass. For weak scale DM masses and couplings of the order $\alpha_D \sim 10^{-3}$ the χ-γ_D kinetic decoupling occurs at temperatures of $\mathcal{O}$(MeV). This implies that the minimal DM halo mass is too small to be tested with current observations [189]. In summary we can conclude that the massless dark photon in the current setup is not in conflict with cosmological observations.

Let us now turn to DM phenomenology. Compared to the pure pNGB DM, which annihilates exclusively to SM final states through the derivative Higgs portal, we have an additional annihilation channel into dark photons, i.e. $\chi^*\chi \to \gamma_D\gamma_D$. This annihilation channel occurs via the couplings in Eq. (4.62) and leads to a thermally averaged annihilation cross-section of the size

$$\langle \sigma_{\gamma_D\gamma_D} v_{\rm rel} \rangle = \frac{2\pi\alpha_D^2}{m_\chi^2}\,, \tag{4.65}$$

where we only kept the leading term in the velocity expansion. There is also an additional annihilation channel into both the dark and visible sector $\chi\chi^* \to \gamma_D h$, which is however p-wave suppressed and therefore almost negligible for setting the relic abundance: it has to vanish for $m_{\gamma_D} = 0$ on-threshold due to spin-conservation.[21]. Requiring to obtain the observed relic abundance via the freeze-out mechanism fixes a relation between the three model parameter, which defines a two dimensional manifold. In the following we will study the parameter space for slices of fixed f.

In the absence of the dark photon all annihilation proceeds through the derivative Higgs portal and the model reduces to the pure pNGB scenario. In this case there is exactly one DM mass which produces the observed relic abundance for a given value of f. For $f = 1\,(1.4)$ TeV e.g. this is $m_\chi^{(f)} \approx 122\,(194)$ GeV. Larger DM masses $m_\chi > m_\chi^{(f)}$ increase the coupling strength of the derivative portal, which results in DM underabundance. Adding the $\chi^*\chi \to \gamma_D\gamma_D$ annihilation channel makes the situation worse for $m_\chi > m_\chi^{(f)}$, but can provide enough annihilation strength, for an appropriate value of α_D, to compensate the reduced derivative portal in the $m_\chi < m_\chi^{(f)}$ region. In order to find the required value for α_D we can compare Eq. (4.65) to the annihilation cross-section in the pure derivative portal scenario in Eq. (3.7). They are roughly of the same size if $\alpha_D^2 \sim m_\chi^2/(2\pi^2 f^4)$, which suggests for $m_\chi/f \sim 1/10$ that α_D should be of the order $\alpha_D \sim 2\times 10^{-3}$. For very light DM, i.e. $m_\chi \ll m_h/2$, the derivative portal is negligible and only the annihilation into dark photons is relevant. This can set the observed relic abundance for $\alpha_D \approx 7\times 10^{-4}\,(m_\chi/30\text{ GeV})$. This behavior is clearly visible in the left panel of Figure 4.15, which shows the relic abundance contour in the (m_χ, α_D) plane for various values of the symmetry breaking scale. We also show how the contribution of invisible annihilations into dark photons compares to the full annihilation cross-section along the relic abundance contour. As we have discussed above the annihilation to dark photons becomes increasingly important for lighter DM. Note that in the region 55 GeV $\lesssim m_\chi \lesssim$ 62.5 GeV the DM is always underabundant, no matter how small α_D. This is the case since for the current value of f the annihilation through the derivative Higgs portal alone, close to the Higgs resonance, is already too large too reproduce the relic abundance. We also show as dotted lines the contours of constant vector resonance masses, which enters the computation of the DM mass in Eq. (4.63).[22] One usually expects

[21] The p-wave suppression applies also for $m_{\gamma_D} \neq 0$, since the longitudinal polarization does not contribute to the amplitude due to $U(1)_{\rm DM}$ invariance.

[22] Precisely, we employed Eq. (I.D.25) with $f_\rho = f$.

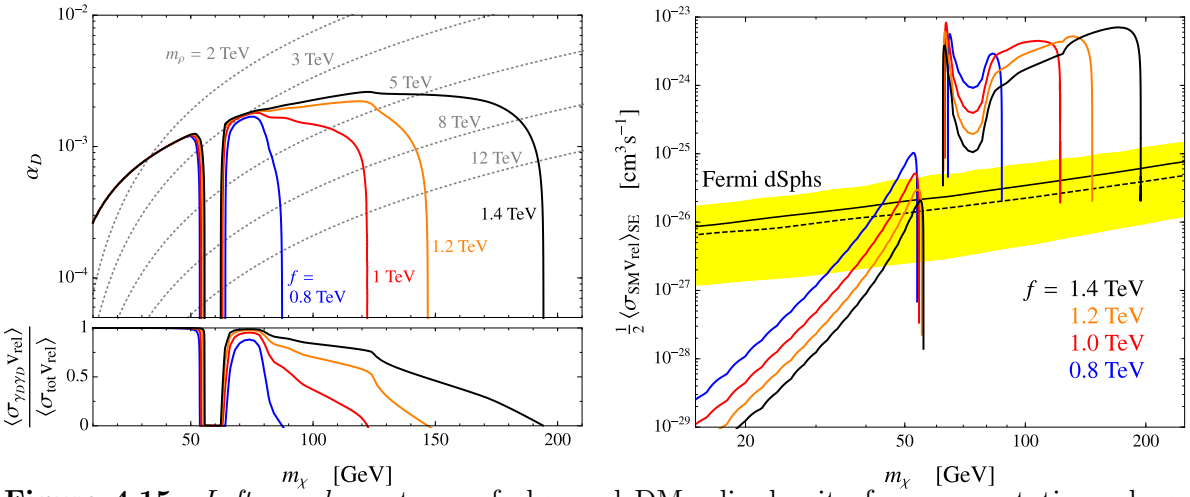

Figure 4.15: *Left panel:* contours of observed DM relic density for representative values of f. The inset shows the fraction of annihilations to dark photons. Contours of constant vector resonance mass m_ρ are also shown, as dashed grey lines. *Right panel:* the colored curves show $\langle\sigma_{\rm SM}v_{\rm rel}\rangle_{\rm SE}$, the present-day annihilation cross section to SM particles including Sommerfeld enhancement, calculated along the relic density contours shown in the left panel. The black line is the observed 95% CL upper limit from the dSphs analysis in [7]. The yellow band corresponds to 95% uncertainty on the expected limit in the same analysis. We also show, as dashed black line, the observed limit from the analysis of a smaller dSphs sample [145]. The quoted experimental limits were obtained assuming DM annihilation to $b\bar{b}$. This Figure was adopted from [29].

$1 \lesssim m_\rho/f \lesssim 4\pi$, but stronger lower bounds can arise from electroweak precision tests or direct searches for vector resonances.

As it turns out some of the strongest constraints in this scenario originate from DM indirect detection. This is the case because the dark photon mediates a long-range force between DM particles, what non-perturbatively boosts the annihilation of non-relativistic DM particles today via Sommerfeld enhancement (SE) [190]. The annihilation cross-section times velocity therefore contains a SE factor, which for s-wave annihilation takes the form

$$(\sigma v_{\rm rel})_{\rm SE} = (\sigma v_{\rm rel})_0\, S(\alpha_D/v_{\rm rel}), \qquad S(\zeta) = \frac{2\pi\zeta}{1-e^{-2\pi\zeta}}\,, \tag{4.66}$$

where $(\sigma v_{\rm rel})_0$ is the result from the perturbative calculation. SE is an important effect if $\alpha_D/v_{\rm rel}$ is an $\mathcal{O}(1)$ number. In this case ladder diagrams with the repeated exchange of dark photons between the DM are all of the same order and have to be resummed. For $\alpha_D/v_{\rm rel} \gtrsim 1/2$ the enhancement factor scales as $S \simeq 2\pi\alpha_D/v_{\rm rel}$. Eq. (4.66) still has to be folded with the phase space distribution of the DM particles. Assuming a Maxwell-Boltzmann distribution the thermally averaged cross-section times relative velocity including SE has the approximate form [191]

$$\langle\sigma v_{\rm rel}\rangle_{\rm SE} = (\sigma v_{\rm rel})_0\, \overline{S}_{\rm ann}\,, \qquad \overline{S}_{\rm ann} = \sqrt{\frac{2}{\pi}}\frac{1}{v_0^3 N}\int_0^{v_{\rm max}} dv_{\rm rel}\, S(\alpha_D/v_{\rm rel}) v_{\rm rel}^2\, e^{-\frac{v_{\rm rel}^2}{2v_0^2}} \tag{4.67}$$

with v_0 being the most probable velocity. The maximal velocity in a galaxy halo is determined by the escape velocity $v_{\rm esc}$, i.e. $v_{\rm max} = 2\,v_{\rm esc}$, and the normalization is given by $N = {\rm erf}(z/\sqrt{2}) - \sqrt{2/\pi}\, z\, e^{-z^2/2}$, $z \equiv v_{\rm max}/v_0$. In the early universe $v_{\rm esc} = \infty$ and consequently $N = 1$. We have also checked that the approximation Eq. (4.67) always agrees within a few percent with the full

numeric treatment. At freeze-out the typical relative DM velocity is of the order $v_0 = \sqrt{2/x_{\rm fo}} \sim 0.3$, for which we used $x_{\rm fo} = m_\chi/T_{\rm fo} \sim 25$, and SE is completely negligible for typical dark photon couplings of the size $\alpha_D \sim 10^{-3}$ (recall that $\alpha_D/v_{\rm rel}$ has to be of order one for SE to be important). However, today the DM particles are significantly slower with typical relative velocities of $v_{\rm rel} \sim 10^{-3}$ in the Milky Way (MW) and $v_{\rm rel} \lesssim 10^{-4}$ in dwarf galaxies. Taking $v_0 = 220$ km/s and $v_{\rm esc} = 533$ km/s for the MW [192], we obtain a SE factor of $\overline{S}_{\rm ann} \approx 6.9$ for $\alpha_D = 10^{-3}$. In dwarf galaxies with representative values of $v_0 = 10\,{\rm km/s}$ and $v_{\rm esc} = 15\,{\rm km/s}$ [193] the SE factor is significantly larger $\overline{S}_{\rm ann} \approx 150$, again for $\alpha_D = 10^{-3}$. This implies that if DM annihilates to a large extent into SM final states, the large SE can lead to conflicts with indirect detection bounds, especially from dwarf galaxies.

The strongest relevant bounds are from the Fermi-Lat collaboration [7, 145], which tries to observe excess gamma rays from DM annihilations in dSphs. The current sensitivity on $\langle\sigma v_{\rm rel}\rangle$ for $m_\chi \sim 100$ GeV is already of a similar size as the canonical thermal relic value. In the right panel of Figure 4.15 we show the expected thermally averaged annihilation cross-section times relative velocity into the visible sector including SE, which one would expect to observe from present-day DM annihilations in dSphs. The cross-sections are computed along the contours in the (m_χ, α_D) plane for which the observed relic abundance is reproduced, and which are also shown for various values of f in the left panel of Figure 4.15. Note that for $m_\chi > m_h/2$, where an $\mathcal{O}(1)$ fraction of the annihilation is into SM particles, this region is ruled out by dSphs analysis due to the large SE. The experimental limit shown in Figure 4.15 assumes that the DM exclusively annihilates into $b\bar{b}$. In our scenario χ annihilates into a combination of SM final states (see e.g. the right panel of Figure 3.1 for an overview). The uncertainty of this approximation is mild and cannot change the conclusion that $m_\chi > m_h/2$ is excluded. Also note that we have completely neglected the effect of bound state formation, which is expected to further enhance the dSphs signal by an $\mathcal{O}(1)$ number (see e.g. [193]). At the same time bound state formation has negligible impact on DM freeze-out due to the relatively low DM mass of $m_\chi \sim 100$ GeV, which we consider here [194].

Another class of important constraints on long-range DM self-interaction comes from the observations of DM halos. The triaxial structure of galaxy halos, and in particular the well-measured non-zero ellipticity of the halo of NGC720 [195], yields strong constraints on the dark photon. Strong self-interactions would have reduced the anisotropy in the DM velocity distribution due to many soft scatterings [189]. The non-relativistic limit of DM-DM scattering is dominated by dark photon exchange, yielding a differential scattering cross-section in the center of mass frame of the following form

$$\frac{d\sigma}{d\Omega} \simeq \frac{\alpha_D^2}{4m_\chi^2 v_{\rm cm}^4 (1-\cos\theta_{\rm cm})^2}\,, \tag{4.68}$$

where we only kept the leading term for small $\theta_{\rm cm}$, which is identical for $\chi\chi \to \chi\chi$ and $\chi\chi^* \to \chi\chi^*$ scattering. The strong $v_{\rm cm}^{-4}$ dependence on the relative velocity implies that the strongest bounds come from galaxies, where the DM is slower than in clusters. The authors of [189] derived a bound by requiring that the relaxation time to obtain an isotropic DM velocity distribution be longer than the age of the universe

$$\tau_{\rm iso} \equiv \langle E_k\rangle/\langle \dot{E}_k\rangle = \mathcal{N} m_\chi^3 v_0^3 (\log\Lambda)^{-1}/(\sqrt{\pi}\alpha_D^2\rho_\chi) > 10^{10}\,{\rm years} \tag{4.69}$$

where $E_k = m_\chi v^2/2$, $\dot{E}_k$ is the rate of energy transfer proportional to $d\sigma/d\Omega$, $\mathcal{N}$ is an $O(1)$ numerical factor, v_0 is the velocity dispersion (very roughly 250 km/s in NGC720), $\rho_\chi = m_\chi n_\chi$ is the χ energy density and the "Coulomb logarithm" $\log\Lambda$ is an artifact of cutting off the infrared divergence arising from Eq. (4.68). The ellipticity bound was reconsidered in a more

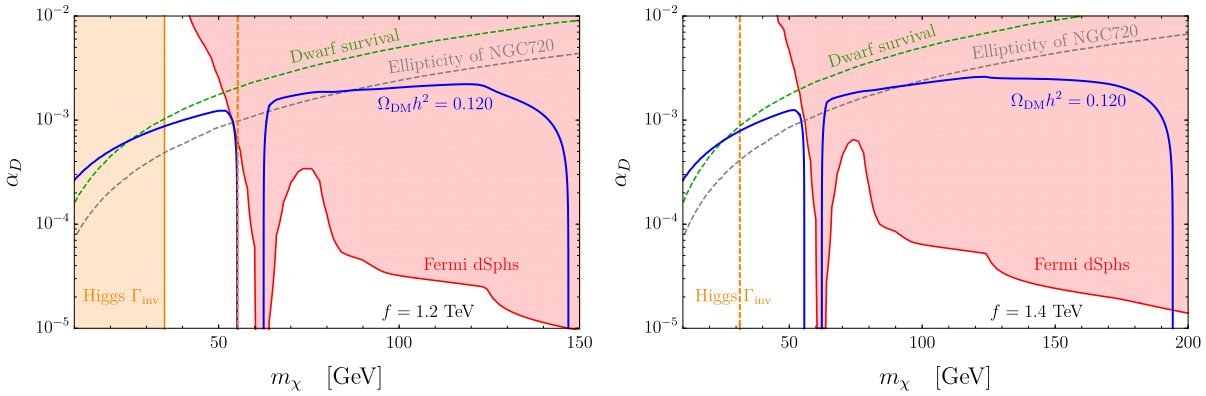

Figure 4.16: Parameter space of the model where the gauging of $U(1)_{\mathrm{DM}}$ gives the leading breaking of the DM shift symmetry, for $f = 1.2$ TeV (left panel) and $f = 1.4$ TeV (right panel). The coefficients of the effective Lagrangian are set to $c_d = 1$, $c_t^\chi = c_b^\chi = \lambda = 0$, $m_{\gamma_D} = 0$. The exclusions from Fermi dwarfs were drawn assuming that all of the observed DM is composed of χ particles, irrespective of the thermal value of the χ density predicted at each point in parameter space. The shaded orange region shows the exclusion from measurements of the Higgs invisible width at the time the results were published in [29]. The dashed orange line shows a more recent updated bound of $\mathrm{BR}(h \to \chi^*\chi) < 0.13$ [183].

recent study [196], where it was argued that it actually is significantly weaker than in the original calculation of [189]. Their result bounds the dark photon coupling to be

$$\alpha_D < 2.4 \times 10^{-3} \left(\frac{m_\chi}{100\ \mathrm{GeV}}\right)^{3/2}. \qquad \text{(ellipticity)} \tag{4.70}$$

The bound in [196] was derived for Dirac fermion DM, but it directly applies to our model, since the leading term of the self-scattering cross-section is the same for fermions and scalars.[23] However, there are several reasons [196] to take even this weaker and more conservative bound with caution, including the fact that it relies only on a single galaxy and that the measurement of the ellipticity is sensitive to unobservable initial conditions. E.g. a galaxy which has recently merged with another galaxy may have a sizeable ellipticity even in the presence of strong long-range self-interactions. For this reason we also show the next most stringent constraint, which is obtained by demanding that the MW dSphs have not evaporated until the present day as they traveled through the Galactic DM halo [197]. This gives a somewhat more robust bound than the ellipticity measurement, despite not being free from caveats either [196]. This bounds dark photon couplings of the size

$$\alpha_D < 5 \times 10^{-3} \left(\frac{m_\chi}{100\ \mathrm{GeV}}\right)^{3/2}. \qquad \text{(dwarf survival)} \tag{4.71}$$

A summary of the above discussion is shown in Figure 4.16 for two representative values of the symmetry breaking scale $f = 1.2, 1.4$ TeV. As mentioned before, the region $m_\chi > m_h/2$ is robustly ruled out by gamma ray observations from dSphs. In the low mass region the constraints from the ellipticity of NGC720 and the survival of dwarf galaxies yield the strongest bound. However, due to the aforementioned doubts on their robustness we do not view them as strict

[23] Notice that Figure 4 in [196] was drawn requiring $\Omega_X = 0.265$ for the DM density, instead of the correct $2\,\Omega_X = 0.265$. As a result, for $m_X < 200$ GeV (where the SE is negligible) their relic density contour should be multiplied by $\sqrt{2}$. We thank P. Agrawal for clarifications about this point.

$m_{\gamma_D} < 6 \times 10^{-4}$ eV	✓ / X	γ_D is dark radiation today, strong constraints from SE of $\chi\chi^* \to$ SM
6×10^{-4} eV $< m_{\gamma_D} \lesssim 3m_\chi/25$	X	γ_D is relativistic at freeze-out, ruled out by warm DM bounds/overabundant
$3m_\chi/25 < m_{\gamma_D} < m_\chi$	X	γ_D is non-relativistic at freeze-out, overabundant
$m_\chi \lesssim m_{\gamma_D} < 2m_\chi$	✓	both γ_D and χ are cold DM
$2m_\chi < m_{\gamma_D}$	✓	γ_D is unstable

Figure 4.17: Summary of the qualitatively different regions in the dark photon mass parameter space. In the second column we indicate with (✓) or (X) if the corresponding regions satisfy or conflict experimental constraints. The third column contains key features of the respective region.

exclusions but note that they will in the future be an important probe for DM self-interactions mediated by a dark photon. Self-interactions of this kind are also an interesting approach to solve small-scale issues of the collisionless cold DM paradigm [198]. A complementary probe are also invisible decays of the Higgs into DM, i.e. $h \to \chi^*\chi$, which can be measured at the LHC.[24] By the end of the high-luminosity phase the LHC will be sensitive to $f \lesssim 1.6$ TeV. Figure 4.16 shows two bounds from invisible Higgs decays: the shaded orange region corresponds to $\mathrm{BR}(h \to \chi^*\chi) < 0.24$ [199], which was the strongest bound available at the time these results were published in [29]. The dashed orange line shows a more recent updated bound of $\mathrm{BR}(h \to \chi^*\chi) < 0.13$ [183]. This updated bound essentially rules out the full remaining parameter space for $f = 1.2$ TeV.

4.5.2 Phenomenology for massive dark photon

The dark photon mass m_{γ_D} is a free parameter in our model. In the previous section we extensively studied the simplest scenario of a massless dark photon and now turn to a discussion on the massive case. The phenomenology crucially depends on the mass hierarchy of dark photon and DM. The region $m_{\gamma_D} < m_\chi$ is essentially ruled out, unless γ_D is light enough to still be relativistic today. A particularly interesting region is $m_\chi \leq m_{\gamma_D} \leq 2m_\chi$ as it leads to a two-component DM setup with novel properties. For $m_{\gamma_D} > 2m_\chi$ the dark photon is unstable and plays a subleading role in DM phenomenology. A summary of all qualitatively different regions in the dark photon mass parameter space is shown in Figure 4.17. Our analysis in the following is split into two parts: Section 4.5.2.A discusses the region of light dark photon masses $m_{\gamma_D} < m_\chi$, whereas Section 4.5.2.B concentrates on heavy dark photons with $m_{\gamma_D} > m_\chi$.

[24] The Higgs can also decay to $\gamma_D\gamma_D$ via a χ loop. The decay width for $m_{\gamma_D} = 0$ is $\Gamma(h \to \gamma_D\gamma_D) = m_h^3 \alpha_D^2 c_d^2 v^2 |F(\frac{m_h^2}{4m_\chi^2})|^2/(64\pi^3 f^4)$, where $F(\tau)$ is given in Eq. (I.F.17). Numerically, for $m_\chi < m_h/2$ this is negligible compared to $\Gamma(h \to \chi^*\chi)$, while for $m_\chi > m_h/2$ it is too small to be observable: e.g. for $m_\chi = 100$ GeV and $f = 1$ TeV we have $\Gamma(h \to \gamma_D\gamma_D) \sim 10^{-12}$ GeV.

A Light dark photon: $m_{\gamma_D} < m_\chi$

The abundance of light dark photons with $m_{\gamma_D} < m_\chi$ effectively freezes out simultaneously with the χ abundance. If the dark photon is still relativistic at DM freeze-out, which is approximately the case if its mass satisfies $m_{\gamma_D} \lesssim 3T_{\mathrm{fo}}^{\chi} \approx 3m_\chi/25$, it freezes out with the abundance n_{γ_D} of a relativistic species. After this there are no γ_D-number-changing interactions in equilibrium (the scattering $\gamma_D\chi \to (h^* \to f\bar{f})\chi$ is extremely suppressed) and therefore the number density simply dilutes due to the expansion of the universe. In order to estimate the abundance today we consider the ratio of the γ_D number density at freeze-out to the SM entropy density $s_{\mathrm{SM}} = (2\pi^2/45)g_{*s,\mathrm{vis}}T^3$. This ratio is $r_{\gamma_D} = n_{\gamma_D}/s_{\mathrm{SM}} = 45\,\zeta(3)g_{\gamma_D}/(2\pi^4 g_{*s,\mathrm{vis}}) \approx 0.01$, where we assumed that the dark and visible sectors are still in kinetic equilibrium at freeze-out, and took $g_{\gamma_D} = 3$, $g_{*s,\mathrm{vis}} \sim 80$. Since both n_{γ_D} and s_{SM} only change due to the expansion of the universe r_{γ_D} is conserved.[25] Assuming that the dark photon becomes non-relativistic as the universe cools, this allows us to estimate the energy density of the dark photon today $\Omega_{\gamma_D} = m_{\gamma_D} r_{\gamma_D} s_{\mathrm{SM}}$. We have to require that this is smaller than the observed DM abundance, what yields

$$\Omega_{\gamma_D} < \Omega_{\mathrm{DM}} \qquad \to \qquad m_{\gamma_D} < 40\ \mathrm{eV} \qquad \text{(dark photon over-abundance)} \tag{4.72}$$

where we used $g_{*s,\mathrm{vis}}(T_0) = 3.91$.

Note that if the dark photon freezes out relativistically it constitutes a hot DM component in addition to the cold component made up by χ. Hot or non-cold DM in general is strongly constrained and can at most constitute a small fraction of the total DM, since it can free stream and wash out small-scale fluctuations. A recent bound on the fraction of the non-cold DM component f_{ncdm} was derived in [200], assuming a thermal relic, by combining observations of CMB, data from baryon acoustic oscillations (BAO) and the number of dwarf satellite galaxies of the MW. The temperature of the dark photon in our model at late times can be obtained from entropy conservation $T_{\gamma_D}/T = [g_{*s,\mathrm{vis}}(T)/g_{*s,\mathrm{vis}}(T_{\mathrm{dec}})]^{1/3} \approx 0.37$, where T is the SM photon temperature and we took $g_{*s,\mathrm{vis}}(T_{\mathrm{dec}}) = 75.75$. The fraction of non-cold DM is

$$f_{\mathrm{ncdm}} \simeq \frac{\Omega_{\mathrm{ncdm}}}{\Omega_{\mathrm{DM}}} = \frac{\rho_{\gamma_D,0}}{\rho_{\mathrm{crit},0}\Omega_{\mathrm{DM}}} = \frac{r_{\gamma_D} s_{\mathrm{SM},0}}{\rho_{\mathrm{crit},0}\Omega_{\mathrm{DM}}} \begin{cases} \frac{\pi^4 T_{\gamma_D,0}}{30\,\zeta(3)} \\ m_{\gamma_D} \end{cases} \approx \begin{cases} 5.8\times 10^{-6} & m_{\gamma_D} \lesssim 3\,T_{\gamma_D,0} \\ 0.024\left(\frac{m_{\gamma_D}}{1\,\mathrm{eV}}\right) & m_{\gamma_D} \gtrsim 3\,T_{\gamma_D,0} \end{cases} \tag{4.73}$$

with the first (second) expression corresponds to the case of the dark photon being still relativistic (non-relativistic) today and $3\,T_{\gamma_D,0} \approx 2.6\times 10^{-4}$ eV. In the first equality we assumed $\Omega_{\mathrm{ncdm}} \ll \Omega_{\mathrm{DM}}$, which is justified since the non-cold component is constrained to be small. Figure 4.18 compares the prediction of our model in Eq. (4.73) with the bounds in [200], after correcting for the fact that it was assumed in [200] that the non-cold relic has the same temperature as the SM neutrinos (the mass has to be rescaled by $T_{\gamma_D}/T_\nu \approx 0.52$). From this we can infer a 95% CL bound on the dark photon bound

$$m_{\gamma_D} < 6\times 10^{-4}\ \mathrm{eV}, \qquad (\mathrm{CMB} + \mathrm{BAO} + \mathrm{MW\ satellites}) \tag{4.74}$$

which roughly requires the dark photon to be relativistic today. Note that for dark photons which satisfy the simple overclosure bound in Eq. 4.72 the bound is mainly driven by CMB and BAO. The MW satellite count is only relevant for larger masses of the order $m_{\gamma_D} \geq$ keV [200]. For very light dark photons, i.e. $m_{\gamma_D} \leq 1$ eV (the dark photon still behaves as radiation at photon decoupling), the resulting bound is stronger than the one from ΔN_{eff} alone. This

[25] Before kinetic decoupling of the dark and visible sectors only $n_{\gamma_D}/s_{\mathrm{tot}}$ is conserved, where s_{tot} is the total entropy, but $s_{\mathrm{tot}} \approx s_{\mathrm{SM}}$ since $g_{\gamma_D} \ll g_{*s,\mathrm{vis}}$.

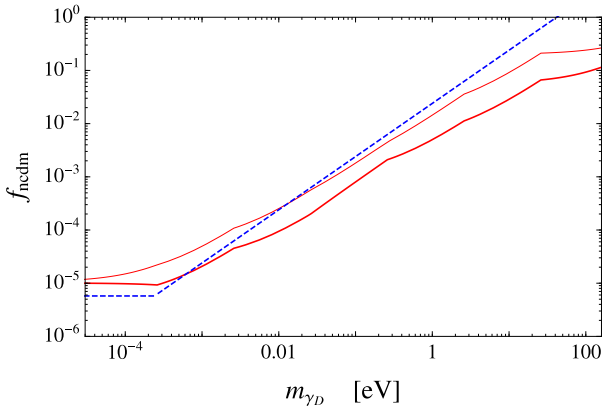

Figure 4.18: The fraction of non-cold DM embodied by the dark photon as predicted by our model in Eq. (4.73) (dashed blue), compared to the 2σ (thick red) and 3σ (thin red) upper bounds from [200]. This Figure was adopted from [29].

improvement is due to the inclusion of BAO data, which is sensitive to the suppression of the matter power spectrum on small-scales caused by the free streaming of the hot DM component.

Dark photons, which satisfy the bound in Eq. (4.74), are still relativistic today and their mass can be neglected. Thus the DM phenomenology for $m_{\gamma_D} = 0$ in Section 4.5.1 still applies. In particular χ annihilation is unaffected, including SE, as the force mediated by the dark photon is effectively long-range: its wavelength is much larger than the Bohr radius of the $(\chi^*\chi)$ bound state $m_{\gamma_D} \ll \alpha_D m_\chi/2$. Additionally Eq. (4.66) is still valid, since the average momentum transfer is much larger than the mediator mass, i.e. $m_{\gamma_D} \ll m_\chi v_{\rm rel}/2$ [201]. The ellipticity bound is affected by the dark photon mass through the IR cutoff from integrating the DM scattering cross-section in Eq. (4.68). While this was taken to be the inter-particle distance $\lambda_P = (m_\chi/\rho_\chi)^{1/3} \sim 5$ cm (for a DM mass of $m_\chi = 100$ GeV and density $\rho_\chi \sim 1$ GeV/cm^3 in the DM-dominated outer region (r $\geq$ 6 kpc) of NGC720 [202]) in the massless case, this has to be $1/m_{\gamma_D}$ if $m_{\gamma_D} > 1/\lambda_P \sim 4 \times 10^{-6}$ eV in the massive case. However, the dependence on the IR cutoff is only logarithmic and thus the bound discussed for m_{γ_D} is essentially unchanged, what also applies to the bound from dwarf galaxy survival.[26]

The last mass region $3T_{\rm fo}^\chi \approx 3m_\chi/25 \lesssim m_{\gamma_D} < m_\chi$ corresponds to the dark photon being non-relativistic during freeze-out. This scenario is ruled out as the dark photon is always overabundant.

B Heavy dark photon: $m_\chi < m_{\gamma_D}$

In the region $m_\chi \lesssim m_{\gamma_D} < 2m_\chi$ the dark photon is still stable and freezes out non-relativistic. This region therefore naturally features a two-component DM model. The simplest way to explain the DM phenomenology in this part of parameter space is to fix a value for f and $m_\chi > m_\chi^{(f)}$, s.t. DM consisting of χ alone would be under-abundant. The remaining part of DM consists of the heavier dark photon. Requiring that the combination of dark photons and χ gives the observed relic abundance fixes a contour in the $(m_{\gamma_D}/m_\chi, \alpha_D)$ plane, which we show in the

[26] The small dark photon masses in Eq. (4.74) are legitimate from an EFT standpoint. Still, it has recently been conjectured [203] that quantum gravity forbids arbitrarily small Stückelberg masses: local quantum field theory would break down at $\Lambda_{\rm UV} \sim (m_{\gamma_D} M_{\rm Pl}/g_D)^{1/2}$. Taking $g_D \sim 0.1$ as needed to obtain the observed relic density for χ, Eq. (4.74) corresponds then to a troublesome $\Lambda_{\rm UV} \lesssim 4$ TeV. The conjecture does not apply, however, if m_{γ_D} arises from a dynamical symmetry breaking [203]. This topic is currently under debate [204].

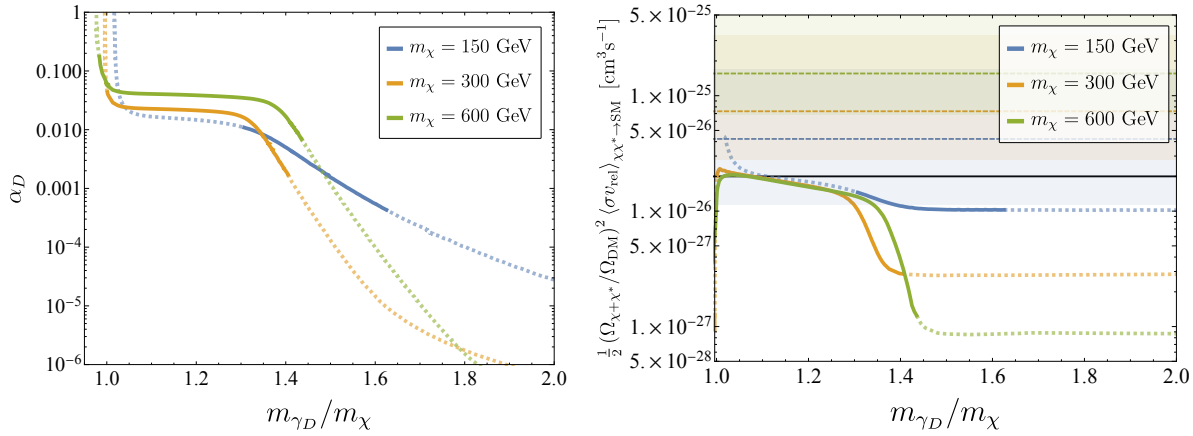

Figure 4.19: *Left panel:* contours in the $(m_{\gamma_D}/m_\chi, \alpha_D)$ plane where the sum of the χ and γ_D densities matches the observed total DM density, $\Omega_{\chi+\chi^*} + \Omega_{\gamma_D} = \Omega_{\mathrm{DM}}$, assuming $f = 1$ TeV and for representative values of $m_\chi > m_\chi^{(f)} \approx 122$ GeV. The solid portions highlight the range of α_D where m_χ can be obtained from dark photon loops cut off at 2.5 TeV $< m_\rho < 4\pi f$ (see Eq. (I.D.25)), where the lower bound comes from the S parameter, $\widehat{S} \sim m_W^2/m_\rho^2 \lesssim 10^{-3}$ (see e.g. [122]). *Right panel:* effective cross-section for present-day DM annihilation to SM particles, calculated along the relic density contours in the left panel. Also shown are the observed 95% CL limits from dSphs in the WW channel [145] (dashed lines), together with the 95% CL uncertainties on the expected limits (colored regions). For reference, the black solid line shows $\langle\sigma v_{\mathrm{rel}}\rangle_{\mathrm{can}}$, the cross-section expected for a single thermal relic that annihilates entirely to SM particles. This Figure was first published in [29].

left panel of Figure 4.19 for $f = 1$ TeV and various values of m_χ. The exact relic abundances were computed by numerically solving the coupled Boltzmann equations of the $\gamma_D - \chi$ system using `micrOMEGAs` [123]. In order to gain a qualitative understanding of Figure 4.19-left, we assume as a first order approximation that the freeze-outs of χ and γ_D are decoupled. In this approximation the freeze-out of χ is completely determined by the annihilation into SM via the derivative portal $\chi^*\chi \to$ SM, thus completely fixing its abundance in terms of f and m_χ. In some parts of the parameter space this approximation receives important corrections, which we will discuss below.

Let us first focus on the contour for $m_\chi = 300$ GeV in the left panel of Figure 4.19. This scenario consists of four qualitatively different regions:

(a) The non-degenerate region, $2m_\chi - m_h \approx 1.6\, m_\chi < m_{\gamma_D} < 2m_\chi$. The dark photon freeze-out is determined by the semi-annihilation process $\gamma_D h \to \chi\chi^*$, which is kinematically allowed at zero temperature, since $m_{\gamma D} + m_h > 2m_\chi$. This dominates over the pair annihilation into χ, i.e. $\gamma_D\gamma_D \to \chi^*\chi$, as for $m_{\gamma_D} > m_h$ the dark photon abundance is exponentially suppressed compared to the Higgs abundance, s.t. the probability of a dark photon to find a Higgs to annihilate with is exponentially larger than to find another dark photon. This implies that the shape of the relic abundance contour is determined by the relation $n_h^{\mathrm{eq}} \langle\sigma_{\gamma_D h\to\chi\chi^*} v_{\mathrm{rel}}\rangle =$ constant, where the LHS is evaluated at the γ_D freeze-out temperature, $T_{\gamma_D}^{\mathrm{fo}} \approx m_{\gamma_D}/25$, and the thermally averaged cross-section is given in Eq. (I.F.20). For lighter dark photons, i.e. decreasing m_{γ_D}/m_χ the non-relativistic Higgs number density follows its equilibrium value n_h^{eq} and gets exponentially suppressed. This has to be compensated by an exponentially growing dark photon cou-

pling, s.t. $\alpha_D \propto \exp\left(\frac{m_h}{m_\chi}\frac{25}{m_{\gamma_D}/m_\chi}\right)$, where we dropped subleading power corrections. Note that the importance of semi-annihilation processes, in which the number of DM particles is changed by one unit in contrast to the more common two units in typical pair annihilation, was discussed first in [205].

(b) The intermediate region, $1.3\,m_\chi \lesssim m_{\gamma_D} \lesssim 1.6\,m_\chi \approx 2m_\chi - m_h$, does not allow the semi-annihilation at zero temperature, since $m_{\gamma D} + m_h < 2m_\chi$. However, semi-annihilation $\gamma_D\gamma_D \to \chi^*\chi$ is still the dominant process to set the relic abundance. In this case the shape of the relic abundance contour can be determined using detailed balance. It is given by the relation $n_h^{\rm eq}\langle\sigma_{\gamma_D h\to\chi\chi^*}v_{\rm rel}\rangle = (n_\chi^{\rm eq\,2}/n_{\gamma_D}^{\rm eq})\langle\sigma_{\chi\chi^*\to\gamma_D h}v_{\rm rel}\rangle = \text{constant}$, where the LHS is evaluated at $T_{\gamma_D}^{\rm fo} \approx m_{\gamma_D}/25$ and the cross-section can be found in Eq. (I.F.21). The Higgs is now slightly less abundant than the dark photon, which has to be compensated by faster increase of the dark photon coupling α_D, which depends exponentially on m_{γ_D}/m_χ. The growth is therefore faster than in the non-degenerate region and is of the form $\alpha_D \propto \exp\left[\left(2-\frac{m_{\gamma_D}}{m_\chi}\right)\frac{25}{m_{\gamma_D}/m_\chi}\right]$, where power corrections were neglected.

(c) The degenerate region, $m_\chi \lesssim m_{\gamma_D} \lesssim 1.3\,m_\chi$. As m_{γ_D}/m_χ decreases further the semi-annihilation is more and more Boltzmann suppressed and the pair annihilation $\gamma_D\gamma_D \to \chi\chi^*$ becomes the dominant process to maintain equilibrium. Therefore the dark photon freezes out when the annihilation into $\chi^*\chi$ goes out of equilibrium. This implies that the relic abundance contour is now approximately determined by $\langle\sigma_{\gamma_D\gamma_D\to\chi\chi^*}v_{\rm rel}\rangle = \text{constant}$, where the cross-section is given in Eq. (I.F.19). The annihilation cross-section $\langle\sigma_{\gamma_D\gamma_D\to\chi\chi^*}v_{\rm rel}\rangle$ increases only as α_D^2, which explains why the variation in α_D is very slow and the contour appears almost flat in this part of parameter space, compared to the regions dominated by semi-annihilations. Note that the evolution of the χ and γ_D number densities is tightly coupled in this region. The annihilation $\gamma_D\gamma_D \to \chi\chi^*$ injects a large number of χ particles, leading to a larger χ abundance as in the simplified decoupling picture. This interesting type of system was first studied numerically in [206]. Here we provide analytical insight into its dynamics. After the yields Y_{χ,γ_D} become much larger than their equilibrium values, they obey the simplified Boltzmann equations ($x \equiv m_\chi/T$)

$$\widehat{\lambda}^{-1}x^2\,\frac{dY_\chi}{dx} = -\langle\sigma v_{\rm rel}\rangle_{\rm SM}Y_\chi^2 + \tfrac{1}{2}\langle\sigma v_{\rm rel}\rangle_{\gamma_D\gamma_D}Y_{\gamma_D}^2 \tag{4.75a}$$

$$\widehat{\lambda}^{-1}x^2\,\frac{dY_{\gamma_D}}{dx} = -\langle\sigma v_{\rm rel}\rangle_{\gamma_D\gamma_D}Y_{\gamma_D}^2 \tag{4.75b}$$

where $\widehat{\lambda} \equiv (2\sqrt{10}\,\pi/15)(g_{*s}m_\chi M_{\rm Pl}/\sqrt{g_*})$, while $\langle\sigma v_{\rm rel}\rangle_{\rm SM}$ refers to $\chi\chi^* \to$ SM and $\langle\sigma v_{\rm rel}\rangle_{\gamma_D\gamma_D}$ to $\gamma_D\gamma_D \to \chi\chi^*$. At $x \gg 1$ the analytic solution of the system satisfies

$$\frac{1}{a_\sigma}\left(\frac{2Y_\chi}{Y_{\gamma_D}}\right)^2 \simeq 1 + \tfrac{1}{2}\left(a_\sigma + \sqrt{a_\sigma(a_\sigma+4)}\right), \qquad a_\sigma \equiv \frac{\langle\sigma v_{\rm rel}\rangle_{\gamma_D\gamma_D}}{\langle\sigma v_{\rm rel}\rangle_{\rm SM}/2}\,, \tag{4.76}$$

where a_σ is approximately constant, since both processes are s-wave. In order to obtain this result we have made the ansatz $Y_\chi = C\,Y_{\gamma_D}$ with C being a constant, which is motivated by numerical results in the $x \gg 1$ region. Plugging the ansatz into the Eq. (4.75), yields a quadratic equation for the constant C

$$C^2 - \frac{1}{2}a_\sigma C - \frac{1}{4}a_\sigma = 0\,, \tag{4.77}$$

which has the solutions

$$C_\pm = \frac{1}{4}\left(a_\sigma \pm \sqrt{a_\sigma(a_\sigma+4)}\right). \tag{4.78}$$

The negative root yields $dY_\chi/dx > 0$ and is therefore unphysical and has to be dropped. The positive root directly leads to Eq. (4.76). In the $m_\chi = 300, 600$ GeV examples $a_\sigma \ll 1$ and the RHS in Eq. (4.76) asymptotes 1. Taking into account the $1/a_\sigma$ factor on the LHS we immediately see that this expresses the equality of fluxes entering and leaving the χ population, i.e. $Y_{\gamma_D}^2 \langle \sigma v_{\mathrm{rel}} \rangle_{\gamma_D \gamma_D} = (2Y_\chi)^2 \langle \sigma v_{\mathrm{rel}} \rangle_{\mathrm{SM}}/2$. Thus the χ density is only slightly larger than in the simplified decoupling limit $2n_\chi/n_{\gamma_D} \simeq a_\sigma^{1/2}$. However, the situation is different for $m_\chi = 150$ GeV. In this case a_σ is of $\mathcal{O}(1)$ and the annihilation into the SM is consequently not as efficient. This results in an accumulation of χ particles, due to the larger annihilation rate of $\gamma_D \gamma_D \to \chi^* \chi$, s.t. the relative χ abundance is larger by $2n_\chi/n_{\gamma_D} \simeq$ few.

(d) The very degenerate and forbidden [207] region, $m_{\gamma_D} \lesssim m_\chi$. The dark photon freeze-out is still set by $\gamma_D \gamma_D \to \chi^* \chi$, but this processes becomes increasingly kinematically suppressed when m_{γ_D}/m_χ approaches and eventually slightly passes below 1. This has to be compensated by a rapid increase of α_D.

While we have mainly focused on $m_\chi = 300$ GeV in the previous discussion, the qualitative features of the relic abundance contour are very similar for $m_\chi = 600$ GeV. For $m_\chi = 150$ GeV the intermediate region is absent since $2m_\chi - m_h \approx 1.2 m_\chi$ and we observe a direct transition from the non-degenerate to the degenerate region.

The right panel of Figure 4.19 shows the present-day effective annihilation cross-section into the SM along the relic density contours shown in the left panel. While we have included all allowed channels, the cross-section is always dominated by $\chi^* \chi \to$ SM with the subleading channels, such as $\gamma_D \chi \to h \chi$ and $\gamma_D \gamma_D \to$ SM, the latter of which proceeds at one loop, contributing at the sub-percent level.[27] We observe two different regimes: in the non-degenerate regime where the decoupling of χ and γ_D can be treated as being independent from each other, the effective cross-section is reduced compared to the standard thermal value $\langle \sigma v_{\mathrm{rel}} \rangle_{\mathrm{can}} \approx 2 \times 10^{-26}\,\mathrm{cm}^3\,\mathrm{s}^{-1}$ by a factor $\langle \sigma v_{\mathrm{rel}} \rangle_{\mathrm{can}} / (\frac{1}{2} \langle \sigma v_{\mathrm{rel}} \rangle_{\chi \chi^* \to \mathrm{SM}}) < 1$. This suppression can be as large as one order of magnitude for $m_\chi = 600$ GeV. In the opposite scenario, i.e. the degenerate region, where there is a significant injection of χ from dark photon annihilation, the effective cross-section is numerically close to $\langle \sigma v_{\mathrm{rel}} \rangle_{\mathrm{can}}$.

The last remaining dark photon mass region is $2m_\chi < m_{\gamma_D}$. In this case the dark photon is unstable and decays into χ particles with decay width $\Gamma(\gamma_D \to \chi^* \chi) = (\alpha_D m_{\gamma_D}/12)(1 - 4m_\chi^2/m_{\gamma_D}^2)^{3/2}$. This process and its inverse maintain chemical equilibrium in the dark sector until the inverse decay rate drops below the expansion rate of the universe, which roughly happens when $H \sim \langle \Gamma \rangle n_{\gamma_D}/n_\chi$. At this time the ratio of number densities is of the size

$$\frac{n_{\gamma_D}}{n_\chi} \sim \frac{H}{\Gamma} \sim \frac{10\,T^2}{M_{\mathrm{Pl}} \alpha_D m_{\gamma_D}} < 10^{-12} \left(\frac{m_{\gamma_D}}{100\ \mathrm{GeV}} \right) \left(\frac{10^{-3}}{\alpha_D} \right), \tag{4.79}$$

where we assumed that $T < m_{\gamma_D}$ at this point, and neglected $O(1)$ factors. The impact of the subsequent decay of dark photons on the χ abundance is negligible. Thus the full DM abundance is set by the annihilation of χ into the SM. In this region the only phenomenological impact of the dark photon is the generation of the mass for χ at one loop, which we estimated in Eq. (4.63). At low energies this constitutes a perfect realization of the pure pNGB DM scenario, which was discussed in Section 3.1.

[27] Note that due to the large mass of the dark photon, in this case the Sommerfeld enhancement of the $\chi \chi^* \to$ SM annihilation is negligible.

Chapter 5

pNGB dark matter at colliders

In the previous chapters we have argued that pNGB DM is a compelling WIMP candidate. It is not only naturally compatible with the strong constraints from direct detection experiments, as we have discussed in Section 3.1, but is also well-motivated by theories in which the DM arises as a pNGB together with the Higgs, thus solving both the naturalness and DM problem. In Chapter 3 we discussed general features of pNGB DM from an EFT point of view, motivated by realizations in the CH framework. We also presented explicit CH models with complex scalar pNGB DM, based on the $SO(7)/SO(6)$ symmetry breaking structure, in Chapter 4 and verified that the assumptions we made in Chapter 3 are justified. But pNGB DM does not only appear in the realm of CH models. Simple alternative realization, in which only the DM is a pNGB and not the Higgs, can be obtained by adding a complex scalar to the SM with a $U(1)$ invariant potential, which is softly broken by the mass term of the scalar [129, 130] (see the discussion in Section 3.3).

The irreducible feature of all these models is the derivative Higgs portal. For a real scalar ϕ as DM candidate, stabilized by a Z_2 symmetry, the relevant Lagrangian with the derivative portal between the DM and Higgs is given by

$$\mathcal{L}_{\text{derivative}} = \mathcal{L}_{\text{SM}} + \frac{1}{2}(\partial_\mu \phi)^2 - \frac{1}{2} m_\phi^2 \phi^2 + \frac{c_d}{2f^2} \partial_\mu \phi^2 \partial^\mu |H|^2, \tag{5.1}$$

where H is the Higgs doublet, f the common decay constant of the pNGBs and c_d an $\mathcal{O}(1)$ coefficient. As we have discussed at length in Chapter 3, this gives a viable DM candidate for $m_\chi \sim \mathcal{O}(100)$ GeV and $f = \mathcal{O}(1)$ TeV, which is practically invisible in direct detection experiments.

In this chapter we want to probe the derivative Higgs portal at colliders, which constitutes one of the most important direct tests of this class of models due to the structural suppression of direct detection signals. Here we study the derivative Higgs portal in ϕ pair production via an s-channel Higgs boson in the vector boson fusion (VBF) production channel, which is expected to be the most sensitive channel both at hadron and lepton colliders (see Section 5.1). The corresponding Feynman diagram is shown in Figure 5.1. Our study concentrates on the well-motivated Higgs off-shell region $m_\chi \geq m_h/2$. In the following we assume that ϕ escapes the detector and manifests as missing momentum.

Throughout the whole analysis we will also consider the marginal (or renormalizable) Higgs portal [51–53]

$$\mathcal{L}_{\text{marginal}} = \mathcal{L}_{\text{SM}} + \frac{1}{2}(\partial_\mu \phi)^2 - \frac{1}{2} M_\phi^2 \phi^2 - \frac{\lambda}{2} \phi^2 |H|^2 \,, \tag{5.2}$$

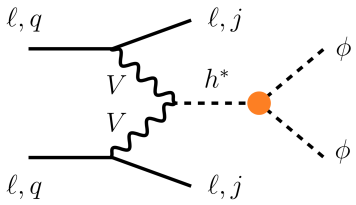

Figure 5.1: Feynman diagram for the signal studied in this work. The orange dot represents either of the portals in Eqs. (5.1) and (5.2). This Figure was taken from [31].

which serves as an important term of comparison.[1] Even though ϕ in the marginal Higgs portal model constitutes a valid DM candidate, the model is mostly ruled out by direct detection [54]. However, such new scalars are not only discussed in the context of DM, but may also appear in models addressing electroweak baryogenesis [208] or naturalness. In particular in neutral naturalness scenarios scalar top partners, neutral under the SM gauge symmetries, couple to the Higgs with coupling strength y_t^2 [209, 210] leading to an interaction of the form $\mathcal{L} \ni -y_t^2|H|^2(|\tilde{u}_1^c|^2 + |\tilde{u}_2^c|^2)$, which can be probed through VBF.

	HL-LHC	CLIC 1.5	HE-LHC	CLIC 3	FCC 100	μC 6	μC 14
Center of mass energy [TeV]	14	1.5	27	3	100	6	14
Integrated luminosity [ab^{-1}]	3	1.5	15	3	30	6	14

Table 5.1: Collider parameters used in our off-shell Higgs projections.

We start this chapter with a short discussion of the on-shell region and some selected previous studies in Section 5.1. Afterwards we describe our analysis in Section 5.2, which we performed for current and future lepton and hadron colliders. A summary of all colliders we consider in this work, together with their center of mass energies and integrated luminosities, is shown in Table 5.1. Finally in Section 5.3 we present our results.

This chapter is based on results which were published in [31],[2] from where all Figures and parts of the text were taken.

5.1 The on-shell Higgs portal and previous studies

Let us start with a brief discussion of the reach on light DM with $m_\phi \leq m_h/2$ in Higgs mediated DM production. In this case the DM constitutes an invisible decay channel of the Higgs, s.t. the most sensitive probes of this scenario are searches for invisible decays of the on-shell Higgs boson. Note that the on-shell Higgs-DM coupling, and therefore the analysis of on-shell decays, is not sensitive to the specific portal. The currently strongest bounds on the branching ratio of Higgs decays into invisible particles[3] at the LHC originate from VBF production [211], see e.g. Refs. [162, 212] for early analyses. A significant improvement of the sensitivity will be obtained in future Higgs factories by exploiting the Zh production channel and an even stronger bound

[1] Note that the normalization of the marginal portal coupling in Eq. (5.2) is different than in Chapter 3 and Chapter 4. Furthermore the physical mass of the scalar is $m_\phi^2 = M_\phi^2 + \lambda v^2/2$, where $v \approx 246$ GeV.

[2] [31]: M. Ruhdorfer, E. Salvioni and A. Weiler, *A Global View of the Off-Shell Higgs Portal.*

[3] Notice that the SM predicts an invisible Higgs branching fraction of $\mathrm{BR}(h \to ZZ^* \to 4\nu)_{\mathrm{SM}} \approx 1.1 \cdot 10^{-3}$.

can be achieved at FCC-hh. A bound on BR($h \to$ inv) can be straightforwardly converted to a limit on λ or $f/c_d^{1/2}$ by using the expression for the decay width of the Higgs into DM

$$\Gamma(h \to \phi\phi) = \frac{v^2}{32\pi m_h}\Big(\lambda - c_d \frac{m_h^2}{f^2}\Big)^2 \Big(1 - \frac{4m_\phi^2}{m_h^2}\Big)^{1/2}. \tag{5.3}$$

In Table 5.2 we summarize the current and projected sensitivities to BR($h \to$ inv) and report the corresponding bounds on λ and $f/c_d^{1/2}$.

	LHC current [183]	HL-LHC	ILC 250 [213]	FCC-ee 240 [213]	FCC-hh [214]
	(VBF)	VBF [215] [Zh] [184]	(Zh)	(Zh)	(inclusive)
BR($h \to$ inv)	0.13	0.035 [0.08]	$1.3 \cdot 10^{-3}$	$8 \cdot 10^{-4}$	$2.5 \cdot 10^{-4}$
$f/c_d^{1/2}$ [TeV]	1.2	1.7 [1.3]	3.8	4.3	5.8
λ [10^{-2}]	1.1	0.55 [0.86]	0.10	0.082	0.046

Table 5.2: 95% CL exclusion limits on the coefficients of the derivative and marginal Higgs portal operators, obtained from *on-shell* invisible Higgs decays, assuming $m_\phi \ll m_h/2$. See text for details.

Heavier DM with $m_\phi > m_h/2$ has to be produced through an off-shell Higgs. In contrast to the on-shell region, the momentum dependence of the derivative portal coupling has an important impact on the signal kinematic distributions. Hence one cannot simply recast searches for DM through the marginal Higgs portal coupling, but a dedicated analysis is required, which we will perform in Section 5.2 for VBF production. Note that [216] previously considered the derivative Higgs portal in the monojet channel at the LHC, but no results were provided for the theory in Eq. (5.1). Instead they considered an extended model with momentum-dependent interactions, finding increased sensitivity in comparison to the momentum-independent case. In our analysis of the VBF channel we confirm this behavior, see in particular Figure 5.7.

While there is no previous dedicated collider analysis of the derivative Higgs portal model of Eq. (5.1), there exist several studies of the off-shell marginal Higgs portal model in Eq. (5.2). The sensitivity to λ at lepton colliders was analyzed in [213] for $\sqrt{s} \leq 1$ TeV, where Zh associated production is the dominant channel (see also [217, 218] for related studies), and in [219] for $\sqrt{s} = 1, 5$ TeV, considering ZZ fusion production.[4] The sensitivity at LHC and FCC-hh was examined in [1], considering the VBF, monojet and $t\bar{t}h$ production modes.

In Section 5.2 and 5.3 we study the VBF production channel for the derivative and marginal Higgs portal at lepton and hadron colliders. The VBF channel is the dominant production mode at lepton colliders for $\sqrt{s} \gtrsim 1$ TeV and was found to be superior to monojet and $t\bar{t}h$ at hadron colliders [1]. We derive the first collider bounds on the derivative Higgs portal and provide projections for a wide range of future lepton and hadron colliders (see Table 5.1). Our second goal is to extend previous findings for the marginal Higgs portal and include high-energy lepton collider proposals, such as CLIC and a muon collider. Additionally we perform a refined analysis for hadron colliders with improved background predictions and we also assess the impact of trigger thresholds on missing transverse energy (MET).

[4] At lepton colliders WW fusion leads to an undetectable final state if ϕ is invisible, hence one must rely on ZZ fusion.

5.2 The off-shell Higgs portal in vector boson fusion

Let us now consider ϕ pair production via VBF in the off-shell Higgs regime, i.e. for $m_\phi \geq m_h/2$. This process proceeds through the Feynman diagram in Figure 5.1. The cross-section for V fusion ($V = W, Z$) can be written as

$$\sigma(f_1 f_2 \to \phi\phi f_1' f_2')[s] = \int_{4m_\phi^2/s}^1 d\tau\, \hat{\sigma}_{VV\to\phi\phi}(\tau s)\, \mathcal{C}_{V_L V_L}^{f_1 f_2}(\tau), \qquad \tau \equiv \hat{s}/s\,, \tag{5.4}$$

where $\hat{s} = M_{\phi\phi}^2$. The parton luminosity is given by

$$\mathcal{C}_{V_L V_L}^{f_1 f_2}(\tau) = \int_\tau^1 \frac{dx}{x} f_{V_L/f_1}(x) f_{V_L/f_2}(\tau/x), \tag{5.5}$$

where we only include the parton distribution functions (PDFs) for the longitudinal polarizations of the vector bosons, since only these couple to the Higgs. In the limit $\hat{s} \gg m_V^2$ they read [220]

$$f_{V_L/f}(x) = \frac{(C_v^f)^2 + (C_a^f)^2}{4\pi^2} \frac{1-x}{x} \tag{5.6}$$

where for the W, $C_v^f = -C_a^f = g/(2\sqrt{2})$, and for the Z, $C_v^f = g_Z(T_L^{3f}/2 - s_w^2 Q^f)$ and $C_a^f = -g_Z T_L^{3f}/2$. Therefore

$$\mathcal{C}_{W_L W_L}(\tau) = \frac{g^4}{256\pi^4\tau}\left[2(\tau-1) - (\tau+1)\log\tau\right], \qquad \frac{\mathcal{C}_{Z_L Z_L}^{f_1 f_2}}{\mathcal{C}_{W_L W_L}} = \frac{R_{f_1} R_{f_2}}{4c_w^4} \equiv \mathcal{R}_w^{f_1 f_2} \tag{5.7}$$

where $R_f = 4(T_L^{3f})^2 - 8 s_w^2 T_L^{3f} Q^f + 8 s_w^4 (Q^f)^2$. The partonic cross-sections for the derivative and marginal Higgs portal are

$$\begin{aligned}
\hat{\sigma}_{VV\to\phi\phi}^{\text{deriv}}(\hat{s}) &= \frac{1}{32\pi}\frac{c_d^2\,\hat{s}}{f^4}\left(1 - \frac{m_h^2}{\hat{s}}\right)^{-2}\left(1 - \frac{4m_\phi^2}{\hat{s}}\right)^{1/2}, \\
\hat{\sigma}_{VV\to\phi\phi}^{\text{marg}}(\hat{s}) &= \frac{1}{32\pi}\frac{\lambda^2}{\hat{s}}\left(1 - \frac{m_h^2}{\hat{s}}\right)^{-2}\left(1 - \frac{4m_\phi^2}{\hat{s}}\right)^{1/2},
\end{aligned} \tag{5.8}$$

where we took the high-energy limit $\hat{s} \gg m_V^2$. Notice that at high energies the derivative portal is enhanced w.r.t. the marginal portal by $\hat{\sigma}^{\text{deriv}}/\hat{\sigma}^{\text{marg}} \propto \hat{s}^2$. With this theoretical background we will first describe our analysis at high-energy lepton colliders in Section 5.2.1, before turning to hadron colliders in Section 5.2.2.

5.2.1 High-energy lepton colliders

At lepton colliders the full center of mass energy of the collider is at our disposal in the collision, apart from initial state radiation effects, which we will neglect in the following. Assuming high energies $\hat{s} \gg m_h^2$, we can obtain an analytic result for the integral in Eq. (5.4). The resulting cross-section for the derivative portal is given by

$$\sigma(e^- e^+ \to \phi\phi e^- e^+) = \frac{\mathcal{R}_w^{e\bar{e}} g^4 c_d^2\, s}{49152\pi^5 f^4}\left[\frac{3}{2} - \frac{2m_\phi^2}{s}\left(3\log^2\frac{s}{m_\phi^2} - 6\log\frac{s}{m_\phi^2} + 12 - \pi^2\right) + O(m_\phi^4/s^2)\right], \tag{5.9}$$

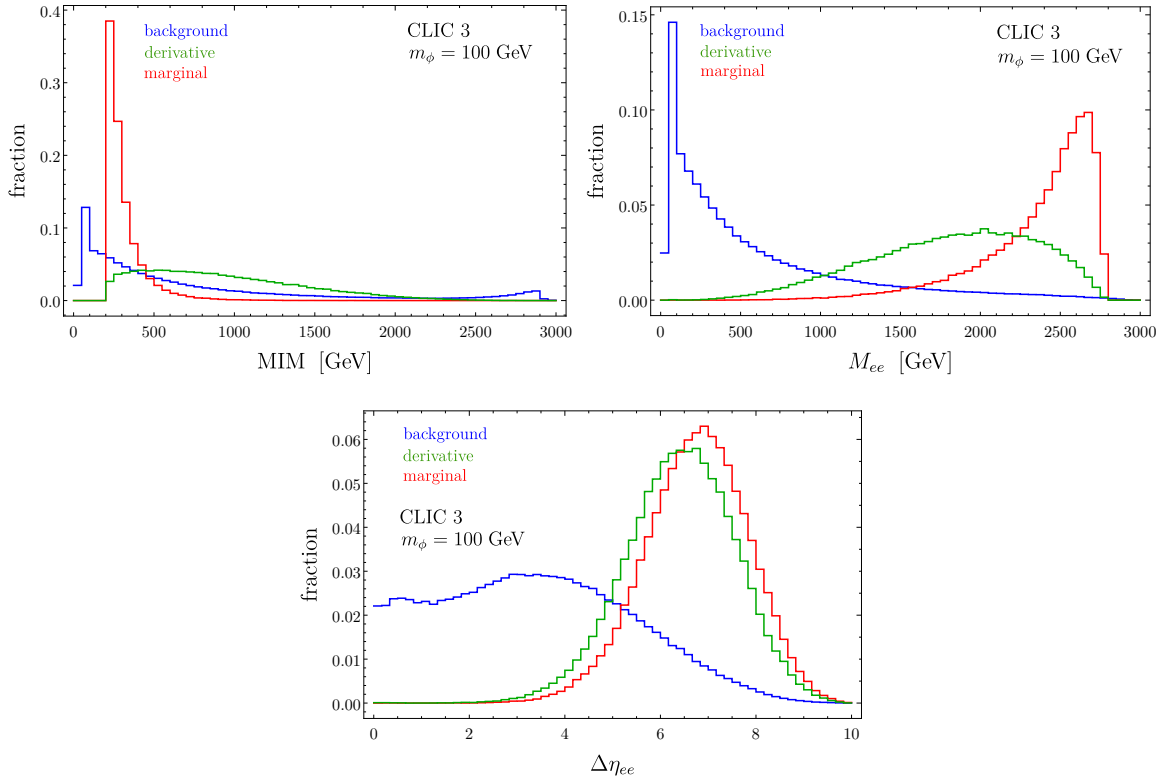

Figure 5.2: Normalized distributions for the signals and background at CLIC with $\sqrt{s} = 3$ TeV. The ϕ mass is set to 100 GeV. This Figure was previously published in [31]

where $\mathcal{R}_w^{e\bar{e}} \approx 0.11$ and we have expanded for $m_\phi^2/s \ll 1$. For the marginal portal one finds instead [221][5]

$$\sigma(e^-e^+ \to \phi\phi e^- e^+) = \frac{\mathcal{R}_w^{e\bar{e}} g^4 \lambda^2}{49152\pi^5 m_\phi^2}\left[\log\frac{s}{m_\phi^2} - \frac{14}{3} + \frac{m_\phi^2}{s}\left(3\log^2\frac{s}{m_\phi^2} + 18 - \pi^2\right) + O(m_\phi^4/s^2)\right]. \tag{5.10}$$

Note that the two cross-sections have a very different scaling in the center of mass energy and DM mass. At high energies $s \gg m_\phi^2$ the cross-section for the derivative portal $\sigma \propto c_d^2\, s/f^4$ grows very quickly with $\sqrt{s}$ and is approximately independent of the DM mass. In contrast the marginal portal yields $\sigma \propto \lambda^2 \log(s/m_\phi^2)/m_\phi^2$, what is only weakly dependent on the center of mass energy, but drops rapidly for increasing DM masses. Also note that Eq. (5.9) and Eq. (5.10) are only an accurate approximation if $m_\phi \gg m_h/2$, since the partonic cross-section receives an important contribution from the on-shell region $\hat{s} \approx 4m_\phi^2$. In our analysis we always use the exact cross-section, which we compute with `MadGraph5` [222] using a `FeynRules 2.0` [164] implementation of Eqs. (5.1) and (5.2).

At lepton colliders we perform a parton-level analysis with `MadGraph5`, which is a decent approximation due to the extremely clean final state with two leptons and missing momentum. The main background for this analysis is $e^-e^+ \to \nu\bar{\nu}e^-e^+$. When generating events with `MadGraph5` we require $p_T^e > 10$ GeV, $|\eta_e| < 5$ and $\Delta R_{ee} > 0.4$. In order to discriminate signal

[5]Notice some typos in [221]: the second expression in Eq. (15) should have coefficient 256 instead of 4096, and the first expression should have 1/16 instead of 1/64. In addition, in the last expression of Eq. (14), $\hat{s}x/s \to \hat{s}/(sx)$. However, their numerical results are correct. We thank A. Tesi for correspondence about this point.

from background we impose cuts on the kinematic distributions. Among the most useful and sensitive variables are MET and missing invariant mass (MIM)

$$\not{E}_T = (\not{p}_x^2 + \not{p}_y^2)^{1/2}, \qquad \text{MIM} = (\not{p}_\mu \not{p}^\mu)^{1/2}, \tag{5.11}$$

where $\not{p} = (\sqrt{s}, \mathbf{0}) - p_{e^-} - p_{e^+}$. Additionally we consider the invariant mass M_{ee} and pseudorapidity separation $\Delta\eta_{ee} = |\eta_{e^-} - \eta_{e^+}|$ of the electron-positron pair. Normalized distributions of MIM, M_{ee} and $\Delta\eta_{ee}$ for CLIC 3, which we chose as a representative example, are shown in Figure 5.2. In the analysis we optimize the cuts to maximize the significance $\mathcal{S} \equiv S/\sqrt{S+B}$, where S and B are the signal and background events after the cuts have been applied. An exemplary flow of optimized cuts for $m_\phi = 100$ GeV at CLIC 3 is displayed in Table 5.3. As can be seen the discriminating power of M_{ee} is weaker for the derivative portal, which is however compensated by a more restrictive cut on MIM. After the selection cuts the dominant contribution to the background is $\nu_e \bar{\nu}_e e^- e^+$, which includes an $O(10)\%$ contribution from on-shell WW production.

CLIC 3	signal, $m_\phi = 100$ GeV $f/c_d^{1/2} = 500$ GeV [$\lambda = 1$]	$\nu\bar{\nu}e^-e^+$ background
Generation cuts	0.084 [0.139]	754
MIM > 560 [200] GeV	0.061 [0.139]	311 [541]
$\Delta\eta_{ee} > 5.5$ [6]	0.046 [0.106]	3.49 [19.4]
$\not{E}_T > 80$ [80] GeV	0.028 [0.071]	0.472 [2.76]
$M_{ee} > 1100$ [2200] GeV	0.026 [0.058]	0.391 [0.501]

Table 5.3: Cross-sections in fb. For 3 ab^{-1} we have $\mathcal{S} = 2.2\,[4.2]$ for the derivative [marginal] portal. No EFT consistency condition is applied.

Another important aspect is to ensure that our analysis of the derivative portal consistently takes into account the limited range of validity of the EFT when setting limits. For this reason we follow the strategy proposed in [223]: in addition to the regular selection cuts on the kinematic variables we exclude events with characteristic energy $E > g_* f/c_d^{1/2}$, where $g_* \leq 4\pi$ is a coupling, as they lie outside the region of validity of the EFT. As characteristic energy scale we choose the energy flowing through the effective coupling, which is given by $E = M_{\phi\phi}$. Thus for a given value of g_* we derive the exclusion contour in the plane $(m_\phi, f/c_d^{1/2})$ using only events with $M_{\phi\phi} < g_* f/c_d^{1/2}$ and requiring that the significance $\mathcal{S} \equiv S/\sqrt{S+B} = \sqrt{2}\,\mathrm{erf}^{-1}(1-2p)$ (Gaussian approximation, one-sided test), where for 95% CL ($p = 0.05$) the right-hand side equals 1.64. The results for $g_* = 4\pi$ are presented in Section 5.3.

Finally we also assess the sensitivity of a future muon collider. The analysis is very similar to the analysis at electron-positron colliders with the main difference being a higher center of mass energy [224] (we take $\sqrt{s} = 6$ and 14 TeV as benchmarks, see Table 5.1), which causes the produced muons in the signal to be very forward with an extremely large pseudorapidity. This problem is especially severe for $\sqrt{s} = 14$ TeV. As can be seen in the top left panel of Figure 5.3, a detector coverage limited to $|\eta_\mu| < 5$ loses an $\mathcal{O}(1)$ fraction of the signal, what causes a significant reduction of the sensitivity. In order to capture most of the signal with only a mild increase of background, an extended detector coverage of $|\eta_\mu| < 6$ is required. The resulting gain in sensitivity is shown in the top right and bottom panel of Figure 5.3 for the derivative and marginal Higgs portal, respectively.

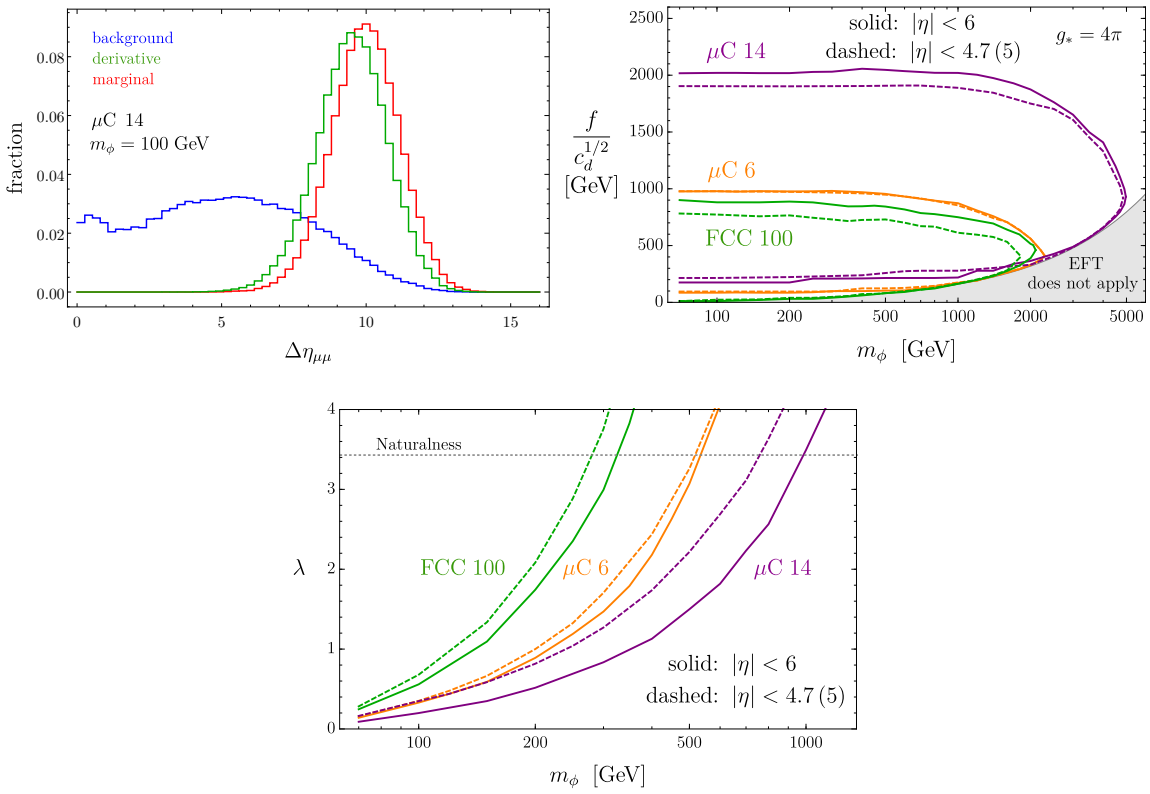

Figure 5.3: *Top Left:* normalized $\Delta\eta_{\mu\mu}$ distributions for the signals with $m_\phi = 100$ GeV and the background at a muon collider with $\sqrt{s} = 14$ TeV. Only for this plot, the generation-level cut on the muon pseudorapidity was relaxed to $|\eta_\mu| < 8$. *Top Right:* projected 95% CL constraints on the derivative portal at FCC 100 and at a muon collider, assuming the forward detector coverage extends up to $|\eta| = 6$ (solid) or $|\eta| = 4.7\,[5]$ for the FCC [muon collider] (dashed). *Bottom:* same as the middle panel, for the marginal portal. This Figure is adopted from [31].

5.2.2 Hadron colliders

The cross-sections at hadron colliders are obtained by convoluting Eq. (5.4) with the parton luminosities in the proton

$$\sigma(pp \to \phi\phi jj) = \sum_{q_1,\,q_2} \int_{4m_\phi^2/S}^1 dT\, L_{q_1q_2}(T,Q)\, \sigma(q_1q_2 \to \phi\phi q_1' q_2')[TS], \tag{5.12}$$

with

$$L_{q_1q_2} = \int_T^1 \frac{dx}{x} [q_1(x) q_2(T/x)]_Q\,. \tag{5.13}$$

$\sqrt{S}$ is the collider center of mass energy, Q the factorization scale and the sum extends over all relevant quarks and antiquarks. Eq. (5.12) is a sensible estimate for $m_\phi \gg m_V/2$: the agreement with the exact result improves from 30% for $m_\phi = 100$ GeV to better than 10% for $m_\phi > 200$ GeV.

At HL-LHC our analysis can be seen as an extension of recent searches for invisible Higgs decays in the VBF production channel at CMS [225] and ATLAS [226]. Our simulation pipeline

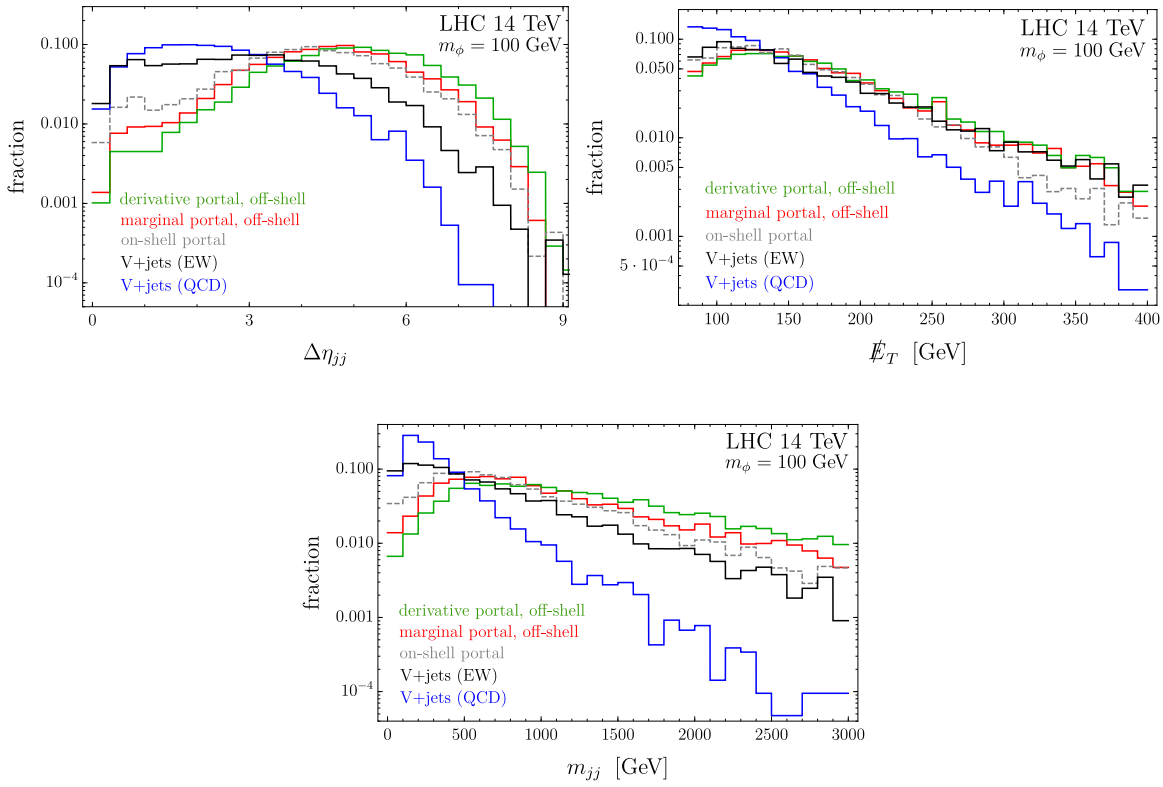

Figure 5.4: Normalized distributions at the 14 TeV LHC for the signals with $m_\phi = 100$ GeV and the main backgrounds, after the baseline cuts. For reference we also show normalized distributions for the on-shell signal. This Figure is adopted from [31].

starts with the generation of parton level events with `MadGraph5_aMC@NLO`, which are subsequently showered with `Pythia8` [227] and finally passed through a fast detector simulation using `Delphes3` [228] with the CMS card. The main background for our signal process $pp \to jj\phi\phi$, which is characterized by large MET and very forward jets j, what is typical for the VBF topology, are $Z_{\nu\nu}$+jets and $W_{\ell\nu}$+jets. Each of the backgrounds can be separated into a QCD and an electroweak (EW) part, which differ by the production mode of the jets. The interference between both contributions is negligible [226]. Even though the EW contributions have a smaller cross-section their inclusion is important, since their kinematics closely resembles that of the signal. For this reason the EW contributions to $Z_{\nu\nu}$+jets and $W_{\ell\nu}$+jets constitute an $\mathcal{O}(1)$ fraction of the total background after the selection cuts have been applied. For the QCD induced contribution to background processes we generate $V + 2$ jets at NLO, whereas the EW contributions are a matched sample of $V + 2, 3$ jets. The overall normalization of each background sample is fixed by comparing our generated events for 13 TeV with the expected event yields of the CMS shape analysis, reported in Table 3 of [225]. After rescaling all samples we find agreement with the CMS expectations at the order of 10%, what we demonstrate in the top left panel of Figure I.G.2 in Appendix I.G. In our 14 TeV analysis we apply the same rescaling factors, which we found from matching to the CMS expectations at 13 TeV. Additionally we include the $t\bar{t}$+jets background, which we generate at LO matched with up to 2 additional partons and normalized to the NNLO+NNLL cross-section of 974 pb [229].

HL-LHC	signal, $m_\phi = 100$ GeV $f/c_d^{1/2} = 500$ GeV $[\lambda = 1]$	$Z_{\nu\nu}$ QCD	$W_{\ell\nu}$ QCD	$Z_{\nu\nu}$ EW	$W_{\ell\nu}$ EW	$t\bar{t}$
Baseline cuts	0.164 [0.618]	$1.4 \cdot 10^4$	$1.7 \cdot 10^4$	330	330	$1.7 \cdot 10^3$
$\Delta\eta_{jj} > 4.8$ [4.2]	0.090 [0.366]	440 [960]	890 [1700]	46 [78]	50 [80]	12 [29]
$\not{E}_T > 180$ GeV	0.028 [0.110]	58 [140]	38 [100]	14 [26]	7.8 [15]	1.5 [4.4]
$m_{jj} > 1.97$ [1.30] TeV	0.015 [0.075]	12 [56]	5.0 [32]	7.4 [18]	3.9 [11]	– [1.5]

Table 5.4: Cross-sections in fb. The baseline cuts are given in Eq. (5.14). For 3 ab^{-1} we have $\mathcal{S} = 0.15\,[0.38]$ for the derivative [marginal] portal. A dash indicates that our MC statistics is insufficient to estimate the cross-section. No EFT consistency condition is applied.

The baseline cuts in our 14 TeV analysis are

$$\begin{aligned} \not{E}_T > 80 \text{ GeV}, \qquad N_j \geq 2\,, \qquad p_T^{j_1,j_2} > 50 \text{ GeV}, \qquad |\eta_{j_1,j_2}| < 4.7\,, \qquad \eta_{j_1} \cdot \eta_{j_2} < 0\,, \\ N_\ell = 0\,, \qquad N_j^{\text{central}} = 0\,, \qquad \Delta\phi(j_1, j_2) < 2.2\,, \qquad \Delta\phi(\not{p}_T, j) > 0.5\,. \end{aligned} \tag{5.14}$$

We implement the lepton veto in the same way as in the CMS analysis [225]. The central jet veto forbids events with an additional jet, which satisfies $p_T^j > 30$ GeV and $\min \eta_{j_1,j_2} < \eta_j < \max \eta_{j_1,j_2}$, while the $\Delta\phi(\not{p}_T, j)$ requirement is applied to any jet with $p_T^j > 30$ GeV. We show normalized distributions of the signal and background after the baseline cuts for $m_\phi = 100$ GeV in Figure 5.4. For comparison we include the portal independent signal for the on-shell Higgs region. As can be clearly seen $\Delta\eta_{jj}$, which is displayed in the top left panel of Figure 5.4, is an important discriminating variable, especially for the derivative portal. Its behavior is in fact opposite to what happens at lepton colliders, where the $\Delta\eta_{\ell\ell}$ distribution is harder for the marginal portal. In our analysis we select events with $\Delta\eta_{jj} > 4.8$ [4.2] for the derivative [marginal] portal. We additionally impose a stronger cut on $\not{E}_T$ and a cut on m_{jj}. The variation of the significance for different values of the $\not{E}_T$ and m_{jj} cut is shown in Figure 5.5. From this it is apparent that a relatively mild cut on $\not{E}_T$ would be preferred by both portals. However, as event selection has to be done with a missing energy trigger, we have to impose a rather stringent requirement on $\not{E}_T$. Following the ATLAS analysis [226] we set $\not{E}_T > 180$ GeV. Also note that the shape of the missing energy distribution of the electroweak backgrounds have a close resemblance with the signal distribution. We finally choose the m_{jj} cut separately for the marginal and derivative portal by maximizing the significance of the signal. A complete cut flow for $m_\phi = 100$ GeV is reported in Table 5.4. The contribution of the $t\bar{t}$ background is small and subleading after the selection cuts, which is why we neglect it in our HL-LHC projections. In contrast the EW V+jets background is very important, constituting 40% of the total background to the signal from the derivative portal. We keep all cuts identical for each m_ϕ hypothesis, except for m_{jj}, which we optimize in each case.

As we mentioned above and show in Figure 5.5, even though the signal prefers a mild $\not{E}_T$ cut we are forced to take a more stringent cut due to the degrading trigger efficiency for lower $\not{E}_T$. For this reason it is interesting to examine how much the significance is affected by varying the missing energy cut. As benchmarks we take $\not{E}_T > 150$ GeV, which corresponds to a trigger efficiency of $\sim 90\%$ on signal events at ATLAS [230] (to be compared with 98% for the reference choice $\not{E}_T > 180$ GeV [226]) and $\not{E}_T > 250$ GeV, as required in the CMS analysis [225]. Considering the derivative portal with $m_\phi = 100$ GeV the bound on $f/c_d^{1/2}$ varies from 290 to 260 GeV, whereas the reach on m_ϕ for the marginal portal with naturalness inspired coupling strength decreases from 135 to 117 GeV.

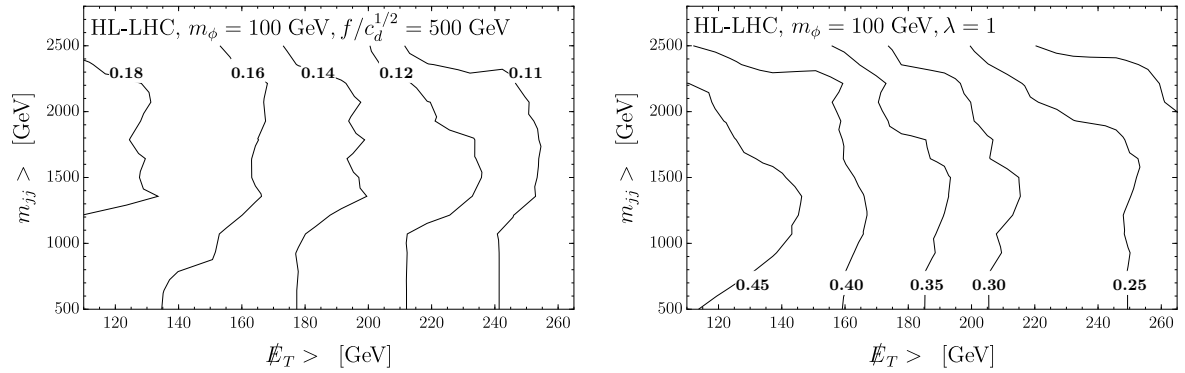

Figure 5.5: Isocontours of the significance $\mathcal{S}$ in the plane of the $(\not{E}_T, m_{jj})$ cuts, at the HL-LHC. Baseline and $\Delta\eta_{jj}$ cuts have already been applied. This Figure is adopted from [31].

The analysis for HE-LHC proceeds along similar lines. The V+jets backgrounds are rescaled with the same factor, which we determined from the comparison to CMS at 13 TeV, and $t\bar{t}$+jets is normalized to the theoretical prediction of 3.73 nb [231]. For the fast detector simulation we use the HL-LHC card for `Delphes3`. The baseline cuts are identical to Eq. (5.14), except that we impose $|\eta_{j_1,j_2}| < 4.9$. As additional selection cuts we apply $\Delta\eta_{jj} > 5.2$ [4.2] for the derivative [marginal] signal, fix $\not{E}_T > 200$ GeV, and as before we optimize the m_{jj} cut for each m_ϕ and portal hypothesis.

In the FCC analysis we again apply the 13 TeV rescaling factors for the V+jets background, normalize $t\bar{t}$+jets to 34.7 nb [232] and use the FCC `Delphes` card. As baseline cuts we keep Eq. (5.14) but increase the requirement on the jet pseudorapidity to $|\eta_{j_1,j_2}| < 6$. As is also emphasized in the FCC-hh Conceptual Design Report [233], extending detector coverage up to $|\eta_j| = 6$ would be important for the measurement of VBF processes. This is explicitly verified and also quantified in Figure 5.3, where we visualize the gain in sensitivity if the pseudorapidity acceptance in the forward jet measurement is extended from the LHC range $|\eta_j| < 4.7$ to the expected FCC design $|\eta_j| < 6$ (note that the FCC 100 bounds shown in Figure 5.6 assume coverage up to $|\eta_j| = 6$). Further selection cuts are $\Delta\eta_{jj} > 5.5$ [4.2] for the derivative [marginal] portal and $\not{E}_T > 200$ GeV [214]. We show the complete cut flow for $m_\phi = 100$ GeV in Table 5.5. Note that for the marginal portal the $t\bar{t}$+jets background is not negligible, thus we consistently include it in the FCC projections.

FCC 100	signal, $m_\phi = 100$ GeV $f/c_d^{1/2} = 1$ TeV $[\lambda = 1]$	$Z_{\nu\nu}$ QCD	$W_{\ell\nu}$ QCD	$Z_{\nu\nu}$ EW	$W_{\ell\nu}$ EW	$t\bar{t}$
Baseline cuts	7.6 [114] $\cdot 10^{-4}$	170	220	3.5	3.7	49
$\Delta\eta_{jj} > 5.5$ [4.2]	5.9 [90] $\cdot 10^{-4}$	12 [38]	24 [64]	0.79 [1.5]	0.97 [1.9]	2.0 [6.6]
$\not{E}_T > 200$ GeV	2.1 [29] $\cdot 10^{-4}$	1.7 [6.0]	1.6 [5.4]	0.24 [0.51]	0.17 [0.37]	0.11 [0.50]
$m_{jj} > 6.62$ [2.30] TeV	0.87 [17] $\cdot 10^{-4}$	0.062 [1.3]	0.060 [1.3]	0.053 [0.29]	0.032 [0.22]	– [0.12]

Table 5.5: Cross-sections in pb. The baseline cuts are in Eq. (5.14), except that $|\eta_{j_1,j_2}| < 6$. For 30 ab^{-1} we have $\mathcal{S} = 1.0\,[5.2]$ for the derivative [marginal] portal. A dash indicates that our MC statistics is insufficient to estimate the cross-section. No EFT consistency condition is applied.

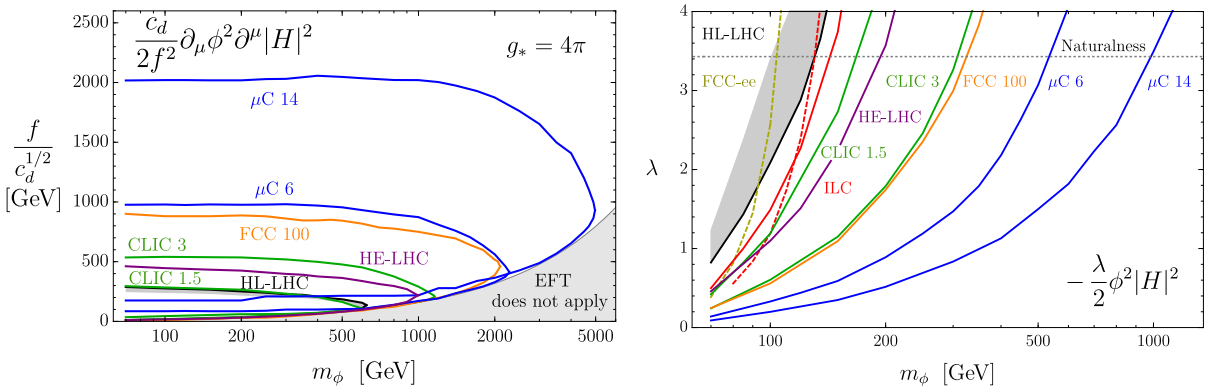

Figure 5.6: Projected 95% CL constraints on the Higgs portal couplings at future colliders. *Left:* derivative Higgs portal. To remain within the regime of validity of the EFT we only retain events with $M_{\phi\phi} < g_* f / c_d^{1/2}$, where g_* is set to 4π. This requirement cannot be satisfied in the gray region $2m_\phi > g_* f / c_d^{1/2}$. The excluded region is the one enclosed by each line. All limits are derived from VBF. *Right:* marginal Higgs portal. The excluded region is the one above each line. Solid lines correspond to VBF processes: in addition to the benchmarks in Table 5.1, we show ILC 1 TeV with 1 ab^{-1} (solid red). Dashed lines correspond to Zh production from [213]: ILC 500 GeV with 1 ab^{-1} (dashed red) and FCC-ee at 350 GeV and 2.5 ab^{-1} (dashed yellow). The dotted line labeled "Naturalness" corresponds to $\lambda = \sqrt{4N_c}\, y_t^2$, namely two degenerate scalar top partners. In both panels, for the HL-LHC we also show a gray band whose weaker limit boundary corresponds to adding a 1% systematic uncertainty on the background. This Figure is adopted from [31].

Let us finally comment on the role of systematic uncertainties, which we have so far neglected in our analysis. S/B at lepton colliders is at least several per-cent (see e.g. Table 5.3), therefore the effect of systematics is expected to be minor. However, at hadron colliders S/B is below the per-mille (cf. Tables 5.4 and 5.5) implying that systematics will have an important impact on the analysis. In order to quantify this effect we repeat the HL-LHC analysis with the assumption of a 1% systematic uncertainty on the total background (see e.g. [234] for the theoretical advancement in the precise predictions of the dominant V+jets backgrounds). The selection cuts remain the same as listed in Table 5.4, except for the m_{jj} cut, whose optimization drives it to larger values in order to suppress the background to the largest extent possible, as can be seen in the top right panel of Figure I.G.2. The resulting limits are shown by the gray bands in Figure 5.6. A more comprehensive discussion of systematics lies beyond the scope of this first study.

5.3 Results and discussion

The results of our analysis are summarized in Figure 5.6 for the marginal and derivative portals as defined in Eq. (5.2) and Eq. (5.1), respectively. Note that the results in Figure 5.6 can be straightforwardly extended to the case of N real, degenerate scalars with identical couplings. Their effect on the signal is equivalent to that of a single field with $\{c_d, \lambda\} \to \sqrt{N}\{c_d, \lambda\}$. In particular for complex pNGB DM χ with derivative portal $\partial_\mu|\chi|^2\partial^\mu|H|^2/f^2 \in \mathcal{L}$, which we have considered in the previous chapters, we should take $c_d = \sqrt{2}$. For degenerate scalar top partners (two complex scalars in the $SU(N_c)$ fundamental, with y_t^2 coupling to the Higgs) we have $\lambda = \sqrt{4N_c}\, y_t^2$, what is our benchmark coupling strength for the marginal portal in Table 5.6.

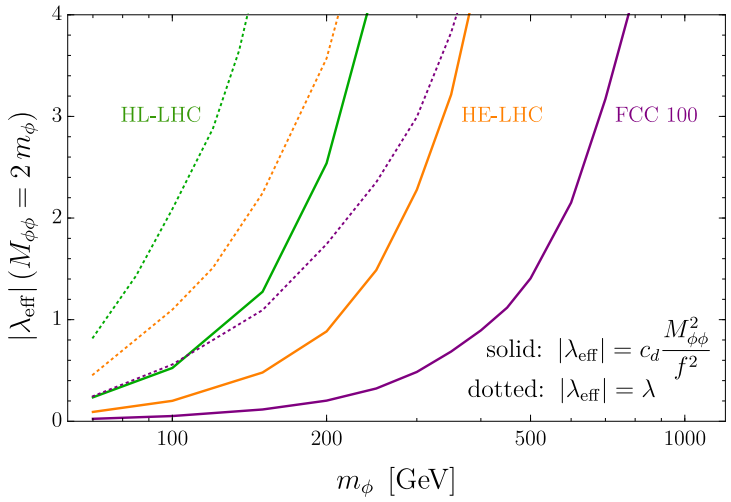

Figure 5.7: Hadron collider sensitivity on the effective coupling evaluated at the threshold $M_{\phi\phi} = 2m_\phi$, for the derivative and marginal portals, as obtained from our analysis. The figure quantifies the sensitivity gain that follows from the relative scaling $\propto \hat{s}^2$ in Eq. (5.8). This Figure is adopted from [31].

Note also that if the integrated luminosity of a future collider turns out to be L' instead of the L (see Table 5.1), neglecting systematic uncertainties the reach on $f/c_d^{1/2}$ scales as $(L'/L)^{1/8}$ and as $(L'/L)^{1/4}$ for λ.

To allow for an easy comparison of the sensitivities at different colliders we present the reach along benchmark slices of the parameter space in Table 5.6. For the derivative portal we take as benchmark a ϕ mass of $m_\phi = 100$ GeV and compare the reach on $f/c_d^{1/2}$ for this mass hypothesis. The benchmark for the marginal portal is a naturalness inspired effective coupling strength of $\lambda = \sqrt{4N_c}\,y_t^2$, for which we compare the reach on m_ϕ at different collider scenarios.

	HL-LHC	CLIC 1.5	HE-LHC	CLIC 3	FCC 100	μC 6	μC 14
derivative, $m_\phi = 100$ GeV: $f/c_d^{1/2}$ [GeV]	280	280	450	540	880	980	2000
marginal, $\lambda = \sqrt{4N_c}\,y_t^2$: m_ϕ [GeV]	130	170	190	310	330	540	990

Table 5.6: 95% CL exclusion limits obtained from our off-shell Higgs analysis.

Let us now discuss a few aspects of the results and the analysis. As a first comment we note that hadron colliders have a stronger sensitivity to the derivative Higgs portal than the marginal Higgs portal due to the harder kinematic distributions in the derivative portal scenario, which allows for a more efficient background suppression (see e.g. Tables 5.4 and 5.5). In order to quantify this statement we compare the bounds on the absolute value of the effective coupling strength of both portals on threshold $M_{\phi\phi} = 2m_\phi$, which is $c_d 4m_\phi^2/f^2$ and λ, respectively. For hadron colliders the threshold is a reasonable point of comparison, due to the PDF suppression at higher $M_{\phi\phi}$. The resulting bounds in Figure 5.7 clearly show that there is a better reach on the derivative portal thanks to the more pronounced tail at higher invariant masses. For $m_\phi = 100$ GeV, the ratio of the effective coupling bounds is $\sim 1/4.0$ at the HL-LHC, $\sim 1/5.5$ at the HE-LHC and $\sim 1/11$ at the FCC. This explains why FCC 100, for example, gives projected bounds comparable to a 6 TeV muon collider for the derivative portal, but similar to CLIC 3

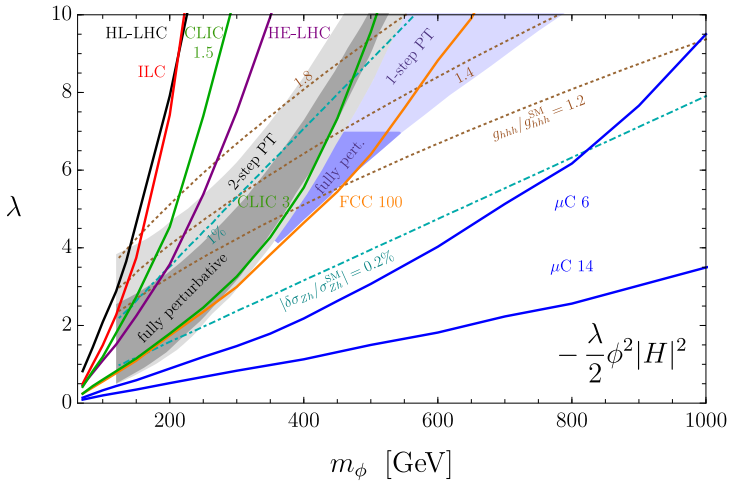

Figure 5.8: Comparison of the VBF sensitivity on the marginal portal derived in this work with the regions where a first-order EW PT may be possible as given in [221]. Solid lines show projected 95% CL VBF constraints, extended to larger λ with respect to the right panel of Figure 5.6. Dotted brown contours indicate the deviation of the Higgs trilinear coupling from the SM (see Eq. (5.15)) while dot-dashed cyan contours show the deviation of the $\ell^+\ell^- \to Zh$ cross-section (see Eq. (5.16)). This Figure was previously published in [31].

for the marginal portal.

The key motivation for the derivative portal is pNGB DM. As we have discussed at length in Chapter 3, the requirement of obtaining the observed DM relic abundance fixes a relation between m_χ and f. From the resulting relic abundance contour in the (m_χ, f) plane (see e.g. Figure 3.2), we can extract that for $m_\chi > m_h/2$ a symmetry breaking scale of $f \gtrsim 500$ GeV is needed for complex DM. Comparing this to Figure 5.6 we conclude that this region is out of reach at HL-LHC and CLIC 1.5 and can only be probed to a very limited extent at HE-LHC and CLIC 3. In order to truly explore this interesting region FCC 100 or a muon collider would be needed, with a μC 14 being able to test DM masses up to 600 GeV.

A representative example for the marginal coupling are scalar top partners with coupling strength fixed by naturalness. In this scenario even FCC 100 will have a limited sensitivity, which will not extend beyond masses of approximately 300 GeV. A muon collider would again have a superior reach, extending all the way up to $m_{\tilde{u}^c} \approx 1$ TeV for center of mass energy of 14 TeV, which would represent an impressive, model-independent test of the possibility that the little hierarchy is stabilized by scalar top partners, regardless of their decay pattern.

Another theoretically well-motivated scenario for scalar singlets coupled to the Higgs through a sizable marginal Higgs portal is the possibility of a first-order electroweak phase transition (EW PT), which would allow for electroweak baryogenesis (see e.g. [208]). In Figure 5.8 we compare our results for the sensitivity on λ to the region of parameter space, where a first-order EW PT can occur. This region has been reproduced from [221], where a detailed description can be found. The results in Figure 5.8 imply that only a muon collider could fully test this scenario for electroweak baryogenesis with an invisible singlet. CLIC 3 and FCC 100 can, however, cover parts of the relevant parameter space. In Figure 5.8 we also show the deviation of the Higgs trilinear from its SM value, which we obtain from Eq. (5.2) by integrating out the scalar ϕ at

one-loop

$$\frac{g_{hhh}}{g_{hhh}^{\rm SM}} \simeq 1 + \frac{\lambda^2 v^2}{96\pi^2 m_\phi^2}\Big(\frac{\lambda v^2}{m_h^2} - \frac{3}{4}\Big)\,, \qquad g_{hhh}^{\rm SM} = \frac{m_h^2}{2v}\,. \tag{5.15}$$

We have checked that this is a reasonable approximation in the parameter space of interest by comparing to [235]. However, some corrections arise for $m_\phi \lesssim 250$ GeV. Note also that there is a modification of the $\ell^+\ell^- \to Zh$ cross-section at one-loop

$$\frac{\delta\sigma_{Zh}}{\sigma_{Zh}^{\rm SM}} \simeq -\frac{\lambda^2 v^2}{192\pi^2 m_\phi^2}\,. \tag{5.16}$$

A precise measurement of this cross-section would provide an alternative test for the marginal Higgs portal [236].

Appendices part I

I.A SO(7)/SO(6) model: CCWZ construction

For the generators of the fundamental representation of $SO(7)$ we take

$$\begin{aligned}
(T^{\alpha}_{L,R})_{IJ} &= -\frac{i}{2}\left[\frac{1}{2}\epsilon^{\alpha\beta\gamma}(\delta^{\beta}_{I}\delta^{\gamma}_{J}-\delta^{\beta}_{J}\delta^{\gamma}_{I})\pm(\delta^{\alpha}_{I}\delta^{4}_{J}-\delta^{\alpha}_{J}\delta^{4}_{I})\right], \qquad \alpha=1,2,3,\\
T^{ab}_{IJ} &= -\frac{i}{\sqrt{2}}(\delta^{a}_{I}\delta^{b}_{J}-\delta^{a}_{J}\delta^{b}_{I}), \qquad b=5,6;\ a=1,\dots,b-1,\\
X^{a}_{IJ} &= -\frac{i}{\sqrt{2}}(\delta^{a}_{I}\delta^{7}_{J}-\delta^{a}_{J}\delta^{7}_{I}), \qquad a=1,\dots,6,
\end{aligned} \tag{I.A.1}$$

where the indices I,J take the values $1,\dots,7$. $T^{\alpha}_{L,R}$ and T^{ab} are the generators of $SO(6)$, collectively denoted by $T^{\hat{a}}$ ($\hat{a}=1,\dots,15$), with $T^{\alpha}_{L,R}$ spanning the custodial $SO(4)\cong SU(2)_L\times SU(2)_R$ subgroup, while X^a are the broken generators that parameterize the coset space $SO(7)/SO(6)$. Notice that the unbroken generators are block-diagonal in our basis,

$$T^{\hat{a}}=\begin{pmatrix} t^{\hat{a}} & 0\\ 0 & 0\end{pmatrix}, \qquad t^{\hat{a}}\in SO(6). \tag{I.A.2}$$

All generators T^A ($A=1,\dots,21$) are normalized such that $\mathrm{Tr}\left[T^AT^B\right]=\delta^{AB}$. Under the unbroken $SO(6)$, the six GBs π^a transform linearly and in the fundamental representation, whose decomposition under $SO(4)$ is $\mathbf{6}=\mathbf{4}\oplus\mathbf{1}\oplus\mathbf{1}$. The Higgs doublet $H=(h_u,h_d)^T$ is identified with the $\mathbf{4}$, so that

$$\boldsymbol{\pi}=\frac{1}{\sqrt{2}}\left(-i(h_u-h_u^*),\quad h_u+h_u^*,\quad i(h_d-h_d^*),\quad h_d+h_d^*,\quad \sqrt{2}\,\eta,\quad \sqrt{2}\,\kappa\right)^T. \tag{I.A.3}$$

In unitary gauge, i.e. $h_u=0$, $h_d=\tilde{h}/\sqrt{2}$, this has the expression in Eq. (4.2) and the Goldstone matrix $U(\boldsymbol{\pi})=\exp\left(i\sqrt{2}\pi^aX^a/f\right)$ can be written, after performing the convenient field redefinition [37]

$$\frac{\sin(\pi/f)}{\pi}\,\pi^a\to\frac{\pi^a}{f} \qquad \text{with} \qquad \pi=\sqrt{\boldsymbol{\pi}^T\boldsymbol{\pi}}\,, \tag{I.A.4}$$

in the following form

$$U=\begin{pmatrix} \mathbf{1}_{3\times3} & & & & \\ & 1-\frac{\tilde{h}^2}{f^2(1+\Omega)} & -\frac{\tilde{h}\eta}{f^2(1+\Omega)} & -\frac{\tilde{h}\kappa}{f^2(1+\Omega)} & \frac{\tilde{h}}{f}\\ & -\frac{\tilde{h}\eta}{f^2(1+\Omega)} & 1-\frac{\eta^2}{f^2(1+\Omega)} & -\frac{\eta\kappa}{f^2(1+\Omega)} & \frac{\eta}{f}\\ & -\frac{\tilde{h}\kappa}{f^2(1+\Omega)} & -\frac{\eta\kappa}{f^2(1+\Omega)} & 1-\frac{\kappa^2}{f^2(1+\Omega)} & \frac{\kappa}{f}\\ & -\frac{\tilde{h}}{f} & -\frac{\eta}{f} & -\frac{\kappa}{f} & \Omega \end{pmatrix}, \qquad \Omega=\frac{1}{f}\sqrt{f^2-\tilde{h}^2-\eta^2-\kappa^2}\,. \tag{I.A.5}$$

Under $g \in SO(7)$, the GB matrix transforms as

$$U(\boldsymbol{\pi}) \to g\, U(\boldsymbol{\pi})\; h(\boldsymbol{\pi}; g)^T\,, \tag{I.A.6}$$

where $h(\boldsymbol{\pi}; g)$ is block-diagonal in our basis,

$$h(\boldsymbol{\pi}; g) = \begin{pmatrix} h_6 & 0 \\ 0 & 1 \end{pmatrix}, \qquad h_6 \in SO(6). \tag{I.A.7}$$

The d_μ and e_μ symbols are defined via[6]

$$iU^\dagger D_\mu U \equiv d_\mu^a X^a + e_\mu^{\hat{a}} T^{\hat{a}}\,, \tag{I.A.8}$$

where $D_\mu U = \partial_\mu U - iA_\mu^{\hat{a}} T^{\hat{a}} U$. Notice that we took the gauge fields as belonging to the $SO(6)$ subalgebra, since this is the relevant case. Explicitly, for $SU(2)_L \times U(1)_Y$ we have $A_\mu^{\hat{a}} T^{\hat{a}} = \bar{g} \bar{W}_\mu^\alpha T_L^\alpha + \bar{g}' \bar{B}_\mu T_R^3$. If the $U(1)_{\rm DM}$ were also gauged, then $A_\mu^{\hat{a}} T^{\hat{a}} \to A_\mu^{\hat{a}} T^{\hat{a}} + g_D A_{D\mu} \sqrt{2}\, T^{56}$, with A_D the associated vector field and g_D its coupling. Under $g \in SO(7)$,

$$d_\mu^a \to (h_6)^a{}_b\, d_\mu^b\,, \qquad e_\mu \equiv e_\mu^{\hat{a}} t^{\hat{a}} \to h_6\, (e_\mu + i\partial_\mu)\, h_6^T\,, \tag{I.A.9}$$

where h_6 was defined in Eq. (I.A.7). To leading order in $1/f$, we have

$$d_\mu^a = -\frac{\sqrt{2}}{f}\, D_\mu \pi^a + O(1/f^3), \qquad e_\mu^{\hat{a}} = A_\mu^{\hat{a}} + O(1/f^2)\,, \tag{I.A.10}$$

where $D_\mu \pi^a = \partial_\mu \pi^a - i A_\mu^{\hat{a}} (t^{\hat{a}})^a{}_b \pi^b$. The fermion covariant derivatives that appear in Eq. (4.15) read

$$D_\mu q_L = \Big(\partial_\mu - i\bar{g} \bar{W}_\mu^\alpha \frac{\sigma^\alpha}{2} - i\bar{g}' \frac{1}{6} \bar{B}_\mu\Big) q_L\,, \qquad D_\mu \Psi = \Big(\partial_\mu - i \frac{2}{3} \bar{g}' \bar{B}_\mu\Big) \Psi\,, \tag{I.A.11}$$

where $\Psi = t_R, Q_i, S_j$, and in all cases the color $SU(3)$ component is understood.

I.B SO(7)/SO(6) model: fermion sector

Here we shortly summarize the embeddings of the elementary fermions and top partner couplings for the different scenarios we discuss in Chapter 4.

DM shift symmetry broken by top quark
This scenario is discussed in Section 4.3 and assumes an embedding of q_L and t_R into the $\mathbf{7}_{2/3}$ representation of $SO(7) \times U(1)_X$. The explicit form of the embedding is

$$\xi_L = \frac{1}{\sqrt{2}} \big(ib_L,\ \ b_L,\ \ it_L,\ \ -t_L,\ \ 0,\ \ 0,\ \ 0\big)^T\,, \quad \xi_R = \big(0,\ \ 0,\ \ 0,\ \ 0,\ \ 0,\ \ 0,\ \ t_R\big)^T\,. \tag{I.B.1}$$

Since $\mathbf{7}_{2/3}$ decomposes as $\mathbf{7}_{2/3} = \mathbf{6}_{2/3} \oplus \mathbf{1}_{2/3}$ under $SO(6) \times U(1)_X$, we consider fermionic resonances Q in the $\mathbf{6}_{2/3}$ and S in the $\mathbf{1}_{2/3}$ representation of the unbroken group. The explicit form of the Q multiplet in the fundamental representation can be written as

$$Q = \frac{1}{\sqrt{2}} \big(iB - iX_{5/3},\ \ B + X_{5/3},\ \ iT + iX_{2/3},\ \ -T + X_{2/3},\ \ -i\mathcal{Y} + i\mathcal{Z},\ \ \mathcal{Y} + \mathcal{Z}\big)^T\,, \tag{I.B.2}$$

where the doublet $(T, B)^T$ transforms as $\mathbf{2}^0_{1/6}$ under $(SU(2)_L)^{\rm DM}_Y$, the exotic doublet $(X_{5/3}, X_{2/3})^T \sim \mathbf{2}^0_{7/6}$ contains an exotic fermion with electric charge equal to 5/3 and the two states $\mathcal{Y}, \mathcal{Z} \sim \mathbf{1}^{\pm 1}_{2/3}$ share the SM quantum numbers of the t_R, but are additionally charged under $U(1)_{\rm DM}$. For the leading Lagrangian of the fermion mixing see Eq. (4.15).

[6] Notice that we define the d_μ and e_μ symbols with opposite sign compared to, e.g., [152].

DM shift symmetry preserved by top quark

This scenario for the top quark is assumed in Section 4.4 and 4.5. The choice of DM shift symmetry-preserving top quark embeddings that we have made is

$$\mathbf{7}_{2/3} \sim \xi_L^{(t)} = \frac{1}{\sqrt{2}} \left(i b_L, \quad b_L, \quad i t_L, \quad -t_L, \quad \mathbf{0}_3^T \right)^T, \qquad \mathbf{21}_{2/3} \sim \xi_R^{(t)} = \frac{i\, t_R}{2} \begin{pmatrix} 0 & -1 & & & \\ 1 & 0 & & & \\ & & 0 & 1 & \\ & & -1 & 0 & \\ & & & & \mathbf{0}_{3\times 3} \end{pmatrix}, \tag{I.B.3}$$

where empty entries in the expression of $\xi_R^{(t)}$ are zeros. Since $\mathbf{7} = \mathbf{6} \oplus \mathbf{1}$ and $\mathbf{21} = \mathbf{15} \oplus \mathbf{6}$ under $SO(6)$, in the top sector we expect fermionic resonance multiplets $G \sim \mathbf{15}_{2/3}$, $Q \sim \mathbf{6}_{2/3}$ and $S \sim \mathbf{1}_{2/3}$ under $SO(6) \times U(1)_X$. The decomposition and component expression of Q was given in Sec. II of [28], whereas G decomposes as $\mathbf{15} = [(\mathbf{3},\mathbf{1}) + (\mathbf{1},\mathbf{3})]_0 \oplus (\mathbf{1},\mathbf{1})_0 \oplus (\mathbf{2},\mathbf{2})_{\pm 1}$ under $SU(2)_L \times SU(2)_R \times U(1)_{\rm DM}$, where the $X = 2/3$ charge is understood. In components,

$$G = \frac{1}{2} \begin{pmatrix} 0 & -iT_+^{12} & B_+^{12} - X_+^{12} & -i(B_-^{12} + X_-^{12}) & -\mathcal{B}_- - \mathcal{X}_{5/3\,-} & -i(\mathcal{B}_+ + \mathcal{X}_{5/3\,+}) \\ & 0 & -i(B_+^{12} + X_+^{12}) & -B_-^{12} + X_-^{12} & i(\mathcal{B}_- - \mathcal{X}_{5/3\,-}) & -\mathcal{B}_+ + \mathcal{X}_{5/3\,+} \\ & & 0 & -iT_-^{12} & -\mathcal{T}_- - \mathcal{X}_{2/3\,-} & -i(\mathcal{T}_+ + \mathcal{X}_{2/3\,+}) \\ & & & 0 & -i(\mathcal{T}_- - \mathcal{X}_{2/3\,-}) & \mathcal{T}_+ - \mathcal{X}_{2/3\,+} \\ & & & & 0 & -i\sqrt{2}\,\widetilde{S} \\ & & & & & 0 \end{pmatrix}, \tag{I.B.4}$$

where the lower triangle is determined by antisymmetry. We have made the definitions $T_\pm^{12} \equiv \widetilde{T}_1 \pm \widetilde{T}_2$, $Q_\pm^{12} \equiv (\widetilde{Q}_1 \pm \widetilde{Q}_2)/\sqrt{2}$ $(Q = X, B)$ and $\mathcal{Q}_\pm \equiv (\mathcal{Q}^{(+)} \pm \mathcal{Q}^{(-)})/\sqrt{2}$ $(\mathcal{Q} = \mathcal{T}, \mathcal{B}, \mathcal{X}_{2/3}, \mathcal{X}_{5/3})$. Here $(\widetilde{X}_i, \widetilde{T}_i, \widetilde{B}_i)^T$ is a $(\mathbf{3},\mathbf{1})_0$ for $i = 1$ and a $(\mathbf{1},\mathbf{3})_0$ for $i = 2$, $\widetilde{S} \sim (\mathbf{1},\mathbf{1})_0$, and the fields with calligraphic names compose the $(\mathbf{2},\mathbf{2})_{\pm 1}$.[7] The elementary-composite mixing Lagrangian for the top sector is

$$\begin{aligned} \mathcal{L}_{\rm mix}^{(t)} = {} & \epsilon_{qS}^i \bar{\xi}_L^{(t)A} U_{A7} S_{R,i} + \epsilon_{qQ}^j \bar{\xi}_L^{(t)A} U_{Aa} Q_{R,j}^a + \epsilon_{tQ}^j \bar{\xi}_R^{(t)BA} U_{Aa} U_{B7} Q_{L,j}^a \\ & + \epsilon_{tG}^k \bar{\xi}_R^{(t)BA} U_{Aa} U_{Bb} G_{L,k}^{ab} + \text{h.c.}, \end{aligned} \tag{I.B.5}$$

where repeated indices are summed. Here $\{i, j, k\}$ count the multiplicities of resonances and therefore run from 1 to $\{N_S, N_Q, N_G\}$, respectively, while A, B are $SO(7)$ indices and a, b are $SO(6)$ indices. Calculability of the one-loop scalar potential is obtained via generalized Weinberg sum rules (WSRs), see Appendix I.D for more details. The minimal field content that gives a completely ultraviolet (UV)-finite one-loop Higgs potential is $N_S = N_Q = N_G = 1$, which we adopt in the main text. The embeddings in Eq. (I.B.3) yield a Higgs potential with "double tuning" structure [168], where parametrically $\Delta^{-1} \sim (v^2/f^2)(\epsilon^t)^2$.

DM shift symmetry broken by b quark

This refers to the scenario discussed in Section 4.4. The simplest embedding of the bottom quark which breaks the DM shift symmetry is

$$\mathbf{7}_{-1/3} \sim \xi_L^{(b)} = \frac{1}{\sqrt{2}} \left(-i t_L, \quad t_L, \quad i b_L, \quad b_L, \quad \mathbf{0}_3^T \right)^T, \qquad \mathbf{7}_{-1/3} \sim \xi_R^{(b)} = b_R \left(\mathbf{0}_6^T, \quad 1 \right)^T. \tag{I.B.6}$$

[7] Fields with calligraphic names have the same $SO(4)$ quantum numbers as their non-calligraphic versions. For example $\mathcal{X}_{5/3}^{(\pm)}$ transforms as $X_{5/3}$ under $SO(4)$, but has in addition charge ± 1 under $U(1)_{\rm DM}$.

We thus expect resonances $Q^{(b)} \sim \mathbf{6}_{-1/3}$ and $S^{(b)} \sim \mathbf{1}_{-1/3}$ under $SO(6)\times U(1)_X$. The component expression of $Q^{(b)}$ is

$$Q^{(b)} = \frac{1}{\sqrt{2}}\left(iU_{-4/3} - i\widetilde{T}, U_{-4/3} + \widetilde{T}, iU_{-1/3} + i\widetilde{B}, -U_{-1/3} + \widetilde{B}, -i\mathcal{V} + i\mathcal{W}, \mathcal{V} + \mathcal{W}\right)^T, \quad \text{(I.B.7)}$$

where under $(SU(2)_L)^{\rm DM}_Y$ we have $(U_{-1/3}, U_{-4/3})^T \sim \mathbf{2}^0_{-5/6}$, $(\widetilde{T}, \widetilde{B})^T \sim \mathbf{2}^0_{1/6}$ and $\mathcal{V}, \mathcal{W} \sim \mathbf{1}^{\pm 1}_{-1/3}$. The elementary-composite mixing Lagrangian for this scenario is given in Eq. (4.55).

DM shift symmetry preserved by b quark
In Section 4.5 we assume that both the top and bottom embeddings preserve the DM shift symmetry. In this case we embed b_R as

$$\mathbf{21}_{2/3} \sim \xi^{(b)}_R = \frac{b_R}{2\sqrt{2}} \begin{pmatrix} & & 1 & i & \\ & \mathbf{0}_{2\times 2} & -i & 1 & \\ -1 & i & & & \\ -i & -1 & & \mathbf{0}_{2\times 2} & \\ & & & & \mathbf{0}_{3\times 3} \end{pmatrix}, \quad \text{(I.B.8)}$$

where empty entries are zeros. Therefore the embedding of q_L in Eq. (I.B.1) or Eq. (I.B.3) is sufficient to generate the bottom mass, and an $X = -1/3$ sector needs not be introduced. The Lagrangian that mixes the b_R with the composite resonances reads

$$\widetilde{\mathcal{L}}^{(b)}_{\rm mix} = \epsilon^j_{bQ}\bar{\xi}^{(b)BA}_R U_{Aa}U_{B7}Q^a_{L,j} + \epsilon^k_{bG}\bar{\xi}^{(b)BA}_R U_{Aa}U_{Bb}G^{ab}_{L,k} + \text{h.c.}, \quad \text{(I.B.9)}$$

and the complete fermionic Lagrangian is $\mathcal{L}_f = (\text{kin. terms}) + (\text{resonance masses}) + \mathcal{L}^{(t)}_{\rm mix} + \widetilde{\mathcal{L}}^{(b)}_{\rm mix}$.

I.C SO(7)/SO(6) model: gauge sector

At the leading order in derivatives, the Lagrangian describing the vector resonances $\rho_\mu \equiv \rho^{\hat{a}}_\mu t^{\hat{a}} \sim \mathbf{15}$ and $a_\mu \equiv a^a_\mu X^a \sim \mathbf{6}$ reads

$$\mathcal{L}_V = -\frac{1}{4}\text{Tr}\left(\rho_{\mu\nu}\rho^{\mu\nu}\right) + \frac{f^2_\rho}{2}\text{Tr}\left(g_\rho\rho_\mu - e_\mu\right)^2 - \frac{1}{4}\text{Tr}\left(a_{\mu\nu}a^{\mu\nu}\right) + \frac{f^2_a}{2\Delta^2}\text{Tr}\left(g_a a_\mu - \Delta d_\mu\right)^2, \quad \text{(I.C.1)}$$

where $f_{\rho,\,a}$ are decay constants, $g_{\rho,\,a}$ are couplings, and Δ is a dimensionless parameter. The field strengths are given by

$$\rho_{\mu\nu} = \partial_\mu\rho_\nu - \partial_\nu\rho_\mu - ig_\rho\left[\rho_\mu, \rho_\nu\right], \qquad a^a_{\mu\nu} = \nabla_\mu a^a_\nu - \nabla_\nu a^a_\mu, \quad \nabla_\mu = \partial_\mu - ie_\mu\,. \quad \text{(I.C.2)}$$

In the limit where the external gauge fields are neglected, the masses of the ρ and a read

$$m^2_\rho = g^2_\rho f^2_\rho\,, \qquad m^2_a = \frac{g^2_a f^2_a}{\Delta^2}\,. \quad \text{(I.C.3)}$$

Neglecting EWSB, only ρ_μ can mix with the $SU(2)_L \times U(1)_Y$ gauge fields. The mass eigenstates are obtained via the rotations

$$\begin{pmatrix}\bar{W}^\alpha \\ \rho^\alpha_L\end{pmatrix} \to \frac{1}{\sqrt{g^2_\rho + \bar{g}^2}}\begin{pmatrix} g_\rho & -\bar{g} \\ \bar{g} & g_\rho\end{pmatrix}\begin{pmatrix}W^\alpha \\ \rho^\alpha_L\end{pmatrix}, \qquad \begin{pmatrix}\bar{B} \\ \rho^3_R\end{pmatrix} \to \frac{1}{\sqrt{g^2_\rho + \bar{g}'^2}}\begin{pmatrix} g_\rho & -\bar{g}' \\ \bar{g}' & g_\rho\end{pmatrix}\begin{pmatrix}B \\ \rho^3_R\end{pmatrix}, \quad \text{(I.C.4)}$$

with W^α and B identified with the SM states. The associated SM couplings are $g = g_\rho \bar{g}/\sqrt{g_\rho^2 + \bar{g}^2}$ and $g' = g_\rho \bar{g}'/\sqrt{g_\rho^2 + \bar{g}'^2}$.

Gauging $U(1)_{\rm DM}$
In Section 4.5 we consider a model where the stabilizing $U(1)_{\rm DM}$ symmetry is gauged. In this case the CCWZ construction has to be slightly modified in order to include the additional gauge field. In the case when $SU(2)_L \times U(1)_Y \times U(1)_{\rm DM} \subset SO(6)$ are gauged the covariant derivative of the GB matrix in Eq. (I.A.8) is of the form $D_\mu U = \partial_\mu U - i A_\mu^{\hat{a}} T^{\hat{a}} U$, with

$$A_\mu^{\hat{a}} T^{\hat{a}} = \bar{g} \bar{W}_\mu^\alpha T_L^\alpha + \bar{g}' \bar{B}_\mu T_R^3 + \sqrt{2}\, \bar{g}_D \bar{A}_{D\mu} T^{\rm DM} \,. \tag{I.C.5}$$

The normalization of the $U(1)_{\rm DM}$ gauge coupling is chosen in such a way that the χ kinetic term obtained from the two-derivative GB Lagrangian

$$\mathcal{L}_\pi = \frac{f^2}{4}\, d_\mu^a d^{a\,\mu} \tag{I.C.6}$$

is $|(\partial_\mu - i\bar{g}_D \bar{A}_{D\mu})\chi|^2$. Through Eq. (I.C.1) $\bar{A}_D$ mixes with an $SO(4) \times U(1)_{\rm DM}$ singlet contained in ρ_μ. The mass matrix and the rotation that diagonalizes it are

$$\frac{f_\rho^2}{2} (\bar{A}_D, \rho_D) \begin{pmatrix} 2\bar{g}_D^2 & -\sqrt{2}\bar{g}_D g_\rho \\ -\sqrt{2}\bar{g}_D g_\rho & g_\rho^2 \end{pmatrix} \begin{pmatrix} \bar{A}_D \\ \rho_D \end{pmatrix}, \; \begin{pmatrix} \bar{A}_D \\ \rho_D \end{pmatrix} \to \begin{pmatrix} \frac{g_\rho}{\sqrt{g_\rho^2 + 2\bar{g}_D^2}} & -\frac{\sqrt{2}\bar{g}_D}{\sqrt{g_\rho^2 + 2\bar{g}_D^2}} \\ \frac{\sqrt{2}\bar{g}_D}{\sqrt{g_\rho^2 + 2\bar{g}_D^2}} & \frac{g_\rho}{\sqrt{g_\rho^2 + 2\bar{g}_D^2}} \end{pmatrix} \begin{pmatrix} A_D \\ \rho_D \end{pmatrix}, \tag{I.C.7}$$

hence the physical dark photon coupling is $g_D = g_\rho \bar{g}_D / \sqrt{g_\rho^2 + 2\bar{g}_D^2}$.

I.D SO(7)/SO(6) model: scalar potential and parameter scan

Integrating out the vector resonances at tree level, we obtain the effective Lagrangian containing the gauge fields $\bar{W}^\alpha, \bar{B}$ and the Higgs,

$$\mathcal{L}_g^{\rm eff} = \frac{1}{2}\Big(g^{\mu\nu} - \frac{p^\mu p^\nu}{p^2}\Big) \left(2\Pi_{+-} \bar{W}_\mu^+ \bar{W}_\nu^+ + \Pi_{33} \bar{W}_\mu^3 \bar{W}_\nu^3 + \Pi_{BB} \bar{B}_\mu \bar{B}_\nu + 2\Pi_{3B} \bar{W}_\mu^3 \bar{B}_\nu\right) \tag{I.D.1}$$

where

$$\Pi_{+-} = \Pi_{33} = \Pi_0 + \frac{\tilde{h}^2}{4f^2}\Pi_1^g \,, \quad \Pi_{BB} = \Pi_B + \frac{\bar{g}'^2}{\bar{g}^2}\frac{\tilde{h}^2}{4f^2}\Pi_1^g \,, \quad \Pi_{3B} = -\frac{\bar{g}'}{\bar{g}}\frac{\tilde{h}^2}{4f^2}\Pi_1^g \,. \tag{I.D.2}$$

The dynamics of the strong sector resonances are encoded in the momentum-dependent form factors, which read in Euclidean space

$$\Pi_{0(B)} = p^2\left(1 + \frac{\bar{g}^{(\prime)\,2} f_\rho^2}{p^2 + m_\rho^2}\right), \qquad \Pi_1^g = \bar{g}^2 \left[f^2 + 2p^2\left(\frac{f_a^2}{p^2 + m_a^2} - \frac{f_\rho^2}{p^2 + m_\rho^2}\right)\right]. \tag{I.D.3}$$

The effective potential for the Higgs has the expression

$$V_g(\tilde{h}) = \frac{3}{2}\int \frac{d^4p}{(2\pi)^4} \log\left[\Pi_{+-}^2 (\Pi_{33}\Pi_{BB} - \Pi_{3B}^2)\right]. \tag{I.D.4}$$

The gauge contribution is rendered finite by introducing generalized WSRs of the form

$$2f_\rho^2 - 2f_a^2 = f^2\,, \qquad f_\rho^2 m_\rho^2 = f_a^2 m_a^2\,, \qquad (\text{WSR } 1+2)_g\,. \tag{I.D.5}$$

The first relation removes the quadratic sensitivity to the cutoff in the Higgs mass squared $\mu_{h,\,g}^2$ and makes the Higgs quartic $\lambda_{h,\,g}$ finite, whereas the second relation cancels the remaining logarithmic divergence in $\mu_{h,g}^2$.

Integrating out the fermionic resonances at tree level we obtain an effective Lagrangian containing the top quark, the b_L and the GBs as degrees of freedom,

$$\mathcal{L}_t^{\text{eff}} = \Pi_L^b\, \bar{b}_L \not{p} b_L + \Pi_R^b \bar{b}_R \not{p} b_R + \Pi_L^t \bar{t}_L \not{p} t_L + \Pi_R^t \bar{t}_R \not{p} t_R - \left(\Pi_{LR}^t\, \bar{t}_L t_R + \Pi_{LR}^b\, \bar{b}_L b_R + \text{h.c.}\right), \tag{I.D.6}$$

In the following we specialize to the different scenarios we have discussed in Chapter 4.

A) DM shift symmetry broken by the top couplings
This scenario is discussed in Section 4.3 and assumes an embedding of q_L and t_R into the $\mathbf{7}_{2/3}$ of $SO(7)\times U(1)_X$. The RH bottom b_R is not introduced in this scenario, since it gives a subleading contribution to the effective potential. Integrating out the resonances in Eq. (4.15) we obtain the form factors in Eq. (I.D.6). We find that $\Pi_R^b = \Pi_{LR}^b = 0$ and $\Pi_L^b = \Pi_{L_0}$ for the bottom. For the top quark we find

$$\Pi_L^t = \Pi_{L_0} + \frac{\tilde{h}^2}{2f^2}\,\Pi_{L_1}\,, \quad \Pi_R^t = \Pi_{R_0} + \left(\frac{\tilde{h}^2}{f^2} + \frac{2\chi^*\chi}{f^2}\right)\Pi_{R_1}\,, \quad \Pi_{LR}^t = \frac{\tilde{h}}{\sqrt{2}f}\sqrt{1 - \frac{\tilde{h}^2}{f^2} - \frac{2\chi^*\chi}{f^2}}\;\Pi_1^t\,. \tag{I.D.7}$$

The momentum-dependent form factors read, in Euclidean space,

$$\begin{aligned}
\Pi_{L_0} &= 1 + \sum_{i=1}^{N_Q} \frac{|\epsilon_{qQ}^i|^2}{p^2 + m_{Q_i}^2}\,, \qquad \Pi_{L_1} = \sum_{j=1}^{N_S} \frac{|\epsilon_{qS}^j|^2}{p^2 + m_{S_j}^2} - \sum_{i=1}^{N_Q} \frac{|\epsilon_{qQ}^i|^2}{p^2 + m_{Q_i}^2}\,,\\
\Pi_{R_0} &= 1 + \sum_{j=1}^{N_S} \frac{|\epsilon_{tS}^j|^2}{p^2 + m_{S_j}^2}\,, \qquad \Pi_{R_1} = \sum_{i=1}^{N_Q} \frac{|\epsilon_{tQ}^i|^2}{p^2 + m_{Q_i}^2} - \sum_{j=1}^{N_S} \frac{|\epsilon_{tS}^j|^2}{p^2 + m_{S_j}^2}\,,\\
\Pi_1^t &= \sum_{j=1}^{N_S} \frac{\epsilon_{tS}^{*j}\epsilon_{qS}^j m_{S_j}}{p^2 + m_{S_j}^2} - \sum_{i=1}^{N_Q} \frac{\epsilon_{tQ}^{*i}\epsilon_{qQ}^i m_{Q_i}}{p^2 + m_{Q_i}^2}\,.
\end{aligned} \tag{I.D.8}$$

The effective potential for the GBs reads

$$V_f(\tilde{h},\chi) = -2N_c \int \frac{d^4p}{(2\pi)^4} \log\left(p^2\Pi_L^t\Pi_R^t + |\Pi_{LR}^t|^2\right). \tag{I.D.9}$$

Expanding Eqs. (I.D.4) and (I.D.9) to quartic order in the fields and matching with Eq. (4.17), we obtain the expressions of the parameters $\mu_h^2, \lambda_h, \mu_{\text{DM}}^2, \lambda_{\text{DM}}$ and λ as integrals over the form factors. For the dominant fermion contribution we find

$$\begin{aligned}
\mu_{h,f}^2 &= -\frac{N_c}{8\pi^2 f^2}\int_0^\infty dp^2 p^2 \left(\frac{\Pi_{L_1}}{\Pi_{L_0}} + \frac{2\Pi_{R_1}}{\Pi_{R_0}} + \frac{(\Pi_1^t)^2}{p^2\Pi_{L_0}\Pi_{R_0}}\right),\\
\lambda_{h,f} &= \frac{N_c}{4\pi^2 f^4}\int_{\mu_{\text{IR}}^2}^\infty dp^2 p^2 \left[\frac{1}{4}\left(\frac{\Pi_{L_1}}{\Pi_{L_0}} + \frac{2\Pi_{R_1}}{\Pi_{R_0}} + \frac{(\Pi_1^t)^2}{p^2\Pi_{L_0}\Pi_{R_0}}\right)^2 + \frac{(\Pi_1^t)^2 - p^2\Pi_{L_1}\Pi_{R_1}}{p^2\Pi_{L_0}\Pi_{R_0}}\right],
\end{aligned}$$

$$\mu^2_{\rm DM} = -\frac{N_c}{4\pi^2 f^2}\int_0^\infty dp^2 p^2 \frac{\Pi_{R_1}}{\Pi_{R_0}}\,, \qquad \lambda_{\rm DM} = \frac{N_c}{4\pi^2 f^4}\int_0^\infty dp^2 p^2 \frac{\Pi^2_{R_1}}{\Pi^2_{R_0}}\,,$$
$$\lambda = \frac{N_c}{8\pi^2 f^4}\int_0^\infty dp^2 p^2 \left[2\,\frac{\Pi^2_{R_1}}{\Pi^2_{R_0}} + \frac{(\Pi^t_1)^2}{p^2\Pi_{L_0}\Pi_{R_0}}\left(1+\frac{\Pi_{R_1}}{\Pi_{R_0}}\right)\right], \tag{I.D.10}$$

where we assumed real mixing parameters ϵ. Notice that the integral for the Higgs quartic $\lambda_{h,f}$ is IR divergent; the same happens for the (small) gauge contribution $\lambda_{h,g}$. The IR divergence signals that the potential is non-analytic at $\tilde{h}=0$, due to the contribution of the light degrees of freedom (the top quark and SM gauge bosons). To remove this issue, the expansion of the potential in Eq. (4.17) is extended to include an additional term $\Delta V = (\delta_h/2)\tilde{h}^4\log(\tilde{h}^2/f^2)$, which captures the non-analytic contribution to the Higgs quartic. Then all the coefficients of $V+\Delta V$ are IR-finite, including δ_h. The Higgs VEV $\langle\tilde{h}\rangle = v$ is obtained by solving the equation $\langle\tilde{h}\rangle^2 = -\mu_h^2/[\lambda_h + \delta_h(1+2\log(\langle\tilde{h}\rangle^2/f^2))]$, and the Higgs mass is $m_h^2 = (1-\xi)2v^2(\lambda_h + 3\delta_h + 2\delta_h\log\xi)$.

B) DM shift symmetry broken by the bottom couplings

The scenario where the dominant source of DM shift symmetry breaking is the coupling of the bottom quarks to the strong sector is discussed in Section 4.4 and assumes that q_L, t_R, b_R couple to operators $\mathcal{O}_q \sim \mathbf{7}_{2/3}, \mathcal{O}_t \sim \mathbf{21}_{2/3}$ and $\mathcal{O}_{q',b} \sim \mathbf{7}_{-1/3}$ under $SO(7)\times U(1)_X$. Integrating out the top in Eq. (I.B.5) and the bottom partners in Eq. (4.55) we can match to Eq. (I.D.6). For the top we obtain

$$\Pi^t_L = \Pi_{L_0} + \frac{\tilde{h}^2}{2f^2}\Pi^t_{L_1}\,, \quad \Pi^t_R = \Pi^t_{R_0} + \frac{\tilde{h}^2}{4f^2}\Pi^t_{R_1}\,, \quad \Pi^t_{LR} = \frac{\tilde{h}}{2\sqrt{2}f}\Pi^t_1\,. \tag{I.D.11}$$

with the momentum-dependent form factors in Euclidean space,

$$\Pi_{L_0} = 1 + \sum_{i=1}^{N_Q}\frac{|\epsilon^i_{qQ}|^2}{p^2+m^2_{Q_i}} + \sum_{n=1}^{N_Q^{(b)}}\frac{|\epsilon^n_{qQ^{(b)}}|^2}{p^2+m^2_{Q^{(b)}_n}}\,, \qquad \Pi^t_{L_1} = \sum_{j=1}^{N_S}\frac{|\epsilon^j_{qS}|^2}{p^2+m^2_{S_j}} - \sum_{i=1}^{N_Q}\frac{|\epsilon^i_{qQ}|^2}{p^2+m^2_{Q_i}}\,,$$
$$\Pi^t_{R_0} = 1 + \sum_{k=1}^{N_G}\frac{|\epsilon^k_{tG}|^2}{p^2+m^2_{G_k}}\,, \qquad \Pi^t_{R_1} = \sum_{i=1}^{N_Q}\frac{|\epsilon^i_{tQ}|^2}{p^2+m^2_{Q_i}} - 2\sum_{k=1}^{N_G}\frac{|\epsilon^k_{tG}|^2}{p^2+m^2_{G_k}}\,,$$
$$\Pi^t_1 = -\sum_{i=1}^{N_Q}\frac{\epsilon^{*i}_{tQ}\epsilon^i_{qQ}m_{Q_i}}{p^2+m^2_{Q_i}}\,. \tag{I.D.12}$$

The top contributes only to the Higgs potential parameters, which after expanding Eq. (I.D.9) in the fields with the above form factors yields

$$\mu^2_{h,t} = -\frac{N_c}{8\pi^2 f^2}\int dp_E^2 p_E^2\left(\frac{\Pi^t_{L_1}}{\Pi_{L_0}} + \frac{\Pi^t_{R_1}}{2\Pi^t_{R_0}} + \frac{(\Pi^t_1)^2}{4p_E^2\Pi_{L_0}\Pi^t_{R_0}}\right),$$
$$\lambda_{h,t} = \frac{N_c}{16\pi^2 f^4}\int dp_E^2 p_E^2\left[\left(\frac{\Pi^t_{L_1}}{\Pi_{L_0}} + \frac{\Pi^t_{R_1}}{2\Pi^t_{R_0}} + \frac{(\Pi^t_1)^2}{4p_E^2\Pi_{L_0}\Pi^t_{R_0}}\right)^2 - \frac{\Pi^t_{L_1}\Pi^t_{R_1}}{\Pi_{L_0}\Pi^t_{R_0}}\right]. \tag{I.D.13}$$

$\mu^2_{h,t}$ and $\lambda_{h,t}$ can be made fully calculable if we require two sets of WSRs

$$\sum_{j=1}^{N_S}|\epsilon^j_{qS}|^2 = \sum_{i=1}^{N_Q}|\epsilon^i_{qQ}|^2\,, \qquad 2\sum_{k=1}^{N_G}|\epsilon^k_{tG}|^2 = \sum_{i=1}^{N_Q}|\epsilon^i_{tQ}|^2\,, \qquad \text{(WSR 1)}_t \tag{I.D.14}$$

$$\sum_{i=1}^{N_Q} m_{Q_i}^2 \left(2|\epsilon_{qQ}^i|^2 - |\epsilon_{tQ}^i|^2\right) + 2\sum_{k=1}^{N_G} m_{G_k}^2 |\epsilon_{tG}^k|^2 - 2\sum_{j=1}^{N_S} m_{S_j}^2 |\epsilon_{qS}^j|^2 = 0\,. \qquad \text{(WSR 2)}_t \qquad \text{(I.D.15)}$$

For the bottom we obtain

$$\Pi_L^b = \Pi_{L_0} + \frac{\tilde{h}^2}{2f^2}\Pi_{L_1}^b\,, \quad \Pi_R^b = \Pi_{R_0}^b + \left(\frac{\tilde{h}^2}{f^2} + \frac{2\chi^*\chi}{f^2}\right)\Pi_{R_1}^b\,, \quad \Pi_{LR}^b = \frac{\tilde{h}}{\sqrt{2}f}\sqrt{1 - \frac{\tilde{h}^2}{f^2} - \frac{2\chi^*\chi}{f^2}}\,\Pi_1^b\,. \tag{I.D.16}$$

In this case the Euclidean form factors are,

$$\begin{aligned}
\Pi_{L_0} &= 1 + \sum_{i=1}^{N_Q} \frac{|\epsilon_{qQ}^i|^2}{p^2 + m_{Q_i}^2} + \sum_{n=1}^{N_Q^{(b)}} \frac{|\epsilon_{qQ^{(b)}}^n|^2}{p^2 + m_{Q_n^{(b)}}^2}\,, & \Pi_{L_1}^b &= \sum_{m=1}^{N_S^{(b)}} \frac{|\epsilon_{qS^{(b)}}^m|^2}{p^2 + m_{S_j^{(b)}}^2} - \sum_{n=1}^{N_Q^{(b)}} \frac{|\epsilon_{qQ^{(b)}}^n|^2}{p^2 + m_{Q_n^{(b)}}^2}\,,\\
\Pi_{R_0}^b &= 1 + \sum_{m=1}^{N_S^{(b)}} \frac{|\epsilon_{bS^{(b)}}^m|^2}{p^2 + m_{S_m^{(b)}}^2}\,, & \Pi_{R_1}^b &= \sum_{n=1}^{N_Q} \frac{|\epsilon_{bQ^{(b)}}^n|^2}{p^2 + m_{Q_n^{(b)}}^2} - \sum_{m=1}^{N_S^{(b)}} \frac{|\epsilon_{bS^{(b)}}^m|^2}{p^2 + m_{S_m^{(b)}}^2}\,,\\
\Pi_1^b &= \sum_{m=1}^{N_S^{(b)}} \frac{\epsilon_{bS^{(b)}}^{*m}\epsilon_{qS^{(b)}}^m m_{S_m^{(b)}}}{p^2 + m_{S_m^{(b)}}^2} - \sum_{n=1}^{N_Q^{(b)}} \frac{\epsilon_{bQ^{(b)}}^{*n}\epsilon_{qQ^{(b)}}^n m_{Q_n^{(b)}}}{p^2 + m_{Q_n^{(b)}}^2}\,.
\end{aligned} \tag{I.D.17}$$

The resulting contributions to the scalar potential are

$$\begin{aligned}
\mu_{h,b}^2 &= -\frac{N_c}{8\pi^2 f^2}\int_0^\infty dp_E^2 p_E^2 \left(\frac{\Pi_{L_1}^b}{\Pi_{L_0}} + \frac{2\Pi_{R_1}^b}{\Pi_{R_0}^b} + \frac{(\Pi_1^b)^2}{p_E^2 \Pi_{L_0}\Pi_{R_0}^b}\right),\\
\lambda_{h,b} &= \frac{N_c}{4\pi^2 f^4}\int_{\mu_{\rm IR}^2}^\infty dp_E^2 p_E^2 \left[\frac{1}{4}\left(\frac{\Pi_{L_1}^b}{\Pi_{L_0}} + \frac{2\Pi_{R_1}^b}{\Pi_{R_0}^b} + \frac{(\Pi_1^b)^2}{p_E^2\Pi_{L_0}\Pi_{R_0}^b}\right)^2 + \frac{(\Pi_1^b)^2 - p_E^2\Pi_{L_1}^b\Pi_{R_1}^b}{p_E^2\Pi_{L_0}\Pi_{R_0}^b}\right],\\
\mu_{\rm DM}^2 &= -\frac{N_c}{4\pi^2 f^2}\int_0^\infty dp_E^2 p_E^2 \frac{\Pi_{R_1}^b}{\Pi_{R_0}^b}\,, \qquad \lambda_{\rm DM} = \frac{N_c}{4\pi^2 f^4}\int_0^\infty dp_E^2 p_E^2 \frac{(\Pi_{R_1}^b)^2}{(\Pi_{R_0}^b)^2}\,,\\
\lambda &= \frac{N_c}{8\pi^2 f^4}\int_0^\infty dp_E^2 p_E^2 \left[2\frac{(\Pi_{R_1}^b)^2}{(\Pi_{R_0}^b)^2} + \frac{(\Pi_1^b)^2}{p_E^2\Pi_{L_0}\Pi_{R_0}^b}\left(1 + \frac{\Pi_{R_1}^b}{\Pi_{R_0}^b}\right)\right].
\end{aligned} \tag{I.D.18}$$

The contributions to the Higgs potential are subleading compared to the ones generated by the top. However, these are the dominant sources for $\mu_{\rm DM}^2, \lambda_{\rm DM}$ and λ. In order to get a finite result we also have to impose a set of WSRs for the bottom sector

$$\sum_{m=1}^{N_S^{(b)}} |\epsilon_{qS^{(b)}}^m|^2 = \sum_{n=1}^{N_Q^{(b)}} |\epsilon_{qQ^{(b)}}^n|^2\,, \qquad \sum_{m=1}^{N_S^{(b)}} |\epsilon_{bS^{(b)}}^m|^2 = \sum_{n=1}^{N_Q^{(b)}} |\epsilon_{bQ^{(b)}}^n|^2\,, \qquad \text{(WSR 1)}_b \tag{I.D.19}$$

$$\sum_{n=1}^{N_Q^{(b)}} m_{Q_n^{(b)}}^2 |\epsilon_{qQ^{(b)}}^n|^2 = \sum_{m=1}^{N_S^{(b)}} m_{S_m^{(b)}}^2 |\epsilon_{qS^{(b)}}^m|^2\,, \quad \sum_{n=1}^{N_Q^{(b)}} m_{Q_n^{(b)}}^2 |\epsilon_{bQ^{(b)}}^n|^2 = \sum_{m=1}^{N_S^{(b)}} m_{S_m^{(b)}}^2 |\epsilon_{bS^{(b)}}^m|^2\,. \quad \text{(WSR 2)}_b \tag{I.D.20}$$

The minimal model with a completely calculable potential and non-vanishing $\mu_{\rm DM}^2$ requires $N_S = N_Q = N_G = N_Q^{(b)} = 1$ and $N_S^{(b)} = 2$. In Section 4.4 we are content with a partially

calculable potential, which allows for a parametrically simpler understanding of the parameter space, and only impose the first set of bottom sum rules Eq. (I.D.19). This makes the marginal couplings finite but leaves a residual logarithmic divergence, which we regularize with a hard cutoff Λ.

C) DM shift symmetry broken by the gauging of $\mathbf{U(1)_{DM}}$

This scenario assumes that both the top and bottom couplings only break the Higgs, but preserve the DM shift symmetry. The DM shift symmetry is only broken by the gauging of $U(1)_{\rm DM}$, under which all SM particles are uncharged. Thus the generation of the Higgs and DM potential are fully decoupled. For this reason we assume that the fermion and $SU(2)_L \times U(1)_Y$ part of of the gauge sector take care of generating a realistic Higgs potential and only concentrate on the potential for the DM, which is generated by dark photon loops.

In order to compute the DM effective potential we integrate out the vector resonances. This generates and effective Lagrangian for the gauge sector, but he we will only keep the part containing the dark photon

$$\mathcal{L}^{\rm eff}_{A_D} = \frac{1}{2}\Big(g^{\mu\nu} - \frac{p^\mu p^\nu}{p^2}\Big)\Pi_{AA}\bar{A}_{D\mu}\bar{A}_{D\nu}, \qquad \Pi_{AA} = \Pi_A + \frac{2\bar{g}_D^2}{\bar{g}^2}\frac{\chi^*\chi}{f^2}\,\Pi_1^g, \tag{I.D.21}$$

with Euclidean-space form factors

$$\Pi_A = p^2\left(1 + \frac{2\bar{g}_D^2 f_\rho^2}{p^2+m_\rho^2}\right), \qquad \Pi_1^g = \bar{g}^2\left[f^2 + 2p^2\left(\frac{f_a^2}{p^2+m_a^2} - \frac{f_\rho^2}{p^2+m_\rho^2}\right)\right]. \tag{I.D.22}$$

The contribution to the one-loop effective potential is $V_{A_D}(\chi)$, which is given by

$$V_{A_D}(\chi) = \frac{3}{2}\int\frac{d^4p}{(2\pi)^4}\log\left[1 + \frac{\bar{g}_D^2}{\bar{g}^2}\frac{2\chi^*\chi}{f^2}\frac{\Pi_1^g}{\Pi_A}\right]. \tag{I.D.23}$$

Note that, importantly, the one-loop potential does not contain a Higgs portal term $\sim \lambda\tilde{h}^2\chi^*\chi$. Expanding the logarithm in Eq. (I.D.23) and matching to Eq. (3.11) gives for the χ mass term

$$\mu^2_{\rm DM} = \frac{3\bar{g}_D^2}{16\pi^2\bar{g}^2 f^2}\int_0^\infty dp^2 p^2\frac{\Pi_1^g}{\Pi_A}, \tag{I.D.24}$$

which is in general quadratically UV-divergent, but is automatically rendered finite after the two WSRs in Eq. (I.D.5) that ensure finiteness of $V_g(\tilde{h})$ are imposed. After the WSRs are used to express f_a, m_a in terms of f_ρ, m_ρ, and f, we find $\Pi_1^g > 0$, which guarantees that $U(1)_{\rm DM}$ is never spontaneously broken. Performing the integral and taking the leading order in $\bar{g}_D^2 f^2/m_\rho^2, \bar{g}_D^2 f_\rho^2/m_\rho^2 \ll 1$ we arrive at

$$\mu^2_{\rm DM} \simeq \frac{3\alpha_D}{2\pi}\frac{f_\rho^2}{f^2}\,m_\rho^2\log\left(\frac{2f_\rho^2/f^2}{2f_\rho^2/f^2 - 1}\right). \tag{I.D.25}$$

The results above assume a massless dark photon. A Stückelberg mass can be obtained by extending the coset to $SO(7)\times U(1)'/SO(6)$ and gauging the diagonal combination of $U(1)_{\rm DM}\times U(1)'$, namely $\sqrt{2}\,T^{\rm DM} + Z'$. All SM fields are assumed to be uncharged under $U(1)'$. The extended Goldstone matrix is $U = \exp(i\sqrt{2}\pi^a X^a/f)\exp(i\hat{\pi}Z'/f')$ and the two-derivative Lagrangian becomes $\mathcal{L}_\pi + (f'^2/2)\hat{d}_\mu\hat{d}^\mu$, where $\hat{d}_\mu = -(\partial_\mu\hat{\pi} - \bar{g}_D f'\bar{A}_{D\mu})/f'$ to all orders in $1/f'$. The additional piece is precisely the Stückelberg Lagrangian, which gives a mass $m_A = \bar{g}_D f'$ to

$\bar{A}_D$. In the effective Lagrangian of Eq. (I.D.21) we must then replace $\Pi_A \to \Pi_A + m_A^2$, which in turn leads to a suppression of the χ mass: taking for simplicity $f_\rho = f$, Eq. (I.D.25) becomes

$$\frac{\mu^2_{\rm DM}(m_A^2)}{\mu^2_{\rm DM}(0)}\Big|_{f_\rho = f} = \frac{1 + \frac{y}{2(1-y)}\frac{\log y}{\log 2}}{1 - \frac{y}{2}}\,, \qquad y \equiv \frac{m_A^2}{m_\rho^2}\,. \tag{I.D.26}$$

Numerically, the suppression is small: for example $\mu^2_{\rm DM}(m_A^2)/\mu^2_{\rm DM}(0) \approx 0.97$ for $m_A/m_\rho = 1/10$. As long as m_A^2/m_ρ^2, $\bar{g}_D^2/g_\rho^2 \ll 1$, after m_A^2 is included in the mass matrix in Eq. (I.C.7) the diagonalization is still obtained through a rotation of angle $\theta \sim \sqrt{2}\bar{g}_D/g_\rho$.

Parameter scans

In Chapter 4 we often used numeric parameter scans to get an intuition for the parameter space and to justify estimates. Here we briefly summarize our procedure for the parameter scan on the example of the two-layer model in Section 4.3. All other scans were performed in a similar fashion.

We start from Eq. (4.31) and requiring that $0 \le s^2_{\theta,\phi} \le 1$, what leads to the constraints

$$\frac{m^2_{S_1} - m^2_{Q_1}}{m^2_{Q_2} - m^2_{Q_1}} \le s^2_{\alpha,\beta} \le \frac{m^2_{S_2} - m^2_{Q_1}}{m^2_{Q_2} - m^2_{Q_1}}\,. \tag{I.D.27}$$

These can be satisfied only for $m_{S_2} > m_{Q_1}$, which we therefore assume. Taking into account that Π_1^t is the only form factor that is sensitive to the signs of the mixing parameters ϵ, and that furthermore the scalar potential is unaffected by $\Pi_1^t \to -\Pi_1^t$, the angles are restricted to the following ranges

$$\theta, \alpha \in [-\pi/2, \pi/2], \qquad \phi \in [0, \pi/2], \qquad \beta \in [0, \pi]. \tag{I.D.28}$$

We summarize here the procedure adopted in the parameter scan of the two-layer model with WSRs (the procedure for the scan of the one-layer model is analogous).

1. The following parameters are randomly selected: $\epsilon_t \in [f/10, 8f]$, $m_{S_1,Q_1} \in [0, 6f]$, $m_{S_2,Q_2} \in [m_{Q_1}, 6f]$, $f_\rho \in \left[f/\sqrt{2}, 2f\right]$;
2. The angles α and β are randomly picked, compatibly with the restrictions in Eqs. (I.D.27) and (I.D.28). Then ϕ is completely fixed, while the sign of $\sin\theta$ is picked randomly.
3. ϵ_q is fixed by solving the following equation

$$m_t^2 = \frac{\left|\Pi_{LR}(m_t^2)\right|^2}{\Pi_L(m_t^2)\Pi_R(m_t^2)}\bigg|_{\tilde{h}=v,\,\chi=0}\,, \tag{I.D.29}$$

   where the numerical value of the top mass is set to $m_t = m_t^{\overline{MS}}(2\text{ TeV}) = 150$ GeV.
4. m_ρ is fixed by requiring the Higgs VEV to match the observed value, $\langle\tilde{h}\rangle = v \simeq 246$ GeV.

In the two-layer model, the compositeness fraction s_L (s_R) of the left (right) handed top is computed by diagonalizing analytically the fermion mass matrix for $v \to 0$, and taking the projection onto the composite fermions of the normalized eigenvector that corresponds to the physical t_L (t_R). For example, the compositeness fraction of t_R is defined as

$$s_R \equiv \sqrt{\frac{a_2^2 + a_3^2}{a_1^2 + a_2^2 + a_3^2}} \qquad \text{with} \qquad t_R^p = \frac{1}{\sqrt{a_1^2 + a_2^2 + a_3^2}}\,(a_1 t_R + a_2 S_1 + a_3 S_2), \tag{I.D.30}$$

where t_R^p denotes the mass-eigenstate right-handed top (for $v \to 0$). The compositeness fractions satisfy $0 \leq s_{L,R} \leq 1$. In the one-layer model, they are identified with the sine of the elementary-composite mixing angles.

I.E SO(7)/SO(6) model: $U(1)_Y$ - $U(1)_{\rm DM}$ kinetic mixing

In this appendix we show that kinetic mixing of $U(1)_Y$ and $U(1)_{\rm DM}$ (in short, Y-DM kinetic mixing) can vanish exactly in the $SO(7)/SO(6)$ model, thus motivating the choice $\varepsilon = 0$ made throughout our discussion.

As first step, we neglect the explicit $\mathcal{G}$ breaking in the fermion sector and consider the bosonic Lagrangian including the gauging of $SU(2)_L \times U(1)_Y \times U(1)_{\rm DM}$. At $O(p^2)$ this is simply given by Eq. (I.C.6), and the kinetic mixing operators arise at $O(p^4)$. The four-derivative bosonic Lagrangian was first written down for the $SO(5)/SO(4)$ model in [237]. To obtain a basis of operators for our model we find it convenient to follow [238], where the $O(p^4)$ Lagrangian for $SO(5)/SO(4)$ was discussed by parametrizing the GBs with the matrix $\Sigma(\boldsymbol{\pi}) = U(\boldsymbol{\pi})^2$. This alternative, but equivalent, description is possible for *symmetric* cosets such as $SO(N+1)/SO(N)$, which admit an automorphism (grading) $\mathcal{R}$ of the algebra that flips the sign of only the broken generators, $T^{\hat{a}} \to +T^{\hat{a}}$ and $X^a \to -X^a$. The three building blocks that are used to construct invariant operators, all transforming in the adjoint of $\mathcal{G}$, are

$$V_\mu = (D_\mu \Sigma)\Sigma^{-1}, \qquad A_{\mu\nu} = \partial_\mu A_\nu - \partial_\nu A_\mu - i[A_\mu, A_\nu], \qquad \Sigma A^{\mathcal{R}}_{\mu\nu}\Sigma^{-1}, \tag{I.E.1}$$

where $A^{\mathcal{R}}_{\mu\nu} \equiv \mathcal{R}(A_{\mu\nu})$ and we formally took the whole of $\mathcal{G}$ to be gauged by $A_\mu = g_{\mathcal{G}} A^A_\mu T^A$, hence the covariant derivative is $D_\mu \Sigma = \partial_\mu \Sigma - i(A_\mu \Sigma - \Sigma A^{\mathcal{R}}_\mu)$. In this formalism, the two-derivative Lagrangian is $\mathcal{L}_\pi = -(f^2/16)\mathrm{Tr}\big[V_\mu V^\mu\big]$.

In our model the physical sources are given by Eq. (I.C.5), which satisfies $A^{\mathcal{R}}_\mu = A_\mu$. By constructing a complete basis for the $O(p^4)$ Lagrangian $\mathcal{L}_4$, we find that Y-DM kinetic mixing is encoded by the operators

$$\mathrm{Tr}\big[\bar{\mathbf{B}}_{\mu\nu}\bar{\mathbf{F}}_D^{\mu\nu}\big], \qquad \mathrm{Tr}\big[\Sigma\bar{\mathbf{B}}_{\mu\nu}\Sigma^{-1}\bar{\mathbf{F}}_D^{\mu\nu}\big], \tag{I.E.2}$$

where $\bar{\mathbf{B}}^{\mu\nu} \equiv \bar{g}' \bar{B}^{\mu\nu} T^3_R$ and $\bar{\mathbf{F}}^{\mu\nu}_D \equiv \sqrt{2}\,\bar{g}_D \bar{F}^{\mu\nu}_D T^{\rm DM}$. Both operators in Eq. (I.E.2) vanish identically. In fact, we have checked that the whole $\mathcal{L}_\pi + \mathcal{L}_4$ is invariant under the parity $P_6 = \mathrm{diag}\,(1,1,1,1,1,-1,1) \in O(7)$. Recalling that $T^{\rm DM}$ generates rotations in the $(5,6)$ plane $[\sqrt{2}\,T^{\rm DM} = \mathrm{diag}\,(\mathbf{0}_{4\times4}, \sigma^2, 0)]$, P_6 is identified with the charge conjugation C_D that we referred to in the main text. The action of P_6 on the $SO(7)$ generators is

$$P_6\, T P_6 = +T, \quad T = \Big\{T^\alpha_{L,R}, T^{a5}, X^b\Big\} \qquad \text{and} \qquad P_6\, \mathcal{T} P_6 = -\mathcal{T}, \quad \mathcal{T} = \big\{T^{\rm DM}, T^{a6}, X^6\big\} \tag{I.E.3}$$

where $a = 1, \ldots, 4$ and $b = 1, \ldots, 5$. As a consequence, the GBs and the elementary gauge fields transform as

$$\chi \to -\chi^*, \qquad \bar{A}_D \to -\bar{A}_D\,, \qquad \{h_i, \bar{W}, \bar{B}\} \to +\{h_i, \bar{W}, \bar{B}\} \qquad (i = 1, \ldots, 4), \tag{I.E.4}$$

which shows that if P_6 is exact, Y-DM kinetic mixing is forbidden. Furthermore, "higher-derivative kinetic mixing" operators (i.e. operators that mix $\bar{B}^{\mu\nu}$ and $\bar{F}^{\mu\nu}_D$, but with the insertion of additional derivatives) also have to be built out of the objects in Eq. (I.E.1), and are found to vanish. Summarizing our results thus far, the explicit breaking of $SO(7)$ due to the weak gauging does not generate Y-DM kinetic mixing.

As second step, we turn on the explicit $\mathcal{G}$ breaking in the fermion sector. Since $[T^{\rm DM}, P_6] \neq 0$, the SM fermions cannot be simultaneously assigned a nonzero $U(1)_{\rm DM}$ charge and definite P_6 parity. Therefore if the SM fermions were taken to have $Q_{\rm DM} \neq 0$, then fermion loops would generate Y-DM kinetic mixing: for example, this would happen if q_L were embedded in the $(\mathbf{2},\mathbf{2})_{+1} \subset \mathbf{21}_{2/3}$ of $SO(7)\times U(1)_X$ and t_R in the $(\mathbf{1},\mathbf{1})_{+1} \subset \mathbf{7}_{2/3}$. However, for our purposes we must take $Q_{\rm DM} = 0$ for all SM fields, in order for χ to be the lightest $U(1)_{\rm DM}$-charged particle and therefore stable. In this case each elementary fermion can be assigned definite parity (all the fermion embeddings employed in this paper have in fact $P_6 = +1$), which guarantees that fermion loops do not generate Y-DM kinetic mixing.

Note that the last conclusion can be altered by subleading spurions, if a single elementary fermion couples to operators with different P_6. As a concrete example we can imagine that t_R has, in addition to the embedding in the $(\mathbf{1},\mathbf{3})_0 \subset \mathbf{21}_{2/3}$ given in Eq. (I.B.3), a second embedding in the $(\mathbf{1},\mathbf{1})_0 \subset \mathbf{21}_{2/3}$, namely $\xi_R^{\prime(t)} = t_R T^{\rm DM}$. Then it is clear from Eq. (I.E.3) that the first spurion has $P_6 = +1$ while the second has $P_6 = -1$, so t_R cannot be assigned a definite parity. Nonetheless, P_6 invariance of the fermionic Lagrangian can still be *enforced*, by imposing that each elementary field couples to only even operators (or only odd ones, although we are not interested in that possibility here).

Notice that from Eq. (I.E.3) it follows that P_6 also acts on the resonances: taking as examples the S, Q and G fermionic multiplets, we have

$$\mathcal{Y} \leftrightarrow -\mathcal{Z}\,, \qquad \widetilde{S} \to -\widetilde{S}, \qquad \{\mathcal{T}^{(+)}, \mathcal{B}^{(+)}, \mathcal{X}^{(+)}_{2/3}, \mathcal{X}^{(+)}_{5/3}\} \leftrightarrow -\{\mathcal{T}^{(-)}, \mathcal{B}^{(-)}, \mathcal{X}^{(-)}_{2/3}, \mathcal{X}^{(-)}_{5/3}\}, \quad \text{(I.E.5)}$$

while all the other components are left invariant. One can similarly derive the transformation properties of the other fermionic resonances and of the vector multiplets, where in particular $\rho_D \to -\rho_D$.

I.F Details on DM phenomenology

In this appendix we collect details relevant for DM phenomenology in the different scenarios.

Global view on pNGB DM

The equations we give here refer to the most general EFT of pNGB DM given in Section 3.3.

To calculate the cross section for DM scattering on nuclei, we first match Eq. (3.17) to the following effective DM-SM interactions,

$$\begin{aligned}\sum_{\psi=u,d,c,s,t,b} &\Big(m_\psi a_\psi |\chi|^2\, \overline{\psi}\psi + i(\chi^* \overleftrightarrow{\partial_\mu} \chi)\, \overline{\psi}\gamma^\mu(\lambda^V_\psi + \lambda^A_\psi \gamma_5)\psi\Big) \\ &+ \frac{ie}{m_*^2} c_B (\chi^* \overleftrightarrow{\partial_\mu}\chi)\partial_\nu F^{\mu\nu} + \frac{d_G\, y^2}{16\pi^2}\frac{g_s^2}{m_*^2}|\chi|^2 G^a_{\mu\nu} G^{a\,\mu\nu}\end{aligned} \qquad \text{(I.F.1)}$$

with coefficients

$$a_\psi = \frac{2\,\lambda}{m_h^2} + \frac{c^\chi_\psi}{f^2} \qquad \lambda^V_\psi = \frac{b_{\psi_R} + b_{q_L}}{2f^2}\,, \qquad \lambda^A_\psi = \frac{b_{\psi_R} - b_{q_L}}{2f^2}\,. \qquad \text{(I.F.2)}$$

From these we derive the spin-independent DM-nucleon cross section up to one loop (see Sec-

tion 2.4.3 for more details),

$$\sigma_{\rm SI}^{\chi N,\,\chi^* N} = \frac{1}{\pi}\left(\frac{m_\chi m_N}{m_\chi+m_N}\right)^2 \frac{1}{A^2}\Bigg\{Z\Bigg[\frac{m_p}{2m_\chi}\Big(\sum_{\psi=u,d,s} f^p_{T_\psi}\,a_\psi + \frac{2}{27}f^p_{T_g}\Big(\sum_{\psi=c,b,t} a_\psi - 3\frac{d_G\,y^2}{m_*^2}\Big)\Big) \pm \sum_{\psi=u,d} f^p_{V_\psi}(\lambda^V_\psi + \delta\lambda^V_\psi)\Bigg] + \{p\to n, Z\to A-Z\}\Bigg\}^2 \tag{I.F.3}$$

where $\delta\lambda^V_\psi = c_B e^2 Q_\psi/m_*^2$ and $m_N = (m_p+m_n)/2$. The form factors averaged over proton and neutron take the values $f_{T_{u,d}} \approx 0.020, 0.043$ [120, 239] (see also [119]), $f_{T_s} = 0.043$ [121] (also [240]) and $f_{T_g} \approx 0.89$. It is important to note that for the vector current operators proportional to λ^V_ψ, the form factors simply count the valence content of the nucleons, namely $f^p_{V_u} = f^n_{V_d} = 2$ and $f^p_{V_d} = f^n_{V_u} = 1$. The additional term proportional to $\delta\lambda^V_\psi$ originates from t-channel photon exchange.

As for DM annihilation, the last two operators in the first line of Eq. (3.17) contribute to the p-wave, while all other operators contribute to the s-wave. For $m_\chi \gtrsim m_W$ the $\chi\chi^* \to WW, ZZ, hh$ channels dominate and the b_Ψ and c_B operators are subleading to the unsuppressed Higgs portal. Conversely, for $m_\chi \lesssim m_W$ the $\chi\chi^* \to \psi\overline{\psi}$ channel (where ψ is a SM fermion) dominates and the b_Ψ and c_B operators are important at freeze-out, when their velocity suppression can be less severe than the m_ψ-suppression that characterizes the other operators. As an example we consider $\chi\chi^* \to b\bar{b}$, for which we find a cross section

$$\sigma(\chi\chi^*\to b\bar{b})v_{\rm rel} = \frac{N_c}{4\pi s}\sqrt{1-\tfrac{4m_b^2}{s}}\Big\{A^2(s)m_b^2(s-4m_b^2) + \frac{2}{3}(s-4m_\chi^2)\big[B^2(s)(s+2m_b^2)+C^2(s)(s-4m_b^2)\big]\Big\} \tag{I.F.4}$$

with

$$A = \Big(\frac{c_d s}{f^2}-\lambda\Big)\frac{c_{hbb}}{s-m_h^2} + \frac{c^\chi_{d3}}{f^2}, \tag{I.F.5}$$

$$B = \frac{c_B}{m_*^2}\Big(e^2Q_b - \frac{g_Z^2 s_w^2 v_b s}{s-m_Z^2}\Big) + \frac{b^3_{q_L}+b^3_{d_R}}{2f^2}, \tag{I.F.6}$$

$$C = -\frac{c_B}{m_*^2}\frac{g_Z^2 s_w^2 a_b s}{s-m_Z^2} + \frac{b^3_{q_L}-b^3_{d_R}}{2f^2}\,, \tag{I.F.7}$$

where $c_{hbb} = g_{hbb}/g^{\rm SM}_{hbb}$ and the coupling of the SM fermion ψ to the Z is defined as $ig_Z\gamma^\mu(v_\psi - a_\psi\gamma_5)$. Taking the thermal average and considering for simplicity the limit $m_\chi \gg m_b$ we arrive at

$$\langle\sigma v_{\rm rel}\rangle(T) \simeq \frac{N_c}{4\pi}\Big\{m_b^2A^2(4m_\chi^2) + 4m_\chi T\big[B^2(4m_\chi^2)+C^2(4m_\chi^2)\big]\Big\}\,. \tag{I.F.8}$$

At the freeze-out temperature $\sim m_\chi/25$, for $A^2 \sim B^2 + C^2$ we have parametrically

$$\frac{\langle\sigma v_{\rm rel}\rangle_{p\text{-wave}}}{\langle\sigma v_{\rm rel}\rangle_{s\text{-wave}}} \sim \frac{4}{25}\frac{m_\chi^2}{m_b^2}\,. \tag{I.F.9}$$

Shift symmetry broken by top couplings

The explicit values of the $SO(7)/SO(6)$ sigma model couplings in the electroweak broken phase in Eqs. (3.11, 4.33) are

$$\begin{aligned} a_{hhh} = b_{h\chi\chi} = \frac{\xi}{\sqrt{1-\xi}}\,, \qquad a_{hh\chi\chi} = \frac{\xi^2}{1-\xi}\,, \qquad b_{hh\chi\chi} = \xi\,\frac{1+\xi}{1-\xi}\,, \\ a_{hVV} = d_{h\chi\chi} = d_{hhh} = \sqrt{1-\xi}\,, \qquad d_{hh\chi\chi} = 1-\xi\,. \end{aligned} \tag{I.F.10}$$

The couplings between the scalars and the top quark in Eq. (4.35) can be easily computed by matching with Eq. (I.D.6), where the top partners have been integrated out in the original field basis. However, the results of the parameter scan show that the "composite" mass of the lightest singlet, m_{S_1}, can in some cases be as low as few hundred GeV (while the physical mass of the lightest singlet is still above the experimental lower bound of 1 TeV, because it receives a large contribution from the elementary-composite mixing parameters $\sim \epsilon_t$), thus invalidating the simple effective theory approach in this basis. Therefore we proceed as follows: Starting from the UV Lagrangian in Eq. (4.15), after exact, numerical diagonalization of the fermion mass matrices we consider the following terms

$$\begin{aligned} \mathcal{L}_f \;\ni\; & i\bar{t}\not{\partial}t - m_t\bar{t}t\Big(\tilde{c}_{tth}\frac{h}{v} + 2\,\tilde{c}_{tt\chi\chi}\frac{\chi^*\chi}{v^2}\Big) \\ & + \sum_{i=1}^{N_Q}\Big[\overline{\mathcal{Y}}_i\left(i\not{\partial} - m_{Q_i}\right)\mathcal{Y}_i + \overline{\mathcal{Z}}_i\left(i\not{\partial} - m_{Q_i}\right)\mathcal{Z}_i + \bar{t}(b_L^i P_L + b_R^i P_R)(\mathcal{Y}_i\chi^* + \mathcal{Z}_i\chi) + \text{h.c.}\Big], \end{aligned} \tag{I.F.11}$$

where we introduced the coefficients $\tilde{c}_{tth}, \tilde{c}_{tt\chi\chi}, b_L^i$ and b_R^i, which are real if $\mathcal{CP}$ invariance is imposed. After integrating out the $\mathcal{Y}_i$ and $\mathcal{Z}_i$ and matching to Eq. (4.35), we find that $c_{tth} = \tilde{c}_{tth}$, whereas

$$c_{tt\chi\chi} = \tilde{c}_{tt\chi\chi} - \frac{v^2}{m_t}\sum_{i=1}^{N_Q}\left[\frac{b_L^i b_R^i}{m_{Q_i}} + \frac{m_t}{2m_{Q_i}^2}(b_L^{i\,2} + b_R^{i\,2})\right]. \tag{I.F.12}$$

We have verified that for parameter choices where the EFT approximation is justified, the values of c_{tth} and $c_{tt\chi\chi}$ obtained from Eq. (I.D.6) agree with those computed with this semi-numerical method.

The annihilation cross-sections needed to compute the DM relic abundance according to Eqs. (2.91) and (2.92) were calculated analytically in terms of the parameters of the effective Lagrangian in Eq. (4.32), and found to agree with those of [8] in the limit $c_{tth} = c_{tth}^{\text{nl}\sigma\text{m}}$, $c_{tt\chi\chi} = c_{tt\chi\chi}^{\text{nl}\sigma\text{m}}$. Eq. (4.38) provides a naive solution of the Boltzmann equation, which is nevertheless useful for a qualitative understanding.

The SI DM-nucleon cross section is given in Eq. (I.F.3). In our case we typically have that $m_\chi \gg m_N$ and the vector current couplings vanish. If we additionally define $k_g^t = -3d_G\,y^2/m_*^2$ and integrate out the top, s.t. it contributes to k_g^t the DM-nucleon scattering cross-section takes the form

$$\sigma_{\text{SI}}^{\chi N} \approx \frac{1}{4\pi}\frac{m_N^4}{m_\chi^2}\left[\sum_{q=u,d,s} f_{T_q} a_q + \frac{2}{27} f_{T_g}\Big(\sum_{q=c,b} a_q + k_g^t\Big)\right]^2, \tag{I.F.13}$$

with m_N the average nucleon mass, and the form factors are this time averaged over proton and neutron take the values $f_{T_{u,d}} \approx 0.020, 0.043$ [120, 239] (see also [119]), $f_{T_s} = 0.043$ [121] (also [240]) and $f_{T_g} \approx 0.89$. The first term represents the tree-level coupling to the light quarks u, d, s, while the second term parameterizes the coupling to gluons via loops of heavy fermions. In the second term we have further singled out the contribution mediated by the top and top

partners, k_g^t, from the one coming from the charm and bottom, because we want to keep track on the contributions from the top partner loops to the coupling of the Higgs to the gluons. The contribution from the top sector can be easily computed using the low-energy theorem for the GBs,

$$k_g^t = \frac{2\,\lambda v}{m_h^2}\, d_{h\chi\chi} D_h - D_{\chi\chi^*} \tag{I.F.14}$$

with the definitions

$$\begin{aligned} D_h &\equiv \sqrt{1-\xi}\,\left(\frac{\partial}{\partial\tilde{h}}\log|\det\mathcal{M}_t(\tilde{h},\chi)|\right)_{\tilde{h}=v,\,\chi=0} = \frac{1}{v}\frac{1-2\xi}{\sqrt{1-\xi}}\,, \\ D_{\chi\chi*} &\equiv \left(\frac{\partial^2}{\partial\chi\partial\chi^*}\log|\det\mathcal{M}_t(\tilde{h},\chi)|\right)_{\tilde{h}=v,\,\chi=0} = -\frac{1}{f^2(1-\xi)}\,, \end{aligned} \tag{I.F.15}$$

where $\mathcal{M}_t$ is the field-dependent mass matrix for the top sector. Even though k_g^t receives contributions from the top partners, its final expression depends only on f and is insensitive to the resonance parameters. This cancellation can be traced to the fact that with our choice of fermion embeddings, $q_L, t_R \sim \mathbf{7}$ of $SO(7)$, there is only one $SO(6)$ invariant that generates the top mass [241,242].[8] We remark that our computation based on Eq. (I.F.14) is only approximate for the box diagrams that contain $\mathcal{Y}, \mathcal{Z}$ propagators, and could be improved through an exact computation of the $\chi g \to \chi g$ scattering amplitude, see [243] for an extensive discussion in the similar case of neutralino-nucleon scattering. However, we have checked that for realistic parameter points the contribution of the box diagrams to k_g^t is $\lesssim 10\%$, hence we estimate that the corrections to our approximation would only affect $\sigma_{\rm SI}^{\chi N}$ at the percent level.

The contribution of the light SM quarks is encoded by the coefficients a_q ($q = u, d, c, s, b$) in Eq. (I.F.1). It is somewhat model-dependent, being determined by the choice of the corresponding embeddings, which we have not specified so far since they do not affect any other aspect of the phenomenology. For concreteness, we assume all left-handed light quarks to be embedded in the **7**, whereas for the right-handed light quarks we take $b_R \sim \mathbf{7}$, leading to a contribution identical to the one of the top sector, and $q_R \sim \mathbf{1}$ ($q = u, d, c, s$), yielding a vanishing coefficient for the $\chi^*\chi\bar{q}q$ contact term. In summary, we have

$$k_g^t = a_b = \frac{2\,\lambda}{m_h^2}(1-2\xi) + \frac{1}{f^2(1-\xi)}\,, \qquad a_{u,d,c,s} = \frac{2\,\lambda}{m_h^2}(1-\xi). \tag{I.F.16}$$

For realistic parameters the Higgs exchange dominates and the cross section can be approximated by the simple expression in Eq. (4.45), with $f_N \equiv 2/9 + (7/9)\sum_{q=u,d,s} f_{T_q}^{p,n} \simeq 0.30$.

Shift symmetry broken by bottom couplings
The scenario discussed in Section (4.4), where the DM shift symmetry is broken by the bottom couplings, the situation is almost identical to previous scenario. The main difference is that the marginal Higgs portal coupling λ is negligible and the cross section takes the form in Eq. (4.61), where $\tilde{f}_N = (2/27) f_{T_g} \approx 0.066$ in case I and $\tilde{f}_N = f_{T_d} + f_{T_s} + (2/27) f_{T_g} \approx 0.15$ in case II. See Section 4.4.2 for more details.

Shift symmetry broken by gauging of $U(1)_{\rm DM}$
The DM phenomenology for this scenario was thoroughly discussed in Section 4.5. Here we

[8] Notice that the expression of k_g^t is identical to that obtained in $SO(6)/SO(5)$ when $q_L, t_R \sim \mathbf{6}$ [8].

merelye give some supporting formulas.
The loop function for the $h \to \gamma_D\gamma_D$ decay is, for $m_{\gamma_D} = 0$,

$$F(\tau) = \frac{\tau}{3}A_0(\tau), \quad A_0(\tau) = \frac{3}{\tau^2}[f(\tau)-\tau], \quad f(\tau) = \begin{cases} \arcsin^2\sqrt{\tau}\,, & \tau \le 1\,, \\ -\frac{1}{4}\left[\log\left(\frac{1+\sqrt{1-1/\tau}}{1-\sqrt{1-1/\tau}}\right) - i\pi\right]^2, & \tau > 1\,. \end{cases} \tag{I.F.17}$$

Note that $A_0(\tau) = 1 + O(\tau)$ for small τ.

Finally we report the thermally averaged cross sections relevant to the region $m_\chi \lesssim m_{\gamma_D} < 2m_\chi$. The one for $\chi\chi^* \to \gamma_D\gamma_D$ is

$$\langle\sigma_{\chi\chi^*\to\gamma_D\gamma_D}v_{\rm rel}\rangle = \frac{2\pi\alpha_D^2}{m_\chi^2}\sqrt{1-R}\,\frac{1-R+3R^2/8}{(1-R/2)^2}\,, \qquad R \equiv \frac{m_{\gamma_D}^2}{m_\chi^2}\,, \tag{I.F.18}$$

whereas

$$\langle\sigma_{\gamma_D\gamma_D\to\chi\chi^*}v_{\rm rel}\rangle = \frac{22\pi\alpha_D^2}{9m_{\gamma_D}^2}(1-\widetilde{R})^{1/2}\left(1-\frac{24\widetilde{R}}{11}+\frac{16\widetilde{R}^2}{11}\right), \qquad \widetilde{R} \equiv \frac{m_\chi^2}{m_{\gamma_D}^2}\,. \tag{I.F.19}$$

For the semi-annihilation

$$\langle\sigma_{\gamma_D h\to\chi\chi^*}v_{\rm rel}\rangle = \frac{\alpha_D v^2 m_h(m_{\gamma_D}+m_h)^2}{6f^4m_{\gamma_D}^3}\left[1-\frac{4m_\chi^2}{(m_{\gamma_D}+m_h)^2}\right]^{3/2}, \tag{I.F.20}$$

while for the inverse process we have

$$\langle\sigma_{\chi\chi^*\to\gamma_D h}v_{\rm rel}\rangle = \frac{\alpha_D v^2 m_h^4 T}{8f^4m_\chi^5}\,\beta_{h\gamma_D}\,\frac{1-(\frac{3}{2}R_{\gamma_D}+2R_h)+R_h(R_h+3R_{\gamma_D})+\frac{1}{2}R_{\gamma_D}(R_{\gamma_D}-R_h)^2}{(1-R_h-R_{\gamma_D})^4}\,, \tag{I.F.21}$$

where $\beta_{h\gamma_D} \equiv [1+(R_h-R_{\gamma_D})^2-2(R_h+R_{\gamma_D})]^{1/2}$ and $R_i \equiv m_i^2/(4m_\chi^2)$. Notice the additional factor T/m_χ coming from the p-wave suppression.

Lastly,

$$\langle\sigma_{\gamma_D\chi\to h\chi}v_{\rm rel}\rangle = \frac{\alpha_D v^2 m_h^4\,G(m_{\gamma_D},m_h;m_\chi)}{24f^4m_\chi m_{\gamma_D}^3}\,, \quad \langle\sigma_{h\chi\to\gamma_D\chi}v_{\rm rel}\rangle = \frac{\alpha_D v^2 m_h m_{\gamma_D}^2 G(m_h,m_{\gamma_D};m_\chi)}{8f^4m_\chi(m_h+2m_\chi)^2}\,,$$
$$G(m_1,m_2;m_\chi) = \frac{\left[(m_1^2-m_2^2)((m_1+2m_\chi)^2-m_2^2)\right]^{3/2}}{(m_1+m_\chi)^2[m_\chi(m_1+2m_\chi)-m_2^2]^2}\,. \tag{I.F.22}$$

I.G Details of the analysis and comparison with previous works

At lepton colliders we cut on four kinematic variables, namely MIM, $\Delta_{\ell\ell}$, $\not{E}_T$ and $M_{\ell\ell}$:

- The cuts on the MIM are summarized in the left-most panel of Figure I.G.1 for the derivative portal. For the marginal portal we always take MIM $> 2m_\phi$, and in a few cases we also impose an upper bound: at ILC 1, MIM $< \{175, 280, 300, 380, 450\}$ GeV for $m_\phi = \{70, 85, 100, 120, 150\}$ GeV; at CLIC 1.5 and 3, MIM $< \{250, 300\}$ GeV for $m_\phi = \{70, 85\}$ GeV.
- The cuts on $\Delta\eta_{\ell\ell}$ are shown in the middle-left panel of Figure I.G.1. For the marginal portal at ILC 1 this cut is replaced by $H_T(ee) < 260$ GeV, as in [213].

- The cuts on $\not{E}_T$ = MET are shown in the middle-right panel of Figure I.G.1 (the points that are not immediately visible in this plot all have $\not{E}_T > 80$ GeV, e.g. the marginal portal at CLIC 3).
- The cuts on $M_{\ell\ell}$ are shown in the right-most panel of Figure I.G.1.

For hadron colliders, we show in the middle panel of Figure I.G.2 the cuts on m_{jj}.

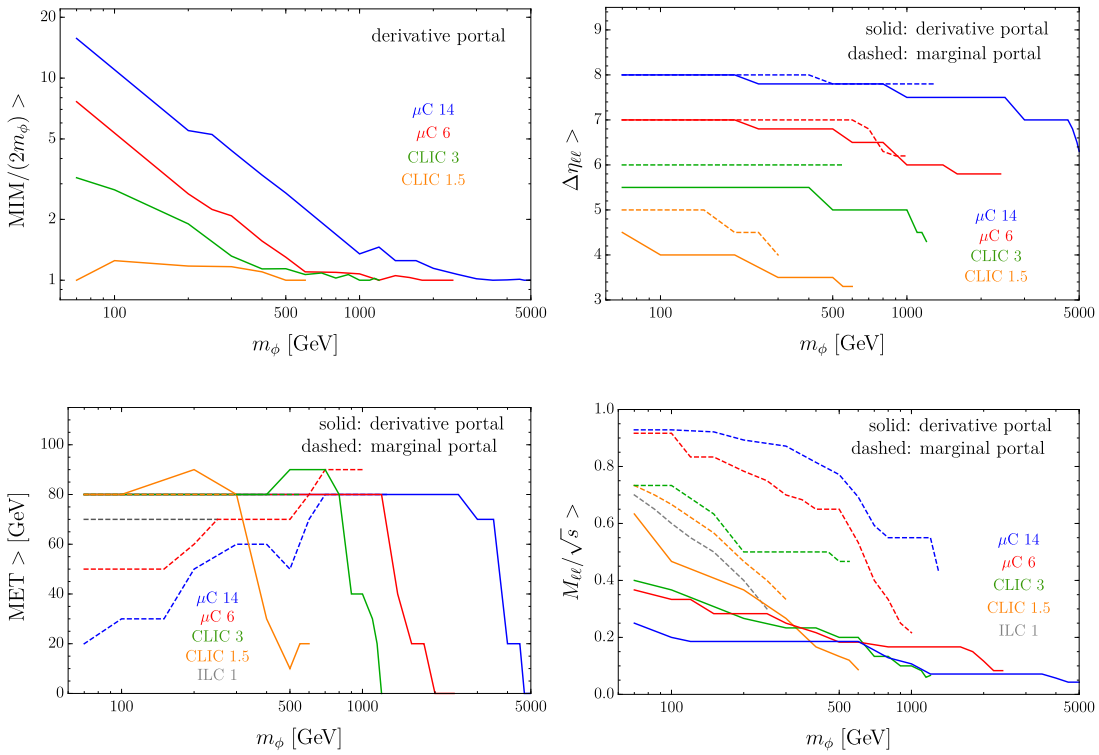

Figure I.G.1: Summary of the cuts we apply at lepton colliders. The cuts not shown here are discussed in the text.

I.G.1 Comparison to Ref. [1]

We deem it useful to provide a thorough comparison of our results for the marginal portal at hadron colliders to those of [1]. For this purpose we have tried to reproduce their VBF analysis as closely as possible, given the available information. The results are shown in the right panel of Figure I.G.2, together with the bounds quoted in [1] and those obtained in our main analysis.[9] We are able to reproduce well the results of [1], agreement being excellent for the FCC and good for the HL-LHC. This exercise helps us to pinpoint the differences between our analysis and that of [1]:

1) In [1] the EW components of V+jet were neglected, while the QCD components were generated at LO and normalized to the `MadGraph5` cross sections. In this work we have included EW production and generated the QCD part at NLO; normalizations were fixed by comparison with the 13 TeV CMS results [225].

[9] Only for this plot, following [1] we adopt the coupling normalization $c_\phi = \lambda/2$ and use a two-sided test to determine the exclusion bounds, i.e. we require $\mathcal{S} = \sqrt{2}\,\mathrm{erf}^{-1}(1-p) \approx 1.96$ for $p = 0.05$ (95% CL).

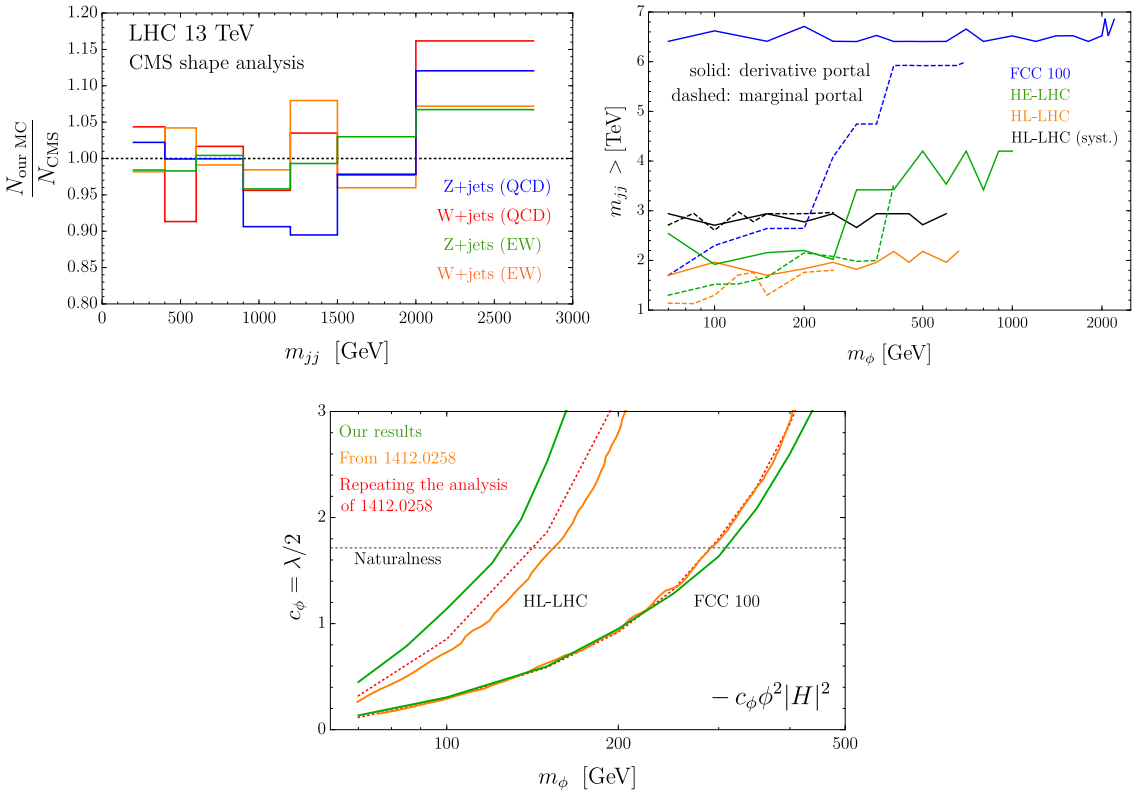

Figure I.G.2: *Left:* comparison of our MC predictions to the expected yields in the CMS shape analysis (reported in Table 3 of [225]). Each of our MC samples has been normalized to the total expected yield quoted by CMS. The required rescaling factors are $1.18, 1.08$ for $Z_{\nu\nu}(\text{QCD}), W_{\ell\nu}(\text{QCD})$, and $1.74, 1.63$ for $Z_{\nu\nu}(\text{EW}), W_{\ell\nu}(\text{EW})$. We do not show the $m_{jj} \in [2.75, 3.5]$ TeV and $m_{jj} > 3.5$ TeV bins because there the statistical uncertainty of our MC is large. *Middle:* summary of the optimized m_{jj} cut we adopt at hadron colliders. For the HL-LHC with 1% systematic uncertainty we take $m_{jj} > 3$ TeV as the strongest possible cut, due to the limited MC statistics. *Right:* comparison of our results for the marginal portal at hadron colliders with those of [1]. See text for further details.

2) In [1] both the $\not{E}_T$ and m_{jj} cuts were optimized, without imposing a trigger-motivated lower limit on the former. As a result the optimal values were $\not{E}_T \gtrsim 120$ GeV at the HL-LHC and $\not{E}_T \gtrsim 100$-160 GeV at the FCC. In this work we have fixed $\not{E}_T > 180$ and 200 GeV, respectively, and optimized only the m_{jj} cut.

3) In our FCC analysis we have assumed forward jet tagging up to $|\eta| = 6$, to be compared with 4.7 used in [1].

Owing to the points 1) and 2) our HL-LHC sensitivity is weaker, while at the FCC the point 3) more than compensates for the first two, allowing us to derive slightly more stringent limits.

Part II

Small instanton contributions to the axion mass

Chapter 6

Motivation and introduction

Let us now shift our attention from WIMP DM, which was our focus in Part I, to axions, another well-motivated DM candidate. Axions and ALPs have received increasing attention in the past decades. From the QCD axion, which constitutes the most plausible solution for the strong $\mathcal{CP}$ problem [9–12] while being a natural DM candidate, to ALPs in string theory, axions appear in many contexts in BSM model building.

The couplings of the QCD axion are determined by the BSM sector, which spontaneously breaks the Peccei-Quinn (PQ) symmetry and its strength is set by the generally large symmetry breaking scale f_a of the PQ symmetry. Even though both the PQ sector and the symmetry breaking scale are unknown, the mass of the QCD axion is surprisingly well predicted. The mass is generated by non-perturbative QCD effects, which can be quantified using chiral symmetry which relates the uncalculable axion mass to the pion mass according to the well-known relation (see e.g. [244])

$$m_a^2 = \frac{m_u m_d}{(m_u + m_d)^2} \frac{m_\pi^2 f_\pi^2}{f_a^2} \,. \tag{6.1}$$

Eq. (6.1) suggests that the axion mass is completely fixed in terms of measurable IR observables in addition to the axion decay constant f_a. This relation seems to be a robust prediction: the axion mass is completely determined by strongly coupled QCD intanton effects, which are expected to dominate over the weakly coupled, and hence suppressed, UV instantons. The suppression of UV instantons is indeed a general feature of the simplest UV completions of QCD, in which QCD remains weakly coupled in the UV. However, it is possible to enhance the contributions from small instantons, e.g. by modifying the running of the QCD coupling in such a way that QCD gets strong again in the UV [245–247]. A particularly appealing realization is the embedding of QCD into a higher dimensional theory, e.g. in 5D small instanton contributions can be naturally enhanced [248] and give the dominant contribution to the axion mass [249].

However, it was recently realized by Agrawal and Howe (AH) [18, 19] that in a specific kind of UV completion based on product groups the effects from small and weakly coupled (and thus fully calculable) instantons can dominate over the one from large and strongly coupled QCD instantons, what can result in a significant enhancement of the axion mass away from the pure low-energy QCD prediction of Eq. (6.1). This surprising and unexpected result admits new regions in the $(m_a^2,\ f_a)$ parameter space for the QCD axion. Various models which implement the mechanism of [18] include [250–255]. For reasons of completeness let us also mention that there are other approaches to modify the axion mass within QCD which were proposed in [256–259] while in [260–266] the axion mass is raised by coupling it to a new confining gauge group.

In this part of the thesis we want to re-examine the class of models which were presented in [18, 19] to identify the underlying dynamics which causes the enhancement of the small in-

stanton effects. Additionally we aim to present an accurate estimate of the small instanton contributions to the axion mass by performing a detailed one-instanton calculation including all $\mathcal{O}(1)$ factors, s.t. we can identify specific models which successfully implement the enhancement mechanism of [18, 19].

We start in Chapter 7 by giving a short introduction to the strong $\mathcal{CP}$ problem and the axion. Chapter 8 introduces instantons and the instanton calculus in broken and unbroken gauge theories. Using this foundation, in Chapter 9 we finally turn to small instanton contributions to the axion mass in partially broken gauge groups, such as the ones proposed in [18, 19]. We identify the non-trivial index of embedding of QCD into a UV gauge group as the reason for the enhancement of small instantons and explicitly compute their contribution to the axion mass in product group models where QCD is imbedded in the diagonal subgroup.

The second part of Chapter 8 and Chapter 9 are based on [32], from where all Figures and parts of the text have been taken.

Chapter 7

Strong $\mathcal{CP}$ problem and the axion

In this chapter we start the discussion with a short introduction to the strong $\mathcal{CP}$ problem and the axion as its solution. The foundation of the strong $\mathcal{CP}$ problem is the non-trivial vacuum structure of QCD which we will discuss in Section 7.1. Building on this background we formulate the strong $\mathcal{CP}$ problem in Section 7.2, before we discuss its solution in terms of the axion in Section 7.3. For a further pedagogical introduction to the strong $\mathcal{CP}$ problem and the axion see [267–269].

7.1 Yang-Mills vacuum

After the discovery of the instanton solution in Euclidean Yang-Mills theory by Belavin et al [270] it was soon realized that Yang-Mills theories have a discrete set of degenerate classical vacua [271, 272], which allow us to interpret the instanton solution as quantum tunneling paths between degenerate vacua. In order to understand this result and to find the set of minima we consider a $SU(N)$ Yang-Mill theory described by the Lagrangian[1]

$$\mathcal{L}_{\rm YM} = -\frac{1}{4} G^a_{\mu\nu} G^{a\,\mu\nu}\,, \tag{7.1}$$

where a are color indices in the adjoint representation of $SU(N)$ and $G^a_{\mu\nu} = \partial_\mu A^a_\nu - \partial_\nu A^a_\mu + g\, f^{abc} A^b_\mu A^c_\nu$ is the field strength with gauge coupling g and $SU(N)$ structure constants f^{abc}. The emergence of the discrete set of classical vacua is most easily seen in temporal gauge $A_0 = 0$, which we will use in the following. In temporal gauge the Hamiltonian, which represents the classical energy of a field configuration, takes the form

$$\mathcal{H} = \frac{1}{2} \int d^3x \big(E^a_i E^a_i + B^a_i B^a_i \big), \tag{7.2}$$

where we defined the chromoelectric and chromomagnetc field $E^a_i = \dot{A}^a_i = G^a_{0i}$ and $B^a_i = -\frac{1}{2}\epsilon_{ijk} G^a_{jk}$, respectively.[2] Eq. (7.2) directly implies that the vacuum or minimal energy solutions are given by $E^a_i = B^a_i = 0$, i.e. $G^a_{\mu\nu} = 0$. Note that temporal gauge does not entirely fix the

[1] Note that there is one additional renormalizable operator of the form $\theta\, G^a_{\mu\nu} \tilde{G}^{a\,\mu\nu}$ with $\tilde{G}^{a\,\mu\nu} = \frac{1}{2}\epsilon^{\mu\nu\alpha\beta} G^a_{\alpha\beta}$ which should be added to the Lagrangian according to the EFT paradigm. This operator is a total derivative and has no effect in perturbation theory. However, we will see in the following that it naturally emerges and can have observable consequences in non-perturbative transition amplitudes.

[2] Note that the theory described by the Hamiltonian in Eq. (7.2) is not completely equivalent to the one of the Lagrangian in Eq. (7.1) as its equations of motion lack the analog of Gauss's law $(D_i E_i)^a = 0$, which must be enforced by hand.

gauge and still allows for time-independent gauge transformations $U = U(\mathbf{x})$. This means that the gauge field in vacuum, corresponding to $G^a_{\mu\nu} = 0$, is a pure gauge configuration, i.e.

$$A_i(\mathbf{x})|_{\text{vac}} = \frac{i}{g} U(\mathbf{x}) \partial_i U(\mathbf{x}) \,, \tag{7.3}$$

where we absorbed the $SU(N)$ generators T^a into the gauge field $A_\mu = A^a_\mu T^a$.[3] Our goal is to study local effects and therefore we require

$$\lim_{|\mathbf{x}|\to\infty} U(\mathbf{x}) = 1 \,. \tag{7.4}$$

This effectively compactifies $\mathbb{R}^3$ to $\mathbb{R}^3 \cup \{\infty\} \simeq S_3$, which is topologically equivalent to the three sphere S_3. The gauge maps $U(\mathbf{x})$ are therefore maps $U : S_3 \to G$ from the three sphere into the group. Maps $S_3 \to G$ can be divided into topologically distinct classes which are characterized by the elements of the homotopy group $\pi_3(G)$, which for $G = SU(N)$ is given by (see e.g. [273])

$$\pi_3(SU(N)) = \mathbb{Z} \,. \tag{7.5}$$

The gauge transformations and consequently the classical vacua therefore fall into disconnected sets labeled by integers $\nu[U(\mathbf{x})] \in \mathbb{Z}$, which are the so-called winding number, i.e. the number of times the space S_3 covers the group manifold. Only $U(\mathbf{x})$ in the same homotopy class, i.e. maps with the same winding number, can be continuously deformed into each other. For $G = SU(2)$ the winding number is defined as

$$\nu[U(\mathbf{x})] = \frac{1}{24\pi^2} \epsilon^{ijk} \int d^3x \, \mathrm{Tr}\big[U^{-1}\partial_i U U^{-1} \partial_j U U^{-1} \partial_k U\big] \,. \tag{7.6}$$

Note that the winding number is additive, i.e. $\nu[U_1 U_2] = \nu[U_1] + \nu[U_2]$.

Now let us define the Chern-Simons current j^μ_A

$$j^\mu_A = \frac{g^2}{8\pi^2} \epsilon^{\mu\nu\alpha\beta} \mathrm{Tr}\big(A_\nu \partial_\alpha A_\beta - \frac{2ig}{3} A_\nu A_\alpha A_\beta\big) \tag{7.7}$$

$$= \frac{g^2}{16\pi^2} \epsilon^{\mu\nu\alpha\beta} \mathrm{Tr}\big(A_\nu G_{\alpha\beta} + \frac{2ig}{3} A_\nu A_\alpha A_\beta\big) \,, \tag{7.8}$$

where $G_{\alpha\beta} = G^a_{\alpha\beta} T^a$ in the second equality. Note that even though j^μ_A is not gauge invariant its divergence is manifestly gauge invariant

$$\partial_\mu j^\mu_A = \frac{g^2}{16\pi^2} \mathrm{Tr}\; G_{\mu\nu} \tilde{G}^{\mu\nu} \,, \tag{7.9}$$

where $\tilde{G}^{\mu\nu} = \frac{1}{2} \epsilon^{\mu\nu\alpha\beta} G_{\alpha\beta}$ is the dual field strength. The corresponding charge Q_A, given by

$$Q_A = \int d^3x \, j^0_A = \frac{g^2}{16\pi^2} \int d^3x \, \epsilon^{ijk} \mathrm{Tr}\; \big(A_i F_{jk} + \frac{2ig}{3} A_i A_j A_k\big) \tag{7.10}$$

cannot be expected to be conserved since the current's divergence does not vanish in general. However, Q_A has an important interpretation: it gives the winding number of the vacuum configuration $A_i = i/g \, U^{-1} \partial_i U$

$$Q_A = \nu[U] \,. \tag{7.11}$$

[3] Our convention is that the generators in the fundamental representation are normalized as $\mathrm{Tr}[T^a T^b] = \frac{1}{2}\delta^{ab}$.

This is straightforward to verify for $G = SU(2)$ by plugging $A_i = i/g\, U^{-1}\partial_i U$ and $F_{jk} = 0$ into Eq. (7.10), what recovers Eq. (7.6). Note that there is no adiabatic and energy-conserving evolution connecting vacua with different winding number. This can be seen by noticing that any such evolution would have to be a continuous gauge transformation which, however, cannot connect topologically distinct sectors. This implies that all paths between vacua in different equivalence classes must cross an energy barrier in real time (see e.g. [271]).

Now that we have established the existence of a discrete set of vacuum solutions and that we have found the topological charge Q_A which classifies the vacua according to the winding number of the gauge map, we are faced with the task of interpreting this result. Does the discrete set of vacua imply that there are many possible disconnected Hilbert spaces, each with a theory only invariant under small gauge transformations, i.e. gauge transformations which do not change the winding number? Clearly the answer to this question crucially depends on the existence of transition amplitudes between sectors with different winding number or topological charge. Indeed if there is a sequence of finite-energy solutions $A_\mu(\mathbf{x}, t)$ interpolating vacua with different winding numbers, Q_A is not conserved

$$\frac{g^2}{16\pi^2}\int d^4x\, \mathrm{Tr}\; G_{\mu\nu}\tilde{G}^{\mu\nu} = \int d^4x\big(\partial_0 j^0_A + \partial_i j^i_A\big) = \int d^3x\big(\, j^0_A\big|_{t_2} - j^0_A\big|_{t_1}\,\big) = Q^{(2)}_A - Q^{(1)}_A = \nu_2 - \nu_1\,, \tag{7.12}$$

where we dropped the spatial surface term for j^i_A, which should vanish for finite energy configurations in the limit $r \to \infty$. These finite energy configurations are the already mentioned instantons which are exact solutions of the Euclidean equations of motion and exist as valid paths in the Euclidean path integral. Instantons can thus be interpreted as tunneling solutions between vacua with different winding number in Minkowski spacetime (ST).

Since all degenerate vacua $|\nu\rangle$ can be reached in transition amplitudes the true vacuum should be a superposition of all $|\nu\rangle$ vacua. In order to find the real vacuum it is helpful to define an operator T which changes the winding number by one unit, i.e.

$$T:\, T|\nu\rangle \to |\nu + 1\rangle\,. \tag{7.13}$$

Since T can be identified with a large gauge transformation it commutes with the Hamiltonian $[H, T] = 0$ and thus it can only change the true vacuum by a phase, i.e. $T|\theta\rangle = e^{i\theta}|\theta\rangle$. The θ-vacuum defined as

$$|\theta\rangle = \sum_{\nu=-\infty}^{\infty} e^{-i\nu\theta}|\nu\rangle \tag{7.14}$$

has this property. θ in the above is an angle which is periodic with 2π. θ is a constant of nature and vacua corresponding to a different θ' are not accessible to us

$$\begin{aligned}\langle\theta'|e^{-iHt}|\theta\rangle &= \sum_{\nu_1,\nu_2} e^{i\nu_2\theta'}e^{-i\nu_1\theta}\langle\nu_2|e^{-iHt}|\nu_1\rangle = \sum_{\nu_1,\nu_2} e^{i\nu_2(\theta'-\theta)}e^{i(\nu_2-\nu_1)\theta}\langle\nu_2|e^{-iHt}|\nu_1\rangle \\ &= \sum_{\nu_2,\Delta\nu} e^{i\nu_2(\theta'-\theta)}e^{i\Delta\nu\theta}\langle\Delta\nu|e^{-iHt}|0\rangle = \delta(\theta-\theta')\sum_{\Delta\nu} e^{i\Delta\nu\theta}\langle\Delta\nu|e^{-iHt}|0\rangle\,,\end{aligned} \tag{7.15}$$

where we used in the third step that the Hamiltonian commutes with large gauge transformations and thus the amplitude only dependes on the change in winding number $\Delta\nu$. Note also that by using the definition of the generating functional and Eq. (7.12) the effect of the instanton can be absorbed into the Lagrangian by adding the so-called θ term

$$\langle\theta'|e^{-iHt}|\theta\rangle = \delta(\theta-\theta')\int\sum_{\Delta\nu,a}\mathcal{D}A^a_{\Delta\nu}\exp\left[i\int d^4x\big(-\frac{1}{2}\mathrm{Tr}\; G_{\mu\nu}G^{\mu\nu} + \theta\frac{g^2}{16\pi^2}\mathrm{Tr}\; G_{\mu\nu}\tilde{G}^{\mu\nu}\big)\right], \tag{7.16}$$

which we already mentioned in Footnote 1. Thus when considering topologically non-trivial field configurations one should work with the modified Yang-Mills Lagrangian

$$\mathcal{L}_{\text{eff}} = \mathcal{L}_{\text{YM}} + \mathcal{L}_\theta = \mathcal{L}_{\text{YM}} + \theta \frac{g^2}{16\pi^2} \text{Tr}\, G_{\mu\nu}\tilde{G}^{\mu\nu} \,. \tag{7.17}$$

The θ-term does not affect the equations of motion and is a total derivative and therefore has no effect in perturbation theory. However, in theories that include fermions it induces measurable effects, which will be the topic of the next section.

Before concluding this section note that there is an alternative but equivalent interpretation of the distinct set of degenerate Yang-Mills vacua. In this interpretation all vacua with different winding number are considered as the same physical vacuum, since they only differ by a gauge transformation [274]. This scenario is analogous to the quantum mechanical treatment of the pendulum, where paths $A_i(\mathbf{x}, t)$ that start and end at the physical vacuum might not be continuously contractable, i.e. the situation is topologically equivalent to the gauge field winding around a circle. Since these solutions have to leave the physical vacuum during their path they are finite-energy solutions. This means that evolutions along such a path at zero energy cost is only possible via quantum tunneling, which leads us back to the instanton.

7.2 Strong $\mathcal{CP}$ problem

Let us now turn to QCD, i.e. Yang-Mills based on $G = SU(3)$, and explore the implications of $\mathcal{L}_\theta$ as defined in Eq. (7.17). In terms of the chromomagnetic and chromoelectric field it is of the form $\mathbf{E}^a \cdot \mathbf{B}^a$, which is manifestly odd under the discrete symmetries $\mathcal{P}$ and $\mathcal{T}$ and consequently violates $\mathcal{CP}$. In order to extract physical consequences and see the $\mathcal{CP}$ violation the theory needs to be coupled to fermions, in which case the θ terms is closely related to the anomaly of the axial current. In order to visualize this connection let us consider a single quark q in the fundamental representation of QCD, i.e.

$$\mathcal{L} \supset i\bar{q}\not{D}q - m_q\bar{q}q \,, \tag{7.18}$$

where $D_\mu q = (\partial_\mu - igA^a_\mu T^a)q$ is the covariant derivative. In the massless limit $m_q \to 0$ this Lagrangian is invariant under global $U(1)_V \times U(1)_A$ transformations

$$U(1)_V : q \to e^{i\alpha}q \,, \qquad U(1)_A : q \to e^{i\alpha\gamma_5}q \tag{7.19}$$

at the classical level. However, the axial $U(1)_A$ is not only broken by the mass term, but also by quantum effects in the form of the Adler-Bell-Jackiew chiral anomaly (see e.g. [275]). The divergence of the chiral current $j^\mu_5 = \bar{q}\gamma^\mu\gamma_5 q$ is therefore of the form

$$\partial_\mu j^\mu_5 = 2i\, m_q\bar{q}\gamma_5 g + \frac{g^2}{8\pi^2} \text{Tr}\, G_{\mu\nu}\tilde{G}^{\mu\nu} \,, \tag{7.20}$$

which is non-vanishing in the instanton background even for vanishing quark masses. Thus the axial $U(1)_A$ is explicitly broken by the topology of the QCD vacuum. A chiral transformation of the form $q \to e^{i\alpha\gamma_5}q$ changes the QCD Lagrangian as

$$\mathcal{L}_{\text{eff}} \supset -m_q\bar{q}q + \theta\frac{g^2}{16\pi^2} \text{Tr}\, G_{\mu\nu}\tilde{G}^{\mu\nu} \to -m_q\bar{q}e^{-2i\alpha\gamma_5}q + (\theta - 2\alpha)\frac{g^2}{16\pi^2} \text{Tr}\, G_{\mu\nu}\tilde{G}^{\mu\nu} \,. \tag{7.21}$$

This implies that chiral transformations shift the θ parameter by $\theta \to \theta - 2\alpha$. This has two important implications: i) the vacuum θ angle can be completely rotated into the quark masses and therefore its effects can be studied by considering QCD with θ-dependent quark masses. ii)

if just one quark in the theory is massless the θ angle can be completely eliminated through a chiral rotation. Or put slightly differently, for $m_q = 0$ there exists an exact shift symmetry $\theta \to \theta - 2\alpha$ which makes θ unphysical and therefore eliminates any $\mathcal{CP}$ violation from the QCD Lagrangian. This is the idea behind the massless up-quark solution of the strong $\mathcal{CP}$ problem, which we will formulate momentarily.

Note that so far we have neglected the possibility that the quark mass contains a complex phase, i.e. $m_q = |m_q|e^{i\theta_q}$ with

$$-(\bar{q}_L m_q q_R + \bar{q}_R m_q^* q_L) = -|m_q|\bar{q}e^{i\theta_q\gamma_5}q\,. \tag{7.22}$$

In this case the chiral transformation has the effect of shifting $\theta_q \to \theta_q - 2\alpha$ and $\theta \to \theta - 2\alpha$. This means that the bare vacuum angle θ is not observable and only the shift-invariant combination $\bar{\theta} = \theta - \theta_q$ is physical and will turn out to determine the amount of $\mathcal{CP}$ violation. In a scenario with multiple quarks with the mass matrix M, $\bar{\theta}$ is given by

$$\bar{\theta} = \theta - \arg\ \det\ M\,. \tag{7.23}$$

With these tools we are finally able to quantify the amount of $\mathcal{CP}$-violation in QCD. We can use chiral rotations to eliminate $\mathcal{L}_\theta$. Assuming that $\bar{\theta} \ll 1$, which is justified from experimental input, in low-energy QCD with three quark flavors (u, d, s) this transformation induces the manifestly $\mathcal{CP}$ violating operator [276]

$$\delta\mathcal{L}_{\mathcal{CP}} = i\bar{\theta}\frac{m_u m_d m_s}{m_u m_d + m_u m_s + m_d m_s}(\bar{u}\gamma_5 u + \bar{d}\gamma_5 d + \bar{s}\gamma_5 s)\,. \tag{7.24}$$

This contributes to the neutron electric dipole moment $|d_n|$, which is predicted to be (see e.g. [267, 268, 276])

$$|d_n| \sim 4.5 \cdot 10^{-15}\bar{\theta}\, e \cdot \mathrm{cm}\,. \tag{7.25}$$

The experimental upper bound on the neutron electric dipole moment is of the order [277–279]

$$|d_n| \leq 10^{-26}\, e \cdot \mathrm{cm}\,, \tag{7.26}$$

what implies that $\bar{\theta}$ has to be smaller than

$$\bar{\theta} \leq 10^{-10}\,. \tag{7.27}$$

This small value of $\bar{\theta}$ is the origin of the so-called strong $\mathcal{CP}$ problem: $\bar{\theta}$ could take any value between 0 and π but it appears to be close to zero or exactly zero. The strong $\mathcal{CP}$ problem is the endaviour of finding a reason why $\bar{\theta}$ is so unnaturally small.

There are a number of possible solutions to the strong $\mathcal{CP}$ problem and we have already encountered the simplest one. If the mass of the lightest quark, i.e. the up-quark, vanishes the θ angle is unphysical and there is no $\mathcal{CP}$ violation, as can also be seen from Eq. (7.24), which vanishes for $m_u = 0$. This can also be understood from the QCD vacuum structure. In the presence of massless quarks the instanton tunneling amplitude between $|\nu\rangle$ vacua vanishes [280], which means the potential barrier is infinite and any $|\nu\rangle$ vacuum is a good vacuum. However, the massless up-quark solution is strongly disfavored by experiment and lattice results. A very interesting dynamical solution can be obtained by adding a new particle, the axion, which will be the focus of study in the next section.

7.3 Axion solution to the strong $\mathcal{CP}$ problem

A particularly elegant solution of the strong $\mathcal{CP}$ problem requires the introduction of a new light particle, the axion. It is based on the observation that the QCD vacuum energy density E depends on $\bar{\theta}$, i.e. $E = E(\bar{\theta})$. Explicit calculation in two-flavor chiral perturbation theory reveals that the vacuum energy density depends on $\bar{\theta}$ as [244]

$$E(\bar{\theta}) = -m_\pi^2 f_\pi^2 \sqrt{1 - \frac{4 m_u m_d}{(m_u + m_d)^2} \sin^2 \frac{\bar{\theta}}{2}}\,, \tag{7.28}$$

where m_π, f_π are the pion mass and decay constant and m_u, m_d are the up and down quark masses. Eq. (7.28) implies that $E(\bar{\theta})$ is minimized at $\bar{\theta} = 0 \bmod 2\pi$.[4] Thus if $\bar{\theta}$ is a dynamical variable it will be naturally driven to the $\mathcal{CP}$ conserving vacuum with $\bar{\theta} = 0$.

A mechanism realizing this idea is due to Peccei and Quinn (PQ) [9, 10] and is essentially a simple extension of the massless up-quark solution: in a theory with a non-linearly realized $U(1)_{\rm PQ}$ chiral symmetry the vacuum angle retains the shift symmetry $\theta \to \theta - 2\alpha$. Soon afterwards Weinberg and Wilczek [11, 12] realized that the spontaneously broken symmetry implies the existence of a Goldstone boson, the so-called axion a with decay constant f_a, which also shifts under this symmetry as

$$\frac{a}{f_a} \to \frac{a}{f_a} + \alpha\,, \tag{7.29}$$

similar to the phases in the quark masses but with the important difference that the axion is not a constant angle but a dynamical field. Through the $U(1)_{\rm PQ}$-QCD-QCD chiral anomaly the axion couples to $\tilde{G}G$ as[5]

$$\mathcal{L}_a = \left(\bar{\theta} + \frac{a}{f_a}\right) \frac{g^2}{16\pi^2} \mathrm{Tr}\; G_{\mu\nu} \tilde{G}^{\mu\nu}\,. \tag{7.30}$$

In the instanton background this coupling breaks the axion shift symmetry and therefore instantons generate a potential for the axion. Treating $\bar{\theta} + a/f_a$ as an effective θ-angle the vacuum energy density in Eq. (7.28) can be straightforwardly generalized to the case with an axion such that the axion potential is of the form[6] [244]

$$V(a) = -m_\pi^2 f_\pi^2 \sqrt{1 - \frac{4 m_u m_d}{(m_u + m_d)^2} \sin^2 \left(\frac{a}{2 f_a} + \frac{\bar{\theta}}{2}\right)}\,. \tag{7.31}$$

Classical motion will drive the axion field to the minimum of the potential such that

$$\bar{\theta}_{\rm eff} = \frac{\langle a \rangle}{f_a} + \bar{\theta} = 0\,, \tag{7.32}$$

what would explain why there is no observable $\mathcal{CP}$ violation in the strong interaction.

The original Peccei-Quinn model was a two-Higgs doublet model, which contained the axion as a linear combination of the angular degrees of freedom of the two Higgs fields. Consequently the $U(1)_{\rm PQ}$ symmetry breaking was related to the breaking of the electroweak symmetry

[4] See [281] for a proof not relying on chiral perturbation theory.

[5] Note that in general the axion appears together with a model dependent anomaly coefficient. However, for simplicity we will set it to unity in the following.

[6] The axion potential is dominated by contributions from large, non-perturbative QCD instantons and is therefore non-calculable. The potential in Eq. (7.31) is an extrapolation into the non-perturbative region and therefore an order of magnitude estimate. A more accurate form is obtained in chiral perturbation theory.

$SU(2)_L \times U(1)_Y$ and introduced a weak scale f_a. This model was ruled out soon after its proposal [282]. Nowadays one dominantly considers so-called invisible axion models in which the axion arises from a $SU(2)_L \times U(1)_Y$ singlet scalar field, which leads to light and feebly coupled axions. The two most famous UV completions of such models go back to Kim, Shifman, Vainshtein, Zakharov (KSVZ) [283, 284] and Dine, Fischler, Srednicki, Zhitnitskii (DFSZ) [285, 286].

7.3.1 Peccei-Quinn mechanism at work: KSVZ axion model

It is instructive to see the PQ mechanism at work in a concrete example. For this reason we will now explicitly demonstrate the PQ mechanism for the KSVZ axion [283, 284], which is one of the simplest UV complete axion models.

In the KSVZ model the SM is extended with a complex scalar σ and a heavy quark Q, which are both $SU(2)_L \times U(1)_Y$ singlets

$$\mathcal{L}_{\text{KSVZ}} = -y_Q\, \sigma\, \bar{Q}_L Q_R + h.c. - V(|\sigma|^2) + \bar{\theta}\frac{g^2}{16\pi^2}\text{Tr}\; G_{\mu\nu}\tilde{G}^{\mu\nu}\,, \tag{7.33}$$

where $V(|\sigma|^2)$ is the scalar potential and y_Q the Yukawa coupling for the heavy quark.[7] At the classical level this Lagrangian is invariant under the axial $U(1)_{\text{PQ}}$ transformation

$$U(1)_{\text{PQ}}: \quad Q \to e^{i\gamma_5\alpha} Q\,, \qquad \sigma \to e^{-2i\alpha}\sigma\,. \tag{7.34}$$

As we saw in the previous section the chiral anomaly breaks this symmetry and shifts $\bar{\theta} \to \bar{\theta} - 2\alpha$, therefore allowing us to eliminate $\bar{\theta}$ with a $U(1)_{\text{PQ}}$ transformation. Up to this point this coincides with the massless quark solution. The new ingredient is that we can now introduce a mass for the quark Q without explicitly breaking the chiral symmetry by choosing $V(|\sigma|^2)$ such that $U(1)_{\text{PQ}}$ is spontaneously broken at a large scale $f_a \gg v_{\text{EW}}$. In this case we parameterize the σ field as

$$\sigma = \frac{1}{\sqrt{2}}(f_a + \rho)\, e^{ia/f_a}\,, \tag{7.35}$$

where ρ is the massive radial mode and a the massless Goldstone boson from the broken symmetry, the axion. This will introduce a large mass for Q of the form $m_Q = y_Q f_a/\sqrt{2}$ and also for the radial mode ρ of similar size. Note that under $U(1)_{\text{PQ}}$ the axion field shifts in the same way as $\bar{\theta}$, i.e. $a/f_a \to a/f_a - 2\alpha$ and therefore behaves exactly like a phase of the quark mass matrix with the important difference that it is a dynamical field. In complete analogy to the phase of the quark mass we can apply a chiral redefinition of the quark field $Q \to e^{-i\gamma_5 \frac{a}{2f_a}} Q$ to rotate the axion field to the $\bar{\theta}$ angle

$$\mathcal{L} \to -y\frac{f_a+\rho}{\sqrt{2}}\bar{Q}_L Q_R + h.c. - V((f_a+\rho)^2/2) + \frac{\partial_\mu a}{2f_a}\bar{Q}\gamma^\mu\gamma_5 Q + \left(\bar{\theta} + \frac{a}{f_a}\right)\frac{g^2}{16\pi^2}\text{Tr}\; G_{\mu\nu}\tilde{G}^{\mu\nu}\,. \tag{7.36}$$

All couplings of the axion in the above Lagrangian, except the one to Tr $G_{\mu\nu}\tilde{G}^{\mu\nu}$, are derivative and preserve the Goldstone shift symmetry. This allows us to eliminate $\bar{\theta}$ by redefining the axion field as $\tilde{a} = a + f_a\,\bar{\theta}$, effectively making the axion a dynamical $\bar{\theta}$ angle. The last term in the above Lagrangian violates the Goldstone shift symmetry in the instanton background and therefore generates a potential for the axion field, which is nothing else but the QCD vacuum energy with the identification $\bar{\theta} \to \tilde{a}$. As we have seen before this is minimized for $\langle\tilde{a}\rangle = \bar{\theta} + \frac{\langle a\rangle}{f_a} = 0$ (see Eq. 7.31), such that the classical motion of the axion field relaxes the effective vacuum angle to zero, what naturally explains the non-observation of $\mathcal{CP}$ violation in QCD.

[7] Note that one can forbid a bare mass term for Q by imposing a discrete symmetry $R: Q_L \to -Q_L\,,\, Q_R \to +Q_R\,,\, \sigma \to -\sigma$ under which all SM fields are invariant [283]. In general σ also couples to the Higgs as $\lambda_{\sigma H}|H|^2|\sigma|^2$, but for the following we will assume that $\lambda_{\sigma H} = 0$.

7.3.2 Effective axion Lagrangian

At energies much below the PQ breaking scale f_a and the electroweak scale $v_{\rm EW}$, we can write an effective Lagrangian for the axion coupled to QCD. At leading order in $1/f_a$, without loss of generality, this Lagrangian takes the form [244]

$$\mathcal{L} = \mathcal{L}_{\rm QCD} + \mathcal{L}_a \tag{7.37}$$

$$\mathcal{L}_{\rm QCD} = -\frac{1}{2}\text{Tr } G_{\mu\nu}G^{\mu\nu} + \bar{q}i\not{D}q - \bar{q}_L M_q q_R + h.c. \tag{7.38}$$

$$\mathcal{L}_a = \frac{1}{2}(\partial_\mu a)^2 + \frac{a}{f_a}\frac{g^2}{16\pi^2}\text{Tr } G_{\mu\nu}\tilde{G}^{\mu\nu} + \frac{1}{4}a\, g^{(0)}_{a\gamma\gamma}F_{\mu\nu}\tilde{F}^{\mu\nu} + \frac{\partial_\mu a}{2f_a}j^\mu_{a,0}\,, \tag{7.39}$$

where $g^{(0)}_{a\gamma\gamma}$ and $j^\mu_{a,0}$ are model dependent couplings to the photon field strength via the anomaly of the $U(1)_{\rm PQ}$ and the equally model dependent PQ current. The N_f quarks are combined into a N_f vector and the masses are combined into a $N_f \times N_f$ mass matrix M_q. In the above Lagrangian we assumed that any occurrence of the axion field in the phase of the quark masses is rotated into the Tr $G_{\mu\nu}\tilde{G}^{\mu\nu}$ term. We also used the shift symmetry of the axion field in the remaining Lagrangian to absorb the $\bar{\theta}$ angle in the definition of the axion field.

Note that the form of the Lagrangian is not unique. Axion dependent chiral redefinitions of the quark fields shift the coefficients (see [267] for a thorough discussion). Each such Lagrangian is equivalent and physical observables should only depend on reparameterization invariant combinations of the coefficients. The axion mass for example must be proportional to all quark masses and the instanton contribution from the Tr $G_{\mu\nu}\tilde{G}^{\mu\nu}$ term at the same time, since it can be rotated from one into the other.

Let us now consider low-energy QCD, which is well described by considering only two quark flavors, i.e. $q = (u, d)^T$ and $M_q = \text{diag}(m_u, m_d)$. The axion in the $G\tilde{G}$ term can be rotated into the quark mass matrix using a chiral rotation of the form

$$q \to e^{i\gamma_5 \frac{a}{2f_a}Q_a}q\,, \tag{7.40}$$

where $Tr(Q_a) = 1$. This yields an axion dependent QCD Lagrangian

$$\mathcal{L}_{{\rm QCD},a} = -\frac{1}{2}\text{Tr } G_{\mu\nu}G^{\mu\nu} + \bar{q}i\not{D}q - \bar{q}_L M_a q_R + h.c. \tag{7.41}$$

where we defined

$$M_a = e^{i\frac{a}{2f_a}Q_a}M_q e^{i\frac{a}{2f_a}Q_a} = e^{i\frac{a}{2f_a}Q_a}\begin{pmatrix} m_u & \\ & m_d \end{pmatrix}e^{i\frac{a}{2f_a}Q_a}\,. \tag{7.42}$$

This axion dependent mass matrix is now the sole source of the axion shift symmetry breaking and can be used as a spurion for constructing the axion potential. The largest contribution to the axion potential comes from the strongly-coupled low-energy region of QCD. This contribution is non-perturbative and is therefore not calculable within the QCD Lagrangian. However, symmetry arguments enable us to construct an effective Lagrangian for the low-energy degrees of freedom, i.e. mesons and baryons instead of quarks and gluons. In this effective framework, which is commonly denoted chiral perturbation theory, we can compute the axion potential in terms of low-energy QCD observables such as the pion mass and pion decay constant, what we will shortly demonstrate in the following.

In the massless limit the two-flavor QCD Lagrangian in Eq. (7.38) is invariant under $U(1)_V \times SU(2)_L \times SU(2)_R$,[8] i.e. independent $SU(2)$ transformations of the left-handed and right-handed quark components and the combined rescaling with a phase. From experimental observations we know that the low-energy QCD spectrum does not exhibit this symmetry, only a vectorial $U(1)_V \times SU(2)_V$ symmetry is observed. This implies that low-energy QCD spontaneously breaks $SU(2)_L \times SU(2)_R \to SU(2)_V$ due to a non-vanishing chiral condensate $\langle \bar{q}q \rangle \neq 0$, which is the order parameter of chiral symmetry breaking. The low-energy spectrum contains one massless Goldstone boson for each broken symmetry generator, which can be parameterized in the Goldstone matrix Σ as excitations along the broken directions in the group, i.e.

$$\Sigma = e^{i\sigma^a \pi^a / f_\pi} = e^{i\Pi/f_\pi}\,, \qquad \Pi = \begin{pmatrix} \pi^0 & \sqrt{2}\pi^+ \\ \sqrt{2}\pi^- & -\pi^0 \end{pmatrix}\,, \tag{7.43}$$

where σ^a are the Pauli matrices, π^a the Goldstones and f_π their decay constant. The Goldstone bosons can be identified with the pions, as indicated above. Under $SU(2)_L \times SU(2)_R$ transformations Σ transforms as a bif-undamental $\Sigma \sim (\mathbf{2}, \bar{\mathbf{2}})$

$$\Sigma \to U_L \Sigma U_R^{-1}\,, \tag{7.44}$$

with its vacuum expectation value (VEV) $\langle \Sigma \rangle = \mathbb{1}_2$ breaking it to the diagonal combination. The small explicit breaking from the quark mass term can be included by treating M_q as a spurion: if M_q were to transform as $M_q \to U_L M_q U_R^{-1}$, i.e. as a bi-fundamental $M_q \sim (\mathbf{2}, \bar{\mathbf{2}})$, the quark mass term would be invariant under $SU(2)_L \times SU(2)_R$. Promoting M_q to a dynamical field with these transformation properties we construct all invariant terms including Σ and M_q, before setting it to its actual value (which effectively can be viewed as the VEV of the dynamical field). This will capture the symmetry breaking effects due to the mass term. At leading order the chiral Lagrangian takes the form

$$\mathcal{L}_{\chi PT} = \frac{f_\pi^2}{4} \mathrm{Tr}\big[\partial_\mu \Sigma^\dagger \partial^\mu \Sigma\big] + B_0 \frac{f_\pi^2}{2} \mathrm{Tr}\big[U M^\dagger + M U^\dagger\big]\,, \tag{7.45}$$

where the first term contains the kinetic terms and derivative interactions among the Goldstone bosons and the second term generates a potential. B_0 is a constant related to the chiral condensate and can be fixed in terms of the pion mass.

The axion field can be included in this construction by simply replacing $M_q \to M_a$ and using the mass matrix dressed with the axion field. In order to find the axion potential it is sufficient to include the neutral pion fields such that the potential takes the form

$$V(a, \pi^0) = -B_0 \frac{f_\pi^2}{2} \mathrm{Tr}\big[U M_a^\dagger + M_a U^\dagger\big] \tag{7.46}$$

$$= -B_0 f_\pi^2 \left[m_u \cos\left(\tfrac{\pi^0}{f_\pi} - \tfrac{a}{2f_a}\right) + m_d \cos\left(\tfrac{\pi^0}{f_\pi} + \tfrac{a}{2f_a}\right) \right]. \tag{7.47}$$

Integrating out the pion field one arrives at the axion potential in Eq. (7.31). In order to obtain the axion mass it is sufficient to expand the potential to second order in the fields

$$V(a) = -\frac{1}{2} B_0 f_\pi^2 \begin{pmatrix} \pi^0 & a \end{pmatrix} \begin{pmatrix} \frac{m_u+m_d}{f_\pi^2} & -\frac{m_u-m_d}{2f_\pi f_a} \\ -\frac{m_u-m_d}{2f_\pi f_a} & \frac{m_u+m_d}{4f_a^2} \end{pmatrix} \begin{pmatrix} \pi^0 \\ a \end{pmatrix} + \dots\,. \tag{7.48}$$

[8] At the classical level the QCD Lagrangian is also invariant under axial $U(1)_A$ transformations. However, as we have discussed at length before this symmetry is actually badly broken at the quantum level due to instanton effects and is therefore no symmetry at all. This explains the absence of the corresponding would-be Goldstone boson, commonly denoted as η'. 't Hooft solved this so-called $U(1)$ problem [287] by noticing that instantons contribute to the η' mass making it much heavier than the other pseudo-Goldstone bosons.

The eigenvalues of the mass matrix to leading order in $1/f_a$ are given by

$$m_a^2 = B_0 f_\pi^2 \frac{m_u m_d}{f_a^2 (m_u + m_d)}\,, \qquad m_\pi^2 = B_0 f_\pi^2 \frac{m_u + m_d}{f_\pi^2}\,. \tag{7.49}$$

Fixing B_0 using the pion mass, we finally obtain the prediction for the axion mass

$$m_a^2 = \frac{m_u m_d}{(m_u + m_d)^2} \frac{m_\pi^2 f_\pi^2}{f_a^2}\,, \tag{7.50}$$

which is completely determined by f_a and low-energy observables.

In the next sections we will focus on the axion potential and mass from the instanton point of view, but we will always use Eq. (7.50) as the axion mass predicted by low-energy QCD.

Chapter 8

Instanton calculus

In the previous chapter we discussed the vacuum structure of QCD and the strong-$\mathcal{CP}$ problem. The introduction of the θ-vacuum and also the strong-$\mathcal{CP}$ problem crucially depended on the existence of transition amplitudes between topologically distinct QCD vacua. These transition amplitudes are caused by instantons, which are solutions of the Yang-Mills equation of motion in Euclidean ST and can therefore be interpreted as quantum tunnelling between QCD vacua with different winding number.

In this chapter we introduce the instanton calculus in broken and unbroken gauge groups. For this reason we will start by discussing the Euclidean formulation of QCD along the lines of [288], before we shortly present the one-instanton solution as found by Belavin, Polyakov, Schwartz and Tyupkin (BPST) [270]. Based on these tools we will finally show how to perform the path-integral in the instanton background in $SU(N)$ theories [280,289]. The derivation of the instanton density will loosely follow [290]. For a further pedagogical introduction to instantons we refer the reader to [288, 291–293].

8.1 Euclidean formulation of QCD

In order to describe instanton effects one has to work in Euclidean ST. For this reason we will now discuss how to formulate a Euclidean version of the QCD Lagrangian. We will follow the conventions of [288] in which quantities in Euclidean ST are marked with a caret, e.g. $\hat{v}_\mu$, for which the indices take values $\mu, \nu, \ldots = 1, 2, 3, 4$. For the corresponding quantity in Minkowski ST v_μ the indices run from 0 to 3. Latin letters $i, j, \ldots = 1, 2, 3$ denote spatial indices. Note that in Euclidean ST there is no difference between upper and lower indices.

One can pass from complexified Minkowski ST to Euclidean ST via a Wick rotation. This leaves the spatial coordinates unchanged, i.e. $\hat{x}_i = x^i$ but effectively substitutes the time component by $x_0 = -i\hat{x}_4$. This obviously also affects the vector potential, for which we define a Euclidean version as

$$A^i = -\hat{A}_i\,, \qquad A_0 = i\hat{A}_4\,. \tag{8.1}$$

With this definition the covariant derivative takes the form

$$\hat{D}_\mu = \frac{\partial}{\partial \hat{x}_\mu} - ig\hat{A}^a_\mu T^a\,, \tag{8.2}$$

which is related to the covariant derivative in Minkowski ST via $D^i = -\hat{D}_i$ and $D_0 = i\hat{D}_4$. This way the field strength tensor $\hat{G}^a_{\mu\nu}$ has exactly the same form as in Minkowski ST, just

with A_μ, $\partial/\partial x_\mu$ replaced by $\hat{A}_\mu$ and $\partial/\partial\hat{x}_\mu$, which amounts to the identification $G^a_{ij} = \hat{G}^a_{ij}$ and $G^a_{0j} = i\hat{G}^a_{4j}$.

In order to formulate QCD in Euclidean ST we also need a Euclidean formulation for the fermion fields. In contrast to Minkowski space, the Dirac fermions ψ and $\bar{\psi}$ are independent anticommuting variables in Euclidean space. The corresponding Euclidean spinor fields are defined as

$$\psi = \hat{\psi}\,, \qquad \bar{\psi} = -i\hat{\bar{\psi}}\,. \tag{8.3}$$

Note also that $\hat{\bar{\psi}}$ does not transform like its Minkowskian counterpart as $\psi^\dagger\gamma_0$, but instead as $\hat{\psi}^\dagger$, such that $\hat{\psi}_1^\dagger\hat{\psi}_2$ transforms as a scalar and $\hat{\psi}_1^\dagger\hat{\gamma}_\mu\hat{\psi}_2$ as a vector. Last but not least we have to define the Euclidean analogs of the γ matrices

$$\hat{\gamma}_4 = \gamma_0\,, \quad \hat{\gamma}_i = -i\gamma^i\,, \qquad \{\hat{\gamma}_\mu, \hat{\gamma}_\nu\} = 2\delta_{\mu\nu}\,. \tag{8.4}$$

With these ingredients we can formulate the Euclidean action for QCD [288]

$$iS = -\hat{S}\,, \tag{8.5}$$

$$S = \int d^4x \left[-\frac{1}{2}\mathrm{Tr}\; G_{\mu\nu}G^{\mu\nu} + \bar{\psi}(i\gamma^\mu D_\mu - m)\psi + \theta\frac{g^2}{16\pi^2}\mathrm{Tr}\; G_{\mu\nu}\tilde{G}^{\mu\nu}\right], \tag{8.6}$$

$$\hat{S} = \int d^4\hat{x} \left[\frac{1}{2}\mathrm{Tr}\; \hat{G}_{\mu\nu}\hat{G}^{\mu\nu} + \hat{\bar{\psi}}(-i\hat{\gamma}^\mu\hat{D}_\mu - im)\hat{\psi} + i\theta\frac{g^2}{16\pi^2}\mathrm{Tr}\; \hat{G}_{\mu\nu}\hat{\tilde{G}}^{\mu\nu}\right], \tag{8.7}$$

where the Levi-Civita tensor in $\hat{\tilde{G}}$ is defined such that $\epsilon_{1234} = 1$. Since we will work almost exclusively in Euclidean ST in the following, we will omit the carets and implicitly assume that all quantities are defined in Euclidean ST.

8.2 The BPST instanton

As we have mentioned before, instantons mediate tunneling transitions between topologically distinct Yang-Mills vacua. Therefore they are by definition solutions of the Euclidean equations of motion

$$D_\mu G_{\mu\nu} = 0 \tag{8.8}$$

with finite action (solutions with infinite action lead to vanishing transition amplitudes due to the e^{-S} factor in the partition function). From Eq. (8.7) it is straightforward to see that $G^a_{\mu\nu}$ has to decrease faster than $1/x^2$ for $|x| \to \infty$ for the action to be finite. This implies that A^a_μ is pure gauge far away from the instanton center, i.e.

$$A_\mu = A^a_\mu T^a \xrightarrow{|x|\to\infty} \frac{i}{g} S\partial_\mu S^\dagger\,, \tag{8.9}$$

such that the large $|x|$ behavior is determined by the gauge transformation S at the boundary of four-dimensional spacetime, which can be taken to be the three-dimensional sphere S_3. Thus the classification of finite action solutions is equivalent to the classification of gauge transformations S. As we have seen in Section 7.1, when we classified vacuum solutions, the gauge maps $S : S_3 \to G$ can be characterized in terms of elements of the homotopy group $\pi_3(G)$, which for $SU(N)$ theories is given by

$$\pi_3(SU(N)) = \mathbb{Z}\,. \tag{8.10}$$

As the reader might have noticed this discussion is extremely similar to the classification of vacuum states. But note that the interpretation is slightly different: in Section 7.1 we characterized different vacuum solutions, i.e. minimum energy solutions, by their winding number ν.

However, here we classify trajectories in field space which interpolate between a vacuum with winding number ν_1 at $x_4 = -\infty$ and a different vacuum with winding number ν_2 at $x_4 = +\infty$. Thus the finite action solutions are classified by the topological charge Q, which is the change in winding number of the vacuum due to the tunneling solution, and whose form follows from Eq. (7.12)

$$Q = \frac{g^2}{16\pi^2}\int d^4x \,\mathrm{Tr}\; G_{\mu\nu}\tilde{G}^{\mu\nu} = \nu(x_4 = +\infty) - \nu(x_4 = -\infty)\,. \tag{8.11}$$

Now let us construct the explicit form of the instanton solution. In order to simplify the construction it is helpful to note that in order to find a finite action solution of the Euclidean equations of motion it is sufficient to find a minimum of the action (which is by definition a solution of the equations of motion). Through a simple trick it is straightforward to find the minimum value of the action and in the process identify the properties of the corresponding field configurations. With the so-called Bogomol'nyi completion we can rewrite the Yang-Mills action

$$\begin{aligned}\int d^4x \frac{1}{2}\mathrm{Tr}\; G_{\mu\nu}^2 &= \int d^4x \frac{1}{4}\mathrm{Tr}\; \left[G_{\mu\nu}^2 + \tilde{G}_{\mu\nu}^2\right] \\ &= \int d^4x \frac{1}{4}\mathrm{Tr}\; \left[G_{\mu\nu} \mp \tilde{G}_{\mu\nu}\right]^2 \pm \int d^4x \frac{1}{2}\mathrm{Tr}\; G_{\mu\nu}\tilde{G}_{\mu\nu} \\ &= \pm\left(\frac{8\pi^2}{g^2}\right)Q + \int d^4x \frac{1}{4}\mathrm{Tr}\; \left[G_{\mu\nu} \mp \tilde{G}_{\mu\nu}\right]^2 \\ &\geq \left(\frac{8\pi^2}{g^2}\right)|Q|\,,\end{aligned} \tag{8.12}$$

where we used Eq. (8.11). Therefore the minimum of the action for a fixed Q is $S = 8\pi^2|Q|/g^2$, which is saturated for:

- self-dual field configurations $G_{\mu\nu} = \tilde{G}_{\mu\nu}$ for $Q > 0$,
- anti-self-dual field configurations $G_{\mu\nu} = -\tilde{G}_{\mu\nu}$ for $Q < 0$.

The self-dual solutions are termed instantons, whereas the anti-self-dual solutions are commonly referred to as anti-instantons. Note that this discussion implies that field strengths which satisfy the self-duality or anti-self-duality condition automatically satisfy the equations of motion, since they are minima of the action. This can also be seen directly by applying the Bianchi identity

$$D_\mu G_{\mu\nu} = \pm D_\mu \tilde{G}_{\mu\nu} = \pm\frac{1}{2}\epsilon_{\mu\nu\rho\sigma} D_\mu G_{\rho\sigma} = 0\,. \tag{8.13}$$

The (anti-)self-duality equations are useful, since they are simpler to solve than the second order equations of motion.

We will now focus on $G = SU(2)$ and construct the explicit form of the BPST instanton [270] in the $Q = 1$ sector. The straightforward generalization to $G = SU(N)$ will be discussed at the end of the section. We have already found that the asymptotic form of the instanton at $|x| \to \infty$ is pure gauge

$$A_\mu^{Q=1} \xrightarrow{|x|\to\infty} \frac{i}{g} S_1 \partial_\mu S_1\,, \tag{8.14}$$

where S_1 is a gauge map with unit winding number. An example of such a map is

$$S_1 = \frac{i\tau_\mu^+ x_\mu}{\sqrt{x^2}}\,, \tag{8.15}$$

where $\tau_\mu^\pm = (\boldsymbol{\tau}, \mp i)$ with $\boldsymbol{\tau}$ being a vector of Pauli matrices. Note that it is straightforward to obtain gauge maps S_n with winding number n from S_1 by exploiting the additivity of the winding number: $S_n = (S_1)^n$. In order to write Eq. (8.14) in terms of A_μ^a we introduce the 't Hooft symbols $\eta_{a\mu\nu}$[1]

$$\eta_{a\mu\nu} = \begin{cases} \epsilon_{a\mu\nu}\,, & \mu,\nu = 1,2,3 \\ -\delta_{a\nu}\,, & \mu = 4 \\ \delta_{a\mu}\,, & \nu = 4 \\ 0\,, & \mu = \nu = 4 \end{cases}\,, \tag{8.16}$$

with which we can write Eq. (8.14) as

$$A_\mu^a \xrightarrow{|x|\to\infty} \frac{2}{g}\eta_{a\mu\nu}\frac{x_\nu}{x^2}\,. \tag{8.17}$$

Based on this asymptotic form and assuming A_μ^a has the same angular behavior for all x we make the following ansatz for the instanton solution with center at $x = 0$

$$A_\mu^{a,\,Q=1} = \frac{2}{g}\eta_{a\mu\nu}\frac{x_\nu}{x^2}f(x^2)\,. \tag{8.18}$$

$f(x^2)$ must have the asymptotic behavior

$$f(x^2) \xrightarrow{|x|\to\infty} 1 \tag{8.19}$$

$$f(x^2) \xrightarrow{|x|\to 0} \text{const.}\cdot x^2\,, \tag{8.20}$$

where the second condition makes sure that the solution is regular at the origin. The self-duality condition $G_{\mu\nu}^a = \tilde{G}_{\mu\nu}^a$ yields a first order differential equation for the profile function

$$f(1-f) - x^2 f' = 0\,, \tag{8.21}$$

which is solved by

$$f(x^2) = \frac{x^2}{x^2+\rho^2}\,, \tag{8.22}$$

with the free parameter ρ^2 that is identified with the instanton size. In order to obtain the full familiy of solutions for instantons centered at x_0 we can simply shift the solution by $x \to x - x_0$, such that the full solution is given by

$$A_\mu^{a,\,Q=1} = \frac{2}{g}\eta_{a\mu\nu}\frac{(x-x_0)_\nu}{(x-x_0)^2+\rho^2}\,. \tag{8.23}$$

It is sometimes useful to shift the non-trivial behavior of the gauge field from infinity to the instanton center. This can be done with a singular gauge-transformation of the form

$$U = \frac{i\tau_\mu^+(x-x_0)_\mu}{\sqrt{(x-x_0)^2}}\,, \tag{8.24}$$

which yields the instanton in singular gauge[2]

$$\bar{A}_\mu^{a,\,Q=1} = \frac{2\rho^2}{g}\bar{\eta}_{a\mu\nu}\frac{(x-x_0)_\nu}{(x-x_0)^2\big[(x-x_0)^2+\rho^2\big]}\,. \tag{8.25}$$

[1] For properties of the 't Hooft symbols see e.g. [288].

[2] This is obtained by gauge transforming the vector potential $g\frac{\tau^a}{2}A_\mu^a \to U^\dagger g\frac{\tau^a}{2}A_\mu^a U + iU^\dagger\partial_\mu U$.

A generalization of the instanton to $Q > 1$ is also possible and a simple recipe for obtaining such solutions goes back to 't Hooft (see e.g. [294]). However, $Q > 1$ instantons are suppressed as long as the theory is perturbative and will therefore be neglected in the following.

The instanton solution in Eq. (8.25) was derived for $SU(2)$. However, the extension to larger gauge groups is straightforward. Instantons in $SU(N)$ are obtained by embedding the $SU(2)$ instanton into $SU(N)$. The simplest way of embedding the $SU(2)$ instanton is the so-called minimal embedding, in which one embeds the instanton into a $SU(2)$ subgroup with generators in the fundamental representation. For instance we can embed the $SU(2)$ in the 2×2 upper-left-hand corner of the $N \times N$ matrices which generate the fundamental representation of $SU(N)$, i.e.

$$A_\mu^{SU(N)} = \begin{pmatrix} A_\mu^{SU(2)} & 0 \\ 0 & 0 \end{pmatrix} . \tag{8.26}$$

Note that this embedding is not unique. One can generate a new embedding by acting on Eq. (8.26) with a general $SU(N)$ element. But not all $SU(N)$ transformations lead to new embeddings, since there are group elements which leave Eq. (8.26) invariant. This set of $SU(N)$ elements forms the stability group of the instanton embedding, which is $T_N = SU(N-2) \times U(1)$ for the minimal embedding. This means that only $SU(N)/T_N$ transformations yield new embeddings, corresponding to a $4N-5$ (which is the dimension of the coset) parameter family of instanton solutions. These $4N-5$ parameters in addition to the position and scale of the instanton will be identified with the collective coordinates in the next section.

The minimal embedding is not the only way of embedding the instanton into $SU(N)$. Instead of embedding the 2×2 matrix representation, i.e. the fundamental representation of the $SU(2)$ generators, into the $N \times N$ matrix representation of the $SU(N)$ generators, one can also choose a different representation of the $SU(2)$ generators (see e.g. [295]).[3] However, in the following we will stick to the minimal embedding.

8.3 Instantons in broken $SU(N)$ gauge groups

Now we finally have the tools to formulate and compute the Euclidean path integral in the instanton background. In this section we determine the instanton density in completely broken $SU(N)$ theories.[4] Instantons in completely broken $SU(N)$ theories will be important in the next chapter, where we will consider contributions to the axion mass in product group theories broken to a diagonal subgroup, for example, $SU(N)_1 \times SU(N)_2 \to SU(N)_D$. From the point of view of the instantons which live in only one of the individual $SU(N)$ factors, the $SU(N)$ of the corresponding factor is completely broken.

This section loosely follows the instanton calculation in supersymmetric QCD by Cordes [290] with slight modifications due to the non-sypersymmetric nature of the problem at hand. In instanton calculations it is common practice to use Pauli-Villars (PV) regularization in calculations, which we will also do here. However, in perturbative calculations dimensional regularization and the MS or $\overline{\text{MS}}$ scheme are more common. The formulae needed to convert from PV to $\overline{\text{MS}}$ scheme are collected in Appendix II.B.

In the following we consider an $SU(N)$ gauge theory with a matter sector consisting of

[3] These embeddings do not correspond to unit winding number instantons in $SU(N)$, since the winding number is proportional to Tr $T^a T^b$ which is in turn proportional to the quadratic Casimir and the dimension of the representation. E.g. embedding the spin-1 representation of $SU(2)$ into $SU(3)$ yields instantons with topological charge $Q = \pm 4$.

[4] Note that the instanton density for unbroken gauge theories is obtained by setting the scalar VEVs to zero.

$S \geq N-1$ scalars[5] ϕ_n, $n = 1, \ldots, S$ and F (approximately) massless fermions ψ_f, $f = 1, \ldots, F$ all in the fundamental representation of $SU(N)$. The Euclidean action for this model is given by

$$S_E = S_G + S_\phi + S_\psi \,, \tag{8.27}$$

where

$$S_G = \int d^4x \left[\frac{1}{2} \text{Tr } G_{\mu\nu} G_{\mu\nu} + i\theta \frac{g^2}{16\pi^2} \text{Tr } G_{\mu\nu} \tilde{G}_{\mu\nu} + \mathcal{L}_{\text{ghost}}(\eta, \bar{\eta}) \right], \tag{8.28}$$

$$S_\phi = \int d^4x \left[(D_\mu \phi_n)^\dagger D_\mu \phi_n + V(\phi_n) \right], \tag{8.29}$$

$$S_\psi = \int d^4x \, \bar{\psi}_f (-i\gamma_\mu D_\mu) \psi_f \,, \tag{8.30}$$

with $D_\mu \phi_n = (\partial_\mu - i g A_\mu^A T^A)\phi_n$. T^A, $A = 1, \ldots, N^2-1$ are the $SU(N)$ generators. A sum over the scalar and fermion generations is implied. The scalar potential $V(\phi_f)$ is such that the scalars develop a VEV which breaks the $SU(N)$ gauge symmetry completely.

As we saw in the previous section, in the absence of scalar VEVs the Euclidean Yang-Mills action S_G possesses exact instanton solutions for the classical equations of motion, with the one instanton solution in $SU(2)$, centered at x_0, with unit topological charge ($Q = 1$) in singular gauge given by Eq. (8.25). In the minimal embedding the $SU(N)$ instanton takes the form

$$A_\mu^{Q=1} = \frac{2\rho^2}{g} \bar{\eta}_{a\mu\nu} \frac{(x-x_0)_\nu}{(x-x_0)^2 \left[(x-x_0)^2 + \rho^2 \right]} J^a \,, \tag{8.31}$$

where we dropped the bar over the gauge field. J^a, $a = 1, 2, 3$ are the generators of the $SU(2)$ subgroup in the 2×2 upper-left-hand corner of the $N \times N$ matrices which generate the fundamental representation of $SU(N)$ into which the instanton is embedded.

Once the scalars obtain a VEV $|\langle \phi_n \rangle| > 0$ and break $SU(N)$ completely, no exact instanton solutions exist[6]. However, the expectation is that for small instantons, $g\rho|\langle \phi_n \rangle| \ll 1$, the solution in Eq. (8.31) remains a good approximation and the path integral is still dominated by instanton-like configurations. In this scenario the path integral can still be performed by using the constrained instanton formalism of Affleck [296]. In the constrained instanton formalism the scalars satisfy the equation of motion in the classical instanton background, $D^2(A_{cl})\phi = 0$, s.t. the scalar profile to leading order in $g\rho|\langle \phi \rangle|$ is given by

$$\phi_{in}(x) = \begin{cases} \left(\frac{x^2}{x^2+\rho^2} \right)^{1/2} \langle \phi_{in} \rangle & \text{for } i = 1, 2 \\ \langle \phi_{in} \rangle & \text{for } i = 3, \ldots, N \end{cases} , \tag{8.32}$$

where i is the $SU(N)$ index of the scalar multiplets.

The classical action in the constrained instanton framework with a $Q = 1$ instanton background in the presence of the scalar profile evaluates to

$$S_0(\rho) = \frac{8\pi^2}{g^2} + 2\pi^2 \rho^2 \sum_{i=1}^{2} \sum_{n=1}^{S} |\langle \phi_{in} \rangle|^2 + i\theta \,. \tag{8.33}$$

[5] In order to break $SU(N)$ completely one needs at least $N-1$ scalar fields.

[6] If $SU(N)$ is only partially broken with an unbroken residual $SU(2)$ subgroup, i.e. $\text{rank}(\langle \phi_{in} \rangle) < N-1$, exact instanton solutions still exist in the unbroken $SU(2)$.

Thus large instantons ($g\rho|\langle\phi_f\rangle| \gg 1$) are exponentially suppressed. This provides a natural IR cutoff for the instanton size and makes instanton contributions to observables calculable.

Let us in the following consider the one-instanton vacuum-to-vacuum amplitude in $W_{SU(N)}$

$$W_{SU(N)} \equiv \langle 0|0\rangle_{\Delta Q=1} = \frac{\int_{1-\text{inst}} \mathcal{D}A_\mu \mathcal{D}\eta \mathcal{D}\bar{\eta} \mathcal{D}\phi_f \mathcal{D}\phi_f^\dagger \mathcal{D}\psi \mathcal{D}\bar{\psi}_n \, e^{-S_E}}{\int_{A_\mu^{\text{cl}}=0} \mathcal{D}A_\mu \mathcal{D}\eta \mathcal{D}\bar{\eta} \mathcal{D}\phi_f \mathcal{D}\phi_f^\dagger \mathcal{D}\psi \mathcal{D}\bar{\psi}_n \, e^{-S_E}} \,. \tag{8.34}$$

We evaluate Eq. (8.34) in the semi-classical approximation by expanding the Euclidean action to second order in the fields around the classical solutions given in Eq. (8.32) and (8.31)

$$S_E = S_0(\rho) + \int d^4x \left[\frac{1}{2} A_\mu M_A A_\mu + \bar{\eta} M_{\text{ghost}} \eta + \phi^\dagger M_\phi \phi + \bar{\psi} M_\psi \psi \right], \tag{8.35}$$

where $\phi = (\phi_1, \ldots, \phi_S)^T$ and $\psi = (\psi_1, \ldots, \psi_F)^T$ are vectors containing all scalar and fermion generations, and perform the functional integral.

We will thoroughly discuss the contributions to the generating functional from the different sectors in the following, but here we already give the final result for the vacuum-to-vacuum amplitude with the above field content

$$W_{SU(N)} = e^{-i\theta} \int \frac{d^4x_0 d\rho}{\rho^5} d_N(\rho) \int d\tilde{\mu} \, e^{-2\pi^2\rho^2 \sum_{i=1}^{2} \sum_{n=1}^{S} |\langle \tilde{\phi}_{in} \rangle(\tilde{\mu})|^2} \int \prod_{f=1}^{2F} \rho^{1/2} d\xi_f^{(0)} \,, \tag{8.36}$$

where $d_N(\rho)$ is the instanton density in vacuum

$$d_N(\rho) = \frac{C_1 e^{-(S-2F)\alpha(1/2)}}{(N-1)!(N-2)!} \left(\frac{8\pi^2}{g^2} \right)^{2N} e^{-\frac{8\pi^2}{g^2(1/\rho)} - C_2 N} \,. \tag{8.37}$$

C_1 and C_2 are defined as

$$C_1 = \frac{2e^{5/6}}{\pi^2} \approx 0.466 \,, \tag{8.38}$$

$$C_2 = \frac{5}{3}\ln 2 - \frac{17}{36} + \frac{1}{3}(\ln 2\pi + \gamma) + \frac{2}{\pi^2} \sum_{s=1}^{\infty} \frac{\ln s}{s^2} \approx 1.678 \,. \tag{8.39}$$

$\alpha(t)$ is defined in [280] (with $\alpha(0) = 0$, $\alpha(1/2) = 0.145873$, $\alpha(1) = 0.443307$), $\int d\tilde{\mu}$ is the integral over the already mentioned $4N-5$ collective coordinates corresponding to the orientation of the instanton within $SU(N)$ normalized to unity, and $\int d\xi_f^{(0)}$ is the integral over the fermion zero modes. $\langle \tilde{\phi}_{in} \rangle(\tilde{\mu})$ are the scalar VEVs rotated in group space to account for the arbitrary location of the instanton $SU(2)$ inside $SU(N)$.

8.3.1 Bosonic contributions

Let us first consider the bosonic sector of the theory. Performing the integral in Eq. (8.34) for the gauge, scalar and ghost fields one obtains

$$W_{SU(N)} = \int \prod_i d\gamma_i J(\gamma) e^{-S_0(\rho)} I_\psi(\gamma) \frac{(\det' M_A(\gamma))^{-1/2} (\det' M_{\text{ghost}}(\gamma)) (\det' M_\phi(\gamma))^{-2}}{((\det M_A)^{-1/2} (\det M_{\text{ghost}}) (\det M_\phi)^{-2})_{A_\mu^{\text{cl}}=0}} \,, \tag{8.40}$$

where we encode the contribution from the fermions in I_ψ, which we will discuss later, and the determinants $\det'$ are taken over non-zero modes only.

Zero modes are flat directions in the action and can be parameterised in terms of collective coordinates γ_i

$$\gamma_i = \begin{cases} (x_0)_i & i = 1, \ldots, 4 \\ \rho & i = 5 \\ t^A & i = A + 5 = 6, \ldots, N^2 + 4 \end{cases} \tag{8.41}$$

where x_0 is the instanton position, ρ its size and t^A are the N^2-1 parameters describing general $SU(N)$ transformations. As we discussed in the previous section, the number of group theoretic zero modes does not coincide with the N^2-1 parameters of general $SU(N)$ transformations, but depend on the embedding of the $SU(2)$ instanton into $SU(N)$. In the minimal embedding the J^a generators of the $SU(2)$ subgroup in which the instanton is embedded transform as singlets under the stability group $T_N = SU(N-2) \times U(1) \subset SU(N)$. There are no normalizable zero modes corresponding to singlet generators, what implies that the number of group theoretic zero modes is given by the $4N-5$ parameters that characterize transformations in $SU(N)/T_N$, i.e. $SU(N)$ transformations which do not live in the stability group. In combination with the 5 zero-modes from the instanton position and size, $SU(N)$ instantons possess $4N$ normalizable zero modes in total.

The functional integral over the zero modes can be cast into an integration over collective coordinates. The change of integration variables induces the Jacobian $J(\gamma)$ in Eq. (8.40). With the normalization of the zero modes one obtains (see e.g. [290] and [289])[7]

$$\int \prod_i^{4N} d\gamma_i \, J(\gamma) = \int d^4x_0 \, d\rho \, d\mu \, \frac{2^7}{\rho^5} \left(\frac{\pi\rho^2}{g^2} \right)^{2N} , \tag{8.42}$$

where $d\mu$ is the Haar measure of the quotient group $SU(N)/T_N$. In [290] Cordes showed that for integrands invariant under T_N, the group integration can be recast into

$$\begin{aligned} \int_{SU(N)/T_N} d\mu &= \frac{V(SU(N-1))}{V(T_N)} \int_{SU(N)/SU(N-1)} d\mu \\ &= \frac{2^{4N-6}\pi^{N-2}}{(N-2)!} \int_{S^{2N-1}} \delta(\sqrt{\sum |y_i|^2} - 1) \, d^2y_1 \ldots d^2y_N \, . \end{aligned} \tag{8.43}$$

Let us define Ω to be a general element of the coset $SU(N)/SU(N-1)$. We could parameterise Ω in terms of the y_i [290], but we will not need the explicit form of Ω in the following. Using that the surface of the S^{2N-1} sphere is given by $S(S^{2N-1}) = 2\pi^N/(N-1)!$, we define a normalized integration measure

$$\int d\tilde{\mu} = \frac{(N-1)!}{2\pi^N} \int_{S^{2N-1}} \delta(\sqrt{\sum |y_i|^2} - 1) \, d^2y_1 \ldots d^2y_N \, . \tag{8.44}$$

Finally we have to evaluate the functional determinants over the non-zero modes. This calculation has been done by 't Hooft [280] for an $SU(2)$ gauge theory. The generalization of his results to $SU(N)$ is straightforward (see e.g. [289]) and yields in Pauli-Villars regularization

$$\begin{aligned} &\frac{(\det' M_A(\gamma))^{-1/2} (\det' M_{\text{ghost}}(\gamma)) (\det' M_\phi(\gamma))^{-2}}{((\det M_A)^{-1/2} (\det M_{\text{ghost}}) (\det M_\phi)^{-2})_{A_\mu^{\text{cl}}=0}} \\ &= \exp\left[-\left(\tfrac{1}{3}N + \tfrac{1}{6}\sum_t S(t)C(t)\right) \ln(\mu_0\rho) - \alpha(1) - 2(N-2)\alpha(1/2) - \sum_t S(t)\alpha(t) \right] , \end{aligned} \tag{8.45}$$

[7] Cordes [290] and Bernard [289] use different normalizations for the $SU(N)$ generators, which is reflected in their different results for the zero-mode normalization (apart from the missing factor of ρ in $||A_\mu^{(\text{isodoub})}||$ in Eq. (5.7) of [290], which is clearly a typo). In the following we will follow Cordes' conventions.

where t denotes the isospin representation under the instanton $SU(2)$. $S(t)$ is the number of scalar multiplets with isospin t, where each complex multiplet counts as 1 and each real multiplet as 1/2 and $C(t) = \frac{2}{3}t(t+1)(2t+1)$. Each scalar fundamental contributes one multiplet in the isospin 1/2 representation and $(N-2)$ singlets.

Substituting Eqs. (8.42), (8.43), (8.44) and (8.45) into Eq. (8.40) and recalling that in Pauli-Villars regularization each zero-mode yields a factor μ_0 of the regulator field, we obtain

$$W_{SU(N)} = \frac{C_1\, e^{-N_S\alpha(1/2)}}{(N-1)!(N-2)!} e^{-i\theta}\left(\frac{8\pi^2}{g^2}\right)^{2N} \int \frac{d^4x_0\, d\rho}{\rho^5}(\mu_0\rho)^{b_0} e^{-8\pi^2/g^2 - C_2 N} \times \int d\tilde{\mu}\, I_\psi(\gamma)\, e^{-2\pi^2\rho^2 \sum_{i=1}^{2}\sum_{n=1}^{S}|\langle\phi_{in}\rangle|^2}\,, \tag{8.46}$$

where $b_0 = \frac{11}{3}N - \frac{1}{6}S$ is the bosonic contribution to the β-function and

$$C_1 = \frac{4\, e^{-\alpha(1)+4\alpha(1/2)}}{\pi^2}\,, \qquad C_2 = 2\,\ln 2 + 2\,\alpha(1/2)\,. \tag{8.47}$$

When we plug in the explicit expression for $\alpha(t)$, the above definition of C_1 and C_2 agrees with Eqs. (8.38) and (8.39).

The group integration $\int d\tilde{\mu}$ in Eq. (8.46) corresponds to rotating the instanton embedding in $SU(N)$. An equivalent way of proceeding is to keep the instanton position within $SU(N)$ fixed and instead rotate all other fields, in particular the scalar fields and their VEVs, by a general $SU(N)/SU(N-1)$ group element Ω, i.e. in Eq. (8.46) we should make the replacement

$$\langle\phi_{in}\rangle \to \langle\tilde{\phi}_{in}\rangle(\tilde{\mu}) = \sum_{j=1}^{N}\Omega_{ij}\langle\phi_{jn}\rangle\,. \tag{8.48}$$

8.3.2 Fermionic contributions

Now let us turn to the fermionic contributions to the vacuum-to-vacuum amplitude and isolate the zero modeds in the functional integral over the fermion fields, i.e.

$$\mathcal{D}\psi\mathcal{D}\bar{\psi} = \prod_f ||\psi_f^{(0)}||^{-1}\, d\xi_f^{(0)} \prod_{f'} ||\bar{\psi}_{f'}^{(0)}||^{-1}\, d\bar{\xi}_{f'}^{(0)}\, \mathcal{D}\psi'\, \mathcal{D}\bar{\psi}'\,, \tag{8.49}$$

where $\psi_f^{(0)}$ and $\bar{\psi}_f^{(0)}$ are the zero mode wave functions of the Dirac operator $M_\psi^{mn} = -i\delta^{mn}\gamma_\mu D_\mu$ and $d\xi_f^{(0)}, d\bar{\xi}_f^{(0)}$ are Grassmann integration measures with mass dimension $[d\xi_f^{(0)}] = [d\bar{\xi}_f^{(0)}] = \frac{1}{2}$. The explicit form of the normalized zero-modes in singular gauge, for an instanton centered at x_0, is given by [288]

$$\psi_f^{(0)}(x)_{\alpha i} = \frac{\rho}{\pi}\frac{(x-x_0)_\mu}{((x-x_0)^2)^{1/2}((x-x_0)^2+\rho^2)^{3/2}}\begin{pmatrix}0\\ i(\tau_\mu^+)_i^j\varphi_{\alpha j}\end{pmatrix}\epsilon_{\alpha k}\,, \tag{8.50}$$

where $\alpha, i, j = 1, 2$ are the spinor and $SU(N)$ indices (restricted to the instanton $SU(2)$ with $\psi_f^{(0)}(x)_{\alpha i} = 0$ for $i = 3, \ldots, N$), respectively.[8] $\varphi_{\alpha j}$ is a two component Weyl spinor with $\varphi_{\alpha j} = \epsilon_{\alpha j}$. Note that for small instantons, far from the instanton center, the zero mode wavefunction

[8] Note that the zero modes naively seem to have the wrong dimension (mass dimension 2 instead of 3/2), but the combination with the corresponding Grassmann variable $\xi_f^{(0)}$ in the expansion $\psi_f(x) = \sum_k \psi_f^{(k)}(x)\,\xi_f^{(k)}$ has the right dimension ($[\xi_f^{(k)}] = -1/2$, s.t. $\int d\xi_f^{(k)}\,\xi_f^{(k)} = 1$).

is proportional to the free fermion propagator $S_F(x) = \frac{\gamma_\mu x_\mu}{2\pi^2(x^2)^2}$. Each massless Dirac fermion in the fundamental representation possesses two zero modes, one for each chirality, in the one instanton background. This implies that in a model with F fermion flavors we have $2F$ fermionic zero modes.

The integral over the non-zero modes can be directly performed, which yields

$$I_\psi = \int \prod_{f=1}^{2F} d\xi_f^{(0)} \mu_0^{-F} \left(\frac{\det' M_\psi^\dagger M_\psi}{(\det M_\psi^\dagger M_\psi)_{A_\mu^{\rm cl}=0}} \right)^{1/2}, \tag{8.51}$$

where we assumed normalized zero modes and collectively denoted the zero mode integration measure as $d\xi_f^{(0)}$. Additionally we inserted a factor $\mu_0^{-1/2}$ of the regulator field for each of the $2F$ zero modes, since we work in Pauli-Villars regularization scheme.

The non-zero mode determinant was computed by 't Hooft [280]

$$\left(\frac{\det' M_\psi^\dagger M_\psi}{(\det M_\psi^\dagger M_\psi)_{A_\mu^{\rm cl}=0}} \right)^{1/2} = \exp\left[\tfrac{1}{3} F \ln(\rho\mu_0) + 2F\alpha(1/2) \right]. \tag{8.52}$$

Combining Eqs. (8.51) and (8.52), we obtain the full fermionic contribution to $W_{SU(N)}$

$$I_\psi = \rho^F e^{-\frac{2}{3}F\ln(\rho\mu_0)+2F\alpha(1/2)} \int \prod_{f=1}^{2F} d\xi_f^{(0)}. \tag{8.53}$$

Plugging this result into Eq. (8.46), one obtains the vacuum to vacuum amplitude for a broken $SU(N)$ gauge theory in a one instanton background, which we already anticipated in Eq. (8.36).

Chapter 9

Small instanton contribution to the axion mass in partially broken gauge groups

We now finally turn to the study of small instanton contributions to the axion mass. Our main interest will be theories where QCD is embedded in a larger gauge group in the UV, similar to the class of models proposed by Agrawal and Howe [18] where QCD is the diagonal combination of a product of k $SU(3)$ factors. Before diving into a full instanton calculation we present in Section 9.1 a back-of-the-envelope estimate for the size of small instanton corrections for various non-trivial UV completions of QCD. Along the way we identify a non-trivial index of embedding as the main reason for the enhancement of small instanton contributions in partially broken gauge groups. Having obtained this insight we perform in Sections 9.2 and 9.3 a complete one-instanton calculation of the small instanton contribution in one of the simplest classes of partially broken gauge groups with a non-trivial index of embedding which are product groups broken to their diagonal, i.e. $SU(N)_1 \times \cdots SU(N)_k \to SU(N)_D$. As a last step we revisit the model by Agrawal and Howe [18] and reexamine their estimates in the light of our full calculation.

The results of this chapter have been published before in [32][1] from where all of the Figures and parts of the text are taken.

9.1 Order of magnitude estimate

Before performing the full instanton calculation we will present a back-of-the-envelope estimate for the size of small instanton contributions to the axion mass in various UV completions of QCD. The model of [18] contains two novel aspects which are due to the fact that we are considering small instantons of the size $\rho \ll \Lambda_{QCD}^{-1}$.

- The Higgs boson(s) become propagating particles at high energies what allows us to also consider the effects of closing up the fermion legs of the instanton vertex using Higgs loops (rather than Higgs VEV insertions as is usually done)

- There may be non-trivial embeddings of QCD into the UV theory where the small instantons of the UV theory correspond to "fractional instantons" of QCD.

[1] [32]: C. Csáki, M. Ruhdorfer and Y. Shirman, *UV Sensitivity of the Axion Mass from Instantons in Partially Broken Gauge Groups.*

In the following we will estimate small instanton effects using both the traditional Higgs VEV insertions and the new Higgs loop diagrams. It will turn out that for the simplest embeddings of QCD into the UV gauge theory all such effects are negligible. However, in models with a non-trivial embedding there can be an enhancement of small instanton contributions to the axion mass by some power of the ratio M/Λ_{QCD}, where M is the scale where the UV gauge theory is broken to QCD. Due to this enhancement small instantons can potentially dominate over the IR contributions from large QCD intantons. As we will see the model in [18] which features dominant contributions to the axion mass from small instantons falls into this category of non-trivial embeddings.

Let us assume that the high energy gauge group G is broken to the low energy group H (in phenomenological applications we will, of course, choose H to be $SU(3)_{QCD}$) at the scale M by the VEV of some heavy scalars. We will assume that the theory has F flavors of matter fields in the fundamental representation of G. In expectation of our results to the Standard Model we will choose F to be even. In addition, we will introduce gauge singlet scalars H coupled to the matter fields through Yukawa couplings y. These scalars will eventually be identified with the Higgs scalar(s) of the SM. Thus we will assume that in the low-energy theory H has both a VEV and a mass of order v. Finally, we will assume that the Yukawa couplings of H are small. This leads us to consider the following hierarchy of scales

$$yv \ll \Lambda_{QCD} \ll v \ll \Lambda \ll M\,, \tag{9.1}$$

where Λ and Λ_{QCD} denote RG invariant scales of high and low energy theories respectively. When the embedding of the low energy group into G is trivial the matching relation between these scales is given by

$$\left(\frac{\Lambda_{QCD}}{M}\right)^{b_{QCD}} = \left(\frac{\Lambda}{M}\right)^{b_G}\,. \tag{9.2}$$

Our choice of the hierarchy of scales leads to several important consequences. First, the contributions of the instantons in the broken group (i.e. instantons of size $\rho \lesssim 1/M$) to the effective action are completely calculable. Furthermore, the contributions of small instantons with size $\rho \ll 1/\Lambda_{QCD}$ (and, in particular, of size $\rho \lesssim 1/v$) within the low energy theory but still above the QCD scale are also calculabe. Finally, the Higgses H decouple from the low energy physics within the weak coupling regime while the matter fields are effectively massless[2] even at the strong coupling scale Λ_{QCD}.

To obtain a simple estimate of the magnitudes of the effects of the small instantons we use an effective Lagrangian below the symmetry breaking scale M. Integrating over the instantons of size $\rho < 1/M$ generates a 't Hooft operator which must be included in the Lagrangian of the effective theory

$$\frac{\Lambda^{b_G}}{M^{b_G+3F-4}}\prod_i^F \psi_i\bar{\psi}_i\,. \tag{9.3}$$

These 't Hooft operators will also contribute to the mass of the axion once the fermion legs are closed up with Higgs VEV insertions or via Higgs loops. Such contributions can be represented by the diagrams in Figure 9.1. One important issue to consider is which of these diagrams can possibly contribute to the axion mass. The axion is the Goldstone boson resulting from the spontaneous breaking of the anomalous $U(1)_{PQ}$ symmetry at a high scale f_a. However if the classical action possesses additional exact anomalous unbroken symmetries, one can always

[2]To streamline the analysis we assume here that all the matter fields are light compared to Λ_{QCD}. Accounting for the mass of heavy SM flavors, t, b, c, will not affect the relative importance of contributions from different energy scales.

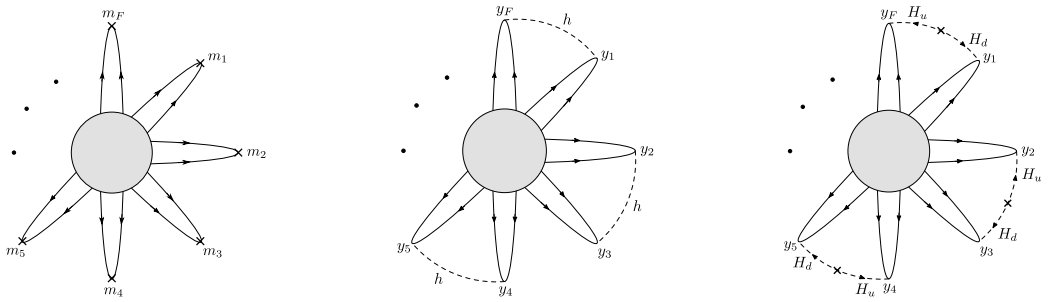

(a) (b) (c)

Figure 9.1: Contributions to the axion mass obtained from closing up the instanton induced 't Hooft operators. On the left we use Higgs VEV insertions, in the middle we use loops of a dynamical Higgs boson in a single Higgs theory, while on the right we use Higgs loops in a 2HDM. Note that the arrows correspond to chiralities. This Figure has been adopted from [32].

redefine the broken $U(1)_{PQ}$ to be anomaly free and the axion remains exactly massless (this is for example the case when one of the SM quarks are exactly massless). As usual the presence of an exact anomalous symmetry will also imply that the QCD θ angle is unphysical. The Yukawa coupling of the SM fermions breaks any additional global symmetries, hence to obtain a contribution to the axion mass one needs to have a diagram proportional to all SM Yukawa couplings. In models with a single Higgs (like the KSVZ-type axion models [283, 284])

$$\sum_{i=1}^{F/2} yH\psi_i\bar{\psi}_i + \sum_{i=F/2+1}^{F} yH^\dagger\psi_i\bar{\psi}_i + \text{h.c.} \tag{9.4}$$

we can obtain a contribution either through Higgs insertions or via closing up the diagrams using Higgs loops as already depicted in Figure 9.1(a) and 9.1(b). In other common axion models like DFSZ [285, 286] there are two Higgs doublets (2HDM), with Yukawa couplings of the sort

$$\sum_{i=1}^{F/2} yH_u\psi_i\bar{\psi}_i + \sum_{i=F/2+1}^{F} yH_d\psi_i\bar{\psi}_i + \text{h.c.} \tag{9.5}$$

In this case we can still use Higgs insertions, however in order to be able to produce diagrams with Higgs loops one needs an additional B_μ-like term $f_a H_u H_d + h.c.$ Such terms are usually readily present in complete axion models like the DFSZ axion [285, 286], and the actual diagram will be of the sort presented in Figure 9.1(c). The effective theory below f_a will be a one-Higgs doublet model of the sort (9.4). As long as $f_a > M$ we can work in the effective one-Higgs doublet model. However if $f_a < M$ one expects the loop diagrams in 2HDMs to be suppressed by powers of f_a/M.

We can now compare the contributions to the axion mass from the Higgs VEV insertion diagram

$$m_M^2 f_a^2 = \left(\frac{yv}{M}\right)^F \frac{\Lambda^{b_G}}{M^{b_G-4}}\,, \tag{9.6}$$

to the contributions from the diagram obtained by closing the Higgs loops:

$$m_M'^2 f_a^2 = \left(\frac{y}{4\pi}\right)^F \frac{\Lambda^{b_G}}{M^{b_G-4}}\,. \tag{9.7}$$

where m_M^2 and $m_M'^2$ represent the contributions of small instantons[3] ($\rho \lesssim 1/M$) to the axion mass obtained from VEV-insertion and loop-induced diagrams respectively. For sufficiently large symmetry breaking scale, the suppression of (9.6) by $(v/M)^F$ may easily overcome the suppression of the loop-induced contribution by loop factors, making (9.7) the dominant contribution from this regime.

There will be similar small instanton contribution to the axion mass from instantons of size $1/M \lesssim \rho \lesssim 1/v$:

$$\begin{aligned} m_v^2 f_a^2 &= y^F \frac{\Lambda_{QCD}^{b_{QCD}}}{v^{b_{QCD}-4}} \\ m_v'^2 f_a^2 &= \left(\frac{y}{4\pi}\right)^F \frac{\Lambda_{QCD}^{b_{QCD}}}{v^{b_{QCD}-4}}\,, \end{aligned} \tag{9.8}$$

where m_v^2 and and $m_v'^2$ denote the VEV insertion and the Higgs loop induced contributions respectively[4]. It is easy to see that loop-induced contributions in (9.7) are small both compared to VEV-insertion and loop-induced contributions in (9.8).

Below the Higgs mass v the Higgs decouples from the theory and loop-induced contributions are absent. However, given our choice of small Yukawas, the fermions remain light and the instanton diagrams with Higgs VEV insertions still contribute both to the 't Hooft operator and the axion potential. These contributions remain calculable in the $1/v < \rho \ll 1/\Lambda_{QCD}$ regime and at the renormalization scale μ satisfying $\Lambda_{QCD} \ll \mu \ll v$ are given by

$$m_\mu^2 f_a^2 = (yv)^F \frac{\Lambda_{QCD}^{b_{QCD}}}{\mu^{b_{QCD}-4}}\,. \tag{9.9}$$

Once again, instanton contributions from lower scales in (9.9) dominate over the instantons of size $1/v$ in (9.8) and instantons of size $1/M$ in (9.6)and (9.7). As the renormalization scale μ approaches the actual strong coupling scale Λ_{QCD}, the perturbative calculation in the one instanton background becomes unreliable. In this regime the contributios of the non-perturbative dynamics to the axion mass are a priori incalculable, however they can be obtained from chiral perturbation theory by relating the axion mass to the pion mass. Nevertheless, one can estimate the final axion mass by taking a naive $\mu \to \Lambda_{QCD}$ limit:

$$m_{QCD}^2 f_a^2 = (yv)^F \Lambda_{QCD}^{4-F} = m^F \Lambda_{QCD}^{4-F}\,, \tag{9.10}$$

where F is the number of flavors that remain light at Λ_{QCD} and m_{QCD} represents the QCD contribution to the axion mass.

We can now estimate the ratio of loop-induced small instanton and QCD contributions to the axion mass:

$$\frac{m_M'^2}{m_{QCD}^2} \sim \frac{1}{(4\pi)^F} \left(\frac{\Lambda_{QCD}}{v}\right)^F \left(\frac{\Lambda_{QCD}}{M}\right)^{b_{QCD}-4}\,. \tag{9.11}$$

As expected the axion mass is dominated by strong coupling QCD contributions while the contributions of small instantons are highly suppressed by powers of Λ/M and otherwise are UV independent. Indeed, every term in (9.11) is smaller than one. As a reminder, b_{QCD} is the QCD beta function just below the matching scale with all flavors assumed to be massless: $b_{QCD} = \frac{11}{3}N_c - \frac{2}{3}F = 7$ for QCD with 6 flavors, but most importantly $b_{QCD} > 4$ implying a strong suppression by powers of Λ_{QCD}/M.

[3] These effects are dominated by instantons of inverse size M.

[4] These effects are dominated by instantons of inverse size v.

There is however an important caveat in the above argument, which is what Agrawal and Howe have exploited [18, 19]. The matching relation (9.2) can be modified if the embedding of QCD into the bigger group G is non-trivial. In fact, (9.2) has a very simple and intuitive interpretation: the one-instanton solution of the low-energy H theory is also a one-instanton solution of the high-energy G theory (with additional bosonic zero modes of the high energy theory lifted by spontaneous symmetry breaking). However, other kinds of embedding are possible [297] – for example, the one-instanton solution of the low energy theory may represent a 2-instanton, or in general a k-instanton configuration in the high energy theory. The first examples of non-trivial effects due to such instantons were identified in the context of exact results in SUSY gauge theories by Intriligator, Seiberg and Leigh [298]. In this case the matching relation (9.2) would be modified to

$$\left(\frac{\Lambda}{M}\right)^{kb_G} = \left(\frac{\Lambda_{QCD}}{M}\right)^{b_{QCD}} \tag{9.12}$$

where the integer k is usually referred to as the index of embedding, first identified in [298–300] and explained extensively in [297]. Such a non-trivial factor usually appears when there are instantons in the partially broken gauge group [297], meaning that the instantons of the unbroken group do not map one-to-one to the instantons of the high energy theory. Topologically it is the homotopy group $\pi_3(G/H)$ that will be relevant, and when both G and H are simple one can show that $\pi_3(G/H) = Z_k$, where k is the index of embedding. In this paper we are interested in models where one breaks a product group to its diagonal subgroup. For example, when the symmetry breaking pattern is given by $SU(N) \times SU(N) \to SU(N)_D$ the one-instanton of the low-energy theory actually corresponds to a $(1, 1)$ of the UV theory, while for $SU(N)^k \to SU(N)_D$ the one-instanton will be a $(1, 1, 1, \ldots, 1)$ instanton. For the product group case the relevant homotopy group will be $\pi_3(SU(N)^k/SU(N)_D) = Z \times Z \times \ldots Z$ with $k - 1$ Z-factors. Either way, if dynamical scales and beta function coefficients of all UV gauge group factors are equal, the matching relation will be given by Eq. (9.12). More generally the scale matching relation (9.12) is replaced by a relation where factors of dynamical scale on the right-hand side are replaced by a product of one-instanton weights of UV gauge group factors:

$$\prod_i^k \left(\frac{\Lambda_i}{M}\right)^{b_i} = \left(\frac{\Lambda_D}{M}\right)^{b_D} . \tag{9.13}$$

We can see now how this non-trivial mapping of instantons (and matching of dynamical scales) would possibly lead to an enhancement of the small instanton contributions. When one has a non-trivial index of embedding, some of the broken instantons are actually topologically distinct from those eventually giving rise to the QCD instanton corrections, hence they will scale differently. From the point of view of scaling they will appear as "fractional" $1/k$ instantons, and their contributions may be enhanced compared to the usual QCD instantons. For a case with index of embedding k while the expression of the contribution of the small instantons from the partially broken group are still given by (9.7), the use of the modified matching (9.12) will result in

$$\frac{m_M'^2}{m_{QCD}^2} \sim \frac{1}{(4\pi)^F} \left(\frac{\Lambda_{QCD}}{v}\right)^F \left(\frac{\Lambda_{QCD}}{M}\right)^{\frac{b_{QCD}}{k}-4} . \tag{9.14}$$

Already for $k = 2$ the sign of the exponent of Λ_{QCD}/M will flip, and lead to the possibility of these terms dominating over the ordinary QCD contributions when M is taken to be large.

In the rest of this chapter we will present a detailed calculation of the small instanton effects in the partially broken gauge group to replace (9.14) with a more precise expression, paying careful

attention to all the relevant $\mathcal{O}(1)$ factors and perturbation of the classical instanton action in the presence of spontaneous symmetry breaking. This will give us a better understanding of models and parameter regions in which small instanton contributions are dominant.

9.2 Axion mass in broken $SU(N)$ gauge groups

As we have seen in the previous section, not all instantons in the broken UV gauge group are matched to instantons in the unbroken IR gauge group if the index of embedding is non-trivial. In the case of $SU(N)^k \to SU(N)_D$ one instanton solutions in the individual $SU(N)$ factors, i.e. solutions of the form $(1, 0, \ldots, 0)$ are absent in the low-energy $SU(N)_D$ gauge theory and have to be integrated out. This means that in order to construct the low-energy theory we have to perform the path integral over these broken individual one-instanton solutions. From the point of view of the instanton solutions which live entirely in one group factor the $SU(N)$ is completely broken and the path integral is exactly calculable, as we have seen in Section 8.3.

These instanton contributions in the vacuum to vacuum amplitude contribute to the vacuum energy and generate a potential for the θ angle and therefore also for the axion which can be viewed as a dynamical θ angle. The effective potential can be obtained from the one instanton vacuum to vacuum amplitude $W_{SU(N)}$ by summing over all instanton and anti-instanton configurations in the dilute instanton gas approximation [291, 301], where one assumes that a winding number Q instanton configuration is made up of Q well-separated $Q = 1$ instantons. The resulting effective potential is

$$\begin{aligned} \exp\left[-\int d^4x\, \mathcal{L}(\theta)\right] = \langle\theta|e^{-HT}|\theta\rangle &\approx \sum_{n_+,n_-=0}^{\infty} \frac{1}{n_+!}\frac{1}{n_-!} W_{SU(N)}^{n_+} \bar{W}_{SU(N)}^{n_-} \\ &= \exp\left[W_{SU(N)} + \bar{W}_{SU(N)}\right], \end{aligned} \tag{9.15}$$

where $\bar{W}_{SU(N)}$ is the contribution to the vacuum to vacuum amplitude of the one anti-instanton solution with $Q = -1$. Using that $\bar{W}_{SU(N)} = W_{SU(N)}^{\dagger}$ and plugging in Eq. (8.36) for $W_{SU(N)}$ we obtain the effective potential for the θ angle or respectively the axion. In a theory without massless fermions this potential is simply given by

$$-\delta\mathcal{L}^{F=0} = 2\int \frac{d\rho}{\rho^5} \int d\tilde{\mu}\, C_N(\rho)\cos(\theta)\,, \tag{9.16}$$

where $C_N(\rho)$ contains the instanton density and the action of the Higgs scalars

$$C_N(\rho) = d_N(\rho)\, e^{-2\pi^2\rho^2 \sum_{i=1}^{2}\sum_{n=1}^{S} |\langle\tilde{\phi}_{in}\rangle|^2}\,. \tag{9.17}$$

If the theory contains massless fermions, Eq. (8.53) implies that due to the $\xi_f^{(0)}$ integration any correlation function, including the vacuum to vacuum amplitude, which does not include the full set of $2F$ chiral fermions vanishes. Effectively the integration projects out the zero mode wave functions, i.e. for a fermion field expanded in eigenmodes $\psi_f = \psi_f^{(0)}\xi_f^{(0)} + \ldots$, the integration yields $\int d\xi_f^{(0)}\psi_f = \psi_f^{(0)}$. Thus the effect of massless fermions in the instanton background is captured by an effective $2F$-fermion operator, the so called 't Hooft operator.

However, even in the presence of massless fermions instantons can still generate a potential for the θ angle if the theory contains further interactions. The easiest way to see this is by working in the effective theory with a 't Hooft operator and closing up the external legs using the

additional interaction terms forming a vacuum bubble (see Figure 9.1), which contributes to the vacuum energy. Alternatively one can calculate the non-vanishing contribution to the vacuum to vacuum amplitude directly from the path integral by including higher orders in the interaction that includes all massless fermions. In the following we will pursue the second approach, which corresponds to the full calculation. We do expect the effective 't Hooft operator approach to be a good approximation to the full calculation, which we will indeed verify in Appendix II.A where we present the 't Hooft operator method and also compare the results of the two approaches.

Let us assume the theory contains an additional scalar H (which we will later identify with the SM Higgs), which couples to the massless fermions via Yukawa interactions, i.e. let us add the following term to the Euclidean action

$$\Delta S = S_0[H] - i\int d^4x \sum_{f=1}^{F} \frac{y_f}{\sqrt{2}} H(x)\bar{\psi}_f(x)\psi_f(x)\,, \tag{9.18}$$

where $S_0[H]$ is the free action for the scalar H. With this addition the vacuum to vacuum amplitude now takes the form

$$\begin{aligned} W_{SU(N)} = e^{-i\theta}\int d^4x_0 \int d\tilde{\mu} \int \frac{d\rho}{\rho^5} C_N(\rho) \int \mathcal{D}H\, e^{-S_0[H]} \\ \times \int \prod_{f=1}^{F} \rho\, d\xi_f^{(0)} d\bar{\xi}_f^{(0)} e^{i\int d^4x \sum_{f=1}^{F} \frac{y_f}{\sqrt{2}} H(x)\bar{\psi}_f(x)\psi_f(x)}\,. \end{aligned} \tag{9.19}$$

At order F in the Yukawa couplings, the expansion of the exponential contains a term with all $2F$ massless fermions. The integration over $\xi_f^{(0)}$ and $\bar{\xi}_f^{(0)}$ projects out the corresponding zero mode wave functions and all lower order terms vanish due to this integration. The leading contribution to $W_{SU(N)}$, assuming F is even so that the path integral of the Higgs field does not vanish (ie. the Higgs loops can be closed up), is therefore[5]

$$W_{SU(N)} = e^{-i\theta}\int d^4x_0 \int d\tilde{\mu} \int \frac{d\rho}{\rho^5} C_N(\rho) \int \mathcal{D}H\, e^{-S_0[H]} \prod_{f=1}^{F} \left(\frac{i y_f \rho}{\sqrt{2}} \int d^4x H(x) \bar{\psi}_f^{(0)}(x)\psi_f^{(0)}(x) \right). \tag{9.20}$$

Performing the path integral for H, only fully contracted Higgs fields survive, each contraction giving a Feynman propagator

$$W_{SU(N)} = e^{-i\theta}\int d^4x_0 \int d\tilde{\mu} \int \frac{d\rho}{\rho^5} C_N(\rho)\, \kappa_F \prod_{f=1}^{F} \left(\frac{y_f \rho}{\sqrt{2}}\right) \mathcal{I}^{F/2}\,, \tag{9.21}$$

where $\kappa_F = (F-1)\cdot(F-3)\cdots 1$ counts the number of equivalent contractions and $\mathcal{I}$ is the integral over the fermion zero modes and scalar Feynman propagators $\Delta_F(x_1 - x_2)$

$$\mathcal{I} = -\int d^4x_1 \int d^4x_2\, \bar{\psi}_f^{(0)}(x_1)\psi_f^{(0)}(x_1)\bar{\psi}_{f'}^{(0)}(x_2)\psi_{f'}^{(0)}(x_2)\Delta_F(x_1 - x_2)\,. \tag{9.22}$$

Using the explicit form for the fermion zero modes[6] $\psi_f^{(0)}$ in Eq. (8.50) $\mathcal{I}$ simplifies to

$$\mathcal{I} = \frac{\rho^4}{4\pi^8}\int d^4x_1 \int d^4x_2 \int d^4p \frac{1}{p^2 + m_H^2} \frac{e^{-ipx_1}}{(x_1^2+\rho^2)^3} \frac{e^{ipx_2}}{(x_2^2+\rho^2)^3}\,. \tag{9.23}$$

[5]Note that the $1/F!$ from the expansion of the exponential is compensated by $F!$ terms which are identical after renaming the integration variables.

[6]Note that similarly to the scalars ϕ_{in} one should rotate $\psi_f^{(0)}$ with the general $SU(N)/SU(N-1)$ coset element Ω. However, due to the $SU(N)$ invariant Yukawa interaction, the Ω dependence cancels out and $\mathcal{I}$ is independent of $\tilde{\mu}$.

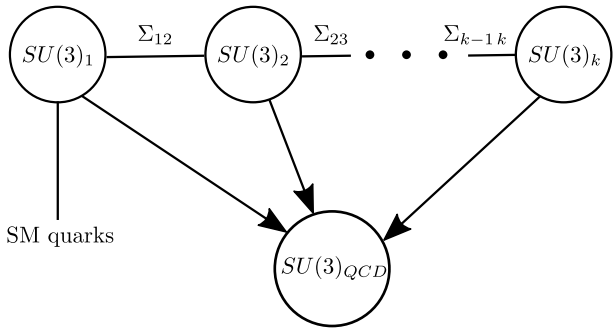

Figure 9.2: Illustration of the product gauge group model introduced in [18] to enhance small instanton contributions to the axion mass. The k $SU(3)$ factors are broken at a scale M by scalar link fields $\Sigma_{i\,i+1}$ in the bifundamental representation of $SU(3)_i \times SU(3)_{i+1}$ to their diagonal combination which is identified with $SU(3)_{QCD}$. We further assume that the SM quarks are only charged under $SU(3)_1$. This Figure has been adopted from [32].

Using the identity

$$\int d^4x \frac{e^{-ipx}}{(x^2+\rho^2)^3} = \frac{\pi^2}{2\rho^2}(p\rho)K_1(p\rho)\,, \tag{9.24}$$

where K_1 is a modified Bessel function of the second kind, we can evaluate $\mathcal{I}$ explicitly in the limit $\rho \ll 1/m_H$

$$\mathcal{I} \simeq \frac{1}{12\pi^2\rho^2}\,. \tag{9.25}$$

Plugging this into Eq. (9.21) we can immediately write down the leading contribution to the potential for the θ angle, generated by 1-(anti)instanton configurations, for theories with massless fermions and a Yukawa interaction

$$-\delta\mathcal{L}^F = 2\int \frac{d\rho}{\rho^5}\int d\tilde{\mu}\, C_N(\rho)\,\kappa_F \prod_{f=1}^{F}\left(\frac{y_f}{\sqrt{24}\pi}\right)\cos(\theta)\,. \tag{9.26}$$

It is worth emphasizing that $\mathcal{I}$ could be estimated in the effective field theory by soaking up fermion legs of the 't Hooft operator with the Higgs propagators. However, the EFT result would be cutoff dependent while the above computation is completely convergent and calculable. For more on the correct value of the cutoff scale see Appendix II.A.

9.3 Product group models

Let us now turn to an explicit example of a model with a non-trivial index of embedding. We will consider the class of models proposed by Agrawal and Howe [18, 19], in which a product gauge group consisting of k $SU(3)$ factors is spontaneously broken at a scale M to its diagonal subgroup by $k-1$ link fields $\Sigma_{i\,i+1}$

$$SU(3)_1 \times SU(3)_2 \times \ldots \times SU(3)_k \to SU(3)_{QCD}\,. \tag{9.27}$$

The diagonal subgroup can then be identified with $SU(3)_{QCD}$. In the following we will assume that all SM quarks are only charged under $SU(3)_1$. For a diagrammatic depiction of the model see Figure 9.2. The individual $SU(3)$ factors by themselves are completely broken and therefore the one-instanton effects are calculable and finite. The one-instanton configuration in low-energy

QCD corresponds to k-instantons of the UV theory with one instanton in each $SU(3)$ factor. In the following we will first discuss some details of the model before we explicitly compute the small instanton contributions to the axion potential in the two simplest realizations with $k = 2, 3$ and compare the results to [18]. Note that in this section we work in Minkowski space.

9.3.1 Axions in product group models

Each of the $SU(3)$ gauge factors comes with its own $\mathcal{CP}$ violating θ angle. Therefore we assume that there is also one anomalous $U(1)_{PQ}$ for each factor, which is spontaneously broken at $f_{a_i} > M$. This yields one axion for each $SU(3)$

$$\mathcal{L} = \sum_{i=1}^{k} \mathcal{L}_i \,, \qquad \mathcal{L}_i = -\frac{1}{4} G_i^a G_i^{a\,\mu\nu} + \frac{g_i^2}{32\pi^2}\left(\frac{a_i}{f_{a_i}} - \theta_i\right) G_{i\,\mu\nu}^a \tilde{G}_i^{a\,\mu\nu} \,. \tag{9.28}$$

As depicted in Figure 9.2, the gauge group is broken to $SU(3)_{QCD}$ by higgsing it with $k-1$ scalar link fields $\Sigma_{i\,i+1}$, which transform as a bifundamental $(3, \bar{3})$ under $SU(3)_i \times SU(3)_{i+1}$. A potential[7] of the form [18, 302]

$$V(\Sigma) = -m_\Sigma^2 \mathrm{Tr}(\Sigma\Sigma^\dagger) + \frac{\lambda}{2}[\mathrm{Tr}(\Sigma\Sigma^\dagger)]^2 + \frac{\kappa}{2}\mathrm{Tr}(\Sigma\Sigma^\dagger\Sigma\Sigma^\dagger) \tag{9.29}$$

for each of the link fields induces a VEV

$$\langle\Sigma\rangle = \frac{m_\Sigma}{\sqrt{\kappa + 3\lambda}} \mathbb{1}_3 \equiv v_\Sigma \mathbb{1}_3 \,, \tag{9.30}$$

which for simplicity we take to be the same for all link fields. Each symmetry breaking VEV results in one massive gauge and one massive scalar multiplet in the adjoint representation of the unbroken diagonal group. The masses of gauge and scalar multiplets are of the order[8] $g_i v_\Sigma$ and κv_Σ and they can be integrated out. The dynamical scale of the low energy effective field theory is given by

$$\Lambda_{QCD}^{b_{QCD}} = \frac{\prod_i^k \Lambda_i^{b_i}}{M^{\sum_i b_i - b_{QCD}}} \,, \tag{9.31}$$

where the matching scale M is the geometric mean of the eigenvalues of the mass matrix for the heavy states. In terms of the QCD coupling constant g_s this implies the usual matching relation at M

$$\frac{1}{g_s^2(M)} = \sum_{i=1}^{k} \frac{1}{g_i^2(M)} \,, \tag{9.32}$$

The QCD θ angle is simply the sum of the individual $SU(3)_i$ θ angles

$$\bar{\theta}_{QCD} = \sum_{i=1}^{k} \bar{\theta}_i \,, \tag{9.33}$$

where $\bar{\theta} = \theta + \arg\det M_f$ is the physical theta angle, which contains a possible $\mathcal{CP}$ violating phase from the fermion mass matrix. At the same time one also has to integrate out the small

[7] One can add $U(1)$ factors to forbid terms like $\mu \det\Sigma$ [18].

[8] For simplicity we will assume that $g^2/\kappa \sim 1$ and will not distinguish between the gauge boson and scalar thresholds.

instantons in the UV theory, which generate a potential for the axions. Thus the effective Lagrangian for the axion fields takes the form[9]

$$\mathcal{L}_a = \sum_{i=1}^{k} m_{a_i}^2 f_{a_i}^2 \cos\left(\frac{a_i}{f_{a_i}} - \bar{\theta}_i\right) + \frac{g_s^2}{32\pi^2} \sum_{i=1}^{k} \left(\frac{a_i}{f_{a_i}} - \bar{\theta}_i\right) G_{\mu\nu}^a \tilde{G}_i^{\mu\nu} \,. \tag{9.34}$$

One can see $\bar{\theta}_{QCD}$ is relaxed to zero due to two independent effects. First, small instanton contributions in broken gauge factors relax each individual $\bar{\theta}_i$ to zero. In addition, once QCD confines, the potential is generated for the linear combination $a/f_a = \sum_i a_i/f_{a_i}$ which relaxes $\bar{\theta}_{QCD}$ to zero just like the usual axion would. In contrast to standard axion models there is not just one but k axions in the IR spectrum and it is the lightest mass eigenstate which plays the role of the QCD axion. When small instanton contributions are dominant the mass of this lightest state can be significantly higher than the standard QCD prediction in Eq. (6.1).

9.3.2 Small instanton contributions

When working in the EFT one has to take into account the instanton configurations which are not mapped to the low energy theory, i.e. QCD. These are the independent one-instanton contributions from $SU(3)_1, \ldots, SU(3)_k$. Since they are broken to their diagonal combination each $SU(3)$ factor considered separately is completely broken and therefore we can use the formalism of Section 8.3 with three Higgs scalars ϕ_n, $n = 1, 2, 3$ for each link field, which develop a VEV[10]

$$\langle \phi_{in} \rangle = v_\Sigma \, \delta_{in} \,, \tag{9.35}$$

where $i = 1, 2, 3$ are the $SU(3)$ indices. This allows us to evaluate the classical action for the Higgs scalars from one of the link fields in the instanton background explicitly

$$S_0^\phi(\rho) = 2\pi^2\rho^2 \sum_{i=1}^{2}\sum_{n=1}^{3} |\langle \tilde{\phi}_{in} \rangle|^2 = 2\pi^2\rho^2 v_\Sigma^2 \sum_{i=1}^{2}\sum_{n=1}^{3} |\Omega_{in}|^2 = 4\pi^2\rho^2 v_\Sigma^2 \,, \tag{9.36}$$

where we considered the rotated VEVs (see Eq. (8.48)) to account for arbitrary instanton locations inside $SU(3)$.[11] The result is independent of $\tilde{\mu}$ and we can therefore do the now trivial group integration in the results of Section 9.2. Note that the scalar action for $SU(3)_2, \ldots, SU(3)_{k-1}$ is twice as large, since each of them couples to two link fields.

We begin by considering the $SU(3)$ sectors without fermions. The last of these sectors, i.e. $SU(3)_k$, has only one scalar link, i.e. $S = 3$ scalars in the fundamental representation, and the beta function coefficient $b_k = 21/2$. For this sector the vacuum-vacuum amplitude contributes directly to the axion potential (see Eq. (9.16)) with a mass scale m_{a_k} of

$$m_{a_k}^2 f_{a_k}^2 = \left(\frac{\Lambda_k}{M}\right)^{b_k} \left(\frac{M}{2\pi v_\Sigma}\right)^{b_k - 4} M^4 \,, \tag{9.37}$$

where the factor $(M/2\pi v_\Sigma)^{b_k-4}$ converts between the physical mass threshold at M and the effective cutoff of the instanton size integral at $1/\rho \sim 2\pi v_\Sigma$, while the RG invariant scale of $SU(3)_k$ sector is defined by

$$\Lambda_k^{b_k} = d_3(M)|_{S_k, F=0} \, \Gamma[b_k/2 - 2] M^{b_k} \,, \tag{9.38}$$

[9] In [18] the mass scale of the potential $m_{a_i}^2 f_{a_i}^2$ was denoted Λ_i^4.

[10] From the point of view of one of the $SU(3)_i$ factors the bifundamental $\Sigma_{i\,i+1}$ looks like three scalars in the fundamental representation.

[11] Note that the explicit form of Ω in $SU(3)$ is not needed to obtain the factor of 2. $\sum_{i=1}^{2}\sum_{f=1}^{3} |\Omega_{if}|^2$ sums the norms of the first two row vectors in Ω and since $\Omega \in SU(3)$ each row vector is normalized to unity.

and the instanton weight $d_3(M)|_{S_k,F=0}$ is given in (8.37). The remaining sectors $i = 2, \ldots, k-1$ have two link fields, i.e. $S = 6$ scalars in the fundamental representation and the beta function coefficient $b_i = 10$. The vacuum-vacuum amplitude contributes to the axion potential in these sectors with a mass scale m_{a_i} which is given by Eq. (9.37) after the replacement $k \to i$ and $v_\Sigma \to \sqrt{2}\, v_\Sigma$. The additional suppression by $2^{2-b_i/2}$ originates from the scalar action which is twice as large, since all of these sectors couple to two link fields.

All the SM quarks are charged under the $SU(3)_1$ sector. Thus its particle content is characterized by $F = 6$ approximately massless fermions[12] and $S = 3$ scalars in the fundamental representation, corresponding to a beta function coefficient of $b_1 = 13/2$. Taking the result for the vacuum energy in the instanton background with massless quarks and a Yukawa interaction from Eq. (9.26) for $N = 3$ and $\theta = \bar{\theta}_1 - \frac{a_1}{f_{a_1}}$ and matching it to the axion potential in Eq. (9.34) we obtain the scale $m_{a_1}^2 f_{a_1}^2$

$$m_{a_1}^2 f_{a_1}^2 = K \int \frac{d\rho}{\rho^5}\, 2C_3(\rho)\,. \tag{9.39}$$

where K is given by

$$K = \frac{40}{9} \frac{y_u y_d y_s y_c y_b y_t}{(16\pi^2)^3}\,. \tag{9.40}$$

Note that K reproduces a loop factor expected from an EFT diagram in Figure 9.1(b) and included in the results of [18]. However, the full calculation of correlation functions in the instanton background performed in Sec. 9.2 allows us to extract the exact numerical coefficient multiplying this loop factor. Performing the ρ integral in Eq. (9.39) we find

$$m_{a_1}^2 f_{a_1}^2 = K \left(\frac{\Lambda_1}{M}\right)^{b_1} \left(\frac{M}{2\pi v_\Sigma}\right)^{b_1-4} M^4\,, \tag{9.41}$$

where the dynamical scale of $SU(3)_1$ is defined by

$$\Lambda_1^{b_1} = d_3(M)|_{S=3,F=6}\, \Gamma[b_1/2-2] M^{b_1}\,, \tag{9.42}$$

and once again the instanton weight $d_3(M)|_{S=3,F=6}$ is given in (8.37). Note that these results are in agreement with the qualitative discussion of Section 9.1.

The unusual scaling of the axion mass with the physical QCD scale can be seen from the fact that $d_3(M) \sim \exp(-\frac{8\pi^2}{g_i^2(M)})$ where g_i^2 is the coupling of the ith SU(3) factor rather than the actual QCD coupling, implying that $\Lambda_i^{b_i}$ will be a fractional power of $\Lambda_{QCD}^{b_{QCD}}$, where the actual fraction depends on the ratios of coupling strengths and the distribution of the matter fields among the different group factors.

However the full expression of the corrections to the axion mass Eqs. (9.37)-(9.42) also includes an additional suppression factor of the form $(M/2\pi v_\Sigma)^{b_i-4}$. Indeed the presence of this factor implies that, up to an order one coefficient, our results for $m_{a_i}^2 f_{a_i}^2$ are smaller than the previous estimates $(\tilde{m}_{a_i}^2 f_{a_i}^2)$ in [18] by a factor of

$$\frac{m_{a_i}^2}{\tilde{m}_{a_i}^2} \simeq 2^{-6} \cdot \left(\frac{M}{2\pi v_\Sigma}\right)^{b_i-4}\,. \tag{9.43}$$

This suppression is due to two independent reasons:

[12] To a good approximation all SM quarks are massless at scales $M \gg$ TeV.

- Our vacuum instanton density $d_N(\rho)|_{S=F=0}$ is smaller by a factor of 2^{-2N} than the one used in [18]. This discrepancy originates from a small error in 't Hooft's original calculation [280], which was later corrected in an Erratum. However, the source for the instanton density [301] cited in [18] still contains this error.
- In [18] the ρ integration was cut off at $\rho = 1/M$ by hand. However, when working in the constrained instanton framework the ρ integral is convergent and we find that the actual cutoff is roughly $\rho \sim 1/(2\pi v_\Sigma)$ (see also [251]).

The actual size of the suppression depends on the relation between the matching scale M and the VEV v_Σ. Since M corresponds to the mass scale of the massive gauge bosons, it scales like $M = g_{\text{eff}}\, v_\Sigma$, where g_{eff} is some combination of $g_1, \ldots, g_k$. For couplings of $\mathcal{O}(1)$ this leads to a suppression of $(2\pi)^{4-b_i}$, which is strongest for the $SU(3)$ group factors that do not couple to fermions. As we will show momentarily, this suppression is significant in the minimal model with only two group factors, but is less important once more $SU(3)$ factors are included and the matching relation in Eq. (9.32) allows larger couplings in the individual $SU(3)$ factors.

9.3.3 Example $SU(3)^2, SU(3)^3 \to SU(3)_{QCD}$

Let us now have a look at the minimal model with $k = 2$. In this case the matching scale is directly set by masses of the heavy gauge bosons (and scalars)

$$M^2 = (g_1^2 + g_2^2) v_\Sigma^2 \,. \tag{9.44}$$

In order to do the matching we use the RG equation to run the $\overline{\text{MS}}$ QCD coupling from the top mass at $\alpha_s(m_t) = 0.10$ to the matching scale M. The small instanton contribution to the axion mass relative to the QCD contribution can now be computed using the mass scales $m_{a_2}^2 f_{a_2}^2$ and $m_{a_1}^2 f_{a_1}^2$ from Eqs. (9.37) and (9.42), respectively. For simplicity we will assume that $f_{a_1} = f_{a_2} = f_a$ and use Eq. (6.1) to obtain a numerical value for $f_a m_a = (75.5\text{ MeV})^2$.

This ratio is shown for both axions (solid for m_{a_1}/m_a and dashed for m_{a_2}/m_a) for the choice of $M = 10^{14}$ GeV for the symmetry breaking scale in Figure 9.3(a). In contrast to previous estimates [18] (shown in red), the full calculation shows that there is no region in parameter space where both axion masses are enhanced by more than an $\mathcal{O}(1)$ factor compared to the pure QCD prediction at the same time. One of the axions might be heavy, but then the other will be dominated by the QCD contribution to its potential and will therefore be like the standard QCD axion. The largest effect of small instanton contributions to both axion masses is found at the intersection of the two curves where both axions have the same mass which is about $M_a/m_a = 2.4$ times heavier than the standard QCD axion. Figure 9.3(b) shows the maximal enhancement of the axion mass due to small instantons as a function of the symmetry breaking scale M. This shows that even taking M to be at the Planck scale the axion mass cannot deviate by more than a factor of ~ 100 from the QCD prediction. Due to the suppression factor in Eq. (9.43) the enhancement is lower by about two orders of magnitude than the initial prediction in [18].

We can therefore conclude that it is hard to get significant contributions from small instantons to the axion mass in the minimal model. However, according to our parametric estimate in Section 9.1, we expect a larger mass enhancement in models with more $SU(3)$ factors. In the following we demonstrate that this conclusion is indeed correct by considering the next to minimal model with $k = 3$ factors.

In the model with $k = 3$ group factors $SU(3)^3$ is broken by the VEVs of two link fields, which we both take to be $\langle \Sigma \rangle = v_\Sigma \mathbb{1}_3$. Note that since $SU(3)_2$ couples to both link fields, not all gauge

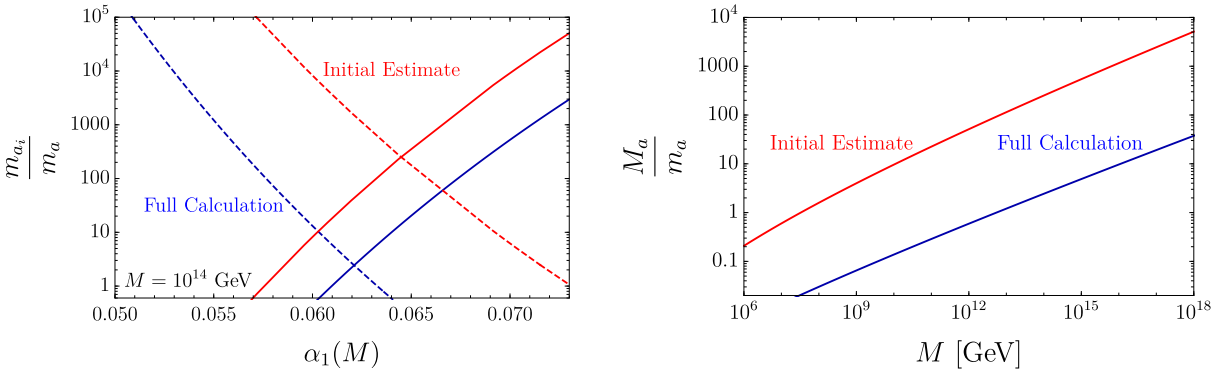

Figure 9.3: Small instanton contribution to the axion mass relative to the IR QCD contributions in the model based on the symmetry breaking structure $SU(3) \times SU(3) \to SU(3)_{QCD}$. On the left we show our results for the full calculation in blue compared to the initial estimates in previous work [18] in red at a breaking scale of $M = 10^{14}$ GeV as a function of $\alpha_1 = \frac{g_1^2}{4\pi}$. The solid (dashed) curves show m_{a_1}/m_a (m_{a_2}/m_a), which intersect at $M_a/m_a = 2.4$ in the full calculation and at $M_a/m_a = 251$ in previous estimates. On the right we show the values for M_a/m_a at the intersection point of m_{a_1}/m_a and m_{a_2}/m_a for a wide range of breaking scales M. In both plots we took $f_{a_1} = f_{a_2} = f_a$. This Figure has been adopted from [32].

bosons get the same masses. One linear combination, corresponding to the QCD gluons, stays massless as before, whereas the masses of the other two linear combinations are given by

$$M^2_{V_{1/2}} = \frac{v_\Sigma^2}{2}\left(g_1^2 + 2g_2^2 + g_3^2 \pm \sqrt{4g_2^4 + (g_1^2 - g_3^2)^2}\right). \tag{9.45}$$

The matching threshold is given by the geometric mean of these two mass eigenvalues

$$M = (g_1^2 g_2^2 + g_2^2 g_3^2 + g_1^2 g_3^2)^{1/4} v_\Sigma \,. \tag{9.46}$$

As in the minimal model we take $f_{a_1} = f_{a_2} = f_{a_3} = f_a$ and show our result (blue) in Figure 9.4 for the small instanton contributions to the axion mass compared to the estimates in [18] (red), fixing in both cases $g_2 = g_3$. In Figure 9.4(a) we again show m_{a_1}/m_a (solid) and m_{a_2}/m_a (dashed) at a breaking scale of $M = 10^{14}$ GeV. Note that m_{a_3} is always larger than m_{a_2} for identical couplings, since m_{a_2} is suppressed by an additional factor of $2^{2-b_2/2}$. As can be seen, even though the mass enhancement is again smaller in the full calculation than in the initial estimate, small instantons can still enhance the mass of all three axions simultaneously by up to a factor of $4 \cdot 10^{10}$ compared to the QCD contribution at the intersection point. Figure 9.4(b) shows that small instantons give dominant contributions to the axion mass also at smaller breaking scales M, making the axion considerably heavier than in the standard QCD axion scenario. Note that at small M, m_{a_1}/m_a and m_{a_2}/m_a do not intersect anymore. When this is the case $m_{a_1}/m_a < m_{a_2}/m_a$ due to its suppression by the Yukawa couplings and therefore we take the maximum of m_{a_1}/m_a as an estimate for the maximal simultaneous enhancement of all axion masses. This is the reason for the kink in the curves in the Figure 9.4(b).

Adding additional $SU(3)$ factors increases the possible enhancement of the axion mass even further. It was already noted in [18] that for $k \gg 1$ the axion masses scale as $m_{a_i} \sim M^2/f_{a_i}$ for $i = 2, \ldots, k$ and $m_{a_1} \sim \sqrt{K} M^2/f_{a_1}$, where the first axion mass is parametrically suppressed

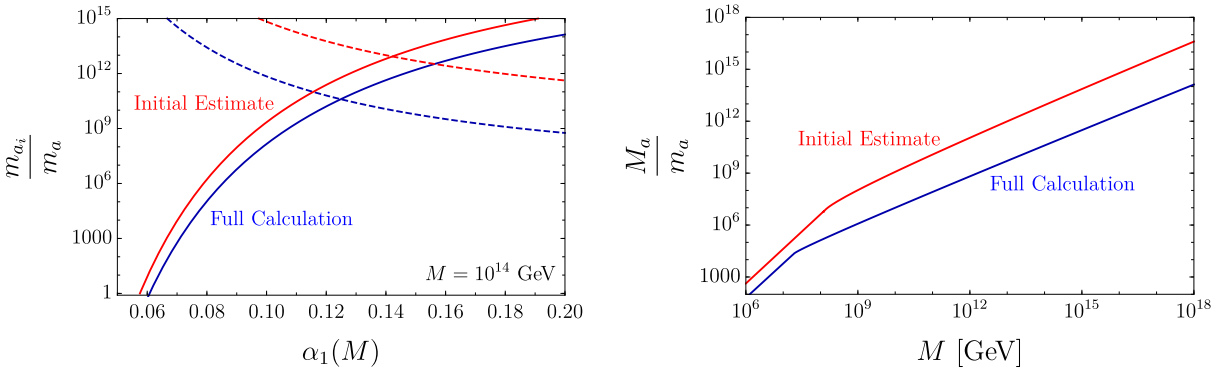

Figure 9.4: Small instanton contribution to the axion mass relative to the IR QCD contributions in the model based on the symmetry breaking structure $SU(3) \times SU(3) \times SU(3) \to SU(3)_{QCD}$. On the left we show the results for the full calculation in blue compared to the initial estimates in previous work [18] in red at a breaking scale of $M = 10^{14}$ GeV as a function of $\alpha_1 = \frac{g_1^2}{4\pi}$. The solid (dashed) curves show m_{a_1}/m_a (m_{a_2}/m_a), which intersect at $M_a/m_a \simeq 4 \cdot 10^{10}$ in the full calculation and at $M_a/m_a = 9 \cdot 10^{12}$ in previous estimates. On the right we show the values for M_a/m_a at the intersection point of m_{a_1}/m_a and m_{a_2}/m_a or at the maximum of m_{a_1}/m_a if they do not intersect for a wide range of breaking scales M. In both plots we took $f_{a_1} = f_{a_2} = f_{a_3} = f_a$ and fixed $g_2 = g_3$, which implies that m_{a_3} is always slightly larger than m_{a_2}. This Figure previously appeared in [32].

relative to the others by the Yukawa couplings and loop factors $\sqrt{K} \approx 10^{-12}$. With the help of Eq. (9.14) we can now understand the scaling of the axion mass with M^2 as the limit $b_{QCD}/k \xrightarrow{k\to\infty} 0$ in Eq. (9.14).

Appendices part II

II.A 't Hooft operator approach

In this appendix we compute the small instanton contribution to the vacuum energy or axion potential in the presence of massless fermions using the 't Hooft operator approximation and compare it to the full calculation in Section 9.2.

In a gauge theory with F massless fermion flavors in the fundamental representation of $SU(N)$ the pure vacuum-vacuum amplitude in the instanton background vanishes and the instanton configuration only contributes to correlation functions in which each fermion flavor and chirality appears at least once, i.e. for example $\langle 0|\prod_f(\bar{\psi}_f\psi_f)|0\rangle_{\Delta Q=1}\neq 0$. The effect of the instanton can thus be captured by the 't Hooft operator, which is an effective $2F$ fermion operator of the form (see e.g. [280])

$$-\delta\mathcal{L}^F = e^{-i\theta}\int\frac{d\rho}{\rho^5}C_N(\rho)\rho^{3F}\left(\kappa_N^{(N_f)}\right)^{i_1\cdots i_{2F}}\det_{f,f'}(\bar{\psi}_{R\,f}(x_0)\psi_{L\,f'}(x_0))_{i_1\cdots i_{2F}}+h.c.\,, \qquad \text{(II.A.1)}$$

where the determinant goes over flavor indices and the hermitian conjugate results from the anti-instanton configuration. $C_N(\rho)$ is defined in Eq. (9.17) and $\left(\kappa_N^{(N_f)}\right)^{i_1\cdots i_{2F}}$ is obtained by computing the $2F$ fermion correlation function in the instanton background and matching the result to the above effective operator. Note that the integration over the instanton location inside $SU(N)$, for which we assumed that $\sum_{i=1}^{2}\sum_{n=1}^{3}|\langle\tilde{\phi}_{in}\rangle|^2$ inside $C_N(\rho)$ is independent of the instanton position, projects out all invariant contractions of the fermion $SU(N)$ indices $i_1,\ldots,i_F$. For one fermion flavor the matching is straightforward (see [303] for an example in $SU(2)$ and $SU(3)$) and gives

$$-\delta\mathcal{L}^{F=1} = e^{-i\theta}\int\frac{d\rho}{\rho^5}C_N(\rho)\rho^3\kappa_N^{(1)}\bar{\psi}_{R\,1}(x_0)\psi_{L\,1}(x_0)+h.c.\,, \qquad \text{(II.A.2)}$$

where we used that $\left(\kappa_N^{(1)}\right)^{i_1i_2}=\kappa_N^{(1)}\delta^{i_1i_2}$ (for example for $SU(3)$: $\kappa_3^{(1)}=\frac{4\pi^2}{3}$).

Since we want to close the 't Hooft operator with Higgs loops, we are only interested in flavor diagonal $SU(N)$ contractions of the form $(\bar{\psi}_R\psi_L)^F$. Therefore we will consider the effective Lagrangian

$$-\delta\mathcal{L}^F \simeq e^{-i\theta}\int\frac{d\rho}{\rho^5}C_N(\rho)(\rho^3\kappa_N^{(1)})^F\prod_{f=1}^{F}\bar{\psi}_{R\,f}(x_0)\psi_{L\,f}(x_0)+h.c.\,. \qquad \text{(II.A.3)}$$

Note that due to Fierz relations among $SU(N)$ invariants, the prefactor $(\kappa_N^{(1)})^F$ is not exact, but will deviate from the full prefactor by an $\mathcal{O}(1)$ factor.

Such a 't Hooft operator contributes to the axion potential if one closes the fermion legs with loops. The leading contribution arises from closing the operator with Higgs loops via Yukawa couplings to the fermions as shown in Figure 9.1(b). This is the case since the diagram

only includes marginal couplings and therefore scales as M_{cut}^{3F} where M_{cut} is the cutoff for the divergent loop integrals.

Focusing on $SU(3)$ and identifying $\theta = \bar{\theta} - a_1/f_{a_1}$, we can match the resulting operator to the effective Lagrangian in Eq. (9.34) to obtain $m_{a_1} f_{a_1}$

$$m_{a_1}^2 f_{a_1}^2 = 2K \int \frac{d\rho}{\rho^5} C_3(\rho) (4\pi^2 M^3 \rho^3)^F \,, \tag{II.A.4}$$

where K contains the Yukawa couplings and loop factors

$$K = \prod_{f=1}^{F} \frac{y_f}{4\pi} \,. \tag{II.A.5}$$

Note that we canceled a factor $N = 3$ from the sum over colors in the loop for each fermion flavor with the 3^{-F} from $(\kappa_3^{(1)})^F$. Computing the ρ integral one obtains

$$m_{a_1}^2 f_{a_1}^2 = K \; d_3(M)|_{S=3,F} \, (4\pi^2)^F \Gamma\left[\frac{3F + b_0^{(1)} - 4}{2}\right] \left(\frac{M}{2\pi v_\Sigma}\right)^{b_0^{(1)}-4} \left(\frac{M_{\text{cut}}}{2\pi v_\Sigma}\right)^{3F} M^4 \,, \tag{II.A.6}$$

where M is the matching scale for the couplings.

Comparing this result to Eq. (9.42), which was obtained by including the SM Higgs and Yukawa couplings directly in the path integral evaluation of the vacuum-vacuum amplitude, one finds that with M_{cut}, the cutoff of the loop integrals, an additional scale appears. However, the exact definition of M_{cut} is ambiguous and always introduces an uncertainty. Since M_{cut} enters $m_{a_1}^2 f_{a_1}^2$ with a large power, even $\mathcal{O}(1)$ changes in the definition of M_{cut} can have a significant impact on $m_{a_1}^2 f_{a_1}^2$. This ambiguity is removed in the calculation in Section 9.2, since the result is manifestly finite.

Both methods are equivalent and therefore we can use the result from Sec. 9.2 to infer the appropriate definition of M_{cut} for this process. We find that both approaches yield the same result, up to an $\mathcal{O}(1)$ factor, if one identifies $M_{\text{cut}} \simeq v_\Sigma$, in nice agreement with our intuitive expectations.

II.B Converting results to $\overline{\text{MS}}$ scheme

All results in Section 8.3 were derived in the Pauli-Villars regularization scheme. However, in perturbative calculations dimensional regularization and the MS or $\overline{\text{MS}}$ scheme are more common. In this appendix we briefly summarize how to convert the results to these schemes.

Already in [280] 't Hooft showed that in order to convert the results to dimensional regularization one has to do the substitutions

$$\ln \mu_0 \to \frac{1}{4-n} - \frac{1}{2}\gamma + \frac{1}{2}\ln 4\pi \qquad \text{(zero-modes)} \,, \tag{II.B.1}$$

$$\ln \mu_0 \to \frac{1}{4-n} - \frac{1}{2}\gamma + \frac{1}{2}\ln 4\pi - \frac{1}{2} \qquad \text{(kinetic terms)} \,, \tag{II.B.2}$$

where the first substitution has to be made for the μ_0 originating from gauge and fermion zero-modes and the second for μ_0 from kinetic terms, i.e. from the non-zero modes and scalar fields.[13]

[13] In [280] 't Hooft found $-\frac{5}{12}$ instead of the $-\frac{1}{2}$ in Eq. (II.B.2). This mistake was noted by Hasenfratz and Hasenfratz [304] and reconciled the disagreement with Shore, who did the instanton calculation using dimensional regularization [305]. 't Hooft corrected the $-\frac{5}{12}$ in Eq. (B12) of [287] to -1. However, this was later again corrected by Shifman [288] to the $-\frac{1}{2}$ we use in Eq. (II.B.2).

This substitution only affects the running coupling in the exponential

$$-\frac{8\pi^2}{g^2(1/\rho)} = -\frac{8\pi^2}{g_B^2(\mu_0)} + \ln(\mu_0\rho)\big[(4N-F) + (\tfrac{1}{3}F - \tfrac{1}{3}N - \tfrac{1}{6}S)\big] \tag{II.B.3}$$

$$\to \frac{8\pi^2}{g_B^2(n)} + \left(\ln\rho + \frac{1}{4-n} + \frac{1}{2}(\ln 4\pi - \gamma)\right)b_0 - \frac{1}{2}\left(\tfrac{1}{3}F - \tfrac{1}{3}N - \tfrac{1}{6}S\right), \tag{II.B.4}$$

where we separated in Eq. (II.B.3) the contributions to b_0 originating from zero modes (first bracket) from the ones from non-zero modes (second bracket). The renormalized coupling now depends on the renormalization scheme. Here we will consider MS and $\overline{\text{MS}}$ scheme which are define by

$$\frac{8\pi^2}{g^2_{\text{MS}}(1/\rho)} = \frac{8\pi^2}{g_B^2(n)} + \left(\ln\rho + \frac{1}{4-n}\right)b_0\,, \tag{II.B.5}$$

$$\frac{8\pi^2}{g^2_{\overline{\text{MS}}}(1/\rho)} = \frac{8\pi^2}{g_B^2(n)} + \left(\ln\rho + \frac{1}{4-n} + \frac{1}{2}(\ln 4\pi - \gamma)\right)b_0\,. \tag{II.B.6}$$

Note that in the above we have to identify [280]

$$g_B(n) \to g_{\text{MS}}(\mu) \qquad \text{and} \qquad \ln\rho + \frac{1}{4-n} \to \ln(\rho\mu)\,, \tag{II.B.7}$$

$$g_B(n) \to g_{\overline{\text{MS}}}(\mu) \qquad \text{and} \qquad \ln\rho + \frac{1}{4-n} + \frac{1}{2}(\ln 4\pi - \gamma) \to \ln(\rho\mu)\,, \tag{II.B.8}$$

where μ is the renormalization scale in dimensional regularization. Thus to convert our results to $\overline{\text{MS}}$ scheme we have to replace

$$e^{-8\pi^2/g^2(1/\rho) - C_2 N} \to e^{-\frac{1}{12}(2F-S)} e^{-8\pi^2/g^2_{\overline{\text{MS}}}(1/\rho) - C_2^{\overline{\text{MS}}} N}\,, \tag{II.B.9}$$

with $C_2^{\overline{\text{MS}}}$ given by

$$C_2^{\overline{\text{MS}}} = C_2 - \frac{1}{6}\,. \tag{II.B.10}$$

Using this the instanton density in $\overline{\text{MS}}$ scheme is given by

$$d_N^{\overline{\text{MS}}}(\rho)\Big|_{F,S} = e^{-\frac{1}{12}(2F-S)+\frac{1}{6}N}\; d_N(\rho)|_{F,S}\;. \tag{II.B.11}$$

Part III

EFT of the SM and gravity

Chapter 10

Motivation and introduction

The focus of Part I and II of this thesis were DM candidates in well-motivated extensions of the SM. However, the search for DM is not the only place where NP could appear. For this reason it is crucial to look for effects of BSM physics as globally as possible. Especially in the light of null results in DM and collider experiments it is important to analyze the data in a model independent way, s.t. no hints of NP are missed due to theoretical bias. Such a model independent approach is the EFT framework.[1]

EFTs really lie at the core of our modern understanding of the fundamental interactions in nature. They encode the dynamics of the relevant degrees of freedom at the scales of interest, and enable the systematic exploration of the effects of heavy states via an infinite set of local operators built out of the light fields. Crucially, the higher the operator's dimension, the smaller the departure it introduces from the leading order dynamics.

While EFTs, and the SMEFT in particular, offer a model-independent parameterization of departures from a leading theory, it can still be useful or even necessary to refer to possible UV completions as guidelines and for the interpretation of future deviations in observables from their SM prediction. For this reason one needs a dictionary between UV complete theories and SMEFT operators they generate when the heavy physics is integrated out. In Chapter 12 we contribute to this effort by performing the one-loop matching of the SM with a new heavy singlet scalar, one of the simplest renormalizable extensions of the SM, onto the dimension six SMEFT Lagrangian. We identify terms which have been missed in previous matching calculations [20,21] and present the first complete one-loop result for this model. We believe that this result is not only relevant for a future publication in the context of pNGB DM [306], but also as an important and simple benchmark scenario for EFT interpretations.

The SM and consequently also the SMEFT offers an excellent description of all known fundamental interaction, with the exception of gravity. The low-energy description of gravity, Einstein's theory of GR, is one of the most successful field theories, it has survived all experimental tests since its formulation in 1915. However, many of the contemporary puzzles in high energy physics and cosmology are intimately tied to gravitational interactions. E.g. DM has so far only been observed through its gravitational interactions. Thus an important question is how one can systematically test departures from GR, or even at a more basic level, what is the set of independent IR departures one could possibly test. Since all of our current probes of GR are on macroscopic scales or low energies, much below the Planck mass $(4\pi)M_{\rm pl}$, which is the intrinsic

[1] It has to be kept in mind that while the EFT framework encompasses a large variety of possible UV complete theories, it is not free of theoretical bias. An EFT expansion typically assumes a separation of scales, which can be used to define an expansion in a small parameter. Thus when using the SMEFT one implicitly assumes that NP enters at a high energy scale, which is not currently reachable at experiments.

energy scale of gravity up to which one could envision it to be a valid description of gravitational phenomena, it is natural to work in an EFT language in order to answer these questions. In Chapter 13 we develop a method to count and construct independent operators for EFTs with gravity, based on a Hilbert series approach. A basis of non-redundant EFT operators exactly corresponds to the full set of physical IR departures due to heavy NP. We also use our method to construct for the first time a non-redundant set of EFT operators of GR coupled to the SM, which we call the GRSMEFT. This EFT is the true most general low-energy parameterization of all fundamental interaction known to date.

Finding an operator basis is only the first step in the exploration of an EFT. Understanding quantum effects, such as operator renormalization and mixing, is a crucial ingredient to relate physics at different scales. From studies within the SMEFT we know that operator mixing is very constrained at one-loop. There exist many zeroes in the anomalous dimension matrix of the mass dimension six operators [24–26]. A physically transparent explanation for these zeroes has recently been obtained with the help of helicity selection rules [27] and angular momentum selection rules [307]. Similar non-trivial non-renormalization results also appear in EFTs with gravity. In Chapter 14 we extend the helicity selection rules of [27] to gravitational theories and use them to formulate non-renormalization theorems. We additionally compute the anomalous dimensions at mass dimension six in a toy SM coupled to gravity, using amplitude methods.

We start this part of the thesis with a short introduction to modern EFT methods, including one-loop matching and the Hilbert series, in Chapter 11. In Chapter 12 we present our results on the one-loop matching of the scalar, based on [33]. We continue in Chapter 13 with the construction of operator bases of EFTs with gravity. These results were also published in [30]. Finally we show preliminary results on the non-renormalization of gravitational operators in Chapter 14. This is based on work in progress [34].

All Figures and parts of the text are taken from the above publications.

Chapter 11

Effective field theories

The main idea behind EFTs is the concept of decoupling. Decoupling is a very useful property of nature, according to which details of small scale phenomena are in general (but not always) irrelevant when describing dynamics on much larger scales. This means that it is not necessary to know the microscopic most fundamental theory to do computations and to make predictions. It is sufficient to have an effective theory with a limited range of validity, which describes the degrees of freedom at the relevant energies. The effect of small scale phenomena are absorbed into low-energy parameters, which can be measured at macroscopic scales. E.g. while the proton mass is sensitive to the top quark mass, this is completely irrelevant in condensed matter physics, since the proton mass can be fixed by a low-energy measurement.

Decoupling is also naturally implemented in quantum field theory (QFT): for instance in a momentum dependent renormalization scheme one finds that heavy particles of mass M decouple and do not contribute to the running of couplings at scales $\mu \ll M$. This example of the Appelquist-Carazzone decoupling theorem [308] is already a first hint that it should be enough to consider only degrees of freedom accessible at the relevant scale, i.e. particles which can be produced on-shell, and local interactions among these particles, parameterized by low-energy constants. But why should this work in general? We know that heavy degrees of freedom, even if they cannot be produced on-shell, can appear as virtual particles in tree graphs and in loops. However, this does not spoil the decoupling. In order to see how this works one has to remember that observables in QFTs are expressed in terms of correlation functions. It is well known that correlation functions are analytic in the external momenta except for poles or branch cuts, which appear when the kinematics allow for the on-shell production of physical intermediate states. This implies that if the available energy is far below the mass threshold of a heavy particle with mass M, the correlation function in a hypothetical UV theory is analytic in p^2/M^2 and can be expanded for $p^2 \ll M^2$. At tree-level this simply corresponds to the Taylor expansion of internal heavy-particle propagators, i.e.

$$\frac{1}{p^2 - M^2} = -\frac{1}{M^2}\left(1 + \frac{p^2}{M^2} + \mathcal{O}(p^4/M^4)\right). \tag{11.1}$$

The expanded correlators can thus be described by local terms in the Lagrangian, which only involve light degrees of freedom.

Let us make two comments about this observation. First of all, while trading a non-local interaction for an infinite tower of local terms in the Lagrangian seems like a complication, in actual applications and measurements one is only sensitive to a limited precision δ in the observables. Therefore only a finite number of terms with $(p^2/M^2)^n \gtrsim \delta$ is relevant and the EFT is a fully predictive QFT. A scheme which organizes the operators according to an expansion

in a small parameter is usually referred to as a power counting scheme. As a second comment we note that the above observation goes two ways: a QFT with a separation of scales can be matched to an EFT at low-energies, which contains only the low-energy degrees of freedom and reproduces the analytic structure of correlation functions of the full theory at low energies. This is the top-down view on EFTs, which we will discuss in Section 11.1. Alternatively one can start from a low scale and construct a QFT for the accessible degrees of freedom with the observed symmetries. Possible effects of heavy new physics can then be included by adding operators which are higher order in the power counting scheme. This is the bottom-up point of view, which we will comment on in Section 11.3.

Besides discussing bottom-up and top-down EFTs we also shortly introduce the concept of operator running and mixing in Section 11.2. Afterwards we turn to the importance of fixing a non-redundant and complete operator basis in Section 11.4. Finally we introduce the Hilbert series as a convenient method to count and construct EFT basis in Section 11.5. For a more thorough pedagogic introduction to EFTs we refer the reader to [309–313].

11.1 Top-down EFTs

Even when the UV theory is known it can be useful or even necessary to construct a low-energy EFT for some applications. Reasons for this can be that computations in the EFT are simpler or the appearance of large logarithms $\log m/M$ with $m \ll M$ in a multi-scale QFT, which can be efficiently resummed in the EFT framework. Another reason can be that the high-energy degrees of freedom are not the same as in the IR. An example of this is QCD, where the quarks and gluons condense into baryons and mesons at low-energies.

The process of constructing the EFT Lagrangian from a known UV theory is called matching or integrating out heavy particles. It fixes the EFT parameters by equating correlation functions of purely light particles in the full and effective theory. The minimal requirement is that observables, i.e. on-shell scattering amplitudes in the UV and effective theory match to the required precision

$$\langle q_1, \dots, q_m | \mathcal{S}_{\text{UV}} | p_1, \dots, p_n \rangle = \langle q_1, \dots, q_m | \mathcal{S}_{\text{EFT}} | p_1, \dots, p_n \rangle + \text{truncation errors}\,, \tag{11.2}$$

where the p_i, q_i are light particle states and $\mathcal{S}_{\text{UV}}, \mathcal{S}_{\text{EFT}}$ are the $\mathcal{S}$-matrix of the UV theory and the EFT, respectively. A stronger version of matching requires that also the off-shell Green's functions coincide, which is achieved by matching the one-light-particle effective action in the UV with the effective action for the EFT, i.e. the generating functionals of connected, irreducible light particle Green's functions[1]

$$\Gamma_{\text{L,UV}}[\phi] = \Gamma_{\text{EFT}}[\phi] + \text{truncation errors}\,, \tag{11.3}$$

where ϕ stands for the light particles. Both approaches are equivalent and fully agree after a field redefinition (see Section 11.4). Even though off-shell matching requires a larger operator basis in the EFT, the so called Green's basis, which includes operators that vanish on-shell, it is often simpler because the matching can be performed at unphysical kinematic configurations. After the matching the Green's basis can be reduced to a non-redundant minimal basis, which up to higher dimensional operators gives the same result as the on-shell matching in Eq. (11.2).

The matching itself can be performed either diagrammatically or using functional methods. Functional matching using the covariant derivative expansion [314–317] has received a lot of

[1] The effective action $\Gamma[\phi]$ is obtained from the generating functional $Z[J] = \exp(iW[j]) = \mathcal{N} \int \mathcal{D}\phi \exp(iS[\phi] + i \int d^d x J(x)\phi(x))$ via a Legendre transformation $\Gamma[\phi] = W[J] - \int d^d x J(x)\phi(x)$, where J is determined by solving $\phi(x) = \delta W[J]/\delta J(x)$ for $J(x)$.

attention lately [318–320] with the goal of constructing a full one-loop universal effective action [320]. For an overview of the current status see e.g. [321] and references therein. Functional matching has the advantage that an explicit operator basis for the EFT is not required and that it can be performed algorithmically [322, 323]. However, functional one-loop matching is in general very technical and intransparent, which is why diagrammatic matching is often the preferred choice. An exception to this is tree-level matching, which is very straightforward using functional methods. The path integral over the heavy field Φ is dominated by the saddle point at tree-level $(\delta S_{\rm UV}[\Phi,\phi]/\delta\Phi)|_{\Phi=\Phi_c[\phi]}=0$, i.e. it corresponds to replacing Φ in the effective action of the UV theory by its equation of motion $\Phi=\Phi_c[\phi]$. Thus Eq. (11.3) is at tree-level given by [321]

$$\left.\begin{aligned}\Gamma^{(\rm tree)}_{\rm L,UV}[\phi] &= S_{\rm UV}[\Phi,\phi]|_{\Phi=\Phi_c[\phi]}\\ \Gamma^{(\rm tree)}_{\rm EFT}[\phi] &= S^{(\rm tree)}_{\rm EFT}[\phi]\end{aligned}\right\} \quad\Rightarrow\quad \mathcal{L}^{(\rm tree)}_{\rm EFT}[\phi]=\mathcal{L}_{\rm UV}[\Phi,\phi]|_{\Phi=\Phi_c[\phi]}\,, \tag{11.4}$$

where $S=\int d^dx\,\mathcal{L}$ is the action and the equation of motion $\Phi_c[\phi]$ can be expanded to the required precision. At one-loop the identification of the matching contribution is not as simple, since some one-loop contributions from the UV-theory correspond to one-loop contributions in the EFT constructed from couplings matched at tree-level. In the following we will focus on diagrammatic matching, for which we show a simple example in Section 11.1.1.

11.1.1 Example: diagrammatic matching of scalar theory

Here we demonstrate the matching procedure for a theory of real scalars $\{\Phi,\phi\}$ with mass M and $m\ll M$, respectively. The Lagrangian of the UV theory is given by[2]

$$\mathcal{L}_{\rm UV}[\Phi,\phi]=\frac{1}{2}\partial_\mu\Phi\partial^\mu\Phi-\frac{1}{2}M^2\Phi^2+\frac{1}{2}\partial_\mu\phi\partial^\mu\phi-\frac{1}{2}m^2\phi^2-\frac{1}{4!}\lambda\,\phi^4-\frac{1}{3!}\kappa\,\phi^3\Phi\,, \tag{11.5}$$

where κ and λ are parameters of the scalar potential. In our setup the power counting parameter is $\lambda=m/M\ll 1$. We assume that the momenta of the external ϕ are small and scale as $p_\phi\sim M\lambda$, s.t. ϕ and ∂_μ in the effective Lagrangian scale as $\phi,\partial_\mu\sim\lambda$. This implies that an expansion in terms of mass dimension in the effective Lagrangian is also ordered according to our power counting. Our goal is to match Eq. (11.5) to an EFT for ϕ, which we truncate at mass dimension six. Our parameterization of the effective Lagrangian is given by

$$\mathcal{L}_{\rm EFT}[\phi]=\frac{Z_\phi}{2}\partial_\mu\phi\partial^\mu\phi-\frac{1}{2}\tilde{m}^2\phi^2+\frac{1}{4!}C_4\phi^4+\frac{1}{6!}\frac{C_6}{M^2}\phi^6+\frac{1}{4}\frac{C_{\partial\phi}}{M^2}\phi^2\partial^2\phi^2\,, \tag{11.6}$$

where we used the Z_2 symmetry $\{\phi,\Phi\}\to-\{\phi,\Phi\}$ of Eq. (11.5) to exclude odd powers in the ϕ field. Note that the operator $\phi^2\partial^2\phi^2$ is not independent and can be removed with a field redefinition, which will yield contributions to C_4 and C_6 (see Section 11.4). Also note that the matching in general gives contributions to the kinetic term of ϕ and the mass term, s.t. $Z_\phi\neq 1$ and $\tilde{m}\neq m$.

In order to perform the matching we have to specify amplitudes with exclusively ϕ as external states and compute them both in the EFT and the UV theory. Expanding the UV theory amplitude to the required order in the power counting, we can fix the EFT Wilson coefficients C_i. For our scenario it is sufficient to consider the three processes $\phi\to\phi$, $\phi\phi\to\phi\phi$ and $\phi\phi\phi\to\phi\phi\phi$

[2]Note that the same theory is treated as an example for functional matching in [320]. We have checked that the results we show here agree with the functional matching in [320].

in order to fix all Wilson coefficients. Note that we should only consider amputated one-light-particle irreducible diagrams in the UV theory, i.e. the UV amplitude should not contain light-particle propagators. Diagrams with internal light particles are matched to reducible EFT diagrams and therefore give no new information for the matching.

In the following we will determine the Wilson coefficients order by order in perturbation theory by performing a loop expansion

$$C_k = C_k^{(0)} + \frac{C_k^{(1)}}{(4\pi)^2} + \dots \,, \tag{11.7}$$

where $C_k^{(0)}$ and $C_k^{(1)}$ denote the tree-level and one-loop coefficients, respectively.

A Tree-level matching

The matching calculation at tree-level is very straightforward. The two-point function is in both cases simply a free propagator of a canonically normalized scalar. This fixes $Z_\phi^{(0)} = 1$ and $\tilde{m}^{(0)} = m$. $C_4^{(0)}$ and $C_{\partial\phi}^{(0)}$ are fixed by requiring that the four-point functions are identical

$i\,\mathcal{A}_{\text{Full}} =$ 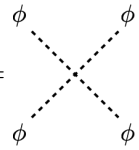 $= -i\lambda \quad \overset{!}{=} \quad i\,C_4^{(0)} - 2\,i\frac{C_{\partial\phi}^{(0)}}{M^2}(s+t+u) =$ 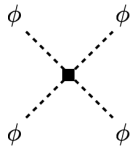 $= i\,\mathcal{A}_{\text{EFT}}\,,$ (11.8)

where we have kept the external lines off-shell and depicted tree-level EFT interactions with a box. The Mandelstam variables are defined as $s = (p_1+p_2)^2$, $t = (p_1-p_3)^2$ and $u = (p_1-p_4)^2$. This equality fixes $C_4^{(0)} = -\lambda$ and $C_{\partial\phi}^{(0)} = 0$. The matching of the six-point amplitude works analogously

$i\,\mathcal{A}_{\text{Full}} =$ 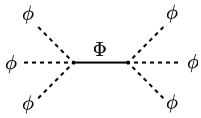 $+$ crossed legs $= 10\,i\frac{\kappa^2}{M^2} + \mathcal{O}(M^{-4}) \overset{!}{=} i\frac{C_6^{(0)}}{M^2} =$ 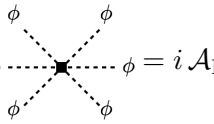 $= i\,\mathcal{A}_{\text{EFT}}\,,$ (11.9)

where we expanded the heavy Φ propagator to leading order in $1/M$. This fixes $C_6^{(0)} = 10\,\kappa^2$. As a simple cross-check we can compare this to what one obtains from integrating out Φ at tree-level following Eq. (11.4), i.e. using the equation of motion for Φ

$$\Phi_c[\phi] = -\frac{1}{\Box + M^2}\frac{\kappa}{6}\phi^3\,, \tag{11.10}$$

where $1/(\Box + M^2)$ is the inverse of the differential operator. Plugging this into the Lagrangian of the full theory and expanding $1/(\Box + M^2)$ in a series of local operators we obtain

$$\begin{aligned}\mathcal{L}_{\text{EFT}}[\phi] = \mathcal{L}_{\text{UV}}[\Phi,\phi]|_{\Phi=\Phi_c[\phi]} &= \frac{1}{2}\partial_\mu\phi\partial^\mu\phi - \frac{1}{2}m^2\phi^2 - \frac{1}{4!}\lambda\,\phi^4 + \frac{\kappa^2}{72}\phi^3\frac{1}{\Box+M^2}\phi^3 \\ &= \frac{1}{2}\partial_\mu\phi\partial^\mu\phi - \frac{1}{2}m^2\phi^2 - \frac{1}{4!}\lambda\,\phi^4 + \frac{\kappa^2}{72\,M^2}\phi^6 + \mathcal{O}(M^{-4})\,,\end{aligned} \tag{11.11}$$

which agrees with the results from the diagrammatic matching.

B One-loop matching

The matching at one-loop level is completely analogous to the tree-level computation with a few added complications. For once the n-point functions are in general divergent. We regularize the divergences with dimensional regularization in $d = 4 - 2\epsilon$ dimensions and use the $\overline{\text{MS}}$ scheme to absorb the divergences into local counterterms in the EFT and full theory separately. Effectively this corresponds to simply dropping the $1/\epsilon$ poles, what we will do in the following. Additionally we have to choose a renormalization scale μ at which we will perform the matching. As we will see a convenient choice is $\mu = M$.

In the full theory there is no one-loop contribution to the ϕ two-point function, which includes heavy particles. This implies that it automatically matches the two-point function in the EFT, since we have already matched the tree-level couplings which enter the computation. The four-point function in the UV theory gets contributions from three different classes of diagrams

$$
\begin{aligned}
i\,\mathcal{A}_{\text{Full}} = {} & \\
& = i\frac{\lambda^2}{32\pi^2}\left(f(s,m)+f(t,m)+f(u,m)+6+3\,\ln\frac{\mu^2}{m^2}\right)+i\frac{\kappa^2}{32\pi^2}\frac{s+t+u}{M^2} \\
& \quad + i\frac{\kappa^2}{16\pi^2}\left(3+3\ln\frac{\mu^2}{M^2}-2\frac{m^2}{M^2}-2\frac{m^2}{M^2}\ln\frac{\mu^2}{m^2}+3\frac{m^2}{M^2}\ln\frac{m^2}{M^2}\right)+\mathcal{O}(M^{-4})\,,
\end{aligned}
\tag{11.12}
$$

where the result is expanded up to order $m^2/M^2, p^2/M^2$ and $f(s,m)$ is defined as

$$
f(s,m) = \sqrt{1-\frac{4m^2}{s}}\,\ln\left(\frac{2m^2-s+\sqrt{s(s-4m^2)}}{2m^2}\right). \tag{11.13}
$$

Note that the third class of diagrams is not one-particle irreducible but one-light-particle irreducible, which is why we have to include it in the matching. The same amplitude in the EFT takes the form

$$
\begin{aligned}
i\,\mathcal{A}_{\text{EFT}} = {} & \\
& = i\,\frac{C_4^{(1)}}{(4\pi)^2} - 2\,i\frac{C_{\partial\phi}^{(1)}}{(4\pi)^2M^2}(s+t+u) - i\frac{5\,\kappa^2}{16\pi^2}\frac{m^2}{M^2}\left(1+\ln\frac{\mu^2}{m^2}\right) \\
& \quad + i\frac{\lambda^2}{32\pi^2}\left(f(s,m)+f(t,m)+f(u,m)+6+3\,\ln\frac{\mu^2}{m^2}\right),
\end{aligned}
\tag{11.14}
$$

where we already inserted the tree-level values for the Wilson coefficients in the loop diagrams and took the same renormalization scale μ in the EFT and UV theory. The interaction due to the one-loop Wilson coefficient in the EFT is depicted with a dot. Comparing Eq. (11.12) with Eq. (11.14) we obtain

$$
C_4^{(1)}(\mu) = -3\,\kappa^2\left(1+\frac{m^2}{M^2}\right)\left(1+\ln\frac{\mu^2}{M^2}\right), \qquad C_{\partial\phi}^{(1)}(\mu) = -\frac{\kappa^2}{4}\,. \tag{11.15}
$$

The natural choice for the matching scale is therefore $\mu = M$, where the logarithm vanishes. Before going on let us make a few remarks on the result above. As can be seen when comparing

Eq. (11.12) with Eq. (11.14), loops within the EFT generate the full non-analytic dependence on the light mass m which cancels in the matching procedure. For this reason the non-analytic contributions to the Wilson coefficients can only be of the form $\ln(\mu^2/M^2)$, which can be kept small for $\mu \sim M$ and exactly vanishes for $\mu = M$. Note that this is fundamentally different in the full theory result, which contains large logarithms of the form $\log(m^2/M^2)$, no matter what we choose for μ. Such large logarithms can substantially worsen the convergence of perturbation theory. The EFT framework therefore provides a natural way to deal with large logarithms. The idea is to split the logarithm at the matching scale μ

$$\ln \frac{m^2}{M^2} = -\ln \frac{M^2}{\mu^2} + \ln \frac{m^2}{\mu^2}\,, \tag{11.16}$$

where the first contribution can be made small by performing the matching at $\mu = M$ and the second can be resummed with the renormalization group running within the EFT.

The observation that the EFT reproduces the full non-analytic contributions in the light mass m from loops of tree-level Wilson coefficients helps us to devise a more efficient matching procedure. All we need are the analytic contributions in m from the UV theory. This is straightforward to obtain with the method of regions [324], according to which the full loop integral in dimensional regularization can be obtained by summing the contributions from all momentum regions in the full integral. In this case there is a soft region, where the loop momentum scales as $k \sim m$, and a hard region, where it scales as $k \sim M$. The analytic contributions in m come from the hard region, where one can expand the integrand in powers of $m \ll k, M$. Thus we directly obtain the matching contribution by expanding the loop integrals in the UV theory for small m (see e.g. [312, 313] for a thorough discussion).

Applying this method it is easy to obtain the matching correction to $C_6^{(1)}$ from the six-point function

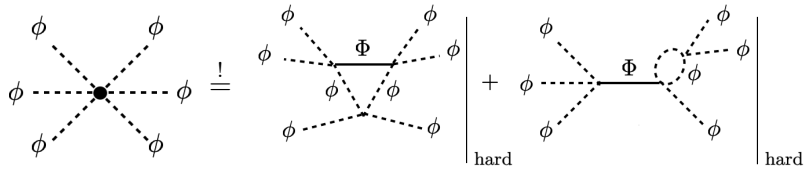

$$= i\frac{45\,\kappa^2\lambda}{16\pi^2 M^2}\left(1 + \ln\frac{\mu^2}{M^2}\right), \tag{11.17}$$

where additional diagrams with crossed legs are implicit. Note that the second class of diagrams in the UV theory does not yield any hard contribution, since the loop contains only light particles and becomes scaleless when the integrand is expanded. From this we find that

$$C_6^{(1)}(\mu) = 45\,\kappa^2\lambda\left(1 + \ln\frac{\mu^2}{M^2}\right), \tag{11.18}$$

what concludes the one-loop matching.

Note that the logarithmic contributions in Eqs.(11.15) and (11.18) do not capture the full scale dependence of the Wilson coefficients. It lacks the scale dependence of the UV theory parameters. Once they are included the logarithmic contributions only depend on parameters of the low-energy EFT and agree with the anomalous dimensions, which can be determined within the EFT. For a related discussion in the context of one-loop matching of the SM extended by a singlet scalar to the SMEFT see Appendix III.B.

11.2 Renormalization group and anomalous dimensions

The renormalization group (RG) provides a framework to sum large logarithms in perturbation theory and goes hand in hand with the top down EFT approach. We saw in the previous

section that in a multi-scale QFT integrating out heavy particles and matching to a low-energy EFT allowed us to split large logarithms of the form $\ln(m^2/M^2)$ into two qualitatively different contributions (cf. Eq. (11.16)). The matching contribution, which only depends on the heavy scale M, can be made small by performing the matching at a scale $\mu \sim M$. The remaining contribution is only non-analytic in the low mass scale m and is fully reproduced by loops within the EFT. This makes it possible to employ well-known RG methods to evolve the EFT coefficients from the matching scale down to a lower scale and thus resum these logarithms.

The renormalization scale dependence enters in the EFT through one-loop divergences, which have to be absorbed by the Wilson coefficients. In dimensional regularization with $d = 4 - 2\epsilon$ and $\overline{\text{MS}}$ scheme the renormalized Wilson coefficient $C(\mu)$ is related to the bare one $\tilde{C}$ by

$$\tilde{C} = \mu^{n\epsilon} Z_C \, C(\mu) \,, \tag{11.19}$$

where we have introduced $\mu^{n\epsilon}$, with n being determined by the mass dimension of the effective operator, to keep $C(\mu)$ dimensionless. $Z_C = 1+\delta_C$ is the renormalization constant, which can be determined perturbatively by requiring that the counterterm interaction proportional to δ_C cancels the divergences. The independence of the bare Wilson coefficient $\tilde{C}$ on the renormalization scale allows us to derive the RG equation for $C(\mu)$

$$\frac{d}{d\ln\mu} C(\mu) \equiv \gamma_{C,C} \, C(\mu) \qquad \text{with} \qquad \gamma_{C,C} = -\left(n\,\epsilon + \frac{1}{Z_C} \frac{dZ_C}{d\log\mu} \right) , \tag{11.20}$$

where $\gamma_{C,C}$ is the anomalous dimension.[3] $Z_C = Z_C(\{g_i\})$ is a function of the coupling constants g_i, which in turn depend on the renormalization scale $g_i = g_i(\mu)$. This implies that $d/(d\ln\mu) Z_C = \sum_i \partial\, Z_C/\partial g_i \cdot d\, g_i/d\ln\mu$. Note that in EFTs with more than one effective operator Z_C in general also depends on additional Wilson coefficients, i.e. $Z_C = Z_C(\{C_j\})$. In this case the RG equation becomes a matrix equation of the form

$$\frac{d}{d\ln\mu} C_i(\mu) \equiv \gamma_{ij} C_j(\mu) \,, \tag{11.21}$$

where γ_{ij} is now the so-called anomalous dimension matrix. This implies that Wilson coefficients mix under RG evolution, i.e. an interaction which is not generated at matching might be generated radiatively through RG evolution. In EFTs with exclusively massless particles Wilson coefficients can only get renormalized by equal or lower dimensional interactions. E.g. at mass dimension six the Wilson coefficients $C^{(6)}$ can receive divergent contributions either from two insertions of dimension five interactions $C^{(5)}$ or one dimension six interaction, s.t. the RG equation is given by

$$\frac{d}{d\ln\mu} C_i^{(6)}(\mu) = \gamma_{ij}^{(6)} C_j^{(6)}(\mu) + \gamma_{ijk}\, C_j^{(5)}(\mu) C_k^{(5)}(\mu) \,. \tag{11.22}$$

In massive EFTs Wilson coefficients can also get renormalized by higher dimensional operators with a mass insertion. However, if the suppression scale of the operators is considerably higher than the mass of the EFT particles, these contributions are usually negligible. Also note that

[3] Note that the definition of the anomalous dimension in Eq. (11.20) already introduces the anomalous dimension matrix, where $\gamma_{C,C}$ denotes the entry on the diagonal, which corresponds to the self-renormalization of C. In the following we will always refer to the matrix notation if γ_{ij} has to indices. If γ_C has only one index it stands for $\gamma_C \equiv \sum_j \gamma_{C,j} C_j$. It is sometimes useful to define the anomalous dimension without the loop factor $(4\pi)^{-2}$ similar to Eq. (11.7). This definition will be used in Chapter 12, where it will be marked with a tilde, i.e. $d/(d\ln\mu)\, C(\mu) = \tilde{\gamma}_C/(4\pi)^2$.

operator mixing in general gives contributions to redundant operators, which after the RG evolution can be reduced to a non-redundant basis with the methods in Section 11.4.

While RG evolution is closely related to the top down view on EFTs, it also has important implications for bottom up EFTs, which we will discuss momentarily. Operator mixing implies that independent of the matching conditions at the UV scale, practically any operator allowed by symmetries will be present in the IR with in general no hierarchies in the Wilson coefficients if the running is over many orders of magnitude. For this reason one should always include a full set of operators in the EFT and justify hierarchies in the values of Wilson coefficients with symmetries or the structure of the class of UV theories that one wants to study.

11.3 Bottom-up EFTs

The bottom up approach to EFTs does not start from a specific full theory in the UV. Instead the only inputs are the accessible degrees of freedom and manifest symmetries at the relevant energy scale. Starting from these ingredients one constructs all local interactions between the low-energy degrees of freedom, which are allowed by the symmetries. The resulting Lagrangian parameterizes the most general theory of the low-energy particles with the parameters being fixed by experimental observations.

According to this reasoning any theory is morally an EFT and renormalizable theories, such as the SM, can be viewed as the leading terms in an EFT expansion. As we saw in the previous section, at low energies the effect of heavy new particles with masses far above the electroweak scale $m_* \gg v$ looks like higher dimensional operators suppressed by the heavy scale. This implies that a consistent way of including generic contributions from heavy new physics is to extend the SM, or any other renormalizable theory, by higher dimensional operators, which are invariant under the low-energy symmetries and only contain the low-energy particle content. The SMEFT Lagrangian can therefore be written as

$$\mathcal{L}_{\text{SMEFT}} = \mathcal{L}_{\text{SM}} + \sum_{n\geq 5} \sum_i \frac{c_{n,i}}{m_*^{n-4}} \mathcal{O}_{n,i} \,, \tag{11.23}$$

where m_* is the scale of new physics, $c_{n,i}$ are the Wilson coefficients and $\mathcal{O}_{n,i}$ are local operators of mass dimension $n \geq 5$. This has the advantage that the Lagrangian parameterizes a vast class of UV theories, allowing for model independent searches for new physics by probing the effect of the higher dimensional operators. Note that from the above reasoning it is obvious that the EFT Lagrangian has a limited range of validity. Once the energy gets close to the mass scale of the heavy particles, the non-locality of the heavy-particle interactions shows up as the breakdown of the EFT expansion (all operators are of the same order in the power counting). At the latest when the energy is large enough to produce the heavy particles on-shell, the EFT has to be replaced by a more fundamental theory. Also note that if one defines $\mathcal{O}(1)$ Wilson coefficients $\tilde{c}_{n,i}$, i.e. $\tilde{c}_{n,i}/\Lambda^{n-4} = c_{n,i}/m_*^{n-4}$, the suppression scale Λ of the effective operators is not necessarily the mass of a heavy particle, which has been integrated out. In general it is a combination of the coupling and mass of the heavy particle.

By probing processes, which are sensitive to the higher dimensional operators, one can bound $c_{n,i}/m_*^{n-4}$. The interpretation of such bounds is, however, model dependent. Since $c_{n,i}/m_*^{n-4}$ is a combination of masses and couplings of hypothetical heavy particles, the interpretation of a bound can be dramatically different for a weakly coupled and a strongly coupled UV theory. In order to estimate the natural size of Wilson coefficients a power counting scheme is required. A particularly simple one is the one-scale one-coupling scheme, which assumes that heavy new

physics is characterized by one new scale m_* and one new coupling g_*. From dimensional analysis one finds that this implies the following scaling of the Wilson coefficients

$$c_{n,i} \sim g_*^{N_i-2}\left(\frac{g_*^2}{16\pi^2}\right)^L, \tag{11.24}$$

where N_i is the number of fields in $\mathcal{O}_{n,i}$ and L is the number of loops at which this operator is assumed to be generated. For the derivation of the one-scale and one-coupling power counting scheme in the Composite Higgs context see Section 2.2.3.

11.4 Operator basis

Especially in the context of bottom-up EFTs, it is essential to construct a full operator basis. The set of higher dimensional effective operators parameterizes all possible IR departures from the leading order Lagrangian, which enter the computation of observables. An incomplete operator basis might therefore falsely predict that some observables are not sensitive to heavy new physics. The solution to this problem seems obvious: simply write down all possible Lorentz and gauge invariant operators of the low-energy degrees of freedom. However, there is a considerable freedom in rewriting the effective action in equivalent ways such that the brute-force approach in general vastly over-counts the possible number of interactions. On closer inspection many of the operators can turn out to be degenerate with other operators in physical observables or they might not even influence observables at all. Thus in order to properly identify the independent directions in the space of all possible UV completions of the EFT, it is essential to construct a full and non-redundant operator basis. Redundant operators in this context are operators, which do not have new physical effects on observables.

Identifying a non-redundant operator basis is a non-trivial task due to many redundancies. These include 1) redundancies in the group invariants, 2) the integration by parts (IBP) redundancy and 3) the equation of motion (EOM) redundancy. The construction of a complete and non-redundant operator basis for the SMEFT at operator dimension six took around 30 years from its starting point in 1979 by Weinberg [325] until 2010 [326]. Today there exist several equivalent operator bases. The most relevant ones for our purpose are the Warsaw basis [326] and the SILH basis [122]. In the remainder of this section we give an overview of the aforementioned three classes of operator redundancies, before we introduce the Hilbert Series as a convenient tool to count and construct independent operators in Section 11.5.

1) Redundancies among symmetry group invariants
Operators have to be invariants under both internal symmetries and the Lorentz spacetime symmetry. However, not all invariants are independent and there are relations between invariants, so-called syzygies. Such relations include Fierz-identities, the Schouten identity, the Levi-Civita identity and the Jacobi identity. The Levi-Civita identity for instance

$$\epsilon^{\mu\nu\rho\sigma}\epsilon_{\alpha\beta\gamma\delta} = -24\delta^{[\mu}_{\alpha}\delta^{\nu}_{\beta}\delta^{\rho}_{\gamma}\delta^{\sigma]}_{\delta}\,, \tag{11.25}$$

where $A^{[a_1\cdots a_n]} = \frac{1}{n!}(A^{a_1\cdots a_n} + (-1)^{\sigma_n}\text{ permutations})$ denotes anti-symmetrization of the indices, relates invariants of four $U(1)$ field-strength tensors $B_{\mu\nu}$

$$B_{\mu\nu}B^{\nu\rho}B_{\rho\sigma}B^{\sigma\mu} = \frac{1}{2}\big(B_{\mu\nu}B^{\mu\nu}\big)^2 + \frac{1}{4}\big(B_{\mu\nu}\tilde{B}^{\mu\nu}\big)^2\,, \tag{11.26}$$

with the dual field strength $\tilde{B}^{\mu\nu} = \frac{1}{2}\epsilon^{\mu\nu\rho\sigma}B_{\rho\sigma}$. As we will see in Section 11.5, such relations are naturally taken into account by the Hilbert Series construction.

2) Integration by parts redundancy
The integration by parts redundancy is based on the fact that total derivatives in the Lagrangian do not affect physical observables in perturbation theory. A total derivative term in the action evaluates to an integral over the boundary of spacetime after the use of Stoke's theorem. Assuming that the quantum fields vanish at spatial and timelike infinity, the boundary term vanishes. This implies that operators $\mathcal{O}_1$ and $\mathcal{O}_2$ are equivalent if they only differ by a total derivative, i.e.

$$\mathcal{O}_1 \sim \mathcal{O}_2 \quad \text{if} \quad \mathcal{O}_1 = \mathcal{O}_2 + \partial_\mu \mathcal{O}_3^\mu \,. \tag{11.27}$$

In practice this implies that $\mathcal{O}_2$ can be obtained from $\mathcal{O}_1$ by integration by parts. As an example consider the operators $\mathcal{O}_1 = \phi\partial_\mu\phi\partial^\mu\phi$ and $\mathcal{O}_2 = \phi^2\partial^2\phi$. They are clearly related through a total derivative

$$\partial_\mu(\phi^2\partial^\mu\phi) = 2\,\phi\partial_\mu\phi\partial^\mu\phi + \phi^2\partial^2\phi = 2\,\mathcal{O}_1 + \mathcal{O}_2 \,. \tag{11.28}$$

3) EOM redundancy
The last redundancy, which we have to take into account, is the EOM redundancy. In practical terms it states that operators proportional to the leading order EOM are redundant and can be removed. This is based on the observation that physical observables do not change under field redefinitions [327–330] (see [331] for a recent discussion). The fundamental degrees of freedom in the theory are particles. Quantum fields $\phi(x)$ are chosen such that they interpolate between the vacuum and a one-particle state $|p\rangle$, i.e. they can create a particle from the vacuum

$$\langle p|\phi(x)|0\rangle \neq 0 \,. \tag{11.29}$$

The explicit form of the interpolating field is not relevant and many choices are possible. The only requirement is Eq. (11.29), i.e. that $\phi(x)|0\rangle$ has a non-vanishing overlap with the one-particle state. The physical external states in a scattering process can then be projected out from correlation functions of the quantum fields $\langle 0|T\{\phi(x_1)\cdots\phi(x_n)\}|0\rangle$ with the LSZ reduction formula [332]. This implies that any local field redefinition of the form

$$\phi \to \phi' = F[\phi] \quad \text{with} \quad \langle p|F[\phi(x)]|0\rangle \neq 0 \,, \tag{11.30}$$

leaves the S-matrix unaffected. In particular this includes perturbative field redefinitions where $F[\phi] = \phi + \lambda G[\phi]$, with $\lambda \ll 1$. After the field redefinition the theory is described by the action

$$S'[\phi] = S[F[\phi]] \,, \tag{11.31}$$

where $S[\phi]$ is the action for the original field variable.[4] In order to see how this helps to remove redundant operators which are proportional to the EOM consider an effective action of the form

$$S_{\text{eff}}[\phi] = S_0[\phi] + \lambda S_1[\phi] + \lambda^2 S_2[\phi] + \dots \,, \tag{11.32}$$

where ϕ stands for the field variables, $S_0[\phi]$ is the leading order action and $S_i[\phi]$ is suppressed by λ^i in a small power counting parameter $\lambda \ll 1$. Performing a perturbative field redefinition

$$\phi' = \phi + \delta\phi = \phi + \lambda^k f_k[\phi] + \lambda^{k+1} f_{k+1}[\phi] + \dots \,, \tag{11.33}$$

[4]Note that the field redefinition introduces a Jacobian in the generating functional. If one uses dimensional regularization this Jacobian is trivial for local field redefinitions, with the exception of fermionic chiral transformations. Also note that the theory described by $S'[\phi]$ is only equivalent to a theory with the action $S[\phi]$ on-shell. Off-shell Green's functions differ in both theories (see e.g. [313, 331]).

where $f_i[\phi]$ are functions of the fields and their derivatives, we find that the action changes as

$$\delta S_{\text{eff}} = \int d^4x \left(\frac{\delta S_0}{\delta\phi(x)} + \lambda \frac{\delta S_1}{\delta\phi(x)} + \lambda^2 \frac{\delta S_2}{\delta\phi(x)} + \dots \right) \delta\phi \tag{11.34}$$

$$= \int d^4x \left(\lambda^k \left[\frac{\delta S_0}{\delta\phi(x)} f_1 \right] + \lambda^{k+1} \left[\frac{\delta S_0}{\delta\phi(x)} f_2 + \frac{\delta S_1}{\delta\phi(x)} f_1 \right] + \dots \right). \tag{11.35}$$

This implies that f_1 can be used to eliminate any operator at order λ^k proportional to $\delta S_0/\delta\phi(x)$, i.e. the leading order EOM, without affecting any operators at lower orders. The cost of this simplification is to introduce higher dimensional operators of the form $\lambda^{k+i}\, \delta S_i/\delta\phi(x)\, f_1$ for $i \geq 1$. However, if they are again proportional to the leading order EOM, they can in turn be eliminated with a further field redefinition. Repeating this process order by order in the power counting we can iteratively remove all operators proportional to the EOM, which are therefore redundant.

11.5 Counting operators with the Hilbert series

As we discussed in the previous section, it is important to construct complete and non-redundant operator bases for EFTs. Due to the redundancies, which we introduced above, this is usually a non-trivial task: one can never be sure if all operators and redundancies have been found. For this reason it is helpful to have a tool, which counts the number of independent operators for a given field content and number of derivatives. This is exactly what the Hilbert Series does: it counts the number of group invariants. [22,23] applied Hilbert series methods to count operators in the SMEFT. In this section we introduce the basic features of the Hilbert series and review some key results of [22,23].[5] This section is based on [30].

11.5.1 Hilbert Series

The Hilbert series $\mathcal{H}(q)$ is a generating function that counts the number of independent group invariants that can be built out of a spurion q in a given representation of the group. It is formally defined as a power series in q

$$\mathcal{H}(q) = \sum_{r=0}^{\infty} c_r\, q^r\,, \tag{11.36}$$

where c_r denotes the number of invariants involving r spurions, with $c_0 = 1$ by definition. By including multiple spurions q_i, one can construct the multi-graded Hilbert series, which provides information on the structure of the invariants. In a field theoretical setting, the spurions stand for field operators ϕ_i and derivatives $\mathcal{D}$, i.e. the Hilbert series in general has the form

$$\mathcal{H}(\mathcal{D}, \{\phi_i\}) = \sum_{r_1,\dots,r_n,k} c_{r_1,\dots,r_n,k}\, \phi_1^{r_1} \cdots \phi_n^{r_n} \mathcal{D}^k\,, \tag{11.37}$$

where $c_{r_1,\dots,r_n,k}$ now indicates the number of invariants of order k in derivates and order r_i in ϕ_i. As an explicit example, consider a complex scalar field ϕ charged under a $U(1)$ symmetry. Any invariant in the scalar potential can be written as a polynomial in the monomial $(\phi^*\phi)$, with each power appearing exactly once. In this case it is straightforward to compute the Hilbert

[5] For a physics oriented introduction to the Hilbert series technique we recommend [333] (see also [334]) . For a mathematically more rigorous presentation refer to [335, 336].

series for the scalar potential, which even has a closed form expression if we formally take the spurions to be small, $(\phi^*\phi) < 1$,

$$\mathcal{H}(\phi,\phi^*) = 1 + (\phi^*\phi) + (\phi^*\phi)^2 + \ldots = \sum_{r=0}^{\infty}(\phi^*\phi)^r = \frac{1}{1-\phi^*\phi}\,. \tag{11.38}$$

Obtaining the Hilbert series in this example was simple only because we already knew the form of the invariants. However, when multiple spurions in different representations of a group G are involved, it is no longer straightforward to find all the invariants. This task can be greatly simplified using group characters. The character of a representation $\mathbf{R}$ of a group G is defined as $\chi_{\mathbf{R}}(g) = \mathrm{Tr}_{\mathbf{R}}(g)$ with $g \in G$. Group characters of compact Lie groups are orthonormal w.r.t. the integration over the group's Haar measure, i.e. $\int d\mu_G(g)\,\chi_{\mathbf{R}}(g)\,\chi^*_{\mathbf{R}'}(g) = \delta_{\mathbf{R}\,\mathbf{R}'}$. Therefore, taking all possible tensor products of the spurions, which amounts to multiplying their characters, and projecting them onto the trivial representation yields all the group invariants. For a bosonic spurion $\phi_{\mathbf{R}}$ in the representation $\mathbf{R}$, the generating function for the characters of all the symmetric tensor products is the plethystic exponential (PE) [337, 338]

$$\mathrm{PE}[\phi_{\mathbf{R}}\,\chi_{\mathbf{R}}(z)] = \sum_{n=0}^{\infty}\phi^n_{\mathbf{R}}\,\chi_{\mathrm{Sym}^n(\mathbf{R})}(z) = \exp\left[\sum_{r=1}^{\infty}\frac{1}{r}\phi^r_{\mathbf{R}}\,\chi_{\mathbf{R}}(z^r)\right], \tag{11.39}$$

where $\mathrm{Sym}^n(\mathbf{R})$ is the symmetric tensor product of n representations $\mathbf{R}$ and $z = \{z_1,\ldots,z_{\mathrm{rank(G)}}\}$ are the $\mathrm{rank}(G)$ variables parameterizing the group. For a short derivation of this formula see appendix III.E. The fermionic plethystic exponential (PEF) [339] is the counterpart for fermionic spurions, where the antisymmetric tensor product has to be taken,

$$\mathrm{PEF}[\phi_{\mathbf{R}}\,\chi_{\mathbf{R}}(z)] = \sum_{n=0}^{\infty}\phi^n_{\mathbf{R}}\,\chi_{\wedge^n(\mathbf{R})}(z) = \exp\left[\sum_{r=1}^{\infty}\frac{(-1)^{r+1}}{r}\phi^r_{\mathbf{R}}\,\chi_{\mathbf{R}}(z^r)\right]. \tag{11.40}$$

In the following our notation will not differentiate between the fermionic and bosonic version of the PE, as it will be clear from the context which one is meant. For more than one spurion we define the PE as $\mathrm{PE}[\phi_{\mathbf{R}},\ldots,\varphi_{\mathbf{R}'}] = \mathrm{PE}[\phi_{\mathbf{R}}]\cdots\mathrm{PE}[\varphi_{\mathbf{R}'}]$, where from now on we omit the characters for the spurions in the argument of the PE to ease the notation. From the PE one can obtain the Hilbert series by projecting onto the trivial representation $\mathbf{1}$, with character $\chi_{\mathbf{1}} = 1$, and integrating over the group

$$\mathcal{H}(\phi_{\mathbf{R}},\ldots,\varphi_{\mathbf{R}'}) = \int d\mu_G\,\mathrm{PE}[\phi_{\mathbf{R}},\ldots,\varphi_{\mathbf{R}'}]\,. \tag{11.41}$$

In the literature this is often referred to as the Molien-Weyl formula (see e.g. [336]). Let us illustrate how this machinery works by looking at a simple example with a bosonic spurion $\phi_{\mathbf{2}}$ that transforms in the fundamental representation of $SU(2)$ and its complex conjugate $\phi^\dagger_{\bar{\mathbf{2}}}$. $SU(2)$ has rank one and therefore its characters are a function of one complex variable y. The characters for the fundamental $\mathbf{2}$ and adjoint $\mathbf{3}$ representations of $SU(2)$ are $\chi_{\bar{\mathbf{2}}}(y) = \chi_{\mathbf{2}}(y) = y + 1/y$ and $\chi_{\mathbf{3}}(y) = y^2+1+1/y^2$ [340], while the $SU(2)$ Haar measure can be expressed as a contour integral in the complex plane [340]

$$\int d\mu_{SU(2)}(y) = \frac{1}{2\pi i}\oint_{|y|=1}\frac{dy}{y}\big(1-y^2\big)\,. \tag{11.42}$$

Up to $\mathcal{O}(\phi^2)$, the PE for the spurion ϕ is given by

$$\mathrm{PE}[\phi_{\mathbf{2}}] = \exp\left[\sum_{r=1}^{\infty}\frac{1}{r}\phi^r_{\mathbf{2}}\,\chi_{\mathbf{2}}(y^r)\right] \;=\; 1 + \chi_{\mathbf{2}}(y)\,\phi + \frac{1}{2}(\chi_{\mathbf{2}}(y^2) + \chi_{\mathbf{2}}(y)^2)\,\phi^2 + \mathcal{O}(\phi^3)$$

$$= \quad 1 + \chi_{\mathbf{2}}(y)\,\phi + \chi_{\mathbf{3}}(y)\phi^2 + \mathcal{O}(\phi^3)\,, \tag{11.43}$$

where note that we recover the symmetric part of the $SU(2)$ tensor decomposition $\mathbf{2}\otimes\mathbf{2} = \mathbf{1}_A\oplus\mathbf{3}_S$ from the characters. The PE for $\phi^\dagger_{\mathbf{2}}$ is obtained from Eq. (11.43) after the substitution $\phi_{\mathbf{2}} \to \phi^\dagger_{\mathbf{2}}$. Combining these ingredients and using Eq. (11.41), the Hilbert series up to second order in the fields is given by

$$\begin{aligned}\mathcal{H}(\phi_{\mathbf{2}}, \phi^\dagger_{\mathbf{2}}) &= \int d\mu_{SU(2)}(y)\left(1 + (\phi_{\mathbf{2}} + \phi^\dagger_{\mathbf{2}})\chi_{\mathbf{2}}(y) + (\phi^2_{\mathbf{2}} + \phi^{\dagger\,2}_{\mathbf{2}})\chi_{\mathbf{3}}(y) + (\phi_{\mathbf{2}}\phi^\dagger_{\mathbf{2}})\chi_{\mathbf{2}}(y)\chi_{\mathbf{2}}(y) + \dots\right)\\ &= 1 + \phi_{\mathbf{2}}\phi^\dagger_{\mathbf{2}} + \mathcal{O}(\phi_{\mathbf{2}}, \phi^\dagger_{\mathbf{2}})^3\,,\end{aligned} \tag{11.44}$$

where only the $\phi_{\mathbf{2}}\phi^\dagger_{\mathbf{2}}$ term survives the integration, since the tensor product contains one singlet as can be seen from $\chi_{\mathbf{2}}(y)\chi_{\mathbf{2}}(y) = \chi_{\mathbf{1}}(y) + \chi_{\mathbf{3}}(y)$. This result tells us that there is no invariant at the first order in the fields, and exactly one at the second order. This may seem trivial, however by continuing the expansion of the PE to higher orders one can derive the multiplicity and structure of each invariant order by order.

11.5.2 Hilbert series for EFTs

The main principle for constructing EFTs is to include all Lorentz and gauge invariant local operators built out of the degrees of freedom accessible at the relevant energy scale. However, to find an operator basis $\mathcal{K} = \{\mathcal{O}_i\}$, i.e. the minimal set of operators that lead to physically distinct phenomena, is considerably more difficult than just finding all invariants, since in general redundancies appear among operators, which need to be taken care of. As we have discussed at length in Section 11.4, such redundancies appear in three ways: (1) operators proportional to the free field EOM, which can be removed by a field redefinition that leaves the S-matrix invariant, (2) operators related by a total derivative, which can be transformed into each other using IBP, and (3) operators which are related by relations among group invariants. The problem of relations among group invariants is automatically solved by the Hilbert series. The basic building blocks for local operators are fields and derivatives acting on them. For example, for a single scalar field ϕ, any local EFT operator can be written as a polynomial in $\mathbb{C}[\phi, \partial_\mu\phi, \partial_\mu\partial_\nu\phi, \dots]$. Monomials such as $\partial_\mu\partial_\nu\phi$ have to be understood as the tensor product of two derivatives acting on the field and therefore still contain a term which is proportional to the free EOM $\partial^2\phi = -m^2\phi$. These redundant terms (ϕ is already a building block) can be avoided by taking only the symmetrized, traceless combination of the derivatives, which we denote as $\partial_{\{\mu_1}\cdots\partial_{\mu_n\}}$.[6] This leads to the single particle module R_ϕ as the basic building block [23]

$$R_\phi = \begin{pmatrix} \phi \\ \partial_\mu\phi \\ \partial_{\{\mu_1}\partial_{\mu_2\}}\phi \\ \vdots \end{pmatrix}\,. \tag{11.45}$$

One could now use the Molien-Weyl formula with each component of the single particle module as an independent spurion. Using their group characters for the Lorentz representations and integrating over the Lorentz group, one could project out all scalar operators.[7] This would yield

[6] Note that this remains true even if we replace the derivatives by covariant derivatives. Antisymmetric combinations of covariant derivatives are related to the gauge field strength via $[D_\mu, D_\nu] \sim F_{\mu\nu}$. Therefore, the antisymmetric contributions are already accounted for when constructing operators with $F_{\mu\nu}$ and ϕ.

[7] The Lorentz group is not a compact Lie group and therefore its characters are not orthonormal. However, since we are not interested in dynamics but only want to enumerate the operators, we can work in Euclidean space, where the Lorentz group $SO(4) \simeq [SU(2)_L \otimes SU(2)_R]/Z_2$ is compact. In addition, since we will be considering fermions, we in fact work with the covering group $Spin(4)$.

an operator basis with the EOM redundancy removed, but the IBP redundancy still present. A procedure which additionally takes care of the IBP redundancy was first proposed in [23], their main insight the realization that the single particle modules coincide with unitary conformal representations of free fields. The conformal group in four dimensions is isomorphic to $SO(4,2) \simeq SO(6,\mathbb{C})$ and its representations consist of a primary operator $\mathcal{O}_l$ and an infinite tower of derivatives acting on it, its descendants. Schematically, they are of the form

$$R_{[\Delta;l]} \sim \begin{pmatrix} \mathcal{O}_l \\ \partial\mathcal{O}_l \\ \partial^2\mathcal{O}_l \\ \vdots \end{pmatrix} . \tag{11.46}$$

The representations are labeled by the scaling dimension Δ and the Lorentz representation $l = (l_1, l_2) \in SU(2)_L \times SU(2)_R$ of the primary operator, where l_i denotes the $2\,l_i + 1$ dimensional representation. For a conformal representation to be unitary its scaling dimension Δ has to satisfy a lower bound Δ_l [341]

$$\begin{aligned} &\Delta \geq \Delta_l = l_1 + l_2 + 2 \qquad && l_1 \neq 0, \quad l_2 \neq 0\,, \\ &\Delta \geq \Delta_l = l_1 + l_2 + 1 \qquad && l_1 l_2 = 0\,. \end{aligned} \tag{11.47}$$

Conformal representations of free fields saturate the unitarity bound, i.e. $\Delta = \Delta_l$ [341–343], which causes some of its descendants to be absent (avoiding negative-norm descendants). Such descendants are exactly those that vanish due to the free EOM. This implies that any local operator can now be constructed by taking tensor products of single particle modules, i.e. tensor products of unitary conformal representations. These tensor products can in turn be decomposed into irreducible conformal representations $\mathcal{O}'$

$$\begin{pmatrix} \mathcal{O}_l \\ \partial\mathcal{O}_l \\ \partial^2\mathcal{O}_l \\ \vdots \end{pmatrix}^{\otimes n} = \sum_{\mathcal{O}'} \begin{pmatrix} \mathcal{O}' \\ \partial\mathcal{O}' \\ \partial^2\mathcal{O}' \\ \vdots \end{pmatrix} . \tag{11.48}$$

The set of all scalar primaries in the tensor product are independent operators with both the IBP and EOM redundancy removed. Therefore, in order to obtain a basis of operators for the EFT, one only has to consider all possible tensor products and project out the scalar $[\Delta, (0,0)]$ representations for all Δ. The corresponding primaries form the EFT basis. Using conformal group characters $\chi_{[\Delta;l]}$, the Hilbert series is schematically

$$\mathcal{H} \sim \int d\mu_{\text{conformal}} \sum_{\Delta} \chi_{[\Delta;(0,0)]}\, \text{PE}[\{\phi_a\}]\,. \tag{11.49}$$

Including the integral over possible gauge groups to project out the gauge invariant operators and performing the integral associated with the dilatations one obtains the expression for the Hilbert series[8] (see [23] for details)

$$\mathcal{H}(\mathcal{D}, \{\phi_i\}) = \mathcal{H}_0(\mathcal{D}, \{\phi_i\}) + \Delta\mathcal{H}(\mathcal{D}, \{\phi_i\})\,, \tag{11.50}$$

[8] Note that Eq. (11.51) still holds even if the single particle module is not a unitary conformal representation [23]. However, a closed form expression for $\Delta\mathcal{H}(\mathcal{D}, \{\phi_i\})$ exists only for unitary conformal representations.

with $\mathcal{H}_0(\mathcal{D},\{\phi_i\})$ given by

$$\mathcal{H}_0(\mathcal{D},\{\phi_i\}) = \int d\mu_{\text{Lorentz}}(x) \int d\mu_{\text{gauge}}(y) \frac{1}{P(\mathcal{D},x)} \prod_i \text{PE}\left[\frac{\phi_i}{\mathcal{D}^{\Delta_i}}\right], \tag{11.51}$$

where we denoted the single particle modules by their primaries (i.e. ϕ_i for R_{ϕ_i}), and recall that ϕ_i comes with its character χ_{ϕ_i} in the PE. The group characters for the single particle modules are a product of the conformal and gauge group characters

$$\chi_{\phi_i}(\mathcal{D};x,y) = \chi_{[\Delta_{\phi_i};l_i]}(\mathcal{D};x)\cdot\chi_{\text{gauge}}(y)\,. \tag{11.52}$$

Furthermore, $\Delta\mathcal{H}(\mathcal{D},\{\phi_i\})$ in Eq. (11.50) contains terms of at most scaling dimension 4, and arises from subtleties regarding the orthonormality of the group characters of conformal representations saturating the unitarity bound; basically, the absence of descendants of the form $\Box\mathcal{O}$ and/or $\partial_\mu\mathcal{O}^\mu$ (associated with the EOMs). An explicit expression can be found in [23]. The $1/P(\mathcal{D},x)$ factor corrects for the IBP redundancy, with $P(\mathcal{D},x)$ being the momentum generating function that encodes the information about the symmetric tensor products of derivatives ($\mathcal{D}$ transforming in the fundamental $(\frac{1}{2},\frac{1}{2})$ representation of the Lorentz group) and is given by (see Appendix III.E for symmetric tensor products)

$$P(\mathcal{D},x) = \sum_{d=0}^{\infty} \mathcal{D}^d\, \chi_{\text{Sym}^d(1/2,1/2)}(x) = \frac{1}{\det_{(1/2,1/2)}(1-\mathcal{D}\,g)}\,. \tag{11.53}$$

The conformal characters are obtained by tracing over the sum of Lorentz representations in the single particle module weighted with the corresponding scaling dimensions. For instance, for a scalar field with primary scaling dimension $\Delta_\phi = 1$ for the primary and single particle module given in Eq. (11.45), the conformal character is

$$\chi_{[1;(0,0)]}(\mathcal{D};x) = \mathcal{D}(1-\mathcal{D}^2)\sum_{d=0}^{\infty}\mathcal{D}^d\,\chi_{\text{Sym}^d(1/2,1/2)}(x) = \mathcal{D}\,P(\mathcal{D},x)(1-\mathcal{D}^2)\,. \tag{11.54}$$

The $\mathcal{D}^1$ factor in Eq. (11.54) is due to the scaling dimension of the primary, while each additional power of $\mathcal{D}$ corresponds to a derivative (the subtraction of $\mathcal{D}^2$ in the parenthesis is due to $\Delta_\phi = \Delta_0$ saturating the unitarity bound). Therefore, if each spurion ϕ_i in Eq. (11.51) is weighted by $\mathcal{D}^{-\Delta_{\phi_i}}$, any occurrence of $\mathcal{D}$ in the Hilbert series will be associated with a derivative. Let us finally note that generically the Hilbert series cannot be computed in full but only as an expansion following a given grading. A common grading is to use the mass dimension $[\phi_i]$ of the operators, i.e. we rescale the spurions $\phi_i \to \epsilon^{[\phi_i]}\phi_i$, $\mathcal{D}\to\epsilon\mathcal{D}$ and expand the Hilbert series in powers of ϵ

$$\mathcal{H}(\mathcal{D},\{\phi_i\};\epsilon) = \sum_n \epsilon^n\,\mathcal{H}_n(\mathcal{D},\{\phi_i\})\,. \tag{11.55}$$

Explicit expressions for $P(\mathcal{D},x)$ and for the conformal and gauge characters and the integration measures, which will be relevant in the following, can be found in Appendix III.C.

We wish to note at this point that the Hilbert series systematically counts the operators at a given order in fields and derivatives, yet it does not explicitly construct them. While knowing the number of operators is exceedingly useful for the latter task, algorithms to directly construct the operators are being developed in the context of the S-matrix [344, 345].

11.5.3 Example: generalized Euler-Heisenberg Lagrangian

Let us end this section with the discussion of a simple and instructive example, the generalization of the well-known Euler-Heisenberg Lagrangian, i.e. we construct the most general EFT for an abelian gauge field.[9] The basic building block is the gauge invariant abelian field strength $F_{\mu\nu}$, which satisfies the free EOM

$$\partial_\mu F^{\mu\nu} = 0\,. \tag{11.56}$$

From the Bianchi identity $\partial_{[\alpha}F_{\mu\nu]} = 0$ it also follows that

$$\partial^2 F_{\mu\nu} = 0\,. \tag{11.57}$$

Therefore, the single particle module contains only symmetric and traceless combinations of derivatives of the field strength tensor [23]

$$R_F = \begin{pmatrix} F_{\mu\nu} \\ \partial_{\{\mu_1}F_{\mu\}\nu} \\ \partial_{\{\mu_1}\partial_{\mu_2}F_{\mu\}\nu} \\ \vdots \end{pmatrix}\,. \tag{11.58}$$

The field strength transforms in the reducible $(1,0)\oplus(0,1)$ representation of the Lorentz group. We will therefore work with the combinations $F^{L,R}_{\mu\nu} = \frac{1}{2}(F_{\mu\nu} \pm i\tilde{F}_{\mu\nu})$ of the field strength and its dual $\tilde{F}_{\mu\nu} = \frac{1}{2}\epsilon_{\mu\nu\rho\sigma}F^{\rho\sigma}$ which live in the $(1,0)$ and $(0,1)$ representations, respectively. The conformal character associated with $F^{L,R}_{\mu\nu}$ is the sum of the characters for the Lorentz representations of the elements in the single particle module in Eq. (11.58), weighted by the scaling dimension ($\Delta_{F_{L,R}} = 2$), i.e. for $F^L_{\mu\nu}$

$$\chi_{[2;(1,0)]}(\mathcal{D};x) = \mathcal{D}^2\,P(\mathcal{D},x)\big(\chi_{(1,0)}(x) - \chi_{(1/2,1/2)}(x)\,\mathcal{D} + \mathcal{D}^2\big)\,, \tag{11.59}$$

and the same with $\chi_{(1,0)}(x)$ replaced by $\chi_{(0,1)}(x)$ for $F^R_{\mu\nu}$. The first term in the parenthesis is the Lorentz representation of the conformal primary, i.e. the field strength, with a tower of symmetrized derivatives generated by $P(\mathcal{D},x)$. The second term subtracts all the descendants where one derivative is contracted with the field strength, corresponding to the Lorentz representation $\partial_\mu F^{L,\mu\nu} \sim (\frac{1}{2},\frac{1}{2})\otimes_A(1,0) = (\frac{1}{2},\frac{1}{2})$. However, this means that also the term $\partial_\mu\partial_\nu F^{L,\mu\nu} \sim (0,0)$ and derivatives thereof are being subtracted, even though they vanish due to the antisymmetry of the field strength and thus were never there from the beginning. For this reason they are added back in the form of the third term in the parenthesis. The structure of Eq. (11.59) can also be understood directly in terms of conformal representations [342]. Since abelian field strengths are gauge invariant, the full group characters are $\chi_{F_L} = \chi_{[2;(1,0)]}(\mathcal{D};x)$ and $\chi_{F_R} = \chi_{[2;(0,1)]}(\mathcal{D};x)$ and the integral over the gauge group is trivial $\int d\mu_{\text{gauge}} = \int d\mu_{U(1)} = 1$. The Hilbert series in the mass dimension grading scheme, i.e. $F_{L,R} \to \epsilon^2\,F_{L,R}$ and $\mathcal{D} \to \epsilon\,\mathcal{D}$, is thus given by

$$\begin{aligned}\mathcal{H}_0(\mathcal{D},F_L,F_R;\epsilon) &= \int d\mu_{\text{Lorentz}}(x)\frac{1}{P(\epsilon\,\mathcal{D},x)}\text{PE}\left[\frac{F_L}{\mathcal{D}^2},\frac{F_R}{\mathcal{D}^2}\right] \\ &= \epsilon^8\big(F_L^4 + F_L^2F_R^2 + F_R^4\big) + \epsilon^{10}\big(F_L^4 + F_L^3F_R + F_L^2F_R^2 + F_LF_R^3 + F_R^4\big)\mathcal{D}^2 + \dots\,.\end{aligned} \tag{11.60}$$

Eq. (11.60) gives the structure and multiplicity of the operator basis at mass dimension 5 and higher, but it does not reveal how the Lorentz (and gauge) indices of the field strengths and

[9] The original Euler-Heisenberg Lagrangian [346] is the EFT for QED at energies much below the electron mass. The $\mathcal{CP}$ symmetry of QED forbids $\mathcal{CP}$ breaking terms in the Euler-Heisenberg Lagrangian; here we extend it by including $\mathcal{CP}$ violating operators.

derivatives are contracted. However, if the field content of an operator is known, it is usually straightforward to build Lorentz and gauge invariants. This is especially true if the multiplicity of a given structure is one, since then any non-vanishing contraction can be used as a basis element. The operator basis implied by the Hilbert series in Eq. (11.60) can be expressed in terms of $F_{\mu\nu}$ and $\tilde{F}_{\mu\nu}$. At mass dimension 8 this is, explicitly,

$$\mathcal{L} = \frac{c_1}{\Lambda^4}(F_{\mu\nu}F^{\mu\nu})^2 + \frac{c_2}{\Lambda^4}(F_{\mu\nu}\tilde{F}^{\mu\nu})^2 + \frac{ic_3}{\Lambda^4}(F_{\mu\nu}F^{\mu\nu})(F_{\rho\sigma}\tilde{F}^{\rho\sigma}) + \dots\,, \tag{11.61}$$

where the first two terms also appear in the Euler-Heisenberg Lagrangian. The operator proportional to c_3 is $\mathcal{CP}$ violating and therefore constitutes an extension of the Euler-Heisenberg Lagrangian. Finally, we note that this method automatically takes algebraic identities, such as $F_{\mu\nu} = -F_{\nu\mu}$ in this simple case, into account. This is because the Hilbert series directly uses group representations to build the invariants, instead of explicitly contracting indices.

Chapter 12

One-loop matching of a singlet scalar

As we have argued in Section 11.3, it is natural to view the renormalizable SM Lagrangian as merely the leading order contribution of an EFT, the so-called SMEFT. The EFT framework, which we introduced in Chapter 11, provides a well-defined and model-independent way to characterize and constrain heavy new physics. However, a completely unbiased approach is hardly feasible: already at mass dimension six there are 2499 independent baryon number conserving operators [22, 23]. In order to reduce this number to a manageable amount, one has to make assumptions about the UV theory, such as for instance flavor symmetries. In order to justify such assumptions it is of utmost importance to build a dictionary of possible UV complete theories and the SMEFT Wilson coefficients, which are generated when integrating out the heavy physics. This information is not only useful to estimate the expected size of Wilson coefficients, but will be crucial to identify the nature of new physics when a deviation from the SM prediction is found in an observable.

Such a dictionary for tree-level matching of UV theories with general scalar, spinor and vector field content and arbitrary interactions has been presented in [347]. One-loop matching calculations are, however, only available for a small set of specific models, but there is an ongoing effort to unify the computation of one-loop matching contributions in the so-called universal one-loop effective action (UOLEA) approach [318] that generalises methods based on a covariant derivative expansion [317] (see also the discussion in Section 11.1).

The arguably simplest renormalizable extension of the SM is the addition of a real singlet scalar ϕ, which we will call SSM in the following. The corresponding Lagrangian can be written as

$$\mathcal{L}_{\text{SSM}} = \mathcal{L}_{\text{SM}} + \frac{1}{2}(\partial_\mu \phi)^2 - \frac{1}{2}M^2\phi^2 - A|H|^2\phi - \frac{1}{2}\kappa|H|^2\phi^2 - \frac{1}{3!}\mu\phi^3 - \frac{1}{4!}\lambda_\phi\phi^4\,, \tag{12.1}$$

where we have ignored a potential tadpole contribution, meaning that the field ϕ in Eq. (12.1) corresponds to the excitation around a possible non-zero vacuum expectation value. The parameters M^2, A, κ, μ and λ_ϕ appearing in Eq. (12.1) are treated as independent in what follows.

Due to its simplicity the SSM is a perfect benchmark scenario for studies within the SMEFT. However, its importance extends far beyond the use as a benchmark scenario. Many well-motivated BSM theories contain singlet scalars which couple to the Higgs. They appear e.g. in the context of electroweak baryogenesis [208], as scalar top partners in neutral naturalness [209, 210] and in scalar DM models. A particularly interesting scenario concerns pNGB DM, which can be realized in simple scalar extensions of the SM (see e.g. [129, 131] and the discussion in Section 3.3). In order to arrive at the pNGB DM Lagrangian, which we discussed at length in Chapter 3, a heavy radial mode with couplings to the SM Higgs as in Eq. (12.1) has to be integrated out. This does not only generate the derivative Higgs portal but also pure SMEFT

operators. The knowledge of these effective operators is crucial when one wants to explore one-loop probes of the pNGB DM in SM processes, such as for instance off-shell Higgs production, employing an EFT for the SM plus the DM candidate. This will be studied in an upcoming publication [306], for which the matching calculation in this chapter is an important ingredient.

For all of the above applications a precise matching calculation to the SMEFT Lagrangian is required. The first one-loop matching corrections at dimension-six for the SSM have been obtained in [21], using a combination of the UOLEA master formulae of [20] and Feynman calculus. In this chapter, we repeat the calculation of [21] from scratch, relying entirely on the use of Feynman diagrams. With the help of our independent computation we are able to identify terms that have been missed in the existing calculations [20, 21] — small discrepancies in the latter publications have already been noted in the presentation [348]. We want to stress that these discrepancies are due to oversights, and not due to structural limitations of the UOLEA approach. See Appendix III.A for further explanations.

In Section 12.1 we set the notation for our computation, before we perform the one-loop matching in Section 12.2. These results were previously published in [33][1] from where all Figures and parts of the text are taken.

12.1 Setup and notation

In order to set up our notation and conventions, let us first define the EW part of the SM. Before spontaneous EW symmetry breaking the tree-level EW SM Lagrangian takes the following familiar form,

$$\begin{aligned}\mathcal{L}_{\text{SM}} = (D_\mu H)^\dagger (D^\mu H) + \mu_h^2 |H|^2 - \frac{1}{2}\lambda_h |H|^4 - \frac{1}{4} B_{\mu\nu} B^{\mu\nu} - \frac{1}{4} W^a_{\mu\nu} W^{a\,\mu\nu} \\ + \sum_{f\,=\,q,u,d,\ell,e} \bar{f} i \not{D} f - \left(y_u \bar{q} \widetilde{H} u + y_d \bar{q} H d + y_e \bar{\ell} H e + \text{h.c.} \right) .\end{aligned} \tag{12.2}$$

Here H denotes the SM Higgs doublet and the shorthand notation $\widetilde{H}_i = \epsilon_{ij} (H_j)^*$ with ϵ_{ij} totally antisymmetric and $\epsilon_{12} = 1$ has been used. The covariant derivative is defined as

$$D_\mu = \partial_\mu - i g_1 Y B_\mu - i g_2 \frac{\sigma^a}{2} W^a_\mu \,, \tag{12.3}$$

with g_1 and g_2 the $U(1)_Y$ and $SU(2)_L$ gauge coupling, respectively, and B_μ and W^a_μ ($B_{\mu\nu}$ and $W^a_{\mu\nu}$) the corresponding gauge fields (field strength tensors). The hypercharge operator is denoted by Y with eigenvalues $\{Y_H, Y_q, Y_u, Y_d, Y_\ell, Y_e\} = \{1/2, 1/6, 2/3, -1/3, -1/2, -1\}$ and σ^a are the Pauli matrices. The Yukawa couplings y_u, y_d and y_e are matrices in flavour space and a sum over flavour indices is implicit in Eq. (12.2). Finally, the symbols q and ℓ denote left-handed quark and lepton doublets, while u, d and e are right-handed fermion singlets.

As stated before, the goal of this chapter is to calculate the complete matching corrections up to one-loop order that arise in the SSM. At the renormalizable level, Lorentz and gauge invariance allow a real singlet scalar to couple to the SM exclusively through $|H|^2$. The resulting Lagrangian is shown in Eq. (12.1).

[1] [33]: U. Haisch, M. Ruhdorfer, E. Salvioni, E. Venturini and A. Weiler, *Singlet night in Feynman-ville: one-loop matching of a real scalar.*

12.2 Matching calculation

By integrating out the field ϕ that appears in the SSM Lagrangian Eq. (12.1) one can determine the Wilson coefficients C_k that multiply the operators Q_k in the SMEFT

$$\mathcal{L}_{\text{SMEFT}} = \sum_k C_k Q_k \,, \tag{12.4}$$

order by order in perturbation theory by performing a loop expansion $C_k = C_k^{(0)} + C_k^{(1)}/(4\pi)^2 + \ldots$ (cf. Eq. (11.7)). This notation will also be used when expanding other quantities of interest. The full set of dimension-six SMEFT operators has been presented in the so-called Warsaw basis in [326]. Up to the one-loop level, it turns out that matching the theory described by the Lagrangian Eq (12.1) to the SMEFT Lagrangian Eq. (12.4) generates non-zero Wilson coefficients for the following set of 18 effective operators:

$$\begin{aligned}
Q_{H\Box} &= |H|^2 \Box |H|^2 \,, & Q_{Hu} &= (H^\dagger i\overset{\leftrightarrow}{D}_\mu H)(\bar{u}\gamma^\mu u) \,, \\
Q_{H} &= |H|^6 \,, & Q_{Hd} &= (H^\dagger i\overset{\leftrightarrow}{D}_\mu H)(\bar{d}\gamma^\mu d) \,, \\
Q_{HD} &= (H^\dagger D_\mu H)^* (H^\dagger D^\mu H) \,, & Q_{Hud} &= (i\widetilde{H}^\dagger D_\mu H)(\bar{u}\gamma^\mu d) \,, \\
Q_{HB} &= |H|^2 B_{\mu\nu} B^{\mu\nu} \,, & Q_{He} &= (H^\dagger i\overset{\leftrightarrow}{D}_\mu H)(\bar{e}\gamma^\mu e) \,, \\
Q_{HW} &= |H|^2 W^a_{\mu\nu} W^{a\,\mu\nu} \,, & Q^{(1)}_{Hq} &= (H^\dagger i\overset{\leftrightarrow}{D}_\mu H)(\bar{q}\gamma^\mu q) \,, \\
Q_{HWB} &= (H^\dagger \sigma^a H) W^a_{\mu\nu} B^{\mu\nu} \,, & Q^{(3)}_{Hq} &= (H^\dagger i\overset{\leftrightarrow}{D}^a_\mu H)(\bar{q}\gamma^\mu \sigma^a q) \,, \\
Q_{uH} &= |H|^2 (\bar{q}\widetilde{H} u) \,, & Q^{(1)}_{H\ell} &= (H^\dagger i\overset{\leftrightarrow}{D}_\mu H)(\bar{\ell}\gamma^\mu \ell) \,, \\
Q_{dH} &= |H|^2 (\bar{q} H d) \,, & Q^{(3)}_{H\ell} &= (H^\dagger i\overset{\leftrightarrow}{D}^a_\mu H)(\bar{\ell}\gamma^\mu \sigma^a \ell) \,, \\
Q_{eH} &= |H|^2 (\bar{\ell} H e) & Q_{2y} &= \left|\bar{q}_j y_u u \epsilon^{ji} + \bar{d} y_d^\dagger q^i + \bar{e} y_e^\dagger \ell^i\right|^2 .
\end{aligned} \tag{12.5}$$

Here $\Box = \partial_\mu \partial^\mu$, $H^\dagger i\overset{\leftrightarrow}{D}_\mu H = iH^\dagger\big(D_\mu - \overleftarrow{D}_\mu\big)H$ and $H^\dagger i\overset{\leftrightarrow}{D}^a_\mu H = iH^\dagger\big(\sigma^a D_\mu - \overleftarrow{D}_\mu \sigma^a\big)H$. For the operators $Q_{\psi H}$ with $\psi = u, d, e$, as well as for Q_{Hud}, the sum of the hermitian conjugate in Eq. (12.4) is understood.

The matching of Eq. (12.1) onto Eq. (12.4) can be performed using either Feynman diagrams or functional methods. In fact, the work [20] employed the UOLEA approach to calculate the heavy (i.e. only ϕ loops) and the heavy-light (i.e. loops with both ϕ and Higgs exchange) one-loop matching corrections for the Wilson coefficients $C_{H\Box}$ and C_H. Based on the results of that article, the paper [21] then presented the complete one-loop matching corrections in the model described by Eq. (12.1), computing the missing heavy-light contributions involving a ϕ scalar and a gauge boson or a fermion, by means of traditional Feynman diagram techniques.[2]

In contrast to [20,21] our calculation of the Wilson coefficients $C_k^{(0)}$ and $C_k^{(1)}$ relies on Feynman diagrams only, and therefore represents an independent cross-check of the results obtained earlier. To allow for a direct comparison with the expressions given in the publications [20, 21], we regularize UV divergences using dimensional regularization (DR) in $d = 4 - 2\epsilon$ dimensions and renormalize the results in the $\overline{\text{MS}}$ scheme supplemented by the renormalization scale μ_R. IR divergences have also been regularized dimensionally. The matching corrections can therefore be found by simply Taylor expanding the corresponding scattering amplitudes in powers

[2] The correction to the operator Q_{Hud} was not given in [21]. It was also missed in previous versions of [33].

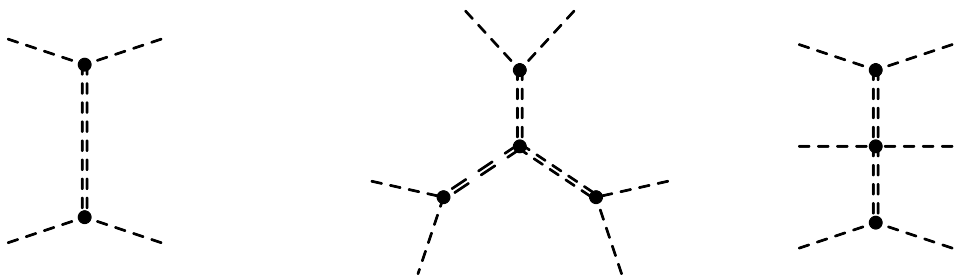

Figure 12.1: Example diagrams that contribute to the tree-level matching coefficients $\lambda_h^{(0)}$ and $C_{H\Box}^{(0)}$ (left) and $C_H^{(0)}$ (right), respectively. Double-dashed lines represent virtual exchange of the heavy real singlet scalar field ϕ, while single-dashed lines stand for H or $H^\dagger$ fields. This Figure was adopted from [33].

of external momenta squared divided by M^2 before performing any loop integration (see discussion in Section 11.1.1.B). On the other hand, SMEFT loop graphs do not contribute to the matching, because after Taylor expansion of the integrands they involve only scaleless integrals which vanish in DR — see e.g. [349,350] for further technical details. The actual generation and computation of the off-shell amplitudes made use of the `Mathematica` packages `FeynArts` [351], `FeynRules` [164], `FormCalc` [352] and `Package-X` [353], and part of the one-loop matching corrections obtained by computer were also verified with pen and paper.

12.2.1 Tree-level results

In the SM extension Eq. (12.1) only the Higgs quartic $|H|^4$ $\big($cf. Eq. (12.2)$\big)$ and the two effective operators $Q_{H\Box}$ and Q_H $\big($see Eq. (12.5)$\big)$ receive a non-zero matching correction at tree level. The corresponding Feynman diagrams are shown in Figure 12.1. For the additive shift $\lambda_h^{(0)}$ of the quartic Higgs coupling, i.e. $\lambda_h \to \lambda = \lambda_h + \lambda_h^{(0)}$, in agreement with [21] we find

$$\lambda_h^{(0)} = -\frac{A^2}{M^2}\,, \tag{12.6}$$

while in the case of the Wilson coefficients we obtain

$$C_{H\Box}^{(0)} = -\frac{A^2}{2M^4}\,, \tag{12.7}$$

$$C_H^{(0)} = \frac{A^3\mu}{6M^6} - \frac{A^2\kappa}{2M^4}\,. \tag{12.8}$$

The results Eq. (12.7) and Eq. (12.8) are well-known and agree with the analytic expressions reported for instance in the works [21,317,347].

12.2.2 One-loop results

In order to determine the one-loop matching corrections $C_k^{(1)}$ to the Wilson coefficients of the dimension-six SMEFT operators Q_k as given in Eq. (12.5), we consider only Feynman diagrams that are one-particle-irreducible in the light fields, i.e. we work in the so-called Green's basis defined in [21], subsequently projecting our off-shell results onto the Warsaw basis using the operator identities given in Appendix A of the latter paper.

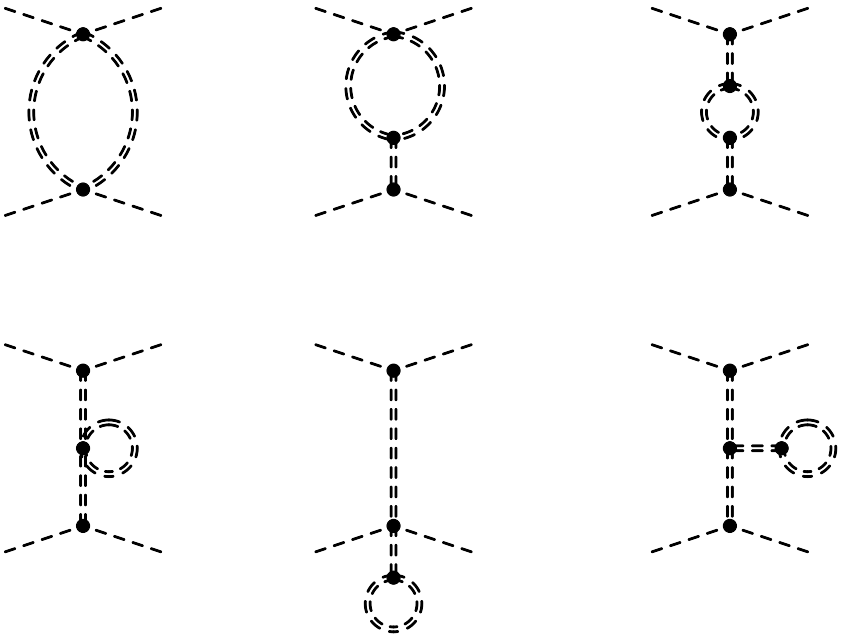

Figure 12.2: Examples of heavy contributions to the one-loop matching correction $C_{H\Box}^{(1)}$. The line styles and their meanings resemble those of Figure 12.1. This Figure is taken from [33].

The one-loop matching corrections of the tree-level operators $Q_{H\Box}$ and Q_H receive contributions from three sources that we describe in the following. The first two types encode the threshold effects at a matching scale μ_M around M. The first kind of threshold corrections arise from heavy loops. For the case of $C_{H\Box}^{(1)}$, the relevant graphs are shown in Figure 12.2. Notice that diagrams with ϕ tadpoles in general contribute to this type of corrections, hence the analytic expressions for the heavy contributions to the Wilson coefficients $C_{H\Box}^{(1)}$ and $C_H^{(1)}$ depend on how the tadpole contributions are fixed. In our diagrammatic calculation, as well as in the UOLEA approach described in Appendix III.A, we renormalize ϕ tadpoles minimally [354, 355] and Eqs. (12.10), (12.12), (III.A.8) and (III.A.9) therefore correspond to the $\overline{\text{MS}}$ scheme. Notice that in the $\overline{\text{MS}}$ scheme the effective one-loop scalar potential contains a term linear in the ϕ field, which by definition would be absent in the on-shell scheme where the tadpole counterterm is fixed such that all tadpole diagrams vanish [356] — see also [357–359] for excellent discussions of the different treatments of tadpoles.

The second type of threshold corrections to $C_{H\Box}^{(1)}$ and $C_H^{(1)}$ stem from heavy-light loop diagrams involving either a H or a B_μ (W_μ^a) field. Universal effects related to the wave function renormalization of the Higgs field belong to this class. In fact, after the field redefinition $H \to \left(1 - Z_H^{(1)}/(4\pi)^2\right)H$ the Wilson coefficients $C_{H\Box}$ and C_H receive a one-loop contribution proportional to $C_{H\Box}^{(0)}$ and $C_H^{(0)}$, respectively. The relevant wave function renormalization constant $Z_H^{(1)}$ is determined by calculating the one-loop corrections to the Higgs kinetic term $(D_\mu H)^\dagger (D^\mu H)$ that arises from the graph displayed on the left in Figure 12.3. In agreement with [21] we obtain

$$Z_H^{(1)} = \frac{A^2}{4M^2}\,. \tag{12.9}$$

In addition to the wave function renormalization contributions, non-universal heavy-light cor-

Figure 12.3: Higgs wave function renormalization effects. Left: heavy-light contribution to $Z_H^{(1)}$ in (12.9). Right: gauge-boson and fermionic contributions to the anomalous dimensions of the SSM parameters A and κ in Eq. (III.B.3) and Eq. (III.B.4). The wiggly line corresponds to a B_μ or W_μ^a field, the solid straight lines represent fermion fields, while the rest of the line styles and their meanings are identical to those employed in Figure 12.1. This Figure is taken from [33].

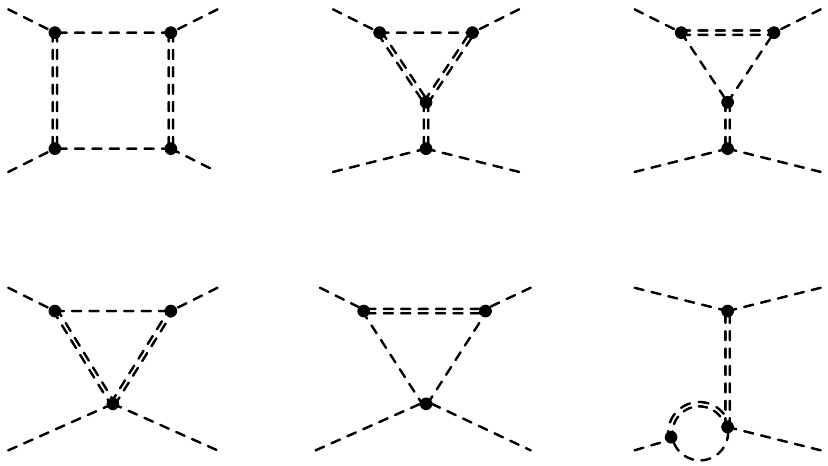

Figure 12.4: Examples of heavy-light scalar contributions to the one-loop matching correction $C_{H\Box}^{(1)}$. Diagrams with loops that contain only H fields are not shown, since they evaluate to zero in DR if the H fields are taken to be massless before Taylor expanding the corresponding loop integrals. The line styles and their meanings resemble those of Figure 12.1. This Figure has been adopted from [33].

rections arise. The corresponding scalar and gauge-boson contributions to $C_{H\Box}^{(1)}$ are displayed in Figure 12.4 and Figure 12.5, respectively. Notice that when IR divergences are regulated dimensionally, SSM diagrams involving only light particles in the loop do not need to be considered, because such graphs result in scaleless integrals after Taylor expanding the associated off-shell amplitudes in powers of external momenta squared divided by M^2. This should be contrasted to methods that use small external momenta or small light-field masses as IR regulators (cf. for instance [360–362]). In these cases, SSM diagrams with only light particles in the loop give non-zero IR divergent corrections but their contributions are exactly cancelled by the corresponding SMEFT graphs. As a result, the one-loop matching corrections $C_{H\Box}^{(1)}$ and $C_H^{(1)}$ turn out to be independent of the procedure that is used to regulate IR divergences (as they should), and in our calculation we have employed DR to regulate both UV and IR divergences simply because it is technically the easiest method to implement.

The third type of corrections to $C_{H\Box}^{(1)}$ and $C_H^{(1)}$ arise instead from the renormalization of the

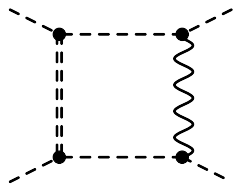

Figure 12.5: Example of a heavy-light gauge-boson contribution to the one-loop matching correction $C_{H\Box}^{(1)}$. Graphs with loops of only H and B_μ, or H and W_μ^a fields are not displayed, because such diagrams do not contribute if IR divergences are regulated dimensionally. The line styles and their meanings mirror those in Figure 12.3. This Figure is taken from [33].

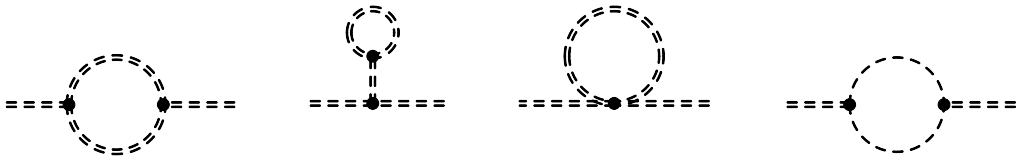

Figure 12.6: One-loop contributions to the propagator of the real singlet scalar. In the $\overline{\text{MS}}$ scheme the UV poles of the first and second diagram cancel against each other. The line styles and their meanings are identical to those employed in Figure 12.1. This Figure has been adopted from [33].

SSM parameters that enter the tree-level Wilson coefficients (see e.g. [312] for a pedagogical discussion). These contributions are, therefore, purely logarithmic in the $\overline{\text{MS}}$ scheme. The logarithmic terms proportional to the SM couplings generate a RG flow that extends below the matching scale, providing one of the contributions to the anomalous dimensions of the SMEFT Wilson coefficients. These effects, coming from light loops, give the same corrections to both the SSM and SMEFT amplitudes. On the other hand, the RG-flow contributions proportional to UV SSM parameters appear only above μ_M. The anomalous dimension of M^2 is obtained from the Feynman diagrams shown in Figure 12.6, while Figure 12.7, Figure 12.8 and Figure 12.9 display example graphs of contributions to the running of A, κ and μ, respectively. Notice that the anomalous dimensions that describe the RG flow of the SSM parameters A and κ also contain pieces arising from the light contributions to the Higgs wave function displayed on the right-hand side in Figure 12.3, since the corresponding operators contain two powers of the H field. See Appendix III.B for further details and explanations.

In the case of the dimension-six SMEFT operator $Q_{H\Box}$, we find after combining the three different types of contributions described above the following result for the one-loop matching correction:

$$\begin{aligned} C_{H\Box}^{(1)} = &-\frac{\kappa^2}{24M^2} + \frac{25A^2\kappa - 6A^2\lambda_\phi - 5A\kappa\mu}{12M^4} + \frac{38A^4 - 26A^3\mu + 11A^2\mu^2}{24M^6} \\ &- \frac{31A^2\left(g_1^2 + 3g_2^2\right)}{72M^4} + \tilde{\gamma}_{H\Box,H\Box}\, C_{H\Box}^{(0)} \ln\frac{\mu_M}{M}\,. \end{aligned} \tag{12.10}$$

Here

$$\tilde{\gamma}_{H\Box,H\Box} = 12\lambda - \frac{4}{3}\left(g_1^2 + 3g_2^2\right) + 4y_2\,, \tag{12.11}$$

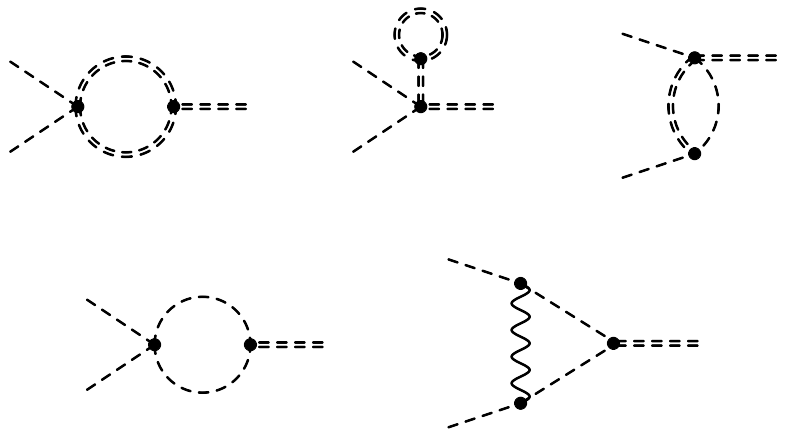

Figure 12.7: Examples of one-loop contributions to the renormalization of the coupling A. The UV poles of the first and second graph cancel against each other in the $\overline{\text{MS}}$ scheme. The line styles and their meanings are analogue to those of Figure 12.5. This Figure has been taken from [33].

with λ denoting the quartic Higgs coupling that includes the tree-level shift of Eq. (12.6) and the objects $C_{H\Box}^{(0)}$ and y_2 defined in Eq. (12.7) and Eq. (III.B.8), respectively. Notice that all mass and coupling parameters in Eq. (12.10), Eq. (12.11) as well as in the tree-level expression Eq. (12.7) are renormalized at the scale M. Also note that we use a different normalization of the anomalous dimension as in Section 11.2. We define $d/(d\ln\mu)\,C(\mu) = \tilde{\gamma}_C/(4\pi^2)$ and mark the anomalous dimensions according to this definition with a tilde to differentiate them from the definition in Section 11.2.

A couple of comments concerning our result Eq. (12.10) seem to be in order. The rational terms in Eq. (12.10) receive contributions from the Higgs wave function renormalization constant Eq. (12.9) and heavy and heavy-light diagrams (see Figure 12.2, Figure 12.4 and Figure 12.5), while the logarithmic terms result from the combination of heavy and heavy-light graphs as well as the renormalization of M^2 and A according to Eq. (III.B.2) and Eq. (III.B.3). In fact, the logarithmic pieces proportional to SM couplings combine to give the anomalous dimension $\tilde{\gamma}_{H\Box,H\Box}$, whereas the remaining terms cancel, because they do not run below the matching scale (see Appendix III.B for further details). The anomalous dimension describes the self-mixing of the dimension-six operator $Q_{H\Box}$, and our expression Eq. (12.11) agrees with the results of the direct calculation of $\tilde{\gamma}_{H\Box,H\Box}$ presented in [24–26] — the found agreement constitutes a non-trivial cross-check of our computation. We add that the logarithmic corrections in Eq. (12.10) are scheme-independent, while the rational terms in $C_{H\Box}^{(1)}$ depend on the choice of renormalization scheme, including the specific treatment of ϕ tadpoles. Notice that the cancellation in Eq. (12.10) of logarithms that are not proportional to SM couplings is crucial to achieve the correct factorisation of short-distance and long-distance effects. In fact, in the SMEFT only the combination of SSM parameters that forms a Wilson coefficient has a non-trivial RG flow, together with the SM couplings λ, g_1, g_2 and y_f. Thus, the correct description of long-distance physics has to be formulated in terms of the SM couplings and the Wilson coefficient $C_{H\Box}$ evaluated at the low-energy scale. Let us finally mention that Eq. (12.10) differs from the expression for $C_{H\Box}^{(1)}$ given in both [20] and [21]. The disagreement has two sources. First, as shown in Appendix III.A, the latter calculations miss certain heavy-loop contributions,

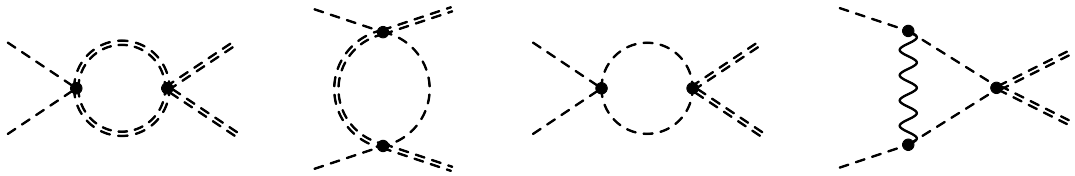

Figure 12.8: Examples of one-loop contributions to the renormalization of the coupling κ. The line styles and their meanings are analogue to those of Figure 12.5. This Figure has been adopted from [33].

Figure 12.9: Examples of one-loop contributions to the renormalization of the coupling μ. The line styles and their meanings resemble those of Figure 12.1. This Figure has been taken from [33].

and second, RG effects associated to the running of SSM parameters have not been explicitly included in the existing computations.

In the case of the operator Q_H, we have calculated the $H \to H$, $HHH \to HHH$, $HH^\dagger \to W_\mu^a$ and $HH \to HHW_\mu^a W_\nu^b$ scattering amplitudes to find the following expression for the one-loop correction to the Wilson coefficient C_H:

$$\begin{aligned} C_H^{(1)} = &-\frac{\kappa^3}{12M^2} - \frac{6A^2\kappa\lambda_\phi + 162A^2\kappa\lambda - 66A^2\kappa^2 - 164A^2\lambda^2 + 3A\kappa^2\mu}{12M^4} \\ &+ \frac{87A^4\kappa - 6A^4\lambda_\phi - 72A^4\lambda - 60A^3\kappa\mu + 4A^3\mu\lambda_\phi + 78A^3\lambda\mu + 6A^2\kappa\mu^2}{12M^6} \\ &- \frac{8A^6 + 21A^5\mu - 12A^4\mu^2 + 2A^3\mu^3}{12M^8} - \frac{31A^2\lambda g_2^2}{18M^4} \\ &+ \left(\tilde{\gamma}_{H,H\Box} C_{H\Box}^{(0)} + \tilde{\gamma}_{H,H} C_H^{(0)}\right) \ln\frac{\mu_M}{M}\,. \end{aligned} \tag{12.12}$$

The anomalous dimensions entering Eq. (12.12) read

$$\tilde{\gamma}_{H,H\Box} = -40\lambda^2 + \frac{20\lambda g_2^2}{3}\,, \tag{12.13}$$

$$\tilde{\gamma}_{H,H} = 54\lambda - \frac{9}{2}\left(g_1^2 + 3g_2^2\right) + 6y_2\,, \tag{12.14}$$

while Eqs. (12.7), (12.8) and (III.B.8) contain the explicit expressions for $C_{H\Box}^{(0)}$, $C_H^{(0)}$ and y_2. All mass and coupling parameters that appear in Eqs. (12.12) to (12.14) as well as in the tree-level expressions Eq. (12.7) and Eq. (12.8) are renormalized at the scale M.

Like in the case of Eq. (12.10), one observes that the logarithmic corrections in Eq. (12.12) involve only anomalous dimensions that depend on SM couplings, but not on SSM parameters.

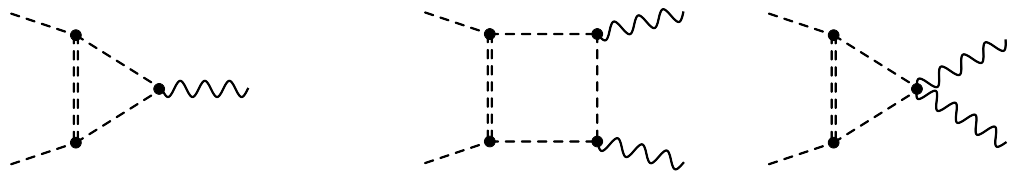

Figure 12.10: Examples of one-loop heavy-light scalar diagrams that need to be considered to extract the one-loop matching corrections of the bosonic dimension-six SMEFT operators in Eq. (12.5) that do not receive a tree-level Wilson coefficient. The line styles and their meanings resemble those of Figure 12.5. This Figure has been adopted from [33].

In fact, our expressions Eq. (12.13) and Eq. (12.14) for $\tilde{\gamma}_{H,H\Box}$ and $\tilde{\gamma}_{H,H}$ agree with the results obtained in [24–26]. The source of the difference between the first four terms in Eq. (12.12) and the rational terms of $C_H^{(1)}$ as quoted in [20, 21] is unraveled in Appendix III.A. In addition, the existing calculations do not explicitly include effects stemming from the renormalization of SSM parameters — cf. Eqs. (III.B.2) to (III.B.5) — and therefore the logarithmic corrections given in Eq. (12.12) differ from the corresponding terms specified in [20, 21] as well.

In the case of the 16 dimension-six SMEFT operators in Eq. (12.5) that do not receive a tree-level Wilson coefficient, only heavy-light Feynman diagrams contribute to the one-loop matching. To extract the relevant one-loop corrections of the bosonic operators, we have calculated the off-shell amplitudes for $HH \to HH$, $HH^\dagger \to V_\mu$ and $HH^\dagger \to V_\mu V'_\nu$ scattering with $V_\mu^{(\prime)} = B_\mu, W_\mu^a$. See Figure 12.10 for the processes with external gauge bosons. We obtain

$$C_{HD}^{(1)} = -\frac{31A^2g_1^2}{18M^4} + \tilde{\gamma}_{HD,H\Box}\, C_{H\Box}^{(0)} \ln\frac{\mu_M}{M}\,, \tag{12.15}$$

$$C_{HB}^{(1)} = \frac{A^2g_1^2}{12M^4}\,, \tag{12.16}$$

$$C_{HW}^{(1)} = \frac{A^2g_2^2}{12M^4}\,, \tag{12.17}$$

$$C_{HWB}^{(1)} = \frac{A^2g_1g_2}{6M^4}\,. \tag{12.18}$$

Here

$$\tilde{\gamma}_{HD,H\Box} = \frac{20g_1^2}{3}\,, \tag{12.19}$$

and the expression for the tree-level Wilson coefficient $C_{H\Box}^{(0)}$ has already been given in Eq. (12.7). We emphasise that our results Eqs. (12.15) to (12.18) agree with Eqs. (A.20) to (A.23) of [21] and that the anomalous dimension Eq. (12.19) matches that calculated in [26]. Notice that in contrast to $C_{HD}^{(1)}$, the Wilson coefficients $C_{HB}^{(1)}$, $C_{HW}^{(1)}$ and $C_{HWB}^{(1)}$ do not receive logarithmic corrections. This feature is expected, because the tree-level operators $Q_{H\Box}$ and Q_H do not mix into Q_{HB}, Q_{HW} and Q_{HWB} at the one-loop level [24–26].

In order to determine the one-loop matching corrections of the fermionic dimension-six SMEFT operators appearing in Eq. (12.5), we have computed the heavy-light scalar contributions to the $HH^\dagger \to \bar{f}f$ and $HH \to H\bar{f}f$ off-shell amplitudes with $f = q, u, d, \ell, e$, as well as to $HH \to u\bar{d}$. Examples of the corresponding diagrams are shown in Figure 12.11. We find

$$C_{\psi H}^{(1)} = -\frac{A^2y_\psi}{36M^4}\left(27\kappa - 87\lambda - \frac{9A\mu}{M^2} + 31g_2^2 - 45y_\psi^\dagger y_\psi\right) + \tilde{\gamma}_{\psi H,H\Box}\, C_{H\Box}^{(0)} \ln\frac{\mu_M}{M}\,, \tag{12.20}$$

Figure 12.11: Examples of one-loop heavy-light scalar diagrams that need to be considered to extract the one-loop matching corrections of the fermionic dimension-six SMEFT operators in Eq. (12.5). The line styles and their meanings duplicate those of Figure 12.3. This Figure has been taken from [33].

$$C_{Hu}^{(1)} = -\frac{A^2}{216M^4}\left(34g_1^2 - 135y_u^\dagger y_u\right) + \tilde{\gamma}_{Hu,H\Box}\, C_{H\Box}^{(0)} \ln\frac{\mu_M}{M}\,, \tag{12.21}$$

$$C_{Hd}^{(1)} = \frac{A^2}{216M^4}\left(17g_1^2 - 135y_d^\dagger y_d\right) + \tilde{\gamma}_{Hd,H\Box}\, C_{H\Box}^{(0)} \ln\frac{\mu_M}{M}\,, \tag{12.22}$$

$$C_{Hud}^{(1)} = -\frac{5A^2}{4M^4}\, y_u^\dagger y_d + \tilde{\gamma}_{Hud,H\Box}\, C_{H\Box}^{(0)} \ln\frac{\mu_M}{M}\,, \tag{12.23}$$

$$C_{He}^{(1)} = \frac{A^2}{72M^4}\left(17g_1^2 - 45y_e^\dagger y_e\right) + \tilde{\gamma}_{He,H\Box}\, C_{H\Box}^{(0)} \ln\frac{\mu_M}{M}\,, \tag{12.24}$$

$$C_{Hq^{(1)}}^{(1)} = -\frac{A^2}{432M^4}\left[17g_1^2 + 135\left(y_u y_u^\dagger - y_d y_d^\dagger\right)\right] + \tilde{\gamma}_{Hq^{(1)},H\Box}\, C_{H\Box}^{(0)} \ln\frac{\mu_M}{M}\,, \tag{12.25}$$

$$C_{Hq^{(3)}}^{(1)} = -\frac{A^2}{144M^4}\left[17g_2^2 - 45\left(y_u y_u^\dagger + y_d y_d^\dagger\right)\right] + \tilde{\gamma}_{Hq^{(3)},H\Box}\, C_{H\Box}^{(0)} \ln\frac{\mu_M}{M}\,, \tag{12.26}$$

$$C_{H\ell^{(1)}}^{(1)} = \frac{A^2}{144M^4}\left(17g_1^2 + 45y_e y_e^\dagger\right) + \tilde{\gamma}_{H\ell^{(1)},H\Box}\, C_{H\Box}^{(0)} \ln\frac{\mu_M}{M}\,, \tag{12.27}$$

$$C_{H\ell^{(3)}}^{(1)} = -\frac{A^2}{144M^4}\left(17g_2^2 - 45y_e y_e^\dagger\right) + \tilde{\gamma}_{H\ell^{(3)},H\Box}\, C_{H\Box}^{(0)} \ln\frac{\mu_M}{M}\,, \tag{12.28}$$

$$C_{2y}^{(1)} = \frac{A^2}{6M^4}\,. \tag{12.29}$$

The one-loop anomalous dimensions appearing in the above expressions are

$$\tilde{\gamma}_{\psi H,H\Box} = -y_\psi\left(2\lambda - \frac{10g_2^2}{3} + 6y_\psi^\dagger y_\psi\right)\,, \tag{12.30}$$

$$\tilde{\gamma}_{Hu,H\Box} = \frac{2g_1^2}{9} - y_u^\dagger y_u\,, \tag{12.31}$$

$$\tilde{\gamma}_{Hd,H\Box} = -\frac{g_1^2}{9} + y_d^\dagger y_d\,, \tag{12.32}$$

$$\tilde{\gamma}_{Hud,H\Box} = 2y_u^\dagger y_d\,, \tag{12.33}$$

$$\tilde{\gamma}_{He,H\Box} = -\frac{g_1^2}{3} + y_e^\dagger y_e\,, \tag{12.34}$$

$$\tilde{\gamma}_{Hq^{(1)},H\Box} = \frac{g_1^2}{18} + \frac{1}{2}\left(y_u y_u^\dagger - y_d y_d^\dagger\right)\,, \tag{12.35}$$

$$\tilde{\gamma}_{Hq^{(3)},H\Box} = \frac{g_2^2}{6} - \frac{1}{2}\left(y_u y_u^\dagger + y_d y_d^\dagger\right) , \tag{12.36}$$

$$\tilde{\gamma}_{H\ell^{(1)},H\Box} = -\frac{g_1^2}{6} - \frac{1}{2} y_e y_e^\dagger , \tag{12.37}$$

$$\tilde{\gamma}_{H\ell^{(3)},H\Box} = \frac{g_2^2}{6} - \frac{1}{2} y_e y_e^\dagger . \tag{12.38}$$

A sum over flavour indices is implicit in the above equations and the index ψ in Eqs. (12.20) to (12.30) can take the values $\psi = u, d, e$. Our results Eqs. (12.20) to (12.22) and Eqs. (12.24) to (12.29) for the one-loop matching corrections of the fermionic dimension-six SMEFT operators agree with Eqs. (A.24) to (A.34) as given in [21]. On the other hand, the correction in Eq. (12.23) was missed in [21]. In addition, the anomalous dimension expressions Eqs. (12.30) to (12.38) fulfill the one-loop SMEFT RG equations collected in [24–26]. Finally, note that the operator Q_{2y} is a linear combination of several four-fermion operators in the Warsaw basis [363]. The Wilson coefficient C_{2y} does not receive a logarithmic correction, since the (purely bosonic) tree-level operators $Q_{H\Box}$ and Q_H obviously cannot mix into four-fermion operators at one loop.

Chapter 13

Effective theory of gravity to all orders

According to the EFT paradigm one should include all low-energy degrees of freedom (DOF) in the construction of an EFT. In the previous chapters of this part, and Chapter 12 in particular, we worked in an EFT for the SM particles only. However, the SM particles are not the full spectrum of low-energy DOF. Gravity, the fourth of the fundamental interactions, is mediated by a massless helicity two particle, the graviton, which is not included in the SM. Its leading order interactions are described by Einstein's theory of GR and just as for the SM, deviations due to heavy new physics can be systematically encoded in higher dimensional operators. Thus the true most general parameterization of all physically distinct low-energy deviations from the established description of all known fundamental interactions, i.e. the SM Lagrangian and the Einstein-Hilbert action, must be an EFT of all low-energy DOF, including gravity. In this chapter we develop a method, based on Hilbert series techniques (see Section 11.5), to construct the EFT of GR coupled to the SM, which we call GRSMEFT, to all orders in the EFT expansion.

We start this chapter with a short introduction to the Einstein-Hilbert action of GR, the leading contribution of the EFT of gravity [364–366], in Section 13.1. In contrast to the SM, GR is manifestly non-renormalizable, which makes an EFT interpretation unavoidable. In Section 13.2 we identify the independent building blocks for constructing gravitational effective operators and show that the Hilbert series methods from Section 11.5 can be directly applied. With these ingredients we construct a non-redundant operator basis for several EFTs with gravity: the EFT of gravity in vacuum in Section 13.3, the EFT of a shift-symmetric scalar coupled to gravity in Section 13.4 and the EFT of the SM coupled to gravity in Section 13.5. Finally we demonstrate in Section 13.6 how our method is straightforwardly extended to $d > 4$ spacetime dimensions and explicitly construct the EFT for gravity in vacuum in $d = 5$ dimensions.

In the following we adopt the metric and curvature conventions of [366, 367]. This chapter is based on [30][1] from where parts of the text are taken.

[1] [30]: M. Ruhdorfer, J. Serra and A. Weiler, *Effective Field Theory of Gravity to All Orders.*

13.1 General Relativity as an EFT

GR as a classical theory provides an excellent description of gravitational phenomena at large distances. However, once the Einstein-Hilbert action[2] is quantized

$$S_{\rm EH} = -\frac{M_{\rm pl}^2}{2}\int d^4x\sqrt{-g}R\,, \tag{13.1}$$

where $M_{\rm pl} = (8\pi G)^{-1/2}$ is the reduced Planck mass and R the Ricci scalar, it becomes clear that this can only be the leading term in a low-energy EFT. GR as a quantum field theory is non-renormalizable and quantum corrections induce higher-dimensional operators with higher powers of the Riemann tensor [368–370] (the same conclusion is reached when quantum effects from matter fields are considered [368, 369, 371–373]). According to the EFT paradigm, all operators invariant under general coordinate transformations, the gauge symmetry of GR, should be included in a systematic expansion in derivatives over a cutoff scale Λ, i.e.

$$S_{eff} = \int d^4x\sqrt{-g}\Big[-\frac{M_{Pl}^2}{2}R + a\,R^2 + b\,R_{\mu\nu}R^{\mu\nu} + c\,R_{\mu\nu\rho\sigma}R^{\mu\nu\rho\sigma} + d\,\Box R + \frac{e}{\Lambda^2}{\rm Riem}^3 + \dots\Big]\,, \tag{13.2}$$

where Riem^3 stands for terms with three Riemann tensors and $\Box = \nabla_\mu\nabla^\mu$ is the contraction of two covariant derivatives. As we have discussed in Section 11.4, not all invariants one can write are independent. Operators proportional to the free EOM can be removed by means of field redefinitions. The EOM for GR are the Einstein equations, which can be written in their trace-reversed form as

$$R_{\mu\nu} = \frac{1}{M_{\rm pl}^2}(T_{\mu\nu} - \frac{1}{2}T g_{\mu\nu})\,, \tag{13.3}$$

where we included a possible contribution from matter fields through the energy momentum tensor $T^{\mu\nu} = \frac{-2}{\sqrt{-g}}\frac{\delta S_{\rm matter}}{\delta g_{\mu\nu}}$, with its trace $T = g^{\mu\nu}T_{\mu\nu}$. The free EOM, i.e. the Einstein equations in vacuum ($T_{\mu\nu} = 0$), have the simple solution

$$R_{\mu\nu} = 0\,. \tag{13.4}$$

This implies that any higher-dimensional operator containing $R_{\mu\nu}$ or $R = g^{\mu\nu}R_{\mu\nu}$ can be eliminated by performing a perturbative field redefinition of the metric

$$g_{\mu\nu} \to g_{\mu\nu} + \frac{2}{M_{\rm pl}^2}\delta g_{\mu\nu}\,, \tag{13.5}$$

which to leading order in $\delta g_{\mu\nu}$ modifies the Einstein-Hilbert action by

$$\delta S_{\rm EH} = \int d^4x\sqrt{-g}\big[R^{\mu\nu} - \frac{1}{2}Rg^{\mu\nu}\big]\delta g_{\mu\nu} = \int d^4x\sqrt{-g}R^{\mu\nu}\delta\bar{g}_{\mu\nu}\,, \tag{13.6}$$

where we introduced the trace-reversed metric perturbation

$$\delta\bar{g}_{\mu\nu} = \delta g_{\mu\nu} - \frac{1}{2}g_{\mu\nu}\,\delta g\,, \tag{13.7}$$

with $\delta g = g^{\mu\nu}\delta g_{\mu\nu}$. From Eq. (13.6) it is clear that by choosing an appropriate $\delta\bar{g}_{\mu\nu}$, any operator including $R_{\mu\nu}$ can indeed be removed. Coming back to the effective action in Eq. (13.2), several redundant operators can now be identified (see also [365]). Furthermore, we can drop

[2] In the following discussion we will always implicitly assume that the cosmological constant is set to zero.

$\sqrt{-g}\,\Box R = \partial_\mu(\sqrt{-g}\,\nabla^\mu R)$, since it is a total derivative. The term proportional to $R_{\mu\nu\rho\sigma}R^{\mu\nu\rho\sigma}$ can be expressed in terms of $R_{\mu\nu}R^{\mu\nu}$ and R^2 because the Gauss-Bonnet term $\mathcal{L}_{GB} = R^2 - 4R_{\mu\nu}R^{\mu\nu} + R_{\mu\nu\rho\sigma}R^{\mu\nu\rho\sigma}$ is a total derivative in four dimensions; this shifts the Wilson coefficients $a \to \tilde{a} = a - c$ and $b \to \tilde{b} = b + 4c$. Finally, performing the metric redefinition in Eq. (13.5) with $\delta\bar{g}_{\mu\nu} = -\tilde{b}R_{\mu\nu} - \tilde{a}Rg_{\mu\nu}$, gets rid of all the operators with two Riemann structures. The first non-trivial contribution to the gravity EFT appears only at dimension 6 with three Riemann tensors.

In the presence of matter fields, a redefinition of the metric such as Eq. (13.5) also affects the matter action

$$\delta S_{\rm EH} + \delta S_{\rm matter} = \int d^4x\sqrt{-g}\left[R^{\mu\nu} - \frac{1}{M_{\rm pl}^2}(T^{\mu\nu} - \frac{1}{2}Tg^{\mu\nu})\right]\delta\bar{g}_{\mu\nu}\,. \tag{13.8}$$

We can still use this redefinition to remove any pure gravity terms involving $R_{\mu\nu}$ or R, but this will in general introduce mixed curvature-matter operators, such as $R_{\mu\nu}T^{\mu\nu}$. These however usually have a higher mass dimension than the removed operators and can therefore be further removed by an independent redefinition. More care has to be taken when a massive scalar field ϕ is involved, since its energy-momentum tensor at leading order in fields and derivatives is $T^{\mu\nu} = \frac{1}{2}m^2\phi^2 g^{\mu\nu} + \ldots$, thus one always introduces new mixed curvature-scalar operators with the same mass dimension as the removed ones. This is in fact not an issue, since the redefinition of the metric can be generalized to include matter fields. To make this clear, consider again the field transformation with $\delta\bar{g}_{\mu\nu} = -\tilde{b}R_{\mu\nu} - \tilde{a}Rg_{\mu\nu}$, which removes the $\tilde{a}R^2 + \tilde{b}R_{\mu\nu}R^{\mu\nu}$ terms in Eq. (13.2), now in the presence of a massive scalar field ϕ. The change of the action is

$$\delta S_{\rm EH} + \delta S_{\rm matter} = \int d^4x\sqrt{-g}\left[-\tilde{a}\,R^2 - \tilde{b}\,R_{\mu\nu}R^{\mu\nu} - \frac{m^2}{2M_{\rm pl}^2}(\tilde{b} + 4\tilde{a})\phi^2 R + \ldots\right], \tag{13.9}$$

where we dropped higher-dimensional operators. The last term in Eq. (13.9) is a non-minimal coupling of the scalar field to gravity, which could in fact have been there from the beginning. As anticipated, this term can be removed by a further metric redefinition with $\delta\bar{g}_{\mu\nu} \propto \phi^2 g_{\mu\nu}$. This is a Weyl transformation which takes us to the Einstein frame, where the leading order EOM of the scalar field and gravity are decoupled.

The recipe above lets us, order-by-order in mass dimension, remove any occurrence of $R_{\mu\nu}$ and R in the Lagrangian.[3] This implies that the only non-redundant gravitational operators are those built out of the traceless components of the Riemann tensor $R_{\mu\nu\rho\sigma}$. Still, even such operators might not all be independent, due to algebraic identities. The Riemann tensor is cyclic

$$R_{\mu\nu\rho\sigma} + R_{\mu\rho\sigma\nu} + R_{\mu\sigma\nu\rho} = 0 \tag{13.10}$$

and it satisfies the Bianchi identity

$$\nabla_\alpha R_{\mu\nu\rho\sigma} + \nabla_\rho R_{\mu\nu\sigma\alpha} + \nabla_\sigma R_{\mu\nu\alpha\rho} = 0\,. \tag{13.11}$$

Additionally, there are the so-called dimensionally dependent tensor identities, which are obtained by antisymmetrizing tensor indices [379], and can be used to simplify tensor contractions.

[3] Another comment in this regard is that the same procedure also holds in the presence of classical (gravitational) sources and one is interested in how gravity affects their dynamics; once operators with $R_{\mu\nu}$ and R are removed, one should properly include contact terms between the sources [365]. Besides, we note that in these situations it might be more convenient to work with a non-covariant EFT on the corresponding background metric, as for example in [374–378].

Once all the redundancies in the gravitational sector are removed, it is clear that field redefinitions of the matter fields can be used to simplify the matter Lagrangian, just as in flat spacetime.

Let us finally briefly comment on spacetimes with torsion. If one is not restricted to a torsion-free spacetime, coupling fermions to gravity will in general induce a non-vanishing torsion tensor $T_{\mu\nu}{}^{\rho}$. However, even if we chose to include the torsion tensor explicitly as a building block of the EFT, torsion vanishes in vacuum, i.e. in the free theory, and at the lowest order in derivatives, i.e. from the leading EOM. Therefore, we conclude that in the presence of matter one can use field redefinitions and work with a torsion-free theory, with shifted coefficients in the matter action [380, 381]. In other words, no generality is lost in our EFT by considering a torsion-free spacetime.

13.2 Building blocks for the gravity EFT

The Riemann tensor does not transform in an irreducible representation of the Lorentz group. It can be decomposed as

$$R_{\mu\nu\rho\sigma} \sim (1,1) \oplus (2,0) \oplus (0,2) \oplus (0,0)\,, \tag{13.12}$$

where the $(1,1)$ is a symmetric rank-two traceless tensor, identified with the traceless part of the Ricci tensor $R_{\mu\nu}$, the singlet $(0,0)$ is the Ricci scalar R, and the component transforming as $(2,0)\oplus(0,2)$ is the Weyl or conformal tensor $C_{\mu\nu\rho\sigma}$. The Weyl tensor is the traceless part of the Riemann tensor and is given by

$$C_{\mu\nu\rho\sigma} \equiv R_{\mu\nu\rho\sigma} - \left(g_{\mu[\rho}R_{\sigma]\nu} - g_{\nu[\rho}R_{\sigma]\mu}\right) + \frac{1}{3}g_{\mu[\rho}g_{\sigma]\nu}R\,, \tag{13.13}$$

where the brackets denote index antisymmetrization, e.g. $A_{[\mu\nu]} = \frac{1}{2}(A_{\mu\nu} - A_{\nu\mu})$ for arbitrary tensors A. It possesses the same symmetries as the Riemann tensor and satisfies the cyclicity and Bianchi identity of Eqs. (13.10) and (13.11) up to terms involving $R_{\mu\nu}$ and R. As discussed in the previous section, any occurrence of $R_{\mu\nu}$ and R can always be eliminated by an appropriate field redefinition. This leaves the Weyl tensor as the only independent object for constructing gravitational EFT operators. The Einstein equations do not directly constrain the traceless components of the Riemann tensor, but the contracted Bianchi identities imply an EOM for the Weyl tensor, which can be expressed in terms of the Ricci tensor and scalar,

$$\nabla^{\mu}C_{\mu\nu\rho\sigma} = \nabla_{[\rho}R_{\sigma]\nu} + \frac{1}{6}g_{\nu[\rho}\nabla_{\sigma]}R\,. \tag{13.14}$$

For the free theory, i.e. in vacuum, this simplifies to

$$\nabla^{\mu}C_{\mu\nu\rho\sigma} = 0\,, \tag{13.15}$$

in analogy to the EOM for the field strength tensor of gauge fields in Eq. (11.56). Additionally, the Bianchi identity in combination with the EOM implies that also $\nabla^2 C_{\mu\nu\rho\sigma}$ is not an independent object, since in vacuum

$$\nabla^2 C_{\mu\nu\rho\sigma} = -2C^{\lambda}{}_{\mu\rho\alpha}C_{\lambda\nu\sigma}{}^{\alpha} - 2C^{\lambda}{}_{\nu\rho\alpha}C_{\mu\lambda\sigma}{}^{\alpha} - C^{\lambda}{}_{\alpha\rho\sigma}C_{\mu\nu\lambda}{}^{\alpha} \tag{13.16}$$

plus terms that can be removed due to the EOM. Consequently, the EOM redundancy is taken care of if we consider, similarly to the case of the spin-1 field strength, $C_{\mu\nu\rho\sigma}$ and symmetric

traceless combinations of covariant derivatives acting on $C_{\mu\nu\rho\sigma}$ as the basic building blocks for EFT operators. This implies that the single particle module is of the form

$$R_C = \begin{pmatrix} C_{\mu\nu\rho\sigma} \\ \nabla_{\{\mu_1} C_{\mu\}\nu\rho\sigma} \\ \nabla_{\{\mu_1}\nabla_{\mu_2} C_{\mu\}\nu\rho\sigma} \\ \vdots \end{pmatrix} . \tag{13.17}$$

We consider only symmetric combinations of the covariant derivatives, since antisymmetric combinations are related to the Riemann tensor via $[\nabla_\mu, \nabla_\nu]V^\rho = R_{\mu\nu\sigma}{}^\rho V^\sigma$. An operator containing an antisymmetric combination of covariant derivatives is therefore always equivalent to the tensor product of the Weyl tensor with a descendant that contains fewer derivatives. Analogously to the gauge field strength, we can identify the irreducible representations of the Lorentz group with

$$C^{\mu\nu\rho\sigma}_{L/R} = \frac{1}{2}\Big(C^{\mu\nu\rho\sigma} \pm i\, \tilde{C}^{\mu\nu\rho\sigma} \Big) , \tag{13.18}$$

where we introduced the dual Weyl tensor $\tilde{C}^{\mu\nu\rho\sigma} = \epsilon^{\mu\nu\alpha\beta} C_{\alpha\beta}{}^{\rho\sigma}/2$.[4] $C_{L/R}$ transform in the $(2,0)$ and $(0,2)$ representations of the Lorentz group, respectively. Note that the single particle modules $R_{C_{L/R}}$ cannot be identified with unitary conformal representations in four dimensions. The mass dimension of the Weyl tensor is $[C_{L/R}] = 2$, which violates the unitarity bound for the scaling dimension $\Delta \geq \Delta_{(2,0)} = \Delta_{(0,2)} = 3$ in Eq. (11.47). However, since our aim is only to enumerate and construct operators, we can formally assign a conformal scaling dimension of $\Delta_{C_{L/R}} = 3$ to the spurion representing the Weyl tensor.[5] When expanding the Hilbert series we can choose a grading in which the spurion for the Weyl tensor is assigned a weight according to the Weyl tensor's actual mass dimension in four dimensions. The conformal representations $[3;(2,0)]$ and $[3;(0,2)]$ saturate the unitarity bound and therefore are representations with all descendants proportional to the free EOM $\nabla^\mu C_{\mu\nu\rho\sigma} = 0$ (as well as $\nabla^2 C_{\mu\nu\rho\sigma}$) being absent. This is exactly of the form of the single particle module in Eq. (13.17). The corresponding conformal character is

$$\chi_{[3;(2,0)]}(\mathcal{D};x) = \mathcal{D}^3\, P(\mathcal{D},x)\big(\chi_{(2,0)}(x) - \chi_{(3/2,1/2)}(x)\,\mathcal{D} + \chi_{(1,0)}(x)\,\mathcal{D}^2\big) , \tag{13.19}$$

and equivalently for $[3;(0,2)]$. Note that here and in the following the spurion $\mathcal{D}$ denotes covariant derivatives ∇_μ. The structure of Eq. (13.19) is completely analogous to that of the conformal character for a gauge field strength, Eq. (11.59). Using this character, in the next section we will construct the operator basis for EFTs which involve gravity. Note that similarly to the example in Section 11.5.3, the Hilbert series method automatically factors in redundancies due to Bianchi identities, cyclicity of indices or dimensionally dependent identities, since we do not construct index contractions but work directly with group representations and form invariants. At the end of this chapter in Section 13.6 we generalize Eq. (13.19) to d spacetime dimensions, pointing out the main difference with respect to the derivation for $d = 4$, namely that the single particle module for the Weyl tensor, R_C in Eq. (13.17), cannot be embedded for $d > 4$ in a free field unitary conformal representation. We count and identify as well the basis of effective operators for pure gravity in $d = 5$.

[4] The normalization of the Levi-Civita tensor is such that $\epsilon^{0123} = 1/\sqrt{-g}$.

[5] Besides, note that Eq. (11.51) for the construction of the Hilbert series also holds for single particle modules that are not conformal representations [23]. The advantage of promoting the Weyl tensor to be formally a unitary conformal representation is that in this case there is a closed form expression for $\Delta\mathcal{H}$ in Eq. (11.50).

With the help of the formalism outlined in this section we are in a position to use Hilbert series techniques to first enumerate and subsequently construct operator bases for EFTs involving gravity. In Section 13.3 we verify and extend the operator basis for gravity in vacuum as given in e.g. [382]. Next in Section 13.4, as a first step towards including matter fields, we build the EFT for a shift-symmetric scalar coupled to gravity and point out redundancies in the operator basis of [383]. Finally, we list for the first time the complete basis of the SM coupled to gravity in Section 13.5.

13.3 Gravity in vacuum

In vacuum the only independent operators that do not vanish on-shell are the Weyl tensor and its dual, which can be used to form the chiral combinations $C_{L/R}^{\mu\nu\rho\sigma}$, as shown in Eq. (13.18). The building blocks are therefore their corresponding single particle modules, which can be embedded into conformal representations if we formally assign to $C_{L/R}$ a conformal scaling dimension of $\Delta_{C_{L/R}} = 3$. Hence, their group characters are

$$\chi_{C_L}(\mathcal{D};x) = \chi_{[3,(2,0)]}(\mathcal{D};x)\,, \qquad \chi_{C_R}(\mathcal{D};x) = \chi_{[3,(0,2)]}(\mathcal{D};x)\,, \tag{13.20}$$

with the explicit form of the conformal characters given in Eq. (13.19) and Appendix III.C. Grading the spurions according to their actual mass dimension, i.e. $C_{L/R} \to \epsilon^2\, C_{L/R}$ and $\mathcal{D} \to \epsilon\,\mathcal{D}$, the Hilbert series can be computed as an expansion in mass dimension using Eq. (11.50)[6]

$$\begin{aligned}\mathcal{H}(\mathcal{D},C_L,C_R;\epsilon) &= \int d\mu_{\text{Lorentz}}(x)\frac{1}{P(\epsilon\,\mathcal{D},x)}\text{PE}\left[\frac{C_L}{\epsilon\,\mathcal{D}^3},\frac{C_R}{\epsilon\,\mathcal{D}^3}\right] + \Delta\mathcal{H}(\mathcal{D},C_L,C_R;\epsilon)\\ &= \epsilon^4\left(C_L^2+C_R^2\right)+\epsilon^6\left(C_L^3+C_R^3\right)+\epsilon^8\left(C_L^4+C_L^2C_R^2+C_R^4\right)\\ &\quad+\epsilon^{10}\left(C_L^5+C_L^3C_R^2+C_L^2C_R^3+C_R^5+C_L^4\mathcal{D}^2+C_L^2C_R^2\mathcal{D}^2+C_R^4\mathcal{D}^2\right)+\dots\,.\end{aligned} \tag{13.21}$$

The terms at $\mathcal{O}(\epsilon^4)$ correspond to the operators $C_{\mu\nu\rho\sigma}\tilde{C}^{\mu\nu\rho\sigma}$ and $C_{\mu\nu\rho\sigma}C^{\mu\nu\rho\sigma}$. Both can be dropped, since the first is a total derivative and the second can be related to $R_{\mu\nu}R^{\mu\nu}$ and R^2 because the Gauss-Bonnet term is a total derivative in four dimensions (see Section 13.1). These operators were misidentified as being non-redundant, since they are in fact related to gravitational topological terms. That topological terms are misidentified by our method was already realized in [23], being a consequence of working with covariant field strengths instead of gauge fields. The operators $C_{\mu\nu\rho\sigma}\tilde{C}^{\mu\nu\rho\sigma}$ and $C_{\mu\nu\rho\sigma}C^{\mu\nu\rho\sigma}$ give rise, respectively, to the four-dimensional Pontryagin and Euler densities [384]. The other terms in Eq. (13.21) indicate the structure and multiplicity of the basis of operators for the most general gravity Lagrangian in vacuum up to mass dimension 10. In terms of the Weyl tensor and its dual the basis can be written as

$$\begin{aligned}S = \int d^4x\sqrt{-g}\Big[&- \frac{M_{\text{pl}}^2}{2}R + \frac{c_1}{\Lambda^2}\mathcal{I} + \frac{c_2}{\Lambda^2}\tilde{\mathcal{I}} + \frac{d_1}{\Lambda^4}\mathcal{C}^2 + \frac{d_2}{\Lambda^4}\mathcal{C}\tilde{\mathcal{C}} + \frac{d_3}{\Lambda^4}\tilde{\mathcal{C}}^2\\ &+ \frac{e_1}{\Lambda^6}\mathcal{I}\mathcal{C} + \frac{e_2}{\Lambda^6}\tilde{\mathcal{I}}\mathcal{C} + \frac{e_3}{\Lambda^6}\mathcal{I}\tilde{\mathcal{C}} + \frac{e_4}{\Lambda^6}\tilde{\mathcal{I}}\tilde{\mathcal{C}} + \frac{e_5}{\Lambda^6}\mathcal{F}\mathcal{C} + \frac{e_6}{\Lambda^6}\mathcal{F}\tilde{\mathcal{C}} + \frac{e_7}{\Lambda^6}\tilde{\mathcal{F}}\tilde{\mathcal{C}} + \dots\Big]\,,\end{aligned} \tag{13.22}$$

with the basic invariants

$$\mathcal{I} = C_{\mu\nu}{}^{\rho\sigma}C^{\mu\nu\alpha\beta}C_{\alpha\beta\rho\sigma}\,, \qquad \tilde{\mathcal{I}} = C_{\mu\nu}{}^{\rho\sigma}C^{\mu\nu\alpha\beta}\tilde{C}_{\alpha\beta\rho\sigma}\,, \tag{13.23}$$

[6] For unitary conformal representations, as it is the case here, $\Delta\mathcal{H}$ can be evaluated explicitly [23] and yields $-\epsilon^4\mathcal{D}^4$, which cancels the $+\epsilon^4\mathcal{D}^4$ that one obtains from evaluating the integral over the group measure.

$$\mathcal{C} = C_{\mu\nu\rho\sigma}C^{\mu\nu\rho\sigma}\,, \qquad \tilde{\mathcal{C}} = C_{\mu\nu\rho\sigma}\tilde{C}^{\mu\nu\rho\sigma}\,, \tag{13.24}$$

$$\mathcal{F} = (\nabla_\alpha C_{\mu\nu\rho\sigma})(\nabla^\alpha C^{\mu\nu\rho\sigma})\,, \qquad \tilde{\mathcal{F}} = (\nabla_\alpha C_{\mu\nu\rho\sigma})(\nabla^\alpha \tilde{C}^{\mu\nu\rho\sigma})\,. \tag{13.25}$$

The first line of Eq. (13.22) is equivalent to the effective action in Eq. (1.1) of [382].[7] The second line of Eq. (13.22) shows for the first time the basis of gravitational operators at dimension 10. We used the `Invar` package [385] to explicitly construct and classify the ($\mathcal{CP}$ even) operators and to check that they are indeed independent. We note that in general the basis of operators without derivatives corresponds to the most general polynomial of the invariants $\mathcal{C}$, $\tilde{\mathcal{C}}$, $\mathcal{I}$ and $\tilde{\mathcal{I}}$, these being the four scalar quantities that completely determine the spacetime curvature in four dimensions (see e.g. the discussion in [386]). This fact is further verified by computing the Hilbert series for the left- and right-handed Weyl tensors $C_{L/R}$ without derivatives, which according to the Molien-Weyl formula Eq. (11.41) yields

$$\mathcal{H}(C_L, C_R) = \frac{1}{(1-C_L^2)(1-C_R^2)(1-C_L^3)(1-C_R^3)}\,. \tag{13.26}$$

Therefore all operators without derivatives are generated by the four basic invariants C_L^2, C_R^2, C_L^3 and C_R^3, corresponding to the invariants in Eqs. (13.23) and (13.24).

It is straightforward to compute even higher order contributions to the Hilbert series with this formalism. Finding the explicit form for the corresponding basis of operators can be more involved. However, since we know how many independent operators appear in each category, one does not need to classify all invariants. It is sufficient to find as many operators as the multiplicity in the Hilbert series predicts and check that they are independent.

Let us finally comment on some important aspect of the gravity EFT in vacuum. At one loop GR is finite [369], a fact that from the EFT perspective follows from NDA and the absence of non-redundant operators at $O(\epsilon^4)$. At two loops the Einstein-Hilbert term induces RG evolution of the $\mathcal{CP}$ preserving cubic curvature term in Eq. (13.22), with running coefficient [370,387,388]

$$\mu\frac{\partial c_1}{\partial \mu} = \frac{1}{120}\frac{\Lambda^2}{M_{\rm pl}^2}\frac{1}{(4\pi)^4}\,. \tag{13.27}$$

Heavy matter fields (scalars, fermions or vectors) contribute at one loop to the gravity EFT [389, 390], giving rise to a finite contribution to c_1, which for e.g. a Dirac fermion of mass Λ reads $c_1 = -\frac{1}{7560}(1/4\pi)^2$, as well as to contributions to several other operators that are not present in our basis being dependent on $R_{\mu\nu}$, R.[8] Gravitational UV completions, such as (super-)string theories, generate as well a specific pattern of Wilson coefficients below the string scale, see e.g. [391]. In a generic gravity effective Lagrangian, the Wilson coefficients are arbitrary $\mathcal{O}(1)$ numbers. To be more precise, the size of the coefficient can be estimated following NDA as

$$\mathcal{L}_{eff} = \frac{m_*^4}{g_*^2}L\left(\frac{R_{\mu\nu\rho\sigma}}{m_*^2}, \frac{\nabla_\mu}{m_*}\right) - \frac{\hat{M}_{\rm pl}^2}{2}R\,, \tag{13.28}$$

where m_* and g_* broadly characterize, respectively, the typical mass scale and coupling of the UV resonances that have been integrated out. We have explicitly included a "fundamental" Einstein-Hilbert term, to distinguish between a bona fide completion of GR such as string theory, which would correspond to $M_{\rm pl} \sim \hat{M}_{\rm pl} \sim m_*/g_*$, and the case where the graviton can be considered

[7] In [382] the operator basis is given in terms of the Riemann tensor, which after the decomposition in Eq. (13.13) coincides with the operators we found in Eq. (13.22) modulo terms with $R_{\mu\nu}$ and R, which can be removed by field redefinitions as explained in Section 13.1.

[8] Matter fields also contribute to the RG running of $M_{\rm pl}$ and the cosmological constant.

external, i.e. "elementary", to the dynamics giving rise to L, e.g. loops of N matter particles of mass m_*, for which $g_* \sim 4\pi/\sqrt{N}$. The simple power counting of Eq. (13.28) implies then $c_1 = \mathcal{O}(1)$ for $\Lambda \sim g_* m_*$, and similarly for the rest of Wilson coefficients. Interestingly, several works have derived constraints on the sign and size of such coefficients based on causality, unitarity and analyticity. For instance, positivity of the coefficients of the $\mathcal{CP}$ even dimension 8 operators, i.e. $d_1, d_3 > 0$, has been derived based on causality of graviton propagation [392], or unitarity and analyticity of graviton scattering amplitudes [393,394], while [382] extended the former causality analysis to the $\mathcal{CP}$ odd operator, concluding $d_2 \lesssim d_1 d_3$. We should recall however that these arguments are delicate when applied to gravitational interactions, in particular [393,394] neglect the universal t-channel singularity due to graviton exchange, a fact that could be justified by e.g. the rationale presented in [395]. Besides, [396] argues that in a weakly coupled theory of gravity, with $g_* \sim m_*/M_{\rm pl} \ll 1$, avoiding causality violation originating from cubic curvature terms ($\mathcal{I}$ and $\tilde{\mathcal{I}}$ in Eq. (13.22), with coefficients c_1 and c_2 effectively of tree-level size), requires an infinite tower of higher-spin states to appear at or near the EFT cutoff m_*, regardless of the coefficients sign. Instead, for other types of UV completions where the graviton is elementary, with $M_{\rm pl} \gg m_*/g_*$ such as from loops of matter particles [390], acausality lies beyond the validity of the EFT.

13.4 Shift-symmetric scalar coupled to gravity

As a second application of our method we consider a shift-symmetric scalar ϕ coupled to gravity. The shift symmetry $\phi \to \phi + \alpha$ implies that the scalar can only couple derivatively, i.e. it will always appear with at least one derivative acting on it. The scalar can be thought of as the massless Nambu-Goldstone boson of a spontaneously broken $U(1)$ symmetry. Because of this interpretation, it is no surprise that the single particle module for the shift-symmetric scalar has the same form as for non-linear field realizations as given in [23][9]

$$R_{d\phi} = \begin{pmatrix} \nabla_\mu \phi \\ \nabla_{\{\mu_1} \nabla_{\mu\}} \phi \\ \nabla_{\{\mu_1} \nabla_{\mu_2} \nabla_{\mu\}} \phi \\ \vdots \end{pmatrix} . \tag{13.29}$$

In Eq. (13.29) we already imposed the scalar's EOM $\nabla_\mu \nabla^\mu \phi = 0$. Therefore, the weighted character for the single particle module is identical to the one for non-linear realizations [23]

$$\chi_{d\phi}(\mathcal{D}; x) = \mathcal{D}\big[\big(1 - \mathcal{D}^2\big) P(\mathcal{D}; x) - 1\big] . \tag{13.30}$$

Note that this single particle module is not a conformal representation since the primary field is a total derivative. However, we can still use Eq. (11.51) to construct the Hilbert series for higher-dimensional operators, which are the ones we are interested in. To obtain the full Hilbert series, i.e. including also operators of dimension 4 and lower, we have to rely on the results of [23] for non-linear realizations. A basis for the $\mathcal{CP}$ even operators, up to 6 derivatives, was constructed in [383]. We compute the Hilbert series for operators with 6 and 8 derivatives and compare our basis to their results. The Hilbert series as an expansion in derivatives can be

[9] [23] used the decomposition of the Maurer-Cartan form $U^{-1}\partial_\mu U = u^i_\mu X^i + v^a_\mu T^a = u_\mu + v_\mu$ into components along broken generators X^i and unbroken generators T^a to obtain a linearly transforming building block u_μ from the non-linearly transforming Goldstone matrix $U = \exp(i\phi^i X^i / f_\phi)$. For a spontaneously broken $U(1)$ symmetry $u_\mu \propto \partial_\mu \phi$. Here the only difference is in the mass dimension, $[\nabla_\mu \phi] = 2$ whereas $[u_\mu] = 1$.

obtained by rescaling the spurions $C_{L/R} \to \epsilon^2 C_{L/R}$, $\mathcal{D} \to \epsilon\,\mathcal{D}$ and $d\phi \to \epsilon d\phi$ and expanding in ϵ

$$\mathcal{H}_0(\mathcal{D}, C_L, C_R, d\phi; \epsilon) = \int d\mu_{\text{Lorentz}}(x) \int \frac{1}{P(\epsilon\,\mathcal{D}, x)} \text{PE}\left[\frac{C_L}{\epsilon\,\mathcal{D}^3}, \frac{C_R}{\epsilon\,\mathcal{D}^3}, \frac{d\phi}{\epsilon\,\mathcal{D}^2}\right] = \sum_n \epsilon^n \mathcal{H}_n\,. \quad (13.31)$$

The 6-derivative Hilbert series is

$$\mathcal{H}_6 = C_L^3 + C_R^3 + d\phi^3 C_L \mathcal{D} + d\phi^3 C_R \mathcal{D} + d\phi^2 C_L^2 + d\phi^2 C_R^2 + d\phi^6 + d\phi^4 \mathcal{D}^2\,. \quad (13.32)$$

If we restrict to $\mathcal{CP}$ even operators, the EFT operator basis at the 6-derivative level can be written as

$$\begin{aligned} \mathcal{O}_1 = \left[(\nabla_\mu\phi)^2\right]^3\,, \qquad \mathcal{O}_2 = (\nabla_\mu\phi)^2(\nabla_\rho\nabla_\sigma\phi)^2\,, \qquad \mathcal{O}_3 = C_{\mu\nu}{}^{\rho\sigma} C^{\mu\nu\alpha\beta} C_{\alpha\beta\rho\sigma}\,, \\ \mathcal{O}_4 = (C_{\alpha\beta\rho\sigma})^2(\nabla_\mu\phi)^2\,, \qquad \mathcal{O}_5 = C_{\mu\nu\rho\sigma}(\nabla^\mu\phi)(\nabla^\rho\phi)(\nabla^\nu\nabla^\sigma\phi)\,. \end{aligned} \quad (13.33)$$

Note that [383] lists two additional operators in their operator basis (written in terms of the Riemann instead of the Weyl tensor), $(\nabla_\alpha R_{\mu\nu\rho\sigma})^2$ and $R_{\mu\nu\alpha\beta}(\nabla^\mu\nabla^\alpha\phi)(\nabla^\nu\nabla^\beta\phi)$. Both of these operators are redundant: the first is related to $\mathcal{O}_3$, whereas the second to $\mathcal{O}_4$ (see Appendix III.D). Therefore, the correct $\mathcal{CP}$ even operator basis for the 6-derivative Lagrangian is that in Eq. (13.33). At 8 derivatives we find 26 independent operators, with the structures as given in the Hilbert series

$$\begin{aligned} \mathcal{H}_8 = {} & C_L^4 + C_L^2 C_R^2 + C_R^4 + d\phi^8 + 2d\phi^6\mathcal{D}^2 + d\phi^5\mathcal{D}^3 + d\phi^4\mathcal{D}^4 + d\phi^5\mathcal{D}C_L + d\phi^5\mathcal{D}C_R \\ & + d\phi^4 C_L C_R + d\phi^4\mathcal{D}^2 C_L + d\phi^4 C_L^2 + d\phi^4\mathcal{D}^2 C_R + d\phi^4 C_R^2 + 2d\phi^3\mathcal{D}C_L^2 \\ & + 2d\phi^3\mathcal{D}C_R^2 + d\phi^2\mathcal{D}^2 C_L C_R + 2d\phi^2\mathcal{D}^2 C_L^2 + d\phi^2 C_L^3 + 2d\phi^2\mathcal{D}^2 C_R^2 + d\phi^2 C_R^3\,. \end{aligned} \quad (13.34)$$

Finally, we note that there are two operators that respect the shift symmetry that cannot be found by our method (and are missing in [383]):

$$\phi C_{\mu\nu\rho\sigma} C^{\mu\nu\rho\sigma}\,, \qquad \phi C_{\mu\nu\rho\sigma} \tilde{C}^{\mu\nu\rho\sigma}\,. \quad (13.35)$$

Not surprisingly, these operators are related to (gravitational) topological terms.

13.5 Standard Model coupled to gravity

Let us now construct the complete EFT for the SM, i.e. all operators including SM fields and gravity. Operators including gravity are usually omitted in the SMEFT, even though gravity is part of the SM. We work with one generation of fermions and introduce them in the left-handed $(\frac{1}{2}, 0)$ representation of the Euclidean Lorentz group $SO(4) \simeq SU(2)_L \times SU(2)_R$ along with their right-handed conjugates.[10] In the following we adopt the notation of [22] and denote the spurion fields as

$$\{\phi_a\} = \left\{H, H^\dagger, B_L, B_R, W_L, W_R, G_L, G_R, C_L, C_R, Q, Q^\dagger, u, u^\dagger, d, d^\dagger, L, L^\dagger, e, e^\dagger\right\}\,, \quad (13.36)$$

with their representation under the Lorentz and SM gauge group $SU(3)_C \times SU(2)_W \times U(1)_Y$ given in Table 13.1. We can write the Hilbert series as

$$\mathcal{H}(\{\phi_a\}; \mathcal{D}) = \int d\mu_{\text{gauge}}(y) \int d\mu_{\text{Lorentz}}(x)\, \frac{1}{P(\mathcal{D}; x)} \text{PE}\left[\left\{\frac{\phi_a}{\mathcal{D}^{\Delta_a}}\right\}\right]\,, \quad (13.37)$$

[10] This means we work with the charge conjugated fields of the standard SM right-handed fermions, i.e. u^c, d^c, e^c. In the following we will drop the superscript c.

	$SU(2)_L \times SU(2)_R$	$SU(3)_C$	$SU(2)_W$	$U(1)_Y$
H	$(0,0)$	$\mathbf{1}$	$\mathbf{2}$	$1/2$
B_L	$(1,0)$	$\mathbf{1}$	$\mathbf{1}$	0
W_L	$(1,0)$	$\mathbf{1}$	$\mathbf{3}$	0
G_L	$(1,0)$	$\mathbf{8}$	$\mathbf{1}$	0
C_L	$(2,0)$	$\mathbf{1}$	$\mathbf{1}$	0
Q	$(\frac{1}{2},0)$	$\mathbf{3}$	$\mathbf{2}$	$1/6$
u_c	$(\frac{1}{2},0)$	$\bar{\mathbf{3}}$	$\mathbf{1}$	$-2/3$
d_c	$(\frac{1}{2},0)$	$\bar{\mathbf{3}}$	$\mathbf{1}$	$1/3$
L	$(\frac{1}{2},0)$	$\mathbf{1}$	$\mathbf{2}$	$-1/2$
e_c	$(\frac{1}{2},0)$	$\mathbf{1}$	$\mathbf{1}$	1

Table 13.1: Representations of the spurions under the Lorentz and SM gauge groups.

with the integral over the gauge groups given by

$$\int d\mu_{\text{gauge}}(y) = \int d\mu_{U(1)_Y}(v) \int d\mu_{SU(2)_W}(w) \int d\mu_{SU(3)_C}(z_1, z_2)\,, \tag{13.38}$$

with $y = \{v, w, z_1, z_2\}$ being the variables that parameterize the $SU(3)_C \times SU(2)_W \times U(1)_Y$ gauge group. The characters χ_a for the single particle modules of the spurions are a composition of the characters for the conformal and gauge group representation $\mathbf{R}$ of the spurions,

$$\chi_a(\mathcal{D}; x, y) = \chi_{[\Delta_a, l_a]}(\mathcal{D}; x) \cdot \chi^{U(1)_Y}_{\mathbf{R}_a}(v) \cdot \chi^{SU(2)_W}_{\mathbf{R}_a}(w) \cdot \chi^{SU(3)_C}_{\mathbf{R}_a}(z_1, z_2)\,. \tag{13.39}$$

The explicit form of the group measures and characters is given in Appendix III.C. Note that in order to fully describe the flavor structure of the SM we would have to work with three independent instances of each fermion to implement the three fermion generations. This would increase the number of terms in the generating function at each order exponentially. However, we can still get some information about the number of invariants with N_f flavors by simply suppressing the flavor indices and adding the same fermion spurion N_f times, i.e. we can write the complete PE as

$$\text{PE}\left[\left\{\frac{\phi_a}{\mathcal{D}^{\Delta_a}}\right\}\right] = \prod_b \text{PE}\left[\left\{\frac{\phi_b}{\mathcal{D}^{\Delta_b}}\right\}\right] \prod_f \text{PEF}\left[\left\{\frac{\phi_f}{\mathcal{D}^{\Delta_f}}\right\}\right]^{N_f}, \tag{13.40}$$

where the index b runs over all bosons and f over all fermions. Next we expand the Hilbert series according to the mass dimension of the operators. We will neglect all pure SM contributions to the Hilbert series, which are given in [22]. The first gravity operators appear at dimension 6, the Hilbert series being

$$\mathcal{H}_6 = C_L^3 + C_R^3 + B_L^2 C_L + B_R^2 C_R + H C_L^2 H^\dagger + H C_R^2 H^\dagger + C_L G_L^2 + C_R G_R^2 + C_L W_L^2 + C_R W_R^2\,. \tag{13.41}$$

This includes the pure gravity contributions discussed in Section 13.3 plus mixed SM-gravity terms. Note that at this mass dimension, the latter operators only contain SM bosons. An explicit operator basis is given by

$$
\begin{aligned}
\mathcal{L}_6 \;=\;& \frac{c_1}{\Lambda^2} C_{\mu\nu}{}^{\rho\sigma} C^{\mu\nu\alpha\beta} C_{\alpha\beta\rho\sigma} + \frac{\tilde{c}_1}{\Lambda^2} C_{\mu\nu}{}^{\rho\sigma} C^{\mu\nu\alpha\beta} \tilde{C}_{\alpha\beta\rho\sigma} \\
&+ \frac{c_2}{\Lambda^2} H^\dagger H C_{\mu\nu\rho\sigma} C^{\mu\nu\rho\sigma} + \frac{\tilde{c}_2}{\Lambda^2} H^\dagger H C_{\mu\nu\rho\sigma} \tilde{C}^{\mu\nu\rho\sigma} \\
&+ \frac{c_3}{\Lambda^2} B^{\mu\nu} B^{\rho\sigma} C_{\mu\nu\rho\sigma} + \frac{\tilde{c}_3}{\Lambda^2} B^{\mu\nu} B^{\rho\sigma} \tilde{C}_{\mu\nu\rho\sigma} + \frac{c_4}{\Lambda^2} G^{\mu\nu} G^{\rho\sigma} C_{\mu\nu\rho\sigma} + \frac{\tilde{c}_4}{\Lambda^2} G^{\mu\nu} G^{\rho\sigma} \tilde{C}_{\mu\nu\rho\sigma} \\
&+ \frac{c_5}{\Lambda^2} W^{\mu\nu} W^{\rho\sigma} C_{\mu\nu\rho\sigma} + \frac{\tilde{c}_5}{\Lambda^2} W^{\mu\nu} W^{\rho\sigma} \tilde{C}_{\mu\nu\rho\sigma} \,. \qquad (13.42)
\end{aligned}
$$

There are no new gravity operators at mass dimension 7. However, there is a multitude of terms in the Hilbert series at mass dimension 8. This is the first order where operators with SM fermions appear. For one flavor, i.e. $N_f = 1$, the part of the Hilbert series that involves gravity reads

$$
\begin{aligned}
\mathcal{H}_8 \;=\;& C_L^4 + HH^\dagger C_L^3 + H^2 \left(H^\dagger\right)^2 C_L^2 + 2B_L^2 C_L^2 + B_R^2 C_L^2 + C_R^2 C_L^2 + 2G_L^2 C_L^2 + G_R^2 C_L^2 + 2W_L^2 C_L^2 \\
&+ W_R^2 C_L^2 + HQuC_L^2 + H\mathcal{D}^2 H^\dagger C_L^2 + eLH^\dagger C_L^2 + dQH^\dagger C_L^2 + He^\dagger L^\dagger C_L^2 + Hd^\dagger Q^\dagger C_L^2 \\
&+ H^\dagger Q^\dagger u^\dagger C_L^2 + deu^2 C_L + HH^\dagger B_L^2 C_L + HH^\dagger G_L^2 C_L + B_L G_L^2 C_L + HH^\dagger W_L^2 C_L \\
&+ B_L W_L^2 C_L + dQ^2 uC_L + HQ\mathcal{D}^2 uC_L + eLQuC_L + eL\mathcal{D}^2 H^\dagger C_L + dQ\mathcal{D}^2 H^\dagger C_L \\
&+ HQuB_L C_L + d\mathcal{D}d^\dagger B_L C_L + e\mathcal{D}e^\dagger B_L C_L + H\mathcal{D}^2 H^\dagger B_L C_L + eLH^\dagger B_L C_L + dQH^\dagger B_L C_L \\
&+ L\mathcal{D}L^\dagger B_L C_L + Q\mathcal{D}Q^\dagger B_L C_L + \mathcal{D}uu^\dagger B_L C_L + HQuG_L C_L + d\mathcal{D}d^\dagger G_L C_L + dQH^\dagger G_L C_L \\
&+ Q\mathcal{D}Q^\dagger G_L C_L + \mathcal{D}uu^\dagger G_L C_L + HQuW_L C_L + H\mathcal{D}^2 H^\dagger W_L C_L + eLH^\dagger W_L C_L \\
&+ dQH^\dagger W_L C_L + L\mathcal{D}L^\dagger W_L C_L + Q\mathcal{D}Q^\dagger W_L C_L + HH^\dagger B_L W_L C_L + C_R^4 + HH^\dagger C_R^3 \\
&+ H^2 \left(H^\dagger\right)^2 C_R^2 + B_L^2 C_R^2 + 2B_R^2 C_R^2 + HQuC_R^2 + H\mathcal{D}^2 H^\dagger C_R^2 + eLH^\dagger C_R^2 + dQH^\dagger C_R^2 \\
&+ He^\dagger L^\dagger C_R^2 + Hd^\dagger Q^\dagger C_R^2 + H^\dagger Q^\dagger u^\dagger C_R^2 + C_R^2 G_L^2 + 2C_R^2 G_R^2 + HH^\dagger C_R G_R^2 + B_R C_R G_R^2 \\
&+ C_R^2 W_L^2 + 2C_R^2 W_R^2 + HH^\dagger C_R W_R^2 + B_R C_R W_R^2 + d^\dagger e^\dagger \left(u^\dagger\right)^2 C_R + HH^\dagger B_R^2 C_R \\
&+ H\mathcal{D}^2 e^\dagger L^\dagger C_R + H\mathcal{D}^2 d^\dagger Q^\dagger C_R + d^\dagger \left(Q^\dagger\right)^2 u^\dagger C_R + \mathcal{D}^2 H^\dagger Q^\dagger u^\dagger C_R + e^\dagger L^\dagger Q^\dagger u^\dagger C_R \\
&+ d\mathcal{D}d^\dagger B_R C_R + e\mathcal{D}e^\dagger B_R C_R + H\mathcal{D}^2 H^\dagger B_R C_R + L\mathcal{D}L^\dagger B_R C_R + He^\dagger L^\dagger B_R C_R \\
&+ Q\mathcal{D}Q^\dagger B_R C_R + Hd^\dagger Q^\dagger B_R C_R + \mathcal{D}uu^\dagger B_R C_R + H^\dagger Q^\dagger u^\dagger B_R C_R + d\mathcal{D}d^\dagger C_R G_R \\
&+ Q\mathcal{D}Q^\dagger C_R G_R + Hd^\dagger Q^\dagger C_R G_R + \mathcal{D}uu^\dagger C_R G_R + H^\dagger Q^\dagger u^\dagger C_R G_R + H\mathcal{D}^2 H^\dagger C_R W_R \\
&+ L\mathcal{D}L^\dagger C_R W_R + He^\dagger L^\dagger C_R W_R + Q\mathcal{D}Q^\dagger C_R W_R + Hd^\dagger Q^\dagger C_R W_R + H^\dagger Q^\dagger u^\dagger C_R W_R \\
&+ HH^\dagger B_R C_R W_R \,. \qquad (13.43)
\end{aligned}
$$

A classification of the dimension 8 operators of our basis is given in Table 13.2, while an explicit form for all 103 of them for $N_f = 1$ can be found in Tables III.F.1 and III.F.2 of Appendix III.F.[11]

13.5.1 Comments on the GRSMEFT operator basis

Let us comment on some interesting aspects of the GRSMEFT operator basis.

Matching what can be derived based on little group covariance and locality of on-shell massless 3-particle amplitudes (see e.g. [397]), we find in our basis the corresponding EFT operators

[11] As a curiosity, we find a single dimension-8 operator, $\mathcal{O}_{uedC}$ in Table III.F.2, that violates baryon and lepton numbers, by $\Delta B = \Delta L = 1$.

Structure	N_f	$N_f=1$	$N_f=3$	Representative Operator
C^4	3	3	3	$(C_{\mu\nu\rho\sigma}C^{\mu\nu\rho\sigma})^2$
C^3H^2	2	2	2	$H^\dagger H(C_{\mu\nu}{}^{\rho\sigma}C^{\mu\nu\alpha\beta}C_{\alpha\beta\rho\sigma})$
C^2H^4	2	2	2	$(H^\dagger H)^2(C_{\mu\nu\rho\sigma}C^{\mu\nu\rho\sigma})$
C^2X^2	18	18	18	$B_{\mu\nu}B^{\rho\sigma}C^{\mu\nu\alpha\beta}C_{\alpha\beta\rho\sigma}$
CH^2X^2	8	8	8	$H^\dagger H(C^{\mu\nu\rho\sigma}W^a_{\mu\nu}W^a_{\rho\sigma})$
CX^3	4	4	4	$C^{\mu\nu\rho\sigma}W^a_{\mu\nu}W^a_{\rho\alpha}B^\alpha{}_\sigma$
$C^2H\psi^2$	$12N_f^2$	12	108	$\bar{Q}_L H d_R(C_{\mu\nu\rho\sigma}C^{\mu\nu\rho\sigma})$
$CHX\psi^2$	$16N_f^2$	16	144	$C_{\mu\nu\rho\sigma}(\bar{Q}_L\sigma^{\mu\nu}d_R)\tau^a H W^{a,\rho\sigma}$
$C\psi^4$	$\frac{N_f^2}{3}(17N_f^2+3N_f-2)$	6	480	$\epsilon_{jk}C_{\mu\nu\rho\sigma}(\bar{Q}^j_L\sigma^{\mu\nu}u_R)(\bar{L}^k_L\sigma^{\rho\sigma}e_R)$
$CX\psi^2\mathcal{D}$	$20N_f^2$	20	180	$C_{\mu\nu\rho\sigma}(\bar{Q}_L\gamma^\mu\tau^a\nabla^\nu Q_L)W^{a,\rho\sigma}$
$C^2H^2\mathcal{D}^2$	2	2	2	$(\nabla_\mu H)^\dagger(\nabla^\mu H)(C_{\mu\nu\rho\sigma}C^{\mu\nu\rho\sigma})$
$CH^2X\mathcal{D}^2$	4	4	4	$C_{\mu\nu\rho\sigma}(\nabla^\mu H)^\dagger\tau^a(\nabla^\nu H)W^{a,\rho\sigma}$
$CH\psi^2\mathcal{D}^2$	$6N_f^2$	6	54	$C_{\mu\nu\rho\sigma}(\bar{Q}_L\sigma^{\mu\nu}\nabla^\rho d_R)\nabla^\sigma H$
Total	$43+\frac{N_f^2}{3}(17N_f^2+3N_f+160)$	103	1009	

Table 13.2: Classification of dimension-8 operators containing gravity interactions. C denotes the Weyl tensor, whereas H, ψ, X and $\mathcal{D}$ stand for the Higgs, fermions, gauge fields and derivatives respectively. We show the number of operators in each class for N_f fermion flavors and give one exemplary operator for each class.

modifying gravitational trilinear vertices: $C_{\mu\nu}{}^{\rho\sigma}C^{\mu\nu\alpha\beta}\overset{(\sim)}{C}{}_{\alpha\beta\rho\sigma}$ (3 gravitons), $X^{\mu\nu}X^{\rho\sigma}\overset{(\sim)}{C}{}_{\mu\nu\rho\sigma}$ (1 graviton and 2 gauge bosons), and $H^\dagger HC^{\mu\nu\rho\sigma}\overset{(\sim)}{C}{}_{\mu\nu\rho\sigma}$ (2 gravitons and 1 scalar, once the Higgs gets a vacuum expectation value). This one-to-one correspondence follows from the fact that our basis does not include terms that vanish on the free EOMs.

Similar to the EFT of pure gravity in vacuum, the leading dimension-4 Lagrangian induces, at one loop, RG evolution for some of the operators in the GRSMEFT, although in our basis all such operators involve SM fields only [368,369,371–373]. In this regard, the absence of (one-loop) divergences associated with mixed SM-gravity operators, such as $X^{\mu\nu}X^{\rho\sigma}C_{\mu\nu\rho\sigma}$, can be understood, in the particular case of gravity coupled to a $U(1)$ gauge field, by the invariance of the leading Einstein-Maxwell Lagrangian under vector field duality transformation [398], or from supersymmetry in the case of the Einstein-Yang-Mills system [399]. In Chapter 14 we rederive these non-renormalization results from helicity selection rules similar to [27]. Heavy (charged) matter fields give finite contributions [400–402] to the operators of the GRSMEFT, e.g. a Dirac fermion of unit hypercharge and mass Λ generates $c_3=-\frac{1}{90}(g'/4\pi)^2$, as well as contributions to several other operators in the SMEFT. In this regard, one should note that the latter operators, for instance $(B_{\mu\nu}B^{\mu\nu})^2$, receive direct contributions from the heavy dynamics, of $\mathcal{O}(g'^4/\Lambda^4)$, as well as contributions from operators with $R_{\mu\nu}$, R, which when rewritten in our basis are relatively suppressed by powers of $\Lambda/g'M_{\rm pl}$. We note in passing that we have not found in the literature the corresponding calculation for the coefficients of the dimension-6

Higgs-gravity operators in Eq. (13.42).

One can power-count, as in Eq. (13.28) for the pure gravity EFT, the size of the Wilson coefficients in a generic GRSMEFT. Focussing for simplicity on the subclass of operators involving gauge fields and gravity

$$\mathcal{L}_{eff} = \frac{m_*^4}{g_*^2} L\left(\frac{R_{\mu\nu\rho\sigma}}{m_*^2}, \frac{\nabla_\mu}{m_*}, \frac{\epsilon X_{\mu\nu}}{m_*^2}\right) - \frac{\hat{M}_{\rm pl}^2}{2} R - \frac{1}{4\hat{g}^2} X_{\mu\nu} X^{\mu\nu} \,, \tag{13.44}$$

where we introduced a "fundamental" kinetic term for the gauge field, with coupling $\hat{g} \lesssim g_*$, ϵ parametrizes the (multipole) charge of the heavy states that have been integrated out, and $\nabla_\mu = \partial_\mu + i\omega_\mu + i\epsilon' X_\mu$ with ϵ' parametrizing the (monopole) charge of the particles, if any, that remain in the EFT, fixing then the low-energy gauge coupling to $g = \epsilon' \hat{g}$ [128]. From Eq. (13.44) one can conclude that there could be situations in which gravitational operators such as $X^{\mu\nu} X^{\rho\sigma} C_{\mu\nu\rho\sigma}$ are enhanced compared to non-gravitational ones like $(X_{\mu\nu} X^{\mu\nu})^2$, e.g. if $\epsilon \ll \epsilon'$, a pattern that arises for instance from milli-charged particles – an axion would belong to this category. This however does not appear as an optimal (phenomenological) scenario, since the light charged SM particles that remain in the spectrum below m_*, e.g. the electron, would dominate the new EFT coefficients (since $\epsilon' \gg \epsilon$) after being themselves integrated out at even lower energies. This is unless there exists no charged particle below m_*, i.e. $m_* \ll m_e$, for which, while $\epsilon \ll 1$, $\epsilon' = 0$ – for the GRSMEFT, this would mean a very low new physics scale, yet with an interesting and unexplored parameter space in terms of mixed SM-gravity effects. In scenarios where $\epsilon \gg \epsilon' \neq 0$, the non-gravitational operators are instead comparatively enhanced. We also note that from a purely low-energy point of view, there seems to be nothing wrong with taking mixed SM-gravity operators, such as $X^{\mu\nu} X^{\rho\sigma} C_{\mu\nu\rho\sigma}$, of size $\mathcal{O}(g^2/g_*^2 m_*^2)$, as the leading deformation in the EFT, in the sense that quantum corrections within the EFT do not point towards large non-gravitational operators as long as the cutoff, which saturates the loops in the UV, satisfies $m_* \lesssim 4\pi(g_*/g) M_{\rm pl}$, and this even for $g_* \ll g$, although such a condition goes against NDA.[12]

Regardless of these facts, there always remains the obstacle that to probe operators intrinsically sensitive to gravitational physics, by which we mean those that do not depend on $R_{\mu\nu}$, R and therefore do not contribute to the SMEFT, one needs to overcome the $M_{\rm pl}$ suppression that comes with gravitational interactions. This is of course the reason why experimental constraints on the SMEFT are much more stringent than those on the rest of the GRSMEFT. The question of how to test gravitational EFT operators has been partly investigated before, e.g. in [401] for the Einstein-Maxwell system after integrating out the electron, or more recently in [404] for more general situations yet concentrating still on photon propagation around non-trivial gravitational backgrounds. For purely gravitational operators, [382] studied their effects on the gravitational waves from merging black holes. In all these situations, the conclusion is that for the effects of the higher-dimensional operators to be observable, the typical size (e.g. the Schwarzschild radius) and distance from the gravitational source should be of the order of the (inverse) cutoff of the EFT. Leaving aside our preconceptions on the expected size of the mixed SM-gravity operators with respect to non-gravitational ones, one should consider probing the former at high-energy colliders.Finally, we think it is worthwhile to further investigate and extend the theoretical constraints based on causality, unitarity and analyticity to the full set of operators in Eq. (13.42).

[12]However, at least for the mixed SM-gravity operator $X^{\mu\nu} X^{\rho\sigma} C_{\mu\nu\rho\sigma}$ with $X_{\mu\nu}$ associated with a $U(1)$ gauge field, this possibility seems to be in tension with arguments related to the weak gravity conjecture [395, 403].

13.6 Gravity EFT in $d > 4$ spacetime dimensions

All the discussion so far implicitly assumed that we work in four spacetime dimensions. However, our results are more general and it is straightforward to extend them to $d > 4$ spacetime dimensions. The independent building blocks for the EFT of gravity, i.e. the graviton single particle module R_C, which we identified in Section 13.2 for $d = 4$ spacetime dimensions, trivially extends to $d > 4$.[13] The derivation of the graviton single particle module only made use of the Einstein equations and Bianchi identities, which have the same form in any dimension. Consequently, also R_C in Eq. (13.17) is valid in dimensions larger than 4.

In this section we will shortly outline how to obtain the character for the single particle module χ_C and the corresponding Hilbert series for gravity in vacuum in $d > 4$ and explicitly perform the construction for $d = 5$.

13.6.1 Character for the Single Particle Module

We work in Euclidean space, where the Lorentz group in d dimensions is $SO(d)$. The finite dimensional representations of $SO(d)$ can be labeled by partitions $l = (l_1, l_2, \ldots, l_r)$ with $l_1 \geq \cdots \geq l_{r-1} \geq |l_r|$ for $SO(2r)$ and $l_1 \geq \cdots \geq l_r \geq 0$ for $SO(2r+1)$, where r is the rank of the group. These representations are in a one-to-one correspondence with Young diagrams, i.e. they correspond to tensors with $|l| = \sum_i l_i$ indices, which are (anti)symmetrized according to the corresponding Young diagram (in this regard, such a labelling is more convenient than the one we have used for $SO(4)$ in the main text). In this notation, the fundamental representation is labeled by $l = (1, 0, \ldots, 0)$, the antisymmetric tensor with two indices is $l = (1, 1, 0, \ldots, 0)$ and the completely symmetric, traceless tensor with n indices corresponds to $l = (n, 0, \ldots, 0)$. Therefore the Weyl tensor in d dimensions lives in the representation labeled by $l = (2, 2, 0, \ldots, 0)$.[14]

The single particle module in Eq. (13.17) consists of the Weyl tensor and symmetric, traceless combinations of covariant derivatives acting on the Weyl tensor. In the notation we introduced above, it is clear that $\nabla_{\{\mu_1} \cdots \nabla_{\mu_n} C_{\mu\}\nu\rho\sigma}$ transforms in the representation corresponding to $l = (n+2, 2, 0, \ldots, 0)$, which implies that the character of the single particle module is given by

$$\chi_C^{(d)}(\mathcal{D}; x) = \sum_{n=0}^{\infty} \mathcal{D}^{n+2} \chi^{(d)}_{(n+2,2,0,\ldots,0)}(x)\,, \tag{13.45}$$

where $\chi_l^{(d)}(x)$ are the $SO(d)$ characters.

Let us specialize to $d = 5$ dimensions. Eq. (13.45) can be evaluated explicitly using the Weyl character formula for $SO(5)$ characters, which can be found e.g. in Appendix A of [23]

$$\begin{aligned}\chi_C^{(5)}(\mathcal{D}; x) = \mathcal{D}^2 P^{(5)}(\mathcal{D}; x) \Big[&\chi^{(5)}_{(2,2)}(x) - \mathcal{D}\big(\chi^{(5)}_{(2,2)}(x) + \chi^{(5)}_{(2,1)}(x)\big) \\ &+ \mathcal{D}^2\big(\chi^{(5)}_{(2,1)}(x) + \chi^{(5)}_{(1,1)}(x)\big) - \mathcal{D}^3 \chi^{(5)}_{(1,1)}(x) \Big]\,.\end{aligned} \tag{13.46}$$

At this point we want to emphasize that unlike in $d = 4$, the single particle module R_C cannot be identified with a short conformal representation, whose scaling dimension saturates the unitarity bound, by formally assigning this scaling dimension to the Weyl tensor. The character for the conformal representation $[4; (2, 2)]$ in $d = 5$ dimensions is given by (see e.g. [405])

$$\chi^{(5)}_{[4;(2,2)]}(\mathcal{D}; x) = \mathcal{D}^4 P^{(5)}(\mathcal{D}; x) \Big[\chi^{(5)}_{(2,2)}(x) - \mathcal{D}\chi^{(5)}_{(2,1)}(x) + \mathcal{D}^2 \chi^{(5)}_{(1,1)}(x) \Big]\,, \tag{13.47}$$

[13] In $d < 4$ the Weyl tensor identically vanishes, i.e. the graviton is not dynamical.

[14] Note that $SO(2r)$ admits chiral representations if $l_r \neq 0$, which is why in $d = 4$ the Weyl tensor can be decomposed into a left-handed and a right-handed part, which belong to the representations labeled by $(2, 2)$ and $(2, -2)$, respectively.

which clearly differs from Eq. (13.46) even after assigning a scaling dimension of 4 to the Weyl tensor. The reason for this is that the conformal primary, i.e. the equivalent of the Weyl tensor, does not satisfy the second Bianchi identity. The corresponding descendent $\nabla_{[\mu_1} C_{\mu\nu]\rho\sigma}$, which transforms in the representation labeled by $l = (2, 2)$, is therefore not subtracted from the conformal multiplet, as can be explicitly seen in Eq. (13.47).

Note that there is no known expression for $\Delta\mathcal{H}$ in Eq. (11.50) if the single particle modules cannot be identified with conformal representations. However, Eq. (11.51) for $\mathcal{H}_0$ still holds.

13.6.2 Gravity in vacuum in $d = 5$

The Hilbert series for pure gravity in $d = 5$ dimensions can be computed using Eq. (11.51) and the character for the single particle module in Eq. (13.46). Grading the spurions according to their mass dimension, i.e. $C \to \epsilon^2 C$ and $\mathcal{D} \to \epsilon\mathcal{D}$, and expanding up to mass dimension ten we obtain[15]

$$\begin{aligned}\mathcal{H}_0(\mathcal{D}, C; \epsilon) &= \int d\mu_{SO(5)}(x) \frac{1}{P^{(5)}(\epsilon\,\mathcal{D}, x)} \mathrm{PE}\left[\frac{C}{\mathcal{D}^2}\right] \\ &= \epsilon^6 C^3 + \epsilon^8 4\, C^4 + \epsilon^{10}\left(7\, C^4\mathcal{D}^2 + 5\, C^5\right) + \dots\,,\end{aligned} \tag{13.48}$$

where we have dropped terms of mass dimension five or lower, since they also receive contributions from $\Delta\mathcal{H}$. Note that the number of independent operators in $d = 5$ differs from the number of $\mathcal{CP}$ even operators in $d = 4$, i.e. the operators which can be written without the dual of the Weyl tensor. This implies that, beyond chirality, there are genuinely new contractions of Weyl tensors which are linearly dependent or vanish in $d = 4$. The number of independent operators without derivatives can be cross-checked with the number of Weyl invariants given in [406] and we find full agreement.

[15] The explicit expressions for the $SO(5)$ integration measure and characters can be found e.g. in the Appendix of [23].

Chapter 14

(Non-)Renormalization of gravity

In the previous chapter, we developed a method to construct non-redundant operator bases for gravitational EFTs. As was pointed out in Section 13.1, already GR on its own is non-renormalizable. Quantum effects radiatively generate higher-order effective operators and induce mixing among the effective operators. However, at one-loop not all operators which could naively be generated are actually generated and also not all operators which could naively mix, do actually mix. The same phenomenon has been observed in the SMEFT, where it manifests itself as mysterious zeroes in the anomalous dimension matrix at mass dimension six [24–26]. Some of these zeroes can be explained using supersymmetric non-renormalization theorems [407]. A more intuitive explanation is provided by helicity selection rules [27, 408] and more recently angular momentum selection rules [307], which combined explain almost all non-trivial zeroes.

The goal of this chapter is to extend the helicity selection rules of [27] to gravitational EFTs in order to explain the non-renormalization of GRSMEFT operators at one-loop. On the one hand this is interesting from a purely theoretical point of view. But on the other hand it might also be useful in more phenomenological applications: the non-zero anomalous dimensions tell us which operators are generated by RG evolution and are therefore expected to be present at low energy scales.

In the following we first introduce in Section 14.1 the basics of well-established amplitude methods in EFTs. In Section 14.2 we use these methods to derive for the first time helicity bounds on tree-level gravitational amplitudes, which we use in Section 14.3 to formulate helicity selection rules and non-renormalization theorems at one-loop. In Section 14.4 we subsequently compute all non-zero anomalous dimensions in a toy GRSMEFT for all dimension six operators, which induce three- and four-point amplitudes.

The material in Sections 14.2, 14.3 and 14.4 are original results and are based on work in progress [34],[1] which has not been published yet.

14.1 Amplitude formalism in EFTs

The power of amplitude methods originates from working exclusively with physical quantities, i.e. on-shell scattering amplitudes. This bypasses the Lagrangian formulation of QFTs, what requires the introduction of field redundancies in order to describe gauge theories or gravity. These redundancies are an artifact of describing particles, which are in abstract terms irreducible representations of the little group $SO(3)$ for massive and $ISO(2)$ for massless particles, in terms of quantum fields in irreducible representations of the full Lorentz group.

[1] [34]: P. Baratella, D. Haslehner, M. Ruhdorfer, J. Serra and A. Weiler, *(Non-)Renormalization of Gravity*, in preparation.

In Section 14.1.1 we first introduce spinor-helicity variables and then discuss the structure of tree-level amplitudes. Afterwards we point out the relation between EFT operators and contact amplitudes in Section 14.1.2. Finally in Section 14.1.3 we demonstrate how anomalous dimensions can be efficiently computed within the amplitude formalism.

14.1.1 Spinor-helicity variables and tree-level amplitudes

An important ingredient of modern amplitude methods are spinor-helicity variables, which have a well-defined transformation behavior under the little group and make gauge redundancies obsolete. In this section we introduce massless spinor-helicity variables along the lines of [275, 397, 409–411].[2] Our conventions for two-component spinors follow [413], i.e. in particular the gamma matrices are defined as

$$\gamma^\mu = \begin{pmatrix} 0 & (\sigma^\mu)_{\alpha\dot\beta} \\ (\bar\sigma^\mu)^{\dot\alpha\beta} & 0 \end{pmatrix}, \quad \text{with} \quad \sigma^\mu_{\alpha\dot\beta} = (\delta_{\alpha\dot\beta}, \boldsymbol{\sigma}_{\alpha\dot\beta}) \quad \text{and} \quad \bar\sigma^{\mu\,\dot\alpha\beta} = (\delta^{\dot\alpha\beta}, -\boldsymbol{\sigma}^{\dot\alpha\beta}) \tag{14.1}$$

where $\boldsymbol{\sigma}$ is a vector containing the Pauli matrices. We also work with amplitudes, where all external particles are taken as incoming.

The $(1/2, 0)$ and $(0, 1/2)$ spinor representations are the fundamental representations of the complexified Lorentz group $SO(1,3) \simeq [SU(2)_L \times SU(2)_R]/Z_2$. The LH and RH Weyl spinors $\psi_\alpha \sim (1/2, 0)$ and $\tilde\psi_{\dot\alpha} \sim (0, 1/2)$,[3] are therefore the basic building blocks for finite dimensional representations. Thus momenta $P_\mu \sim (1/2, 1/2)$ are more naturally represented as bispinors $P_{\alpha\dot\alpha}$. We can map a four vector into a 2×2 matrix with the Pauli matrices

$$P_{\alpha\dot\alpha} \equiv \sigma^\mu_{\alpha\dot\alpha} P_\mu = \begin{pmatrix} p^0 - p^3 & p^1 + i\,p^2 \\ p^1 - i\,p^2 & p^0 + p^3 \end{pmatrix}. \tag{14.2}$$

Note that $\det(P_{\alpha\dot\alpha}) = P_\mu^2 = m^2$, what vanishes for momenta of massless particles and implies that $P_{\alpha\dot\alpha}$ is not of full rank and therefore can be written as a product of two spinors, i.e.

$$P_{\alpha\dot\alpha} = \lambda_\alpha \tilde\lambda_{\dot\alpha}\,, \tag{14.3}$$

where λ^α and $\tilde\lambda^{\dot\alpha}$ are often called "holomorphic" and "anti-holomorphic" spinors. Note that λ and $\tilde\lambda$ are not Grassmann numbers. For complex momenta λ^α and $\tilde\lambda^{\dot\alpha}$ are independent complex vectors, whereas for real momenta they satisfy

$$\tilde\lambda_{\dot\alpha} = \pm(\lambda_\alpha)^*\,, \tag{14.4}$$

where $+$ corresponds to positive energies. Physical quantities can now be expressed in terms of the spinor variables. It is convenient to introduce a square and angle bracket notation

$$\lambda^\alpha = \langle\lambda|^\alpha\,, \quad \lambda_\alpha = |\lambda\rangle_\alpha\,, \quad \tilde\lambda_{\dot\alpha} = [\tilde\lambda|_{\dot\alpha}\,, \quad \tilde\lambda^{\dot\alpha} = |\tilde\lambda]^{\dot\alpha}\,. \tag{14.5}$$

The indices can be raised and lowered with the epsilon tensor, e.g. $\lambda_\alpha = \epsilon_{\alpha\beta}\lambda^\beta$. Lorentz invariant objects can be formed with the epsilon tensor or equivalently by gluing together the brackets, i.e.

$$\langle\lambda\,\chi\rangle \equiv \epsilon_{\alpha\beta}\lambda^\alpha\chi^\beta = \lambda^\alpha\lambda_\alpha = -\lambda_\alpha\chi^\alpha = -\langle\chi\,\lambda\rangle\,, \tag{14.6}$$

$$[\lambda\,\chi] \equiv \epsilon^{\dot\alpha\dot\beta}\tilde\lambda_{\dot\alpha}\tilde\chi_{\dot\beta} = \tilde\lambda_{\dot\alpha}\tilde\chi^{\dot\alpha} = -\tilde\lambda^{\dot\alpha}\tilde\chi_{\dot\alpha} = -[\tilde\chi\,\tilde\lambda]\,, \tag{14.7}$$

[2] Note that there is a straightforward extension of the formalism to massive particles [412].

[3] $\alpha, \dot\alpha = 1, 2$ denote LH and RH spinor indices, respectively

with the normalization $\epsilon^{12} = \epsilon^{\dot{1}\dot{2}} = -\epsilon_{12} = -\epsilon_{\dot{1}\dot{2}} = 1$ and $\langle \lambda\, \lambda \rangle = [\tilde{\lambda}\, \tilde{\lambda}] = 0$. In our convention undotted indices are always contracted from top to bottom, whereas the reverse holds for dotted indices. The Mandelstam invariants can now be expressed in terms of angle and square brackets

$$s_{ij} = (p_i + p_j)^2 = 2 p_i p_j = \langle i\, j \rangle [j\, i]\,. \tag{14.8}$$

Spinor products satisfy some additional relations. Momentum conservation, taking all particles as ingoing, takes the following form in spinor variables $\sum_j \lambda_\alpha^j \tilde{\lambda}_{\dot{\alpha}}^j = 0$. Sandwiching this inbetween two additional spinors gives

$$\sum_{j=1}^{n} \langle i\, j \rangle [j\, k] = 0\,. \tag{14.9}$$

One obtains additional relations by observing that the spinors live in a two-dimensional vector space and therefore only two of them can be linearly independent. This implies that we can express λ_1^α in terms of some λ_2^α and λ_3^α, i.e.

$$\lambda_1^\alpha = \frac{\langle 1\, 3 \rangle}{\langle 2\, 3 \rangle} \lambda_2^\alpha + \frac{\langle 2\, 1 \rangle}{\langle 2\, 3 \rangle} \lambda_3^\alpha\,, \tag{14.10}$$

and similarly for the square brackets. This can be contracted with additional external spinors to yield the so-called Schouten identities. For four external particles this takes the form

$$\langle 1\, 2 \rangle \langle 3\, 4 \rangle + \langle 1\, 3 \rangle \langle 4\, 2 \rangle + \langle 1\, 4 \rangle \langle 2\, 3 \rangle = 0\,. \tag{14.11}$$

Note that Eq. (14.2) does not fix λ and $\tilde{\lambda}$ uniquely. The momentum is left invariant under

$$\lambda_i^\alpha \to t\, \lambda_i^\alpha\,, \qquad \tilde{\lambda}_i^{\dot{\alpha}} \to t^{-1} \tilde{\lambda}_i^{\dot{\alpha}}\,, \tag{14.12}$$

which corresponds to a little group transformation. For complex momenta λ_i and $\tilde{\lambda}_i$ are independent and t can be any complex number. However, for real momenta the spinors satisfy the reality condition $\lambda_i = (\tilde{\lambda}_i)^*$, s.t. t can only be a phase. In this case one immediately sees that this rescaling freedom is generated by the $U(1)$ generator of helicity

$$\hat{h} = \frac{1}{2} \sum_{i=1}^{n} \left[-\lambda_i^\alpha \frac{\partial}{\partial \lambda_i^\alpha} + \tilde{\lambda}_i^{\dot{\alpha}} \frac{\partial}{\partial \tilde{\lambda}_i^{\dot{\alpha}}} \right], \tag{14.13}$$

which indeed generates the little group for massless particles.[4] This implies that λ and $\tilde{\lambda}$ carry helicity weight of $-1/2$ and $+1/2$, respectively. Note that we marked the helicity generator with a hat in order to differentiate it from the total helicity of an amplitude, which we will denote as $h = \sum_i h_i$ in the following.

Scattering amplitudes transform under little group transformations as (see e.g. [409])

$$\mathcal{A}(1_{h_1}, 2_{h_2}, \ldots, n_{h_n}) \to \prod_{i=1}^{n} t_i^{-2\, h_i} \mathcal{A}(1_{h_1}, 2_{h_2}, \ldots, n_{h_n})\,. \tag{14.14}$$

Thus we can write any scattering amplitude in the form

$$\mathcal{A}(1_{h_1}, \ldots, n_{h_n}) \propto f(\{s_{ij}\}) \prod_{i=1}^{n} \lambda_i^{r_i} \tilde{\lambda}_i^{\bar{r}_i}\,, \qquad \bar{r}_i - r_i = 2\, h_i\,, \tag{14.15}$$

[4] Note that the little group for massless particles is actually $ISO(2)$, generated by A, B and $\hat{h}$. However, in order to avoid continuous spin representations, one has to choose states with eigenvalue 0 under A and B, which effectively reduces the little group to $U(1)$ generated by the helicity operator.

where the spinors have to be contracted in a Lorentz invariant way and $f(\{s_{ij}\})$ is a scalar function purely of the kinematic invariants. In any scattering amplitude we can therefore factor out the full little group scaling of the external particles. Note that while Eq. (14.15) parameterizes all possible scattering amplitudes for a given set of external states, not every possibility is independent, since there are still redundancies due to momentum conservation and Schouten identities.

Despite the remaining ambiguities, the little group scaling is already a very powerful tool and strongly restricts the form of allowed amplitudes. This is especially true for three particle amplitudes, which are completely fixed by their helicity scaling. Momentum conservation requires all kinematic invariants for on-shell three-point amplitudes to vanish, i.e. $s_{12} = s_{13} = s_{14} = 0$. Extending the discussion to complex momenta, where λ_i and $\tilde{\lambda}_i$ are independent, we see that three particle amplitudes only have support on two kinematic configurations, the anti-holomorphic configuration with all vanishing angle brackets

$$\langle 1\,2\rangle = \langle 1\,3\rangle = \langle 1\,4\rangle = 0 \quad \text{i.e.} \quad \lambda_1 \propto \lambda_2 \propto \lambda_3\,, \tag{14.16}$$

or the holomorphic configuration with vanishing square brackets

$$[1\,2] = [1\,3] = [1\,4] = 0 \quad \text{i.e.} \quad \tilde{\lambda}_1 \propto \tilde{\lambda}_2 \propto \tilde{\lambda}_3\,. \tag{14.17}$$

Thus all three particle amplitudes are of the form

$$\mathcal{A}(1_{h_1}, 2_{h_2}, 3_{h_3}) = g \begin{cases} \langle 1\,2\rangle^{h_3-h_1-h_2}\langle 2\,3\rangle^{h_1-h_2-h_3}\langle 3\,1\rangle^{h_2-h_3-h_1}\,, & h \leq 0 \\ [1\,2]^{h_1+h_2-h_3}[2\,3]^{h_2+h_3-h_1}[3\,1]^{h_3+h_1-h_2}\,, & h \geq 0 \end{cases} \tag{14.18}$$

where g is a coupling constant. Note that dimensional analysis relates the mass dimension of the coupling to the total helicity of the amplitude it mediates. Three-point amplitudes in four dimensions have mass dimension $[\mathcal{A}_3] = 1$ and it holds that

$$[\mathcal{A}_3] = [g] + |h| \qquad \Rightarrow \qquad |h| = 1 - [g]\,, \tag{14.19}$$

what implies that relevant couplings, i.e. three scalar interactions, induce $h = 0$ amplitudes and marginal couplings, such as gauge couplings, $|h| = 1$ amplitudes. Higher helicity three-point amplitudes require irrelevant couplings, i.e. only appear in EFTs. Also note that not all three point amplitudes are valid and lead to consistent theories, including all non-scalar $h = 0$ amplitudes. A discussion on consistent three particle amplitudes can be found in [414].

Higher point amplitudes can be obtained from their analyticity properties. It is well-known that scattering amplitudes are analytic in the kinematic invariants, except for simple poles and branch cuts on the real axis. The concept of locality implies that these singularities have the interpretation of particle exchange: poles signify the tree-level exchange of one particle, whereas branch cuts correspond to multi-particle exchange in loops. If we specialize to tree-level amplitudes, there are only simple poles and on the poles, i.e. for kinematic configurations on which the internal particle is on-shell, the amplitude factorizes into lower-point amplitudes. Any pole must correspond to a factorization channel. This implies that higher-point amplitudes can be constructed from lower-point amplitudes by requiring consistent factorization in all channels. For four-point amplitudes this implies that

$$\lim_{s_{12}\to 0} s_{12} \cdot \mathcal{A}_4(1_{h_1}, 2_{h_2}, 3_{h_3}, 4_{h_4}) = \sum_h \mathcal{A}_3(1_{h_1}, 2_{h_2}, P_h)\,\mathcal{A}_3(-P_{-h}, 3_{h_3}, 4_{h_4})\,, \tag{14.20}$$

where $P = -(p_1 + p_2)$ with similar relations for the 13 and 14 channel. The sum goes over all allowed intermediate particles. In general there are additional contact contributions, which

vanish on the factorization channel and therefore cannot be determined from the factorization limits. Theories in which these contact terms vanish are called on-shell constructible, since any n-point amplitude can be constructed iteratively from a set of seed amplitudes. Examples of on-shell constructible theories are gauge theories and pure gravity [415]. For a nice discussion on sufficient criteria for a theory to be on-shell constructible we refer the reader to [416]. There are simple algorithmic recursion relations to efficiently construct amplitudes in on-shell constructible theories, such as the well-known BCFW relations [417, 418] (see e.g. [397] for a more thorough discussion).

14.1.2 EFT amplitudes and the operator basis

As we have discussed in Section 11.4, a non-redundant operator basis parameterizes all physically observable independent IR deformations of a leading theory. In terms of on-shell amplitudes this corresponds to new independent contributions to the amplitude, which cannot be determined from factorization limits. EFT interactions are therefore in one-to-one correspondence with non-factorizable contact amplitudes. The relation is especially clear when one works in an operator basis in which all operators proportional to the free EOM have been removed with field redefinitions, such as the Warsaw basis [419]. Note that the terms in the Hilbert series, e.g. in Eq. (13.43) for the dimension eight GRSMEFT, can be directly matched to amplitudes, since we work with chiral field strengths and Weyl fermions.

The above discussion implies that instead of constructing the operator basis for an EFT, one can equivalently construct a basis of contact amplitudes. In order to do so one starts from Eq. (14.15) and writes down all allowed amplitude structures for a given set of external states. One further imposes Bose or Fermi statistics and applies momentum conservation and the Schouten identities to remove redundancies. These methods have recently been applied to the SMEFT, the electroweak EFT and gravity [419–422] with extensions to massive particles in [423, 424]. An alternative approach is the use of momentum twister variables [425], which trivially staisfy momentum conservation, or the construction of harmonics on the kinematic manifold of scattering amplitudes [344, 345].

14.1.3 Anomalous dimensions from amplitudes

Amplitude methods are not only useful for tree-level computations, but also provide many simplifications at one-loop. As we will show in this section, the study of the RG is tightly connected to properties of the theory at tree-level. UV-divergent parts of loop amplitudes can be related to the product of two tree-level amplitudes with a phase-space integral over the intermediate particles. This simplicity of dealing with loop computations make amplitude methods a useful tool for the determination of anomalous dimensions (see [426–430] for recent work in this direction). In the following we demonstrate how amplitude methods can be used to efficiently compute anomalous dimensions, following the discussion and notation of [426].

Here we define the anomalous dimension of the Wilson coefficients in an effective Lagrangian of the form $\mathcal{L} = \sum_i C_i \mathcal{O}_i$ as[5]

$$\gamma_i \equiv \frac{d\, C_i}{d\, \ln \mu} = \sum_j \gamma_{ij} C_j \,, \tag{14.21}$$

where μ is the renormalization scale. Using the one-to-one correspondence of effective operators

[5]This agrees with the definition in Section 11.2.

to contact amplitude, we call $\mathcal{A}_i$ the minimal amplitude induced by $C_i\mathcal{O}_i$.[6] The full one-loop amplitude for the corresponding process is then given by

$$\mathcal{A} = \mathcal{A}_i + \mathcal{A}_{\text{loop}}\,. \tag{14.22}$$

The combination of the renormalization scale dependent loop amplitude and the contact amplitude with a running Wilson coefficient $C_i(\mu)$ is scale independent, s.t.

$$\gamma_i \frac{\mathcal{A}_i}{C_i} = -\frac{d\,\mathcal{A}_{\text{loop}}}{d\,\ln\mu}\,. \tag{14.23}$$

Note that for non-minimal amplitudes also the beta functions of additional couplings have to be included. The idea behind obtaining the UV scale dependence of the loop amplitude is based on the fact that any one-loop amplitude $\mathcal{A}_{\text{loop}}$ can be decomposed into a basis of scalar integrals I_n

$$\mathcal{A}_{\text{loop}} = \sum_a C_2^{(a)} I_2^{(a)} + \sum_b C_3^{(b)} I_3^{(b)} + \sum_c C_4^{(c)} I_4^{(c)} + R\,, \tag{14.24}$$

where $I_2^{(a)}, I_3^{(b)}$ and $I_4^{(c)}$ are bubble, triangle and box integrals, named after their topology with $n = 2, 3, 4$ propagators in the loop, respectively. Their explicit form is given by

$$I_n = (-1)^n \mu^{4-D} \int \frac{d^D l}{(2\pi)^D i} \frac{1}{l^2 (l-P_1)^2 (l-P_1-P_2)^2 \cdots (l-P_1-\ldots-P_{n-1})^2}\,, \tag{14.25}$$

where the P_i are combinations of external momenta. The $C_n^{(i)}$ in Eq. (14.24) are kinematic dependent coefficients and R is a rational function of kinematic invariants.

UV divergences and therefore contributions to the UV anomalous dimension γ_i come exclusively from bubble integrals I_2, whereas I_3 and I_4 can be seen to be UV finite on dimensional grounds. Consequently the anomalous dimension, which can be determined from the coefficient of the $1/\epsilon$ divergence in the bubble integrals, is proportional to the sum of bubble coefficients

$$\hat{\gamma}_i \frac{\mathcal{A}_i}{C_i} = -\frac{1}{8\pi^2} \sum_a C_2^{(a)}\,, \tag{14.26}$$

where $\hat{\gamma}_i = \gamma_i$ in the absence of IR divergences. In the presence of IR divergences in $\mathcal{A}_{\text{loop}}$, the coefficient of the $1/\epsilon$ pole in the bubble integrals might not contain the full UV divergence of the amplitude. Massless bubble integrals vanish in dimensional regularization due to the cancelation of UV and IR divergences. This implies that $\hat{\gamma}_i$ in Eq. (14.26) is a combination of UV and IR anomalous dimensions

$$\hat{\gamma}_i = \gamma_i - \gamma_{i,\text{coll}}\,, \tag{14.27}$$

where we identified the IR divergences from massless bubble integrals as collinear divergences, encoded in the collinear anomalous dimension $\gamma_{i,\text{coll}}$. Collinear divergences are universal at one-loop and only depend on the external particles, i.e. they can be written as the sum over collinear anomalous dimensions of the external particles j, i.e. $\gamma_{i,\text{coll}} = \sum_j \gamma^j_{i,\text{coll}}$. We will review a method to compute collinear anomalous dimensions in Appendix III.I. Further soft IR divergences from triangle and box integrals do not affect $C_2^{(a)}$.

Let us now turn to a simple method for extracting the bubble coefficients $C_2^{(a)}$ directly from unitarity double cuts (two-cuts), which was first reported in [431]. Here we present a slightly

[6] The minimal amplitude contains only one insertion of $\mathcal{O}_i$ and no other interaction, i.e. it is non-vanishing in the limit of a free theory extended by $\mathcal{O}_i$.

modified version which employs a different parameterization of the two-particle phase space. Performing a two-cut in a channel a of $\mathcal{A}_{\text{loop}}$, we obtain[7]

$$\text{Cut}_2^{(a)}\left[\mathcal{A}_{\text{loop}}\right] = -\frac{C_2^{(a)}}{8\pi^2} + \text{Cut}_2^{(a)}\left[\sum_b C_3^{(b)} I_3^{(b)} + \sum_c C_4^{(c)} I_4^{(c)}\right]. \tag{14.28}$$

The main ingredient to extract $C_2^{(a)}$ from this relation is the fact that two-cuts of massless triangle and box integrals yield non-rational functions of the kinematic invariants, whereas the two-cut of bubble integrals is proportional to $C_2^{(a)}$ and therefore a rational function of the kinematic quantities. Hence dropping all non-rational contributions in the two-cut projects out the bubble coefficients and we can write Eq. (14.26) as

$$\hat{\gamma}_i \frac{\mathcal{A}_i}{C_i} = \sum_a \mathcal{R}\,\text{Cut}_2^{(a)}\left[\mathcal{A}_{\text{loop}}\right], \tag{14.29}$$

where the action of the operator $\mathcal{R}$ is to pick all rational parts of the two-cut. Analyticity and unitarity of the scattering amplitude implies that the one-loop amplitude factorizes into a product of two tree-level amplitudes on the two-cut, s.t.

$$\mathcal{R}\,\text{Cut}_2^{(a)}\left[\mathcal{A}_{\text{loop}}\right] = -\frac{1}{4\pi^3}\sum_{\ell_1,\ell_2}\sigma_{\ell_1\ell_2}\mathcal{R}\int d\text{LIPS}\;\mathcal{A}_L(...-\bar{\ell}_2-\bar{\ell}_1)\,\mathcal{A}_R(\ell_1\ell_2...)\,, \tag{14.30}$$

where the sum is over all possible choices of internal legs, the integral is over the phase space associated with ℓ_1 and ℓ_2 and $\sigma_{\ell_1\ell_2} = (-i)^{F_{\ell_1\ell_2}}$, where $F_{\ell_1\ell_2}$ counts the number of fermions in the list $\{\ell_1,\ell_2\}$. This factor arises from the convention in which $|-\ell\rangle = i|\ell\rangle$ and $|-\ell] = i|\ell]$. There is an additional factor of $1/2$ if ℓ_1 and ℓ_2 are identical particles. Plugging this into Eq. (14.29) we obtain our master formula to compute anomalous dimensions

$$\gamma_i\frac{\mathcal{A}_i(1\dots n)}{C_i} = -\frac{1}{4\pi^3}\sum_{\substack{\text{cuts}\\ \ell_1,\ell_2}}\sigma_{\ell_1\ell_2}\mathcal{R}\int d\text{LIPS}\;\mathcal{A}_L(...-\bar{\ell}_2-\bar{\ell}_1)\,\mathcal{A}_R(\ell_1\ell_2...) + \gamma_{\text{coll}}\mathcal{A}^{\text{tree}}(1\dots n). \tag{14.31}$$

The action of $\mathcal{R}$ can be implemented in an algorithmic way in the evaluation of the phase space integral using Hermite Polynomial Reduction (HPR) (see [431]). In the following we describe the procedure we use to evaluate Eq. (14.30).

For internal momenta ℓ_1 and ℓ_2 satisfying $\ell_1+\ell_2 = p+q$ for some massless external momenta, or combinations of external momenta, p and q with $p^2 = q^2 = 0$ we can parameterize the two-particle phase space by relating $|\ell_1\rangle$ and $|\ell_2\rangle$ to $|p\rangle$ and $|q\rangle$

$$|\ell_1\rangle = \cos\theta\,|p\rangle - \sin\theta\,e^{i\phi}|q\rangle\,, \qquad |\ell_2\rangle = \sin\theta\,e^{-i\phi}|p\rangle + \cos\theta|q\rangle\,, \tag{14.32}$$

with the square brackets given by the complex conjugate of this expression. The phase space integral in this parameterization is given by [432]

$$\int d\text{LIPS} = \frac{\pi}{2}\int_0^{2\pi}\frac{d\phi}{2\pi}\int_0^{\pi/2} d\theta\,2\sin\theta\,\cos\theta\,. \tag{14.33}$$

Substituting $z = e^{i\phi}$ and $t = \tan\theta$, we can write Eq. (14.30) as

$$\mathcal{R}\,\text{Cut}_2^{(a)}\left[\mathcal{A}_{\text{loop}}\right] = -\frac{1}{8\pi^2}\mathcal{R}\oint_{|z|=1}\frac{dz}{2\pi i}\int_0^\infty dt\frac{2\,t}{(1+t^2)^2}f(z,t)\,, \tag{14.34}$$

[7]Note that in our conventions the two-cut is normalized as $\text{Cut}_2[I_2] = -1/(8\pi^2)$.

where we defined

$$f(z,t) = \frac{1}{z}\sum_{\ell_1,\ell_2} \sigma_{\ell_1\ell_2}\, \mathcal{A}_L(... - \bar{\ell}_2 - \bar{\ell}_1)\, \mathcal{A}_R(\ell_1\ell_2...)\,, \tag{14.35}$$

with ℓ_1 and ℓ_2 expressed in terms of p and q according to Eq. (14.32). We first perform the z integral along the contour $|z| = 1$ what yields a sum over the residues of all simple poles $z_i(t)$ of $f(z,t)$, which are within the unit circle

$$\oint_{|z|=1} \frac{dz}{2\pi i} f(z,t) = \sum_i \Theta(|z_i(t)| - 1)\, \mathrm{Res}_{z_i(t)} f(z,t)\,. \tag{14.36}$$

The heaviside step function enforces that the pole $z_i(t)$, whose position is in general a function of t, lies within the unit circle.

Note that $f(z,t)$ and therefore also $\mathrm{Res}_{z_i(t)} f(z,t)$ is a rational function in the kinematic variables and therefore also t, since it is a product of tree-level amplitudes. The primitive of any rational function has a well defined decomposition into a rational and logarithmic part [433]. In our case this has the form

$$\int dt \frac{2\,t}{(1+t^2)^2} \mathrm{Res}_{z_i(t)} f(z,t) = \rho_{z_i(t)}(t) + L_{z_i(t)}(t)\,, \tag{14.37}$$

where $\rho_{z_i(t)}(t)$ and $L_{z_i(t)}(t)$ are the a purely rational and purely logarithmic parts of the indefinite integral in t. $\rho_{z_i(t)}(t)$ can be efficiently obtained without having to solve the integral using HPR [431,433]. A `Mathematica` implementation of the algorithm can be found at [434]. Plugging in the correct integration boundaries $t_{\max}$ and $t_{\min}$ which are determined by the Heaviside function we finally obtain

$$\mathcal{R}\,\mathrm{Cut}_2^{(a)}\left[\mathcal{A}_{\text{loop}}\right] = \sum_i \left[\rho_{z_i(t)}(t_{\max}) - \rho_{z_i(t)}(t_{\min})\right]. \tag{14.38}$$

14.2 Helicity bounds on gravity amplitudes at tree level

In the remainder of this chapter we will consider amplitudes for massless states with definite helicity, and use the all-incoming convention. An n-point amplitude will be denoted by $\mathcal{A}(1_{\Phi_1}, 2_{\Phi_2}, \ldots, n_{\Phi_n})$, where Φ_i specifies the type of particle, *i.e.* ϕ for scalars, $\bar{\psi}$ and ψ for respectively helicity $\pm 1/2$ fermions, $V_\pm$ and $h_\pm$ for positive and negative helicity gauge bosons and gravitons, respectively. When some labels are not necessary, we will suppress them for simplicity, and will often specify amplitudes according to just their number of legs, as $\mathcal{A}_n$.

As we have discussed in the previous sections, the advantages that come from organizing amplitudes according to the helicity of the external states are enormous. Primarily, it allows to systematically take into account the constraints coming from the little group. Another very fruitful observation is that, in a marginal theory (in particular, where no 3-point scalar couplings are present), almost all 4-point amplitudes $\mathcal{A}(\Phi_1, \Phi_2, \Phi_3, \Phi_4)$ that are non-zero satisfy the following condition [27]

$$h_1 + h_2 + h_3 + h_4 = 0\,, \tag{14.39}$$

where h_i is the helicity of Φ_i. The only exception to the above rule are the four fermion amplitude $\mathcal{A}(\psi,\psi,\psi,\psi)$ and its complex conjugate $\mathcal{A}\left(\bar{\psi},\bar{\psi},\bar{\psi},\bar{\psi}\right)$, whose total helicity $h \equiv \sum_i h_i$ is -2 and 2 respectively. These amplitudes can be zero under some group theoretic condition but are in general present (e.g. in the SM). The fact expressed by Eq. (14.39) is highly non-trivial, as we are now going to explain. In a marginal theory all $n \geq 4$ point amplitudes, with the exception

of four scalar amplitudes, are on-shell constructible from lower point amplitudes[8] and therefore their total helicity satisfies

$$h(\mathcal{A}_n) = h(\mathcal{A}_m) + h(\mathcal{A}_{n-m+2})\,, \tag{14.40}$$

where $\mathcal{A}_m$ and $\mathcal{A}_{n-m+2}$ represent any pair of lower point amplitudes to which $\mathcal{A}_n$ factorizes. The fundamental building blocks in this recursive relation are the 3-point amplitudes which are completely fixed by the little-group scaling of the external particles. As we already saw in Eq. (14.19) dimensional analysis additionally relates the total helicity $h(\mathcal{A}_3)$ to the mass dimension of the coupling constant g_3

$$|h(\mathcal{A}_3)| = 1 - [g_3]\,, \tag{14.41}$$

implying that 3-point amplitudes in a marginal theory have total helicity $|h(\mathcal{A}_3)| = 1$. The helicity composition rule in Eq. (14.40) therefore fixes the helicity of 4-point amplitudes to be $|h(\mathcal{A}_4)| = 0, 2$ but does not explain the vanishing of most $|h(\mathcal{A}_4)| = 2$ amplitudes. An explanation requires either direct computation or the use of further tools, such as Supersymmetric Ward identities [435].

Taking $|h(\mathcal{A}_4)| = 0$ as an input, and using that $|h(\mathcal{A}_3)| = 1$ in a marginal theory, Eq. (14.40) yields a non-trivial bound on the helicity of all n-point amplitudes which do not contain the exceptional four fermion amplitude in a factorization channel

$$|h(\mathcal{A}_n)| \leq n - 4 \qquad\qquad (n \geq 4)\,. \tag{14.42}$$

This tree-level helicity bound in marginal theories was successfully employed in [27] to derive powerful non-renormalization theorems for effective field theories (especially the SM EFT). In the following, we are going to provide a very natural generalization of these results –bound on $|h(\mathcal{A}_n)|$ and non-renormalization theorem– to theories involving gravitons and possibly gravitinos as well.

14.2.1 Gravity minimally coupled to marginal theories

Including a minimal coupling of gravity to an otherwise marginal theory changes the above picture. Gravity comes with a dimensionful coupling constant, the inverse Planck mass $1/M_{\rm pl}$, which introduces a new set of 3-point amplitudes with $|h(\mathcal{A}_3^{\rm grav})| = 2$ (see Figure 14.1). Thus a general 4-point amplitude might now have total helicity $|h(\mathcal{A}_4)| = 0, 1, 2, 3, 4$: $|h| = 0, 2$ if it factorizes into two marginal amplitudes, $|h| = 1, 3$ in case it factorizes into one marginal and one gravitational amplitude and $|h| = 0, 4$ if the factorization is into two gravitational amplitudes.[9]

[8] n-point amplitudes have mass dimension $[\mathcal{A}_n] = 4 - n$. In a theory with only marginal couplings the negative mass dimension for $n > 4$ has to be supplied by kinematic invariants. Locality implies that configurations in which these kinematic invariants vanish and the amplitude becomes singular must correspond to a factorization channel of the amplitude into lower point amplitudes. Therefore all $n > 4$ amplitudes are on-shell constructible. At $n = 4$ the only dimensionless amplitude which does not factorize is a constant, corresponding to a four scalar amplitude. From a field theory point of view this can be phrased as the fact that, with the exception of a four scalar operator, there are no marginal local operators comprised of $n \geq 4$ fields which could generate a contact amplitude.

[9] Tree-level minimally coupled gravitational amplitudes with at least one external graviton [415, 436] or $|h(\mathcal{A}_n)| > 2$, $n \geq 4$ [416] are on-shell constructible, implying that Eq. (14.40) is valid and one can proceed as in the marginal scenario when these conditions are met. Note, however, that on-shell constructibility is not needed to infer the possible range of helicities of an n-point amplitude. If it is not a pure contact amplitude, what corresponds to an effective operator in the Lagrangian language, it has to factorize into lower point amplitudes on its poles and the helicity composition rule Eq. (14.40) still holds. Assuming minimal coupling of gravity to a marginal theory, pure contact amplitudes are absent for $n \geq 4$, with the exception of the four scalar amplitude. Hence Eq. (14.40) can be used to bound the helicity in terms of lower point amplitudes.

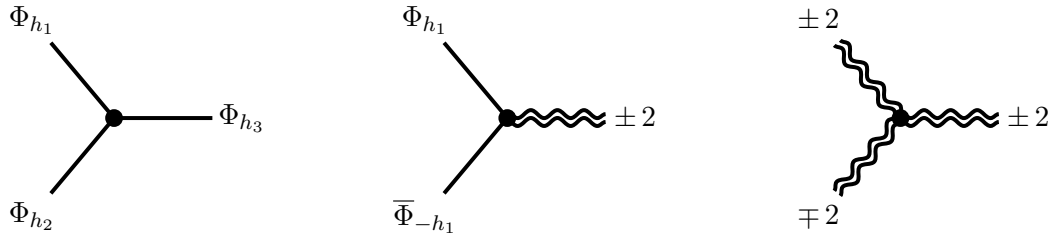

Figure 14.1: Three point amplitudes in a marginal theory minimally coupled to gravity. Amplitudes exclusively among the matter particles – here collectively denoted as Φ –, which can be scalars ϕ, fermions ψ or vectors V, carry total helicity $h = \pm 1$. Gravitational amplitudes in contrast have helicity $h = \pm 2$, the sign being determined by the graviton helicities only. Characterized in terms of a modified helicity $\tilde{h} = h - \frac{1}{2}h^g$, all 3-point amplitudes are on the same footing.

This seems to suggest that a non-trivial bound on the helicity requires a detailed knowledge of all factorization channels and in particular how many of them contain gravitational amplitudes.

A remedy of this shortcoming of the traditional helicity counting approach requires the characterization of amplitudes according to a quantity which treats gravitational and marginal amplitudes on the same footing. Such a quantity can be found by noticing that, due to the parity conserving nature of minimally coupled gravity, all 3-point amplitudes are of the form $\mathcal{A}(1_{\Phi_{h_1}}, 2_{\overline{\Phi}_{-h_1}}, 3_{h_\pm})$ with the total helicity being completely determined by the helicity of the graviton $3_{h_\pm}$. Taking only half of the graviton's helicity would put it on the same footing as an amplitude with gauge bosons (that are always parity preserving and with $h = \pm 1$). Motivated by this observation, we define a modified helicity $\tilde{h}$ which for all particles with $|h| \leq 1$ coincides with the regular helicity $\tilde{h} = h$ but under which gravitons carry $\tilde{h} = \pm 1$. For an arbitrary n-point amplitude the modified helicity can be defined as

$$\tilde{h}(\mathcal{A}_n) = h(\mathcal{A}_n) - \tfrac{1}{2}h^g(\mathcal{A}_n)\,, \tag{14.43}$$

where $h^g(\mathcal{A}_n)$ is the sum of all external graviton helicities in $\mathcal{A}_n$. As is shown in Figure 14.1, the modified helicity puts all 3-point amplitudes on the same footing, s.t.

$$|\tilde{h}(\mathcal{A}_3)| = 1 \qquad \text{for all three point amplitudes} \tag{14.44}$$

in a minimally coupled marginal theory. The benefits of the modified helicity are not limited to 3-point amplitudes: $\tilde{h}$ is additive with respect to factorization in the same way as the regular helicity (cf. Eq. (14.40)). Thus all 4-point amplitudes, including gravitational ones, can only come with $|\tilde{h}| = 0, 2$. As previously discussed all 4-point amplitudes containing exclusively marginal couplings have $\tilde{h} = 0$, with the exception of the four-fermion amplitude. The non-trivial vanishing of $|\tilde{h}| = 2$ amplitudes surprisingly extends to gravitational ones. Through direct calculation, or more elegantly from Supersymmetric Ward identities (see Appendix III.G) one indeed finds that

$$\begin{aligned} 0 &= \mathcal{A}(h_+, h_+, h_+, h_-) = \mathcal{A}(h_+, h_+, \phi, \phi) = \mathcal{A}(h_+, h_+, V_+, V_-) = \mathcal{A}(h_+, h_+, \bar{\psi}, \psi) \\ &= \mathcal{A}(h_+, V_+, V_+, V_-) = \mathcal{A}(h_+, V_+, \phi, \phi) = \mathcal{A}(h_+, \bar{\psi}, \bar{\psi}, \phi) = \mathcal{A}(h_+, V_+, \bar{\psi}, \psi)\,, \end{aligned} \tag{14.45}$$

and the same for the complex conjugated amplitudes, that is those where particles and anti-particles are exchanged. Hence

$$\tilde{h}(\mathcal{A}_4) = 0 \qquad \text{for all four point amplitudes}\,, \tag{14.46}$$

modulo the exceptional one, in a marginal theory minimally coupled to gravity. Recursively constructing n-point amplitudes from their factorization into lower point amplitudes, it is straightforward to generalize Eq. (14.42) to gravitational amplitudes

$$\left|\tilde{h}(\mathcal{A}_n)\right| \leq n-4 \qquad\qquad (n \geq 4)\,. \tag{14.47}$$

This will allow us to formulate unified non-renormalization theorems in the spirit of [27] for EFTs including gravity and in particular the GRSMEFT [30].

Before ending this section let us make a few comments about the modified helicity. The strength of the selection rule in Eq. (14.47) is its generality. It applies to both gravitational and marginal theories and automatically reduces to the selection rule for the regular helicity Eq. (14.42) in the absence of gravity. However, this generality comes with a price: some amplitudes which are allowed by Eq. (14.47) are actually forbidden by regular helicity composition rules. One such example is the graviton-gauge boson amplitude $\mathcal{A}(h_+, h_+, V_-, V_-)$, which has $\tilde{h} = 0$ and therefore seems to be allowed by the selection rule, but whose actual helicity $h = 2$ is not consistent with the fact that it has to factorize into two gravitational 3-point amplitudes (allowing only $|h| = 0, 4$ as discussed previously). The reason for this shortcoming is the fact that gravitons are effectively treated as helicity-one particles. If they appear in amplitudes together with actual helicity-one vectors, an additional piece of information is required to tell if the amplitude is allowed or not. Such information can be provided by h^g, the total helicity in gravitons that the amplitude carries. At four points $|h^g(\mathcal{A}_4)| \leq 2$ and it can at most increase by two units for each additional external state, implying that

$$\left|h^g(\mathcal{A}_n)\right| \leq 2(n-3)\,. \tag{14.48}$$

This additional information forbids the $\mathcal{A}(h_+, h_+, V_-, V_-)$ amplitude. Hence Eq. (14.47) should be seen as a conservative bound which in some cases can be refined by Eq. (14.48) or an explicit study of the factorization channels.

The idea of using a modified helicity to study gravitational amplitudes has some resemblance with the famous KLT relations [437] and the double copy structure of gravity (see [438] for a review), which relate gravity amplitudes to products of two gauge-theory amplitudes. If one of the gauge-theory amplitudes vanishes due to helicity selection rules then so does the gravity amplitude. It seems natural to interpret the modified helicity selection rules in a similar fashion. The modified helicity effectively treats the graviton as a helicity-one particle and preserves the helicity of the remaining matter, what in the double copy language corresponds to a factorization of gravitons into two vectors and each matter particle into a same helicity state and a scalar, similar to the KLT construction in [439]. This is schematically shown in Figure 14.2 for the $\mathcal{A}(h_+, \psi, \psi, \phi)$ amplitude.[10] The first factor is a gauge amplitude with total helicity $\tilde{h}$, which is only non-vanishing for $|\tilde{h}| \leq n-4$ according to the selection rules for marginal theories. This exactly coincides with the modified helicity selection rule. In an explicit KLT construction we would also get an helicity bound from the second factor. However, since the second gauge theory must contain three-scalar couplings, the four-point amplitude can have helicity $|h| = 0, 1$

[10] Note that here we do not try to construct explicit KLT relations for such a factorization of gauge theories. The aim of this discussion is merely to highlight the structural similarity of the modified helicity to double copy constructions.

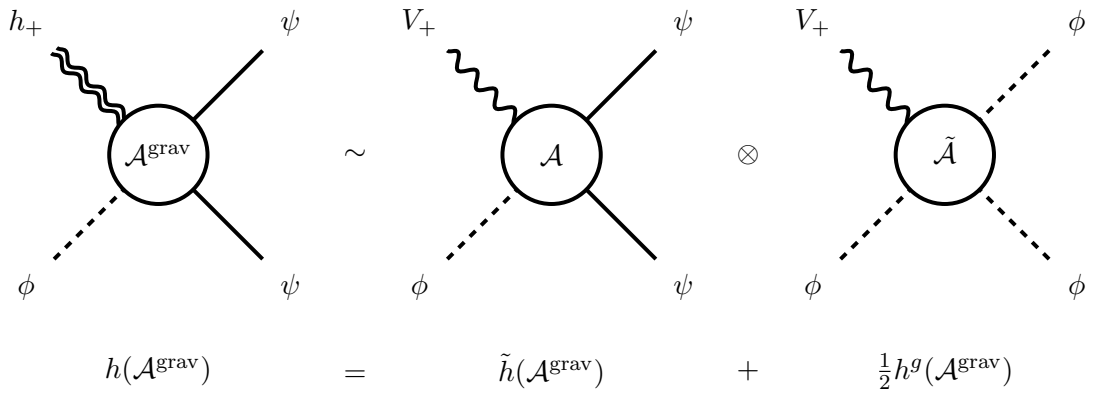

Figure 14.2: Interpretation of the modified helicity selection rules for the $\mathcal{A}(h_+, \psi, \psi, \phi)$ amplitude in terms of double copy relations. The modified helicity treats the graviton as a helicity-one particle and preserves the helicity of $|h| \leq 1$ matter. Thus splitting the helicity as $h = \tilde{h} + \frac{1}{2}h^g$ implies a factorization of the amplitude into a helicity $\tilde{h}$ gauge amplitude $\mathcal{A}$ including all matter particles and a helicity $\frac{1}{2}h^g$ gauge amplitude $\tilde{\mathcal{A}}$ with the matter particles replaced by scalars. The modified helicity selection rule $|\tilde{h}| \leq n-4$ corresponds in this picture to the helicity selection rule for marginal theories applied to $\mathcal{A}$.

resulting in a generally weaker bound of $|h| \leq n-3$. Note that after we identify $h = \frac{1}{2}h^g$ this additional bound coincides with Eq. (14.48).

It is important to point out that, while the modified helicity selection rules are consistent with KLT and double copy constructions and might have an interpretation in terms of such relations, the derivation of the selection rules does not depend on them.

Let us finally mention that it is straightforward to extend the definition of the modified helicity to massless helicity-3/2 particles ζ, that is gravitinos. Note, however, that a consistent theory with massless gravitinos requires superpartners for all matter particles [414], i.e. the theory must be fully supersymmetric. The leading gravitino three-point amplitudes all have total helicity $|h| = 2$ and are of the form $\mathcal{A}(h_+, \zeta_+, \zeta_-)$, $\mathcal{A}(\zeta_+, V_+, \psi)$, $\mathcal{A}(\zeta_-, \psi, \phi)$. These have the same helicity structure as matter amplitudes in a marginal theory if we treat the gravitino as a helicity-1/2 particle, *i.e.* if we assign to it the modified helicity $\tilde{h} = 1/2$. With this the definition the modified helicity of any amplitude $\mathcal{A}_n$ is given by

$$\tilde{h}(\mathcal{A}_n) = h(\mathcal{A}_n) - \tfrac{1}{2}h^g(\mathcal{A}_n) - \tfrac{2}{3}h^\zeta(\mathcal{A}_n)\,, \tag{14.49}$$

where $h^\zeta(\mathcal{A}_n)$ is the sum of external gravitino helicities. At tree-level any four point amplitude satisfies $\tilde{h}(\mathcal{A}_4) = 0$ (see Appendix III.G),[11] implying that the bound in Eq. (14.43) also holds for gravitino amplitudes.

14.2.2 Beyond minimal coupling

So far we have been focusing on amplitudes which are constructed from either marginal interactions or minimal coupling with gravity. Following an EFT point of view, we are now going to include all the interactions that are allowed by the symmetries of the low-energy theory. These new interactions are in one to one correspondence with higher dimensional operators in an effective Lagrangian description.

[11] Note that there is no exception to this rule, since the $|\tilde{h}| = 2$ four-fermion amplitude requires non-holomorphic Yukawa couplings to be non-vanishing. However, in a supersymmetric theory such couplings are absent.

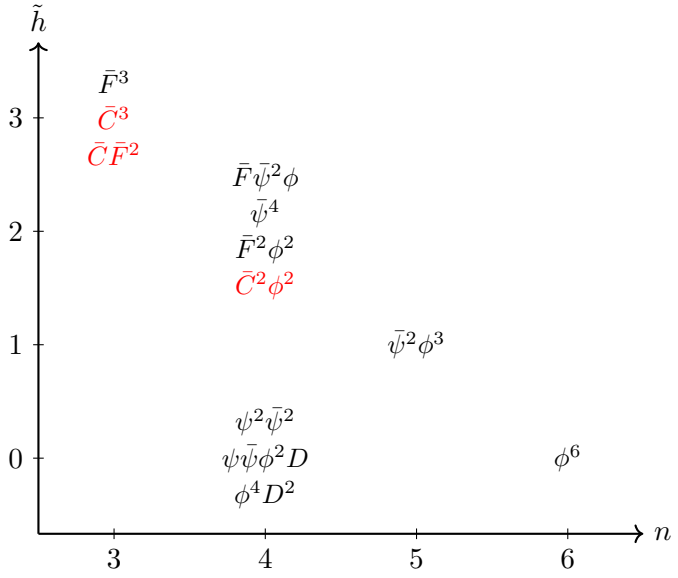

Figure 14.3: Classes of independent dimension six operators in the GRSMEFT labeled according to the modified helicity and number of external particles of the minimal amplitude they induce. $\bar{F}$ stands for the RH gauge field strength and $\bar{C}$ for the RH Weyl tensor. The black operators represent the pure SMEFT basis whereas red operators contain graviton fields. Note that we only show the $\tilde{h} \geq 0$ amplitudes. In order to get the full set one should reflect the diagram around the n axis.

In our approach, "higher dimensional amplitudes" $\mathcal{A}_i$ are defined through their expression in terms of spinor-helicity variables (in an all incoming configuration), and come with a dimensionless coupling C_i that corresponds to a Wilson coefficient in the operator approach. Being new building blocks of the theory, they are not tied to lower point amplitudes by factorization, i.e. they are contact amplitudes.

Similarly as in the operator approach, higher-dimensional amplitudes can be classified according to the inverse power of some UV-theory scale Λ that they carry. Notice that, when involving gravitons as external states, higher dimensional contact amplitudes are also expected to carry a factor $M_{\rm pl}^{-1}$ for each graviton. This is motivated by the Lagrangian formalism, where gravitons only appear in the Weyl tensor as $C \sim \partial^2 h/M_{\rm pl} + \ldots$. Beyond the Λ-scaling, as hinted by the previous analysis, we also find it very convenient to characterize amplitudes by their number of legs n and their modified helicity $\tilde{h}$. In Figure 14.3 we organize accordingly all amplitudes at Λ^{-2} including those with gravitons.

As an example of our method, we list here all contact amplitudes at Λ^{-1} and Λ^{-2} that include at least one graviton. We only list the $\tilde{h} \geq 0$ amplitudes. In a $\mathcal{CP}$ invariant theory, which we will assume in the following, the corresponding negative helicity amplitude can be obtained by complex conjugation. If the theory contains a real scalar, there is one amplitude at order Λ^{-1}

$$\mathcal{A}_{h^2\phi}(1_{h_+}, 2_{h_+}, 3_\phi) = C_{h^2\phi} \frac{[12]^4}{\Lambda\, M_{\rm pl}^2}\,, \tag{14.50}$$

with $n = 3$ and $\tilde{h} = 2$, what corresponds to the dimension five effective operator

$$\mathcal{L}^{(5)}_{\rm eff} \supset \frac{C_{h^2\phi}}{2\,\Lambda} \phi\, C_{\mu\nu\rho\sigma} C^{\mu\nu\rho\sigma}\,. \tag{14.51}$$

At Λ^{-2} we have

$$\mathcal{A}_{hF^2}(1_{h_+}, 2_{F^a_+}, 3_{F^b_+}) = C_{hF^2}\delta^{ab}\frac{[12]^2[13]^2}{\Lambda^2\, M_{\rm pl}}\,, \tag{14.52}$$

$$\mathcal{A}_{h^3}(1_{h_+}, 2_{h_+}, 3_{h_+}) = C_{h^3}\frac{[12]^2[23]^2[13]^2}{\Lambda^2\, M^3_{\rm pl}}\,, \tag{14.53}$$

with $n = 3$ and $\tilde{h} = 3$, the second amplitude being constructed with only gravitons. Finally, we have

$$\mathcal{A}_{h^2\phi^2}(1_{h_+}, 2_{h_+}, 3_{\phi}, 4_{\phi}) = C_{h^2\phi^2}\frac{[12]^4}{\Lambda^2\, M^2_{\rm pl}}\,, \tag{14.54}$$

that has $n = 4$ and $\tilde{h} = 2$. These are equivalent to the dimension six effective operators

$$\mathcal{L}^{(6)}_{\rm eff} \supset \frac{C_{hF^2}}{2\,\Lambda^2}C_{\mu\nu\rho\sigma}F^{A\,\mu\nu}F^{A\,\rho\sigma} + \frac{C_{h^2\phi^2}}{4\,\Lambda^2}C_{\mu\nu\rho\sigma}C^{\mu\nu\rho\sigma}\phi^2 + \frac{C_{h^3}}{6\,\Lambda^2}C_{\mu\nu\rho\sigma}C^{\rho\sigma}{}_{\gamma\delta}C^{\gamma\delta\mu\nu}\,. \tag{14.55}$$

It is straightforward to extend this to complex scalars or abelian gauge fields. Notice that contact amplitudes suppressed by powers of Λ typically do not respect the $\tilde{h}$ bounds in Eq. (14.47).

The Wilson coefficients C_i of higher dimensional amplitudes acquire a scale dependence when loop corrections are included.

14.3 Helicity selection rules at one-loop

According to Eq. (14.31) the anomalous dimension can be determined from unitarity cuts, which correspond to singular kinematic configurations where the loop amplitude factorizes into two on-shell tree-level amplitudes. Neglecting collinear divergences, which will not affect the selection rules, this is schematically of the form

$$\gamma_i\frac{\mathcal{A}_i(1,2,\ldots,n)}{C_i} = -\frac{1}{4\pi^3}\sum_{\rm cuts}\sum_{\ell_1,\ell_2}\sigma_{\ell_1\ell_2}\int d\text{LIPS}\;\mathcal{A}_L(\ldots,-\bar{\ell}_2,-\bar{\ell}_1)\,\mathcal{A}_R(\ell_1,\ell_2,\ldots)\,, \tag{14.56}$$

The advantages that come from using Eq. (14.56) instead of doing a blind loop computation are huge. Primarily, Eq. (14.56) inherits all the transparency and compactness of the on-shell formalism, these qualities being especially manifest when dealing with massless particles with helicity 1 or 2, that in an ordinary Lagrangian approach require the introduction of some degree of gauge redundancy. Second, also partly connected to the on-shellness of the various amplitudes entering the formula, Eq. (14.56) allows to see how properties of $\mathcal{A}_L$ and $\mathcal{A}_R$ are inherited by the "counterterm" $\mathcal{A}_i$, or conversely to constrain the form of relevant amplitudes $\mathcal{A}_{L,R}$ once some a priori knowledge on the form of $\mathcal{A}_i$ is available. Examples of this include "modified helicity" selection rules, as we now explain and will come back to with explicit examples in Section 14.4. This implies that in order for $\mathcal{A}_L$ and $\mathcal{A}_R$ to enter the renormalization of $\mathcal{A}_i$ such a factorization channel must exists. A necessary condition for this is that the total modified helicity and the number and species of external legs of $\mathcal{A}_i$ has to match the ones of the combination of $\mathcal{A}_L$ and $\mathcal{A}_R$. A first, simple but powerful condition coming from Eq. (14.56) is that

$$w_i = w_L + w_R\,. \tag{14.57}$$

where w_i is the total power in dimensional scales or couplings that is carried by $\mathcal{A}_i$, i.e. $\mathcal{A}_i \propto 1/\Lambda^k M_{\rm pl}^{w_i-k}$ in the case of a marginal theory coupled to gravity. A similar yet physically much richer condition holds for the modified helicity $\tilde{h}$, which is additive on the cut and imposes

$$\tilde{h}_i = \tilde{h}_L + \tilde{h}_R\,. \tag{14.58}$$

Its simplicity is key to a couple of very powerful results that we are going to present here and will use in Section 14.4. The first statement is that, when both $\mathcal{A}_L$ and $\mathcal{A}_R$ are amplitudes constructed out of marginal and minimal gravity couplings, we can combine Eq. (14.58) with Eq. (14.47) to get

$$|\tilde{h}_i| = |\tilde{h}_L + \tilde{h}_R| \leq |\tilde{h}_L| + |\tilde{h}_R| \leq (m-4) + [(n-m+4)-4] = n-4\,, \tag{14.59}$$

where in the second step we have used the triangular inequality and in the third step we have used Eq. (14.47) twice, for $\mathcal{A}_{L,R}$ with respectively m and $(n-m+4)$ legs. Thus all divergences in marginal theories minimally coupled to GR must be proportional to operators, which induce contact amplitudes with $|\tilde{h}_i| \leq n-4$. Notice that this remarkable fact is valid at any order in $M_{\rm pl}^{-1}$. We have in particular that

$$\tilde{h}_i^{(1\,\text{loop})} = 0 \qquad\qquad (n=4) \tag{14.60}$$

in any minimally coupled model without trilinear scalar coupling and no exceptional four fermion amplitude.

So far this only includes the renormalization due to the leading theory, i.e. a marginal theory minimally coupled to GR. However, it is straightforward to obtain a similar rule for operator mixing or equivalently renormalization due to contact amplitudes. In this case we assume without loss of generality that $\mathcal{A}_L = \hat{\mathcal{A}}_j$, i.e. that $\mathcal{A}_L$ contains an insertion of the operator $\mathcal{O}_j$. If $\hat{\mathcal{A}}_j = \mathcal{A}_j$, i.e. $\mathcal{A}_L$ is the minimal amplitude induced by $\mathcal{O}_j$, the modified helicity $\tilde{h}_L$ coincides with the one according to which we classify the operator $\tilde{h}_L = \tilde{h}_j$. Otherwise we can use Eqs. (14.40) and (14.44) to find that

$$|\tilde{h}(\hat{\mathcal{A}}_j) - \tilde{h}_j| \leq \hat{n}_j - n_j\,, \tag{14.61}$$

where n_j and $\hat{n}_j$ are the number of external legs of $\mathcal{A}_j$ and $\hat{\mathcal{A}}_j$, respectively. This result simply states that each additional external leg can change the total modified helicity by only one unit. $\mathcal{A}_R$ is an amplitude from the leading theory, which satisfies

$$|\tilde{h}_R| \leq n_R - 4 = (n_i - \hat{n}_j)\,, \tag{14.62}$$

with the exception of the four fermion amplitude, which we will ignore in the following. In Eq. (14.62) we used that $n_i = n_R + n_L - 4$. Combining Eq. (14.58) with Eqs. (14.61) and (14.62), we obtain the range of possible $\tilde{h}_i$, which can be reached from $\mathcal{A}_j$ with $\tilde{h}_j$

$$\begin{aligned} \tilde{h}_i = \tilde{h}(\hat{\mathcal{A}}_j) + \tilde{h}_R &\geq \tilde{h}_j - (\hat{n}_j - n_j) - (n_i - \hat{n}_j) = \tilde{h}_j - (n_i - n_j)\,, \\ &\leq \tilde{h}_j + (\hat{n}_j - n_j) + (n_i - \hat{n}_j) = \tilde{h}_j + (n_i - n_j)\,. \end{aligned} \tag{14.63}$$

This implies that a contact amplitude $\mathcal{A}_i$ can be renormalized by a contact amplitude $\mathcal{A}_j$ if

$$\Delta n_{ij} \geq |\Delta\tilde{h}_{ij}|\,, \tag{14.64}$$

with $\Delta n_{ij} = n_i - n_j$ and $\Delta\tilde{h}_{ij} = \tilde{h}_i - \tilde{h}_j$. As an additional requirement we obtain from Eq. (14.57) that $w_i \geq w_j$. This also implies that the mixing at the same order in $1/\Lambda$, i.e. at the same order in mass dimension in the Lagrangian language, can only increase the number of external gravitons, i.e. $\Delta n_{ij}^g \geq 0$.

Let us make a few remarks before moving on. In the case of purely matter external states the selection rule in Eq. (14.64) trivially reduces to the selection rule of marginal theories, which was found in [27].

In terms of the operator or amplitude classification according to $(n, \tilde{h})$, as it is shown in Figure 14.3, operators can only renormalize other operator within the same $(n, \tilde{h})$ group or operators in the adjacent groups $(n+1, \{\tilde{h}-1, \tilde{h}, \tilde{h}+1\})$ with the above mentioned caveat that $\Delta n^g_{ij} \geq 0$. This implies that e.g. the amplitude corresponding to $\bar{F}^3$ can enter in the renormalization of the one corresponding to $\bar{C}\bar{F}^2$, but the reverse is not possible.

Another important aspect concerns the power counting. Since gravity has a dimensionful coupling, we can make up missing powers of $1/\Lambda$ with powers of $1/M_{\rm pl}$, i.e. an amplitude corresponding to a dimension five operator with scaling $1/\Lambda$ can renormalize a dimension six operator with scaling $1/\Lambda^2$ if $\mathcal{A}_R$ is a gravitational amplitude containing one factor of $1/M_{\rm pl}$. However, for $\Lambda \ll M_{\rm pl}$ these mixing effects are subleading. The leading mixing is always among operators which have the same scaling in $1/\Lambda$.

14.4 Dimension six anomalous dimensions in toy GRSMEFT

Having analyzed the general properties of Eq. (14.56), and with the aim of showing its enormous effectiveness, we now move on and focus on a specific problem. Our purpose in this section is to study the one loop structure of a gauge theory, with scalars and fermions transforming under the gauge group and interacting among themselves through a Yukawa, which is minimally coupled to gravity. This is structurally a close relative of the world we live in. Since the world is quantum, due to the presence of the negative dimensional coupling $M_{\rm pl}^{-1}$ we expect at one loop to generate new interactions that are not present at the minimal coupling level. What is the amplitude/operator spectrum that is required by consistency of the theory at one loop? This is the question we are going to address in the following.

Even though – as the reader should keep in mind – most of the qualitative results do not depend on the details of the model, we are now going to specify it for definiteness. The gauge group is $SU(N)$, with scalars ϕ^i in the fundamental ($i = 1, \ldots, N$) and negative-helicity fermions ψ and χ^i in respectively the singlet and fundamental representations. Gauge bosons will be denoted by $V^a_\pm$ (with $a = 1, \ldots, N^2-1$), the gauge coupling by g. Gravitons will be dubbed $h_\pm$. The field content allows for a Yukawa coupling of the form $\mathcal{A}(1_\chi, 2_\psi, 3_{\bar{\phi}}) = y\langle 12\rangle$ at any N, but only for $N > 3$ this is the only possible Yukawa. We will however set to zero all other Yukawas that can be there at $N = 2, 3$. Positive helicity fermions, as well as anti-scalars, come with a bar. The action of the theory takes the following form

$$S_{\rm toy} = \int d^4x\sqrt{-g}\Big[-\frac{2}{\kappa^2}R - \frac{1}{4}g^{\mu\alpha}g^{\nu\beta}F^a_{\mu\nu}F^a_{\alpha\beta} + g^{\mu\nu}(\nabla_\mu\phi)^\dagger(\nabla_\nu\phi) + \frac{i}{2}\psi^\dagger\bar{\sigma}^\mu\overleftrightarrow{\nabla}_\mu\psi + \frac{i}{2}\chi^\dagger\bar{\sigma}^\mu\overleftrightarrow{\nabla}_\mu\chi - \frac{\lambda}{2}(\phi^\dagger\phi)^2 - y\chi^\dagger\phi\psi^\dagger + h.c.\Big], \tag{14.65}$$

where $\psi^\dagger\overleftrightarrow{\nabla}_\mu\psi = \psi^\dagger\nabla_\mu\psi - (\nabla_\mu\psi^\dagger)\psi$. $F^a_{\mu\nu}$ is the $SU(N)$ field strength tensor and ∇_μ are the covariant derivatives w.r.t. both general coordinate and $SU(N)$ gauge transformations. $\sigma^\mu, \bar{\sigma}^\mu = e^\mu_a\sigma^a, e^\mu_a\bar{\sigma}^a$ with the vierbein field e^μ_a and $\sigma^a = (\mathbb{1}, \sigma^i)^T, \bar{\sigma}^a = (\mathbb{1}, -\sigma^i)^T$. The covariant derivatives are defined as

$$\nabla_\mu\phi = \left(\partial_\mu - i\frac{g}{\sqrt{2}}t^aV^a_\mu\right)\phi\,, \tag{14.66}$$

$$\nabla_\mu\chi = \left(\partial_\mu - i\frac{g}{\sqrt{2}}t^aV^a_\mu - \frac{i}{2}\omega^{mn}_\mu\bar{\sigma}_{mn}\right)\chi\,, \tag{14.67}$$

$$\nabla_\mu\psi = \left(\partial_\mu - \frac{i}{2}\omega^{mn}_\mu\bar{\sigma}_{mn}\right)\psi\,, \tag{14.68}$$

where $\sigma^{mn} = \frac{i}{4}(\sigma^m\bar{\sigma}^n - \sigma^n\bar{\sigma}^m)$ and $\bar{\sigma}^{mn} = \frac{i}{4}(\bar{\sigma}^m\sigma^n - \bar{\sigma}^n\sigma^m)$. Note that in the second order formalism ω_μ^{mn} is not an independent quantity but has to be determined from the vierbein field. Also note that we use the standard normalization of the gauge coupling in the amplitudes context, which differs from the typical normalization in the Lagrangian language by a factor of $1/\sqrt{2}$. In Appendix III.H we give all three-point and four-point amplitudes for the theory specified in Eq. (14.65). Note that the toy model with the above particle content is anomalous. However, the anomaly does not affect any of our one-loop results. Canceling the anomaly simply requires the addition of an additional LH fermion in the anti-fundamental representation. Such an addition does not significantly change the results, which is why we chose to present this simpler but nonetheless incomplete model.

In the following we will analyze the one-loop renormalization of this theory up to $\mathcal{O}(\Lambda^{-2})$, i.e. operator dimension six. Our focus will be renormalization due to gravity, i.e. we will not consider mixing between pure matter operators. The amplitude or operator spectrum at mass dimension six is shown in Figure 14.4. Figure 14.4 also summarizes the one-loop divergence structure of the theory. Structures in green can be generated by the leading marginal theory coupled to gravity according to the selection rule in Eq. (14.59). The arrows show the operator mixings among the dimension six operators, which actually occur. The selection rule in Eq. (14.64) allows more mixings, but these are either forbidden by power counting arguments or there are simply no diagrams. Note that the selection rules are exact for the toy model, since same sign helicity four-fermion amplitudes vanish. For simplicity we will concentrate on the $n = 3, 4$ amplitudes, what is sufficient to present our method.

Note that we have checked all results in this section against a Feynman diagrammatic calculation using `FeynArts` [351] and `FeynCalc` [440, 441] with a model file generated with `FeynRules` [164].

14.4.1 Renormalization from minimal coupling

We present here our results for the renormalization of minimally coupled gravity at 1-loop, $n = 4$ and $\mathcal{O}(\Lambda^{-2})$. These are the first effects when going beyond the renormalizable level.[12] Let us again stress that these contributions to the anomalous dimension are subleading if there is also mixing among dimension six operators. However, the result is still interesting since it is independent of the operators in a specific EFT and will always appear. So to speak the operators, which get generated in this way will be generated in any marginal theory minimally coupled to gravity.

The eight operators at $n = 4$ and $\tilde{h} = 0$ contribute to six different amplitudes. A basis for these is given by

$$\mathcal{A}_\phi(1_{\phi^i}, 2_{\bar{\phi}_j}, 3_{\bar{\phi}_k}, 4_{\phi^l}) = \frac{1}{\Lambda^2}\left[C_\phi\left(s_{12}\delta^i_j\delta^l_k + s_{13}\delta^i_k\delta^l_j\right) + C'_\phi\left(s_{13}\delta^i_j\delta^l_k + s_{12}\delta^i_k\delta^l_j\right)\right], \tag{14.69}$$

$$\mathcal{A}_{\chi\phi}(1_{\chi^i}, 2_{\bar{\chi}_j}, 3_{\bar{\phi}_k}, 4_{\phi^l}) = \frac{1}{\Lambda^2}\langle 1|p_3|2]\left(C_{\chi\phi}(t^a)^i_j(t^a)^l_k + C'_{\chi\phi}\,\delta^i_k\delta^l_j\right), \tag{14.70}$$

$$\mathcal{A}_{\psi\phi}(1_\psi, 2_{\bar{\psi}}, 3_{\bar{\phi}_i}, 4_{\phi^j}) = \frac{C_{\psi\phi}}{\Lambda^2}\langle 1|p_3|2]\,\delta^j_i \tag{14.71}$$

$$\mathcal{A}_\chi(1_{\chi^i}, 2_{\bar{\chi}_j}, 3_{\bar{\chi}_k}, 4_{\chi^l}) = \frac{C_\chi}{\Lambda^2}\langle 14\rangle[23]\left(\delta^i_j\delta^l_k + \delta^i_k\delta^l_j\right), \tag{14.72}$$

$$\mathcal{A}_\psi(1_\psi, 2_{\bar{\psi}}, 3_{\bar{\psi}}, 4_\psi) = \frac{C_\psi}{\Lambda^2}\langle 14\rangle[23], \tag{14.73}$$

[12] There are no contact amplitudes involving gravitons at $\mathcal{O}(\Lambda^{-1})$ for the particle content of the toy model and effects of internal gravitons do not appear before $\mathcal{O}(\Lambda^{-2})$.

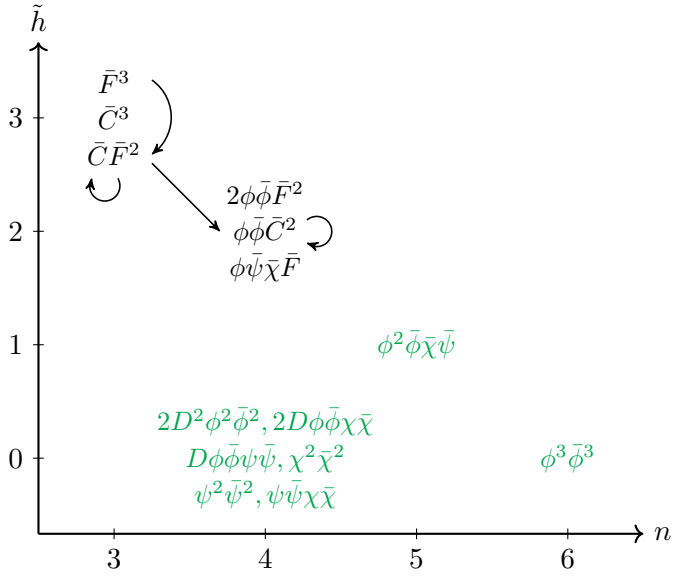

Figure 14.4: Classes of independent dimension six operators, or equivalently contact amplitudes, for the toy model field content labeled according to the modified helicity and number of external particles of the minimal amplitude they induce, limited to $\tilde{h} \geq 0$. For this Figure we took the gauge group to be $SU(4)$ and explicitly show the multiplicity of each structure obtained from a Hilbert series analysis (see Section 11.5). According to the modified helicity selection rule in Eq. (14.59) only the green operators are allowed to receive divergent one-loop contributions from the minimal coupling to gravity. The arrows show the non-zero operator mixings, which involve gravitational operators. The selection rule in Eq. (14.64) allows more mixings, but these are either forbidden by power counting arguments or there are simply no valid factorization channels.

$$\mathcal{A}_{\chi\psi}(1_{\chi^i}, 2_{\bar{\chi}_j}, 3_{\bar{\psi}}, 4_{\psi}) = \frac{C_{\chi\psi}}{\Lambda^2}\langle 14\rangle[23]\,\delta_i^j\,, \tag{14.74}$$

where the first two amplitudes contain two tensor structures each, but for the remaining ones the group structures are completely fixed. The kinematic invariants are defined as $s_{ij} = (p_i + p_j)^2$. Together these give a total of eight independent coefficients that can get a running. In the Lagrangian language the above amplitude basis corresponds to an operator basis of

$$\begin{aligned}\mathcal{L}_6^{\tilde{h}=0} = &-\frac{C_\phi}{2\,\Lambda^2}(\phi^\dagger\phi)\Box(\phi^\dagger\phi) - \frac{C'_\phi}{\Lambda^2}(\phi^\dagger D_\mu\phi)^*(\phi^\dagger D^\mu\phi) - \frac{C'_{\chi\phi}}{2\,\Lambda^2}(\phi^\dagger i\overleftrightarrow{D}_\mu\phi)\chi^\dagger\bar{\sigma}^\mu\chi \\ &- \frac{C_{\chi\phi}}{2\,\Lambda^2}(\phi^\dagger i\overleftrightarrow{D}^a_\mu\phi)\chi^\dagger t^a\bar{\sigma}^\mu\chi - \frac{C_{\psi\phi}}{2\,\Lambda^2}(\phi^\dagger i\overleftrightarrow{D}_\mu\phi)\psi^\dagger\bar{\sigma}^\mu\psi + \frac{c_{\chi\chi}}{\Lambda^2}(\chi_i^\dagger\chi_j^\dagger)(\chi^i\chi^j) \\ &+ \frac{C_\psi}{4\,\Lambda^2}(\psi^\dagger\psi^\dagger)(\psi\psi) + \frac{C_{\chi\psi}}{\Lambda^2}(\chi_i^\dagger\psi^\dagger)(\chi^i\psi)\,,\end{aligned} \tag{14.75}$$

where $\phi^\dagger i\overleftrightarrow{D}_\mu\phi = i\phi^\dagger(D_\mu - \overleftarrow{D}_\mu)\phi$, $\phi^\dagger i\overleftrightarrow{D}^a_\mu\phi = i\phi^\dagger(t^aD_\mu - \overleftarrow{D}_\mu t^a)\phi$ and $(\psi^\dagger\psi^\dagger), (\psi\psi)$ are short forms for $(\psi^\dagger\psi^\dagger) = \psi^\dagger_{\dot{\alpha}}\epsilon^{\dot{\alpha}\dot{\beta}}\psi^\dagger_{\dot{\beta}}$, $(\psi\psi) = \psi^\alpha\epsilon_{\alpha\beta}\psi^\beta$. Note that this is only one basis, which reproduces the above on-shell amplitudes. Equivalent bases can be obtained via field redefinitions and IBP relations.

The anomalous dimensions for the C_i can now be computed with the help of Eq. (14.31), where $\mathcal{A}_L$ and $\mathcal{A}_R$ are amplitudes of the toy model as defined in Eq. (14.65). The corresponding

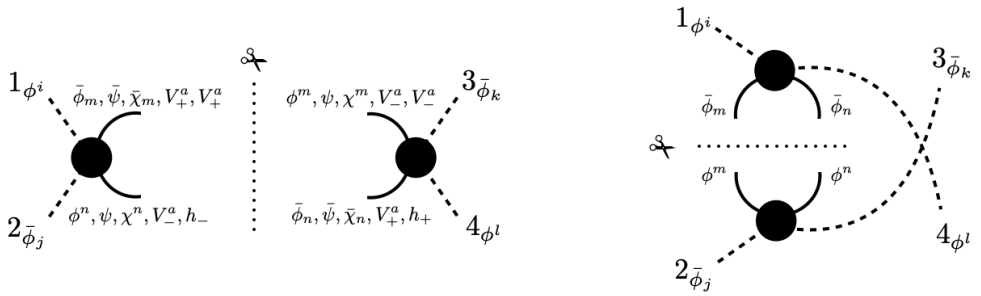

Figure 14.5: Relevant factorization channels of $\mathcal{A}_\phi(1_{\phi^i}, 2_{\bar{\phi}_j}, 3_{\bar{\phi}_k}, 4_{\phi^l})$ to determine the anomalous dimensions for C_ϕ and C'_ϕ. We only show the s- and u-channel. The t-channel cut is identical to the s-channel after the replacement $s_{12} \leftrightarrow s_{13}$ and $j \leftrightarrow k$.

amplitudes are collected in Appendix III.H and the required collinear anomalous dimensions, which also enter Eq. (14.31), are computed in Appendix III.I.

Let us now explicitly demonstrate the computation for the renormalization of C_ϕ and C'_ϕ. In order to determine the anomalous dimensions according to Eq. (14.31) we have to find all valid factorization channels, which contribute to $\mathcal{A}_\phi(1_{\phi^i}, 2_{\bar{\phi}_j}, 3_{\bar{\phi}_k}, 4_{\phi^l})$ at order $1/M_{\rm pl}^2$. These are shown for the s- and u-channel in Figure 14.5. The t-channel contribution can be obtained from the s-channel by replacing $s_{12} \leftrightarrow s_{13}$ and $j \leftrightarrow k$.

Note that there are two Wilson coefficients, i.e. C_ϕ and C'_ϕ, which contribute to the amplitude $\mathcal{A}_\phi(1_{\phi^i}, 2_{\bar{\phi}_j}, 3_{\bar{\phi}_k}, 4_{\phi^l})$. For this reason we have to split $\mathcal{A}_\phi = \mathcal{A}_{C_\phi} + \mathcal{A}_{C'_\phi}$ into the two pieces proportional to C_ϕ and C'_ϕ. In Eq. (14.31) we consequently have to take the sum of both contributions

$$\begin{aligned}\gamma_{C_\phi}\frac{\mathcal{A}_{C_\phi}(1_{\phi^i}, 2_{\bar{\phi}_j}, 3_{\bar{\phi}_k}, 4_{\phi^l})}{C_\phi} + \gamma_{C'_\phi}\frac{\mathcal{A}_{C'_\phi}(1_{\phi^i}, 2_{\bar{\phi}_j}, 3_{\bar{\phi}_k}, 4_{\phi^l})}{C'_\phi} - \gamma_{\rm coll}\,\mathcal{A}^{\rm tree}(1_{\phi^i}, 2_{\bar{\phi}_j}, 3_{\bar{\phi}_k}, 4_{\phi^l})\Big|_{M_{\rm pl}^{-2}} \\ = -\frac{1}{4\pi^3}\sum_{\substack{\text{cuts}\\ \ell_1,\ell_2}}\sigma_{\ell_1\ell_2}\mathcal{R}\int d\text{LIPS}\;\mathcal{A}_L(... - \bar{\ell}_2 - \bar{\ell}_1)\,\mathcal{A}_R(\ell_1\ell_2...)\,,\end{aligned} \tag{14.76}$$

where the contribution from the collinear anomalous dimension is proportional to the $1/M_{\rm pl}^2$ part of the tree-level amplitude in Eq. (III.H.10).

The u-channel contribution to the RHS of Eq. (14.79) contains only one factorization channel and is given by

$$\begin{aligned}-\frac{1}{4\pi^3}\frac{1}{2}\mathcal{R}\int d\text{LIPS}\;\mathcal{A}(1_{\phi^i}, 4_{\phi^l}, -\ell_{2\,\bar{\phi}_m}, -\ell_{1\,\bar{\phi}_n})\,\mathcal{A}(\ell_{1\,\phi^n}, \ell_{2\,\phi^m}, 2_{\bar{\phi}_j}, 3_{\bar{\phi}_k}) \\ = -\frac{4\lambda\, s_{14}}{(4\pi)^2\, M_{\rm pl}^2}\left(\delta_j^i\delta_k^l + \delta_k^i\delta_j^l\right) + \frac{g^2(C_A-1)(C_A-2C_F)s_{14}}{(4\pi)^2\, M_{\rm pl}^2}\left(\delta_j^i\delta_k^l + \delta_k^i\delta_j^l\right),\end{aligned} \tag{14.77}$$

where the $1/2$ is due to the indistinguishable particles in the cut and $C_A = N$ and $C_F = (N^2-1)/(2N)$ are the Casimirs of the adjoint and fundamental representation of $SU(N)$, respectively. In the above we only kept the terms proportional to $1/M_{\rm pl}^2$.

For the s-channel we similarly obtain

$$
\begin{aligned}
&-\frac{1}{4\pi^3}\sum_{\substack{\text{cuts}\\ \ell_1,\ell_2}}\sigma_{\ell_1\ell_2}\mathcal{R}\int d\text{LIPS}\;\mathcal{A}(1_{\phi^i},2_{\bar\phi_j},-\bar\ell_2-\bar\ell_1)\,\mathcal{A}(\ell_1,\ell_2,3_{\bar\phi_k},4_{\phi^l})\\
&\quad=-\frac{2\,\lambda\,s_{12}}{3\,(4\pi)^2\,M_{\text{pl}}^2}\big(6\,\delta^i_k\delta^l_j-(C_A-5)\delta^i_j\delta^l_k\big)+\frac{2\,y^2}{3\,(4\pi)^2\,M_{\text{pl}}^2 s_{12}}\big(s_{12}^2+6s_{12}s_{14}+6s_{14}^2\big)\delta^i_j\delta^l_k\\
&\qquad-\frac{g^2(C_A-2C_F)}{6\,(4\pi)^2\,s_{12}M_{\text{pl}}^2}\Big[\big((3C_A^2+6C_A+11)s_{12}^2+4(6C_A^2+1)s_{12}s_{14}+24(C_A^2-1)s_{14}^2\big)\delta^i_j\delta^l_k\\
&\qquad\qquad-2s_{12}\big((7C_A+3)s_{12}+14C_As_{14}\big)\delta^i_k\delta^l_j\Big]\,,
\end{aligned}
\tag{14.78}
$$

where the sum goes over the factorization channels shown in Figure 14.5. Note that the result contains poles. However, these will be canceled in the full result by the collinear anomalous dimensions. The t-channel can be straightforwardly obtained from this Eq. (14.78).

Summing ovel all channels and taking into account the collinear anomalous dimension $\gamma_{\text{coll}}=4\,\gamma^\phi_{\text{coll}}=-C_Fg^2/(2\pi^2)+y^2/(4\pi^2)$ we indeed obtain a local result

$$
\begin{aligned}
&\gamma_{C_\phi}\frac{\mathcal{A}_{C_\phi}(1_{\phi^i},2_{\bar\phi_j},3_{\bar\phi_k},4_{\phi^l})}{C_\phi}+\gamma_{C'_\phi}\frac{\mathcal{A}_{C'_\phi}(1_{\phi^i},2_{\bar\phi_j},3_{\bar\phi_k},4_{\phi^l})}{C'_\phi}\\
&\quad=\frac{2\,\lambda(C_A+1)}{3\,(4\pi)^2M_{\text{pl}}^2}\big(s_{12}\delta^i_j\delta^l_k+s_{13}\delta^i_k\delta^l_j\big)+\frac{2\,y^2}{3\,(4\pi)^2M_{\text{pl}}^2}\big(s_{13}\delta^i_k\delta^l_j+s_{12}\delta^i_j\delta^l_k\big)\\
&\qquad-\frac{g^2(C_A-2C_F)}{6\,(4\pi)^2M_{\text{pl}}^2}\Big[\big(20(C_A-2)s_{12}+(3C_A^2+40C_A-23)s_{13}\big)\delta^i_k\delta^l_j\\
&\qquad\qquad+\big((3C_A^2+40C_A-23)s_{12}+20(C_A-2)s_{13}\big)\delta^i_j\delta^l_k\Big]\,.
\end{aligned}
\tag{14.79}
$$

From this it is straightforward to obtain the anomalous dimensions

$$\gamma_{C_\phi}=\left(\frac{2}{3}\frac{y^2}{(4\pi)^2}+\frac{2}{3}(1+C_A)\frac{\lambda}{(4\pi)^2}-\frac{1}{6}(40\,C_A+3C_A^2-23)(C_A-2C_F)\frac{g^2}{(4\pi)^2}\right)\frac{\Lambda^2}{M_{\text{pl}}^2}\tag{14.80}$$

$$\gamma_{C'_\phi}=\frac{10}{3}(C_A-2)(C_A-2C_F)\frac{g^2}{(4\pi)^2}\frac{\Lambda^2}{M_{\text{pl}}^2}\,.\tag{14.81}$$

The computation of the remaining anomalous dimensions proceeds along similar lines and we obtain

$$\gamma_{C_{\chi\phi}}=-\frac{21}{2}\frac{g^2}{(4\pi)^2}\frac{\Lambda^2}{M_{\text{pl}}^2}\,,\tag{14.82}$$

$$\gamma_{C'_{\chi\phi}}=-\frac{7}{2}\frac{y^2}{(4\pi)^2}\frac{\Lambda^2}{M_{\text{pl}}^2}\,,\tag{14.83}$$

$$\gamma_{C_{\psi\phi}}=-\frac{7}{2}\frac{y^2}{(4\pi)^2}\frac{\Lambda^2}{M_{\text{pl}}^2}\,,\tag{14.84}$$

$$\gamma_{C_\chi}=\frac{55}{12}(C_A-1)(C_A-2\,C_F)\frac{g^2}{(4\pi)^2}\frac{\Lambda^2}{M_{\text{pl}}^2}\,,\tag{14.85}$$

$$\gamma_{C_\psi} = 0\,, \tag{14.86}$$

$$\gamma_{C_{\chi\psi}} = 0\,. \tag{14.87}$$

These contain additional zeroes, which cannot be explained by the modified helicity selection rules. However, some of these zeroes can be justified with the help angular momentum considerations. We will comment on this in the final publication [34].

14.4.2 Operator mixing at dimension six

Let us finally compute the anomalous dimensions from operator mixing or self-renormalization, which are already shown in Figure 14.4. For these we need the amplitudes induced by $\bar{F}^3$, $\bar{C}\bar{F}^2$ and $\bar{C}^2\phi\bar{\phi}$. The gravitational amplitudes can be taken from Section 14.2.2. Here we repeat them for convenience and adjust them to complex scalars

$$\mathcal{A}_{F^3}(1_{V_+^a}, 2_{V_+^b}, 3_{V_+^b}) = \frac{i\,C_{F^3}}{\Lambda^2 M_{\rm pl}} f^{abc}[12][23][13]\,, \tag{14.88}$$

$$\mathcal{A}_{hF^2}(1_{h_+}, 2_{V_+^a}, 3_{V_+^b}) = \frac{C_{hF^2}}{\Lambda^2 M_{\rm pl}} \delta^{ab}[12]^2[13]^2\,, \tag{14.89}$$

$$\mathcal{A}_{h^2\phi^2}(1_{h_+}2_{h_+}, 3_{\bar{\phi}_j}, 4_{\phi^i}) = \frac{C_{h^2\phi^2}}{\Lambda^2 M_{\rm pl}^2} \delta^i_j[12]^4\,. \tag{14.90}$$

These amplitudes are induced by the following effective operators

$$\mathcal{L}^{(6)}_{\rm eff} \supset \frac{C_{F^3}}{3\sqrt{2}\,\Lambda^2} f^{abc} F^{a\,\mu\nu} F^b_{\nu\rho} F^{c\,\rho}{}_{\mu} + \frac{C_{hF^2}}{2\,\Lambda^2} C_{\mu\nu\rho\sigma} F^{a\,\mu\nu} F^{a\,\rho\sigma} + \frac{C_{h^2\phi^2}}{2\,\Lambda^2} C_{\mu\nu\rho\sigma} C^{\mu\nu\rho\sigma} \phi^\dagger \phi\,. \tag{14.91}$$

Let us now go through all possible mixings.

$\bar{C}\bar{F}^2 \to \bar{C}^2\phi\bar{\phi}$

$\mathcal{A}_{F^3}(1_{V_+^a}, 2_{V_+^b}, 3_{V_+^c})$ cannot directly enter our master formula Eq. (14.31), since this would lead to a scaleless bubble integral, which vanishes in dimensional regularization. The three-vector amplitude therefore has to be embedded into a four-point amplitude, which contributes to $\mathcal{A}_{h^2\phi^2}(1_{h_+}2_{h_+}, 3_{\bar{\phi}_j}, 4_{\phi^i})$ at one-loop. As can be seen in Figure 14.6 $\bar{C}\bar{F}^2$ enters through the amplitude $\hat{\mathcal{A}}_{hF^2}(1_{h_+}2_{V_+^a}, 3_{\bar{\phi}_j}, 4_{\phi^i})$ in the t- and u- channel. This amplitude takes the form

$$\hat{\mathcal{A}}_{hF^2}(1_{h_+}2_{V_+^a}, 3_{\bar{\phi}_j}, 4_{\phi^i}) = \frac{C_{hF^2} g}{\Lambda^2 M_{\rm pl}} (t^a)^i_j \frac{[12]^2[13][1|k_4|3\rangle}{s_{12}}\,. \tag{14.92}$$

With these ingredients, it is straightforward to apply Eq. (14.31) to compute the operator mixing. Using that there are no collinear divergences for non-diagonal mixings, we obtain

$$\gamma_{h^2\phi^2} \frac{\mathcal{A}_{h^2\phi^2}(1_{h_+}2_{h_+}, 3_{\bar{\phi}_j}, 4_{\phi^i})}{C_{h^2\phi^2}} = \frac{1}{(4\pi)^2} \frac{2\,C_{hF^2} g^2 C_F}{\Lambda^2 M_{\rm pl}^2} \delta^i_j [12]^4\,, \tag{14.93}$$

s.t. the anomalous dimension can be identified as

$$\gamma_{hF^2\to h^2\phi^2} = \frac{g^2 C_F}{8\pi^2}\,, \tag{14.94}$$

where $\gamma_{hF^2\to h^2\phi^2}$ actually means $\gamma_{hF^2,h^2\phi^2}$ as in

$$\frac{dC_{h^2\phi^2}}{d\ln\mu} = \sum_j \gamma_{h^2\phi^2,\,j} C_j = \gamma_{h^2\phi^2,hF^2} C_{hF^2} + \dots\,. \tag{14.95}$$

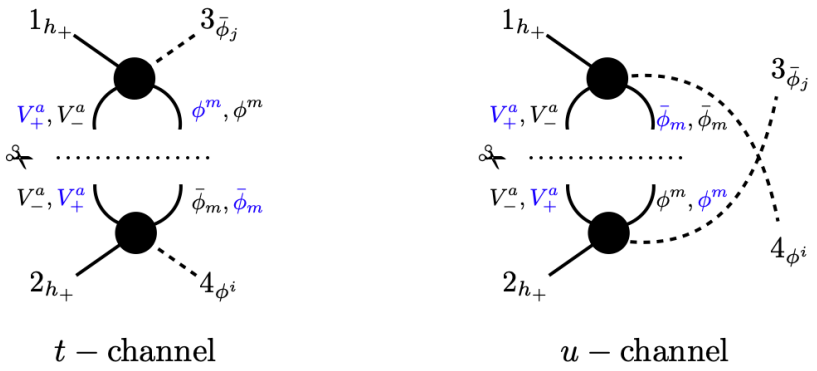

Figure 14.6: Factorization channels of $\mathcal{A}_{h^2\phi^2}(1_{h_+}2_{h_+}, 3_{\bar{\phi}_j}, 4_{\phi^i})$, which contain an insertion of C_{hF^2} through $\hat{\mathcal{A}}_{hF^2}(1_{h_+}2_{V_+^a}, 3_{\bar{\phi}_j}, 4_{\phi^i})$. The blue labels mark the side of the unitarity cut on which the amplitude with the insertion of C_{hF^2} appears.

$\bar{F}^3 \to \bar{C}\bar{F}^2$

The mixing between operators which induce three-point amplitudes cannot be directly computed via unitarity cuts since, as we have mentioned before, on-shell three-point kinematics lead to massless and therefore vanishing bubble integrals. However, we can still determine the mixing indirectly by embedding the operator for which we want to compute the running, i.e. $\bar{C}\bar{F}2$ in our case, into a four-point amplitude. From the contribution of $\bar{F}^3$ to the divergence of this new four point amplitude we can infer the operator mixing $\bar{F}^3 \to \bar{C}\bar{F}^2$. In the following we consider $\hat{\mathcal{A}}_{hF^2}(1_{h_+}2_{V_+^a}, 3_{\bar{\phi}_j}, 4_{\phi^i})$ which we have already computed in Eq. (14.92). The amplitude is a function of the gauge coupling g and the Wilson coefficient C_{hF^2}, i.e. $\hat{\mathcal{A}}_{hF^2} = \hat{\mathcal{A}}_{hF^2}(g, C_{hF^2})$. Using that the full amplitude, i.e. the combination of tree and one-loop, is independent of the renormalization scale we can obtain an equation for the anomalous dimension

$$0 = \frac{d}{d\ln\mu}(\hat{\mathcal{A}}_{hF^2}(g, C_{hF^2}) + \mathcal{A}^{1-\text{loop}}) = \frac{d}{d\ln\mu}\hat{\mathcal{A}}_{hF^2}(g, C_{hF^2}) + \sum_a C_2^{(a)}\frac{dI_2^{(a)}}{d\ln\mu} \tag{14.96}$$

$$= \left(\gamma_{hF^2}\frac{\partial}{\partial C_{hF^2}} - \gamma_{\text{coll}} + \beta_g\frac{\partial}{\partial g}\right)\hat{\mathcal{A}}_{hF^2}(g, C_{hF^2}) + \sum_a C_2^{(a)}\frac{dI_2^{(a)}}{d\ln\mu} \tag{14.97}$$

where we used in the second step that $\mathcal{A}^{1-\text{loop}}$ can be expanded in the Passarino-Veltman basis, where only the bubble integrals I_2 depend on the renormalization scale. In the third step we used that the dependence on the renormalization scale due to the loop amplitude has to be compensated by the running of the Wilson coefficient and gauge coupling.

In order to find the $\gamma_{F^3\to hF^2}$ component of the anomalous dimension matrix it is sufficient to consider the $\mathcal{O}(C_{F^3})$ part of $\mathcal{A}^{1-\text{loop}}(1_{h_+}2_{V_+^a}, 3_{\bar{\phi}_j}, 4_{\phi^i})$. This also has the advantage that we do not have to worry about β_g and the collinear IR divergences since both would be proportional to the tree amplitude $\hat{\mathcal{A}}_{hF^2}(1_{h_+}2_{V_+^a}, 3_{\bar{\phi}_j}, 4_{\phi^i}) \propto C_{hF^2}$. Thus the anomalous dimension can be

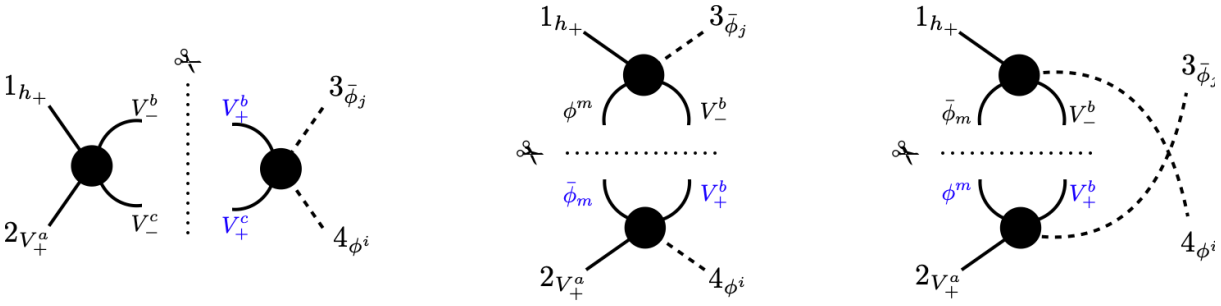

Figure 14.7: Factorization channels of $\hat{\mathcal{A}}_{hF^2}(1_{h_{++}}2_{V_+^a},3_{\bar\phi_j},4_{\phi^i})$, which contains exactly one insertion of C_{F^3} through $\hat{\mathcal{A}}_{F^3}(1_{V_+^a},2_{V_+^b},3_{\bar\phi_j},4_{\phi^i})$. The blue labels mark the side of the unitarity cut on which the amplitude with the insertion of C_{F^3} appears.

determined from

$$\begin{aligned}\gamma_{F^3\to hF^2}\frac{C_{F^3}}{C_{hF^2}}&\hat{\mathcal{A}}_{hF^2}(1_{h_+}2_{V_+^a},3_{\bar\phi_j},4_{\phi^i})\\ &=-\frac{1}{4\pi^3}\sum_{\substack{\text{cuts}\\ \ell_1,\ell_2}}\sigma_{\ell_1\ell_2}\mathcal{R}\int d\text{LIPS}\;\;\mathcal{A}_L(...-\bar\ell_2-\bar\ell_1)\,\mathcal{A}_R(\ell_1\ell_2...)\big|_{\mathcal{O}(C_{F^3})}\\ &=\frac{2\,C_{F^3}g^2C_A}{(4\pi)^2\,\Lambda^2 M_{\text{pl}}}(t^a)^i_j\frac{[12]^3\langle 2|k_3|1]}{s_{12}}\,,\end{aligned}\tag{14.98}$$

where we summed over all possible cuts of the one-loop amplitude with one insertion of C_{F^3}, which are shown in Figure 14.7. In the computation of the cuts we used the four point amplitude $\hat{\mathcal{A}}_{F^3}(1_{V_+^a},2_{V_+^b},3_{\bar\phi_j},4_{\phi^i})$ which contains one insertion of C_{F^3}

$$\hat{\mathcal{A}}_{F^3}(1_{V_+^a},2_{V_+^b},3_{\bar\phi_j},4_{\phi^i})=-g\frac{C_{F^3}}{\Lambda^2}f^{abc}(t^c)^i_j\left(\frac{s_{14}}{s_{12}}+\frac{1}{2}\right)[12]^2\,.\tag{14.99}$$

Comparing Eq. (14.98) to Eq. (14.92), we can identify the anomalous dimension

$$\gamma_{F^3\to hF^2}=\frac{g\,C_A}{8\pi^2}\,.\tag{14.100}$$

$\bar{C}\bar{F}^2\to\bar{C}\bar{F}^2$

In order to compute the self-renormalization $\bar{C}\bar{F}^2\to\bar{C}\bar{F}^2$ we again embed the three point amplitude into $\hat{\mathcal{A}}_{hF^2}(1_{h_+}2_{V_+^a},3_{\bar\phi_j},4_{\phi^i})$. Since this is a diagonal mixing, we now have to include the collinear anomalous dimension and the beta function of the gauge coupling in Eq. (14.97). The anomalous dimension is thus given by

$$\begin{aligned}\left(\gamma_{hF^2\to hF^2}-\gamma_{\text{coll}}+\beta_g\frac{\partial}{\partial g}\right)&\hat{\mathcal{A}}_{hF^2}(1_{h_+}2_{V_+^a},3_{\bar\phi_j},4_{\phi^i})\\ &=-\frac{1}{4\pi^3}\sum_{\substack{\text{cuts}\\ \ell_1,\ell_2}}\sigma_{\ell_1\ell_2}\mathcal{R}\int d\text{LIPS}\;\;\mathcal{A}_L(...-\bar\ell_2-\bar\ell_1)\,\mathcal{A}_R(\ell_1\ell_2...)\big|_{\mathcal{O}(C_{hF^2})}\\ &=\frac{C_{hF^2}g(C_A-2C_F)}{6\,(4\pi)^2\Lambda^2M_{\text{pl}}}\big(g^2(26C_A^2+3C_A-12)-12C_Ay^2\big)(t^a)^i_j\frac{[12]^3\langle 2|k_3|1]}{s_{12}}\,,\end{aligned}\tag{14.101}$$

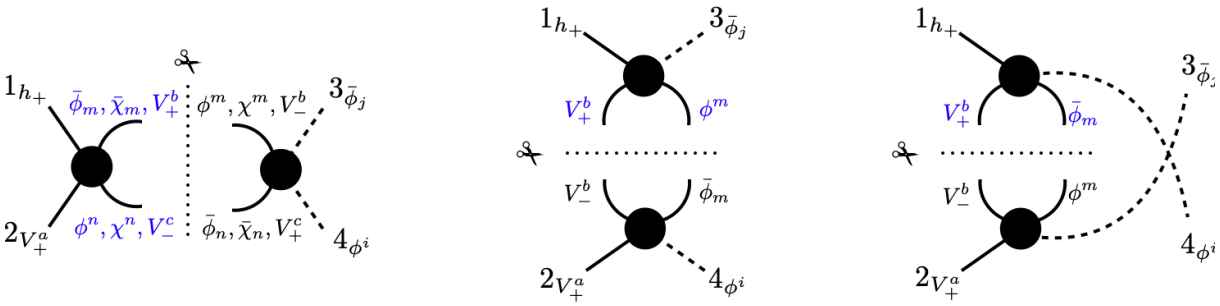

Figure 14.8: Factorization channels of $\hat{\mathcal{A}}_{hF^2}(1_{h_{++}} 2_{V_+^a}, 3_{\bar{\phi}_j}, 4_{\phi^i})$, which contain exactly one insertion of C_{hF^2}. The blue labels mark the side of the unitarity cut on which the amplitude with the insertion of C_{hF^2} appears.

where we have summed over all factorization channels of the one-loop amplitude, which contain one insertion of C_{hF^2}. These are shown in Figure 14.8. In order to extract the UV anomalous dimension we have to subtract the beta function due to the running of the gauge coupling and also have to correct for collinear divergences on the external legs with the collinear anomalous dimensions $\gamma_{\text{coll}} = \gamma_{\text{coll}}^V + 2\,\gamma_{\text{coll}}^\phi$. The beta function β_g is known and given by

$$\beta_g = -\frac{g^3}{32\pi^2}\left(\frac{11C_A}{3} - \frac{n_f}{3} - \frac{n_s}{6}\right) = -\frac{g^3}{32\pi^2}\left(\frac{11C_A}{3} - \frac{1}{2}\right), \tag{14.102}$$

where n_f and n_s are the number of Weyl fermions and scalars charged under the gauge group. Note that β_g is smaller by a factor of 2 compared to the textbook result due to our non-standard normalization of the gauge coupling. Using this in combination with the collinear anomalous dimensions in Appendix III.I we find

$$\gamma_{CF^2\to CF^2} = \frac{(3+14C_A)g^2}{96\pi^2}\,. \tag{14.103}$$

$\bar{C}^2\phi\bar{\phi} \to \bar{C}^2\phi\bar{\phi}$

Finally we compute the self-renormalization of $\bar{C}^2\bar{\phi}\phi$. This can be determined from the divergent one-loop contribution to $\mathcal{A}(1_{h_+}, 2_{h_+}, 3_{\bar{\phi}_j}, 4_{\phi^i})$ proportional to $C_{h^2\phi^2}$. This implies we have to consider all unitarity cuts which contain $\mathcal{A}_{h^2\phi^2}(1_{h_+}, 2_{h_+}, 3_{\bar{\phi}_j}, 4_{\phi^i})$. In this particular case there is only a contribution in the s-channel, since the t- and u-channel would require gravitons in the loop, which would in turn contribute to higher dimensional operators. The only contribution is thus

$$\begin{aligned}
&\left(\gamma_{h^2\phi^2\to h^2\phi^2} - \gamma_{\text{coll}}\right)\mathcal{A}_{h^2\phi^2}(1_{h_+}, 2_{h_+}, 3_{\bar{\phi}_j}, 4_{\phi^i}) \\
&\qquad = -\frac{1}{4\pi^3}\mathcal{R}\int d\text{LIPS}\,\hat{\mathcal{A}}_{h^2\phi^2}(1_{h_{++}}, 2_{h_{++}}, -\ell_{2\,\bar{\phi}_n}, -\ell_{1\,\phi^m})\mathcal{A}(\ell_{1\,\bar{\phi}_m}, \ell_{2\,\phi^n}, 3_{\bar{\phi}_j}, 4_{\phi^i}) \\
&\qquad = \frac{2\,C_{h^2\phi^2}}{(4\pi)^2\Lambda^2 M_{\text{pl}}^2}\left(\frac{C_F}{2}g^2 + (C_A+1)\lambda\right)[12]^4\,,
\end{aligned} \tag{14.104}$$

with $\gamma_{\text{coll}} = 2\gamma_{\text{coll}}^\phi$. Plugging in the explicit expression for $\gamma_{\text{coll}}^\phi$ we find

$$\gamma_{h^2\phi^2\to h^2\phi^2} = \frac{y^2}{8\pi^2} - \frac{3C_F g^2}{16\pi^2} + \frac{(C_A+1)\lambda}{8\pi^2}\,. \tag{14.105}$$

Appendices part III

III.A UOLEA results

In this appendix we apply functional methods to perform the one-loop matching and point out some pieces which were missed in the previous calculation [20]. Once these missing parts are accounted for, the results obtained in the UOLEA framework agree with the expressions of our diagrammatic calculation described in Section 12.2. We demonstrate this agreement explicitly for the contribution from heavy-particle loops to the one-loop matching corrections to the Wilson coefficients $C_{H\Box}$ and C_H. Our discussion follows the general line of reasoning presented in the articles [20,317,318] and we refer to the works [319,320,442] for CDE and UOLEA formulations including heavy-light loops.

Starting from the Lagrangian Eq. (12.1) one can obtain the low-energy effective action by performing the functional integral over the ϕ field. The part originating from heavy particle loops is given by

$$\begin{aligned} S_{\text{eff}}[H] &\simeq S[H,\phi_c] + \frac{i}{2}\text{Tr}\ln\left(-\left.\frac{\delta^2 S}{\delta\phi^2}\right|_{\phi=\phi_c}\right) \\ &\simeq S[H,\phi_c] + \frac{i}{2}\text{Tr}\ln\left(-P^2 + M^2 + U_\phi\right) . \end{aligned} \tag{III.A.1}$$

Here $\phi_c = \phi_c[H]$ is the solution of the classical equation of motion of ϕ, i.e. $\delta S/\delta\phi\big|_{\phi=\phi_c} = 0$, $P_\mu = i\partial_\mu$ and U_ϕ in the case of Eq. (12.1) takes the form

$$U_\phi = \left.\frac{\partial^2 \mathcal{L}_\phi}{\partial\phi^2}\right|_{\phi=\phi_c} = \kappa|H|^2 + \mu\phi_c + \frac{1}{2}\lambda_\phi\phi_c^2 . \tag{III.A.2}$$

In order to find an expression for ϕ_c we perturbatively solve the equation of motion of ϕ, which explicitly reads

$$\left(\Box + M^2 + \kappa|H|^2\right)\phi = -A|H|^2 - \frac{\mu}{2}\phi^2 - \frac{\lambda_\phi}{6}\phi^3 . \tag{III.A.3}$$

Making the ansatz $\phi_c = \phi_c^{(0)} + \phi_c^{(1)} + \phi_c^{(2)} + \ldots$ with $\phi_c^{(k)} = O(\mu^l\lambda_\phi^n)$ and $k = l + n$ it is straightforward to obtain

$$\phi_c^{(0)} = -\frac{1}{\Box + M^2 + \kappa|H|^2}\, A|H|^2 , \tag{III.A.4}$$

$$\phi_c^{(1)} = -\frac{1}{\Box + M^2 + \kappa|H|^2}\left(\frac{\mu}{2}\left(\phi_c^{(0)}\right)^2 + \frac{\lambda_\phi}{6}\left(\phi_c^{(0)}\right)^3\right) , \tag{III.A.5}$$

$$\phi_c^{(2)} = -\frac{1}{\Box + M^2 + \kappa|H|^2}\left(\mu\phi_c^{(0)}\phi_c^{(1)} + \frac{\lambda_\phi}{2}\left(\phi_c^{(0)}\right)^2\phi_c^{(1)}\right) . \tag{III.A.6}$$

Expanding ϕ_c up to four Higgs fields and two derivatives or six Higgs fields and no derivative, we then find the following expression

$$\begin{aligned}\phi_c = &-\frac{A}{M^2}|H|^2+\left(\frac{A\kappa}{M^4}-\frac{A^2\mu}{2M^6}\right)|H|^4+\frac{A}{M^4}\Box|H|^2\\&-\left(\frac{A\kappa}{M^6}-\frac{A^2\mu}{M^8}\right)|H|^2\Box|H|^2-\left(\frac{A\kappa^2}{M^6}-\frac{A^3\lambda_\phi+9A^2\kappa\mu}{6M^8}+\frac{A^3\mu^2}{2M^{10}}\right)|H|^6\,.\end{aligned} \tag{III.A.7}$$

Comparing the above result for ϕ_c to Eq. (4.2) of [20] one observes that while the first three terms of Eq. (III.A.7) agree with the $|H|^2$, $|H|^4$ and $\Box|H|^2$ contributions given in the latter work, the $|H|^2\Box|H|^2$ and $|H|^6$ contain additional pieces, all of which vanish in the limit $\mu \to 0$.

These additional terms affect the matching contributions from heavy loops to the one-loop Wilson coefficients $C^{(1)}_{H\Box}$ and $C^{(1)}_{H}$, which consequently differ from the results presented in the work [20]. Considering the full solution of the classical equation of motion, we find that the heavy-loop contribution to $C^{(1)}_{H\Box}$ is given by

$$\begin{aligned}C^{(1)}_{H\Box}\Big|_{\text{heavy}} = &-\left(\frac{A^2\lambda_\phi+A\kappa\mu}{2M^6}-\frac{A^2\mu^2}{2M^8}\right)\tilde{f}_2\\&+\left(\frac{A\kappa\mu}{M^4}-\frac{A^2\mu^2}{M^6}\right)\tilde{f}_4+\left(\frac{\kappa^2}{2}-\frac{A\kappa\mu}{M^2}+\frac{A^2\mu^2}{2M^4}\right)\tilde{f}_7\\=&-\frac{\kappa^2}{24M^2}-\frac{6A^2\lambda_\phi+5A\kappa\mu}{12M^4}+\frac{11A^2\mu^2}{24M^6}-\frac{A^2\lambda_\phi}{M^4}\ln\frac{\mu_M}{M}\,,\end{aligned} \tag{III.A.8}$$

where to obtain the final result we have inserted the expressions for the universal coefficients $\tilde{f}_N$ reported in Appendix B of [20]. Notice that only the prefactor of $\tilde{f}_2$ in Eq. (III.A.8) differs from the result Eq. (4.10) presented in the article [20]. Diagrammatically the observed difference of $A^2\mu^2\left(1+2\ln\mu_M/M\right)/(2M^6)$ is due to propagator-type tadpole contributions — see the last diagram in Figure 12.2 — that have effectively been missed in the latter calculation.

In the case of the heavy one-loop matching contributions to the Wilson coefficient of the operator Q_H (cf. Eq. (12.4) and Eq. (12.5)), we instead obtain the following expression

$$\begin{aligned}C^{(1)}_{H}\Big|_{\text{heavy}} = &-\left(\frac{A^2\kappa\lambda_\phi+A\kappa^2\mu}{2M^6}-\frac{4A^3\mu\lambda_\phi+9A^2\kappa\mu^2}{12M^8}+\frac{A^3\mu^3}{4M^{10}}\right)\tilde{f}_2\\&+\left(\frac{A^2\kappa\lambda_\phi+2A\kappa^2\mu}{2M^4}-\frac{A^3\mu\lambda_\phi+3A^2\kappa\mu^2}{2M^6}+\frac{A^3\mu^3}{2M^8}\right)\tilde{f}_4\\&+\left(\frac{\kappa^3}{2}-\frac{3A\kappa^2\mu}{2M^2}+\frac{3A^2\kappa\mu^2}{2M^4}-\frac{A^3\mu^3}{2M^6}\right)\tilde{f}_8\\=&-\frac{\kappa^3}{12M^2}-\frac{2A^2\kappa\lambda_\phi+A\kappa^2\mu}{4M^4}+\frac{2A^3\mu\lambda_\phi+3A^2\kappa\mu^2}{6M^6}-\frac{A^3\mu^3}{6M^8}\\&-\left(\frac{A^2\kappa\lambda_\phi}{2M^4}-\frac{A^3\mu\lambda_\phi}{6M^6}\right)\ln\frac{\mu_M}{M}\,.\end{aligned} \tag{III.A.9}$$

Apart from the prefactor of $\tilde{f}_2$, the latter result agrees with Eq. (4.9) of [20]. The resulting difference of $A^2\mu^2\left(A\mu-2M^2\kappa\right)\left(1+2\ln\mu_M/M\right)/(4M^8)$ can again be traced back to propagator-type tadpole contributions that have not been correctly included in the latter article. Our formula Eq. (III.A.9) is in accord with the preliminary results presented in the talk [348], where small discrepancies with the formula for $C^{(1)}_H$ given in [20] were already observed.

The heavy-light contributions to the one-loop matching corrections to the dimension-six SMEFT operators $Q_{H\Box}$ and Q_H are not affected by the additional terms in Eq. (III.A.7). In fact, the operators generated by heavy-light loops that are proportional to ϕ_c appear with at least two additional Higgs fields compared to $Q_{H\Box}$ and Q_H. As a result the missing terms only affect the one-loop matching of operators with a mass dimension of eight or higher. However, when trying to reproduce the results in [20] we discovered an unrelated typo in the heavy-light contribution to $C_H^{(1)}$ that appears in the prefactor of $\tilde{f}_{4A}$ in (4.8) of that work. We find that the actual contribution of the universal coefficient $\tilde{f}_{4A}$ to the Wilson coefficient $C_H^{(1)}$ should read

$$C_H^{(1)}\Big|_{\tilde{f}_{4A}} = \frac{3A^2\kappa^2}{M^4} - \frac{A^3\kappa\mu}{M^6}\,. \tag{III.A.10}$$

Once the additional terms in Eq. (III.A.7) and the correction Eq. (III.A.10) are taken into account we recover the diagrammatic results for $C_{H\Box}^{(1)}$ and $C_H^{(1)}$ originating from heavy and heavy-light pure scalar loops, meaning that our UOLEA calculation reproduced the terms in the first two lines of Eq. (12.10) as well as the terms in the first three lines of Eq. (12.12). Note that the above mistakes and typos are also present in Eq. (3.1) and Eq. (3.2) of [21], which employed the UOLEA master formulas of [20] to obtain the aforementioned results.

III.B RG evolution of SSM parameters

We define the one-loop anomalous dimensions $\tilde{\gamma}_x$ that enter the RG evolution of the parameters x by

$$\frac{dx}{d\ln\mu_R} = \frac{\tilde{\gamma}_x}{(4\pi)^2}\,. \tag{III.B.1}$$

Renormalizing all UV poles including those arising from ϕ tadpoles in the $\overline{\text{MS}}$ scheme, the anomalous dimensions of the parameters M^2, A, κ, μ, λ_ϕ and λ_h read

$$\tilde{\gamma}_{M^2} = M^2\lambda_\phi + 4A^2\,, \tag{III.B.2}$$

$$\tilde{\gamma}_A = A\left(4\kappa + 6\lambda_h - \frac{3}{2}\left(g_1^2 + 3g_2^2\right) + 2y_2\right)\,, \tag{III.B.3}$$

$$\tilde{\gamma}_\kappa = \kappa\left(4\kappa + \lambda_\phi + 6\lambda_h - \frac{3}{2}\left(g_1^2 + 3g_2^2\right) + 2y_2\right)\,, \tag{III.B.4}$$

$$\tilde{\gamma}_\mu = 2\mu\lambda_\phi + 12A\kappa\,, \tag{III.B.5}$$

$$\tilde{\gamma}_{\lambda_\phi} = 12\kappa^2 + 3\lambda_\phi^2\,, \tag{III.B.6}$$

$$\tilde{\gamma}_{\lambda_h} = \kappa^2 + 12\lambda_h^2 - 3\lambda_h\left(g_1^2 + 3g_2^2\right) + \frac{3}{4}\left(g_1^4 + 2g_1^2g_2^2 + 3g_2^4\right) + 4\lambda_h y_2 - 4y_4\,, \tag{III.B.7}$$

with

$$y_2 = \text{Tr}\left(3y_u^\dagger y_u + 3y_d^\dagger y_d + y_e^\dagger y_e\right)\,, \tag{III.B.8}$$

$$y_4 = \text{Tr}\left(3y_u^\dagger y_u y_u^\dagger y_u + 3y_d^\dagger y_d y_d^\dagger y_d + y_e^\dagger y_e y_e^\dagger y_e\right)\,. \tag{III.B.9}$$

Examples of Feynman graphs that contribute to the anomalous dimensions $\tilde{\gamma}_{M^2}$, $\tilde{\gamma}_A$, $\tilde{\gamma}_\kappa$ and $\tilde{\gamma}_\mu$ are shown on the right of Figure 12.3 as well as in Figure 12.6 to Figure 12.9. We add that

the results for $\tilde{\gamma}_{\lambda_\phi}$ and $\tilde{\gamma}_{\lambda_h}$ are not needed in the context of this work, but we provide them for completeness.

In Section 12.2.2 we have presented our final results Eq. (12.10) and Eq. (12.12) for the one-loop matching corrections $C_{H\Box}^{(1)}$ and $C_H^{(1)}$. In both cases we have observed that the logarithmic corrections to the Wilson coefficients involve only anomalous dimensions that depend only on SM couplings but not on SSM parameters. Below we explicitly show how this feature arises. The given formulae should also facilitate a comparison to the existing computations [20, 21] as well as to the preliminary results presented in the talk [348].

In order to derive the logarithmic terms that arise from the renormalization of the SSM parameters, we first notice that if the tree-level Wilson coefficients $C_k^{(0)}$ are expressed through the SSM parameters x one has

$$\frac{dC_k^{(0)}}{d\ln\mu_R} = \sum_x \frac{\partial C_k^{(0)}}{\partial x}\frac{dx}{d\ln\mu_R} = \frac{1}{(4\pi)^2}\sum_x \frac{\partial C_k^{(0)}}{\partial x}\tilde{\gamma}_x\,, \tag{III.B.10}$$

where the sum over x includes M^2, A, κ, μ, λ_ϕ and λ_h, and in the last step we have used the definition Eq. (III.B.1). Integrating Eq. (III.B.10) from μ_M to M then gives rise to the logarithmic corrections that are associated to the renormalization of the SSM parameters.

Applying the master formula Eq. (III.B.10) to the case of the Wilson coefficient $C_{H\Box}^{(1)}$, we find the following logarithmic terms

$$\begin{aligned} C_{H\Box}^{(1)}\Big|_{\ln\frac{\mu_M}{M}} &= \frac{4A^2\kappa - A^2\lambda_\phi}{M^4} + \frac{2A^4}{M^6} - \frac{5A^2\left(g_1^2+3g_2^2\right)}{6M^4} + \frac{A^2\tilde{\gamma}_{M^2}}{M^6} - \frac{A\tilde{\gamma}_A}{M^4} \\ &= \left(12\lambda - \frac{4}{3}\left(g_1^2+3g_2^2\right) + 4y_2\right)\left(-\frac{A^2}{2M^4}\right)\,. \end{aligned} \tag{III.B.11}$$

The first three terms in the first line of Eq. (III.B.11) result from the heavy and heavy-light loop diagrams shown in Figure 12.2 to Figure 12.5. The terms proportional to $\tilde{\gamma}_{M^2}$ and $\tilde{\gamma}_A$ instead arise from the renormalization of the parameters M^2 and A that enter the tree-level Wilson coefficient Eq. (12.7). In the second line of Eq. (III.B.11) we can manifestly see that there is a cancellation of logarithmic terms involving the combinations of SSM parameters that do not form a SMEFT Wilson coefficient, yielding the logarithmic correction quoted in Eq. (12.10) as final result.

In the case of the Wilson coefficient $C_H^{(1)}$ using Eq. (III.B.10) instead leads to

$$\begin{aligned} C_H^{(1)}\Big|_{\ln\frac{\mu_M}{M}} &= -\frac{A^2\kappa\lambda_\phi + 36A^2\kappa\lambda - 12A^2\kappa^2 - 40A^2\lambda^2}{2M^4} \\ &\quad + \frac{18A^4\kappa - 12A^3\kappa\mu + A^3\mu\lambda_\phi + 36A^3\lambda\mu}{6M^6} - \frac{A^5\mu}{M^8} - \frac{10A^2\lambda g_2^2}{3M^4} \\ &\quad + \left(\frac{A^2\kappa}{M^6} - \frac{A^3\mu}{2M^8}\right)\tilde{\gamma}_{M^2} - \left(\frac{A\kappa}{M^4} - \frac{A^2\mu}{2M^6}\right)\tilde{\gamma}_A - \frac{A^2\tilde{\gamma}_\kappa}{2M^4} + \frac{A^3\tilde{\gamma}_\mu}{6M^6} \\ &= \left(-40\lambda^2 + \frac{20\lambda g_2^2}{3}\right)\left(-\frac{A^2}{2M^4}\right) \\ &\quad + \left(54\lambda - \frac{9}{2}\left(g_1^2+3g_2^2\right) + 6y_2\right)\left(\frac{A^3\mu}{6M^6} - \frac{A^2\kappa}{2M^4}\right)\,. \end{aligned} \tag{III.B.12}$$

The first two lines of the above expression correspond to the contributions from heavy and heavy-light graphs, while the terms proportional to the anomalous dimensions $\tilde{\gamma}_{M^2}$, $\tilde{\gamma}_A$, $\tilde{\gamma}_\kappa$ and

$\tilde{\gamma}_\mu$ are the counterterm contributions that are associated to the renormalization of the relevant SSM parameters appearing in the tree-level Wilson coefficient $C_H^{(0)}$. Notice that the final result in Eq. (III.B.12) agrees with the logarithmic correction that we have obtained in Eq. (12.12), and that these terms have the correct form to allow for a resummation of large logarithms using the RG equations of the dimension-six SMEFT operators $Q_{H\Box}$ and Q_H derived in [24–26].

III.C Group characters

In this appendix we summarize the Haar integration measures and group characters, taken from [340], that were used to derive our main results in Chapter 13.

III.C.1 Integration measures

The Haar integration measures over the SM gauge groups can be written as contour integrals in the complex plane of the variables parametrizing the groups

$$\int d\mu_{U(1)_Y}(v) = \frac{1}{2\pi i}\oint_{|v|=1}\frac{dv}{v}\,, \tag{III.C.1}$$

$$\int d\mu_{SU(2)_W}(w) = \frac{1}{2\pi i}\oint_{|w|=1}\frac{dw}{w}\big(1-w^2\big)\,, \tag{III.C.2}$$

$$\int d\mu_{SU(3)_C}(z_1,z_2) = \frac{1}{(2\pi i)^2}\oint_{|z_1|=1}\oint_{|z_2|=1}\frac{dz_1}{z_1}\frac{dz_2}{z_2}\left(1-z_1z_2\right)\left(1-\frac{z_1^2}{z_2}\right)\left(1-\frac{z_2^2}{z_1}\right). \tag{III.C.3}$$

Note that these expressions differ from the ones in [22], since the Haar measures that we use involve only the positive roots and therefore have no Weyl group normalization. This simplified measure can be used when integrating over class functions, i.e. functions $f(g)$ which satisfy $f(hgh^{-1}) = f(g)$ for $h, g \in G$, since they are invariant under the Weyl group. Note that all characters are class functions. For the integration measure over the euclidean Lorentz group $SO(4) \simeq SU(2)_L \otimes SU(2)_R$ we use

$$\int d\mu_{\text{Lorentz}}(x) = \int d\mu_{SU(2)_L\otimes SU(2)_R}(x) = \frac{1}{(2\pi i)^2}\oint_{|x_1|=1}\oint_{|x_2|=1}\frac{dx_1}{x_1}\frac{dx_2}{x_2}\big(1-x_1^2\big)\big(1-x_2^2\big)\,, \tag{III.C.4}$$

where $x = \{x_1, x_2\}$.

III.C.2 Characters for SM gauge representations

The characters for all gauge group representations appearing in the SM are given by

$$\chi_{\mathbf{Q}}^{U(1)_Y}(v) = v^Q\,, \tag{III.C.5}$$

$$\chi_{\mathbf{2}}^{SU(2)_W}(w) = \chi_{\bar{\mathbf{2}}}^{SU(2)_W}(w) = w + \frac{1}{w}\,, \quad \chi_{\mathbf{adj}}^{SU(2)_W}(w) = w^2 + 1 + \frac{1}{w^2}\,, \tag{III.C.6}$$

$$\chi_{\mathbf{3}}^{SU(3)_C}(z_1,z_2) = z_1 + \frac{z_2}{z_1} + \frac{1}{z_2}\,, \quad \chi_{\bar{\mathbf{3}}}^{SU(3)_C}(z_1,z_2) = z_2 + \frac{z_1}{z_2} + \frac{1}{z_1}\,,$$
$$\chi_{\mathbf{adj}}^{SU(3)_C}(z_1,z_2) = z_1z_2 + \frac{z_2^2}{z_1} + \frac{z_1^2}{z_2} + 2 + \frac{z_1}{z_2^2} + \frac{z_2}{z_1^2} + \frac{1}{z_1z_2}\,. \tag{III.C.7}$$

Characters for the Lorentz group are products of $SU(2)$ characters

$$\chi_{(l_1,l_2)}(x) = \chi_{l_1}^{SU(2)_L}(x_1)\cdot\chi_{l_2}^{SU(2)_R}(x_2)\,, \tag{III.C.8}$$

with

$$\chi_{1/2}(x) = x + \frac{1}{x}\,, \qquad \chi_1(x) = x^2 + 1 + \frac{1}{x^2}\,,$$
$$\chi_{3/2}(x) = x^3 + x + \frac{1}{x} + \frac{1}{x^3}\,, \qquad \chi_2(x) = x^4 + x^2 + 1 + \frac{1}{x^2} + \frac{1}{x^4}\,. \tag{III.C.9}$$

III.C.3 Conformal characters

The characters for all unitary conformal representations we use in this work are given by [22, 23, 342]

$$\chi_{[0,(0,0)]}(\mathcal{D};x) = \mathcal{D}\,P(\mathcal{D};x)(1-\mathcal{D}^2)\,, \tag{III.C.10}$$
$$\chi_{[3/2,(1/2,0)]}(\mathcal{D};x) = \mathcal{D}^{\frac{3}{2}}\,P(\mathcal{D};x)\big(\chi_{(1/2,0)}(x) - \mathcal{D}\,\chi_{(0,1/2)}(x)\big)\,, \tag{III.C.11}$$
$$\chi_{[3/2,(0,1/2)]}(\mathcal{D};x) = \mathcal{D}^{\frac{3}{2}}\,P(\mathcal{D};x)\big(\chi_{(0,1/2)}(x) - \mathcal{D}\,\chi_{(1/2,0)}(x)\big)\,, \tag{III.C.12}$$
$$\chi_{[2,(1,0)]}(\mathcal{D};x) = \mathcal{D}^2\,P(\mathcal{D};x)\big(\chi_{(1,0)}(x) - \mathcal{D}\,\chi_{(1/2,1/2)}(x) + \mathcal{D}^2\big)\,, \tag{III.C.13}$$
$$\chi_{[2,(0,1)]}(\mathcal{D};x) = \mathcal{D}^2\,P(\mathcal{D};x)\big(\chi_{(0,1)}(x) - \mathcal{D}\,\chi_{(1/2,1/2)}(x) + \mathcal{D}^2\big)\,, \tag{III.C.14}$$
$$\chi_{[3,(2,0)]}(\mathcal{D};x) = \mathcal{D}^3\,P(\mathcal{D};x)\big(\chi_{(2,0)}(x) - \mathcal{D}\,\chi_{(3/2,1/2)}(x) + \mathcal{D}^2\chi_{(1,0)}(x)\big)\,, \tag{III.C.15}$$
$$\chi_{[3,(0,2)]}(\mathcal{D};x) = \mathcal{D}^3\,P(\mathcal{D};x)\big(\chi_{(0,2)}(x) - \mathcal{D}\,\chi_{(1/2,3/2)}(x) + \mathcal{D}^2\chi_{(0,1)}(x)\big)\,, \tag{III.C.16}$$

with the momentum generating function $P(\mathcal{D};x)$ [22]

$$P(\mathcal{D};x) = \frac{1}{(1-\mathcal{D}x_1x_2)(1-\mathcal{D}/(x_1x_2))(1-\mathcal{D}x_1/x_2)(1-\mathcal{D}x_2/x_1)}\,. \tag{III.C.17}$$

III.D Operator redundancies

In Section 13.4 we identified two redundant operators in the basis of [383] for a shift-symmetric scalar coupled to gravity. Here we show how these can be related to the operator basis in Eq. (13.33). Dropping freely all terms proportional to the free EOM, i.e. any terms containing $R_{\mu\nu}$, R or $\nabla^\mu C_{\mu\nu\rho\sigma}$, the first operator can be rewritten as

$$\begin{aligned}(\nabla_\alpha R_{\mu\nu\rho\sigma})(\nabla^\alpha R^{\mu\nu\rho\sigma}) &= -C_{\mu\nu\rho\sigma}\nabla^2 C^{\mu\nu\rho\sigma} = C_{\mu\nu\rho\sigma}(4\,C^{\lambda\nu\rho\alpha}C^{\mu}{}_{\lambda}{}^{\sigma}{}_{\alpha} + C^{\lambda\alpha\rho\sigma}C^{\mu\nu}{}_{\lambda\alpha}) \\ &= 3\,C_{\mu\nu}{}^{\rho\sigma}C^{\mu\nu\alpha\beta}C_{\alpha\beta\rho\sigma} = 3\,\mathcal{O}_3\,,\end{aligned} \tag{III.D.1}$$

where we used IBP in the first step and Eq. (13.16) in the second. Since there is only one independent $\mathcal{CP}$ even Riemann invariant with three Riemann tensors in four dimensions [406], it is clear that the first line is proportional to $\mathcal{O}_3$. To find the exact relation one has to use dimensionally dependent identities, which can be conveniently implemented with the Invar package [385]. Again throwing away all terms that vanish due to the free EOM, the second operator can be rewritten as

$$\begin{aligned}R_{\mu\nu\alpha\beta}(\nabla^\mu\nabla^\alpha\phi)(\nabla^\nu\nabla^\beta\phi) &= -C_{\mu\nu\alpha\beta}(\nabla^\alpha\phi)(\nabla^\mu\nabla^\nu\nabla^\beta\phi) \\ &= -\frac{1}{2}C_{\mu\nu\alpha\beta}(\nabla^\alpha\phi)((\{\nabla^\mu,\nabla^\nu\} + [\nabla^\mu,\nabla^\nu])\nabla^\beta\phi) \\ &= -\frac{1}{2}C_{\mu\nu\beta\alpha}C^{\mu\nu\beta}{}_{\sigma}(\nabla^\alpha\phi)(\nabla^\sigma\phi)\end{aligned}$$

$$= \quad -\frac{1}{8}(C_{\alpha\beta\rho\sigma})^2(\nabla_\mu\phi)^2 \;= -\frac{1}{8}\mathcal{O}_4\,. \tag{III.D.2}$$

In the first step we used IBP and wrote the covariant derivatives in the last parenthesis as the sum of its commutator and anti-commutator. The term with the anti-commutator vanishes, since it is contracted with $C_{\mu\nu\alpha\beta}$, which is antisymmetric under $\mu \leftrightarrow \nu$. The commutator yields a Riemann tensor, which after removing the $R_{\mu\nu}$ and R components coincides with the Weyl tensor. In the last step we made use of the identity [379]

$$C_{\mu\nu\beta\alpha}C^{\mu\nu\beta}{}_{\sigma} = \frac{1}{4}g_{\alpha\sigma}C_{\mu\nu\gamma\delta}C^{\mu\nu\gamma\delta}\,. \tag{III.D.3}$$

III.E Plethystic exponential

In Section 11.5.1 we introduced the (fermionic) PE as the generating function for the characters of (anti-)symmetric tensor products [337–339]. In the following we give a sketchy derivation to justify the form of the PE which we use here. Readers looking for mathematical rigour should refer to commutative algebra textbooks, such as [335, 336].

III.E.1 Bosonic plethystic exponential

We want to compute the sum over the characters of all symmetric tensor products of a representation $\mathbf{R}$ weighted by a spurion q, i.e.

$$\sum_{d=0}^{\infty} q^d\, \chi_{\mathrm{Sym}^d(\mathbf{R})}(g)\,. \tag{III.E.1}$$

For $g \in G$, let $\mathbf{R}_V(g) \in GL(V)$ be the linear action of the group element g on a n-dimensional vector space V, i.e. $\mathbf{R}$ is a n dimensional group representation. Now let us assume that $\mathbf{R}_V(g)$ can be diagonalized. We take its set of eigenvectors, i.e. $\{e_1, \ldots, e_n\}$ with $\mathbf{R}_V(g)e_i = \lambda_i e_i$, as a basis for V. In this basis the group character is given by the sum over the eigenvalues $\chi_{\mathbf{R}}(g) = \mathrm{Tr}(\mathbf{R}_V(g)) = \sum_{i=1}^n \lambda_i$. The symmetric tensor product $\mathrm{Sym}^d(\mathbf{R})$ is the action of the group element g on the symmetric tensor product of the vector space V, i.e. $\mathrm{Sym}^d(V)$. We denote this linear map by $\mathbf{R}^{\otimes d}_{\mathrm{Sym}^d(V)}(g) \in GL(\mathrm{Sym}^d(V))$.[13] A simple basis for $\mathrm{Sym}^d(V)$ is $\{\frac{1}{d!}\sum_{\sigma\in S_d} e_{i_{\sigma(1)}} \otimes \ldots \otimes e_{i_{\sigma(d)}} | 1 \le i_1 \le \ldots \le i_d \le n\}$, where S_d is the symmetric group. As an explicit example let us write down the basis for $\mathrm{Sym}^2(V)$ and $\dim(V) = 3$

$$\{e_1\otimes e_1\,, e_2\otimes e_2\,, e_3\otimes e_3\,, \tfrac{1}{2}(e_1\otimes e_2 + e_2\otimes e_1)\,, \tfrac{1}{2}(e_1\otimes e_3 + e_3\otimes e_1)\,, \tfrac{1}{2}(e_2\otimes e_3 + e_3\otimes e_2)\}\,. \tag{III.E.2}$$

$\chi_{\mathrm{Sym}^2(\mathbf{R})}(g)$ is obtained by summing over the eigenvalues corresponding to these basis elements

$$\chi_{\mathrm{Sym}^2(\mathbf{R})}(g) = \mathrm{Tr}\big(\mathbf{R}^{\otimes 2}_{\mathrm{Sym}^2(V)}(g)\big) = \lambda_1^2 + \lambda_2^2 + \lambda_3^2 + \lambda_1\lambda_2 + \lambda_1\lambda_3 + \lambda_2\lambda_3 = \tfrac{1}{2}(\chi_{\mathbf{R}}(g)^2 + \chi_{\mathbf{R}}(g^2))\,, \tag{III.E.3}$$

where the trace is a regular matrix trace. In Eq. (III.E.3) we also verified the symmetric square formula for characters that we already found in the explicit example for the Hilbert Series in Eq. (11.43). For general n and d the character can be written as

$$\chi_{\mathrm{Sym}^d(\mathbf{R})}(g) = \mathrm{Tr}\big(\mathbf{R}^{\otimes d}_{\mathrm{Sym}^d(V)}(g)\big) = \sum_{i_1+i_2+\ldots+i_n=d} \lambda_1^{i_1}\lambda_2^{i_2}\cdots\lambda_n^{i_n}\,, \tag{III.E.4}$$

[13] This map is the tensor product representation $\otimes^d\mathbf{R}$ acting on $\mathrm{Sym}^d(\mathbf{V})$.

where the sum is over all partitions $\{i_1, i_2, \ldots, i_n\}$ with $i_1 + i_2 + \ldots + i_n = d$. The i_k indicate the number of times e_k appears in the corresponding basis element and therefore also the power of λ_k in its eigenvalue. Each partition corresponds to a basis element of $\mathrm{Sym}^d(V)$. This is easily seen in our example with $d = 2$ and $n = 3$ with the partitions being $2 = 2+0+0 = 0+2+0 = 0+0+2 = 1+1+0 = 1+0+1 = 0+1+1$. Summing over d in Eq. (III.E.4) yields the generating function

$$\begin{aligned}\sum_{d=0}^{\infty} \chi_{\mathrm{Sym}^d(\mathbf{R})}(g)\, q^d &= \sum_{d=0}^{\infty} q^d \sum_{i_1+i_2+\ldots+i_n=d} \lambda_1^{i_1}\lambda_2^{i_2}\cdots\lambda_n^{i_n} = \Big(\sum_{i_1=0}^{\infty}(\lambda_1 q)^{i_1}\Big)\cdots\Big(\sum_{i_n=0}^{\infty}(\lambda_n q)^{i_n}\Big) \\ &= \frac{1}{\prod_{i=1}^{n}(1-\lambda_i q)} = \frac{1}{\det(\mathbb{1} - \mathbf{R}_V(g)\, q)} = \frac{1}{\det_{\mathbf{R}}(1 - g\, q)}\,, \end{aligned} \tag{III.E.5}$$

where we used the geometric series. Using the matrix identity $\log(\det(A)) = \mathrm{Tr}(\log(A))$ and the logarithmic series $\log(1-x) = -\sum_{k=1}^{\infty} x^k/k$, we obtain the plethystic exponential

$$\sum_{d=0}^{\infty} \chi_{\mathrm{Sym}^d(\mathbf{R})}(g) q^d = \exp\Big[\sum_{k=1}^{\infty} \frac{1}{k} q^k \,\mathrm{Tr}_{\mathbf{R}}(g^k)\Big]\,. \tag{III.E.6}$$

III.E.2 Fermionic plethystic exponential

In the case of fermionic spurions we have to consider the antisymmetric tensor product, i.e. we want to compute

$$\sum_{d=0}^{\infty} q^d\, \chi_{\wedge^d\mathbf{R}}(g)\,, \tag{III.E.7}$$

where $\wedge$ stands for the antisymmetric tensor product. We again pick the system of eigenvectors of $\mathbf{R}_V(g)$ as basis for V and write $\mathbf{R}^{\otimes d}_{\wedge^d V}(g) \in GL(\wedge^d V)$ for the action of the group element g on the vector space formed by the antisymmetric tensor product $\wedge^d V$. A basis for $\wedge^n V$ is $\{\frac{1}{d!}\sum_{\sigma\in S_d}\epsilon(\sigma)\, e_{i_{\sigma(1)}} \otimes \ldots \otimes e_{i_{\sigma(d)}} | 1 \le i_1 < \ldots < i_d \le n\}$, where $\epsilon(\sigma)$ returns the sign of the permutation. Coming back to the example with $d = 2$ and $n = 3$, the basis for $\wedge^2 V$ is

$$\{e_1\wedge e_2, e_1\wedge e_3, e_2\wedge e_3\} = \{\tfrac{1}{2}(e_1\otimes e_2 - e_2\otimes e_1), \tfrac{1}{2}(e_1\otimes e_3 - e_3\otimes e_1), \tfrac{1}{2}(e_2\otimes e_3 - e_3\otimes e_2)\}\,, \tag{III.E.8}$$

with the group character $\chi_{\wedge^2\mathbf{R}}(g)$ given by

$$\chi_{\wedge^2\mathbf{R}}(g) = \mathrm{Tr}\big(\mathbf{R}^{\otimes 2}_{\wedge^2(V)}(g)\big) = \lambda_1\lambda_2 + \lambda_1\lambda_3 + \lambda_2\lambda_3 = \tfrac{1}{2}(\chi_{\mathbf{R}}(g)^2 - \chi_{\mathbf{R}}(g^2))\,. \tag{III.E.9}$$

For general d and n each basis element of $\wedge^d V$ contains d different basis elements e_k. This implies that if $d > n$ then $\wedge^d V$ is an empty space. The group character is the sum over the eigenvalues

$$\chi_{\wedge^d\mathbf{R}}(g) = \mathrm{Tr}\big(\mathbf{R}^{\otimes d}_{\wedge^d V}(g)\big) = \sum_{1\le i_1<\ldots<i_d\le n} \lambda_{i_1}\cdots\lambda_{i_d}\,. \tag{III.E.10}$$

Summing over d we obtain the fermionic plethystic exponential

$$\begin{aligned}\sum_{d=0}^{\infty} q^d\, \chi_{\wedge^d(\mathbf{R})}(g) &= \sum_{d=0}^{\infty} q^d \sum_{1\le i_1<\ldots<i_d\le n} \lambda_{i_1}\cdots\lambda_{i_d} = \prod_{i=1}^{n}(1+\lambda_i\, q) = \det(\mathbb{1} + \mathbf{R}_V(g)\, q) \\ &= \det_{\mathbf{R}}(1 + g\, q) = \exp\Big[\sum_{k=1}^{\infty} \frac{(-1)^{k+1}}{k} q^k \,\mathrm{Tr}_{\mathbf{R}}(g^k)\Big]\,, \end{aligned} \tag{III.E.11}$$

where we again used the matrix identity $\log(\det(A)) = \mathrm{Tr}(\log(A))$ and the logarithmic series $\log(1+x) = \sum_{k=1}^{\infty}(-1)^{k+1}x^k/k$ in the last line.

III.F Dimension 8 GRSMEFT basis

We compile in Tables III.F.1 and III.F.2 the explicit operator basis for the GRSMEFT at mass dimension 8.

We recall that we constructed the Hilbert series in terms of the chiral components of the gauge field strengths ($X_{L/R}$) and the Weyl tensor ($C_{L/R}$), which are related to the standard field strengths and their duals by

$$X^{\mu\nu}_{L/R} = \frac{1}{2}\left(X^{\mu\nu} \pm i\tilde{X}^{\mu\nu}\right), \quad C^{\mu\nu\rho\sigma}_{L/R} = \frac{1}{2}\left(C^{\mu\nu\rho\sigma} \pm i\tilde{C}^{\mu\nu\rho\sigma}\right), \tag{III.F.1}$$

with $\tilde{X}^{\mu\nu} = \frac{1}{2}\epsilon^{\mu\nu\alpha\beta}X_{\alpha\beta}$. For the dual of the Weyl tensor we can define a left- and a right-dual tensor ${}^*C^{\mu\nu\rho\sigma} = \frac{1}{2}\epsilon^{\mu\nu\alpha\beta}C_{\alpha\beta}{}^{\rho\sigma}$ and $C^{\mu\nu\rho\sigma\,*} = \frac{1}{2}\epsilon^{\rho\sigma\alpha\beta}C^{\mu\nu}{}_{\alpha\beta}$, however one can show that ${}^*C^{\mu\nu\rho\sigma} = C^{\mu\nu\rho\sigma\,*}$ and therefore we can define without ambiguity $\tilde{C}^{\mu\nu\rho\sigma} = \frac{1}{2}\epsilon^{\mu\nu\alpha\beta}C_{\alpha\beta}{}^{\rho\sigma}$. Useful relations to trade chiral components for the standard field strength and its dual are

$$C_{L/R\,\mu\nu\rho\sigma}C^{\mu\nu\rho\sigma}_{L/R} = \frac{1}{2}\left(C_{\mu\nu\rho\sigma}C^{\mu\nu\rho\sigma} \pm iC_{\mu\nu\rho\sigma}\tilde{C}^{\mu\nu\rho\sigma}\right), \tag{III.F.2}$$

$$X_{L/R\,\rho\sigma}C^{\mu\nu\rho\sigma}_{L/R} = \frac{1}{2}\left(X_{\rho\sigma}C^{\mu\nu\rho\sigma} \pm i\tilde{X}_{\rho\sigma}C^{\mu\nu\rho\sigma}\right). \tag{III.F.3}$$

We also use that $\epsilon_{i_1\ldots i_n}\epsilon^{j_1\cdots j_n} = n!\delta^{j_1}_{[i_i}\cdots\delta^{j_n}_{i_n]}$ to rewrite pairs of building blocks that both include a dual field strength in terms of contractions without the Levi-Civita tensor.

III.G Selection rules from Supersymmetry

A crucial ingredient for the tree-level modified helicity selection rules in Secion 14.2 is the fact that all $|\tilde{h}| = 2$ four-point amplitudes, with the exception of the four fermion amplitude $\mathcal{A}(1_{\pm\frac{1}{2}}, 2_{\pm\frac{1}{2}}, 3_{\pm\frac{1}{2}}, 4_{\pm\frac{1}{2}})$, vanish on-shell. This non-trivial statement has been shown with a combination of direct computation, supersymmetric Ward identities (SWI) and KLT relations to hold for marginal theories [27, 435], pure gravity [443, 444] and minimally coupled gravity with two external gravitons [445]. Here we complete the proof along the lines of [435] using SWIs and show that all $|\tilde{h}| = 2$ four-point amplitudes with one external graviton vanish, i.e.[14]

$$0 = \mathcal{A}(h^+V^+V^+V^-) = \mathcal{A}(h^+V^+\phi\phi^\dagger) = \mathcal{A}(h^+\psi^+\psi^+\phi) = \mathcal{A}(h^+V^+\psi^+\psi^-)\,. \tag{III.G.1}$$

The proof is based on the observation that a marginal theory minimally coupled to gravity with holomorphic Yukawa couplings can be embedded in a $\mathcal{N} = 1$ supergravity theory with R-parity. For the SM this is the case if either all up-type or down-type Yukawa couplings vanish. Amplitudes in the supersymmetric theory that have only particles of the original marginal theory and gravitons as external states, which are even under R-parity, coincide with amplitudes of the marginal theory minimally coupled to gravity, since the R-parity prevents superpartners to appear in internal lines at tree level. However, global invariance under supersymmetry (SUSY) transformations yields non-trivial relations between amplitudes via SWIs (see e.g. [410,446,447]).

Consider a composite operator $\mathcal{O} = \Phi_1\cdots\Phi_n$ containing a product of arbitrary fields Φ_i and define $Q(\xi) = \bar{\xi}^\alpha Q_\alpha$ as the supercharge multiplied by a Grassmann spinor parameter $\bar{\xi}$. Then the SWI for $\mathcal{O}$ takes the form

$$0 = \langle 0|[Q(\xi), \mathcal{O}]|0\rangle = \sum_i \langle 0|\Phi_1\cdots[Q(\xi), \Phi_i]\cdots\Phi_n|0\rangle\,. \tag{III.G.2}$$

[14] Note that in order to ease the notation, in this Appendix the helicity of a particle is shown as a superscript instead of a subscript as in Chapter 14.

The SUSY transformations of the fields in the normalization of [435] are given by

$$[Q(\xi),\phi^\dagger(k)] = -\theta\,\langle\xi k\rangle\,\psi^+(k)\,, \qquad [Q(\xi),\psi^-(k)] = \theta\,\langle\xi k\rangle\,\phi(k)\,, \tag{III.G.3}$$

$$[Q(\xi),\lambda^+(k)] = -\theta\,\langle\xi k\rangle\,V^+(k)\,, \qquad [Q(\xi),V^-(k)] = \theta\,\langle\xi k\rangle\,\lambda^-(k)\,, \tag{III.G.4}$$

$$[Q(\xi),\zeta^+(k)] = -\theta\,\langle\xi k\rangle\,h^+(k)\,, \qquad [Q(\xi),h^-(k)] = \theta\,\langle\xi k\rangle\,\zeta^-(k)\,, \tag{III.G.5}$$

where particle pairs in the same chiral or vector supermultiplet are denoted by ϕ,ψ and λ,V, respectively. ζ and h are the gravitino and graviton. We also split the Grassmann spinor parameter $\bar{\xi}^\alpha = \theta\,\xi^\alpha$ into a Grassmann parameter θ and a spinor variable ξ^α, corresponding to an arbitrary massless vector ξ. The commutators for the remaining fields are obtained by inverting the helicities, i.e. $\pm\to\mp$ or $\phi\leftrightarrow\phi^\dagger$, and substituting $\langle\xi k\rangle\to-[\xi k]$.

In order to prove Eq. (III.G.1), we consider the two operators $\mathcal{O}_1 = h_1^+V_2^+\lambda_3^+V_4^-$ and $\mathcal{O}_2 = h_1^+\lambda_2^+\phi_3\phi_4^\dagger$. The SWI for the first operator yields

$$\begin{aligned} 0 = &-[\xi k_1]\mathcal{A}(\zeta_1^+V_2^+\lambda_3^+V_4^-) - [\xi k_2]\mathcal{A}(h_1^+\lambda_2^+\lambda_3^+V_4^-) \\ &- \langle\xi k_3\rangle\mathcal{A}(h_1^+V_2^+V_3^+V_4^-) + \langle\xi k_4\rangle\mathcal{A}(h_1^+V_2^+\lambda_3^+\lambda_4^-)\,. \end{aligned} \tag{III.G.6}$$

In a supersymmetrized version of a marginal theory minimally coupled to gravity, there are two classes of three-point amplitudes: graviton and gravitino three-point amplitudes with $|h(\mathcal{A}_3)| = 2$ (see e.g. [414]), and marginal three-point amplitudes with $|h(\mathcal{A}_3)| = 1$. This implies that the first two amplitudes in Eq. (III.G.6), which have total helicity $h = 2$, do not factorize into three-point amplitudes and can only be contact amplitudes, corresponding to a Lorentz invariant higher dimensional effective operator. However, as we assume minimal coupling of gravity to a marginal theory, there are no higher dimensional operators which could give rise to these amplitudes. Hence they must vanish. If we now choose $\xi = k_3$ and $\xi = k_4$ we obtain

$$\mathcal{A}(h_1^+V_2^+V_3^+V_4^-) = 0\,, \qquad \mathcal{A}(h_1^+V_2^+\lambda_3^+\lambda_4^-) = 0\,. \tag{III.G.7}$$

Similarly the Ward identity for $\mathcal{O}_2$

$$\begin{aligned} 0 = &-[\xi k_1]\mathcal{A}(\zeta_1^+\lambda_2^+\phi_3\phi_4^\dagger) - \langle\xi k_2\rangle\mathcal{A}(h_1^+V_2^+\phi_3\phi_4^\dagger) \\ &+ [\xi k_3]\mathcal{A}(h_1^+\lambda_2^+\psi_3^-\phi_4^\dagger) - \langle\xi k_4\rangle\mathcal{A}(h_1^+\lambda_2^+\phi_3\psi_4^+) \end{aligned} \tag{III.G.8}$$

contains two amplitudes with $h = 2$, i.e. $\mathcal{A}(\zeta_1^+\lambda_2^+\phi_3\phi_4^\dagger)$ and $\mathcal{A}(h_1^+\lambda_2^+\psi_3^-\phi_4^\dagger)$, which trivially vanish since there are no interactions that mediate it. Taking $\xi = k_2$ and $\xi = k_4$ we find that also the other two amplitudes vanish

$$\mathcal{A}(h_1^+V_2^+\phi_3\phi_4^\dagger) = 0\,, \qquad \mathcal{A}(h_1^+\lambda_2^+\phi_3\psi_4^+) = 0\,. \tag{III.G.9}$$

In order to complete the proof we note that helicity amplitudes factorize into color and Lorentz structure. This in combination with the fact that gauge groups commute with the SUSY algebra implies that Eqs. (III.G.7) and (III.G.9) do not only hold for gauginos in the adjoint or matter fermions in the fundamental representation, but for fermions in general representations [435]. This completes the proof that all amplitudes in Eq. (III.G.1) vanish.

Gravitino Amplitudes

In Section 14.2.1 we commented on the definition of a modified helicity in the presence of gravitinos. If we define $\tilde{h} = h - \frac{1}{2}h_g - \frac{2}{3}h_\zeta$ all three-point amplitudes satisfy $|\tilde{h}(\mathcal{A}_3)| = 1$, allowing for $|\tilde{h}(\mathcal{A}_4)| = 0, 2$. In the previous discussion we showed that $|\tilde{h}(\mathcal{A}_4)| = 2$ amplitudes with matter

or graviton external states vanish on shell. The same is true for $|\tilde{h}(\mathcal{A}_4)| = 2$ amplitudes with external gravitinos, s.t. $|\tilde{h}(\mathcal{A}_4)| = 0$ for arbitrary amplitudes.[15] A simple proof uses SWI to relate $|\tilde{h}(\mathcal{A}_4)| = 2$ gravitino amplitudes to vanishing graviton amplitudes.

As an explicit example consider the following class of amplitudes $\mathcal{A}(\zeta_1^+ X_2 Y_3 Z_4)$ with X, Y, Z being scalars, fermions or vectors with a combined helicity of $\tilde{h}(XYZ) = +3/2$. This amplitude could naively be constructed but but does not satisfy $|\tilde{h}(\mathcal{A}_4)| = 0$. Using the operator $\mathcal{O} = h_1^+ X_2 Y_3 Z_4$ one obtains the Ward identity

$$0 = -[\xi k_1]\mathcal{A}(\zeta_1^+ X_2 Y_3 Z_4) + \dots \,, \tag{III.G.10}$$

where the ellipsis stand for amplitudes of the form $\mathcal{A}(h_1^+ \cdots)$ with one graviton and three matter particles with combined helicity $\tilde{h}(\cdots) = \{1, 2\}$, s.t. the helicities of the full amplitudes are $\tilde{h} = \{2, 3\}$, which we have shown to vanish in the previous discussion. Thus Eq. (III.G.10) implies that amplitudes of the form $\mathcal{A}(\zeta_1^+ X_2 Y_3 Z_4)$ with $h(XYZ) = +3/2$ vanish on-shell. The remaining $|\tilde{h}(\mathcal{A}_4)| = 2$ amplitudes with additional external gravitinos can be shown to vanish in a similar fashion.

III.H Toy model amplitudes

In this Appendix we collect the three-point and four-point amplitudes, which are induced by the toy model in Eq. (14.65).

III.H.1 Three-point amplitudes

$$\mathcal{A}(1_{\chi^j}, 2_\psi, 3_{\bar{\phi}_i}) = y\,\delta_i^j \langle 12\rangle \quad , \quad \mathcal{A}(1_{\bar{\chi}_j}, 2_{\bar{\psi}}, 3_{\phi^i}) = y\,\delta_j^i [12] \tag{III.H.1}$$

$$\mathcal{A}(1_{V_-^a}, 2_{\phi^i}, 3_{\bar{\phi}_j}) = -g\,(t^a)_j^i \frac{\langle 12\rangle\langle 13\rangle}{\langle 23\rangle} \quad , \quad \mathcal{A}(1_{V_+^a}, 2_{\bar{\phi}_i}, 3_{\phi^j}) = -g\,(t^a)_i^j \frac{[12][13]}{[23]} \tag{III.H.2}$$

$$\mathcal{A}(1_{V_-^a}, 2_{\chi^i}, 3_{\bar{\chi}_j}) = g\,(t^a)_j^i \frac{\langle 12\rangle^2}{\langle 23\rangle} \quad , \quad \mathcal{A}(1_{V_+^a}, 2_{\bar{\chi}_i}, 3_{\chi^j}) = g\,(t^a)_i^j \frac{[12]^2}{[23]} \tag{III.H.3}$$

$$\mathcal{A}(1_{V_-^a}, 2_{V_-^b}, 3_{V_+^c}) = ig\,f^{abc} \frac{\langle 12\rangle^3}{\langle 23\rangle\langle 13\rangle} \quad , \quad \mathcal{A}(1_{V_+^a}, 2_{V_+^b}, 3_{V_-^c}) = -ig\,f^{abc} \frac{[12]^3}{[23][13]} \tag{III.H.4}$$

$$\mathcal{A}(1_{h_-}, 2_{\phi^i}, 3_{\bar{\phi}_j}) = -\frac{1}{M_{\rm pl}}\,\delta_j^i \frac{\langle 12\rangle^2\langle 13\rangle^2}{\langle 23\rangle^2} \quad , \quad \mathcal{A}(1_{h_+}, 2_{\bar{\phi}_i}, 3_{\phi^j}) = -\frac{1}{M_{\rm pl}}\,\delta_i^j \frac{[12]^2[13]^2}{[23]^2} \tag{III.H.5}$$

$$\mathcal{A}(1_{h_-}, 2_{\chi^i}, 3_{\bar{\chi}_j}) = \frac{1}{M_{\rm pl}}\,\delta_j^i \frac{\langle 12\rangle^3\langle 13\rangle}{\langle 23\rangle^2} \quad , \quad \mathcal{A}(1_{h_+}, 2_{\bar{\chi}_i}, 3_{\chi^j}) = \frac{1}{M_{\rm pl}}\,\delta_i^j \frac{[12]^3[13]}{[23]^2} \tag{III.H.6}$$

$$\mathcal{A}(1_{h_-}, 2_\psi, 3_{\bar{\psi}}) = \frac{1}{M_{\rm pl}} \frac{\langle 12\rangle^3\langle 13\rangle}{\langle 23\rangle^2} \quad , \quad \mathcal{A}(1_{h_+}, 2_{\bar{\psi}}, 3_\psi) = \frac{1}{M_{\rm pl}} \frac{[12]^3[13]}{[23]^2} \tag{III.H.7}$$

$$\mathcal{A}(1_{h_-}, 2_{V_-^a}, 3_{V_+^b}) = \frac{1}{M_{\rm pl}}\,\delta_{ab} \frac{\langle 12\rangle^4}{\langle 23\rangle^2} \quad , \quad \mathcal{A}(1_{h_+}, 2_{V_+^a}, 3_{V_-^b}) = \frac{1}{M_{\rm pl}}\,\delta_{ab} \frac{[12]^4}{[23]^2} \tag{III.H.8}$$

$$\mathcal{A}(1_{h_-}, 2_{h_-}, 3_{h_+}) = -\frac{1}{M_{\rm pl}} \frac{\langle 12\rangle^6}{\langle 23\rangle^2\langle 13\rangle^2} \quad , \quad \mathcal{A}(1_{h_+}, 2_{h_+}, 3_{h_-}) = -\frac{1}{M_{\rm pl}} \frac{[12]^6}{[23]^2[13]^2} \tag{III.H.9}$$

[15] A consistent theory with gravitinos must be completely supersymmetric. This forbids non-holomorphic Yukawa couplings, s.t. there is no exceptional four-fermion amplitude which does not respect the helicity selection rule.

III.H.2 Four-point amplitudes

$$\begin{aligned}\mathcal{A}(1_{\phi^i},2_{\bar{\phi}_j},3_{\bar{\phi}_k},4_{\phi^l}) &= -\lambda\left(\delta^i_j\delta^l_k+\delta^i_k\delta^l_j\right)+g^2\left(\left[\frac{s_{14}}{s_{12}}+\frac{1}{2}\right](t^a)^i_j(t^a)^l_k+\left[\frac{s_{14}}{s_{13}}+\frac{1}{2}\right](t^a)^i_k(t^a)^l_j\right)\\ &\quad-\frac{s_{14}}{M_{\rm pl}^2}\left(\frac{s_{14}}{s_{12}}\,\delta^i_j\delta^l_k+\frac{s_{14}}{s_{13}}\,\delta^i_k\delta^l_j\right)+\frac{c_\phi}{M_{\rm pl}^2}\left(s_{12}\,\delta^i_j\delta^l_k+s_{13}\,\delta^i_k\delta^l_j\right)\\ &\quad+\frac{c'_\phi}{M_{\rm pl}^2}\left(s_{12}\,\delta^i_k\delta^l_j+s_{13}\,\delta^i_j\delta^l_k\right),\end{aligned}\tag{III.H.10}$$

$$\begin{aligned}\mathcal{A}(1_{\chi^i},2_{\bar{\chi}_j},3_{\bar{\phi}_k},4_{\phi^l}) &= y^2\delta^i_k\delta^l_j\frac{\langle14\rangle}{\langle24\rangle}-\left(g^2(t^a)^i_j(t^a)^l_k+\frac{s_{13}}{M_{\rm pl}^2}\delta^i_j\delta^l_k\right)\frac{\langle1|p_3|2]}{s_{12}}\\ &\quad+\frac{1}{M_{\rm pl}^2}\langle1|p_3|2]\left(c_{\chi\phi}\,\delta^i_j\delta^l_k+c'_{\chi\phi}\,\delta^i_k\delta^l_j\right),\end{aligned}\tag{III.H.11}$$

$$\mathcal{A}(1_{\psi},2_{\bar{\psi}},3_{\bar{\phi}_i},4_{\phi^j}) = y^2\delta^j_i\frac{\langle14\rangle}{\langle24\rangle}-\frac{1}{M_{\rm pl}^2}\delta^j_i\langle1|p_3|2]\left(\frac{s_{13}}{s_{12}}-c_{\psi\phi}\right),\tag{III.H.12}$$

$$\begin{aligned}\mathcal{A}(1_{\chi^i},2_{\bar{\chi}_j},3_{\bar{\chi}_k},4_{\chi^l}) &= \langle14\rangle[23]\left[g^2\left(\frac{(t^a)^i_j(t^a)^l_k}{s_{12}}+\frac{(t^a)^i_k(t^a)^l_j}{s_{13}}\right)-\frac{s_{14}}{M_{\rm pl}^2}\left(\frac{\delta^i_j\delta^l_k}{s_{12}}+\frac{\delta^i_k\delta^l_j}{s_{13}}\right)\right]\\ &\quad+\frac{c_\chi}{M_{\rm pl}^2}\langle14\rangle[32]\left(\delta^i_j\delta^l_k+\,\delta^i_k\delta^l_j\right),\end{aligned}\tag{III.H.13}$$

$$\mathcal{A}(1_{\psi},2_{\bar{\psi}},3_{\bar{\psi}},4_{\psi}) = -\frac{1}{M_{\rm pl}^2}\langle14\rangle[23]\left(\frac{s_{14}}{s_{12}}+\frac{s_{14}}{s_{13}}-c_{\psi}\right),\tag{III.H.14}$$

$$\mathcal{A}(1_{\chi^i},2_{\bar{\chi}_j},3_{\bar{\psi}},4_{\psi}) = y^2\delta^i_j\frac{\langle14\rangle}{\langle23\rangle}-\frac{1}{M_{\rm pl}^2}\delta^i_j\langle14\rangle[23]\left(\frac{s_{14}}{s_{12}}-c_{\chi\psi}\right),\tag{III.H.15}$$

$$\mathcal{A}(1_{V^a_-},2_{V^b_+},3_{\bar{\phi}_i},4_{\phi^j}) = \langle1|p_3|2]^2\left[\frac{\delta_{ab}\delta^j_i}{M_{\rm pl}^2s_{12}}+g^2\frac{s_{14}(t^at^b)^j_i+s_{13}(t^bt^a)^j_i}{s_{12}s_{13}s_{14}}\right],\tag{III.H.16}$$

$$\mathcal{A}(1_{V^a_-},2_{\bar{\chi}_i},3_{\bar{\psi}},4_{\phi^j}) = yg(t^a)^j_i\frac{\langle13\rangle\langle14\rangle}{\langle23\rangle\langle34\rangle},\tag{III.H.17}$$

$$\mathcal{A}(1_{V^a_-},2_{V^b_+},3_{\bar{\chi}_i},4_{\chi^j}) = -\langle14\rangle[23]\langle1|p_3|2]\left[\frac{\delta_{ab}\delta^j_i}{M_{\rm pl}^2s_{12}}+g^2\frac{s_{14}(t^at^b)^j_i+s_{13}(t^bt^a)^j_i}{s_{12}s_{13}s_{14}}\right],\tag{III.H.18}$$

$$\mathcal{A}(1_{V^a_-},2_{V^b_+},3_{\bar{\psi}},4_{\psi}) = -\frac{1}{M_{\rm pl}^2}\delta_{ab}\frac{\langle14\rangle[23]\langle1|p_3|2]}{s_{12}},\tag{III.H.19}$$

$$\begin{aligned}\mathcal{A}(1_{V^a_-},2_{V^b_+},3_{V^c_+},4_{V^d_-}) &= -\frac{1}{M_{\rm pl}^2}\langle14\rangle^2[23]^2\left(\frac{\delta_{ab}\delta_{cd}}{s_{12}}+\frac{\delta_{ac}\delta_{bd}}{s_{13}}\right)\\ &\quad+g^2\langle14\rangle^2[23]^2\left(\frac{f^{abe}f^{cde}}{s_{12}s_{14}}+\frac{f^{ace}f^{bde}}{s_{13}s_{14}}\right),\end{aligned}\tag{III.H.20}$$

$$\mathcal{A}(1_{h_-},2_{\bar{\chi}_i},3_{\bar{\psi}},4_{\phi^j}) = -\frac{1}{M_{\rm pl}}\mathcal{E}_1^-\mathcal{A}(2_{\bar{\chi}_i},3_{\bar{\psi}},4_{\phi^j}),\tag{III.H.21}$$

$$\mathcal{A}(1_{h_-},2_{V^a_+},3_{\bar{\phi}_i},4_{\phi^j}) = -\frac{1}{M_{\rm pl}}\mathcal{E}_1^-\mathcal{A}(2_{V^a_+},3_{\bar{\phi}_i},4_{\phi^j}),\tag{III.H.22}$$

$$\mathcal{A}(1_{h_-},2_{V^a_+},3_{\bar{\chi}_i},4_{\chi^j}) = -\frac{1}{M_{\rm pl}}\mathcal{E}_1^-\mathcal{A}(2_{V^a_+},3_{\bar{\chi}_i},4_{\chi^j}),\tag{III.H.23}$$

$$\mathcal{A}(1_{h_-},2_{V_+^a},3_{V_+^b},4_{V_-^c}) = -\frac{1}{M_{\rm pl}}\mathcal{E}_1^-\mathcal{A}(2_{V_+^a},3_{V_+^b},4_{V_-^c})\,, \tag{III.H.24}$$

$$\mathcal{A}(1_{h_-},2_{h_+},3_{\bar\phi_i},4_{\phi^j}) = \frac{1}{M_{\rm pl}^2}\delta_i^j\frac{\langle 1|p_3|2]^4}{s_{12}s_{13}s_{14}}\,, \tag{III.H.25}$$

$$\mathcal{A}(1_{h_-},2_{h_+},3_{\bar\chi_i},4_{\chi^j}) = -\frac{1}{M_{\rm pl}^2}\delta_i^j\frac{\langle 14\rangle[23]\langle 1|p_3|2]^3}{s_{12}s_{13}s_{14}}\,, \tag{III.H.26}$$

$$\mathcal{A}(1_{h_-},2_{h_+},3_{\bar\psi},4_{\psi}) = -\frac{1}{M_{\rm pl}^2}\frac{\langle 14\rangle[23]\langle 1|p_3|2]^3}{s_{12}s_{13}s_{14}}\,, \tag{III.H.27}$$

$$\mathcal{A}(1_{h_-},2_{h_+},3_{V_+^a},4_{V_-^b}) = -\frac{1}{M_{\rm pl}^2}\delta_{ab}\frac{\langle 14\rangle^2[23]^2\langle 1|p_3|2]^2}{s_{12}s_{13}s_{14}}\,, \tag{III.H.28}$$

$$\mathcal{A}(1_{h_-},2_{h_+},3_{h_+},4_{h_-}) = \frac{1}{M_{\rm pl}^2}\frac{\langle 14\rangle^4[23]^4}{s_{12}s_{13}s_{14}}\,, \tag{III.H.29}$$

With a Feynman diagram computation, one finds $c_\phi = c'_\phi = 1$, $c_{\chi\phi} = c_{\xi\phi} = c_{\psi\phi} = -1/2$ and $c'_{\chi\phi} = c'_{\xi\phi} = 0$; $c_\chi = c_\xi = -3/4$; $c_\psi = -3/2$; $c_{\chi\xi} = c_{\chi\psi} = c_{\xi\psi} = -3/4$. Another interesting possibility is $c_\phi = 5/6$, that arises when the scalar is conformally coupled to gravity.

For amplitudes involving one graviton, we have used

$$\mathcal{E}_1^- \equiv \frac{\langle 1i\rangle[ij]\langle j1\rangle}{[1j]\langle ji\rangle[i1]} = \frac{\langle 1i\rangle^2[ij]^2\langle j1\rangle^2}{s_{12}s_{13}s_{14}}\,, \tag{III.H.30}$$

with $i,j = 2,3,4$ and $i \neq j$ (its value does not depend on the choice of i and j). When multiplying two matrices, it is important to respect the order as follows

$$M_i^k N_k^j \equiv (MN)_i^j \neq (NM)_i^j\,. \tag{III.H.31}$$

We also have

$$t^a t^b - t^b t^a = i f^{abc} t^c\,. \tag{III.H.32}$$

III.I Collinear Anomalous Dimensions

The computation of UV anomalous dimensions along the lines of Eq. (14.31), which was also thoroughly discussed in Section 14.1.3, is insensitive to soft IR divergences. However, collinear IR divergences originate from massless bubble integrals and have to be subtracted by hand. Fortunately collinear divergences are universal and only depend on the external particles of an amplitude. They can be parameterized in terms of a process independent collinear anomalous dimension $\gamma^j_{\rm coll}$ for each external particle j. In this Appendix we present a method developed in [432] to compute the collinear anomalous dimensions in a physically transparent way.

The authors of [432] determine anomalous dimensions for operators $\mathcal{O}$ via form factors, i.e. the matrix element between an operator and on-shell states $\langle 0|\mathcal{O}|p_1,\ldots,p_n\rangle$. It can be shown (see [432] for details) that at one-loop order the anomalous dimension for a minimal form factor[16] in our conventions is given by

$$\big(\gamma^{(1)}_{\mathcal{O}} - \gamma^{(1)}_{\rm IR}\big)\langle 0|\mathcal{O}|p_1,\ldots,p_n\rangle^{(0)} = -\frac{1}{4\pi^3}\langle 0|\mathcal{O}\otimes\mathcal{M}|p_1,\ldots,p_n\rangle^{(0)}\,, \tag{III.I.1}$$

[16]The minimal form factor of an operator $\mathcal{O}$ is non-vanishing in the free theory. Considering minimal form factors allows us to neglect the contribution from beta functions to the scale dependence of the form factor.

where the superscript shows the order at which the quantities are evaluated, (0) and (1) being tree-level and one-loop, respectively. $\mathcal{O} \otimes \mathcal{M}$ denotes an integration over an intermediate two-particle phase space, i.e.

$$\langle 0|\mathcal{O} \otimes \mathcal{M}|p_1, \ldots, p_n\rangle^{(0)} = \sum_{\ell_1,\ell_2} \int d\text{LIPS}\, \langle 0|\mathcal{O}|\ell_1, \ell_2\rangle^{(0)} \langle \ell_1, \ell_2|\mathcal{M}|p_1, \ldots, p_n\rangle^{(0)}\,, \tag{III.I.2}$$

with an additional factor of $1/2$ if ℓ_1 and ℓ_2 are identical particles. Thanks to momentum conservation in the second matrix element, ℓ_1 and ℓ_2 are related to the external momenta $\ell_1 + \ell_2 = p_1 + \ldots + p_n$, s.t. the phase space integration can be parameterized in a similar manner as in Eq. (14.32) and Eq. (14.33). Projecting out the rational part of Eq. (III.I.1) gives the UV and collinear anomalous dimension. Note that gravitational interactions produce only soft, but no collinear divergences [448] and are therefore irrelevant for the computation of collinear anomalous dimensions.

Since the collinear anomalous dimensions are universal they are identical for any form factor with matching external states. Thus they can be easily determined by considering the form factor of an operator which has vanishing UV divergence. A possible choice is the energy-momentum tensor $T^{\mu\nu}$, or $T^{\alpha\beta,\dot\alpha\dot\beta}$ in spinor notation, such that the collinear anomalous dimensions are given by [432]

$$\gamma^{p_1}_{\text{coll}} + \gamma^{p_2}_{\text{coll}} = \frac{1}{4\pi^3} \frac{\mathcal{R}\,\langle 0|T^{\alpha\beta,\dot\alpha\dot\beta} \otimes \mathcal{M}|p_1, p_2\rangle^{(0)}}{\langle 0|T^{\alpha\beta,\dot\alpha\dot\beta}|p_1, p_2\rangle^{(0)}}\,. \tag{III.I.3}$$

The relevant form factors of the energy-momentum tensor for scalars, fermions and vectors, converted to our notation, are of the form [432]

$$\langle 0|T^{\alpha\beta,\dot\alpha\dot\beta}|1_{\phi^i}, 2_{\bar\phi_j}\rangle = \frac{1}{3}\delta^i_j \big(p_1^{\alpha\dot\alpha} p_1^{\beta\dot\beta} + p_2^{\alpha\dot\alpha} p_2^{\beta\dot\beta} - p_1^{\alpha\dot\alpha} p_2^{\beta\dot\beta} - p_2^{\alpha\dot\alpha} p_1^{\beta\dot\beta} - p_1^{\alpha\dot\beta} p_2^{\beta\dot\alpha} - p_1^{\beta\dot\alpha} p_2^{\alpha\dot\beta}\big)\,, \tag{III.I.4}$$

$$\langle 0|T^{\alpha\beta,\dot\alpha\dot\beta}|1_{\chi^i}, 2_{\bar\chi_j}\rangle = \frac{1}{2}\delta^i_j \big(\lambda_1^\alpha \lambda_1^\beta \tilde\lambda_1^{\dot\alpha} \tilde\lambda_2^{\dot\beta} + \lambda_1^\alpha \lambda_1^\beta \tilde\lambda_1^{\dot\beta} \tilde\lambda_2^{\dot\alpha} - \lambda_1^\alpha \lambda_2^\beta \tilde\lambda_2^{\dot\alpha} \tilde\lambda_2^{\dot\beta} - \lambda_1^\beta \lambda_2^\alpha \tilde\lambda_2^{\dot\alpha} \tilde\lambda_2^{\dot\beta}\big)\,, \tag{III.I.5}$$

$$\langle 0|T^{\alpha\beta,\dot\alpha\dot\beta}|1_{V^a_+}, 2_{V^b_-}\rangle = -2\,\delta^{ab} \lambda_2^\alpha \lambda_2^\beta \tilde\lambda_1^{\dot\alpha} \tilde\lambda_1^{\dot\beta}\,, \tag{III.I.6}$$

where $p_i^{\alpha\dot\alpha} = p_i^\mu \sigma_\mu^{\alpha\dot\alpha}$. With the explicit expression for the form factors it is straightforward to obtain the collinear anomalous dimensions for the toy model particles from Eq. (III.I.3). Let us demonstrate this for the singlet Weyl fermion ψ. There are non-vanishing marginal four-point amplitudes of $\psi\bar\psi$ with $\chi\bar\chi$ and $\phi\bar\phi$, s.t. the numerator in Eq. (III.I.3) takes the form

$$\begin{aligned}
\mathcal{R}\,\langle 0|T^{\alpha\beta,\dot\alpha\dot\beta} \otimes \mathcal{M}|1_\psi, 2_{\bar\psi}\rangle^{(0)} &= \mathcal{R} \int d\text{LIPS} \left[T^{\alpha\beta,\dot\alpha\dot\beta}_{\ell_{1\,\phi^i}\,\ell_{2\,\bar\phi_j}}\, \mathcal{M}_{1_\psi 2_{\bar\psi}\to\ell_{1\,\phi^i}\ell_{2\,\bar\phi_j}} + T^{\alpha\beta,\dot\alpha\dot\beta}_{\ell_{1\,\chi^i}\,\ell_{2\,\bar\chi_j}}\, \mathcal{M}_{1_\psi 2_{\bar\psi}\to\ell_{1\,\chi^i}\,\ell_{2\,\bar\chi_j}}\right] \\
&= \frac{C_A y^2 \pi}{8} \big(\lambda_1^\alpha \lambda_1^\beta \tilde\lambda_1^{\dot\alpha} \tilde\lambda_2^{\dot\beta} + \lambda_1^\alpha \lambda_1^\beta \tilde\lambda_1^{\dot\beta} \tilde\lambda_2^{\dot\alpha} - \lambda_1^\alpha \lambda_2^\beta \tilde\lambda_2^{\dot\alpha} \tilde\lambda_2^{\dot\beta} - \lambda_1^\beta \lambda_2^\alpha \tilde\lambda_1^{\dot\alpha} \tilde\lambda_2^{\dot\beta}\big) \\
&= \frac{C_A y^2 \pi}{4} \langle 0|T^{\alpha\beta,\dot\alpha\dot\beta}|1_\psi, 2_{\bar\psi}\rangle^{(0)}\,,
\end{aligned} \tag{III.I.7}$$

where we defined $T^{\alpha\beta,\dot\alpha\dot\beta}_{ij} \equiv \langle 0|T^{\alpha\beta,\dot\alpha\dot\beta}|p_i, p_j\rangle$ and used that

$$\mathcal{M}_{p_1p_2\to p_3p_4} = \langle p_3, p_4|\mathcal{M}|p_1, p_2\rangle = i^{F_{p_3p_4}} \langle 0|\mathcal{M}|-\bar p_4, -\bar p_3, p_1, p_2\rangle \equiv i^{F_{p_3p_4}} \mathcal{A}(-\bar p_4, -\bar p_3, p_1, p_2)\,, \tag{III.I.8}$$

where we used crossing symmetry and denoted the anti-particle of p_i by $\bar p_i$. The factor $i^{F_{p_3p_4}}$, where $F_{p_3p_4}$ counts the number of fermions in the set $\{p_3, p_4\}$, is required when using the spinor

convention $|-p\rangle, |-p] = i(|p\rangle, |p])$. Plugging Eq. (III.I.7) into Eq. (III.I.3) we immediately obtain $\gamma^{\psi}_{\text{coll}} = C_A y^2/(32\pi^2)$. The collinear anomalous dimensions of the remaining particles in the toy model can be determined through a similar computation. In summary this yields

$$\gamma^{\phi}_{\text{coll}} = -\frac{C_F g^2}{8\pi^2} + \frac{y^2}{16\pi^2}\,, \quad \gamma^{\psi}_{\text{coll}} = \frac{C_A y^2}{32\pi^2}\,, \quad \gamma^{\chi}_{\text{coll}} = -\frac{3C_F g^2}{32\pi^2} + \frac{y^2}{32\pi^2}\,, \quad \gamma^{V}_{\text{coll}} = \frac{(3-22C_A)g^2}{192\pi^2}\,. \tag{III.I.9}$$

C^4		H^2C^3	
$\mathcal{O}_{CC}$	$(C_{\mu\nu\rho\sigma}C^{\mu\nu\rho\sigma})^2$	$\mathcal{O}_{2HC}$	$(H^\dagger H)(C_{\mu\nu\rho\sigma}C^{\rho\sigma\alpha\beta}C_{\alpha\beta}{}^{\mu\nu})$
$\mathcal{O}_{C\tilde{C}}$	$(C_{\mu\nu\rho\sigma}C^{\mu\nu\rho\sigma})(C_{\alpha\beta\gamma\delta}\tilde{C}^{\alpha\beta\gamma\delta})$	$\mathcal{O}_{2H\tilde{C}}$	$(H^\dagger H)(C_{\mu\nu\rho\sigma}C^{\rho\sigma\alpha\beta}\tilde{C}_{\alpha\beta}{}^{\mu\nu})$
$\mathcal{O}_{\tilde{C}\tilde{C}}$	$(C_{\mu\nu\rho\sigma}\tilde{C}^{\mu\nu\rho\sigma})^2$		
H^4C^2		X^3C	
$\mathcal{O}_{4HC}$	$(H^\dagger H)^2(C_{\mu\nu\rho\sigma}C^{\mu\nu\rho\sigma})$	$\mathcal{O}_{GBC}$	$G^A_{\mu\nu}G^A_{\rho\alpha}B^\alpha{}_\sigma C^{\mu\nu\rho\sigma}$
$\mathcal{O}_{4H\tilde{C}}$	$(H^\dagger H)^2(C_{\mu\nu\rho\sigma}\tilde{C}^{\mu\nu\rho\sigma})$	$\mathcal{O}_{GB\tilde{C}}$	$G^A_{\mu\nu}G^A_{\rho\alpha}B^\alpha{}_\sigma \tilde{C}^{\mu\nu\rho\sigma}$
		$\mathcal{O}_{WBC}$	$W^a_{\mu\nu}W^a_{\rho\alpha}B^\alpha{}_\sigma C^{\mu\nu\rho\sigma}$
		$\mathcal{O}_{WB\tilde{C}}$	$W^a_{\mu\nu}W^a_{\rho\alpha}B^\alpha{}_\sigma \tilde{C}^{\mu\nu\rho\sigma}$
X^2C^2			
$\mathcal{O}^{(1)}_{GC}$	$(G^A_{\mu\nu}G^{A\,\mu\nu})(C_{\alpha\beta\rho\sigma}C^{\alpha\beta\rho\sigma})$	$\mathcal{O}^{(1)}_{G\tilde{C}}$	$(G^A_{\mu\nu}G^{A\,\mu\nu})(C_{\alpha\beta\rho\sigma}\tilde{C}^{\alpha\beta\rho\sigma})$
$\mathcal{O}_{\tilde{G}C}$	$(G^A_{\mu\nu}\tilde{G}^{A\,\mu\nu})(C_{\alpha\beta\rho\sigma}C^{\alpha\beta\rho\sigma})$	$\mathcal{O}_{\tilde{G}\tilde{C}}$	$(G^A_{\mu\nu}\tilde{G}^{A\,\mu\nu})(C_{\alpha\beta\rho\sigma}\tilde{C}^{\alpha\beta\rho\sigma})$
$\mathcal{O}^{(2)}_{GC}$	$G^A_{\mu\nu}G^{A\,\rho\sigma}C^{\mu\nu\alpha\beta}C_{\alpha\beta\rho\sigma}$	$\mathcal{O}^{(2)}_{G\tilde{C}}$	$G^A_{\mu\nu}G^{A\,\rho\sigma}C^{\mu\nu\alpha\beta}\tilde{C}_{\alpha\beta\rho\sigma}$
$\mathcal{O}^{(1)}_{WC}$	$(W^a_{\mu\nu}W^{a\,\mu\nu})(C_{\alpha\beta\rho\sigma}C^{\alpha\beta\rho\sigma})$	$\mathcal{O}^{(1)}_{W\tilde{C}}$	$(W^a_{\mu\nu}W^{a\,\mu\nu})(C_{\alpha\beta\rho\sigma}\tilde{C}^{\alpha\beta\rho\sigma})$
$\mathcal{O}_{\tilde{W}C}$	$(W^a_{\mu\nu}\tilde{W}^{a\,\mu\nu})(C_{\alpha\beta\rho\sigma}C^{\alpha\beta\rho\sigma})$	$\mathcal{O}_{\tilde{W}\tilde{C}}$	$(W^a_{\mu\nu}\tilde{W}^{a\,\mu\nu})(C_{\alpha\beta\rho\sigma}\tilde{C}^{\alpha\beta\rho\sigma})$
$\mathcal{O}^{(2)}_{WC}$	$W^a_{\mu\nu}W^{a\,\rho\sigma}C^{\mu\nu\alpha\beta}C_{\alpha\beta\rho\sigma}$	$\mathcal{O}^{(2)}_{W\tilde{C}}$	$W^a_{\mu\nu}W^{a\,\rho\sigma}C^{\mu\nu\alpha\beta}\tilde{C}_{\alpha\beta\rho\sigma}$
$\mathcal{O}^{(1)}_{BC}$	$(B_{\mu\nu}B^{\mu\nu})(C_{\alpha\beta\rho\sigma}C^{\alpha\beta\rho\sigma})$	$\mathcal{O}^{(1)}_{B\tilde{C}}$	$(B_{\mu\nu}B^{\mu\nu})(C_{\alpha\beta\rho\sigma}\tilde{C}^{\alpha\beta\rho\sigma})$
$\mathcal{O}_{\tilde{B}C}$	$(B_{\mu\nu}\tilde{B}^{\mu\nu})(C_{\alpha\beta\rho\sigma}C^{\alpha\beta\rho\sigma})$	$\mathcal{O}_{\tilde{B}\tilde{C}}$	$(B_{\mu\nu}\tilde{B}^{\mu\nu})(C_{\alpha\beta\rho\sigma}\tilde{C}^{\alpha\beta\rho\sigma})$
$\mathcal{O}^{(2)}_{BC}$	$B_{\mu\nu}B^{\rho\sigma}C^{\mu\nu\alpha\beta}C_{\alpha\beta\rho\sigma}$	$\mathcal{O}^{(2)}_{B\tilde{C}}$	$B_{\mu\nu}B^{\rho\sigma}C^{\mu\nu\alpha\beta}\tilde{C}_{\alpha\beta\rho\sigma}$
X^2H^2C			
$\mathcal{O}_{GHC}$	$(H^\dagger H)(G^{A\,\mu\nu}G^{A\,\rho\sigma}C_{\mu\nu\rho\sigma})$	$\mathcal{O}_{GH\tilde{C}}$	$(H^\dagger H)(G^{A\,\mu\nu}G^{A\,\rho\sigma}\tilde{C}_{\mu\nu\rho\sigma})$
$\mathcal{O}_{WHC}$	$(H^\dagger H)(W^{a\,\mu\nu}W^{a\,\rho\sigma}C_{\mu\nu\rho\sigma})$	$\mathcal{O}_{WH\tilde{C}}$	$(H^\dagger H)(W^{a\,\mu\nu}W^{a\,\rho\sigma}\tilde{C}_{\mu\nu\rho\sigma})$
$\mathcal{O}_{BHC}$	$(H^\dagger H)(B^{\mu\nu}B^{\rho\sigma}C_{\mu\nu\rho\sigma})$	$\mathcal{O}_{BH\tilde{C}}$	$(H^\dagger H)(B^{\mu\nu}B^{\rho\sigma}\tilde{C}_{\mu\nu\rho\sigma})$
$\mathcal{O}_{WBC}$	$(H^\dagger\tau^a H)(B^{\mu\nu}W^{a\,\rho\sigma}C_{\mu\nu\rho\sigma})$	$\mathcal{O}_{WB\tilde{C}}$	$(H^\dagger\tau^a H)(B^{\mu\nu}W^{a\,\rho\sigma}\tilde{C}_{\mu\nu\rho\sigma})$
$H^2C^2\mathcal{D}^2$		$XH^2C\mathcal{D}^2$	
$\mathcal{O}_{HC\mathcal{D}}$	$(\nabla_\alpha H)^\dagger(\nabla^\alpha H)(C_{\mu\nu\rho\sigma}C^{\mu\nu\rho\sigma})$	$\mathcal{O}_{WC\mathcal{D}}$	$(\nabla^\mu H)^\dagger\tau^a(\nabla^\nu H)W^{a\,\rho\sigma}C_{\rho\sigma\mu\nu}$
$\mathcal{O}_{H\tilde{C}\mathcal{D}}$	$(\nabla_\alpha H)^\dagger(\nabla^\alpha H)(C_{\mu\nu\rho\sigma}\tilde{C}^{\mu\nu\rho\sigma})$	$\mathcal{O}_{W\tilde{C}\mathcal{D}}$	$(\nabla^\mu H)^\dagger\tau^a(\nabla^\nu H)W^{a\,\rho\sigma}\tilde{C}_{\rho\sigma\mu\nu}$
		$\mathcal{O}_{BC\mathcal{D}}$	$(\nabla^\mu H)^\dagger(\nabla^\nu H)B^{\rho\sigma}C_{\rho\sigma\mu\nu}$
		$\mathcal{O}_{B\tilde{C}\mathcal{D}}$	$(\nabla^\mu H)^\dagger(\nabla^\nu H)B^{\rho\sigma}\tilde{C}_{\rho\sigma\mu\nu}$

Table III.F.1: Bosonic dimension-8 operators of the GRSMEFT including gravitational interactions.

$\psi^2 HC^2$		$\psi^2 XHC$	
$\mathcal{O}_{uHC}$	$(\bar{Q}_L \tilde{H} u_R)(C_{\mu\nu\rho\sigma} C^{\mu\nu\rho\sigma})$	$\mathcal{O}_{uGC}$	$(\bar{Q}_L \sigma^{\mu\nu} T^A u_R) \tilde{H} G^{A\,\rho\sigma} C_{\mu\nu\rho\sigma}$
$\mathcal{O}_{uH\tilde{C}}$	$(\bar{Q}_L \tilde{H} u_R)(C_{\mu\nu\rho\sigma} \tilde{C}^{\mu\nu\rho\sigma})$	$\mathcal{O}_{uWC}$	$(\bar{Q}_L \sigma^{\mu\nu} u_R) \tau^a \tilde{H} W^{a\,\rho\sigma} C_{\mu\nu\rho\sigma}$
$\mathcal{O}_{dHC}$	$(\bar{Q}_L H d_R)(C_{\mu\nu\rho\sigma} C^{\mu\nu\rho\sigma})$	$\mathcal{O}_{uBC}$	$(\bar{Q}_L \sigma^{\mu\nu} u_R) \tilde{H} B^{\rho\sigma} C_{\mu\nu\rho\sigma}$
$\mathcal{O}_{dH\tilde{C}}$	$(\bar{Q}_L H d_R)(C_{\mu\nu\rho\sigma} \tilde{C}^{\mu\nu\rho\sigma})$	$\mathcal{O}_{dGC}$	$(\bar{Q}_L \sigma^{\mu\nu} T^A d_R) H G^{A\,\rho\sigma} C_{\mu\nu\rho\sigma}$
$\mathcal{O}_{eHC}$	$(\bar{L}_L H e_R)(C_{\mu\nu\rho\sigma} C^{\mu\nu\rho\sigma})$	$\mathcal{O}_{dWC}$	$(\bar{Q}_L \sigma^{\mu\nu} d_R) \tau^a H W^{a\,\rho\sigma} C_{\mu\nu\rho\sigma}$
$\mathcal{O}_{eH\tilde{C}}$	$(\bar{L}_L H e_R)(C_{\mu\nu\rho\sigma} \tilde{C}^{\mu\nu\rho\sigma})$	$\mathcal{O}_{dBC}$	$(\bar{Q}_L \sigma^{\mu\nu} d_R) H B^{\rho\sigma} C_{\mu\nu\rho\sigma}$
		$\mathcal{O}_{eWC}$	$(\bar{L}_L \sigma^{\mu\nu} e_R) \tau^a H W^{a\,\rho\sigma} C_{\mu\nu\rho\sigma}$
		$\mathcal{O}_{eBC}$	$(\bar{L}_L \sigma^{\mu\nu} e_R) H B^{\rho\sigma} C_{\mu\nu\rho\sigma}$
$\psi^2 HC\mathcal{D}^2$		$\psi^4 C$	
$\mathcal{O}_{uC\mathcal{D}}$	$(\bar{Q}_L \sigma^{\mu\nu} \nabla^\rho u_R)(\nabla^\sigma \tilde{H}) C_{\mu\nu\rho\sigma}$	$\mathcal{O}_{udC}$	$\epsilon_{ij} (\bar{Q}^i_L \sigma^{\mu\nu} u_R)(\bar{Q}^j_L \sigma^{\rho\sigma} d_R) C_{\mu\nu\rho\sigma}$
$\mathcal{O}_{dC\mathcal{D}}$	$(\bar{Q}_L \sigma^{\mu\nu} \nabla^\rho d_R)(\nabla^\sigma H) C_{\mu\nu\rho\sigma}$	$\mathcal{O}_{ueC}$	$\epsilon_{ij} (\bar{Q}^i_L \sigma^{\mu\nu} u_R)(\bar{L}^j_L \sigma^{\rho\sigma} e_R) C_{\mu\nu\rho\sigma}$
$\mathcal{O}_{eC\mathcal{D}}$	$(\bar{L}_L \sigma^{\mu\nu} \nabla^\rho e_R)(\nabla^\sigma H) C_{\mu\nu\rho\sigma}$	$\mathcal{O}_{uedC}$	$\epsilon^{\alpha\beta\gamma} [(d^\alpha_R)^T C \sigma^{\mu\nu} u^\beta_R][(u^\gamma_R)^T C \sigma^{\rho\sigma} e_R] C_{\mu\nu\rho\sigma}$
$\psi^2 XC\mathcal{D}$			
$\mathcal{O}_{QGC\mathcal{D}}$	$(\bar{Q}_L \gamma^\mu T^A \nabla^\nu Q_L) G^{A\,\rho\sigma} C_{\mu\nu\rho\sigma}$	$\mathcal{O}_{QG\tilde{C}\mathcal{D}}$	$(\bar{Q}_L \gamma^\mu T^A \nabla^\nu Q_L) G^{A\,\rho\sigma} \tilde{C}_{\mu\nu\rho\sigma}$
$\mathcal{O}_{uGC\mathcal{D}}$	$(\bar{u}_R \gamma^\mu T^A \nabla^\nu u_R) G^{A\,\rho\sigma} C_{\mu\nu\rho\sigma}$	$\mathcal{O}_{uG\tilde{C}\mathcal{D}}$	$(\bar{u}_R \gamma^\mu T^A \nabla^\nu u_R) G^{A\,\rho\sigma} \tilde{C}_{\mu\nu\rho\sigma}$
$\mathcal{O}_{dGC\mathcal{D}}$	$(\bar{d}_R \gamma^\mu T^A \nabla^\nu d_R) G^{A\,\rho\sigma} C_{\mu\nu\rho\sigma}$	$\mathcal{O}_{dG\tilde{C}\mathcal{D}}$	$(\bar{d}_R \gamma^\mu T^A \nabla^\nu d_R) G^{A\,\rho\sigma} \tilde{C}_{\mu\nu\rho\sigma}$
$\mathcal{O}_{QWC\mathcal{D}}$	$(\bar{Q}_L \gamma^\mu \tau^a \nabla^\nu Q_L) W^{a\,\rho\sigma} C_{\mu\nu\rho\sigma}$	$\mathcal{O}_{QW\tilde{C}\mathcal{D}}$	$(\bar{Q}_L \gamma^\mu \tau^a \nabla^\nu Q_L) W^{a\,\rho\sigma} \tilde{C}_{\mu\nu\rho\sigma}$
$\mathcal{O}_{LWC\mathcal{D}}$	$(\bar{L}_L \gamma^\mu \tau^a \nabla^\nu L_L) W^{a\,\rho\sigma} C_{\mu\nu\rho\sigma}$	$\mathcal{O}_{LW\tilde{C}\mathcal{D}}$	$(\bar{L}_L \gamma^\mu \tau^a \nabla^\nu L_L) W^{a\,\rho\sigma} \tilde{C}_{\mu\nu\rho\sigma}$
$\mathcal{O}_{QBC\mathcal{D}}$	$(\bar{Q}_L \gamma^\mu \nabla^\nu Q_L) B^{\rho\sigma} C_{\mu\nu\rho\sigma}$	$\mathcal{O}_{QB\tilde{C}\mathcal{D}}$	$(\bar{Q}_L \gamma^\mu \nabla^\nu Q_L) B^{\rho\sigma} \tilde{C}_{\mu\nu\rho\sigma}$
$\mathcal{O}_{uBC\mathcal{D}}$	$(\bar{u}_R \gamma^\mu \nabla^\nu u_R) B^{\rho\sigma} C_{\mu\nu\rho\sigma}$	$\mathcal{O}_{uB\tilde{C}\mathcal{D}}$	$(\bar{u}_R \gamma^\mu \nabla^\nu u_R) B^{\rho\sigma} \tilde{C}_{\mu\nu\rho\sigma}$
$\mathcal{O}_{dBC\mathcal{D}}$	$(\bar{d}_R \gamma^\mu \nabla^\nu d_R) B^{\rho\sigma} C_{\mu\nu\rho\sigma}$	$\mathcal{O}_{dB\tilde{C}\mathcal{D}}$	$(\bar{d}_R \gamma^\mu \nabla^\nu d_R) B^{\rho\sigma} \tilde{C}_{\mu\nu\rho\sigma}$
$\mathcal{O}_{LBC\mathcal{D}}$	$(\bar{L}_L \gamma^\mu \nabla^\nu L_L) B^{\rho\sigma} C_{\mu\nu\rho\sigma}$	$\mathcal{O}_{LB\tilde{C}\mathcal{D}}$	$(\bar{L}_L \gamma^\mu \nabla^\nu L_L) B^{\rho\sigma} \tilde{C}_{\mu\nu\rho\sigma}$
$\mathcal{O}_{eBC\mathcal{D}}$	$(\bar{e}_R \gamma^\mu \nabla^\nu e_R) B^{\rho\sigma} C_{\mu\nu\rho\sigma}$	$\mathcal{O}_{eB\tilde{C}\mathcal{D}}$	$(\bar{e}_R \gamma^\mu \nabla^\nu e_R) B^{\rho\sigma} \tilde{C}_{\mu\nu\rho\sigma}$

Table III.F.2: Dimension-8 operators of the GRSMEFT including gravitational interactions and fermions for $N_f = 1$. We do not show explicitly the h.c. of non self-conjugate operators. $\tilde{H}_i = \epsilon_{ij} H^*_j$ and C is the charge conjugation matrix.

Part IV

Conclusions

Conclusions

Despite conclusive evidence that the SM is incomplete, BSM physics has so far evaded detection. The absence of a signal in combination with an increasing experimental sensitivity puts considerable stress on well-motivated models, such as supersymmetry and Composite Higgs models, and pushes them into a more and more fine-tuned region of parameter space. This requires a careful re-evaluation of the models, which have been the focus of investigation, and the development of new ideas to test the predictions of the SM. In this thesis we have contributed to this effort in several ways: we studied DM in well-motivated models, in particular composite pNGB DM in CH models and the QCD axion, and re-evaluated some of their properties. Additionally we considered EFTs of the SM and gravity and for the first time constructed the EFT of the SM coupled to GR, the GRSMEFT.

In Part I of the thesis we studied composite pNGB DM, a WIMP candidate which naturally arises in the CH framework. In this class of models both the Higgs and DM are pNGBs of a spontaneously broken symmetry of a new strong sector. We started our study with an EFT approach in Chapter 3, where we considered the most general effective Lagrangian of a complex scalar DM χ coupled to the SM with a CH inspired power counting (see Section 2.2.3). This allowed us to identify the derivative Higgs portal $c_d \partial_\mu |H|^2 \partial^\mu |\chi|^2 / f^2$, where f is the symmetry breaking scale of the strong sector, as the characteristic feature of composite pNGB DM. This coupling alone defines a viable and appealing DM scenario: it is strong enough in DM annihilations to produce the observed relic abundance for weak scale DM $m_\chi \sim m_h$ and $f \sim$ TeV, but at the same time highly suppressed at low-energy scattering on nuclei, thus explaining the null results in direct detection experiments. A scenario, where the derivative Higgs portal is the leading coupling to the SM can be seen as the "Goldstone limit", since the coupling preserves the Goldstone symmetry of the DM and Higgs. However, in realistic models this simple picture can be significantly changed, since the generation of a mass for the DM requires an explicit breaking of the χ Goldstone shift symmetry. This introduces in general further model-dependent, non-derivative interactions, such as the marginal Higgs portal coupling $\lambda |H|^2 |\chi|^2$, which is strongly constrained by direct detection experiments. The viability of the model therefore crucially depends on how closely the "Goldstone limit" can be realized.

After this general discussion on composite pNGB DM, the focus of Chapter 4 was on an explicit realization in a fully realistic CH model based on the symmetry breaking structure $SO(7)/SO(6)$. This symmetry breaking structure gives rise to six GBs, the Higgs doublet H and a complex DM candidate χ. This model has the additional appealing feature that the stability of the DM is guaranteed by a global symmetry $U(1)_{\rm DM} \subset SO(6)$ of the strong sector. We identified three qualitatively different sources for the explicit breaking of the DM shift symmetry: shift symmetry breaking by the couplings to the top quark (Section 4.3), shift symmetry breaking by the couplings to the bottom quark (Section 4.4) and shift symmetry breaking by gauging $U(1)_{\rm DM}$ (Section 4.5). All three scenarios successfully implement EWSB

and lead to qualitatively different DM phenomenologies. Let us briefly summarize the main results of these model realizations.

The model where the leading breaking of the DM shift symmetry is due to the top quark couplings does not realize the "Goldstone limit". It predicts a marginal Higgs portal coupling, whose natural size is related to the Higgs quartic by $\lambda \lesssim \lambda_h/2 \approx 0.065$. We find that a moderately tuned version of the model with a symmetry breaking scale of $f = 1.4$ TeV, a DM mass of 200 GeV $\lesssim m_\chi \lesssim$ 400 GeV and a portal coupling of $0.01 \lesssim \lambda \lesssim 0.04$ is still viable although in mild tension with recent XENON1T results. XENON1T in its full lifetime will probe the entire remaining parameter space of the model.

If the couplings of the bottom quark are the leading breaking of the DM shift symmetry, the "Goldstone limit" is realized to a large extent. The marginal Higgs portal coupling is strongly suppressed $\lambda \ll 10^{-3}$, s.t. it is irrelevant for DM phenomenology, and the DM is heavy enough with $m_\chi \sim 100$ GeV for the relic abundance to be produced via annihilations through the derivative Higgs portal. However, in contrast to the pure "Goldstone limit", this model is not completely invisible in direct detection experiments. The shift symmetry breaking by the bottom quark generates a contact interaction of the form $y_b \bar{q}_L H b_R |\chi|^2/f^2$ with $\mathcal{O}(1)$ coefficient, leading to a small but observable direct detection signal, which will be probed in future experiments such as LZ and XENONnT.

The cleanest realization of the "Goldstone limit" is reached if all fermion couplings respect the DM shift symmetry and the DM mass arises purely from gauging the stabilizing $U(1)_{\rm DM}$ symmetry. This does not generate any non-derivative contact interactions to the SM at one loop. Thus the direct detection signal is extremely suppressed and out of reach even at future experiments. However, the dark sector consisting of the DM χ and dark photon γ_D can be tested at colliders and in cosmology and astroparticle experiments. Important probes for a massless or approximately massless dark photon with $m_{\gamma_D} \approx 0$ are the number of relativistic degrees of freedom $\Delta N_{\rm eff}$, which will be sensitive to this scenario in the next generation of CMB measurements, and probes of the long-range DM self-interactions. Heavier dark photons $m_{\gamma_D} \gtrsim m_\chi$ result in an interesting two-component dark matter scenario, which can only be tested in DM indirect detection.

Composite pNGB DM, which realizes the "Goldstone limit", is practically invisible in direct detection experiments. For this reason collider probes, which can fully exploit the energy growth of the derivative couplings, are a crucial ingredient to test pNGB DM. In Chapter 5 we studied both the derivative and marginal Higgs portal in the Higgs off-shell region $m_\chi \gtrsim m_h/2$ in the weak-boson fusion production channel at current and future lepton and hadron colliders. While the derivative Higgs portal allows for a better separation of signal from background than the marginal Higgs portal, due to harder kinematic distributions, a high-energy hadron collider such as FCC-100 or a high-energy muon collider is needed to truly test the region of parameter space, which is relevant for pNGB DM.

In summary, pNGB DM remains an appealing and well-motivated DM candidate, which, especially in the "Goldstone limit", is challenging to probe. For this reason it is important to devise new tests of this scenario. An interesting idea is to look for indirect effects of pNGB DM in precisely measured SM processes. This was done e.g. in [449] for the marginal Higgs portal by considering contributions of DM loops to the $gg \to ZZ(\to 4\ell)$ process in the off-shell Higgs mediated region. We plan to perform a similar study for the derivative Higgs portal [306].

The focus of Part II was the QCD axion, another well-motivated DM candidate. We investigated the robustness of the conventional axion mass prediction, which can be phrased purely in terms of IR observables $m_a f_a \sim m_\pi f_\pi$. This implicitly assumes that the dominant contribution

to the axion mass originates from large instantons, where QCD is strongly coupled. However, in a recent publication by Agrawal and Howe it was pointed out that for a particular type of UV completion based on product groups, small instantons could provide the dominant contribution to the axion mass even if the UV theory remains weakly coupled (and hence fully calculable). The goal of our work was to identify the origin of this enhancement of small instantons.

In Chapter 9 we studied small instanton contributions to the axion mass in partially broken gauge groups and identified the non-trivial index of embedding of QCD into a high-energy gauge group G as the source for the enhancement of small instantons. The index of embedding k characterizes the matching of instantons in the high-energy theory to QCD instantons. This can be written in the form $(\Lambda_G/M)^{k\,b_G} = (\Lambda_{\rm QCD}/M)^{b_{\rm QCD}}$, where M is the symmetry breaking scale and $\Lambda_G, \Lambda_{\rm QCD}$ and $b_G, b_{\rm QCD}$ are the dynamic scales and beta function coefficients of the gauge coupling in the high-energy gauge group G and QCD, respectively. This implies that a one instanton solution in QCD corresponds to a k instanton solution of the UV theory. Besides there are certain small instantons, which live entirely in the broken part of the group G and are therefore not matched to QCD instantons. From the low-energy point of view these scale as $1/k$ fractional instantons and are therefore enhanced compared to regular small QCD instantons. The enhancement increases with a larger index of embedding. In Chapter 9 we additionally performed a full one-instanton calculation for the axion mass and found that in product group models the enhancement with two group factors is numerically not significant, however, already three factors can provide a large enhancement of the axion mass compared to the standard QCD prediction.

In product gauge groups, each of the group factors has in general its own strong $\mathcal{CP}$ problem and requires an independent axion. A linear combination of these then playes the role of the QCD axion at low energies. Now that we have identified the index of embedding as the parameter which governs the enhancement of UV instantons, it would be interesting to construct a model with a single simple UV gauge group, which only needs a single axion to solve the strong $\mathcal{CP}$ problem. This would provide a proof of principle that this mechanism could also enhance the axion mass in the simplest phenomenological models.

The overarching topic of Part III is EFTs of the SM and gravity. We started our journey with one of the simplest renormalizable extension of the SM, a heavy singlet scalar coupled to the SM via the Higgs. In Chapter 12 we performed the one-loop matching of this simple toy UV completion onto the dimension six SMEFT Lagrangian. We exclusively used Feynman diagrammatic methods and found contributions, which were missed in previous studies based on a mixture of diagrammatic and functional methods [20, 21]. With our results the one-loop matching of this simple benchmark scenario is finally complete.

The remainder of Part III is devoted to the study of EFTs with gravity. In Chapter 13 we used Hilbert series methods to construct non-redundant operator bases for EFTs, which can include matter and gravity. As a first step we identified the Weyl tensor $C_{\mu\nu\rho\sigma}$ and symmetric traceless covariant derivatives acting on the Weyl tensor $\nabla_{\{\mu_1}\cdots\nabla_{\mu_n}C_{\mu\}\nu\rho\sigma}$, which can be combined into the so-called single particle module R_C, as the independent building blocks for the gravitational degrees of freedom. All other structures, such as the Ricci tensor $R_{\mu\nu}$ or Ricci scalar R, are redundant and can be removed with field redefinitions. Using this result we constructed the operator basis for the EFT of gravity in vacuum (Section 13.3), a shift-symmetric scalar coupled to gravity (Section 13.4) and the SM coupled to gravity (Section 13.5). The EFT of the SM coupled to gravity, which we call GRSMEFT, is the low-energy description of all fundamental interaction we have observed so far. Finally we extend our results to $d > 4$ spacetime dimension in Section 13.6. This extension is straightforward, since the independent degrees of freedom are

the same as in four dimensions, i.e. the single-particle module R_C.

It is well-known that a theory of matter minimally coupled to GR is non-renormalizable, i.e. quantum effects generate higher-dimensional operators. However, not all operators which could naively be generated at one-loop are actually generated. A similar phenomenon appears in the SMEFT: there are many non-trivial zeroes in the dimension six anomalous dimension matrix. These can be understood in terms of helicity selection rules [27].

In Chapter 14 we examined the one-loop structure of the GRSMEFT using on-shell amplitude methods and spinor-helicity variables with the goal of generalizing the selection rules of [27] to gravitational EFTs. In order to achieve this goal we defined a modified helicity $\tilde{h} = h - 1/2\, h^g$, where h is the regular helicity and h^g the helicity carried by gravitons. $\tilde{h}$ is identical to the regular helicity $\tilde{h} = h$ for matter particles but assigns a modified helicity of $|\tilde{h}| = 1$ to gravitons. We found that if we classify gravitational amplitudes according to the modified helicity we can treat them on the same footing as SM amplitudes. In particular the helicity of a $n \geq 4$ point amplitude of a marginal theory minimally coupled to gravity satisfies the same helicity bound for the modified helicity $|\tilde{h}(\mathcal{A}_n)| \leq n - 4$ as purely marginal theories for the regular helicity. Using this result we derived in Section 14.3 non-renormalization theorems for operators in the GRSMEFT. Marginal theories minimally coupled to gravity can renormalize effective operators $\mathcal{O}$, if the modified helicity of $\mathcal{A}_\mathcal{O}$, the minimal amplitude induced by $\mathcal{O}$, satisfies $|\tilde{h}(\mathcal{A}_\mathcal{O})| \leq n_\mathcal{O} - 4$, where $n_\mathcal{O}$ is the number of external legs of $\mathcal{A}_\mathcal{O}$. Operator mixing of the form $\mathcal{O} \to \tilde{\mathcal{O}}$ is possible if $n_{\tilde{\mathcal{O}}} - n_\mathcal{O} \geq |\tilde{h}(\mathcal{A}_{\tilde{\mathcal{O}}}) - \tilde{h}(\mathcal{A}_\mathcal{O})|$. Similar to [27] these results hold with the exception of loop amplitudes, which contain a $|\tilde{h}| = 2$ four-fermion amplitude in a unitarity cut. Finally in Section 14.4 we apply amplitude methods to compute a selection of anomalous dimensions in a toy SM coupled to gravity at dimension six. The set of operators with non-zero anomalous dimensions must be present in any consistent EFT with gravity, no matter if there is non-gravitational NP or not.

The anomalous dimensions in the toy GRSMEFT contain many zeroes, which cannot be explained with the helicity selection rules alone. In an upcoming publication [34] we will make sense of these results using angular momentum selection rules. Additionally we will comment on the renormalization of dimension eight operators from matter minimally coupled to gravity. These are of particular interest, since there are positivity bounds on dimension eight matter operators. It will be interesting to compare these constraints with the sign of the anomalous dimension induced by gravity.

Acknowledgements

First and foremost I would like to thank my supervisor Andreas Weiler for giving me the chance to pursue my doctoral studies in his group. I am grateful for his support and advice and also for suggesting many interesting research topics. His guidance and encouragement to work on a broad range of topics has certainly made me a better physicist.

I also want to thank Prof. Dr. Csaba Csáki and the whole Cornell theory group for the hospitality and kindness during my visit to Cornell University.

During my PhD I had the pleasure of collaborating with many excellent scientists, including Reuven Balkin, Pietro Baratella, Csaba Csáki, Uli Haisch, Ennio Salvioni, Javi Serra, Yuri Shirman and Elena Venturini. I would like to thank all of them for a stimulating and pleasant work atmosphere and countless fruitful discussions.

The PhD journey would not have been as much fun without my office mates and fellow PhD students of T75 Stefan Stelzl, Konstantin Springmann, Tobias Theil, Reuven Balkin, Michael Stadlbauer, Elena Kaiser, Dominik Haslehner, Jonathan Kley, Johannes Herms and Andreas Rappelt. Thank you for being great colleagues and friends. Without the occasional cold beverage after work and our group excursions into the Alps, to the Christmas market or Andechs, my time at T75 would not have been the same. I hope you keep up the traditions! Special thanks goes to Tobias Theil, Stefan Stelzl, Pietro Baratella and Ennio Salvioni for proofreading parts of this thesis.

Finally I want to thank my parents, siblings, grandparents and nephew for their constant love and support along this journey. Without you this would not have been possible.

This research was supported by the Studienstiftung des Deutschen Volkes and the collaborative research center "Neutrinos and Dark Matter in Astro- and Particle Physics" (SFB 1258) and the DFG under Germany's Excellence Strategy - EXC-2094 - 390783311.

Bibliography

[1] N. Craig, H.K. Lou, M. McCullough and A. Thalapillil, *The Higgs Portal Above Threshold*, *JHEP* **02** (2016) 127 [arXiv:1412.0258].

[2] ATLAS collaboration, *Observation of a new particle in the search for the Standard Model Higgs boson with the ATLAS detector at the LHC*, *Phys. Lett. B* **716** (2012) 1 [arXiv:1207.7214].

[3] CMS collaboration, *Observation of a New Boson at a Mass of 125 GeV with the CMS Experiment at the LHC*, *Phys. Lett. B* **716** (2012) 30 [arXiv:1207.7235].

[4] F. Zwicky, *Die Rotverschiebung von extragalaktischen Nebeln*, *Helv. Phys. Acta* **6** (1933) 110.

[5] XENON collaboration, *Dark Matter Search Results from a One Ton-Year Exposure of XENON1T*, *Phys. Rev. Lett.* **121** (2018) 111302 [arXiv:1805.12562].

[6] AMS collaboration, *Antiproton Flux, Antiproton-to-Proton Flux Ratio, and Properties of Elementary Particle Fluxes in Primary Cosmic Rays Measured with the Alpha Magnetic Spectrometer on the International Space Station*, *Phys. Rev. Lett.* **117** (2016) 091103.

[7] Fermi-LAT, DES collaboration, *Searching for Dark Matter Annihilation in Recently Discovered Milky Way Satellites with Fermi-LAT*, *Astrophys. J.* **834** (2017) 110 [arXiv:1611.03184].

[8] M. Frigerio, A. Pomarol, F. Riva and A. Urbano, *Composite Scalar Dark Matter*, *JHEP* **07** (2012) 015 [arXiv:1204.2808].

[9] R. Peccei and H.R. Quinn, *CP Conservation in the Presence of Instantons*, *Phys. Rev. Lett.* **38** (1977) 1440.

[10] R. Peccei and H.R. Quinn, *Constraints Imposed by CP Conservation in the Presence of Instantons*, *Phys. Rev. D* **16** (1977) 1791.

[11] S. Weinberg, *A New Light Boson?*, *Phys. Rev. Lett.* **40** (1978) 223.

[12] F. Wilczek, *Problem of Strong P and T Invariance in the Presence of Instantons*, *Phys. Rev. Lett.* **40** (1978) 279.

[13] L.F. Abbott and P. Sikivie, *A Cosmological Bound on the Invisible Axion*, *Phys. Lett. B* **120** (1983) 133.

[14] M. Dine and W. Fischler, *The Not So Harmless Axion*, *Phys. Lett. B* **120** (1983) 137.

[15] J. Preskill, M.B. Wise and F. Wilczek, *Cosmology of the Invisible Axion*, *Phys. Lett. B* **120** (1983) 127.

[16] CAST collaboration, *New CAST Limit on the Axion-Photon Interaction*, *Nature Phys.* **13** (2017) 584 [arXiv:1705.02290].

[17] ADMX collaboration, *A SQUID-based microwave cavity search for dark-matter axions*, *Phys. Rev. Lett.* **104** (2010) 041301 [arXiv:0910.5914].

[18] P. Agrawal and K. Howe, *Factoring the Strong CP Problem*, *JHEP* **12** (2018) 029 [arXiv:1710.04213].

[19] P. Agrawal and K. Howe, *A Flavorful Factoring of the Strong CP Problem*, *JHEP* **12** (2018) 035 [arXiv:1712.05803].

[20] S.A.R. Ellis, J. Quevillon, T. You and Z. Zhang, *Extending the Universal One-Loop Effective Action: Heavy-Light Coefficients*, *JHEP* **08** (2017) 054 [arXiv:1706.07765].

[21] M. Jiang, N. Craig, Y.-Y. Li and D. Sutherland, *Complete one-loop matching for a singlet scalar in the Standard Model EFT*, *JHEP* **02** (2019) 031 [arXiv:1811.08878].

[22] B. Henning, X. Lu, T. Melia and H. Murayama, *2, 84, 30, 993, 560, 15456, 11962, 261485, ...: Higher dimension operators in the SM EFT*, *JHEP* **08** (2017) 016 [arXiv:1512.03433].

[23] B. Henning, X. Lu, T. Melia and H. Murayama, *Operator bases, S-matrices, and their partition functions*, *JHEP* **10** (2017) 199 [arXiv:1706.08520].

[24] E.E. Jenkins, A.V. Manohar and M. Trott, *Renormalization Group Evolution of the Standard Model Dimension Six Operators I: Formalism and lambda Dependence*, *JHEP* **10** (2013) 087 [arXiv:1308.2627].

[25] E.E. Jenkins, A.V. Manohar and M. Trott, *Renormalization Group Evolution of the Standard Model Dimension Six Operators II: Yukawa Dependence*, *JHEP* **01** (2014) 035 [arXiv:1310.4838].

[26] R. Alonso, E.E. Jenkins, A.V. Manohar and M. Trott, *Renormalization Group Evolution of the Standard Model Dimension Six Operators III: Gauge Coupling Dependence and Phenomenology*, *JHEP* **04** (2014) 159 [arXiv:1312.2014].

[27] C. Cheung and C.-H. Shen, *Nonrenormalization Theorems without Supersymmetry*, *Phys. Rev. Lett.* **115** (2015) 071601 [arXiv:1505.01844].

[28] R. Balkin, M. Ruhdorfer, E. Salvioni and A. Weiler, *Charged Composite Scalar Dark Matter*, *JHEP* **11** (2017) 094 [arXiv:1707.07685].

[29] R. Balkin, M. Ruhdorfer, E. Salvioni and A. Weiler, *Dark matter shifts away from direct detection*, *JCAP* **11** (2018) 050 [arXiv:1809.09106].

[30] M. Ruhdorfer, J. Serra and A. Weiler, *Effective Field Theory of Gravity to All Orders*, *JHEP* **05** (2020) 083 [arXiv:1908.08050].

[31] M. Ruhdorfer, E. Salvioni and A. Weiler, *A Global View of the Off-Shell Higgs Portal*, *SciPost Phys.* **8** (2020) 027 [arXiv:1910.04170].

[32] C. Csáki, M. Ruhdorfer and Y. Shirman, *UV Sensitivity of the Axion Mass from Instantons in Partially Broken Gauge Groups*, *JHEP* **04** (2020) 031 [arXiv:1912.02197].

[33] U. Haisch, M. Ruhdorfer, E. Salvioni, E. Venturini and A. Weiler, *Singlet night in Feynman-ville: one-loop matching of a real scalar*, *JHEP* **04** (2020) 164 [arXiv:2003.05936].

[34] P. Baratella, D. Haslehner, M. Ruhdorfer, J. Serra and A. Weiler. in preparation.

[35] B. Bellazzini, C. Csáki and J. Serra, *Composite Higgses*, *Eur. Phys. J. C* **74** (2014) 2766 [arXiv:1401.2457].

[36] K. Agashe, R. Contino and A. Pomarol, *The Minimal composite Higgs model*, *Nucl. Phys. B* **719** (2005) 165 [arXiv:hep-ph/0412089].

[37] B. Gripaios, A. Pomarol, F. Riva and J. Serra, *Beyond the Minimal Composite Higgs Model*, *JHEP* **04** (2009) 070 [arXiv:0902.1483].

[38] D. Marzocca and A. Urbano, *Composite Dark Matter and LHC Interplay*, *JHEP* **07** (2014) 107 [arXiv:1404.7419].

[39] M. Chala, *$h \to \gamma\gamma$ excess and Dark Matter from Composite Higgs Models*, *JHEP* **01** (2013) 122 [arXiv:1210.6208].

[40] J. Barnard, T. Gherghetta, T.S. Ray and A. Spray, *The Unnatural Composite Higgs*, *JHEP* **01** (2015) 067 [arXiv:1409.7391].

[41] N. Fonseca, R. Zukanovich Funchal, A. Lessa and L. Lopez-Honorez, *Dark Matter Constraints on Composite Higgs Models*, *JHEP* **06** (2015) 154 [arXiv:1501.05957].

[42] I. Brivio, M.B. Gavela, L. Merlo, K. Mimasu, J.M. No, R. del Rey et al., *Non-linear Higgs portal to Dark Matter*, *JHEP* **04** (2016) 141 [arXiv:1511.01099].

[43] M. Kim, S.J. Lee and A. Parolini, *WIMP Dark Matter in Composite Higgs Models and the Dilaton Portal*, arXiv:1602.05590.

[44] M. Chala, G. Nardini and I. Sobolev, *Unified explanation for dark matter and electroweak baryogenesis with direct detection and gravitational wave signatures*, *Phys. Rev. D* **94** (2016) 055006 [arXiv:1605.08663].

[45] Y. Wu, T. Ma, B. Zhang and G. Cacciapaglia, *Composite Dark Matter and Higgs*, *JHEP* **11** (2017) 058 [arXiv:1703.06903].

[46] G. Ballesteros, A. Carmona and M. Chala, *Exceptional Composite Dark Matter*, *Eur. Phys. J. C* **77** (2017) 468 [arXiv:1704.07388].

[47] R. Balkin, G. Perez and A. Weiler, *Little composite dark matter*, *Eur. Phys. J. C* **78** (2018) 104 [arXiv:1707.09980].

[48] T. Alanne, D. Buarque Franzosi, M.T. Frandsen and M. Rosenlyst, *Dark matter in (partially) composite Higgs models*, *JHEP* **12** (2018) 088 [arXiv:1808.07515].

[49] A. Davoli, A. De Simone, D. Marzocca and A. Morandini, *Composite 2HDM with singlets: a viable dark matter scenario*, *JHEP* **10** (2019) 196 [arXiv:1905.13244].

[50] M. Ramos, *Composite dark matter phenomenology in the presence of lighter degrees of freedom*, *JHEP* **07** (2020) 128 [arXiv:1912.11061].

[51] V. Silveira and A. Zee, *SCALAR PHANTOMS*, *Phys. Lett. B* **161** (1985) 136.

[52] J. McDonald, *Gauge singlet scalars as cold dark matter*, *Phys. Rev. D* **50** (1994) 3637 [arXiv:hep-ph/0702143].

[53] C.P. Burgess, M. Pospelov and T. ter Veldhuis, *The Minimal model of nonbaryonic dark matter: A Singlet scalar*, *Nucl. Phys. B* **619** (2001) 709 [arXiv:hep-ph/0011335].

[54] G. Arcadi, A. Djouadi and M. Raidal, *Dark Matter through the Higgs portal*, *Phys. Rept.* **842** (2020) 1 [arXiv:1903.03616].

[55] E. Hardy, *Higgs portal dark matter in non-standard cosmological histories*, *JHEP* **06** (2018) 043 [arXiv:1804.06783].

[56] G.F. Giudice, *Naturally Speaking: The Naturalness Criterion and Physics at the LHC*, arXiv:0801.2562.

[57] R. Barbieri, *Electroweak theory after the first Large Hadron Collider phase*, *Phys. Scripta T* **158** (2013) 014006 [arXiv:1309.3473].

[58] G. 't Hooft, *Naturalness, chiral symmetry, and spontaneous chiral symmetry breaking*, *NATO Sci. Ser. B* **59** (1980) 135.

[59] S. Dimopoulos and L. Susskind, *Mass Without Scalars*, .

[60] L. Susskind, *Dynamics of Spontaneous Symmetry Breaking in the Weinberg-Salam Theory*, *Phys. Rev. D* **20** (1979) 2619.

[61] G. Panico and A. Wulzer, *The Composite Nambu-Goldstone Higgs*, vol. 913, Springer (2016), 10.1007/978-3-319-22617-0, [arXiv:1506.01961].

[62] S. Dimopoulos and J. Preskill, *Massless Composites With Massive Constituents*, *Nucl. Phys. B* **199** (1982) 206.

[63] D.B. Kaplan and H. Georgi, *SU(2) x U(1) Breaking by Vacuum Misalignment*, *Phys. Lett. B* **136** (1984) 183.

[64] D.B. Kaplan, H. Georgi and S. Dimopoulos, *Composite Higgs Scalars*, *Phys. Lett. B* **136** (1984) 187.

[65] T. Banks, *CONSTRAINTS ON SU(2) x U(1) BREAKING BY VACUUM MISALIGNMENT*, *Nucl. Phys. B* **243** (1984) 125.

[66] H. Georgi, D.B. Kaplan and P. Galison, *Calculation of the Composite Higgs Mass*, *Phys. Lett. B* **143** (1984) 152.

[67] H. Georgi and D.B. Kaplan, *Composite Higgs and Custodial SU(2)*, *Phys. Lett. B* **145** (1984) 216.

[68] M.J. Dugan, H. Georgi and D.B. Kaplan, *Anatomy of a Composite Higgs Model*, *Nucl. Phys. B* **254** (1985) 299.

[69] C. Csáki and P. Tanedo, *Beyond the Standard Model*, in *2013 European School of High-Energy Physics*, pp. 169–268, 2015, DOI [arXiv:1602.04228].

[70] C. Csáki, S. Lombardo and O. Telem, *TASI Lectures on Non-supersymmetric BSM Models*, in *Proceedings, Theoretical Advanced Study Institute in Elementary Particle Physics : Anticipating the Next Discoveries in Particle Physics (TASI 2016): Boulder, CO, USA, June 6-July 1, 2016*, R. Essig and I. Low, eds., pp. 501–570, WSP (2018), DOI [arXiv:1811.04279].

[71] R. Contino, *The Higgs as a Composite Nambu-Goldstone Boson*, in *Theoretical Advanced Study Institute in Elementary Particle Physics: Physics of the Large and the Small*, pp. 235–306, 2011, DOI [arXiv:1005.4269].

[72] D.B. Kaplan, *Flavor at SSC energies: A New mechanism for dynamically generated fermion masses*, *Nucl. Phys. B* **365** (1991) 259.

[73] R. Contino and A. Pomarol, *Holography for fermions*, *JHEP* **11** (2004) 058 [arXiv:hep-th/0406257].

[74] S.R. Coleman, J. Wess and B. Zumino, *Structure of phenomenological Lagrangians. 1.*, *Phys. Rev.* **177** (1969) 2239.

[75] J. Callan, Curtis G., S.R. Coleman, J. Wess and B. Zumino, *Structure of phenomenological Lagrangians. 2.*, *Phys. Rev.* **177** (1969) 2247.

[76] R. Contino, L. Da Rold and A. Pomarol, *Light custodians in natural composite Higgs models*, *Phys. Rev. D* **75** (2007) 055014 [arXiv:hep-ph/0612048].

[77] K. Agashe, R. Contino, L. Da Rold and A. Pomarol, *A Custodial symmetry for $Zb\bar{b}$*, *Phys. Lett. B* **641** (2006) 62 [arXiv:hep-ph/0605341].

[78] S.R. Coleman and E.J. Weinberg, *Radiative Corrections as the Origin of Spontaneous Symmetry Breaking*, *Phys. Rev. D* **7** (1973) 1888.

[79] S. Weinberg, *Precise relations between the spectra of vector and axial vector mesons*, *Phys. Rev. Lett.* **18** (1967) 507.

[80] D. Marzocca, M. Serone and J. Shu, *General Composite Higgs Models*, *JHEP* **08** (2012) 013 [arXiv:1205.0770].

[81] A. Pomarol and F. Riva, *The Composite Higgs and Light Resonance Connection*, *JHEP* **08** (2012) 135 [arXiv:1205.6434].

[82] G. Panico and A. Wulzer, *The Discrete Composite Higgs Model*, *JHEP* **09** (2011) 135 [arXiv:1106.2719].

[83] S. De Curtis, M. Redi and A. Tesi, *The 4D Composite Higgs*, *JHEP* **04** (2012) 042 [arXiv:1110.1613].

[84] V.C. Rubin and W.K. Ford, Jr., *Rotation of the Andromeda Nebula from a Spectroscopic Survey of Emission Regions*, *Astrophys. J.* **159** (1970) 379.

[85] V.C. Rubin, N. Thonnard and W.K. Ford, Jr., *Rotational properties of 21 SC galaxies with a large range of luminosities and radii, from NGC 4605 /R = 4kpc/ to UGC 2885 /R = 122 kpc/*, *Astrophys. J.* **238** (1980) 471.

[86] M. Milgrom, *A Modification of the Newtonian dynamics as a possible alternative to the hidden mass hypothesis*, *Astrophys. J.* **270** (1983) 365.

[87] B. Famaey and S. McGaugh, *Modified Newtonian Dynamics (MOND): Observational Phenomenology and Relativistic Extensions*, *Living Rev. Rel.* **15** (2012) 10 [arXiv:1112.3960].

[88] M. Lisanti, M. Moschella, N.J. Outmezguine and O. Slone, *Testing Dark Matter and Modifications to Gravity using Local Milky Way Observables*, *Phys. Rev. D* **100** (2019) 083009 [arXiv:1812.08169].

[89] M. Persic, P. Salucci and F. Stel, *The Universal rotation curve of spiral galaxies: 1. The Dark matter connection*, *Mon. Not. Roy. Astron. Soc.* **281** (1996) 27 [arXiv:astro-ph/9506004].

[90] D. Clowe, M. Bradac, A.H. Gonzalez, M. Markevitch, S.W. Randall, C. Jones et al., *A direct empirical proof of the existence of dark matter*, *Astrophys. J. Lett.* **648** (2006) L109 [arXiv:astro-ph/0608407].

[91] E.W. Kolb and M.S. Turner, *The Early Universe*, vol. 69, Addison-Wesley (1990).

[92] Planck collaboration, *Planck 2018 results. VI. Cosmological parameters*, *Astron. Astrophys.* **641** (2020) A6 [arXiv:1807.06209].

[93] J.L. Feng, *Dark Matter Candidates from Particle Physics and Methods of Detection*, *Ann. Rev. Astron. Astrophys.* **48** (2010) 495 [arXiv:1003.0904].

[94] M. Lisanti, *Lectures on Dark Matter Physics*, in *Theoretical Advanced Study Institute in Elementary Particle Physics: New Frontiers in Fields and Strings*, pp. 399–446, 2017, DOI [arXiv:1603.03797].

[95] T. Lin, *Dark matter models and direct detection*, *PoS* **333** (2019) 009 [arXiv:1904.07915].

[96] W. Hu, R. Barkana and A. Gruzinov, *Cold and fuzzy dark matter*, *Phys. Rev. Lett.* **85** (2000) 1158 [arXiv:astro-ph/0003365].

[97] L. Hui, J.P. Ostriker, S. Tremaine and E. Witten, *Ultralight scalars as cosmological dark matter*, *Phys. Rev. D* **95** (2017) 043541 [arXiv:1610.08297].

[98] S. Tremaine and J.E. Gunn, *Dynamical Role of Light Neutral Leptons in Cosmology*, *Phys. Rev. Lett.* **42** (1979) 407.

[99] A. Boyarsky, O. Ruchayskiy and D. Iakubovskyi, *A Lower bound on the mass of Dark Matter particles*, *JCAP* **03** (2009) 005 [arXiv:0808.3902].

[100] F.E. Schunck and E.W. Mielke, *General relativistic boson stars*, *Class. Quant. Grav.* **20** (2003) R301 [arXiv:0801.0307].

[101] H. Zhang, *Axion Stars*, *Symmetry* **12** (2019) 25 [arXiv:1810.11473].

[102] B. Carr, F. Kuhnel and M. Sandstad, *Primordial Black Holes as Dark Matter*, *Phys. Rev. D* **94** (2016) 083504 [arXiv:1607.06077].

[103] M. Sasaki, T. Suyama, T. Tanaka and S. Yokoyama, *Primordial black holes—perspectives in gravitational wave astronomy*, *Class. Quant. Grav.* **35** (2018) 063001 [arXiv:1801.05235].

[104] J. Baur, N. Palanque-Delabrouille, C. Yeche, A. Boyarsky, O. Ruchayskiy, E. Armengaud et al., *Constraints from Ly-α forests on non-thermal dark matter including resonantly-produced sterile neutrinos*, *JCAP* **12** (2017) 013 [arXiv:1706.03118].

[105] V. Iršič et al., *New Constraints on the free-streaming of warm dark matter from intermediate and small scale Lyman-α forest data*, *Phys. Rev. D* **96** (2017) 023522 [arXiv:1702.01764].

[106] C. Yèche, N. Palanque-Delabrouille, J. Baur and H. du Mas des Bourboux, *Constraints on neutrino masses from Lyman-alpha forest power spectrum with BOSS and XQ-100*, *JCAP* **06** (2017) 047 [arXiv:1702.03314].

[107] R. Murgia, V. Iršič and M. Viel, *Novel constraints on noncold, nonthermal dark matter from Lyman- α forest data*, *Phys. Rev. D* **98** (2018) 083540 [arXiv:1806.08371].

[108] K. Griest and M. Kamionkowski, *Unitarity Limits on the Mass and Radius of Dark Matter Particles*, *Phys. Rev. Lett.* **64** (1990) 615.

[109] V.A. Rubakov and D.S. Gorbunov, *Introduction to the Theory of the Early Universe: Hot big bang theory*, World Scientific, Singapore (2017), 10.1142/10447.

[110] S. Weinberg, *Gravitation and Cosmology: Principles and Applications of the General Theory of Relativity*, John Wiley and Sons, New York (1972).

[111] M. Bauer and T. Plehn, *Yet Another Introduction to Dark Matter: The Particle Physics Approach*, vol. 959 of *Lecture Notes in Physics*, Springer (2019), 10.1007/978-3-030-16234-4, [arXiv:1705.01987].

[112] P. Gondolo and G. Gelmini, *Cosmic abundances of stable particles: Improved analysis*, *Nucl. Phys. B* **360** (1991) 145.

[113] G. Steigman, B. Dasgupta and J.F. Beacom, *Precise Relic WIMP Abundance and its Impact on Searches for Dark Matter Annihilation*, *Phys. Rev. D* **86** (2012) 023506 [arXiv:1204.3622].

[114] XENON collaboration, *Physics reach of the XENON1T dark matter experiment*, *JCAP* **04** (2016) 027 [arXiv:1512.07501].

[115] B.J. Mount et al., *LUX-ZEPLIN (LZ) Technical Design Report*, arXiv:1703.09144.

[116] LUX-ZEPLIN collaboration, *Projected WIMP sensitivity of the LUX-ZEPLIN dark matter experiment*, *Phys. Rev. D* **101** (2020) 052002 [arXiv:1802.06039].

[117] M. Schumann, *Direct Detection of WIMP Dark Matter: Concepts and Status*, *J. Phys. G* **46** (2019) 103003 [arXiv:1903.03026].

[118] M.W. Goodman and E. Witten, *Detectability of Certain Dark Matter Candidates*, *Phys. Rev. D* **31** (1985) 3059.

[119] J.M. Alarcon, J. Martin Camalich and J.A. Oller, *The chiral representation of the πN scattering amplitude and the pion-nucleon sigma term*, *Phys. Rev. D* **85** (2012) 051503 [arXiv:1110.3797].

[120] M. Hoferichter, J. Ruiz de Elvira, B. Kubis and U.-G. Meißner, *High-Precision Determination of the Pion-Nucleon σ Term from Roy-Steiner Equations*, *Phys. Rev. Lett.* **115** (2015) 092301 [arXiv:1506.04142].

[121] P. Junnarkar and A. Walker-Loud, *Scalar strange content of the nucleon from lattice QCD*, *Phys. Rev. D* **87** (2013) 114510 [arXiv:1301.1114].

[122] G.F. Giudice, C. Grojean, A. Pomarol and R. Rattazzi, *The Strongly-Interacting Light Higgs*, *JHEP* **06** (2007) 045 [arXiv:hep-ph/0703164].

[123] G. Bélanger, F. Boudjema, A. Goudelis, A. Pukhov and B. Zaldivar, *micrOMEGAs5.0 : Freeze-in*, *Comput. Phys. Commun.* **231** (2018) 173 [arXiv:1801.03509].

[124] A. Thamm, R. Torre and A. Wulzer, *Future tests of Higgs compositeness: direct vs indirect*, *JHEP* **07** (2015) 100 [arXiv:1502.01701].

[125] C. Csaki, A. Falkowski and A. Weiler, *The Flavor of the Composite Pseudo-Goldstone Higgs*, *JHEP* **09** (2008) 008 [arXiv:0804.1954].

[126] S. Bruggisser, F. Riva and A. Urbano, *Strongly Interacting Light Dark Matter*, *SciPost Phys.* **3** (2017) 017 [arXiv:1607.02474].

[127] S. Bruggisser, F. Riva and A. Urbano, *The Last Gasp of Dark Matter Effective Theory*, *JHEP* **11** (2016) 069 [arXiv:1607.02475].

[128] D. Liu, A. Pomarol, R. Rattazzi and F. Riva, *Patterns of Strong Coupling for LHC Searches*, *JHEP* **11** (2016) 141 [arXiv:1603.03064].

[129] V. Barger, P. Langacker, M. McCaskey, M. Ramsey-Musolf and G. Shaughnessy, *Complex Singlet Extension of the Standard Model*, *Phys. Rev. D* **79** (2009) 015018 [arXiv:0811.0393].

[130] V. Barger, M. McCaskey and G. Shaughnessy, *Complex Scalar Dark Matter vis-\'{a}-vis CoGeNT, DAMA/LIBRA and XENON100*, *Phys. Rev. D* **82** (2010) 035019 [arXiv:1005.3328].

[131] C. Gross, O. Lebedev and T. Toma, *Cancellation Mechanism for Dark-Matter–Nucleon Interaction*, *Phys. Rev. Lett.* **119** (2017) 191801 [arXiv:1708.02253].

[132] K. Huitu, N. Koivunen, O. Lebedev, S. Mondal and T. Toma, *Probing pseudo-Goldstone dark matter at the LHC*, *Phys. Rev. D* **100** (2019) 015009 [arXiv:1812.05952].

[133] D. Azevedo, M. Duch, B. Grzadkowski, D. Huang, M. Iglicki and R. Santos, *One-loop contribution to dark-matter-nucleon scattering in the pseudo-scalar dark matter model*, *JHEP* **01** (2019) 138 [arXiv:1810.06105].

[134] K. Ishiwata and T. Toma, *Probing pseudo Nambu-Goldstone boson dark matter at loop level*, *JHEP* **12** (2018) 089 [arXiv:1810.08139].

[135] K. Kannike and M. Raidal, *Phase Transitions and Gravitational Wave Tests of Pseudo-Goldstone Dark Matter in the Softly Broken U(1) Scalar Singlet Model*, *Phys. Rev. D* **99** (2019) 115010 [arXiv:1901.03333].

[136] K. Kannike, K. Loos and M. Raidal, *Gravitational wave signals of pseudo-Goldstone dark matter in the $\mathbb{Z}_3$ complex singlet model*, *Phys. Rev. D* **101** (2020) 035001 [arXiv:1907.13136].

[137] M. Gonderinger, H. Lim and M.J. Ramsey-Musolf, *Complex Scalar Singlet Dark Matter: Vacuum Stability and Phenomenology*, *Phys. Rev. D* **86** (2012) 043511 [arXiv:1202.1316].

[138] M. Jiang, L. Bian, W. Huang and J. Shu, *Impact of a complex singlet: Electroweak baryogenesis and dark matter*, *Phys. Rev. D* **93** (2016) 065032 [arXiv:1502.07574].

[139] C.-W. Chiang, M.J. Ramsey-Musolf and E. Senaha, *Standard Model with a Complex Scalar Singlet: Cosmological Implications and Theoretical Considerations*, *Phys. Rev. D* **97** (2018) 015005 [arXiv:1707.09960].

[140] N. Chen, T. Li, Y. Wu and L. Bian, *Complementarity of the future e^+e^- colliders and gravitational waves in the probe of complex singlet extension to the standard model*, *Phys. Rev. D* **101** (2020) 075047 [arXiv:1911.05579].

[141] C. Arina, A. Beniwal, C. Degrande, J. Heisig and A. Scaffidi, *Global fit of pseudo-Nambu-Goldstone Dark Matter*, *JHEP* **04** (2020) 015 [arXiv:1912.04008].

[142] T. Alanne, M. Heikinheimo, V. Keus, N. Koivunen and K. Tuominen, *Direct and indirect probes of Goldstone dark matter*, *Phys. Rev. D* **99** (2019) 075028 [arXiv:1812.05996].

[143] D. Karamitros, *Pseudo Nambu-Goldstone Dark Matter: Examples of Vanishing Direct Detection Cross Section*, *Phys. Rev. D* **99** (2019) 095036 [arXiv:1901.09751].

[144] X.-M. Jiang, C. Cai, Z.-H. Yu, Y.-P. Zeng and H.-H. Zhang, *Pseudo-Nambu-Goldstone dark matter and two-Higgs-doublet models*, *Phys. Rev. D* **100** (2019) 075011 [arXiv:1907.09684].

[145] Fermi-LAT collaboration, *Searching for Dark Matter Annihilation from Milky Way Dwarf Spheroidal Galaxies with Six Years of Fermi Large Area Telescope Data*, *Phys. Rev. Lett.* **115** (2015) 231301 [arXiv:1503.02641].

[146] Fermi-LAT collaboration, *Updated search for spectral lines from Galactic dark matter interactions with pass 8 data from the Fermi Large Area Telescope*, *Phys. Rev. D* **91** (2015) 122002 [arXiv:1506.00013].

[147] A. Cuoco, M. Krämer and M. Korsmeier, *Novel Dark Matter Constraints from Antiprotons in Light of AMS-02*, *Phys. Rev. Lett.* **118** (2017) 191102 [arXiv:1610.03071].

[148] M.-Y. Cui, Q. Yuan, Y.-L.S. Tsai and Y.-Z. Fan, *Possible dark matter annihilation signal in the AMS-02 antiproton data*, *Phys. Rev. Lett.* **118** (2017) 191101 [arXiv:1610.03840].

[149] J.M. Cline and T. Toma, *Pseudo-Goldstone dark matter confronts cosmic ray and collider anomalies*, *Phys. Rev. D* **100** (2019) 035023 [arXiv:1906.02175].

[150] I. Cholis, T. Linden and D. Hooper, *A Robust Excess in the Cosmic-Ray Antiproton Spectrum: Implications for Annihilating Dark Matter*, *Phys. Rev. D* **99** (2019) 103026 [arXiv:1903.02549].

[151] N. Yamatsu, *Finite-Dimensional Lie Algebras and Their Representations for Unified Model Building*, arXiv:1511.08771.

[152] A. De Simone, O. Matsedonskyi, R. Rattazzi and A. Wulzer, *A First Top Partner Hunter's Guide*, *JHEP* **04** (2013) 004 [arXiv:1211.5663].

[153] M. Bando, T. Kugo and K. Yamawaki, *Nonlinear Realization and Hidden Local Symmetries*, *Phys. Rept.* **164** (1988) 217.

[154] C. Grojean, O. Matsedonskyi and G. Panico, *Light top partners and precision physics*, *JHEP* **10** (2013) 160 [arXiv:1306.4655].

[155] C. Csaki, T. Ma and J. Shu, *Maximally Symmetric Composite Higgs Models*, *Phys. Rev. Lett.* **119** (2017) 131803 [arXiv:1702.00405].

[156] J.A. Casas, D.G. Cerdeño, J.M. Moreno and J. Quilis, *Reopening the Higgs portal for single scalar dark matter*, *JHEP* **05** (2017) 036 [arXiv:1701.08134].

[157] O. Matsedonskyi, G. Panico and A. Wulzer, *Light Top Partners for a Light Composite Higgs*, *JHEP* **01** (2013) 164 [arXiv:1204.6333].

[158] R. Barbieri and G.F. Giudice, *Upper Bounds on Supersymmetric Particle Masses*, *Nucl. Phys. B* **306** (1988) 63.

[159] Planck collaboration, *Planck 2015 results. XIII. Cosmological parameters*, *Astron. Astrophys.* **594** (2016) A13 [arXiv:1502.01589].

[160] XENON collaboration, *First Dark Matter Search Results from the XENON1T Experiment*, *Phys. Rev. Lett.* **119** (2017) 181301 [arXiv:1705.06655].

[161] LUX collaboration, *Results from a search for dark matter in the complete LUX exposure*, *Phys. Rev. Lett.* **118** (2017) 021303 [arXiv:1608.07648].

[162] J.M. Cline, K. Kainulainen, P. Scott and C. Weniger, *Update on scalar singlet dark matter*, *Phys. Rev. D* **88** (2013) 055025 [arXiv:1306.4710].

[163] G. Belanger, F. Boudjema, A. Pukhov and A. Semenov, *micrOMEGAs_3: A program for calculating dark matter observables*, *Comput. Phys. Commun.* **185** (2014) 960 [arXiv:1305.0237].

[164] A. Alloul, N.D. Christensen, C. Degrande, C. Duhr and B. Fuks, *FeynRules 2.0 - A complete toolbox for tree-level phenomenology*, *Comput. Phys. Commun.* **185** (2014) 2250 [arXiv:1310.1921].

[165] PAMELA collaboration, *PAMELA results on the cosmic-ray antiproton flux from 60 MeV to 180 GeV in kinetic energy*, *Phys. Rev. Lett.* **105** (2010) 121101 [arXiv:1007.0821].

[166] C. Evoli, D. Gaggero and D. Grasso, *Secondary antiprotons as a Galactic Dark Matter probe*, *JCAP* **12** (2015) 039 [arXiv:1504.05175].

[167] G. Durieux, C. Grojean, J. Gu and K. Wang, *The leptonic future of the Higgs*, *JHEP* **09** (2017) 014 [arXiv:1704.02333].

[168] G. Panico, M. Redi, A. Tesi and A. Wulzer, *On the Tuning and the Mass of the Composite Higgs*, *JHEP* **03** (2013) 051 [arXiv:1210.7114].

[169] R. Contino, T. Kramer, M. Son and R. Sundrum, *Warped/composite phenomenology simplified*, *JHEP* **05** (2007) 074 [arXiv:hep-ph/0612180].

[170] R. Contino and G. Servant, *Discovering the top partners at the LHC using same-sign dilepton final states*, *JHEP* **06** (2008) 026 [arXiv:0801.1679].

[171] J. Mrazek and A. Wulzer, *A Strong Sector at the LHC: Top Partners in Same-Sign Dileptons*, *Phys. Rev. D* **81** (2010) 075006 [arXiv:0909.3977].

[172] J. Serra, *Beyond the Minimal Top Partner Decay*, *JHEP* **09** (2015) 176 [arXiv:1506.05110].

[173] A. Anandakrishnan, J.H. Collins, M. Farina, E. Kuflik and M. Perelstein, *Odd Top Partners at the LHC*, *Phys. Rev. D* **93** (2016) 075009 [arXiv:1506.05130].

[174] M. Chala, *Direct bounds on heavy toplike quarks with standard and exotic decays*, *Phys. Rev. D* **96** (2017) 015028 [arXiv:1705.03013].

[175] CMS collaboration, *Search for single production of vector-like quarks decaying to a Z boson and a top or a bottom quark in proton-proton collisions at 13 TeV*, .

[176] ATLAS collaboration, *Search for new phenomena in $t\bar{t}$ final states with additional heavy-flavour jets in pp collisions at $\sqrt{s} = 13$ TeV with the ATLAS detector*, .

[177] CMS collaboration, *Search for heavy vector-like quarks decaying to same-sign dileptons*, .

[178] S. Kraml, U. Laa, L. Panizzi and H. Prager, *Scalar versus fermionic top partner interpretations of $t\bar{t} + E_T^{\text{miss}}$ searches at the LHC*, *JHEP* **11** (2016) 107 [arXiv:1607.02050].

[179] S. Salam and A. Weiler, *Collider Reach, http://collider-reach.web.cern.ch/collider-reach/*, .

[180] CMS collaboration, *Search for new phenomena with the M_{T2} variable in the all-hadronic final state produced in proton–proton collisions at $\sqrt{s} = 13$ TeV*, *Eur. Phys. J. C* **77** (2017) 710 [arXiv:1705.04650].

[181] D. Ghosh, M. Salvarezza and F. Senia, *Extending the Analysis of Electroweak Precision Constraints in Composite Higgs Models*, *Nucl. Phys. B* **914** (2017) 346 [arXiv:1511.08235].

[182] ATLAS collaboration, *Search for pair production of heavy vector-like quarks decaying to high-p_T W bosons and b quarks in the lepton-plus-jets final state in pp collisions at $\sqrt{s} = 13$ TeV with the ATLAS detector*, *JHEP* **10** (2017) 141 [arXiv:1707.03347].

[183] ATLAS collaboration, *Search for invisible Higgs boson decays with vector boson fusion signatures with the ATLAS detector using an integrated luminosity of 139 fb^{-1}*, .

[184] *Projections for measurements of Higgs boson cross sections, branching ratios and coupling parameters with the ATLAS detector at a HL-LHC*, .

[185] P. Gondolo, J. Hisano and K. Kadota, *The Effect of quark interactions on dark matter kinetic decoupling and the mass of the smallest dark halos*, *Phys. Rev. D* **86** (2012) 083523 [arXiv:1205.1914].

[186] L. Ackerman, M.R. Buckley, S.M. Carroll and M. Kamionkowski, *Dark Matter and Dark Radiation*, *Phys. Rev. D* **79** (2009) 023519 [arXiv:0810.5126].

[187] Topical Conveners: K.N. Abazajian, J.E. Carlstrom, A.T. Lee collaboration, *Neutrino Physics from the Cosmic Microwave Background and Large Scale Structure*, *Astropart. Phys.* **63** (2015) 66 [arXiv:1309.5383].

[188] R. Cooke, M. Pettini, R.A. Jorgenson, M.T. Murphy and C.C. Steidel, *Precision measures of the primordial abundance of deuterium*, *Astrophys. J.* **781** (2014) 31 [arXiv:1308.3240].

[189] J.L. Feng, M. Kaplinghat, H. Tu and H.-B. Yu, *Hidden Charged Dark Matter*, *JCAP* **07** (2009) 004 [arXiv:0905.3039].

[190] A. Sommerfeld, *Über die Beugung und Bremsung der Elektronen*, *Annalen der Physik* **403** (1931) 257.

[191] J.L. Feng, M. Kaplinghat and H.-B. Yu, *Sommerfeld Enhancements for Thermal Relic Dark Matter*, *Phys. Rev. D* **82** (2010) 083525 [arXiv:1005.4678].

[192] T. Piffl et al., *The RAVE survey: the Galactic escape speed and the mass of the Milky Way*, *Astron. Astrophys.* **562** (2014) A91 [arXiv:1309.4293].

[193] M. Cirelli, P. Panci, K. Petraki, F. Sala and M. Taoso, *Dark Matter's secret liaisons: phenomenology of a dark U(1) sector with bound states*, *JCAP* **05** (2017) 036 [arXiv:1612.07295].

[194] B. von Harling and K. Petraki, *Bound-state formation for thermal relic dark matter and unitarity*, *JCAP* **12** (2014) 033 [arXiv:1407.7874].

[195] D.A. Buote, T.E. Jeltema, C.R. Canizares and G.P. Garmire, *Chandra evidence for a flattened, triaxial dark matter halo in the elliptical galaxy ngc 720*, *Astrophys. J.* **577** (2002) 183 [arXiv:astro-ph/0205469].

[196] P. Agrawal, F.-Y. Cyr-Racine, L. Randall and J. Scholtz, *Make Dark Matter Charged Again*, *JCAP* **05** (2017) 022 [arXiv:1610.04611].

[197] F. Kahlhoefer, K. Schmidt-Hoberg, M.T. Frandsen and S. Sarkar, *Colliding clusters and dark matter self-interactions*, *Mon. Not. Roy. Astron. Soc.* **437** (2014) 2865 [arXiv:1308.3419].

[198] S. Tulin and H.-B. Yu, *Dark Matter Self-interactions and Small Scale Structure*, *Phys. Rept.* **730** (2018) 1 [arXiv:1705.02358].

[199] CMS collaboration, *Search for invisible decays of the Higgs boson produced through vector boson fusion at* $\sqrt{s} = 13$ TeV, .

[200] R. Diamanti, S. Ando, S. Gariazzo, O. Mena and C. Weniger, *Cold dark matter plus not-so-clumpy dark relics*, *JCAP* **06** (2017) 008 [arXiv:1701.03128].

[201] K. Petraki, M. Postma and J. de Vries, *Radiative bound-state-formation cross-sections for dark matter interacting via a Yukawa potential*, *JHEP* **04** (2017) 077 [arXiv:1611.01394].

[202] P.J. Humphrey, D.A. Buote, C.R. Canizares, A.C. Fabian and J.M. Miller, *A Census of Baryons and Dark Matter in an Isolated, Milky Way-sized Elliptical Galaxy*, *Astrophys. J.* **729** (2011) 53 [arXiv:1010.6078].

[203] M. Reece, *Photon Masses in the Landscape and the Swampland*, *JHEP* **07** (2019) 181 [arXiv:1808.09966].

[204] N. Craig and I. Garcia Garcia, *Rescuing Massive Photons from the Swampland*, *JHEP* **11** (2018) 067 [arXiv:1810.05647].

[205] F. D'Eramo and J. Thaler, *Semi-annihilation of Dark Matter*, *JHEP* **06** (2010) 109 [arXiv:1003.5912].

[206] G. Belanger and J.-C. Park, *Assisted freeze-out*, *JCAP* **03** (2012) 038 [arXiv:1112.4491].

[207] K. Griest and D. Seckel, *Three exceptions in the calculation of relic abundances*, *Phys. Rev. D* **43** (1991) 3191.

[208] D. Curtin, P. Meade and C.-T. Yu, *Testing Electroweak Baryogenesis with Future Colliders*, *JHEP* **11** (2014) 127 [arXiv:1409.0005].

[209] H.-C. Cheng, L. Li, E. Salvioni and C.B. Verhaaren, *Singlet Scalar Top Partners from Accidental Supersymmetry*, *JHEP* **05** (2018) 057 [arXiv:1803.03651].

[210] T. Cohen, N. Craig, G.F. Giudice and M. Mccullough, *The Hyperbolic Higgs*, *JHEP* **05** (2018) 091 [arXiv:1803.03647].

[211] O.J.P. Eboli and D. Zeppenfeld, *Observing an invisible Higgs boson*, *Phys. Lett. B* **495** (2000) 147 [arXiv:hep-ph/0009158].

[212] V. Barger, P. Langacker, M. McCaskey, M.J. Ramsey-Musolf and G. Shaughnessy, *LHC Phenomenology of an Extended Standard Model with a Real Scalar Singlet*, *Phys. Rev. D* **77** (2008) 035005 [arXiv:0706.4311].

[213] Z. Chacko, Y. Cui and S. Hong, *Exploring a Dark Sector Through the Higgs Portal at a Lepton Collider*, *Phys. Lett. B* **732** (2014) 75 [arXiv:1311.3306].

[214] FCC collaboration, *Higgs and Electro-weak symmetry breaking at the FCC-hh*, .

[215] C. Bernaciak, T. Plehn, P. Schichtel and J. Tattersall, *Spying an invisible Higgs boson*, *Phys. Rev. D* **91** (2015) 035024 [arXiv:1411.7699].

[216] D. Barducci, A. Bharucha, N. Desai, M. Frigerio, B. Fuks, A. Goudelis et al., *Monojet searches for momentum-dependent dark matter interactions*, *JHEP* **01** (2017) 078 [arXiv:1609.07490].

[217] S. Matsumoto, K. Fujii, T. Honda, S. Kanemura, T. Nabeshima, N. Okada et al., *Observing the Coupling between Dark Matter and Higgs Boson at the ILC*, in *International Linear Collider Workshop*, 6, 2010 [arXiv:1006.5268].

[218] P. Ko and H. Yokoya, *Search for Higgs portal DM at the ILC*, *JHEP* **08** (2016) 109 [arXiv:1603.04737].

[219] S. Kanemura, S. Matsumoto, T. Nabeshima and H. Taniguchi, *Testing Higgs portal dark matter via Z fusion at a linear collider*, *Phys. Lett. B* **701** (2011) 591 [arXiv:1102.5147].

[220] S. Dawson, *The Effective W Approximation*, *Nucl. Phys. B* **249** (1985) 42.

[221] D. Buttazzo, D. Redigolo, F. Sala and A. Tesi, *Fusing Vectors into Scalars at High Energy Lepton Colliders*, *JHEP* **11** (2018) 144 [arXiv:1807.04743].

[222] J. Alwall, R. Frederix, S. Frixione, V. Hirschi, F. Maltoni, O. Mattelaer et al., *The automated computation of tree-level and next-to-leading order differential cross sections, and their matching to parton shower simulations*, *JHEP* **07** (2014) 079 [arXiv:1405.0301].

[223] D. Racco, A. Wulzer and F. Zwirner, *Robust collider limits on heavy-mediator Dark Matter*, *JHEP* **05** (2015) 009 [arXiv:1502.04701].

[224] J.P. Delahaye, M. Diemoz, K. Long, B. Mansoulié, N. Pastrone, L. Rivkin et al., *Muon Colliders*, arXiv:1901.06150.

[225] CMS collaboration, *Search for invisible decays of a Higgs boson produced through vector boson fusion in proton-proton collisions at* $\sqrt{s} = 13$ *TeV*, *Phys. Lett. B* **793** (2019) 520 [arXiv:1809.05937].

[226] ATLAS collaboration, *Search for invisible Higgs boson decays in vector boson fusion at* $\sqrt{s} = 13$ *TeV with the ATLAS detector*, *Phys. Lett. B* **793** (2019) 499 [arXiv:1809.06682].

[227] T. Sjöstrand, S. Ask, J.R. Christiansen, R. Corke, N. Desai, P. Ilten et al., *An introduction to PYTHIA 8.2*, *Comput. Phys. Commun.* **191** (2015) 159 [arXiv:1410.3012].

[228] DELPHES 3 collaboration, *DELPHES 3, A modular framework for fast simulation of a generic collider experiment*, *JHEP* **02** (2014) 057 [arXiv:1307.6346].

[229] M. Czakon and A. Mitov, *Top++: A Program for the Calculation of the Top-Pair Cross-Section at Hadron Colliders*, *Comput. Phys. Commun.* **185** (2014) 2930 [arXiv:1112.5675].

[230] ATLAS collaboration, *Performance of the ATLAS Trigger System in 2015*, *Eur. Phys. J. C* **77** (2017) 317 [arXiv:1611.09661].

[231] A. Mitov. Talk at the Workshop on the physics of HL-LHC, and perspectives at HE-LHC (2017).

[232] M.L. Mangano et al., *Physics at a 100 TeV pp Collider: Standard Model Processes*, arXiv:1607.01831.

[233] FCC collaboration, *FCC-hh: The Hadron Collider: Future Circular Collider Conceptual Design Report Volume 3*, *Eur. Phys. J. ST* **228** (2019) 755.

[234] J.M. Lindert et al., *Precise predictions for V+ jets dark matter backgrounds*, *Eur. Phys. J. C* **77** (2017) 829 [arXiv:1705.04664].

[235] C. Englert and J. Jaeckel, *Probing the Symmetric Higgs Portal with Di-Higgs Boson Production*, *Phys. Rev. D* **100** (2019) 095017 [arXiv:1908.10615].

[236] N. Craig, C. Englert and M. McCullough, *New Probe of Naturalness*, *Phys. Rev. Lett.* **111** (2013) 121803 [arXiv:1305.5251].

[237] R. Contino, D. Marzocca, D. Pappadopulo and R. Rattazzi, *On the effect of resonances in composite Higgs phenomenology*, *JHEP* **10** (2011) 081 [arXiv:1109.1570].

[238] R. Alonso, I. Brivio, B. Gavela, L. Merlo and S. Rigolin, *Sigma Decomposition*, *JHEP* **12** (2014) 034 [arXiv:1409.1589].

[239] J. Ruiz de Elvira, M. Hoferichter, B. Kubis and U.-G. Meißner, *Extracting the σ-term from low-energy pion-nucleon scattering*, *J. Phys. G* **45** (2018) 024001 [arXiv:1706.01465].

[240] X.-L. Ren, L.-S. Geng and J. Meng, *Scalar strangeness content of the nucleon and baryon sigma terms*, *Phys. Rev. D* **91** (2015) 051502 [arXiv:1404.4799].

[241] A. Azatov and J. Galloway, *Light Custodians and Higgs Physics in Composite Models*, *Phys. Rev. D* **85** (2012) 055013 [arXiv:1110.5646].

[242] M. Montull, F. Riva, E. Salvioni and R. Torre, *Higgs Couplings in Composite Models*, *Phys. Rev. D* **88** (2013) 095006 [arXiv:1308.0559].

[243] M. Drees and M. Nojiri, *Neutralino - nucleon scattering revisited*, *Phys. Rev. D* **48** (1993) 3483 [arXiv:hep-ph/9307208].

[244] G. Grilli di Cortona, E. Hardy, J. Pardo Vega and G. Villadoro, *The QCD axion, precisely*, *JHEP* **01** (2016) 034 [arXiv:1511.02867].

[245] B. Holdom and M.E. Peskin, *Raising the Axion Mass*, *Nucl. Phys. B* **208** (1982) 397.

[246] B. Holdom, *Strong QCD at High-energies and a Heavy Axion*, *Phys. Lett. B* **154** (1985) 316.

[247] J.M. Flynn and L. Randall, *A Computation of the Small Instanton Contribution to the Axion Potential*, *Nucl. Phys. B* **293** (1987) 731.

[248] E. Poppitz and Y. Shirman, *The Strength of small instanton amplitudes in gauge theories with compact extra dimensions*, *JHEP* **07** (2002) 041 [arXiv:hep-th/0204075].

[249] T. Gherghetta, V.V. Khoze, A. Pomarol and Y. Shirman, *The Axion Mass from 5D Small Instantons*, *JHEP* **03** (2020) 063 [arXiv:2001.05610].

[250] M. Gaillard, M. Gavela, R. Houtz, P. Quilez and R. Del Rey, *Color unified dynamical axion*, *Eur. Phys. J. C* **78** (2018) 972 [arXiv:1805.06465].

[251] J. Fuentes-Martín, M. Reig and A. Vicente, *Strong CP problem with low-energy emergent QCD: The 4321 case*, *Phys. Rev. D* **100** (2019) 115028 [arXiv:1907.02550].

[252] D. Croon, R. Houtz and V. Sanz, *Dynamical Axions and Gravitational Waves*, *JHEP* **07** (2019) 146 [arXiv:1904.10967].

[253] M. Reig, *On the high-scale instanton interference effect: axion models without domain wall problem*, *JHEP* **08** (2019) 167 [arXiv:1901.00203].

[254] M. Gavela, M. Ibe, P. Quilez and T. Yanagida, *Automatic Peccei–Quinn symmetry*, *Eur. Phys. J. C* **79** (2019) 542 [arXiv:1812.08174].

[255] M.A. Buen-Abad and J. Fan, *Dynamical axion misalignment with small instantons*, *JHEP* **12** (2019) 161 [arXiv:1911.05737].

[256] M. Dine and N. Seiberg, *String Theory and the Strong {CP} Problem*, *Nucl. Phys. B* **273** (1986) 109.

[257] K. Choi, C. Kim and W. Sze, *Mass Renormalization by Instantons and the Strong {CP} Problem*, *Phys. Rev. Lett.* **61** (1988) 794.

[258] K. Choi and H.D. Kim, *Small instanton contribution to the axion potential in supersymmetric models*, *Phys. Rev. D* **59** (1999) 072001 [arXiv:hep-ph/9809286].

[259] A. Hook, *Solving the Hierarchy Problem Discretely*, *Phys. Rev. Lett.* **120** (2018) 261802 [arXiv:1802.10093].

[260] V. Rubakov, *Grand unification and heavy axion*, *JETP Lett.* **65** (1997) 621 [arXiv:hep-ph/9703409].

[261] H. Fukuda, K. Harigaya, M. Ibe and T.T. Yanagida, *Model of visible QCD axion*, *Phys. Rev. D* **92** (2015) 015021 [arXiv:1504.06084].

[262] Z. Berezhiani, L. Gianfagna and M. Giannotti, *Strong CP problem and mirror world: The Weinberg-Wilczek axion revisited*, *Phys. Lett. B* **500** (2001) 286 [arXiv:hep-ph/0009290].

[263] A. Hook, *Anomalous solutions to the strong CP problem*, *Phys. Rev. Lett.* **114** (2015) 141801 [arXiv:1411.3325].

[264] N. Blinov and A. Hook, *Solving the Wrong Hierarchy Problem*, *JHEP* **06** (2016) 176 [arXiv:1605.03178].

[265] S. Dimopoulos, A. Hook, J. Huang and G. Marques-Tavares, *A collider observable QCD axion*, *JHEP* **11** (2016) 052 [arXiv:1606.03097].

[266] T. Gherghetta, N. Nagata and M. Shifman, *A Visible QCD Axion from an Enlarged Color Group*, *Phys. Rev. D* **93** (2016) 115010 [arXiv:1604.01127].

[267] J.E. Kim and G. Carosi, *Axions and the Strong CP Problem*, *Rev. Mod. Phys.* **82** (2010) 557 [arXiv:0807.3125].

[268] A. Hook, *TASI Lectures on the Strong CP Problem and Axions*, *PoS* **TASI2018** (2019) 004 [arXiv:1812.02669].

[269] P. Ramond, *Journeys beyond the standard model*, vol. 101 (1999).

[270] A. Belavin, A.M. Polyakov, A. Schwartz and Y. Tyupkin, *Pseudoparticle Solutions of the Yang-Mills Equations*, *Phys. Lett. B* **59** (1975) 85.

[271] R. Jackiw and C. Rebbi, *Vacuum Periodicity in a Yang-Mills Quantum Theory*, *Phys. Rev. Lett.* **37** (1976) 172.

[272] J. Callan, Curtis G., R. Dashen and D.J. Gross, *The Structure of the Gauge Theory Vacuum*, *Phys. Lett. B* **63** (1976) 334.

[273] V. Rubakov, *Classical theory of gauge fields*, Princeton Univ. Press, Princeton, NJ, USA (2002).

[274] N. Manton, *Topology in the Weinberg-Salam Theory*, *Phys. Rev. D* **28** (1983) 2019.

[275] M.D. Schwartz, *Quantum Field Theory and the Standard Model*, Cambridge University Press (3, 2014).

[276] V. Baluni, *CP Violating Effects in QCD*, *Phys. Rev. D* **19** (1979) 2227.

[277] C. Baker et al., *An Improved experimental limit on the electric dipole moment of the neutron*, *Phys. Rev. Lett.* **97** (2006) 131801 [arXiv:hep-ex/0602020].

[278] J.M. Pendlebury et al., *Revised experimental upper limit on the electric dipole moment of the neutron*, *Phys. Rev. D* **92** (2015) 092003 [arXiv:1509.04411].

[279] B. Graner, Y. Chen, E. Lindahl and B. Heckel, *Reduced Limit on the Permanent Electric Dipole Moment of Hg199*, *Phys. Rev. Lett.* **116** (2016) 161601 [arXiv:1601.04339].

[280] G. 't Hooft, *Computation of the Quantum Effects Due to a Four-Dimensional Pseudoparticle*, *Phys. Rev. D* **14** (1976) 3432.

[281] C. Vafa and E. Witten, *Parity Conservation in QCD*, *Phys. Rev. Lett.* **53** (1984) 535.

[282] T. Donnelly, S. Freedman, R. Lytel, R. Peccei and M. Schwartz, *Do Axions Exist?*, *Phys. Rev. D* **18** (1978) 1607.

[283] J.E. Kim, *Weak Interaction Singlet and Strong CP Invariance*, *Phys. Rev. Lett.* **43** (1979) 103.

[284] M.A. Shifman, A. Vainshtein and V.I. Zakharov, *Can Confinement Ensure Natural CP Invariance of Strong Interactions?*, *Nucl. Phys. B* **166** (1980) 493.

[285] M. Dine, W. Fischler and M. Srednicki, *A Simple Solution to the Strong CP Problem with a Harmless Axion*, *Phys. Lett. B* **104** (1981) 199.

[286] A. Zhitnitsky, *On Possible Suppression of the Axion Hadron Interactions. (In Russian)*, *Sov. J. Nucl. Phys.* **31** (1980) 260.

[287] G. 't Hooft, *How Instantons Solve the U(1) Problem*, *Phys. Rept.* **142** (1986) 357.

[288] M. Shifman, *Advanced topics in quantum field theory.: A lecture course*, Cambridge Univ. Press, Cambridge, UK (2, 2012).

[289] C.W. Bernard, *Gauge Zero Modes, Instanton Determinants, and QCD Calculations*, *Phys. Rev. D* **19** (1979) 3013.

[290] S.F. Cordes, *The Instanton Induced Superpotential in Supersymmetric {QCD}*, *Nucl. Phys. B* **273** (1986) 629.

[291] A. Vainshtein, V.I. Zakharov, V. Novikov and M.A. Shifman, *ABC's of Instantons*, *Sov. Phys. Usp.* **25** (1982) 195.

[292] S. Vandoren and P. van Nieuwenhuizen, *Lectures on instantons*, arXiv:0802.1862.

[293] E.J. Weinberg, *Classical solutions in quantum field theory: Solitons and Instantons in High Energy Physics*, Cambridge Monographs on Mathematical Physics, Cambridge University Press (9, 2012), 10.1017/CBO9781139017787.

[294] R. Jackiw, C. Nohl and C. Rebbi, *Conformal Properties of Pseudoparticle Configurations*, *Phys. Rev. D* **15** (1977) 1642.

[295] F. Wilczek, *Inequivalent Embeddings of SU(2) and Instanton Interactions*, *Phys. Lett. B* **65** (1976) 160.

[296] I. Affleck, *On Constrained Instantons*, *Nucl. Phys. B* **191** (1981) 429.

[297] C. Csaki and H. Murayama, *Instantons in partially broken gauge groups*, *Nucl. Phys. B* **532** (1998) 498 [arXiv:hep-th/9804061].

[298] K.A. Intriligator and N. Seiberg, *Duality, monopoles, dyons, confinement and oblique confinement in supersymmetric SO(N(c)) gauge theories*, *Nucl. Phys. B* **444** (1995) 125 [arXiv:hep-th/9503179].

[299] K.A. Intriligator, R. Leigh and N. Seiberg, *Exact superpotentials in four-dimensions*, *Phys. Rev. D* **50** (1994) 1092 [arXiv:hep-th/9403198].

[300] K.A. Intriligator and N. Seiberg, *Phases of N=1 supersymmetric gauge theories in four-dimensions*, *Nucl. Phys. B* **431** (1994) 551 [arXiv:hep-th/9408155].

[301] J. Callan, Curtis G., R.F. Dashen and D.J. Gross, *Toward a Theory of the Strong Interactions*, *Phys. Rev. D* **17** (1978) 2717.

[302] Y. Bai and B.A. Dobrescu, *Minimal $SU(3) \times SU(3)$ Symmetry Breaking Patterns*, *Phys. Rev. D* **97** (2018) 055024 [arXiv:1710.01456].

[303] M.A. Shifman, A. Vainshtein and V.I. Zakharov, *Instanton Density in a Theory with Massless Quarks*, *Nucl. Phys. B* **163** (1980) 46.

[304] A. Hasenfratz and P. Hasenfratz, *The Scales of Euclidean and Hamiltonian Lattice QCD*, *Nucl. Phys. B* **193** (1981) 210.

[305] G. Shore, *Dimensional Regularization and Instantons*, *Annals Phys.* **122** (1979) 321.

[306] U. Haisch, M. Ruhdorfer, E. Salvioni, E. Venturini and A. Weiler, "(Non-)Renormalization of Gravity." in preparation.

[307] M. Jiang, J. Shu, M.-L. Xiao and Y.-H. Zheng, *Partial Wave Amplitude Basis and Selection Rules in Effective Field Theories*, *Phys. Rev. Lett.* **126** (2021) 011601 [arXiv:2001.04481].

[308] T. Appelquist and J. Carazzone, *Infrared Singularities and Massive Fields*, *Phys. Rev. D* **11** (1975) 2856.

[309] H. Georgi, *Effective field theory*, *Ann. Rev. Nucl. Part. Sci.* **43** (1993) 209.

[310] I.Z. Rothstein, *TASI lectures on effective field theories*, arXiv:hep-ph/0308266.

[311] D.B. Kaplan, *Five lectures on effective field theory*, arXiv:nucl-th/0510023.

[312] T. Cohen, *As Scales Become Separated: Lectures on Effective Field Theory*, *PoS* **TASI2018** (2019) 011 [arXiv:1903.03622].

[313] A.V. Manohar, *Introduction to Effective Field Theories*, arXiv:1804.05863.

[314] M.K. Gaillard, *The Effective One Loop Lagrangian With Derivative Couplings*, *Nucl. Phys. B* **268** (1986) 669.

[315] L.-H. Chan, *Derivative Expansion for the One Loop Effective Actions With Internal Symmetry*, *Phys. Rev. Lett.* **57** (1986) 1199.

[316] O. Cheyette, *Effective Action for the Standard Model With Large Higgs Mass*, *Nucl. Phys. B* **297** (1988) 183.

[317] B. Henning, X. Lu and H. Murayama, *How to use the Standard Model effective field theory*, *JHEP* **01** (2016) 023 [arXiv:1412.1837].

[318] A. Drozd, J. Ellis, J. Quevillon and T. You, *The Universal One-Loop Effective Action*, *JHEP* **03** (2016) 180 [arXiv:1512.03003].

[319] B. Henning, X. Lu and H. Murayama, *One-loop Matching and Running with Covariant Derivative Expansion*, *JHEP* **01** (2018) 123 [arXiv:1604.01019].

[320] J. Fuentes-Martin, J. Portoles and P. Ruiz-Femenia, *Integrating out heavy particles with functional methods: a simplified framework*, *JHEP* **09** (2016) 156 [arXiv:1607.02142].

[321] T. Cohen, X. Lu and Z. Zhang, *Functional Prescription for EFT Matching*, *JHEP* **02** (2021) 228 [arXiv:2011.02484].

[322] J. Fuentes-Martin, M. König, J. Pagès, A.E. Thomsen and F. Wilsch, *SuperTracer: A Calculator of Functional Supertraces for One-Loop EFT Matching*, arXiv:2012.08506.

[323] T. Cohen, X. Lu and Z. Zhang, *STrEAMlining EFT Matching*, arXiv:2012.07851.

[324] M. Beneke and V.A. Smirnov, *Asymptotic expansion of Feynman integrals near threshold*, *Nucl. Phys. B* **522** (1998) 321 [arXiv:hep-ph/9711391].

[325] S. Weinberg, *Baryon and Lepton Nonconserving Processes*, *Phys. Rev. Lett.* **43** (1979) 1566.

[326] B. Grzadkowski, M. Iskrzynski, M. Misiak and J. Rosiek, *Dimension-Six Terms in the Standard Model Lagrangian*, *JHEP* **10** (2010) 085 [arXiv:1008.4884].

[327] J.S.R. Chisholm, *Change of variables in quantum field theories*, *Nucl. Phys.* **26** (1961) 469.

[328] S. Kamefuchi, L. O'Raifeartaigh and A. Salam, *Change of variables and equivalence theorems in quantum field theories*, *Nucl. Phys.* **28** (1961) 529.

[329] H. Georgi, *On-shell effective field theory*, *Nucl. Phys. B* **361** (1991) 339.

[330] C. Arzt, *Reduced effective Lagrangians*, *Phys. Lett. B* **342** (1995) 189 [arXiv:hep-ph/9304230].

[331] J.C. Criado and M. Pérez-Victoria, *Field redefinitions in effective theories at higher orders*, *JHEP* **03** (2019) 038 [arXiv:1811.09413].

[332] H. Lehmann, K. Symanzik and W. Zimmermann, *On the formulation of quantized field theories*, *Nuovo Cim.* **1** (1955) 205.

[333] L. Lehman and A. Martin, *Hilbert Series for Constructing Lagrangians: expanding the phenomenologist's toolbox*, *Phys. Rev. D* **91** (2015) 105014 [arXiv:1503.07537].

[334] E.E. Jenkins and A.V. Manohar, *Algebraic Structure of Lepton and Quark Flavor Invariants and CP Violation*, *JHEP* **10** (2009) 094 [arXiv:0907.4763].

[335] M. Neusel, *Invariant Theory*, American Mathematical Society, Providence RI, USA (2007).

[336] B. Sturmfels, *Algorithms in Invariant Theory*, Springer, Vienna, Austria (2008).

[337] S. Benvenuti, B. Feng, A. Hanany and Y.-H. He, *Counting BPS Operators in Gauge Theories: Quivers, Syzygies and Plethystics*, *JHEP* **11** (2007) 050 [arXiv:hep-th/0608050].

[338] B. Feng, A. Hanany and Y.-H. He, *Counting gauge invariants: The Plethystic program*, *JHEP* **03** (2007) 090 [arXiv:hep-th/0701063].

[339] A. Hanany and R. Kalveks, *Highest Weight Generating Functions for Hilbert Series*, *JHEP* **10** (2014) 152 [arXiv:1408.4690].

[340] A. Hanany, N. Mekareeya and G. Torri, *The Hilbert Series of Adjoint SQCD*, *Nucl. Phys. B* **825** (2010) 52 [arXiv:0812.2315].

[341] G. Mack, *All unitary ray representations of the conformal group SU(2,2) with positive energy*, *Commun. Math. Phys.* **55** (1977) 1.

[342] A. Barabanschikov, L. Grant, L.L. Huang and S. Raju, *The Spectrum of Yang Mills on a sphere*, *JHEP* **01** (2006) 160 [arXiv:hep-th/0501063].

[343] B. Grinstein, K.A. Intriligator and I.Z. Rothstein, *Comments on Unparticles*, *Phys. Lett. B* **662** (2008) 367 [arXiv:0801.1140].

[344] B. Henning and T. Melia, *Constructing effective field theories via their harmonics*, *Phys. Rev. D* **100** (2019) 016015 [arXiv:1902.06754].

[345] B. Henning and T. Melia, *Conformal-helicity duality \& the Hilbert space of free CFTs*, arXiv:1902.06747.

[346] W. Heisenberg and H. Euler, *Consequences of Dirac's theory of positrons*, *Z. Phys.* **98** (1936) 714 [arXiv:physics/0605038].

[347] J. de Blas, J.C. Criado, M. Perez-Victoria and J. Santiago, *Effective description of general extensions of the Standard Model: the complete tree-level dictionary*, *JHEP* **03** (2018) 109 [arXiv:1711.10391].

[348] C. Anastasiou, A. Carmona, A. Lazopoulos and J. Santiago, "`Match Maker`, talk given at smeft-tools 2019." https://indico.cern.ch/event/787665/contributions/3374418/attachments/1861555/3059604/JSantiagoSMEFT-TOOLS19.pdf.

[349] C. Bobeth, M. Misiak and J. Urban, *Photonic penguins at two loops and m_t dependence of $BR[B \to X_s l^+ l^-]$*, *Nucl. Phys. B* **574** (2000) 291 [arXiv:hep-ph/9910220].

[350] P. Gambino and U. Haisch, *Complete electroweak matching for radiative B decays*, *JHEP* **10** (2001) 020 [arXiv:hep-ph/0109058].

[351] T. Hahn, *Generating Feynman diagrams and amplitudes with FeynArts 3*, *Comput. Phys. Commun.* **140** (2001) 418 [arXiv:hep-ph/0012260].

[352] T. Hahn and M. Perez-Victoria, *Automatized one loop calculations in four-dimensions and D-dimensions*, *Comput. Phys. Commun.* **118** (1999) 153 [arXiv:hep-ph/9807565].

[353] H.H. Patel, *Package-X: A Mathematica package for the analytic calculation of one-loop integrals*, *Comput. Phys. Commun.* **197** (2015) 276 [arXiv:1503.01469].

[354] F. Jegerlehner, M.Y. Kalmykov and O. Veretin, *MS versus pole masses of gauge bosons: Electroweak bosonic two loop corrections*, *Nucl. Phys. B* **641** (2002) 285 [arXiv:hep-ph/0105304].

[355] F. Jegerlehner, M.Y. Kalmykov and O. Veretin, *MS-bar versus pole masses of gauge bosons. 2. Two loop electroweak fermion corrections*, *Nucl. Phys. B* **658** (2003) 49 [arXiv:hep-ph/0212319].

[356] A. Denner, *Techniques for calculation of electroweak radiative corrections at the one loop level and results for W physics at LEP-200*, *Fortsch. Phys.* **41** (1993) 307 [arXiv:0709.1075].

[357] J. Fleischer and F. Jegerlehner, *Radiative Corrections to Higgs Decays in the Extended Weinberg-Salam Model*, *Phys. Rev. D* **23** (1981) 2001.

[358] A. Denner, L. Jenniches, J.-N. Lang and C. Sturm, *Gauge-independent $\overline{MS}$ renormalization in the 2HDM*, *JHEP* **09** (2016) 115 [arXiv:1607.07352].

[359] J.M. Cullen, B.D. Pecjak and D.J. Scott, *NLO corrections to $h \to b\bar{b}$ decay in SMEFT*, *JHEP* **08** (2019) 173 [arXiv:1904.06358].

[360] A.J. Buras, *Weak Hamiltonian, CP violation and rare decays*, in *Les Houches Summer School in Theoretical Physics, Session 68: Probing the Standard Model of Particle Interactions*, 6, 1998 [arXiv:hep-ph/9806471].

[361] P. Gambino, A. Kwiatkowski and N. Pott, *Electroweak effects in the B0 - anti-B0 mixing*, *Nucl. Phys. B* **544** (1999) 532 [arXiv:hep-ph/9810400].

[362] A.J. Buras, P. Gambino and U.A. Haisch, *Electroweak penguin contributions to nonleptonic Delta F = 1 decays at NNLO*, *Nucl. Phys. B* **570** (2000) 117 [arXiv:hep-ph/9911250].

[363] J.D. Wells and Z. Zhang, *Effective theories of universal theories*, *JHEP* **01** (2016) 123 [arXiv:1510.08462].

[364] J.F. Donoghue, *General relativity as an effective field theory: The leading quantum corrections*, *Phys. Rev. D* **50** (1994) 3874 [arXiv:gr-qc/9405057].

[365] C.P. Burgess, *Quantum gravity in everyday life: General relativity as an effective field theory*, *Living Rev. Rel.* **7** (2004) 5 [arXiv:gr-qc/0311082].

[366] J.F. Donoghue, M.M. Ivanov and A. Shkerin, *EPFL Lectures on General Relativity as a Quantum Field Theory*, arXiv:1702.00319.

[367] M. Gasperini, *Theory of Gravitational Interactions*, UNITEXT for Physics, Springer International Publishing, Cham (2017), 10.1007/978-3-319-49682-5.

[368] G. 't Hooft, *An algorithm for the poles at dimension four in the dimensional regularization procedure*, *Nucl. Phys. B* **62** (1973) 444.

[369] G. 't Hooft and M.J.G. Veltman, *One loop divergencies in the theory of gravitation*, *Ann. Inst. H. Poincare Phys. Theor. A* **20** (1974) 69.

[370] M.H. Goroff and A. Sagnotti, *The Ultraviolet Behavior of Einstein Gravity*, *Nucl. Phys. B* **266** (1986) 709.

[371] S. Deser and P. van Nieuwenhuizen, *One Loop Divergences of Quantized Einstein-Maxwell Fields*, *Phys. Rev. D* **10** (1974) 401.

[372] S. Deser, H.-S. Tsao and P. van Nieuwenhuizen, *One Loop Divergences of the Einstein Yang-Mills System*, *Phys. Rev. D* **10** (1974) 3337.

[373] S. Deser and P. van Nieuwenhuizen, *Nonrenormalizability of the Quantized Dirac-Einstein System*, *Phys. Rev. D* **10** (1974) 411.

[374] W.D. Goldberger and I.Z. Rothstein, *An Effective field theory of gravity for extended objects*, *Phys. Rev. D* **73** (2006) 104029 [arXiv:hep-th/0409156].

[375] C. Cheung, P. Creminelli, A.L. Fitzpatrick, J. Kaplan and L. Senatore, *The Effective Field Theory of Inflation*, *JHEP* **03** (2008) 014 [arXiv:0709.0293].

[376] J.K. Bloomfield, E.E. Flanagan, M. Park and S. Watson, *Dark energy or modified gravity? An effective field theory approach*, *JCAP* **08** (2013) 010 [arXiv:1211.7054].

[377] J. Gleyzes, D. Langlois, F. Piazza and F. Vernizzi, *Essential Building Blocks of Dark Energy*, *JCAP* **08** (2013) 025 [arXiv:1304.4840].

[378] G. Franciolini, L. Hui, R. Penco, L. Santoni and E. Trincherini, *Effective Field Theory of Black Hole Quasinormal Modes in Scalar-Tensor Theories*, *JHEP* **02** (2019) 127 [arXiv:1810.07706].

[379] S.B. Edgar and A. Hoglund, *Dimensionally dependent tensor identities by double antisymmetrization*, *J. Math. Phys.* **43** (2002) 659 [arXiv:gr-qc/0105066].

[380] L.V. Delacrétaz, S. Endlich, A. Monin, R. Penco and F. Riva, *(Re-)Inventing the Relativistic Wheel: Gravity, Cosets, and Spinning Objects*, *JHEP* **11** (2014) 008 [arXiv:1405.7384].

[381] S.M. Carroll, *Spacetime and Geometry*, Cambridge University Press (7, 2019).

[382] S. Endlich, V. Gorbenko, J. Huang and L. Senatore, *An effective formalism for testing extensions to General Relativity with gravitational waves*, *JHEP* **09** (2017) 122 [arXiv:1704.01590].

[383] A.R. Solomon and M. Trodden, *Higher-derivative operators and effective field theory for general scalar-tensor theories*, *JCAP* **02** (2018) 031 [arXiv:1709.09695].

[384] T. Eguchi and P.G.O. Freund, *Quantum Gravity and World Topology*, *Phys. Rev. Lett.* **37** (1976) 1251.

[385] J.M. Martin-Garcia, D. Yllanes and R. Portugal, *The Invar tensor package: Differential invariants of Riemann*, *Comput. Phys. Commun.* **179** (2008) 586 [arXiv:0802.1274].

[386] L.D. Landau, *TEXTBOOK ON THEORETICAL PHYSICS. VOL. 2: CLASSICAL FIELD THEORY. (IN GERMAN)* (1987).

[387] A.E.M. van de Ven, *Two loop quantum gravity*, *Nucl. Phys. B* **378** (1992) 309.

[388] Z. Bern, H.-H. Chi, L. Dixon and A. Edison, *Two-Loop Renormalization of Quantum Gravity Simplified*, *Phys. Rev. D* **95** (2017) 046013 [arXiv:1701.02422].

[389] I.G. Avramidi, *Covariant methods for the calculation of the effective action in quantum field theory and investigation of higher derivative quantum gravity*, other thesis, 1986, [arXiv:hep-th/9510140].

[390] G. Goon, *Heavy Fields and Gravity*, *JHEP* **01** (2017) 045 [arXiv:1611.02705].

[391] D.J. Gross and E. Witten, *Superstring Modifications of Einstein's Equations*, *Nucl. Phys. B* **277** (1986) 1.

[392] A. Gruzinov and M. Kleban, *Causality Constrains Higher Curvature Corrections to Gravity*, *Class. Quant. Grav.* **24** (2007) 3521 [arXiv:hep-th/0612015].

[393] A. Adams, N. Arkani-Hamed, S. Dubovsky, A. Nicolis and R. Rattazzi, *Causality, analyticity and an IR obstruction to UV completion*, *JHEP* **10** (2006) 014 [arXiv:hep-th/0602178].

[394] B. Bellazzini, C. Cheung and G.N. Remmen, *Quantum Gravity Constraints from Unitarity and Analyticity*, *Phys. Rev. D* **93** (2016) 064076 [arXiv:1509.00851].

[395] B. Bellazzini, M. Lewandowski and J. Serra, *Positivity of Amplitudes, Weak Gravity Conjecture, and Modified Gravity*, *Phys. Rev. Lett.* **123** (2019) 251103 [arXiv:1902.03250].

[396] X.O. Camanho, J.D. Edelstein, J. Maldacena and A. Zhiboedov, *Causality Constraints on Corrections to the Graviton Three-Point Coupling*, *JHEP* **02** (2016) 020 [arXiv:1407.5597].

[397] H. Elvang and Y.-t. Huang, *Scattering Amplitudes*, arXiv:1308.1697.

[398] S. Deser, M.T. Grisaru, P. van Nieuwenhuizen and C.C. Wu, *Scale Dependence and the Renormalization Problem of Quantum Gravity*, *Phys. Lett. B* **58** (1975) 355.

[399] S. Deser, *Divergence Cancellations in Gravity - Matter Systems From Supergravity Embedding*, *Phys. Lett. B* **101** (1981) 311.

[400] F.A. Berends and R. Gastmans, *Quantum Electrodynamical Corrections to Graviton-Matter Vertices*, *Annals Phys.* **98** (1976) 225.

[401] I.T. Drummond and S.J. Hathrell, *QED Vacuum Polarization in a Background Gravitational Field and Its Effect on the Velocity of Photons*, *Phys. Rev. D* **22** (1980) 343.

[402] F. Bastianelli, J.M. Davila and C. Schubert, *Gravitational corrections to the Euler-Heisenberg Lagrangian*, *JHEP* **03** (2009) 086 [arXiv:0812.4849].

[403] N. Arkani-Hamed, L. Motl, A. Nicolis and C. Vafa, *The String landscape, black holes and gravity as the weakest force*, *JHEP* **06** (2007) 060 [arXiv:hep-th/0601001].

[404] G. Goon and K. Hinterbichler, *Superluminality, black holes and EFT*, *JHEP* **02** (2017) 134 [arXiv:1609.00723].

[405] F.A. Dolan, *Character formulae and partition functions in higher dimensional conformal field theory*, *J. Math. Phys.* **47** (2006) 062303 [arXiv:hep-th/0508031].

[406] S.A. Fulling, R.C. King, B.G. Wybourne and C.J. Cummins, *Normal forms for tensor polynomials. 1: The Riemann tensor*, *Class. Quant. Grav.* **9** (1992) 1151.

[407] J. Elias-Miro, J.R. Espinosa and A. Pomarol, *One-loop non-renormalization results in EFTs*, *Phys. Lett. B* **747** (2015) 272 [arXiv:1412.7151].

[408] Z. Bern, J. Parra-Martinez and E. Sawyer, *Nonrenormalization and Operator Mixing via On-Shell Methods*, *Phys. Rev. Lett.* **124** (2020) 051601 [arXiv:1910.05831].

[409] C. Cheung, *TASI Lectures on Scattering Amplitudes*, in *Proceedings, Theoretical Advanced Study Institute in Elementary Particle Physics : Anticipating the Next Discoveries in Particle Physics (TASI 2016): Boulder, CO, USA, June 6-July 1, 2016*, R. Essig and I. Low, eds. (2018), DOI [arXiv:1708.03872].

[410] L.J. Dixon, *Calculating scattering amplitudes efficiently*, in *Theoretical Advanced Study Institute in Elementary Particle Physics (TASI 95): QCD and Beyond*, 1, 1996 [arXiv:hep-ph/9601359].

[411] L.J. Dixon, *A brief introduction to modern amplitude methods*, in *Theoretical Advanced Study Institute in Elementary Particle Physics: Particle Physics: The Higgs Boson and Beyond*, 10, 2013, DOI [arXiv:1310.5353].

[412] N. Arkani-Hamed, T.-C. Huang and Y.-t. Huang, *Scattering Amplitudes For All Masses and Spins*, arXiv:1709.04891.

[413] H.K. Dreiner, H.E. Haber and S.P. Martin, *Two-component spinor techniques and Feynman rules for quantum field theory and supersymmetry*, *Phys. Rept.* **494** (2010) 1 [arXiv:0812.1594].

[414] D.A. McGady and L. Rodina, *Higher-spin massless S-matrices in four-dimensions*, *Phys. Rev. D* **90** (2014) 084048 [arXiv:1311.2938].

[415] N. Arkani-Hamed and J. Kaplan, *On Tree Amplitudes in Gauge Theory and Gravity*, *JHEP* **04** (2008) 076 [arXiv:0801.2385].

[416] T. Cohen, H. Elvang and M. Kiermaier, *On-shell constructibility of tree amplitudes in general field theories*, *JHEP* **04** (2011) 053 [arXiv:1010.0257].

[417] R. Britto, F. Cachazo and B. Feng, *New recursion relations for tree amplitudes of gluons*, *Nucl. Phys. B* **715** (2005) 499 [arXiv:hep-th/0412308].

[418] R. Britto, F. Cachazo, B. Feng and E. Witten, *Direct proof of tree-level recursion relation in Yang-Mills theory*, *Phys. Rev. Lett.* **94** (2005) 181602 [arXiv:hep-th/0501052].

[419] T. Ma, J. Shu and M.-L. Xiao, *Standard Model Effective Field Theory from On-shell Amplitudes*, arXiv:1902.06752.

[420] R. Aoude and C.S. Machado, *The Rise of SMEFT On-shell Amplitudes*, *JHEP* **12** (2019) 058 [arXiv:1905.11433].

[421] G. Durieux, T. Kitahara, Y. Shadmi and Y. Weiss, *The electroweak effective field theory from on-shell amplitudes*, *JHEP* **01** (2020) 119 [arXiv:1909.10551].

[422] G. Durieux and C.S. Machado, *Enumerating higher-dimensional operators with on-shell amplitudes*, *Phys. Rev. D* **101** (2020) 095021 [arXiv:1912.08827].

[423] G. Durieux, T. Kitahara, C.S. Machado, Y. Shadmi and Y. Weiss, *Constructing massive on-shell contact terms*, *JHEP* **12** (2020) 175 [arXiv:2008.09652].

[424] Z.-Y. Dong, T. Ma and J. Shu, *Constructing on-shell operator basis for all masses and spins*, arXiv:2103.15837.

[425] A. Falkowski, *Bases of massless EFTs via momentum twistors*, arXiv:1912.07865.

[426] P. Baratella, C. Fernandez and A. Pomarol, *Renormalization of Higher-Dimensional Operators from On-shell Amplitudes*, *Nucl. Phys. B* **959** (2020) 115155 [arXiv:2005.07129].

[427] M. Jiang, T. Ma and J. Shu, *Renormalization Group Evolution from On-shell SMEFT*, *JHEP* **01** (2021) 101 [arXiv:2005.10261].

[428] Z. Bern, J. Parra-Martinez and E. Sawyer, *Structure of two-loop SMEFT anomalous dimensions via on-shell methods*, *JHEP* **10** (2020) 211 [arXiv:2005.12917].

[429] J. Elias Miró, J. Ingoldby and M. Riembau, *EFT anomalous dimensions from the S-matrix*, *JHEP* **09** (2020) 163 [arXiv:2005.06983].

[430] P. Baratella, C. Fernandez, B. von Harling and A. Pomarol, *Anomalous Dimensions of Effective Theories from Partial Waves*, *JHEP* **03** (2021) 287 [arXiv:2010.13809].

[431] P. Mastrolia, *Double-Cut of Scattering Amplitudes and Stokes' Theorem*, *Phys. Lett. B* **678** (2009) 246 [arXiv:0905.2909].

[432] S. Caron-Huot and M. Wilhelm, *Renormalization group coefficients and the S-matrix*, *JHEP* **12** (2016) 010 [arXiv:1607.06448].

[433] M. Bronstein, *Symbolic Integration I*, vol. 2, Springer-Verlag, Berlin Heidelberg (2005), 10.1007/b138171.

[434] S. Blake. `https://demonstrations.wolfram.com/IntegrationUsingHermiteReduction/`.

[435] A. Azatov, R. Contino, C.S. Machado and F. Riva, *Helicity selection rules and noninterference for BSM amplitudes*, *Phys. Rev. D* **95** (2017) 065014 [`arXiv:1607.05236`].

[436] C. Cheung, *On-Shell Recursion Relations for Generic Theories*, *JHEP* **03** (2010) 098 [`arXiv:0808.0504`].

[437] H. Kawai, D.C. Lewellen and S.H.H. Tye, *A Relation Between Tree Amplitudes of Closed and Open Strings*, *Nucl. Phys. B* **269** (1986) 1.

[438] Z. Bern, J.J. Carrasco, M. Chiodaroli, H. Johansson and R. Roiban, *The Duality Between Color and Kinematics and its Applications*, `arXiv:1909.01358`.

[439] Z. Bern, A. De Freitas and H.L. Wong, *On the coupling of gravitons to matter*, *Phys. Rev. Lett.* **84** (2000) 3531 [`arXiv:hep-th/9912033`].

[440] R. Mertig, M. Bohm and A. Denner, *FEYN CALC: Computer algebraic calculation of Feynman amplitudes*, *Comput. Phys. Commun.* **64** (1991) 345.

[441] V. Shtabovenko, R. Mertig and F. Orellana, *FeynCalc 9.3: New features and improvements*, *Comput. Phys. Commun.* **256** (2020) 107478 [`arXiv:2001.04407`].

[442] S.A.R. Ellis, J. Quevillon, T. You and Z. Zhang, *Mixed heavy–light matching in the Universal One-Loop Effective Action*, *Phys. Lett. B* **762** (2016) 166 [`arXiv:1604.02445`].

[443] M.T. Grisaru, H.N. Pendleton and P. van Nieuwenhuizen, *Supergravity and the S Matrix*, *Phys. Rev. D* **15** (1977) 996.

[444] M.T. Grisaru and H.N. Pendleton, *Some Properties of Scattering Amplitudes in Supersymmetric Theories*, *Nucl. Phys. B* **124** (1977) 81.

[445] N.E.J. Bjerrum-Bohr, J.F. Donoghue and P. Vanhove, *On-shell Techniques and Universal Results in Quantum Gravity*, *JHEP* **02** (2014) 111 [`arXiv:1309.0804`].

[446] M.L. Mangano and S.J. Parke, *Multiparton amplitudes in gauge theories*, *Phys. Rept.* **200** (1991) 301 [`arXiv:hep-th/0509223`].

[447] L.J. Dixon, E.W.N. Glover and V.V. Khoze, *MHV rules for Higgs plus multi-gluon amplitudes*, *JHEP* **12** (2004) 015 [`arXiv:hep-th/0411092`].

[448] D.C. Dunbar and P.S. Norridge, *Infinities within graviton scattering amplitudes*, *Class. Quant. Grav.* **14** (1997) 351 [`arXiv:hep-th/9512084`].

[449] D. Goncalves, T. Han and S. Mukhopadhyay, *Off-Shell Higgs Probe of Naturalness*, *Phys. Rev. Lett.* **120** (2018) 111801 [`arXiv:1710.02149`].